

Open-angle glaucoma:
from epidemiology to molecular
aspects and anatomical features

Hendrika Springelkamp

Acknowledgements:

The research described in this thesis was supported by the NWO Graduate Programme 2010 BOO (022.002.023). The Rotterdam Study and ERF were supported by the Netherlands Organisation of Scientific Research (NWO; 91111025); Erasmus Medical Center and Erasmus University, Rotterdam, The Netherlands; Netherlands Organization for Health Research and Development (ZonMw); Uitzicht; the Research Institute for Diseases in the Elderly; the Ministry of Education, Culture and Science; the Ministry for Health, Welfare and Sports; the European Commission (DG XII); the municipality of Rotterdam; the Netherlands Genomics Initiative/NWO; Center for Medical Systems Biology of NGL; Stichting Lijf en Leven; Stichting Oogfonds Nederland; Landelijke Stichting voor Blinden en Slechtzienden; Prof. Dr. Henkes Stichting; Algemene Nederlandse Vereniging ter Voorkoming van Blindheid; MD Fonds; Glaucoomfonds; Medical Workshop; Heidelberg Engineering; Topcon Europe BV. The generation and management of GWAS genotype data for the Rotterdam Study is supported by the Netherlands Organisation of Scientific Research NWO Investments (nr. 175.010.2005.011, 911-03-012). This study is funded by the Research Institute for Diseases in the Elderly (014-93-015; RIDE2), the Netherlands Genomics Initiative (NGL)/Netherlands Organisation for Scientific Research (NWO) project nr. 050-060-810.

The publication of this thesis was financially supported by:

Glaucoomfonds, Prof.Dr. Henkes Stichting, Landelijke Stichting voor Blinden en Slechtzienden, Erasmus MC (Department of Epidemiology), Allergan BV, Bayer B.V., Théa Pharma

Cover & lay-out: Jessy Wijgerde
Printing: Ridderprint BV
ISBN: 9789491462252

© 2016 H. Springelkamp

All rights reserved. No part of this book may be reproduced, stored in a retrieval system, or transmitted in any form or by any means without permission of the author, or, when appropriate, of the publisher of the publications.

OPEN-ANGLE GLAUCOMA:
FROM EPIDEMIOLOGY TO MOLECULAR ASPECTS AND ANATOMICAL FEATURES

Open kamerhoek glaucoom:
van epidemiologie naar moleculaire aspecten en anatomische kenmerken

Proefschrift

ter verkrijging van de graad van doctor aan de
Erasmus Universiteit Rotterdam
op gezag van de
rector magnificus

Prof.dr. H.A.P. Pols

en volgens besluit van het College voor Promoties.

De openbare verdediging zal plaatsvinden op
woensdag 13 januari 2016 om 15.30 uur

door

Hendrika Springelkamp

geboren te Apeldoorn

PROMOTIECOMMISSIE

Promotoren:

Prof.dr.ir. C.M. van Duijn

Prof.dr. N.M. Jansonius

Prof.dr. C.C.W. Klaver

Overige leden:

Prof.dr. R.M.W. Hofstra

Prof.dr. P.J. Foster

Prof.dr. L.R. Pasquale

Voor mijn ouders

TABLE OF CONTENTS

Part 1 Introduction	9
1.1 General introduction	11
1.2 The genetics of primary open-angle glaucoma	17
Part 2 The role of optical coherence tomography in glaucoma	27
2.1 Optimizing the information yield of 3-D OCT in glaucoma	29
2.2 Population-based evaluation of retinal nerve fiber layer, retinal ganglion cell layer, and inner plexiform layer as a diagnostic tool for glaucoma	47
Part 3 Risk factors for intraocular pressure and glaucoma	69
3.1 Incidence of glaucomatous visual field loss after two decades of follow-up: the Rotterdam Study	71
3.2 Relationship between sleep apnea and open-angle glaucoma: a population-based cohort study	85
3.3 Associations with intraocular pressure across Europe: The European Eye Epidemiology (E ³) Consortium	99
Part 4 Genetics of intraocular pressure and optic nerve head measurements	123
4.1 Genome-wide analysis of multi-ancestry cohorts identifies new loci influencing intraocular pressure and susceptibility to glaucoma	125
4.2 Meta-analysis of genome-wide association studies identifies novel loci that influence cupping and the glaucomatous process	139
4.3 Meta-analysis of genome-wide association studies identifies novel loci associated with optic disc morphology	153
4.4 <i>ARHGEF12</i> influences the risk of glaucoma by increasing intraocular pressure	171
4.5 New insights into genetics of primary open-angle glaucoma based on meta-analyses of intraocular pressure and optic disc characteristics	189
Part 5 Functional consequences of genetic variants	245
5.1 Exome sequencing and functional analyses suggest <i>SIX6</i> is a gene involved in an altered proliferation-differentiation balance early in life and optic nerve degeneration at old age	247
Part 6 General discussion	271
Part 7	289
Samenvatting	290
Summary	293
Acknowledgements – Dankwoord	296
PhD Portfolio	300
List of publications	302
About the author	305

PART 1

INTRODUCTION

CHAPTER 1.1

General introduction



Glaucoma

The eye helps us to create vision by gathering, focusing and transmitting light to the brain. Light first passes through the cornea, which refracts the light; then through the pupil, which controls the amount of incoming light; and through the lens, which subsequently focuses the light onto the retina. Photoreceptor cells in the retina convert the light into electric signals. These signals are transferred along the optic nerve and subsequent visual pathways to the brain where they are processed so that we can form an image of the outside world. Each optic nerve contains approximately 1 million nerve fibers. Glaucoma is a disease that affects the optic nerve.

An elevated pressure within the eye (intraocular pressure; IOP) is an important risk factor for glaucoma. Intraocular pressure is the result of a balanced process of secretion and drainage of aqueous humor. Aqueous humor is produced by the ciliary body and goes through the pupil and anterior chamber to the trabecular meshwork in the iridocorneal angle, where it leaves the eye (see Figure 1C). The balance between production and outflow determines the IOP. In glaucoma, changes of the optic nerve lead to irreversible visual field loss which may end in blindness. In 2010, 60 million people were estimated to suffer from glaucoma, of which more than 8 million people were blind, making this disease the most important cause of irreversible blindness worldwide¹. Glaucoma is categorized in several subtypes, based on the cause of elevated IOP. In open-angle glaucoma (OAG) there is no visible damage or obstruction in the iridocorneal angle, in contrast to angle-closure glaucoma in which a blockage of the trabecular outflow consists. The most common form in Europeans is OAG. This can be further divided into primary open-angle glaucoma, i.e., without a detectable underlying disease, and glaucomas in eyes with other abnormalities. Examples of the latter are the pseudoexfoliation and pigment dispersion syndromes.

Imaging

OAG is characterized by various features such as thinning of the retinal nerve fiber layer (RNFL) and retinal ganglion cell layer (RGCL). The best-known characteristic is a change of the appearance of the optic nerve head (ONH), also called optic disc. The ONH is visible by ophthalmoscopy. The center of the ONH is called the cup. The nerve fibers are located in the rim, which surrounds the cup. Loss of RNFL and RGCL leads to an enlarged cup, or cupping. This process can be quantified by, amongst others, the vertical cup-disc ratio (VCDR), which is the vertical diameter of the cup compared to the vertical diameter of the total ONH. The ONH can also be examined by imaging. A commonly used device is the Heidelberg Retina Tomograph (HRT)², a confocal scanning laser ophthalmoscope. A laser light scans the ONH at different depths in a series of sequential scans, allowing the creation of a three-dimensional image of the ONH, which can subsequently be analyzed quantitatively. It can also image the RNFL around the ONH and assess its thickness. Another device, the GDx, is a scanning laser polarimetry^{3,4}. It can also measure the RNFL thickness around the ONH, using the birefringent properties of the RNFL. A lot of studies have been published about the correlation between functional loss (visual field loss) as assessed with perimetry and structural loss as assessed with HRT or GDx, however, this correlation was not very good. New imaging techniques were considered, such as Optical Coherence Tomography (OCT)^{5,6}. This technology is based on low-coherence interferometry of electromagnetic radiation, typically employing the near-infrared part of the spectrum, and the results for OAG diagnosis are promising. Most OAG

studies on OCT were based on selected patients from the clinic. How well OCT performs in a setting free of selection bias is currently unclear.

Epidemiology

Although the glaucomatous characteristics of the ONH are well defined, the pathogenesis of OAG is largely unknown. Other risk factors besides an elevated IOP (see above) include a positive family history, myopia or nearsightedness, higher age, and African descent⁷⁻⁹. Another risk factor is a thin central corneal thickness. This causes an underestimation of the actual IOP, but it was also found that it is a risk factor for progression to glaucoma in patients with ocular hypertension independent of IOP¹⁰⁻¹². The known risk factors cannot explain OAG in all cases. For example, it has been estimated that up to 50% of OAG patients have a normal IOP^{13,14}. The identification of new risk factors may lead to a better understanding of the disease and eventually the development of new therapies.

Genetic epidemiology

It has been known for decades that genetic predisposition plays an important role in glaucoma (see Chapter 1.2). In 1993, the first OAG gene (*MYOC*) was identified by linkage studies¹⁵⁻¹⁷. In the next decades, other genes (*OPTN*, *WDR36*) were identified using this technique¹⁸⁻²⁰. During the last years, the identification of new glaucoma genes has been accelerated by the introduction of genome-wide association studies (GWAS). In GWAS, millions of single nucleotide polymorphisms (SNPs) are determined across the genome. Subsequently, the association between these SNPs and the disease or outcome of interest is determined. The identified genetic variants or genes (*SIX6*, *ATOH7*, *CDKN2B*) explain less than 5% of the variation in risk of OAG²¹. Since the heritability of OAG is higher²², this means that there are probably still genes associated with OAG but not identified at the moment. Identification of new genetic variants can learn us more about the pathways involved in OAG. The discovery of new pathways can be a starting point for further research focusing on new therapeutics for OAG.

Zebrafish

Functional studies are indispensable for the translation of genetic variants into knowledge about the pathophysiology of OAG. The zebrafish appears suitable for testing genes associated with eye diseases and has many advantages: after approximately 100 days they are mature and can produce 200-300 eggs a week, fertilized eggs become a transparent embryo outside the mother, the fish develops rapidly (the eye becomes functional after 1 week), and the zebrafish genome is well known and comparable to the human genome²³. Figure 1 shows that the zebrafish eye has many similarities to the human eye. Although the macula is missing in the zebrafish eye, the retinal structure is comparable. Another advantage is that the genome of zebrafish is easy modifiable: microinjection of antisense morpholinos in the egg yolk will cause a transient knockdown of the protein produced by the targeted gene during embryogenesis. This technique is explained in Figure 2.

Figure 1. The human eye (A) is similar to the zebrafish eye (B), although there are some differences²³. For example, the human lens is more ellipsoid and the macula is absent in zebrafish. Part C shows the outflow pathway of the aqueous humor (the dotted square in A): it is produced in the ciliary body and leaves the eye in the trabecular meshwork (dotted arrow). A small proportion leaves the eye via the uveoscleral pathway (smaller dotted arrow).

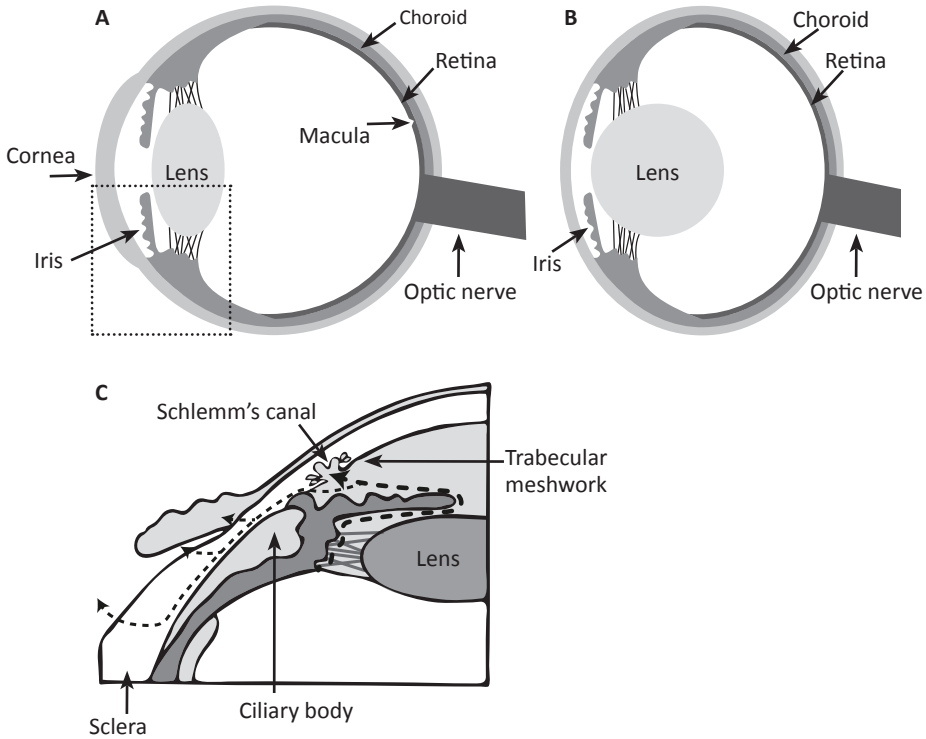
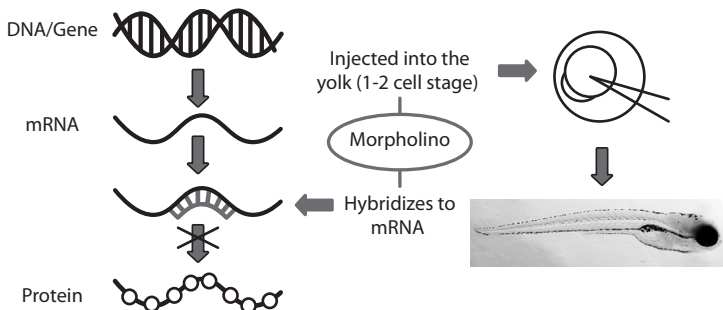


Figure 2. A gene is a structure in the DNA. The order of its nucleotides contains information for one or more proteins. There are two major steps in gene expression: transcription and translation. The gene first makes a copy of itself (transcription), resulting in messenger RNA (mRNA). Subsequently, the nucleotides of mRNA are translated into amino acids of the protein. Morpholinos are molecules that bind to sequences of (messenger) RNA, thereby preventing the translation into a protein. They are often injected in the one or two cell stage of an embryo zebrafish. As a result, the effect of reduced protein formation (i.e., knockdown of the gene) can be studied in the early development stage of the zebrafish.



This thesis and its study populations

The research described in the current thesis addresses several questions related to the topics above. The aims of this research were:

Chapter 2: to address the diagnostic utility of OCT for OAG.

Chapter 3: to elucidate new risk factors for OAG.

Chapter 4: to identify novel genetic variants associated with OAG or its endophenotypes.

Chapter 5: to assess the functional consequences of a gene associated with OAG.

In order to address these aims we used different study populations. The research in Chapter 2 is conducted in the Rotterdam Study. This population-based study consists of almost 15,000 participants aged 45 years and older, living in Ommoord, a district of Rotterdam, the Netherlands²⁴. In Chapter 3, which is also based on the Rotterdam study, I also performed research as part of the European Eye Epidemiology (E³) consortium. This collaborative network of population-based studies across Europe currently includes 38 studies with a total of approximately 150,000 participants. The aim of the E³ consortium is to increase understanding of eye disease and vision loss by creating and analyzing large pooled datasets. This consortium also includes the Erasmus Rucphen Family study, a family based study which was carried out in the South of the Netherlands. In Chapter 4, I used data of another network of studies: the International Glaucoma Genetics Consortium (IGGC). This consortium includes 18 population-based studies from different continents across the world, including the Rotterdam study and the Erasmus Rucphen Family study, with a total of approximately 35,000 participants with data of genotypes and OAG endophenotypes, and OAG case-control studies.

A drawback of using population-based studies is the relatively low number of OAG cases due to the low prevalence. Therefore, I focused on OAG endophenotypes in the studies described in Chapter 3 and Chapter 4. Endophenotypes are phenotypic parameters related to the disease of outcome and include, amongst others, IOP, VCDR, cup area, and disc area for OAG. This makes it possible to study the epidemiology and genetics of OAG on large scale in populations with only a small number of OAG cases. New identified genetic variants for endophenotypes can be subsequently validated in OAG case-control studies to see if they are indeed related to the risk of OAG or normal variation in IOP or VCDR.

References

1. Quigley, H.A. & Broman, A.T. The number of people with glaucoma worldwide in 2010 and 2020. *Br J Ophthalmol* 90, 262-7 (2006).
2. Rohrschneider, K., Burk, R.O., Kruse, F.E. & Volcker, H.E. Reproducibility of the optic nerve head topography with a new laser tomographic scanning device. *Ophthalmology* 101, 1044-9 (1994).
3. Dreher, A.W. & Reiter, K. Retinal laser ellipsometry: a new method for measuring the retinal nerve fibre layer thickness distribution? *Clin Vis Sci* 7, 481-488 (1992).
4. Weinreb, R.N. et al. Histopathologic validation of Fourier-ellipsometry measurements of retinal nerve fiber layer thickness. *Arch Ophthalmol* 108, 557-60 (1990).
5. Hee, M.R. et al. Optical coherence tomography of macular holes. *Ophthalmology* 102, 748-56 (1995).
6. Schuman, J.S. et al. Optical coherence tomography: a new tool for glaucoma diagnosis. *Curr Opin Ophthalmol* 6, 89-95 (1995).
7. Czudowska, M.A. et al. Incidence of glaucomatous visual field loss: a ten-year follow-up from the Rotterdam Study. *Ophthalmology* 117, 1705-12 (2010).
8. Marcus, M.W., de Vries, M.M., Junoy Montolio, F.G. & Jansonius, N.M. Myopia as a risk factor for open-angle glaucoma: a systematic review and meta-analysis. *Ophthalmology* 118, 1989-1994 e2 (2011).
9. Tielsch, J.M. et al. Racial variations in the prevalence of primary open-angle glaucoma. The Baltimore Eye Survey. *JAMA* 266, 369-74 (1991).
10. European Glaucoma Prevention Study, G. et al. Predictive factors for open-angle glaucoma among patients with ocular hypertension in the European Glaucoma Prevention Study. *Ophthalmology* 114, 3-9 (2007).
11. Leske, M.C. et al. Predictors of long-term progression in the early manifest glaucoma trial. *Ophthalmology* 114, 1965-72 (2007).
12. Gordon, M.O. et al. The Ocular Hypertension Treatment Study: baseline factors that predict the onset of primary open-angle glaucoma. *Arch Ophthalmol* 120, 714-20; discussion 829-30 (2002).
13. Anderson, D.R. & Normal Tension Glaucoma, S. Collaborative normal tension glaucoma study. *Curr Opin Ophthalmol* 14, 86-90 (2003).
14. Cheng, J.W., Cai, J.P. & Wei, R.L. Meta-analysis of medical intervention for normal tension glaucoma. *Ophthalmology* 116, 1243-9 (2009).
15. Kubota, R. et al. A novel myosin-like protein (myocilin) expressed in the connecting cilium of the photoreceptor: molecular cloning, tissue expression, and chromosomal mapping. *Genomics* 41, 360-9 (1997).
16. Sheffield, V.C. et al. Genetic linkage of familial open angle glaucoma to chromosome 1q21-q31. *Nat Genet* 4, 47-50 (1993).
17. Stone, E.M. et al. Identification of a gene that causes primary open angle glaucoma. *Science* 275, 668-70 (1997).
18. Monemi, S. et al. Identification of a novel adult-onset primary open-angle glaucoma (POAG) gene on 5q22.1. *Hum Mol Genet* 14, 725-33 (2005).
19. Rezaie, T. et al. Adult-onset primary open-angle glaucoma caused by mutations in optineurin. *Science* 295, 1077-9 (2002).
20. Sarfarazi, M. et al. Localization of the fourth locus (GLC1E) for adult-onset primary open-angle glaucoma to the 10p15-p14 region. *Am J Hum Genet* 62, 641-52 (1998).
21. Ramdas, W.D. et al. Clinical implications of old and new genes for open-angle glaucoma. *Ophthalmology* 118, 2389-97 (2011).
22. Teikari, J.M. Genetic factors in open-angle (simple and capsular) glaucoma. A population-based twin study. *Acta Ophthalmol (Copenh)* 65, 715-20 (1987).
23. Chhetri, J., Jacobson, G. & Gueven, N. Zebrafish--on the move towards ophthalmological research. *Eye (Lond)* 28, 367-80 (2014).
24. Hofman, A. et al. The Rotterdam Study: 2016 objectives and design update. *Eur J Epidemiol* 30, 661-708 (2015).

CHAPTER 1.2

The genetics of primary open-angle glaucoma



Henriët Springelkamp, Gabriëlle H.S. Buitendijk, Lintje Ho, Caroline C.W. Klaver.

In: Scholl HP, Massof RW, West S (Eds). Ophthalmology and the ageing society, (pp68-82). Berlin Heidelberg. Springer.

Familial occurrence of glaucoma has been known for decades; early reports on this topic stem from 1869^{1,2}. It has been estimated that up to 50% of primary open-angle glaucoma (POAG) patients have a positive family history³. The risk for family members was calculated in a population-based familial aggregation study; first degree relatives of an affected individual had an approximately tenfold increased risk of developing POAG compared to first degree relatives of controls (22% versus 2.3%)⁴. During the last two decades, the attention has shifted towards identification of associated genes (Table 1). So far, fifteen chromosomal regions have been identified for POAG (HGNC Database 2011). Several POAG genes are rare but have a major effect on the risk of disease. Other genes are more common but have only minor effects.

Rare genes with high risk of POAG

MYOC

The first gene carrying an important POAG risk was found in a disease-associated locus and named *TIGR* (trabecular meshwork-induced glucocorticoid response protein) or *MYOC* (encoding myocilin)⁵⁻⁷. The name myocilin was chosen because of its similarities with myosin- and olfactomedin-like domains and the abundant appearance in the connecting cilium of photoreceptor cells. Myocilin is expressed in most tissues of the body and in most ocular tissues (including trabecular meshwork, sclera, iris, cornea, lens, ciliary body, retina, optic nerve and vitreous humor)⁸. Mutations in the *MYOC* gene generally lead to an elevated intraocular pressure (IOP). Many disease mechanisms have been suggested, such as an overproduction of myocilin by the trabecular meshwork with subsequent accumulation causing obstruction in the outflow of aqueous humor and elevated IOP⁹. Nevertheless, the precise effect of the mutated gene is still unclear¹⁰. Myocilin-associated glaucoma inherits as an autosomal dominant disease, and carriers of a mutation have a 90% risk of developing POAG¹¹. Most mutations are associated with juvenile or early-adult onset of POAG, although some are associated with the adult-onset phenotype (GLN368STOP mutation⁸). *MYOC* is estimated to play a role in 3-5% of POAG cases.

OPTN

The second well-identified gene with a major effect is *OPTN* (encoding optineurin, i.e. “optic neuropathy inducing” protein)^{12,13}. The site of expression of this protein includes the trabecular meshwork, aqueous humor and retina, and the current hypothesis is that its effect is neuroprotective. A defective optineurin increases the susceptibility of retinal ganglion cells to premature death, but the exact mechanisms behind the mutations are unclear¹⁰. Mutations in optineurin are associated with normal tension glaucoma. The E50K mutation is the most common mutation, and carriers of E50K have a more severe form of glaucoma¹⁴. They are younger at onset, have a worse initial cup-disc ratio, and a faster progression of visual field loss.

WDR36

The third high-risk gene is *WDR36* (WD40-repeat 36)¹⁵. In the initial study, mutations were found in patients with high- and low-pressure glaucoma. In a study with 118 probands from families affected by POAG, patients with a more severe disease more often had a *WDR36* variant, so it was suggested that *WDR36* acts as modifier gene¹⁶. *WDR36* is expressed in non-ocular and numerous ocular tissues (lens, iris, sclera, ciliary muscles, ciliary body, trabecular meshwork, retina and optic nerve). The protein *WDR36* interacts with P53¹⁷. Mouse models show that mutations

in *WDR36* lead to progressive degeneration of retinal ganglion cells in the peripheral retina¹⁸, and *WDR36* depletions in human trabecular meshwork cells lead to apoptotic cell death¹⁹.

NTF4

A mutation in neurotrophin-4 (*NTF4*) was recorded in 1.7% of European POAG patients²⁰. The most frequent *NTF4* mutation leads to decreased activation of tyrosine kinase receptor B and that may cause loss of neurotrophic function¹⁰. *NTF4* mutations are even less frequent in other populations; for instance, it is present in only 0.6% of Chinese POAG patients²¹.

Common genes with minor risk of POAG

CAV 1/CAV 2

A variant (rs4236601) near the Caveolin 1 and 2 genes was associated with POAG²². This variant increased the risk of POAG 1.2x in persons of European ancestry but up to 5x in Chinese. In the eye, *CAV1* and *CAV2* are expressed in the scleral spur cells, trabecular meshwork, and retinal ganglion cells. It is unknown how it plays a role in the pathogenesis.

CDKN2B

This gene was initially discovered as an association with vertical cup-disc ratio (VCDR)²³. Recently, it was shown that the risk variant in this gene increased the risk of POAG 1.5x^{24,25}. *CDKN2B* encodes a protein which plays a role in cell growth regulation²³.

ATOH7

Aside from the involvement in optic disc area and VCDR^{23,26}, risk variants in *ATOH7* are associated with a 1.3x increased risk of POAG²⁵. *ATOH7* is expressed in the retina and plays a role in retinal ganglion cell and optic nerve formation in mice²⁷, but it has not been linked to optic nerve pathology in humans²⁵.

SIX1

A locus between *SIX1* and *SIX6* is associated with VCDR and a 1.2x increased risk of POAG^{23,25}. Variants in *SIX6* are associated with bronchio-oto-renal syndrome. *SIX1* plays a role in eye organogenesis.

TMCO1

SNPs located in *TMCO1* are significantly associated with IOP and a 1.3x increased risk of glaucoma^{24,28}. The function of *TMCO1* is largely unknown. It is highly expressed in the human ciliary body and trabecular meshwork and interacts with *CAV1*.

GAS7

GAS7 has been associated with IOP and a 10% decreased glaucoma risk²⁸. *GAS7* is expressed in the ciliary body and the human trabecular meshwork. It is implicated in cell remodelling. The gene interacts with *MYOC* and other known glaucoma genes such as *OPTN*, *WDR36*, and *CAV1*.

RPGRIP1

Associations between retinitis pigmentosa GTPase regulator-interacting protein 1 (*RPGRIP1*) and POAG have been found in European subjects²⁹. *RPGRIP1* is a scaffold for proteins acting in signaling pathways of different retinal cells. The gene may act as a susceptibility gene.

Copy number variations

Fingert et al. and Davis et al. reported about the association between copy number variations (CNVs) and POAG^{30,31}. Fingert et al. identified a new chromosomal POAG locus and suggested that an extra copy of the *TBK1* gene on this region (chromosome 12q14) is responsible for their normal tension glaucoma cases. It was expressed in microvasculature of the retina, the nerve fiber layer, and in ganglion cells. It interacts with optineurin. Further, a kinase encoded by *TBK1* regulates the expression of genes involved in the NF-kappaB signaling pathway. Processes regulated by this pathway, e.g. apoptosis, have been implicated in the pathogenesis of glaucoma.

Spurious candidates

Many other genetic variants have been related to POAG, but their association is less clear-cut than the genes mentioned above. Tunny et al. suggested that mutations in the atrial natriuretic peptide (*ANP*) gene may play a role in at least a proportion of patients with familial glaucoma due to regulation of intraocular pressure³².

An association between POAG and apolipoprotein E (*APOE*) was suggested in French, Tasmanian, Japanese, and Chinese populations³³⁻³⁶. *APOE* has been involved in Alzheimer's Disease, like glaucoma a neurodegenerative disease. Patients with Alzheimer's Disease have an increased frequency of glaucoma. Functionally, *APOE* is known to interact with myocilin. Although these are interesting findings for the pathogenesis of glaucoma, the role of *APOE* remains controversial³⁷.

Glaucomatous neuropathy is caused by apoptosis. Tumor suppressor protein p53 plays a role in regulation of apoptosis, and it has been suggested that variants in *p53* are a risk factor in the development of POAG in Chinese and Caucasian populations^{38,39}.

Polymorphisms in *OPA1* have been associated with normal tension glaucoma^{40,41}, but it seems that this is not the case in glaucoma phenotypes with elevated intraocular pressure⁴². An association between *CYP1B1* and POAG is also controversial⁴³⁻⁴⁶. Several other variants have been described, such as variants in tumor necrosis factor alpha⁴⁷, insulin-like growth factor⁴⁸, interleukin-1 beta⁴⁹ and interleukin-1 alpha⁵⁰. However, most have not been replicated by other investigators or in other populations⁵¹.

Genes associated with POAG intermediates

An approach that has been recently used in the identification of POAG genes is the focus on quantitative intermediate POAG outcomes, such as VCDR and IOP. The heritability for VCDR ranges from 0.48 to 0.80 and for IOP from 0.29 to 0.50⁵²⁻⁵⁵. Several genes that could be validated as glaucoma genes have been discovered in this way (*CDKN2B*, *ATOH7*, *SIX1*, *TMCO1*, and *GAS7*; see above). So, up to now, this approach appears to be successful.

Optic disc area

SNPs in or near the genes *CDC7*, *TGFBR3*, *SALL1*, and *CARD10* have been associated with optic disc area^{23,56}. *CDC7* encodes a protein which is involved in cell division cyclus. This protein also interacts with the *CDKN2A* protein which is associated with VCDR. A member of the bone morphogenetic protein (BMP) and TGFbeta superfamily is *GDF11*. This gene is

of the same family as *TGFBR3* and interacts with *ATOH7*. *SALL1* defects are a cause of the bronchio-oto-renal syndrome and Townes-Brocks syndrome. Ocular manifestations of the latter include optic nerve atrophy⁵⁷. *CARD10* is involved in the regulation of apoptosis and signals the activation of NF-kappaB. The NF-kappaB signaling pathway is implicated in major neurodegenerative diseases like Alzheimer's Disease.

Vertical Cup-Disc Ratio

Associations with VCDR were found for loci between *FRMD8*, *SCYL1*, and *LTBP3*, in the *DCLK1* gene, *CHEK2* gene, *RERE* gene, and *LRP1B* gene^{23,26,58}. *SCYL1* has been associated with optic nerve atrophy in mice. *LTBP3* is involved in the same signaling pathway as *CDKN2B* for cell growth regulation. It is also homolog to *LTBP2*, which is implicated in primary congenital glaucoma. *DLCK1* may be involved in a calcium signaling pathway. This pathway controls neuronal migration in developing brain and mature brain. Several types of cancer are associated with *CHEK2*. Overexpression of *RERE* leads to apoptosis via triggering of caspase-3 activation. *LRP1B* may be included in a development pathway (with *SIX1*, *SALL1* and *DCLK1*).

Conclusion

A variety of genes have been implicated in the pathogenesis of POAG. Their effect is one of extremes. On one end are mutations in the *MYOC*, *OPTN*, and *WDR36* genes with a large impact on the risk of POAG; however, they occur only in a small number of families. On the other end are frequent variants with only small effects. All mutations in the currently six established POAG genes combined (*MYOC*, *OPTN*, *WDR36*, *ATOH7*, *CDKN2B*, and *SIX1*) explain, together with age, gender, and IOP, only 4-6% of the variation in POAG risk⁵⁹. Hence, there is still much work to do in unraveling the genetic background of this disease.

Table 1. Overview of major genes associated with POAG.

Gene	Location	POAG	VCDR	DA	IOP	Study design	Replication	Gene function
<i>MYOC</i> ^{5,6}	1q23-q24	+	?	?	?	Linkage analysis	+	Unclear
<i>OPTN</i> ^{12,13}	10p13	+	?	?	?	Linkage analysis	+	Loss of neuroprotection in eye and optic nerve
<i>WDR36</i> ^{15,18,19}	5q22.1	+	?	?	?	Mutation screening candidate genes	+	Progressive degeneration of retinal ganglion cells, apoptosis in trabecular meshwork
<i>NTF4</i> ^{20,21}	19q13.3	+	?	?	?	Mutation screening	+	Loss of neurotrophic function
<i>CAV1/2</i> ²²	7q31	+	?	?	?	GWAS	+	Unknown
<i>CDKN2B</i> ²³	9p21	+	+	?	?	GWAS	+	Cell growth regulation
<i>ATOH7</i> ^{23,25,27}	10q21.3-q22.1	+	+	+	?	GWAS	+	Retinal ganglion cell and optic nerve formation in mice
<i>SIX1</i> ^{23,25}	14q22.2-q23	+	+	?	+	GWAS	+	Eye organogenesis
<i>TMC01</i> ^{24,28}	1q24.1	+	?	?	+	GWAS	+	Unknown. Interacts with <i>CAV1</i> .
<i>GAS7</i> ²⁸	17p13.1	+	?	?	?	GWAS	+	Cell remodelling. Interacts with <i>MYOC</i> , <i>OPTN</i> , <i>WDR36</i> and <i>CAV1</i> .
<i>RPGRIP1</i> ²⁹	14q11	+	?	?	?	Mutation screening candidate genes	+	Susceptibility gene. Scaffold for proteins acting in signalling pathways of different retinal cells.
<i>TBK1</i> ^{30,31}	12q14	+	?	?	?	Linkage study	-	Interacts with optineurin. Regulation of genes in the NF-kappaB signaling pathway.
<i>ANP</i> ³²	1p36.21	+	?	?	?	Analysis of <i>ANP</i>	+	Regulation of intraocular pressure
<i>APOE</i> ³³⁻³⁷	19q13.31	+	?	?	?	Analysis of <i>APOE</i>	-	Involved in neurodegenerative diseases like Alzheimer's Disease
<i>TP53</i> ^{38,39,60}	17p13.1	+	?	?	?	Analysis of <i>P53</i>	?	Regulation of apoptosis
<i>OPA1</i> ⁴⁰⁻⁴²	3q28-q29	+	?	?	?	Analysis of <i>OPA1</i>	?	Involved in autosomal dominant optic atrophy

Table 1. (continued)

Gene	Location	POAG	VCDR	DA	IOP	Study design	Replication	Gene function
<i>CYP11B1</i> ⁴³⁻⁴⁶	2p22.2	+	?	?	?	Analysis of <i>CYP11B1</i>	?	Development of iridocorneal angle
<i>TNFα</i> ⁷	6p21.3	+	?	?	?	Analysis of <i>TNFα</i>	?	Apoptosis
<i>IGF-2</i> ⁴⁸	11p15.5	+	?	?	?	Analysis of <i>IGF-2</i>	-	Regulation of apoptosis
<i>IL1α</i> ^{50,61}	2q14	+	?	?	?	Analysis of <i>IL 1α</i>	?	Apoptosis
<i>IL1β</i> ^{49,61}	2q14	+	?	?	?	Analysis of <i>IL 1β</i>	?	Apoptosis
<i>CDC7</i> ²³	1p22	?	?	+	?	GWAS	+	Cell division cyclus Interacts with <i>CDKN2A</i>
<i>TGFB3</i> ²³	1p22	?	?	+	?	GWAS	+	<i>GDF11</i> interacts with <i>ATOH7</i>
<i>SALL1</i> ²³	16q12.1	?	?	+	?	GWAS	+	Involved in bronchio-oto-renal syndrome and Townes-Brocks syndrome
<i>CARD10</i> ⁵⁶	22q13.1	?	?	+	?	GWAS	+	Regulation of apoptosis Signals the activation of NF-kappab
<i>SCYL1</i> ²³	11q11-q12	?	+	?	?	GWAS	+	Associated with optic nerve atrophy in mice
<i>LTBP3</i> ²³	11q12	?	+	?	?	GWAS	+	Cell growth regulation
<i>DCLK1</i> ²³	13q13	?	+	?	?	GWAS	+	Calcium signalling pathway which controls neuronal migration in developing and mature brain
<i>CHEK2</i> ²³	22q12.1	?	+	?	?	GWAS	+	Associated with several types of cancer
<i>RERE</i> ^{23,58}	1p36	?	+	?	?	GWAS, linkage and association analysis	+	Apoptosis via triggering of caspase-3 activation
<i>LRP1B</i> ^{25,58}	2q21.2-q22.2	?	+	?	?	GWAS, linkage and association analysis	+	Developing of the eye

ABBREVIATIONS

DA disc area
GWAS genome-wide association study
IOP intraocular pressure

POAG

VCDR

primary open-angle glaucoma
vertical cup-disc ratio

SYMBOLS IN "REPLICATION" COLUMN

+ replicated
- not replicated
? controversial

References

1. Graefe, A.v. Beitrage zur Pathologie und Therapie des Glaukoms. *Arch Ophthalmol* 15, 108-252 (1869).
2. James, R.R. A Pedigree of a Family Showing Hereditary Glaucoma. *Br J Ophthalmol* 11, 438-43 (1927).
3. Tielsch, J.M., Katz, J., Sommer, A., Quigley, H.A. & Javitt, J.C. Family history and risk of primary open angle glaucoma. The Baltimore Eye Survey. *Arch Ophthalmol* 112, 69-73 (1994).
4. Wolfs, R.C. et al. Genetic risk of primary open-angle glaucoma. Population-based familial aggregation study. *Arch Ophthalmol* 116, 1640-5 (1998).
5. Sheffield, V.C. et al. Genetic linkage of familial open angle glaucoma to chromosome 1q21-q31. *Nat Genet* 4, 47-50 (1993).
6. Stone, E.M. et al. Identification of a gene that causes primary open angle glaucoma. *Science* 275, 668-70 (1997).
7. Kubota, R. et al. A novel myosin-like protein (myocilin) expressed in the connecting cilium of the photoreceptor: molecular cloning, tissue expression, and chromosomal mapping. *Genomics* 41, 360-9 (1997).
8. Fingert, J.H., Stone, E.M., Sheffield, V.C. & Alward, W.L. Myocilin glaucoma. *Surv Ophthalmol* 47, 547-61 (2002).
9. Polansky, J.R. et al. Cellular pharmacology and molecular biology of the trabecular meshwork inducible glucocorticoid response gene product. *Ophthalmologica* 211, 126-39 (1997).
10. Liu, Y. & Allingham, R.R. Molecular genetics in glaucoma. *Exp Eye Res* 93, 331-9 (2011).
11. Alward, W.L. et al. Variations in the myocilin gene in patients with open-angle glaucoma. *Arch Ophthalmol* 120, 1189-97 (2002).
12. Sarfarazi, M. et al. Localization of the fourth locus (GLC1E) for adult-onset primary open-angle glaucoma to the 10p15-p14 region. *Am J Hum Genet* 62, 641-52 (1998).
13. Rezaie, T. et al. Adult-onset primary open-angle glaucoma caused by mutations in optineurin. *Science* 295, 1077-9 (2002).
14. Aung, T. et al. Clinical features and course of patients with glaucoma with the E50K mutation in the optineurin gene. *Invest Ophthalmol Vis Sci* 46, 2816-22 (2005).
15. Monemi, S. et al. Identification of a novel adult-onset primary open-angle glaucoma (POAG) gene on 5q22.1. *Hum Mol Genet* 14, 725-33 (2005).
16. Hauser, M.A. et al. Distribution of WDR36 DNA sequence variants in patients with primary open-angle glaucoma. *Invest Ophthalmol Vis Sci* 47, 2542-6 (2006).
17. Footz, T.K. et al. Glaucoma-associated WDR36 variants encode functional defects in a yeast model system. *Hum Mol Genet* 18, 1276-87 (2009).
18. Chi, Z.L. et al. Mutant WDR36 directly affects axon growth of retinal ganglion cells leading to progressive retinal degeneration in mice. *Hum Mol Genet* 19, 3806-15 (2010).
19. Gallenberger, M. et al. Lack of WDR36 leads to preimplantation embryonic lethality in mice and delays the formation of small subunit ribosomal RNA in human cells in vitro. *Hum Mol Genet* 20, 422-35 (2011).
20. Pasutto, F. et al. Heterozygous NTF4 mutations impairing neurotrophin-4 signaling in patients with primary open-angle glaucoma. *Am J Hum Genet* 85, 447-56 (2009).
21. Vithana, E.N. et al. Identification of a novel mutation in the NTF4 gene that causes primary open-angle glaucoma in a Chinese population. *Mol Vis* 16, 1640-5 (2010).
22. Thorleifsson, G. et al. Common variants near CAV1 and CAV2 are associated with primary open-angle glaucoma. *Nat Genet* 42, 906-9 (2010).
23. Ramdas, W.D. et al. A genome-wide association study of optic disc parameters. *PLoS Genet* 6, e1000978 (2010).
24. Burdon, K.P. et al. Genome-wide association study identifies susceptibility loci for open angle glaucoma at TMCO1 and CDKN2B-AS1. *Nat Genet* 43, 574-8 (2011).
25. Ramdas, W.D. et al. Common genetic variants associated with open-angle glaucoma. *Hum Mol Genet* 20, 2464-71 (2011).
26. Macgregor, S. et al. Genome-wide association identifies ATOH7 as a major gene determining human optic disc size. *Hum Mol Genet* 19, 2716-24 (2010).
27. Brown, N.L., Dagenais, S.L., Chen, C.M. & Glaser, T. Molecular characterization and mapping of ATOH7, a human atonal homolog with a predicted role in retinal ganglion cell development. *Mamm Genome* 13, 95-101 (2002).
28. van Koolwijk, L.M. et al. Common genetic determinants of intraocular pressure and primary open-angle glaucoma. *PLoS Genet* 8, e1002611 (2012).
29. Fernandez-Martinez, L. et al. Evidence for RPGRIP1 gene as risk factor for primary open angle glaucoma. *Eur J Hum Genet* 19, 445-51 (2011).
30. Fingert, J.H. et al. Copy number variations on chromosome 12q14 in patients with normal tension glaucoma. *Hum Mol Genet* 20, 2482-94 (2011).
31. Davis, L.K. et al. Copy number variations and primary open-angle glaucoma. *Invest Ophthalmol Vis Sci* 52, 7122-33 (2011).

32. Tunny, T.J., Richardson, K.A., Clark, C.V. & Gordon, R.D. The atrial natriuretic peptide gene in patients with familial primary open-angle glaucoma. *Biochem Biophys Res Commun* 223, 221-5 (1996).
33. Copin, B. et al. Apolipoprotein E-promoter single-nucleotide polymorphisms affect the phenotype of primary open-angle glaucoma and demonstrate interaction with the myocilin gene. *Am J Hum Genet* 70, 1575-81 (2002).
34. Lam, C.Y. et al. Association of apolipoprotein E polymorphisms with normal tension glaucoma in a Chinese population. *J Glaucoma* 15, 218-22 (2006).
35. Mabuchi, F. et al. The apolipoprotein E gene polymorphism is associated with open angle glaucoma in the Japanese population. *Mol Vis* 11, 609-12 (2005).
36. Vickers, J.C. et al. The apolipoprotein epsilon4 gene is associated with elevated risk of normal tension glaucoma. *Mol Vis* 8, 389-93 (2002).
37. Ressiniotis, T., Griffiths, P.G., Birch, M., Keers, S. & Chinnery, P.F. The role of apolipoprotein E gene polymorphisms in primary open-angle glaucoma. *Arch Ophthalmol* 122, 258-61 (2004).
38. Daugherty, C.L., Curtis, H., Realini, T., Charlton, J.F. & Zarepari, S. Primary open angle glaucoma in a Caucasian population is associated with the p53 codon 72 polymorphism. *Mol Vis* 15, 1939-44 (2009).
39. Lin, H.J., Chen, W.C., Tsai, F.J. & Tsai, S.W. Distributions of p53 codon 72 polymorphism in primary open angle glaucoma. *Br J Ophthalmol* 86, 767-70 (2002).
40. Aung, T. et al. Investigating the association between OPA1 polymorphisms and glaucoma: comparison between normal tension and high tension primary open angle glaucoma. *Hum Genet* 110, 513-4 (2002).
41. Aung, T. et al. A major marker for normal tension glaucoma: association with polymorphisms in the OPA1 gene. *Hum Genet* 110, 52-6 (2002).
42. Liu, Y. et al. No association between OPA1 polymorphisms and primary open-angle glaucoma in three different populations. *Mol Vis* 13, 2137-41 (2007).
43. Bhattacharjee, A. et al. Leu432Val polymorphism in CYP1B1 as a susceptible factor towards predisposition to primary open-angle glaucoma. *Mol Vis* 14, 841-50 (2008).
44. Burdon, K.P., Hewitt, A.W., Mackey, D.A., Mitchell, P. & Craig, J.E. Tag SNPs detect association of the CYP1B1 gene with primary open angle glaucoma. *Mol Vis* 16, 2286-93 (2010).
45. Lopez-Garrido, M.P. et al. Heterozygous CYP1B1 gene mutations in Spanish patients with primary open-angle glaucoma. *Mol Vis* 12, 748-55 (2006).
46. Pasutto, F. et al. Heterozygous loss-of-function variants in CYP1B1 predispose to primary open-angle glaucoma. *Invest Ophthalmol Vis Sci* 51, 249-54 (2010).
47. Lin, H.J. et al. Association of tumour necrosis factor alpha -308 gene polymorphism with primary open-angle glaucoma in Chinese. *Eye (Lond)* 17, 31-4 (2003).
48. Tsai, F.J., Lin, H.J., Chen, W.C., Chen, H.Y. & Fan, S.S. Insulin-like growth factor-II gene polymorphism is associated with primary open angle glaucoma. *J Clin Lab Anal* 17, 259-63 (2003).
49. Lin, H.J. et al. Association of interleukin 1beta and receptor antagonist gene polymorphisms with primary open-angle glaucoma. *Ophthalmologica* 217, 358-64 (2003).
50. Wang, C.Y. et al. Polymorphism in the IL-1alpha (-889) locus associated with elevated risk of primary open angle glaucoma. *Mol Vis* 12, 1380-5 (2006).
51. Allingham, R.R., Liu, Y. & Rhee, D.J. The genetics of primary open-angle glaucoma: a review. *Exp Eye Res* 88, 837-44 (2009).
52. Chang, T.C. et al. Determinants and heritability of intraocular pressure and cup-to-disc ratio in a defined older population. *Ophthalmology* 112, 1186-91 (2005).
53. Klein, B.E., Klein, R. & Lee, K.E. Heritability of risk factors for primary open-angle glaucoma: the Beaver Dam Eye Study. *Invest Ophthalmol Vis Sci* 45, 59-62 (2004).
54. Schwartz, J.T., Reuling, F.H. & Feinleib, M. Size of the physiologic cup of the optic nerve head. hereditary and environmental factors. *Arch Ophthalmol* 93, 776-8 (1975).
55. van Koolwijk, L.M. et al. Genetic contributions to glaucoma: heritability of intraocular pressure, retinal nerve fiber layer thickness, and optic disc morphology. *Invest Ophthalmol Vis Sci* 48, 3669-76 (2007).
56. Khor, C.C. et al. Genome-wide association studies in Asians confirm the involvement of ATOH7 and TGFBR3, and further identify CARD10 as a novel locus influencing optic disc area. *Hum Mol Genet* 20, 1864-72 (2011).
57. Barry, J.S. & Reddy, M.A. The association of an epibulbar dermoid and Duane syndrome in a patient with a SALL1 mutation (Townes-Brocks Syndrome). *Ophthalmic Genet* 29, 177-80 (2008).
58. Axenovich, T. et al. Linkage and association analyses of glaucoma related traits in a large pedigree from a Dutch genetically isolated population. *J Med Genet* 48, 802-9 (2011).
59. Ramdas, W.D. et al. Clinical implications of old and new genes for open-angle glaucoma. *Ophthalmology* 118, 2389-97 (2011).
60. Saglar, E. et al. Association of polymorphisms in APOE, p53, and p21 with primary open-angle glaucoma in Turkish patients. *Mol Vis* 15, 1270-6 (2009).
61. Mookherjee, S. et al. Association of IL1A and IL1B loci with primary open angle glaucoma. *BMC Med Genet* 11, 99 (2010).

PART 2

**THE ROLE OF OPTICAL
COHERENCE TOMOGRAPHY
IN GLAUCOMA**

CHAPTER 2.1

Optimizing the information yield of 3-D OCT in glaucoma



Henriët Springelkamp, Kyungmoo Lee, Wishal D. Ramdas, Johannes R. Vingerling, Albert Hofman, Caroline C. W. Klaver, Milan Sonka, Michael D. Abràmoff, Nomdo M. Jansonius.

ABSTRACT

Purpose. To determine, first, which regions of 3-D optical coherence tomography (OCT) volumes can be segmented completely in the majority of subjects and, second, the relationship between analyzed area and thickness measurement test-retest variability.

Methods. Three-dimensional OCT volumes (6x6 mm) centered around the fovea and optic nerve head (ONH) of 925 Rotterdam Study participants were analyzed; 44 participants were scanned twice. Volumes were segmented into 10 layers, and we determined the area where all layers could be identified in at least 95% (macula) or 90% (ONH) of subjects. Macular volumes were divided in 2x2, 4x4, 6x6, 8x8, or 68 blocks. We placed two circles around the ONH; the ONH had to fit into the smaller circle, and the larger circle had to fit into the segmentable part of the volume. The area between the circles was divided in 3 to 12 segments. We determined the test-retest variability (coefficient of repeatability) of the retinal nerve fiber layer (RNFL) and ganglion cell layer (RGCL) thickness measurements as a function of size of blocks/segments.

Results. Eighty-two percent of the macular volume could be segmented in at least 95% of subjects; for the ONH, this was 65% in at least 90%. The radii of the circles were 1.03 and 1.84 mm. Depending on the analyzed area, median test-retest variability ranged from 8% to 15% for macular RNFL, 11% to 22% for macular RGCL, 5% to 11% for the two together, and 18% to 22% for ONH RNFL.

Conclusions. Test-retest variability hampers a detailed analysis of 3-D OCT data. Combined macular RNFL and RGCL thickness averaged over larger areas had the best test-retest variability.

INTRODUCTION

In open-angle glaucoma (OAG), damage to retinal ganglion cell axons results in visual field loss. Morphological signs of retinal cell damage and death are increased cupping of the optic nerve head (ONH), thinning of the retinal nerve fiber layer (RNFL)¹, and thinning of the retinal ganglion cell layer (RGCL)^{2,3}.

Morphological changes in OAG can be assessed qualitatively by funduscopy and fundus photography. They can also be quantified with the Heidelberg Retina Tomograph (HRT; Heidelberg Engineering, Dossenheim, Germany⁴) and scanning laser polarimetry (GDx Nerve Fiber Analyzer; Carl Zeiss Meditec AG, Jena, Germany^{5,6}). More recently, optical coherence tomography (OCT), and especially spectral-domain OCT^{7,8}, have been added to this armamentarium. Unfortunately, the correspondence between imaging metrics and functional tests such as perimetry (the structure-function correlation) has been low to moderate⁹⁻¹³.

The information yield of 3-D OCT in glaucoma can, theoretically, be improved by quantitative analysis of the entire volume of tissues that are affected morphologically by OAG, the RNFL and the RGCL, over specific regions (Regions of Interest [ROI]) of these tissues. However, though analysis of increasingly smaller ROIs is attractive because it has the potential to better correlate with functional testing, the drawback is that test-retest variability may increase because fewer samples are available. The relationship between test-retest variability and ROI has been studied for peripapillary RNFL thickness measurements (see Discussion section). As far as we know, this relationship has not been studied for thickness measurements of macular RNFL or RGCL.

The aims of the present study were (1) to determine which regions of OCT volumes can be segmented accurately in the majority of subjects using the Iowa Reference Algorithm, which has been validated on the four most widely available commercial OCT scanners¹⁴⁻¹⁶, and (2) to unravel the relationship between ROI and test-retest variability.

METHODS

Study population and data collection

The Rotterdam Study is a prospective population-based cohort study investigating age-related disorders¹⁷. It is conducted in Ommoord, a district of Rotterdam, the Netherlands. The study started in 1990 and is still ongoing. The original cohort comprised 7,983 participants of 55 years or older; ancillary studies were added later on, and in total 14,926 participants were enrolled. The ophthalmic examination as performed at baseline and at all follow-up examinations has been described before¹⁸. Measurements of intraocular pressure (IOP) and linear cup-disc ratio (LCDR), used for this paper, have also been described elsewhere¹⁹. In 2007, OCT scanning of the macular and ONH regions was added to the armamentarium.

All measurements were conducted after the Medical Ethics Committee of the Erasmus University had approved the study protocol and after all participants had provided written informed consent in accordance with the tenets of the Declaration of Helsinki.

OCT data collection

To determine which regions of the OCT volumes could be segmented in what fraction of subjects, the macula and ONH of 925 consecutive subjects were imaged with the Topcon 3-D OCT-1000 (Topcon, Tokyo, Japan). Initially, both eyes were scanned; later, we confined the scanning to only the right eye because of time constraints in our population-based setting. Volume size was 6x6x1.68 mm (512x128x480 voxels). Volumes were centered around the fovea and the ONH and performed in horizontal direction. We excluded volumes with severe motion artifacts due to eye and head movements.

For the test-retest variability analysis, the macula and ONH of the right eye of 43 additional consecutive subjects and of the left eye of one subject were scanned twice on one day with the Topcon 3-D OCT-2000 (Topcon, Tokyo, Japan). Here, volume size was 6x6x2.30 mm (512x128x885 voxels). In between the scans, the head was lifted from the chin rest. We excluded volumes with severe motion artifacts. Volumes with one or more blocks or segments (as defined below; Data analysis, test-retest variability subsection) where the RNFL or RGCL was completely unsegmentable were also excluded.

Data analysis

Iowa Reference Algorithm, segmentable regions

Using our standard automated 3-D graph search approach^{14,20}, all OCT volumes were segmented into 10 layers, demarcated by 11 surfaces. For each A-scan we determined, across subjects, the number of subjects for which all 10 layers could be defined, and then determined, after centering around the fovea and ONH, respectively, the largest continuous region where all layers could be defined in 95% of subjects for the macular region and in 90% of the subjects for the ONH region (see Discussion). Volumes of OS were flipped to get OD data format. A-scans that could be not segmented reliably by the algorithm were marked automatically.

Test-retest variability

We analyzed test-retest variability for a series of ROI grids. For the macula, the area of the volume was divided in 4 (2x2), 16 (4x4), 36 (6x6), 64 (8x8) and 68 (0.6x0.6 mm; following the 10-2 perimetry grid) square ROIs (blocks). For the ONH, we determined the radii of two circles. The radius of the larger circle was chosen so that it provides the largest circle that fit completely into the area that could be segmented in 90% of the subjects (see above) if centered on the x-y center of the volume. The radius of the smaller circle was chosen so that the ONH fit into the smaller circle completely in 95% of the subjects (peripapillary atrophy was allowed outside the smaller circle, as the RNFL can be segmented in areas with peripapillary atrophy). For the analyses, the circles were centered on the center of the individual ONH, and the area between the circles was divided into radially oriented ROIs (segments) of 120° (3 segments), 60° (6 segments), 45° (8 segments), 36° (10 segments) and 30° (12 segments). We determined the position of the segments so that the raphe at the temporal side (assumed to be at the 9 o'clock position for the right eye) was always a demarcation between two segments. If a ROI was partially unsegmentable, the mean thickness of the RNFL or RGCL in the ROI concerned was based on the segmentable part. If one or more ROIs were completely unsegmentable, the volume was excluded (see above, OCT data collection subsection).

As a measure of test-retest variability, we used the coefficient of repeatability²¹, which is defined as two times the standard deviation of the signed differences between test and retest. Test-retest variability was determined for the thickness measurements of the ONH RNFL, macular RNFL, macular RGCL, and the sum of macular RNFL and RGCL. It was calculated both as absolute (in micrometers) and relative to average thickness (in percentages) for all ROIs. We used a general linear model to determine whether the test-retest variability was related to ROI size, mean thickness of the layer concerned, or location within the macular area. Here, the dependent variable was the unsigned relative difference between test and retest.

Normative data

Normative data were based on the macular and ONH volumes of the right eyes of the 925 consecutive participants described above (OCT data collection subsection). We excluded participants with a positive family history of glaucoma, an IOP above 21 mmHg, and participants who received IOP-lowering treatment. We calculated the mean thicknesses with standard deviation and 95% central range (2.5th to 97.5th percentile) for the macular RNFL, macular RGCL, the sum of macular RNFL and RGCL, and the ONH RNFL.

All analyses were performed with IBM SPSS Statistics Release 19.0.0 (IBM Corp., Armonk, NY). A p-value of 0.05 or less was considered statistically significant.

RESULTS

For the segmentable region analysis, 976 macular volumes (897 OD; 79 OS) and 949 ONH volumes (874 OD; 75 OS) were available. The mean (standard deviation) age, IOP and LCDR of these subjects was 57 (7) years, 14 (3) mmHg, and 0.3 (0.2), respectively; 44% were male.

Figures 1A and 1B show the regions of the macular (A) and ONH (B) volumes that could be segmented in the majority of participants. Eighty-two percent of the area of the macular volume could be segmented in at least 95% of the subjects. Sixty-six percent of the area of the ONH volume could be segmented in at least 90% of the subjects. The radii of the inner and outer circles for the ONH volume were 1.03 and 1.84 mm, respectively (Figure 1B). Figures 1C and 1D are similar to A and B but now the volumes were not centered around the fovea/ONH.

For the test-retest variability analysis, 30 pairs of macular volumes and 42 pairs of ONH volumes were available. Here, the mean (standard deviation) age, IOP and LCDR was 71 (5) years, 14 (3) mmHg, and 0.4 (0.2), respectively; 55% were male.

Figure 2 presents the absolute (in micrometers) and relative (in percentages) test-retest variability for the macular RNFL (A) and RGCL (B) thickness measurements per ROI for each grid. Figure 3 shows the test-retest variability for the ONH RNFL thickness measurements per ROI for each grid.

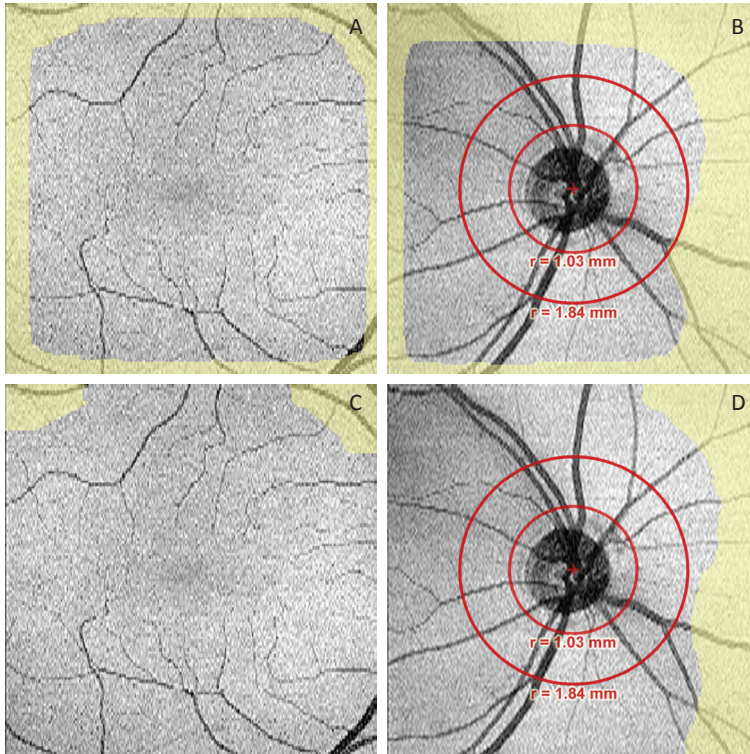


Figure 1. Upper row shows regions of the macular volume that are unsegmentable in $\geq 5\%$ of subjects (A; yellow area) and regions of the optic nerve head volume that are unsegmentable in $\geq 10\%$ of subjects (B; yellow area). Inner circle denotes area where $\geq 95\%$ of optic nerve heads fit in if centered around the center of the optic nerve head (radius = 1.03 mm); outer circle is largest circle that fits in the gray area if centered around the center of the volume (radius = 1.84 mm). Right eye representation. Lower row (C,D) is similar to upper row (A,B) but now the volumes were not centered around the fovea/optic nerve head.

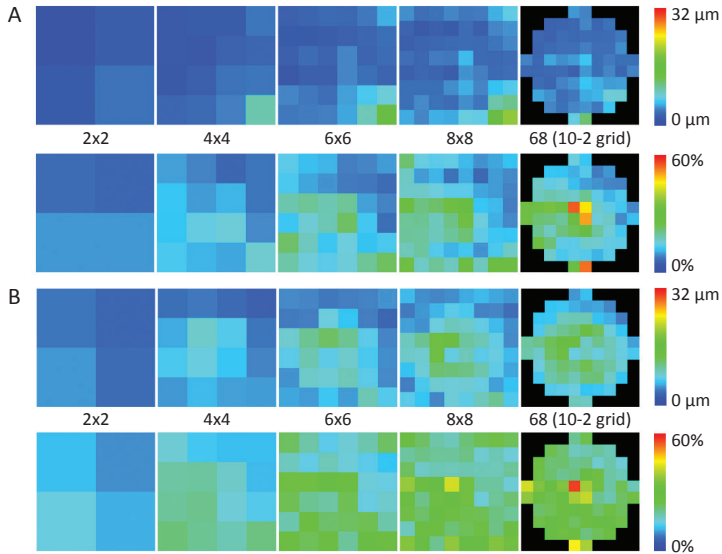


Figure 2. Test-retest variability (twice the standard deviation of the differences) for macular retinal nerve fiber layer (A) and macular retinal ganglion cell layer (B), both absolute (upper row; in micrometers) and relative to average thickness (lower row; in percentages).

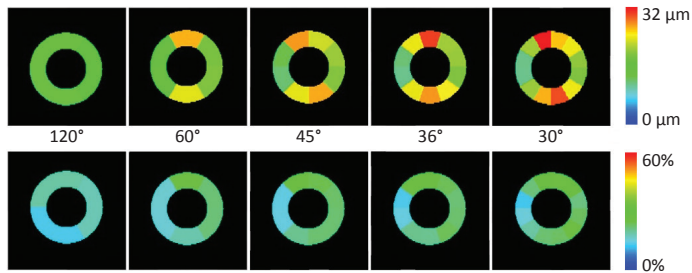


Figure 3. Test-retest variability (twice the standard deviation of the differences) for optic nerve head retinal nerve fiber layer; absolute (upper row; in micrometers) and relative to average thickness (lower row; in percentages).

Figure 4. Test-retest variability of the thickness measurements presented as median with minimum and maximum of the various grids as displayed in Figures 2 and 3. A = macular retinal nerve fiber layer (RNFL); B = macular retinal ganglion cell layer (RGCL); C = macular RNFL and RGCL combined; D = optic nerve head (ONH) retinal nerve fiber layer.

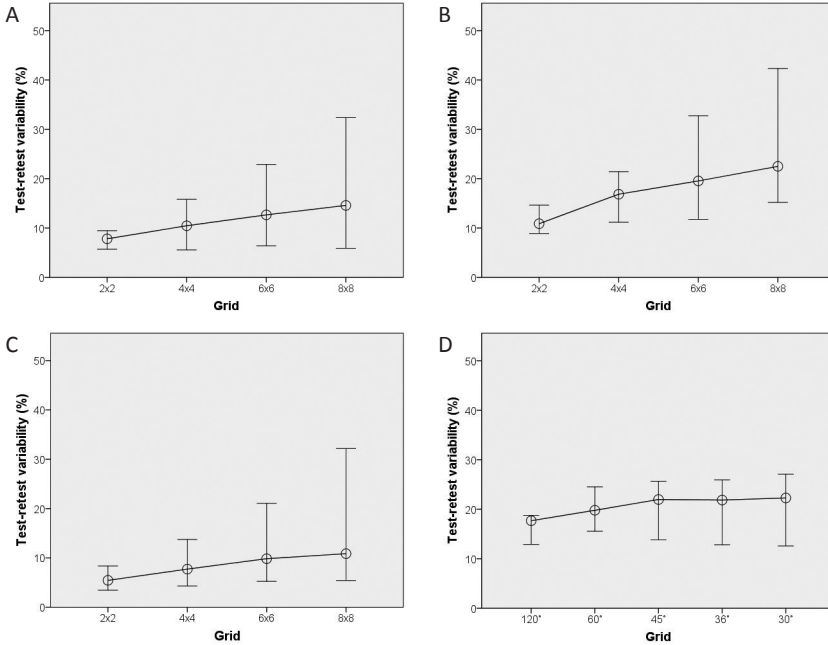


Figure 5. Normative data (color graphs for all grids except the 10-2 grid; in micrometers) for macular retinal nerve fiber layer (A) and macular retinal ganglion cell layer (B).

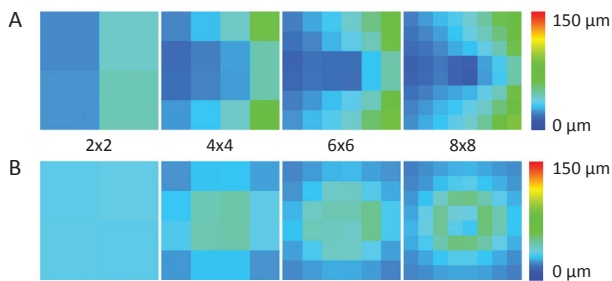


Figure 6. Normative data (color graphs for all grids; in micrometers) for optic nerve head retinal nerve fiber layer.

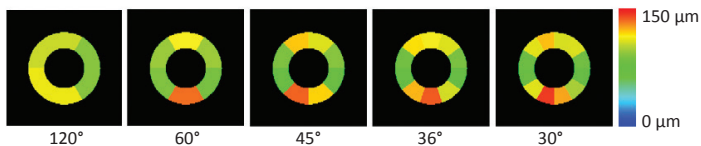


Figure 4 gives the median, minimum and maximum test-retest variability for each grid for the macular RNFL (A), the macular RGCL (B), the macular RNFL and RGCL combined (C), and the ONH RNFL (D). Test-retest variability increased with a more detailed grid. For the individual macula layers, only the 2x2 and 4x4 (RNFL) grids achieved a median test-retest variability of 10% or better. When we combined the two macula layers, the test-retest variability decreased substantially: for the combined layers, the median test-retest variability of the thickness measurements ranged from 5% (2x2 grid) to 11% (8x8 grid). For the ONH, the test-retest variability was <20% only for the 120° and 60° grids. The test-retest variability depended significantly on the ROI size ($P<0.001$ for macular RNFL, RGCL and the two combined; $P=0.02$ for ONH RNFL); the mean thickness of the layer concerned ($P<0.001$ for macular RNFL, $P=0.002$ for macular RGCL, $P<0.001$ for macular RNFL and RGCL combined, and $P<0.001$ for ONH RNFL) and location within the macular area ($P<0.001$).

Figure 5 shows the mean thicknesses for the macular RNFL (A) and macular RGCL (B) as a function of grid size.

Figure 6 presents the mean thicknesses for the ONH RNFL.

Table 1 presents the descriptive statistics of the normative data for the 2x2 macular grid and the 120° ONH segments. These data were based on 795 macular volumes and 781 ONH volumes.

DISCUSSION

The results of this study show that essentially the entire volume of the macula could be segmented and that test-retest variability depends on the size of the ROI. Unsegmentable regions were more common around the ONH, especially on the nasal side. We achieved the best test-retest variability for the combined RNFL/RGCL thickness measurements in the macular area.

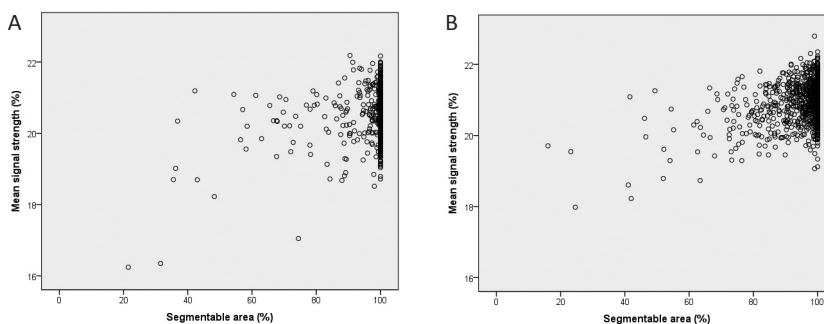
The area of the macular volume that was segmentable in at least 95% of the subjects (Fig. 1A) was initially determined after centering on the fovea. The rationale of this centering is to compare corresponding regions of the retina between subjects. Figure 1A shows a clear vignetting. This might be caused either by poor volume quality towards the borders of the volume or by poor centering during the scanning process. Figure 1C shows the same analysis as Figure 1A but now without centering on the fovea. In this analysis, 96% of the area of the macular volume could be segmented in at least 95% of the subjects (to be compared to 82% in Fig. 1A). Hence, the volume quality does not diminish towards the borders of the volume (except for the two small regions in the upper corners). Rather, centering during the imaging process was suboptimal in our study.

Because many ONH volumes had a large unsegmentable region at the nasal side, we arbitrarily adopted a 90% threshold for determining the segmentable part of the ONH volume. If we had used a 95% threshold for ONH, it would have been possible to segment only 54% of the volume (to be compared to 66% for the 90% threshold). Again, some

Table 1. Normative data for retinal nerve fiber layer (RNFL) thickness, retinal ganglion cell layer (RGCL) thickness and the combined layers for the 2x2 block grid in the macular region and for the RNFL thickness for the 120° segments in the optic nerve head (ONH) region.

	Mean thickness, μm (standard deviation; 95% central range)
Macular RNFL	
Temporal superior	22 (3; 17-27)
Nasal superior	41 (7; 28-54)
Temporal inferior	23 (3; 18-30)
Nasal inferior	44 (8; 29-61)
Macular RGCL	
Temporal superior	34 (5; 24-43)
Nasal superior	35 (4; 27-43)
Temporal inferior	34 (4; 25-43)
Nasal inferior	34 (4; 25-41)
Macular RNFL + RGCL	
Temporal superior	56 (6; 43-67)
Nasal superior	76 (9; 58-92)
Temporal inferior	58 (6; 45-69)
Nasal inferior	78 (10; 58-95)
ONH RNFL	
Temporal superior	105 (18; 55-135)
Nasal	92 (19; 49-129)
Temporal inferior	112 (17; 65-139)

Figure 7. Mean signal strength (percentage of maximum) as a function of segmentable area (percentage of maximum) for the macular area (A) and optic nerve head (B).



vignetting can be seen, which disappeared largely after the removal of centering on the ONH during the data analysis process (Fig. 1D). In Figure 1D, 84% of the area of the ONH volume could be segmented in at least 90% of the subjects (to be compared to 66% in Fig. 1B). The unsegmentable region at the nasal side, however, remained clearly visible, indicating that volume quality is a real issue in this region. Due to imperfect centering during the scanning process, the actual percentage of rings with unsegmentable regions was 12.5% rather than 10%; but in only 4.8%, the unsegmentable part continued up to the inner circle, making it impossible to determine RNFL thickness in part of the circumference. In the remaining 7.7%, the thickness determination was based on the part that was still segmentable. In 80% of the 12.5% with unsegmentable regions within the ring, the unsegmentable regions were located at the nasal side of the ONH.

A possible explanation for the finding that unsegmentable regions were more common in the ONH volumes than in the macular volumes is the fact that the ONH volume has a greater distance to the optical axis of the eye²². The observed higher frequency of unsegmentable regions at the nasal side of the ONH is in line with this explanation. The segmentable area could also be influenced by image quality. Unfortunately, the OCT device used in our study does not provide an image quality parameter. As a proxy, we averaged the signal strength, per subject, over all voxels and plotted the resulting value as a function of the area that could be segmented. Figure 7 shows the results for the macular area (A) and ONH (B). As can be seen in these figures, there is possibly some but no clear relationship between mean signal strength and segmentable area.

For the coarsest grid (2x2 ROIs) of the macular volume, we reached a test-retest variability of 6% to 9% for the RNFL, with the highest values located inferiorly. With more detailed grids, the inferior region and especially the foveal area had the highest test-retest variability. These areas also showed the highest test-retest variability for the RGCL. To our knowledge, only DeBuc et al.²³ have examined the test-retest variability for RNFL in a 6x6 mm macular volume. They found a coefficient of repeatability of 4.6% for the mean RNFL thickness. Mean RNFL thickness test-retest variability for the macular volume as a whole was 4.0% in our data, in good agreement with DeBuc et al. Other studies addressing test-retest variability of OCT thickness measurements focused on the thickness of the entire retina in circular (EDTRS) grids. Neither of these is useful from the point of view of glaucoma.

Table 2 summarizes studies that reported on test-retest variability of peripapillary RNFL thickness measurements. Some of these studies measured at different segment sizes and showed that test-retest variability increased with an increasing number of segments. Test-retest variability was generally highest superiorly (11 to 1 o'clock position) and inferiorly (5 to 6 o'clock position) – the areas where the major vessels can be found. This is in agreement with our data (Fig. 3). Different definitions of test-retest variability have been used in the literature (Table 2). Only studies applying the same definition should be compared. Since we did not look to the quarter grid, we can compare the test-retest variability for only the clock hour grid. Budenz et al.²⁴ showed a median test-retest variability of 14.3 μm in 51 glaucoma patients. In normal eyes, a median test-retest variability of 16.3 μm ²⁵ and 15.9 μm ²⁶ was reported (converted to our definition).

Table 2. Literature overview of test-retest variability for peripapillary retinal nerve fiber layer measurements.

Author	Study population	Mean age (years)	Definition TRV	Median TRV, μm (range), quarter grid	Median TRV, μm (range), clock hour grid	Region(s) with worst TRV
Budenz (2008) ²⁴	Glaucoma (n=51)	69.5	2 x square root of within-day variance components	10 (6.2-12.5)	14.3 (9.3-17.1)	6 and 12 o'clock
Kim (2011) ²⁷	Normal (n=359) and glaucoma (n=263)	49.8 (all)	2 x square root of the variance between two repeated measurements	6.3 (5.8-7.8)	NA	Inferior quadrant
Garas (2010) ²⁸	Normal and ocular hypertensive (n=14) and glaucoma (n=23)	56.7 (normal and hypertensive) and 58.3 (glaucoma)	1.96 x intrasession SD	7.1 (6.5-8.7) (all)	NA	Superior quadrant
Carpineto (2012) ²⁵	Normal (n=68)	29.1	1.96 x SD of differences between measurements	12.9 (7.8-17.0)	16.0 (9.6-30.4)	6 and 12 o'clock
Kim (2009) ²⁶	Normal (14 subjects, 27 eyes)	37.3	SD (approximately the average of all eyes)	8.2 (4.5-9.0), 6.3 (2.2-9.5), 6.8 (2.6-8.8)*	8.0 (3.6-13.6)	5 and 11 o'clock
Paunescu (2004) ²⁹	Normal (n=10)	30.5	Intravisit SD (within-subject, within-date)	2.3 (2.0-3.4)	3.1 (1.5-5.3)	6 and 11 o'clock
Mwanza (2010) ³⁰	Glaucoma (n=55)	70.7	Pooled within-subject test-retest SD (three measurements)	2.5 (2.2-2.8)	3.6 (2.2-4.5)	3, 6 and 11 o'clock
Budenz (2005) ³¹	Normal (n=88) and glaucoma (n=59)	53 (normal) and 68 (glaucoma)	2 x SD of three repeated measurements	9.7 (7.5-10.2) (normal) and 10.4 (5.6-10.7) (glaucoma)	NA	
Hong (2010) ³²	Normal (n=36 eyes of 30 subjects)	28.6	2 x square root of the variance among three repeated measurements	7.5 (5.8-8.1)	10.0 (4.7-13.6)	2 and 6 o'clock

Table 2. (continued)

Author	Study population	Mean age (years)	Definition TRV	Median TRV, μm (range), quarter grid	Median TRV, μm (range), clock hour grid	Region(s) with worst TRV
Lee (2010) ³³	Normal (n=98) and glaucoma (n=79)	51.1 (normal) and 58.7 (glaucoma)	2 x SD of each set of three repeated measurements	7.5 (5.6-8.3) (normal) and 6.7 (4.6-7.2) (glaucoma)	9.5 (7.3-11.5) (normal) and 8.8 (5.0-10.0)	6 and 11 o'clock (normal) and 1 and 5 o'clock (glaucoma)
Savini (2010) ³⁴	Normal (n=32)	59	2 x SD of three repeated measurements	4.4 (2.6-5.6)	7.3 (2.7-9.3)	6 and 12 o'clock
Mansoori (2011) ³⁵	Normal (n=61) and glaucoma (n=41)	38.3 (normal) and 57.2 (glaucoma)	2 x SD of three repeated measurements	2.5 (1.9-3.0) (normal) and 2.4 (1.9-2.9) (glaucoma)	NA	Superior (normal) and nasal (glaucoma)
Nakatani (2011) ³⁶	Normal (n=32) and glaucoma (n=32)	57.3 (normal) and 61.5 (glaucoma)	2 x mean within-participant SD of three repeated measurements	11.7 (10.3-14.0) (normal) and 10.7 (8.7-14.7) (glaucoma)	15.3 (12.8-18.0) (normal) and 13.3 (10.1-18.9) (glaucoma)	8 o'clock (normal) and 4 o'clock (glaucoma)
Leung (2009) ³⁷	Normal (n=16)	52	2.77 x intravisit within-subject SD	8.0 (6.8-9.7)	12.2 (7.5-15.0)	6 and 11 o'clock
Hong (2012) ³⁸	Normal (n=75)	43.7	2.77 x within-subject SD	11.2 (5.4-12.5)	NA	Nasal quadrant
Tan (2012) ³⁹	Normal (n=50)	35.6	2.77 x within-subject SD	8.5 (7.1-11.3) (Cirrus) and 7.8 (6.3-9.1) (Spectralis)	NA	Superior (Cirrus) and temporal (Spectralis)

ABBREVIATIONS

- NA not available
- SD standard deviation
- TRV test-retest variability

*

First TRV is TRV without eye tracking, second and third TRV are TRV with different methods of eye tracking.

Our median test-retest variability of 22.3 μm is somewhat higher. In our study, the two volumes were recorded and analyzed independently; they were not superimposed and aligned before analysing, nor was an eye-tracking system used. For follow-up of a single patient, such measures could lower test-retest variability and thus improve change detection. With our approach, however, the test-retest variability gives a more realistic estimate of the accuracy of single scans, which are often used in screening settings and in population-based studies. A lower test-retest variability after registration of a previous scan was found in the study of Kim et al²⁶. In that study, median test-retest variability decreased after applying two different registration methods (from 8.2 to 6.3 and 6.8 μm , respectively).

A strength of this study is the sample size. Segmentable regions and normative data were based on almost thousand subjects. The population-based setting and the fact that we used volumes of consecutive participants should have made our sample as unbiased as possible. OAG cases previously identified within the study were excluded, as were participants with an increased OAG risk (see Methods section). Together with the low prevalence of OAG in the general population, this should ensure an appropriate dataset for determining normative data.

A limitation of this study is the quality of the scans. Due to limited time for scanning, centering of fovea and ONH was suboptimal, and scans with motion artifacts could not be repeated. Scans performed in a clinical setting (as opposed to our population-based setting) could have larger segmentable areas. This remains to be proven, though. Another drawback is the use of two different OCT devices (Topcon 3-D OCT-1000 and OCT-2000; Topcon) with different volume sizes, due to an update during the course of the study. Within the substudies (segmentable regions and test-retest variability), however, we used the same OCT device for all participants. The older age of the participants in our two substudies (71 and 57 years, respectively) may have made it more difficult to get high-quality scans, due to a higher frequency of ocular morbidity such as cataract. On the other hand, OAG also typically occurs in the elderly, and our scan quality would therefore be representative for the target population.

In the macular volume, a combined thickness measurement of the two layers studied (RNFL and RGCL) improved the repeatability significantly. This indicates that the border between the RNFL and RGCL has a relatively large variability on repeat scanning. However, a good repeatability alone is not sufficient to obtain a good diagnostic performance. Focusing on tissues relevant to the disease of interest is also important. As both the RNFL and the RGCL are involved in OAG, a combined analysis of these two layers seems, a priori, a logical approach. In order to get a first impression of the diagnostic performance (which will be addressed in detail in a further study), we calculated areas under the receiver operating characteristic curves (AUCs) for the average thicknesses of the macular RNFL, the macular RGCL, and both layers together. We found AUCs of 0.89, 0.87 and 0.92, respectively, based on the participants used in this study as controls and 21 eyes of 21 OAG patients as cases. These 21 OAG cases were a random subset of OAG cases identified in the Rotterdam Study before, who had had an OCT scan^{18,40}. The average (range) standard automated perimetry mean deviation was -9.1 dB (-1.4 to -21.8 dB). Although the differences between these AUCs were – possibly related to the small number of OAG cases – not statistically significant, the point estimates indicate that a thorough study of the combined analysis of the two layers is worth the effort.

In conclusion, it is possible to obtain detailed thickness measurements, but there is a balance between the ROI size and variability. In the macular volume, a combined thickness measurement of the two layers studied (RNFL and RGCL) improved the repeatability significantly. The optimal grid size for screening and progression detection in glaucoma can be deduced by comparing cross-sectional measurements in healthy subjects and glaucoma patients, and by performing longitudinal measurements in glaucoma patients, respectively. These issues, including a confirmation of the presumed superiority of a combined analysis of the RNFL and RGCL, should all be addressed before OCT scanning can be optimally used in clinical practice.

References

1. Airaksinen, P.J. & Alanko, H.I. Effect of retinal nerve fibre loss on the optic nerve head configuration in early glaucoma. *Graefes Arch Clin Exp Ophthalmol* 220, 193-6 (1983).
2. Quigley, H.A. Open-angle glaucoma. *N Engl J Med* 328, 1097-106 (1993).
3. Nickells, R.W. Ganglion cell death in glaucoma: from mice to men. *Vet Ophthalmol* 10 Suppl 1, 88-94 (2007).
4. Rohrschneider, K., Burk, R.O., Kruse, F.E. & Volcker, H.E. Reproducibility of the optic nerve head topography with a new laser tomographic scanning device. *Ophthalmology* 101, 1044-9 (1994).
5. Weinreb, R.N. et al. Histopathologic validation of Fourier-ellipsometry measurements of retinal nerve fiber layer thickness. *Arch Ophthalmol* 108, 557-60 (1990).
6. Dreher, A.W. & Reiter, K. Retinal laser ellipsometry: a new method for measuring the retinal nerve fibre layer thickness distribution? *Clin Vis Sci* 7, 481-8 (1992).
7. Hee, M.R. et al. Optical coherence tomography of macular holes. *Ophthalmology* 102, 748-56 (1995).
8. Schuman, J.S. et al. Optical coherence tomography: a new tool for glaucoma diagnosis. *Curr Opin Ophthalmol* 6, 89-95 (1995).
9. Hood, D.C., Anderson, S.C., Wall, M. & Kardon, R.H. Structure versus function in glaucoma: an application of a linear model. *Invest Ophthalmol Vis Sci* 48, 3662-8 (2007).
10. Lee, J.R. et al. Structure-function relationships in normal and glaucomatous eyes determined by time- and spectral-domain optical coherence tomography. *Invest Ophthalmol Vis Sci* 51, 6424-30 (2010).
11. Hood, D.C. & Raza, A.S. Method for comparing visual field defects to local RNFL and RGC damage seen on frequency domain OCT in patients with glaucoma. *Biomed Opt Express* 2, 1097-105 (2011).
12. Rao, H.L. et al. Structure-function relationship in glaucoma using spectral-domain optical coherence tomography. *Arch Ophthalmol* 129, 864-71 (2011).
13. Garvin, M.K. et al. 2-D pattern of nerve fiber bundles in glaucoma emerging from spectral-domain optical coherence tomography. *Invest Ophthalmol Vis Sci* 53, 483-9 (2012).
14. Garvin, M.K. et al. Automated 3-D intraretinal layer segmentation of macular spectral-domain optical coherence tomography images. *IEEE Trans Med Imaging* 28, 1436-47 (2009).
15. Lee, K. et al. Segmentation of the optic disc in 3-D OCT scans of the optic nerve head. *IEEE Trans Med Imaging* 29, 159-68 (2010).
16. Abramoff, M.D. et al. Automated segmentation of the cup and rim from spectral domain OCT of the optic nerve head. *Invest Ophthalmol Vis Sci* 50, 5778-84 (2009).
17. Hofman, A. et al. The Rotterdam Study: 2012 objectives and design update. *Eur J Epidemiol* 26, 657-86 (2011).
18. Wolfs, R.C. et al. Changing views on open-angle glaucoma: definitions and prevalences--The Rotterdam Study. *Invest Ophthalmol Vis Sci* 41, 3309-21 (2000).
19. Ramdas, W.D. et al. Heidelberg Retina Tomograph (HRT3) in population-based epidemiology: normative values and criteria for glaucomatous optic neuropathy. *Ophthalmic Epidemiol* 18, 198-210 (2011).
20. Quilley, G. et al. Three-dimensional analysis of retinal layer texture: identification of fluid-filled regions in SD-OCT of the macula. *IEEE Trans Med Imaging* 29, 1321-30 (2010).
21. Altman, D.G. *Practical statistics for medical research*. London: Chapman & Hall (1991).
22. Gao, W., Cense, B., Zhang, Y., Jonnal, R.S. & Miller, D.T. Measuring retinal contributions to the optical Stiles-Crawford effect with optical coherence tomography. *Opt Express* 16, 6486-501 (2008).
23. DeBuc, D.C. et al. Reliability and reproducibility of macular segmentation using a custom-built optical coherence tomography retinal image analysis software. *J Biomed Opt* 14, 064023 (2009).
24. Budenz, D.L., Fredette, M.J., Feuer, W.J. & Anderson, D.R. Reproducibility of peripapillary retinal nerve fiber thickness measurements with stratus OCT in glaucomatous eyes. *Ophthalmology* 115, 661-666 e4 (2008).
25. Carpineto, P. et al. Reproducibility and repeatability of Cirrus HD-OCT peripapillary retinal nerve fibre layer thickness measurements in young normal subjects. *Ophthalmologica* 227, 139-45 (2012).
26. Kim, J.S. et al. Retinal nerve fibre layer thickness measurement reproducibility improved with spectral domain optical coherence tomography. *Br J Ophthalmol* 93, 1057-63 (2009).
27. Kim, J.H. et al. Effect of signal strength on reproducibility of circumpapillary retinal nerve fiber layer thickness measurement and its classification by spectral-domain optical coherence tomography. *Jpn J Ophthalmol* 55, 220-7 (2011).
28. Garas, A., Vargha, P. & Hollo, G. Reproducibility of retinal nerve fiber layer and macular thickness measurement with the RTVue-100 optical coherence tomograph. *Ophthalmology* 117, 738-46 (2010).
29. Paunescu, L.A. et al. Reproducibility of nerve fiber thickness, macular thickness, and optic nerve head measurements using StratusOCT. *Invest Ophthalmol Vis Sci* 45, 1716-24 (2004).
30. Mwanza, J.C. et al. Reproducibility of peripapillary retinal nerve fiber layer thickness and optic nerve head parameters measured with cirrus HD-OCT in glaucomatous eyes. *Invest Ophthalmol Vis Sci* 51, 5724-30 (2010).
31. Budenz, D.L., Chang, R.T., Huang, X., Knighton, R.W. & Tielsch, J.M. Reproducibility of retinal nerve fiber thickness measurements using the stratus OCT in normal and glaucomatous eyes. *Invest Ophthalmol Vis Sci* 46, 2440-3 (2005).

32. Hong, S., Kim, C.Y., Lee, W.S. & Seong, G.J. Reproducibility of peripapillary retinal nerve fiber layer thickness with spectral domain cirrus high-definition optical coherence tomography in normal eyes. *Jpn J Ophthalmol* 54, 43-7 (2010).
33. Lee, S.H., Kim, S.H., Kim, T.W., Park, K.H. & Kim, D.M. Reproducibility of retinal nerve fiber thickness measurements using the test-retest function of spectral OCT/SLO in normal and glaucomatous eyes. *J Glaucoma* 19, 637-42 (2010).
34. Savini, G., Carbonelli, M., Parisi, V. & Barboni, P. Effect of pupil dilation on retinal nerve fibre layer thickness measurements and their repeatability with Cirrus HD-OCT. *Eye (Lond)* 24, 1503-8 (2010).
35. Mansoori, T., Viswanath, K. & Balakrishna, N. Reproducibility of peripapillary retinal nerve fibre layer thickness measurements with spectral domain optical coherence tomography in normal and glaucomatous eyes. *Br J Ophthalmol* 95, 685-8 (2011).
36. Nakatani, Y., Higashide, T., Ohkubo, S., Takeda, H. & Sugiyama, K. Evaluation of macular thickness and peripapillary retinal nerve fiber layer thickness for detection of early glaucoma using spectral domain optical coherence tomography. *J Glaucoma* 20, 252-9 (2011).
37. Leung, C.K. et al. Retinal nerve fiber layer imaging with spectral-domain optical coherence tomography: a variability and diagnostic performance study. *Ophthalmology* 116, 1257-63, 1263 e1-2 (2009).
38. Hong, J.T. et al. Retinal nerve fiber layer measurement variability with spectral domain optical coherence tomography. *Korean J Ophthalmol* 26, 32-8 (2012).
39. Tan, B.B., Natividad, M., Chua, K.C. & Yip, L.W. Comparison of retinal nerve fiber layer measurement between 2 spectral domain OCT instruments. *J Glaucoma* 21, 266-73 (2012).
40. Czudowska, M.A. et al. Incidence of glaucomatous visual field loss: a ten-year follow-up from the Rotterdam Study. *Ophthalmology* 117, 1705-12 (2010).

CHAPTER 2.2

Population-based evaluation of retinal nerve fiber layer, retinal ganglion cell layer, and inner plexiform layer as a diagnostic tool for glaucoma



Henriët Springelkamp, Kyungmoo Lee, Roger C.W. Wolfs, Gabriëlle H.S. Buitendijk, Wishal D. Ramdas, Albert Hofman, Johannes R. Vingerling, Caroline C.W. Klaver, Michael D. Abràmoff, Nomdo M. Jansonius.

ABSTRACT

Purpose. We determined the glaucoma screening performance of regional optical coherence tomography (OCT) layer thickness measurements in the peripapillary and macular region, in a population-based setting.

Methods. Subjects (n=1,224) in the Rotterdam Study underwent visual field testing (Humphrey Field Analyzer) and OCT of the macula and optic nerve head (Topcon 3-D OCT-1000). We determined the mean thicknesses of the retinal nerve fiber layer (RNFL), retinal ganglion cell layer (RGCL), and inner plexiform layer for regions-of-interest; thus, defining a series of OCT parameters, using the Iowa Reference Algorithms. Reference standard was the presence of glaucomatous visual field loss (GVFL); controls were subjects without GVFL, an intraocular pressure (IOP) of 21 mmHg or less, and no positive family history for glaucoma. We calculated the area under the receiver operating characteristics curve (AUCs) and the sensitivity at 97.5% specificity for each parameter.

Results. After excluding 23 subjects with an IOP >21 mmHg and 73 subjects with a positive family history for glaucoma, there were 1,087 controls and 41 glaucoma cases. Mean RGCL thickness in the inferior half of the macular region showed the highest AUC (0.85; 95% confidence interval [CI] 0.77-0.92) and sensitivity (53.7%; 95% CI, 38.7-68.0%). The mean thickness of the peripapillary RNFL had an AUC of 0.77 (95% CI, 0.69-0.85) and a sensitivity of 24.4% (95% CI, 13.7-39.5%).

Conclusions. Macular RGCL loss is at least as common as peripapillary RNFL abnormalities in population-based glaucoma cases. Screening for glaucoma using OCT-derived regional thickness identifies approximately half of those cases of glaucoma as diagnosed by perimetry.

INTRODUCTION

Glaucoma is a chronic optic neuropathy with associated damage of retinal ganglion cells, which results in visual field loss. This damage is characterized by increased cupping of the optic nerve head (ONH), and thinning of the retinal nerve fiber layer (RNFL) and retinal ganglion cell layer (RGCL), as has been shown with fundus photography, histology, and optical coherence tomography (OCT)¹⁻³. These structures can be assessed with the Heidelberg Retina Tomograph (HRT; Heidelberg Engineering, Dossenheim, Germany)⁴ or with scanning laser polarimetry (GDx Nerve Fiber Analyzer; Carl Zeiss Meditec, Jena, Germany)^{5,6}. These techniques showed an apparently favorable screening performance in some specific study populations^{7,8}. In population-based settings, however, the screening performance of these techniques was rather poor⁹⁻¹². A good screening performance in population-based settings is indispensable for an effective case finding for population-based glaucoma research.

The OCT is a newer technique, which can quantify volumes of different retinal layers through segmentation and detect glaucomatous changes of retina and ONH^{3,13}. Similar to what was found in HRT and GDx, many studies reported a favorable screening performance of OCT in clinical settings. Thus far, only two studies were designed as population-based studies, with relatively small sample sizes and, as a consequence, a very small number of cases (9 cases¹⁴ and 6 cases¹⁵, respectively). Population-based studies are attractive, compared to clinical studies, because of the absence of selection bias.

The aim of this study was to determine, in a population-based setting, the glaucoma screening performance of OCT combined with fully 3D analysis, with glaucomatous visual field loss (GVFL) as the reference standard. Specifically, we evaluated the following metrics: peripapillary RNFL thickness, macular mean RGCL, RNFL, and inner plexiform layer (IPL) thicknesses, and mean RGCL, RNFL, and IPL thicknesses in regions based on the trajectories of the nerve fiber bundles and the macular vulnerability zone¹⁶⁻²⁰.

METHODS

Study Population

The Rotterdam Study is a prospective cohort study investigating age-related disorders²¹. It is conducted in Rotterdam, the Netherlands. It started in 1990 with the original cohort, which comprised 7,983 subjects aged 55 years or older. The study was enlarged with two additional cohorts in 2000 (3,011 subjects aged 55 years or older) and 2006 (3,932 subjects aged 45 years or older). Follow-up examinations are still ongoing. The ophthalmic examinations have been described previously²². All measurements were conducted after the Medical Ethics Committee of the Erasmus Medical Center had approved the study protocol and after all subjects had provided written informed consent in accordance with the tenets of the Declaration of Helsinki.

Cases and controls

We included 1,224 consecutive subjects from the third Rotterdam Study cohort (baseline examinations) and the original Rotterdam Study cohort (fourth follow-up examinations) who had undergone intraocular pressure (IOP) measurement, perimetry, and spectral domain

OCT (see below). After this consecutive inclusion, we continued to include subjects with GVFL to circumvent the low prevalence of glaucoma. Subjects with GVFL (see below) in at least one eye were considered cases, irrespective of their IOP. Subjects without GVFL, an IOP of 21 mmHg or less, and no positive family history for glaucoma were considered controls. If both eyes were eligible, we used data from a random eye. If GVFL was present in one eye, we used data from the eye with GVFL. Due to the extended inclusion of cases, which took place in a younger cohort, the cases and controls were incidentally almost perfectly age-matched (see Results section), even though a difference in age would have been expected²³.

Visual Field Testing

All subjects in the present study were tested for visual field defects using the Humphrey Field Analyzer (HFA; Carl Zeiss Meditec, Jena, Germany). Details of this assessment have been published previously²³. Briefly, each eye was screened using a 52-point supra-threshold test that covered the central visual field with a radius of 24°. If the subject did not respond to the light stimulus (6 dB above a threshold-related estimate of the hill of vision) in at least three contiguous test points (or four including the blind spot) in two supra-threshold tests, full-threshold HFA testing with a 24-2 grid was performed. The full-threshold tests were classified as abnormal if at least one of three criteria was met: 1) a Glaucoma Hemifield Test 'outside normal limits', 2) a minimum of three contiguous points in the pattern deviation probability plot with a sensitivity decreased to $P < 0.05$ of which at least one point to $P < 0.01$, or 3) a Pattern Standard Deviation $P < 5\%$. Visual field loss was considered to be present if it was reproducible, that is, the abnormalities had to be present on the full-threshold test and on both supra-threshold tests. Defects had to be in the same hemifield and at least one depressed test point had to have exactly the same location on all fields. Fundus photographs, ophthalmic examination reports, medical histories, and MRI scans of the brain were checked for disorders that could explain the visual field loss. If no other cause could be identified, and no homonymous defects and artifacts like rim artifacts were found, the visual field loss was considered GVFL. Discrepancies were resolved by consensus.

Optic disc assessment

Subjects underwent optic disc assessment using the HRT. The cutoff values for glaucomatous optic neuropathy (GON) were based on the linear cup-disc ratio (LCDR) and defined as follows: 0.67 for small discs (up to 1.5 mm²), 0.71 for discs 1.5-2.0 mm², and 0.76 for large discs (>2.0 mm²)¹⁰. We excluded HRT scans that exceeded a standard deviation of 50 μm.

Optical Coherence Tomography (OCT)

Since 2007, the macula and ONH of all visiting subjects have been imaged with OCT (Topcon 3-D OCT-1000; Topcon, Tokyo, Japan). At the beginning of the study, only the right eye was scanned in the interest of time. We included $n=883$ subjects during this period. In a later stage, both eyes were scanned. Due to an update during the study, seven glaucoma cases were scanned with the Topcon OCT-2000 instead of the OCT-1000 (the inclusion of cases was extended because of the low prevalence of GVFL, see above). Importantly, the segmentation algorithm corrects for differences between these two devices. To confirm this, we excluded these seven cases and reanalyzed the data (see Results section). Macular and ONH scans were centered around the fovea and the center of the ONH, respectively. Figure 1 shows the scanned areas. The scans were performed in the horizontal direction. Volume size

was 6x6x1.68 mm (512x128x480 voxels). Volumes with severe motion artifacts caused by head or eye movements and macular volumes in which more than 20% of the volume was unsegmentable were excluded. The ONH volumes with one or more clock hour segments (see below) in which the RNFL was completely unsegmentable were also excluded. All included OCT volumes were segmented into 10 layers (11 surfaces), using the Iowa Reference Algorithms (available in the public domain from <http://biomed-imaging.uiowa.edu/downloads>), a fully three-dimensional automated segmentation algorithm²⁴⁻²⁶. We studied the RNFL (between surface 1 and 2), the RGCL (between surface 2 and 3), and the IPL (between surface 3 and 4). For the macula, we calculated the thicknesses of these layers in 100 square blocks of 0.6x0.6 mm each. For the ONH, we calculated the thickness of the RNFL in between two circles with radii of 1.03 and 1.84 mm centered on the manually determined ONH center²⁷. This was done in 12 peripapillary segments of 30° each (one clock hour).

Data Analysis

We calculated the Area Under the receiver operating characteristics Curves (AUC) for different parameters. Starting with the 100 blocks from the macular region and the 12 peripapillary segments, we constructed a series of parameters. These parameters comprised global measures and more detailed measures, based on the pathophysiology of glaucoma. We used the retinal nerve fiber bundle trajectories as described by Jansonius et al.^{18,19} to divide the macular area in 11 subregions. As this subdivision might be too fine-grained given the test-retest variability of OCT measurements²⁷, we divided the macular area in 4 larger scale subregions as well. We focused on a specific region of the macula, the macular vulnerability zone (MVZ)¹⁷ and – related to the MVZ – the inferior half of the macular scan. Table 1 lists all included parameters; Figure 2 presents the 11 and 4 subregions based on the trajectories, and the MVZ.

For AUC analysis, a single variable is needed. For the global measures, there is only one region-of-interest, and, thus, the average thickness of a particular layer in that region is a single variable. For the measures based on a number of subregions, we made a single variable (a score) by counting the number of subregions that had a thickness of a particular layer below a certain percentile. This was repeated for a series of percentiles (P0.5, P1, P2, P5, P10, P20; based on the controls). The percentile yielding the highest AUC was selected. Analyses concerning the macular region were done for the RGCL, and unweighted summations of RGCL + RNFL, and RGCL + RNFL + IPL. Analyses concerning the ONH region were based on the RNFL. The 95 percent confidence intervals (95% CI) were calculated and the highest AUCs from the macula and ONH were compared using a technique described by DeLong et al.²⁸. We performed a cross-validation by calculating an adjusted AUC of the parameter with the highest (uncorrected) AUC and sensitivity using a leave-one-out resampling method.

We calculated the sensitivity at a fixed high specificity of 97.5% for all included parameters, for the best percentile/layer combination – if applicable²⁹. Sensitivities were compared with a McNemar test. For the parameter with the highest AUC and highest sensitivity, the positive and negative predictive values were calculated. For these parameters, we also calculated the sensitivity and AUC for glaucoma defined as HRT-based GON (see above) and as the presence of both GON and GVFL. Analyses were performed with IBM SPSS Statistics Release 21.0.0.1 (IBM Corp., Armonk, NY, USA). The comparisons of AUCs were performed using MedCalc Statistical Software version 12.7.7 (MedCalc Software bvba, Ostend, Belgium;

Figure 1. Schematic overview of the area of the macular scan (left square) and optic nerve head scan (right square).

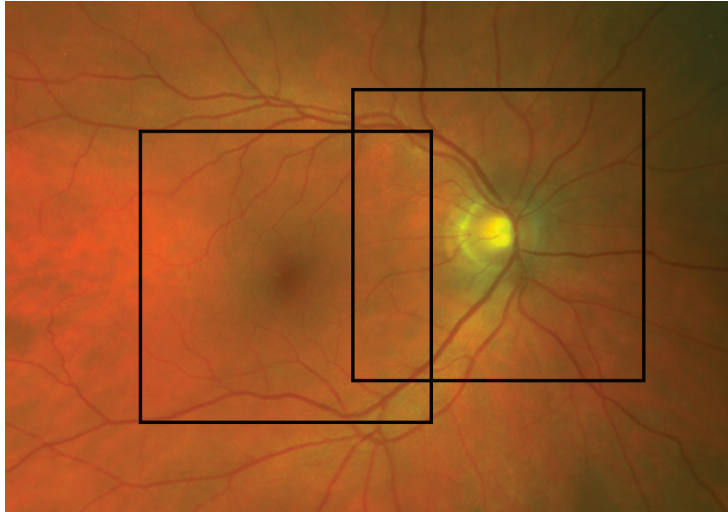


Figure 2. Division of macular scan region in 11 (A) and 4 (B) color-coded subregions, based on the nerve fiber bundle trajectories as described by Jansonius et al.^{18,19}, and the macular vulnerability zone (C) as described by Hood et al.¹⁷. Dark line represents the border between the superior and inferior part of the scan. Division of peripapillary region in 9 color-coded segments (D); * denotes segments that are replaced by macular subregions in the combined variables as described in Table 1).

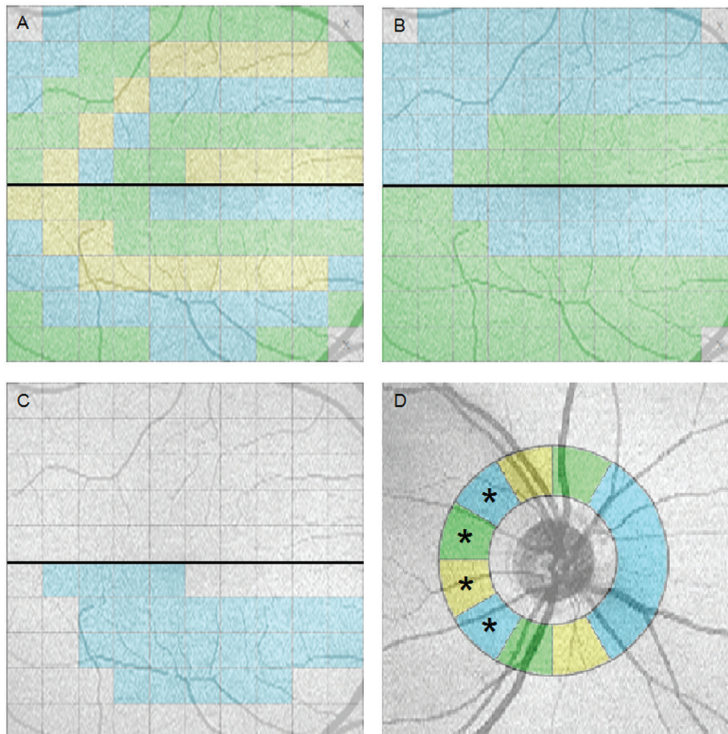


Table 1. Overview of the included OCT parameters.

Region	Parameter	Layer	Measure*
ONH	Mean thickness (µm) in peripapillary region	RNFL	Continuous
	Number of abnormally thin subregions; subregions are peripapillary 30° segments with the 4 nasal segments combined	RNFL	Score 0-9
Macula	Mean thickness (µm) in scan region	RGCL	Continuous
		RGCL+RNFL	
		RGCL+RNFL+IPL	
	Number of abnormally thin subregions; 11 subregions as presented in Figure 2A	RGCL	Score 0-11
		RGCL+RNFL	
		RGCL+RNFL+IPL	
	Number of abnormally thin subregions; 4 subregions as presented in Figure 2B	RGCL	Score 0-4
		RGCL+RNFL	
		RGCL+RNFL+IPL	
	Mean thickness in MVZ (µm; Fig. 2C)	RGCL	Continuous
RGCL+RNFL			
RGCL+RNFL+IPL			
Mean thickness in inferior half of macular scan (µm)	RGCL	Continuous	
	RGCL+RNFL		
	RGCL+RNFL+IPL		
Combined	11 macular subregions (Fig. 2A) with weight factor 4/11 combined with 5 ONH subregions: 2 superior 30° segments, 2 inferior 30° segments, and 1 nasal 120° segment		Score 0-9
	4 macular subregions (Fig. 2B) combined with 5 ONH subregions: 2 superior 30° segments, 2 inferior 30° segments, and 1 nasal 120° segment		Score 0-9

ABBREVIATIONS

IPL inner plexiform layer
MVZ macular vulnerability zone
OCT optical coherence tomography
ONH optic nerve head

RGCL retinal ganglion cell layer
RNFL retinal nerve fiber layer
***** continuous variable or number of subregions with a thickness below a certain percentile

<http://www.medcalc.org>; 2013). The leave-one-out cross-validation was performed using R version 3.0.2 (cvAUC package; R Foundation for Statistical Computing, Vienna, Austria; <http://www.R-project.org/>; 2013). A p-value below 0.05 was considered statistically significant.

RESULTS

We excluded $n=23$ controls with an IOP > 21 mmHg and $n=73$ controls with a positive family history for glaucoma. After this, there were 1,128 subjects left: 1,087 controls and 41 GVFL cases. Controls and cases did not differ in age (74.8 vs. 74.2 years, $P=0.66$) or sex (40.6 vs. 41.5% male, $P=0.91$). The average (median) mean deviation (MD) of the visual field of the cases was -7.5 (-6.5) dB (standard deviation -4.9 dB; interquartile range -3.8 to -10.5 dB).

Table 2 shows the AUCs for the different OCT parameters. None of the parameters had a higher AUC than the mean RGCL thickness in the entire macular region (0.85; 95% CI 0.78 to 0.93). A more detailed analysis did not improve the AUC (0.85 for 11 bundles), nor did confining the analysis to the inferior half of the macular region (0.85). Including additional retinal layers to the thickness measurements (RGCL + RNFL or RGCL + RNFL + IPL), acceptable from an anatomical perspective, yielded lower AUC point estimates. The average RNFL thickness in the ONH volume yielded an AUC of 0.77 (95% CI 0.69 to 0.85; significantly lower than that of the mean RGCL thickness in the entire macular region; $P=0.01$); a detailed analysis of 9 peripapillary segments resulted in essentially the same AUC (0.78). Combined analysis of macular bundles and peripapillary segments did not yield any diagnostic improvement.

Table 3 shows the sensitivity at an approximately 97.5% specificity level for the layer and/or percentile with the highest AUC for each OCT parameter. The mean RGCL thickness in the inferior half of the macular region had the highest sensitivity (53.7%; 95% CI 38.7-68.0%) followed by the mean RGCL thickness in the MVZ (46.3%; 95% CI, 32.1-61.3%). The positive and negative predictive values of the former parameter were 44.9% and 98.2%, respectively. The difference between these two sensitivities was not significant ($P=0.25$). The mean peripapillary RNFL thickness had a sensitivity of 24.4% (95% CI, 13.7-39.5%; $P<0.001$ compared to the mean RGCL thickness in inferior half of the macular region). The corrected AUC for the parameter with the highest AUC and sensitivity (mean RGCL thickness in the inferior half of the macular region; AUC = 0.85) was 0.84 (leave-one-out cross-validation). No significant differences were found for this parameter after exclusion of the subjects who were scanned with the OCT-2000: AUC and sensitivity at 97.5% specificity were 0.83 and 52.9%, respectively.

Of the 41 cases, 19 were not identified by 'mean RGCL thickness in the inferior half of the macular region'. Figure 3 shows the MD and pattern standard deviation (PSD) values of the 41 cases, stratified according to true-positive and false-negative status. The MD and PSD values of the 19 false-negatives seemed to be higher and lower, respectively, than that of the 22 true positives, but the differences were not significant (MD -6.2 vs. -8.6 dB, $P=0.13$; PSD 7.1 vs. 9.0 dB, $P=0.09$). Figure 4 presents the mean sensitivity in the superior half of the visual field (8 superiorly located central test locations of 24-2 grid) as a function of the mean

Table 2. AUCs for the OCT parameters as listed in Table 1.

Region	Parameters	Layer	AUC					
			P0.5	P1	P2	P5	P10	P20
ONH	Mean of all segments	RNFL				0.77		
	Score based on 9 segments	RNFL	0.57	0.64	0.66	0.76	0.78	0.76
Macula	Mean in whole scan	RGCL				0.85		
		RNFL + RGCL				0.83		
		RNFL + RGCL + IPL				0.78		
	Score based on eleven bundles	RGCL	0.68	0.80	0.82	0.85	0.83	0.84
		RNFL + RGCL	0.67	0.76	0.82	0.84	0.84	0.82
		RNFL + RGCL + IPL	0.64	0.71	0.77	0.81	0.81	0.78
	Score based on four bundles	RGCL	0.60	0.71	0.78	0.83	0.83	0.84
		RNFL + RGCL	0.65	0.68	0.78	0.80	0.82	0.81
		RNFL + RGCL + IPL	0.57	0.65	0.73	0.79	0.79	0.76
	Mean in MVZ	RGCL				0.83		
		RNFL + RGCL				0.79		
		RNFL + RGCL + IPL				0.78		
	Mean in inferior scan	RGCL				0.85		
		RNFL + RGCL				0.81		
		RNFL + RGCL + IPL				0.79		
Combined	Score based on ONH RNFL (P10) + eleven macular bundles RGCL (P5)				0.85			
	Score based on ONH RNFL (P10) + four macular bundles RGCL (P20)				0.85			

ABBREVIATIONS

AUC Area Under the receiver operating characteristics Curve
IPL inner plexiform layer
MVZ macular vulnerability zone
OCT optical coherence tomography

ONH optic nerve head
RGCL retinal ganglion cell layer
RNFL retinal nerve fiber layer
 P0.5, P1, P2, P5, P10, and P20 are percentiles based on the controls in this study population that are used as cutoff values to calculate the scores (see Table 1)

Table 3. Sensitivity, at 97.5% specificity*, for the layers and percentiles with the best AUC (Table 2).

Region	Variable	Specificity (*)	Sensitivity
ONH	Mean RNFL of all segments	97.5%	24.4%
	RNFL score: P10	96.1%	29.3%
		98.0%	14.6%
Macula	Mean of whole scan, RGCL	97.5%	36.6%
	11 bundles, RGCL P5	97.2%	29.3%
		98.1%	29.3%
		93.8% (**)	41.5%
	4 bundles, RGCL P20	97.5%	46.3%
	Mean of inferior scan, RGCL	97.5%	53.7%
Combined	ONH RNFL P10 + 4 bundles RGCL P20	97.0%	31.7%
		98.1%	22.0%
	ONH RNFL P10 + 11 bundles RGCL P5	97.5%	26.8%

ABBREVIATIONS

IPL inner plexiform layer**MVZ** macular vulnerability zone**ONH** optic nerve head**RGCL** retinal ganglion cell layer**RNFL** retinal nerve fiber layer

* if none of the cutoff points yielded a specificity of exactly 97.5%, two specificity values were reported that enclose 97.5%

** highest possible specificity for this parameter

Table 4. Sensitivity at 97.5% specificity and AUC for mean RGCL thickness in the inferior half of the macular region and mean RNFL thickness in peripapillary region, for cases with HRT-based GON (n=37), and cases with GON and GVFL (n=10).

		GVFL	GON	GVFL and GON
Mean of macular inferior scan, RGCL	Sensitivity (%)	53.7	24.3	70.0
	AUC	0.85	0.71	0.93
Mean RNFL of all peripapillary segments	Sensitivity (%)	24.4	16.2	40.0
	AUC	0.77	0.78	0.95

ABBREVIATIONS

AUC Area Under the receiver operating characteristics Curve**GON** glaucomatous optic neuropathy (based on HRT, see Methods section)**GVFL** glaucomatous visual field loss**RGCL** retinal ganglion cell layer**RNFL** retinal nerve fiber layer

RGCL thickness in the inferior half of the macular scan, for the 41 cases with GVFL. There was a significant association ($R=0.35$; $P=0.026$). True-positives had on average a lower threshold sensitivity in the central part of the superior visual field compared to false-negatives (19.6 dB versus 24.7 dB, $P=0.042$). There was no difference in axial length between cases and controls (23.8 vs. 23.5 mm, $P=0.09$; based on 33 cases and 903 controls for which axial length data were available), but true-positives had a greater axial length than false-negatives (24.1 vs. 23.4 mm, $P=0.049$). Finally, Figure 5 presents the mean superior macular thickness versus the mean inferior macular thickness for the RGCL, for cases and controls.

Table 4 shows the sensitivity at 97.5% specificity and AUC for patients with HRT-based GON ($n=37$) and GON and GVFL ($n=10$). The sensitivity and AUC of the 'mean RGCL thickness in the inferior half of the macular region' increased from 53.7% to 70.0% and from 0.85 to 0.93, respectively, for cases with GON and GVFL.

Figure 3. Scatterplot of mean deviation versus pattern standard deviation for the 41 cases with glaucomatous visual field loss. White diamonds represent the cases ($n=22$) correctly classified by the mean retinal ganglion cell layer thickness in the inferior half of the macular region (true-positives). Black dots represent the false-negative cases ($n=19$).

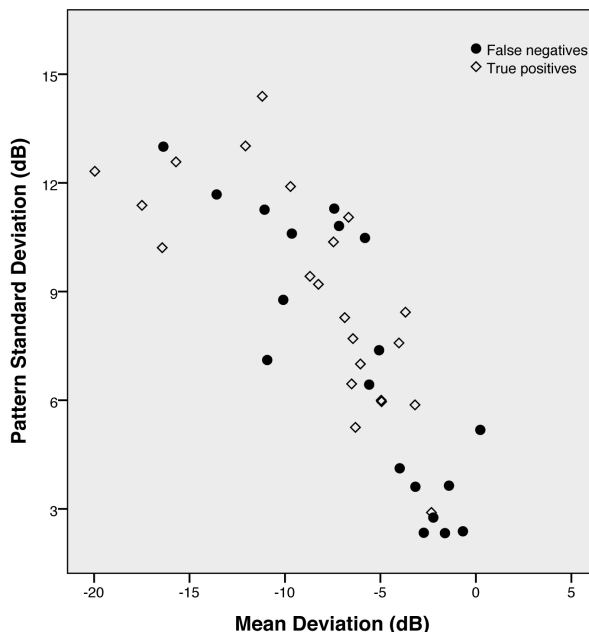


Figure 4. Scatterplot of the mean retinal ganglion cell layer (RGCL) thickness in the inferior half of the macular scan versus the mean sensitivity of the eight superiorly located central test locations of the 24-2 grid for the 41 cases with glaucomatous visual field loss.

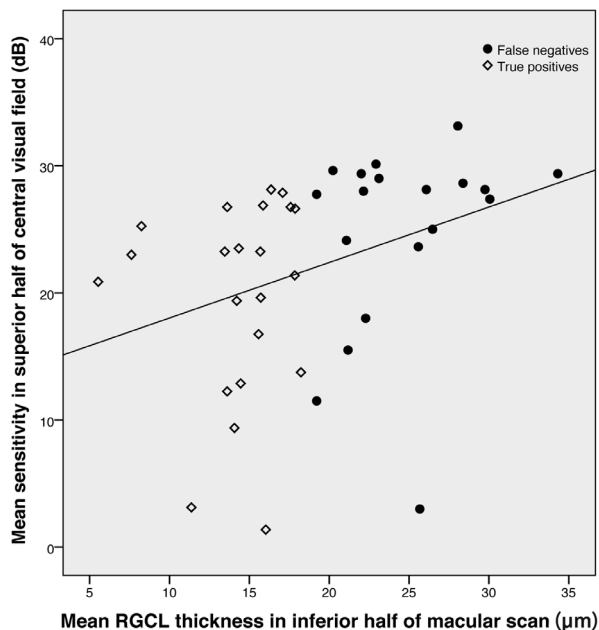
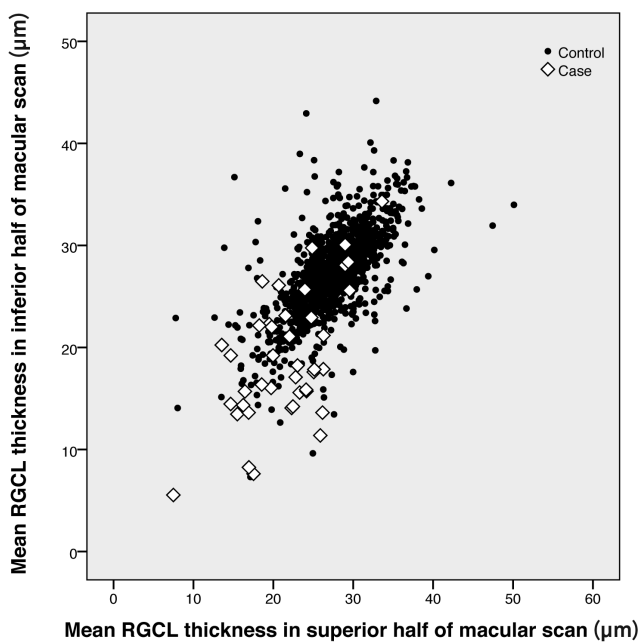


Figure 5. Mean superior macular thickness versus mean inferior macular thickness for the retinal ganglion cell layer (RGCL), for cases (white) and controls (black).



DISCUSSION

Our results showed that the mean RGCL thickness in the inferior half of the macular region has the best performance in terms of AUC and sensitivity at 97.5% specificity in this population-based OCT study. The sensitivity of 53.7% results in missing almost half of GFVL cases if OCT is applied for mass screening for glaucoma, as defined by our criteria of visual field loss.

The AUC is a commonly reported measure for the diagnostic performance of a test. It is a summary measure compiled from the sensitivity and specificity for a range of cutoff values. Given the low prevalence of glaucoma in a population, however, sensitivities at low specificities have diminished relevance. This makes sensitivity at a fixed high specificity a more relevant measure. Therefore, we consider 'mean RGCL thickness in the inferior half of the macular region' the best parameter, despite the fact that many other parameters had comparable AUCs. The 97.5% specificity level has an optimal balance between false-positive and true-positive classification for risk factor analysis²⁹. For screening as part of preventing a disease, the specificity is also a trade-off between yield and cost, and a different cutoff value may be preferred from either perspective. However, a cost-effectiveness analysis is not the purpose of this current study.

Recently, several studies focusing on glaucomatous macular damage have been published³⁰⁻³⁷. The macular ganglion cell complex (GCC, i.e., RNFL + RGCL + IPL) is on average thinner in glaucomatous eyes and correlates with visual field changes. Our study included mainly patients with early and moderate glaucoma (median MD was -6.5 dB) and in this group the macular region was affected in approximately half of the patients (Table 3; sensitivity for the mean RGCL thickness in the inferior half of the macular region 53.7%). This is in agreement with recent studies assessing the macula with perimetry in detail and underlines the importance of macula testing in glaucoma care^{38,39}, something that has been abandoned with the adoption of 6x6 degree perimetric grids. Hood et al. suggested that the RGCL in a specific part of the inferior macula associates with the region of the optic disc where most glaucomatous damage occurs; the macular vulnerability zone¹⁷. In our study, we found a sensitivity of 46.3% for this macular area. Because thickness measurements for this specific area are not available for each OCT device, we calculated the AUC and sensitivity for 'mean RGCL thickness in the inferior half of the macular region' and found a sensitivity that was at least as high as the sensitivity of the MVZ (53.7%; $P=0.25$ compared to the sensitivity of 46.3% of the MVZ). Taking the pathophysiology of glaucoma into account by using the 4 and 11 bundle regions-of-interest approach did not improve performance. Presumably, the large intersubject variability in the retinal nerve fiber bundle trajectories might explain the poor performance of an approach based on the average trajectories¹⁹. We previously found that combined analysis of the RNFL and RGCL thicknesses allowed for analyzing smaller regions-of-interest²⁷. This approach did not increase performance in the current analysis, probably because smaller regions-of-interest were less informative for other reasons, like the intersubject variability of the retinal anatomy mentioned above. Glaucomatous damage causes retinal gliosis⁴⁰, which may mask RNFL thinning on OCT⁴¹.

Table 5 gives an overview of published literature regarding glaucoma screening with OCT. We included studies with information on AUC, and/or sensitivity and specificity and with more than 200 cases and healthy controls in total. Four non population-based studies investigated macular parameters, in various layers, being the GCC⁴², RNFL + RGCL + IPL⁴³, RGCL + IPL⁴⁴, and the RNFL⁴⁵. These macular parameters had AUCs ranging from 0.87 to 0.96; the peripapillary RNFL and ONH parameters in these studies had AUCs varying from 0.78 to 0.99. Obviously, a comparison of these studies is hampered by heterogeneity of the applied glaucoma definitions (reference standards): three of four studies used a glaucoma definition based on visual field loss and GON. In contrast, our reference standard for calling a case glaucoma was based solely on visual field loss (GVFL), that is, on functional changes. This may have biased the results towards a lower agreement with OCT, a technique that measures structural changes. With a more strict glaucoma definition based on GON and GVFL, the sensitivity for mean RGCL thickness in the inferior half of the macular region increased from 53.7% to 70.0%, with an increase in AUC from 0.85 to 0.93 (Table 4), and again the macular region outperformed the peripapillary region (Table 4). Generally, the reported AUCs of other studies seem to surpass that of our study. However, our study is a population-based study and cannot be compared to clinical studies, with their selection bias, directly. In a clinical setting, perimetry is generally confined to those patients who have a suspected ONH appearance. This will induce a selection bias towards abnormal structure, favoring an imaging technique, like OCT. In our population-based setting, perimetry was performed in all subjects. Baskaran et al. included 508 healthy controls from a population-based study, but they selected 184 glaucoma cases from an eye center, where glaucoma diagnosis was based on GON and corresponding visual field loss⁴⁶. Li et al. included community-based volunteer subjects¹⁵, including 204 healthy controls and six cases with definite glaucoma, which was also defined as visual field loss and GON. Their best parameter was the cup diameter (AUC 0.91; 83% sensitivity at 84% specificity). Another study invited individuals randomly from two rural areas¹⁴ and consisted of 129 healthy controls and only nine glaucoma cases. The inclusion criterion for being a case was glaucomatous changes of the optic disc. Their best AUC (0.99) was found for the parameter “ ≥ 1 peripapillary quadrant sectors below P1”; with 100% sensitivity at 96% specificity.

Although the sensitivity we found is lower than in these clinical case-control studies, it is relatively high compared to other imaging techniques used in population-based studies. In the Rotterdam Study, we found a sensitivity of 35% at 97.5% specificity for the best parameter of the HRT (linear cup-disc ratio adjusted for disc area)¹⁰; a similar modest HRT screening performance was found in the Tajimi study and in the Blue Mountains Eye Study^{9,11}. Another study investigated scanning laser polarimetry (GDx-VCC) and found a sensitivity of 25.6% at a specificity of 97.0% for the parameter with the highest AUC (0.89; nerve fiber indicator)¹².

The strength of this study is the large number of subjects. However, the number of cases is a limitation, a consequence of the population-based design. There were 41 cases, which is lower than most clinical studies in Table 5. At the beginning of our study, we scanned only the right eye and, therefore, we missed 15 cases with unilateral GVFL in the left eye. Another strength is the glaucoma reference standard, which is based on visual field loss only. This avoids a selection bias towards abnormal structure (see above). On the other hand,

we have probably missed some glaucoma cases with small macular defects and cases with superficial defects, due to the coarse 6x6 degree grid in combination with the requirement of three contiguous abnormal test locations and the preselection with supra-threshold testing, respectively.

Analyzing a series of parameters bears the risk of chance findings. We tried to avoid this as much as possible by limiting the number of parameters and by focusing on parameters inspired by the anatomy and pathophysiology of glaucoma. In the ideal situation, an external validation is performed. Data for such a validation were not available. For that reason, we performed a cross-validation using a leave-one-out resampling. The resulting adjusted AUC (0.84) of our best parameter, the mean RGCL thickness in the inferior half of the macular region, was essentially equal to the unadjusted AUC (0.85), indicating an unbiased estimate.

Because of the limited number of cases, we did not analyze early, moderate, and severe cases separately. However, we did some exploratory analyses. Correctly identified cases had a lower perimetric threshold sensitivity in the central part of the visual field and a greater axial length compared to cases that were not identified. The difference in axial length could be a technical issue or a real influence of axial length on the pathophysiology of glaucoma⁴⁷.

In conclusion, in this population-based study OCT uncovers abnormalities in the macular region in many cases with early and moderate glaucoma detected with perimetry. Retinal ganglion cell loss in the macular region is at least as common as peripapillary RNFL abnormalities. The OCT-derived regional thickness-based screening only leads to missing approximately half of all glaucoma cases with manifest visual field loss in our population.

Table 5. Overview of published literature regarding glaucoma screening with OCT.

Reference	Definition of glaucoma	Number of cases	Number of controls	OCT device
Baskaran (2012) ⁴⁶	GON + GVFD	184	508	Cirrus HD-OCT
Bengtsson (2012) ¹⁴	GON	138 clinical cases	129 healthy subjects from population	TD Stratus OCT SD Cirrus OCT
Bowd (2008) ⁴⁸	GON and/or GVFD	156	69	Stratus-OCT
Garas (2011) ⁴²	GON + GVFD	111	93	RTVue-100 FD OCT
Huang (2011) ⁴³	GVFD	146	74	RTVue OCT
Jeoung (2013) ⁴⁴	GON + GVFD	142	119	Cirrus HD-OCT
		164	119	Cirrus HD-OCT
Leung (2010) ⁴⁹	GVFD	121	102	TD Stratus OCT SD Cirrus HD-OCT

Table 5. (continued)

Parameter	Best parameter(s)	Sensitivity (%)	Specificity (%)	AUC
RNFL: average, quadrant and clock-hours	Average	x	x	0.92
	Inferior	x	x	0.92
ONH	VCDR	x	x	0.91
RNFL: average, quadrant and clock-hours	Average <P5	78	99	x
	≥1 quadrant sector <P5	93	93	x
	≥1 clock hours <P5	95	81	x
RNFL: average, quadrant and clock-hours	Average <P5	90	95	x
	≥1 quadrant sector <P5	96	81	x
	≥1 clock-hours <P5	94	65	x
RNFL: average, superior and inferior	Average	58	90	0.78
RNFL: average, superior and inferior sectors, 16 segments	Infero-Temporal segment	88.3	97.8	x
Macula: GCC	FLV	92.8	89.1	x
ONH	Cup area or rim area (same results)	85.6	76.3	x
RNFL: 8 segments	Average	81.5	87.8	0.92
ONH	VCDR	71.9	91.9	0.85
Macula: IRL	Inferior hemisphere thickness	74.7	90.5	0.87
RNFL: average, quadrant and clock-hours	Average	83.1	96.6	0.96
	Inferior	86.6	94.6	0.96
ONH	Rim area	80.5	86.6	0.94
Macular GCIPL: average, minimal and 6 sectors	Minimal GCIPL	90.8	88.2	0.96
RNFL: idem	Average	50	96.6	0.90
ONH: idem	Rim area	61	86.6	0.86
Macular GCIPL: idem	Minimal GCIPL	73.2	88.2	0.90
RNFL: clock-hour, quadrant and average	≥1 clock-hour ≤5% level	88.4	89.2	x
	Average	85.1	90	0.94
	Inferior quadrant	86	90	0.93
RNFL: clock-hour, quadrant and average	≥1 clock-hour ≤5% level	93.4	83.3	x
	Average	86.8	90	0.95
	Inferior quadrant	86.8	90	0.95

Table 5. Overview of published literature regarding glaucoma screening with OCT.

Reference	Definition of glaucoma	Number of cases	Number of controls	OCT device
Li (2010) ¹⁵	GON and/or GVFD	6	204	Stratus OCT
Moreno-Montañés (2010) ⁵⁰	GVFD + IOP >21 mmHg	86	130	Stratus OCT Cirrus OCT
Mwanza (2011) ⁵¹	GON + GVFD	73	146	Cirrus HD-OCT
Park (2013) ⁵²	GON + GVFD	146	84	Cirrus HD-OCT
Park (2013) ⁵³	GON + GVFD	144	65	Spectralis SD-OCT
Seo (2012) ⁴⁵	GON + GVFD	84	122	Spectralis SD-OCT
Sihota (2006) ⁵⁴	GON + GVFD + IOP >22 mmHg	61	160	Stratus OCT-3

ABBREVIATIONS

FD	Fourier-domain	GVFD	glaucomatous visual field defect
FLV	total sum of statistically significant GCC volume loss divided by the GCC map area	HD	high definition
GCC	ganglion cell complex	IRL	inner retinal layer (RNFL, ganglion cells layer and inner plexiform layer)
GCIPL	ganglion cell-inner plexiform layer	OCT	optical coherence tomography
GON	glaucomatous optic neuropathy	ONH	optic nerve head

Table 5. (continued)

Parameter	Best parameter(s)	Sensitivity (%)	Specificity (%)	AUC
RNFL: global, superior and inferior average	≥1 parameter <5%	67	85	x
	≥1 parameter <1%	50	94	x
ONH	Cup diameter ≥1.16 mm	83.3	84.4	0.91
RNFL: average, quadrant and clock-hours	Global average	68.9	86.7	0.83
RNFL: average, quadrant and clock-hours	Superior quadrant	68.9	91.4	0.84
RNFL: average, quadrant, clock-hours	Clock-hour lower temporal	x	x	0.96
ONH parameters	Vertical rim thickness	x	x	0.96
RNFL: average, quadrant, clock-hours and RNFL Area Index	RNFL Area Index	x	x	0.99
	Inferior quadrant	x	x	0.97
RNFL: average, quadrants, and four superior and inferior segments	Global average	86	>90	0.95
ONH: laminar thickness; mean of mid-superior, center and mid-inferior	NA	89	>90	0.98
RNFL: average, quadrants and 6 sectors	Abnormality (<1%) in ≥1 sector	85.7	95.1	x
PPAA: central 20° area, 30x25° scan	Number of different cells	x	x	0.96
RNFL: average and quadrant	Average	89.4	80.3	0.91

PPAA posterior pole asymmetry analysis; RNFL thickness value of 8x8 cells --> cell to cell comparison between corresponding cells across the hemisphere (difference ≥30µm)

RNFL retinal nerve fiber layer

RNFL Area Index proportion of normal RNFL area (≥1% age-matched controls)

SD Spectral-domain

TD Time-domain

References

1. Airaksinen, P.J. & Alanko, H.I. Effect of retinal nerve fiber loss on the optic nerve head configuration in early glaucoma. *Graefes Arch Clin Exp Ophthalmol* 220, 193-6 (1983).
2. Nickells, R.W. Ganglion cell death in glaucoma: from mice to men. *Vet Ophthalmol* 10 Suppl 1, 88-94 (2007).
3. Schuman, J.S. et al. Quantification of nerve fiber layer thickness in normal and glaucomatous eyes using optical coherence tomography. *Arch Ophthalmol* 113, 586-96 (1995).
4. Rohrschneider, K., Burk, R.O., Kruse, F.E. & Volcker, H.E. Reproducibility of the optic nerve head topography with a new laser tomographic scanning device. *Ophthalmology* 101, 1044-9 (1994).
5. Dreher AW, R.K. Retinal laser ellipsometry: a new method for measuring the retinal nerve fibre layer thickness distribution? *Clin Vis Sci* 7, 481-488 (1992).
6. Weinreb, R.N. et al. Histopathologic validation of Fourier-ellipsometry measurements of retinal nerve fiber layer thickness. *Arch Ophthalmol* 108, 557-60 (1990).
7. Choplin, N.T. & Lundy, D.C. The sensitivity and specificity of scanning laser polarimetry in the detection of glaucoma in a clinical setting. *Ophthalmology* 108, 899-904 (2001).
8. Oddone, F. et al. Sector-based analysis with the Heidelberg Retinal Tomograph 3 across disc sizes and glaucoma stages: a multicenter study. *Ophthalmology* 116, 1106-11 e1-3 (2009).
9. Healey, P.R., Lee, A.J., Aung, T., Wong, T.Y. & Mitchell, P. Diagnostic accuracy of the Heidelberg Retina Tomograph for glaucoma a population-based assessment. *Ophthalmology* 117, 1667-73 (2010).
10. Ramdas, W.D. et al. Heidelberg Retina Tomograph (HRT3) in population-based epidemiology: normative values and criteria for glaucomatous optic neuropathy. *Ophthalmic Epidemiol* 18, 198-210 (2011).
11. Saito, H., Tsutsumi, T., Araie, M., Tomidokoro, A. & Iwase, A. Sensitivity and specificity of the Heidelberg Retina Tomograph II Version 3.0 in a population-based study: the Tajimi Study. *Ophthalmology* 116, 1854-61 (2009).
12. Toth, M., Kothy, P., Vargha, P. & Hollo, G. Accuracy of combined GDx-VCC and matrix FDT in a glaucoma screening trial. *J Glaucoma* 16, 462-70 (2007).
13. Huang, D. et al. Optical coherence tomography. *Science* 254, 1178-81 (1991).
14. Bengtsson, B., Andersson, S. & Heijl, A. Performance of time-domain and spectral-domain Optical Coherence Tomography for glaucoma screening. *Acta Ophthalmol* 90, 310-5 (2012).
15. Li, G., Fansi, A.K., Boivin, J.F., Joseph, L. & Harasymowycz, P. Screening for glaucoma in high-risk populations using optical coherence tomography. *Ophthalmology* 117, 453-61 (2010).
16. Garvin, M.K. et al. 2-D pattern of nerve fiber bundles in glaucoma emerging from spectral-domain optical coherence tomography. *Invest Ophthalmol Vis Sci* 53, 483-9 (2012).
17. Hood, D.C., Raza, A.S., de Moraes, C.G., Liebmann, J.M. & Ritch, R. Glaucomatous damage of the macula. *Prog Retin Eye Res* 32, 1-21 (2013).
18. Jansonius, N.M. et al. A mathematical description of nerve fiber bundle trajectories and their variability in the human retina. *Vision Res* 49, 2157-63 (2009).
19. Jansonius, N.M., Schiefer, J., Nevalainen, J., Paetzold, J. & Schiefer, U. A mathematical model for describing the retinal nerve fiber bundle trajectories in the human eye: average course, variability, and influence of refraction, optic disc size and optic disc position. *Exp Eye Res* 105, 70-8 (2012).
20. Lee, K. et al. Distribution of damage to the entire retinal ganglion cell pathway: quantified using spectral-domain optical coherence tomography analysis in patients with glaucoma. *Arch Ophthalmol* 130, 1118-26 (2012).
21. Hofman, A. et al. The Rotterdam Study: 2014 objectives and design update. *Eur J Epidemiol* 28, 889-926 (2013).
22. Wolfs, R.C. et al. Changing views on open-angle glaucoma: definitions and prevalences--The Rotterdam Study. *Invest Ophthalmol Vis Sci* 41, 3309-21 (2000).
23. Czudowska, M.A. et al. Incidence of glaucomatous visual field loss: a ten-year follow-up from the Rotterdam Study. *Ophthalmology* 117, 1705-12 (2010).
24. Garvin, M.K. et al. Intraretinal layer segmentation of macular optical coherence tomography images using optimal 3-D graph search. *IEEE Trans Med Imaging* 27, 1495-505 (2008).
25. Garvin, M.K. et al. Automated 3-D intraretinal layer segmentation of macular spectral-domain optical coherence tomography images. *IEEE Trans Med Imaging* 28, 1436-47 (2009).
26. Lee, K. et al. Segmentation of the optic disc in 3-D OCT scans of the optic nerve head. *IEEE Trans Med Imaging* 29, 159-68 (2010).
27. Springelkamp, H. et al. Optimizing the information yield of 3-D OCT in glaucoma. *Invest Ophthalmol Vis Sci* 53, 8162-71 (2012).
28. DeLong, E.R., DeLong, D.M. & Clarke-Pearson, D.L. Comparing the areas under two or more correlated receiver operating characteristic curves: a nonparametric approach. *Biometrics* 44, 837-45 (1988).

29. Ramdas, W.D. et al. Defining glaucomatous optic neuropathy from a continuous measure of optic nerve damage—the optimal cut-off point for risk-factor analysis in population-based epidemiology. *Ophthalmic Epidemiol* 18, 211-6 (2011).
30. Inuzuka, H. et al. Macular Ganglion Cell Complex Thickness in Glaucoma With Superior or Inferior Visual Hemifield Defects. *J Glaucoma* (2013).
31. Kimura, Y. et al. Macular structure parameters as an automated indicator of paracentral scotoma in early glaucoma. *Am J Ophthalmol* 156, 907-917 e1 (2013).
32. Na, J.H. et al. Detection of macular ganglion cell loss in preperimetric glaucoma patients with localized retinal nerve fibre defects by spectral-domain optical coherence tomography. *Clin Experiment Ophthalmol* 41, 870-80 (2013).
33. Nouri-Mahdavi, K. et al. Macular ganglion cell/inner plexiform layer measurements by spectral domain optical coherence tomography for detection of early glaucoma and comparison to retinal nerve fiber layer measurements. *Am J Ophthalmol* 156, 1297-1307 e2 (2013).
34. Rao, H.L. et al. Comparison of different spectral domain optical coherence tomography scanning areas for glaucoma diagnosis. *Ophthalmology* 117, 1692-9, 1699 e1 (2010).
35. Tan, O. et al. Detection of macular ganglion cell loss in glaucoma by Fourier-domain optical coherence tomography. *Ophthalmology* 116, 2305-14 e1-2 (2009).
36. Tan, O. et al. Mapping of macular substructures with optical coherence tomography for glaucoma diagnosis. *Ophthalmology* 115, 949-56 (2008).
37. Wang, M. et al. Combining Information From 3 Anatomic Regions in the Diagnosis of Glaucoma With Time-Domain Optical Coherence Tomography. *J Glaucoma* (2012).
38. Hood, D.C. et al. Initial arcuate defects within the central 10 degrees in glaucoma. *Invest Ophthalmol Vis Sci* 52, 940-6 (2011).
39. Schiefer, U. et al. Spatial pattern of glaucomatous visual field loss obtained with regionally condensed stimulus arrangements. *Invest Ophthalmol Vis Sci* 51, 5685-9 (2010).
40. Wang, L., Cioffi, G.A., Cull, G., Dong, J. & Fortune, B. Immunohistologic evidence for retinal glial cell changes in human glaucoma. *Invest Ophthalmol Vis Sci* 43, 1088-94 (2002).
41. Grieshaber, M.C., Moramarco, F., Schoetzau, A., Flammer, J. & Orguel, S. Detection of retinal glial cell activation in glaucoma by time domain optical coherence tomography. *Klin Monbl Augenheilkd* 229, 314-8 (2012).
42. Garas, A., Vargha, P. & Hollo, G. Diagnostic accuracy of nerve fibre layer, macular thickness and optic disc measurements made with the RTVue-100 optical coherence tomograph to detect glaucoma. *Eye (Lond)* 25, 57-65 (2011).
43. Huang, J.Y., Pekmezci, M., Mesiwala, N., Kao, A. & Lin, S. Diagnostic power of optic disc morphology, peripapillary retinal nerve fiber layer thickness, and macular inner retinal layer thickness in glaucoma diagnosis with fourier-domain optical coherence tomography. *J Glaucoma* 20, 87-94 (2011).
44. Jeoung, J.W., Choi, Y.J., Park, K.H. & Kim, D.M. Macular ganglion cell imaging study: glaucoma diagnostic accuracy of spectral-domain optical coherence tomography. *Invest Ophthalmol Vis Sci* 54, 4422-9 (2013).
45. Seo, J.H. et al. Detection of localized retinal nerve fiber layer defects with posterior pole asymmetry analysis of spectral domain optical coherence tomography. *Invest Ophthalmol Vis Sci* 53, 4347-53 (2012).
46. Baskaran, M. et al. Classification algorithms enhance the discrimination of glaucoma from normal eyes using high-definition optical coherence tomography. *Invest Ophthalmol Vis Sci* 53, 2314-20 (2012).
47. Marcus, M.W., de Vries, M.M., Junoy Montolio, F.G. & Jansonius, N.M. Myopia as a risk factor for open-angle glaucoma: a systematic review and meta-analysis. *Ophthalmology* 118, 1989-1994 e2 (2011).
48. Bowd, C. et al. Bayesian machine learning classifiers for combining structural and functional measurements to classify healthy and glaucomatous eyes. *Invest Ophthalmol Vis Sci* 49, 945-53 (2008).
49. Leung, C.K. et al. Retinal nerve fiber layer imaging with spectral-domain optical coherence tomography: analysis of the retinal nerve fiber layer map for glaucoma detection. *Ophthalmology* 117, 1684-91 (2010).
50. Moreno-Montanes, J., Olmo, N., Alvarez, A., Garcia, N. & Zarranz-Ventura, J. Cirrus high-definition optical coherence tomography compared with Stratus optical coherence tomography in glaucoma diagnosis. *Invest Ophthalmol Vis Sci* 51, 335-43 (2010).
51. Mwanza, J.C., Oakley, J.D., Budenz, D.L., Anderson, D.R. & Cirrus Optical Coherence Tomography Normative Database Study, G. Ability of cirrus HD-OCT optic nerve head parameters to discriminate normal from glaucomatous eyes. *Ophthalmology* 118, 241-8 e1 (2011).
52. Park, H.Y. & Park, C.K. Structure-function relationship and diagnostic value of RNFL Area Index compared with circumferential RNFL thickness by spectral-domain OCT. *J Glaucoma* 22, 88-97 (2013).
53. Park, H.Y. & Park, C.K. Diagnostic capability of lamina cribrosa thickness by enhanced depth imaging and factors affecting thickness in patients with glaucoma. *Ophthalmology* 120, 745-52 (2013).
54. Sihota, R., Sony, P., Gupta, V., Dada, T. & Singh, R. Diagnostic capability of optical coherence tomography in evaluating the degree of glaucomatous retinal nerve fiber damage. *Invest Ophthalmol Vis Sci* 47, 2006-10 (2006).

PART 3

**RISK FACTORS FOR
INTRAOCULAR PRESSURE
AND GLAUCOMA**

CHAPTER 3.1

Incidence of glaucomatous visual field loss after two decades of follow-up: the Rotterdam Study



Henriët Springelkamp, Roger C.W. Wolfs, Wishal D. Ramdas, Albert Hofman, Johannes R. Vingerling, Caroline C.W. Klaver, Nomdo M. Jansonius.

Submitted

ABSTRACT

Objective or Purpose. To determine the incidence of glaucomatous visual field loss (GVFL) two decades after the onset of the Rotterdam Study and to compare known risk factors for open-angle glaucoma (OAG) between the different OAG phenotypes.

Design. Population-based cohort study.

Participants. Participants aged 55 years and older from the Rotterdam Study I.

Methods. Of the 6,806 participants of the Rotterdam Study I, 3,939 participants underwent visual field testing at baseline and at least one follow-up round. The ophthalmic examinations further included optic disc assessment and measurements of intraocular pressure (IOP), refractive error, diastolic blood pressure (DBP), and height and weight. The incidence rate of GVFL was calculated. Risk factors (age, gender, baseline IOP, family history, myopia, DBP, and body mass index [BMI]) were assessed using Cox regression modeling. Outcomes for this analysis (OAG phenotypes) were GVFL with glaucomatous optic neuropathy (GON), GVFL without GON, and GON without GVFL.

Main Outcome Measures. Incidence rate of GVFL and Hazard Ratios of the risk factors for GVFL and/or GON.

Results. Median follow-up was 11.1 (IQR 6.8 to 17.2; range 5.0 to 20.3) years. The incidence rate of GVFL was 2.9 (95% confidence interval 2.4 to 3.4) per 1000 person years. Baseline IOP and age were highly significantly associated with all OAG phenotypes (all $P < 0.001$), BMI showed a non-significant protective effect in all phenotypes ($P = 0.01$ to $P = 0.09$), and gender, myopia, and DBP were not associated with any of the OAG phenotypes.

Conclusions. These data provide an estimate of the long-term incidence of GVFL in a white population. The development of GVFL was strongly associated with baseline IOP and age. The various OAG phenotypes did not differ noticeably in their associations with the OAG risk factors studied.

INTRODUCTION

Glaucoma is a group of diseases that affect the optic nerve. Primary open-angle glaucoma (OAG) is one of the most common forms of glaucoma. It is characterized by loss of retinal ganglion cells (RGCs) and thinning of the retinal nerve fiber layer (RNFL). Another hallmark is excavation of the optic nerve head (ONH), glaucomatous optic neuropathy (GON). These structural changes are visible by fundoscopy or can be assessed with imaging techniques like scanning laser ophthalmoscopy, scanning laser polarimetry, or optical coherence tomography. In general, loss of RGCs and RNFL leads to visual field defects. This functional loss can be measured by perimetry. The surprisingly loose association between structural and functional changes in individual patients is one of the major unsolved issues in glaucoma.

In a general ophthalmology clinical setting, an examination of the ONH and a measurement of the intraocular pressure (IOP) belong to standard care whereas perimetry does not. Perimetry will only be performed in patients with a suspicious appearance of the ONH or an elevated IOP. This biases the clinical OAG phenotype towards high-tension glaucoma (HTG) and/or pronounced ONH abnormalities. The clinical impression that normal tension glaucoma (NTG) patients have more pronounced ONH abnormalities than HTG patients (at a given level of visual field loss) might be the result of this bias, since HTG can, unlike NTG, be detected after an IOP measurement in the absence of a suspicious ONH appearance. Population-based studies that perform perimetry in all subjects avoid this bias. This makes these studies unique for studying the OAG phenotypes, for example differences in structure-function discrepancies between HTG and NTG. Interestingly, NTG cases with glaucomatous visual field loss (GVFL) and an apparently normal ONH appearance are all but rare in a population-based setting¹.

In the Rotterdam Study, a population-based study with participants aged 55 years or above at inclusion, the prevalence of GVFL was 1.4% at baseline. Definite OAG, defined as the presence of both structural (GON) and functional (GVFL) abnormalities, was present in 0.8% of the subjects. After five years of follow-up, the incidence of GVFL and definite OAG were 2.0 and 1.2 per 1000 person-years, respectively². This was 2.9 and 1.2 per 1000 person-years after ten years of follow-up¹.

The aims of our study were 1) to determine the incidence of GVFL two decades after the onset of the Rotterdam Study and 2) to compare the different OAG phenotypes: GVFL without GON, GON without GVFL, and both GVFL and GON. Here, we will determine whether these subgroups are indeed related to glaucoma by studying their associations with IOP, and we will explore differences between these subgroups by studying associations with other known OAG risk factors. With this approach we aim to address the question whether OAG with dominating GVFL or dominating GON are different entities or not.

METHODS

Study population

The Rotterdam Study is a population-based study held in Ommoord, a district of Rotterdam, the Netherlands. The design and background have been published before³. The research described in this paper is based on the Rotterdam Study I (RS-I), which is the originally cohort started in 1990. The RS-I included 7,983 participants aged 55 years and older. The ophthalmic part of the RS-I started in 1991 and comprised 6,806 participants⁴. Follow-up rounds were completed from 1993 to 1995 (RS-I-2; no glaucoma assessments), 1997 to 1999 (RS-I-3)², 2002 to 2004 (RS-I-4)¹ and 2009 to 2011 (RS-I-5). Ophthalmic baseline and follow-up examinations included visual field testing, ONH assessment, and measurements of the intraocular pressure and refractive error. The Rotterdam Study has been approved by the Medical Ethics Committee of the Erasmus MC and by the Ministry of Health, Welfare and Sport of the Netherlands, implementing the “Wet Bevolkingsonderzoek: ERGO (Population Studies Act: Rotterdam Study)”. All participants provided written informed consent in accordance with the Declaration of Helsinki to participate in the study and to obtain information from their treating physicians.

Visual field testing and definition of glaucomatous visual field loss

All participants underwent visual field testing using the Humphrey Field Analyzer (HFA; Carl Zeiss Meditec, Jena, Germany). Details have been published before¹. In short, the visual field of both eyes from each participant was screened with a 52-point supra-threshold test, which tests the 52 points from the Glaucoma Hemifield Test. If a participant did not respond to a light stimulus (6 dB above a threshold-related estimate of the hill of vision) in three or more contiguous points, or four when the defect contained the blind spot, a second supra-threshold test was performed. If the second supra-threshold test showed at least partially (one or more test locations) overlapping abnormalities in the same hemifield, Goldmann kinetic perimetry (RS-I-1 and RS-I-3; Haag Streit) or full-threshold HFA (RS-I-4, RS-I-5) was performed on both eyes. The Goldmann visual fields were classified according to definitions published before⁵. The full-threshold HFA tests were classified as abnormal if at least one of three criteria was met: 1) a Glaucoma Hemifield Test ‘outside normal limits’, 2) a minimum of three contiguous points in the pattern deviation probability plot with a sensitivity decreased to $P < 0.05$ of which at least one point to $P < 0.01$, or 3) a Pattern Standard Deviation $P < 0.05$. Visual field loss was considered to be present if it was reproducible, that is, the abnormalities had to be present on the Goldmann or full-threshold test and on both supra-threshold tests. Defects had to be in the same hemifield and at least one depressed test point had to have exactly the same location on all fields. Fields had to be reliable, that is, false positives and false negatives had to be $< 33\%$ and fixation losses $< 20\%$. Fundus photographs, ophthalmic examination reports, medical histories, and MRI scans of the brain were checked for disorders that could explain the visual field loss. If no other cause could be identified, and no homonymous defects and artifacts like rim artifacts were found, the visual field loss was considered GVFL. Discrepancies were resolved by consensus. Ophthalmic histories were checked for signs of angle-closure and secondary glaucoma. The current study only included GVFL due to OAG, including primary OAG, pseudoexfoliation glaucoma, and pigment dispersion glaucoma.

Hemifield asymmetry was determined by comparing, in the full-threshold HFA tests, the number of abnormal test locations at $P < 0.5\%$ (black squares) in total deviation probability plot between the superior and the inferior hemifield. Scotoma patterns were classified according to SAPCS (Standard Automated Perimetry test result Classification System⁶). In this system, the presence of a scotoma is defined as three adjacent abnormal points in the total deviation probability plot; the subsequent classification of the scotoma is performed in the pattern deviation probability plot (with the exception of a general reduction of sensitivity). The system uses a flow chart with definitions of scotoma patterns based on the 24-2 grid; the first definition that fits a particular visual field is allotted to that field. The subsequent patterns are a general reduction of sensitivity, a homonymous anopia, a bitemporal anopia, a concentric restriction (all edge points in the pattern deviation probability plot affected without any of the 4 central points affected), a (para)central scotoma (scotoma affecting at least 2 of the 4 central points; a zone without any affected points must be present around the scotoma), an enlarged blind spot (scotoma connected to the blind spot on at least 3 points, with at least 1 of these points crossing the horizontal meridian; the scotoma may not cross the vertical meridian), an altitudinal defect (entire superior or inferior hemifield abnormal with the possible exception of the 2 points temporal to the blind spot), and an arcuate scotoma (any other scotoma on one side of the horizontal meridian). Arcuate scotomata may be present in both hemifields.

Optic nerve head assessment and definition of glaucomatous optic neuropathy

During the first follow-up with glaucoma assessment (RS-I-3), simultaneous stereo color photos of the ONH were taken at a fixed angle of 20 degrees and analyzed with a computerized image analyzer (Topcon ImageNet System; ImageNet, Topcon Corporation, Tokyo, Japan). For ImageNet, GON was based on the 97.5th percentile of the vertical cup-disc ratio (VCDR). GON was present if VCDR exceeded 0.69 for small discs (up to 2 mm²), 0.72 for discs 2.0-2.7 mm², and 0.76 for large discs (>2.7 mm²)¹. During the second and third follow-up rounds (RS-I-4 and RS-I-5, respectively), the Heidelberg Retina Tomograph (HRT; Heidelberg Engineering, Dossenheim, Germany) was used to assess the ONH. The GON cutoff values for HRT were based on the 97.5th percentile of the linear cup-disc ratio (LCDR) and defined as follows: 0.67 for small discs (up to 1.5 mm²), 0.71 for discs 1.5-2.0 mm², and 0.76 for large discs (>2.0 mm²)⁷.

Definitions of OAG

Participants without GVFL at baseline who developed GVFL in at least one eye during follow-up were considered incident GVFL (iGVFL) cases. Definite OAG was defined as iGVFL with GON¹. The presence of GON was recorded at the last follow-up examination with both reliable ONH imaging and visual field testing in participants without iGVFL, and at the visit where the iGVFL occurred in participants with iGVFL. Because of the change in ONH assessment technique during the follow-up, we did not study incident GON separately.

Intraocular pressure and refraction

IOP was measured with Goldmann applanation tonometry (Haag-Streit, Bern, Switzerland). For each eye, the median of three measurements was taken. Refraction was measured with the RM-A2000 autorefractor (Topcon, Tokyo, Japan).

Statistical analysis

Incidence of glaucomatous visual field loss and definite open-angle glaucoma

For each participant, we counted the time between the baseline visit (RS-I-1) and the last follow-up visit. For cases with iGVFL, the last follow-up visit was the first visit with GVFL. For controls, the last follow-up visit was the last visit with reliable visual field testing. Participants with GVFL at baseline were excluded, as well as participants with no reliable visual field testing at baseline or follow-up.

We calculated the incidence rate (IR) and used the IR to calculate the overall incidence during the entire follow-up. The IR is calculated as the number of cases with iGVFL divided by the number of person years (the sum of follow-up time of all participants). The overall incidence during the entire follow-up was calculated using the formula $1 - e^{-\langle T \rangle * IR}$, where e is the base of the natural logarithm, $\langle T \rangle$ the mean follow-up of all participants, and IR the incidence rate⁸. The incidence rate and overall incidence during the entire follow-up of definite OAG was calculated similarly, based on iGVFL cases with GON (see above). We further calculated the IR of iGVFL in 10-years age categories. For this analysis we used a dynamic cohort population, i.e., participants could contribute person years to subsequent age categories⁹. In this analysis we also stratified for gender.

Risk factor analysis and OAG phenotypes

The following baseline risk factors were analyzed: age, gender, IOP, IOP treatment, family history for glaucoma, myopia, diastolic blood pressure (DBP), and body mass index (BMI). For IOP, we took the highest value of the medians of both eyes (see above) at baseline. IOP treatment was defined as IOP lowering surgery or laser treatment before baseline or the use of IOP lowering medication at baseline. Medication use was based on a fully automated pharmacy database recording including the ATC code (S01E for IOP lowering medication). Surgery and laser treatment were based on interview data with the participant. Family history was considered positive if the participant reported glaucoma in parents, siblings, or offspring during the interview. Spherical equivalent refraction (SE) was calculated as the spherical refractive error plus half of the cylinder. It was stratified in three categories: high myopia, defined as a SE of -4 D or more myopic; low myopia, defined as a SE between -3.99 and -0.01 D; and no myopia, defined as a SE of 0 D and above. For SE, we used the eye with GVFL in case of unilateral GVFL, and a random eye in case of bilateral GVFL and participants without GVFL. The assessment of DBP has been described before¹⁰. BMI was calculated as mass (in kilograms) divided by the square of height (in meters). Height and weight were measured with indoor clothing and no shoes. In case of missing values for the risk factors, we imputed the missing value to the mean since missing values were present in less than 5% of the participants. In case of cataract extraction in both eyes before baseline, the SE was imputed to the mean; in case of cataract extraction in one eye, the SE of the other eye was taken.

Risk factor analyses were performed using Cox proportional hazards models, with five different outcome measures: (1) iGVFL, (2) GON, (3) iGVFL and GON (definite OAG), (4) iGVFL without GON, and (5) GON without iGVFL. For each analysis, controls were participants without iGVFL and without GON. For this analysis, the last follow-up round with both reliable visual field testing and ONH data was used. Similar to iGVFL (see above, Definitions of OAG),

GON was defined as the presence of GON in at least one eye. A Bonferroni-corrected p-value of 0.01 (0.05/5 analyses) was considered as statistically significant.

In a final comparison, a one-way ANOVA was conducted to compare the mean IOP between participants with GVFL and GON (definitive OAG), GVFL without GON, GON without GVFL, and controls; since there was no homogeneity of variance, the Games-Howell post hoc test was used to compare all groups to each other. A p-value of 0.05 was considered as statistically significant.

All analyses were performed using IBM SPSS Statistics Release 20.0.0 (IBM Corp., Armonk, NY).

RESULTS

After exclusion of participants with GVFL at baseline and participants without visual field testing at follow-up, 3,939 participants were eligible for the study (see Figure 1). Table 1 presents the baseline characteristics with univariable comparisons. Of the 3,939 participants, 140 developed GVFL during one of the follow-up rounds. The median follow-up was 11.1 (IQR 6.8 to 17.2; range 5.0 to 20.3) years, the mean follow-up 12.1 years, and the total follow-up 47,710 person-years. The incidence rate was 2.9 (95% CI 2.4 to 3.4) per 1000 person years; the 12-years incidence was 3.5 (2.9 to 4.0)%. For definite OAG, the incidence rate per 1000 person-years and 12-years incidence were 1.0 (0.7 to 1.3) and 1.2 (0.9 to 1.5)%, respectively. Table 2 presents age- and gender-specific incidence rates of GVFL. The incidence rate increased from 0.8 at age 55 to 64 years to 12.7 per 1000 person years at age 85 and above.

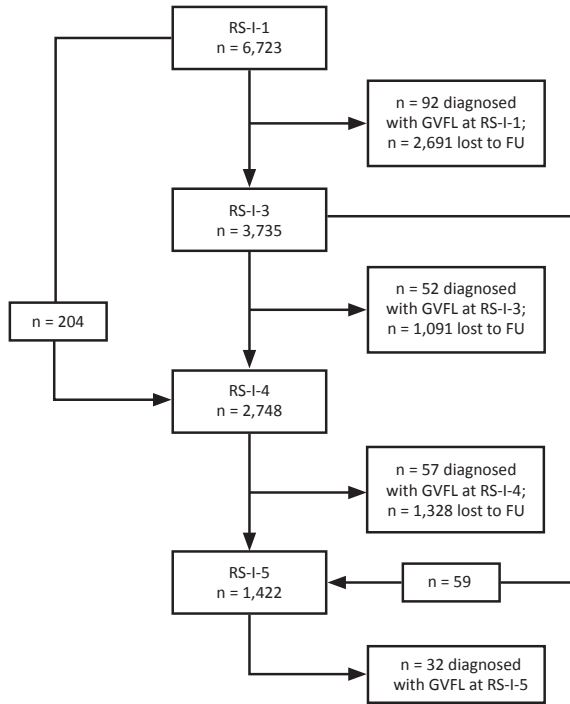
Table 1. Baseline demographic and clinical characteristics of participants with and without iGVFL, presented as mean \pm standard deviation or percentages.

	no GVFL (n=3,799)	iGVFL (n=140)	P-value
Age (years)	65.7 \pm 6.8	67.2 \pm 7.0	0.01
Gender (female)	58.6%	54.3%	0.32
IOP (mmHg)	15.0 \pm 3.1	17.0 \pm 4.4	5.3x10 ⁻⁷
IOP Rx	1.6%	10.0%	1.3x10 ⁻¹²
FH	8.0%	17.9%	5.0x10 ⁻⁵
Myopia			0.56
Low myopia	20.7%	19.3%	
High myopia	5.0%	7.1%	
DBP (mmHg)	73.6 \pm 10.8	72.8 \pm 12.0	0.36
BMI (kg/m ²)	26.3 \pm 3.5	25.7 \pm 3.1	0.03

ABBREVIATIONS

BMI	body mass index	iGVFL	incident glaucomatous visual field loss
DBP	diastolic blood pressure	IOP	intraocular pressure
FH	positive family history for glaucoma	IOP Rx	intraocular pressure lowering treatment

Figure 1. Flow diagram which shows the number of participants with reliable visual field testing in the different follow-up rounds.



ABBREVIATIONS

FU	follow-up	RS-I	Rotterdam Study I	RS-I-4	second follow-up round
GVFL	glaucomatous visual field loss	RS-I-1	baseline examinations	RS-I-5	third follow-up round
		RS-I-3	first follow-up round		

Figure 2. Number of participants with incident glaucomatous visual field loss (iGVFL), glaucomatous optic neuropathy (GON), or both.

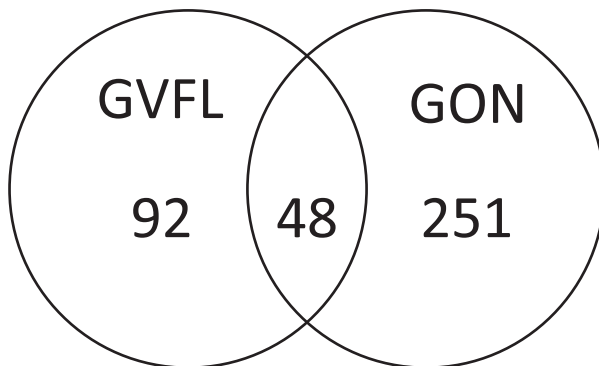


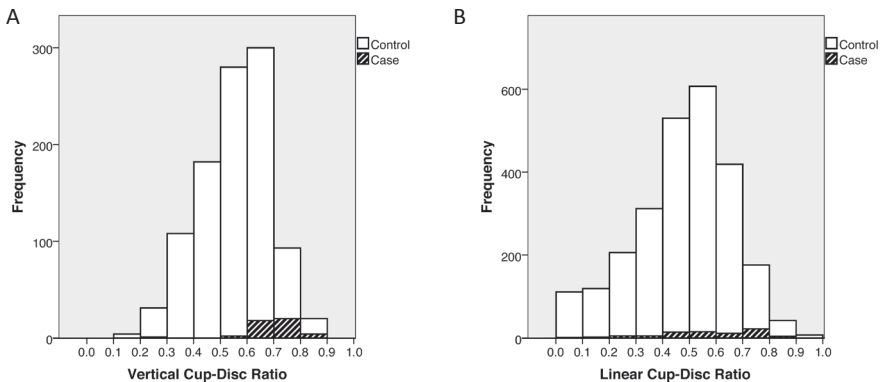
Table 2. Incidence rates of glaucomatous visual field loss as a function of age and gender.

Age group (years)	Number of cases	Person years at risk	IR per 1000 person years (95% CI)	12-years risk (95% CI)
Male				
55-64	2	3950	0.5 (0.0-1.2)	0.6 (-0.2-1.4)%
65-74	23	10180	2.3 (1.3-3.2)	2.7 (1.6-3.7)%
75-84	32	4951	6.5 (4.2-8.7)	7.5 (4.9-9.9)%
85+	7	478	14.6 (3.8-25.5)	16.1 (4.5-26.3)%
Overall	64	19560	3.3 (2.5-4.1)	3.9 (2.9-4.8)%
Female				
55-64	5	5331	0.9 (0.1-1.8)	1.1 (0.1-2.1)%
65-74	17	13615	1.2 (0.7-1.8)	1.5 (0.8-2.2)%
75-84	40	8030	5.0 (3.4-6.5)	5.8 (4.0-7.5)%
85+	14	1174	11.9 (5.7-18.2)	13.3 (6.6-19.6)%
Overall	76	28150	2.7 (2.1-3.3)	3.2 (2.5-3.9)%
Total				
55-64	7	9281	0.8 (0.2-1.3)	0.9 (0.2-1.6)%
65-74	40	23795	1.7 (1.2-2.2)	2.0 (1.4-2.6)%
75-84	72	12982	5.5 (4.3-6.8)	6.4 (5.0-7.9)%
85+	21	1652	12.7 (7.3-18.2)	14.1 (8.4-19.6)%
Overall	140	47710	2.9 (2.4-3.4)	3.5 (2.9-4.0)%

ABBREVIATIONS

CI confidence interval
IR incidence rate

Figure 3. Distribution of vertical cup-disc ratio (A) and linear cup-disc ratio (B) in cases with incident glaucomatous visual field loss (iGVFL; in black pattern) and controls without GVFL (in white).



Of the 140 iGVFL cases, 27 (19.3%) had bilateral iGVFL at the round of diagnosis, 52 (37.1%) had iGVFL in only the right eye, and 61 (43.6%) had iGVFL in only the left eye ($P=0.42$). Of these 113 cases, 8 cases developed GVFL in the second eye during a later follow-up round. Of all the iGVFL cases, 89 were diagnosed with the full threshold HFA (RS-I-4 and RS-I-5) of which 18 had bilateral iGVFL. In 56 of these 107 eyes (52.3%) the upper hemifield was more affected than the lower hemifield (not significantly different from 50%; $P=0.35$). Four eyes (three participants) showed an altitudinal defect; 44 eyes showed an arcuate scotoma in one hemifield and 58 eyes showed an arcuate scotoma in both hemifields.

Of the 140 cases with iGVFL, 24 participants had GON at baseline (as assessed with ImageNet) and 48 had GON at follow-up (as assessed with HRT). Another 251 participants had GON at follow-up but no iGVFL (Figure 2). Of the participants without GON at the time that iGVFL was diagnosed, 10 developed GON in a next follow-up round. Figure 3 shows the VCDR (A; RS-I-3) and LCDR (B; RS-I-4 and RS-I-5) distributions of cases with iGVFL and controls. Although two-third of the cases with iGVFL did not have GON formally, the distributions of the iGVFL cases are clearly shifted towards higher VCDR/LCDR values, when compared to the controls (participants without iGVFL).

The differences in risk factors between participants with iGVFL and/or GON are shown in Table 3. IOP and age were significant risk factors in all subgroups. A positive family history was associated with iGVFL, GON, and definite OAG. Gender, myopia, and DBP were not significantly associated with any of the outcomes; BMI appeared to be associated with various outcomes, but only for GON at the Bonferroni-corrected $P=0.01$.

The mean baseline IOP in participants with definite OAG was 18.4, in iGVFL without GON 16.3, in GON without iGVFL 15.8, and in the controls 15.0 mmHg. Post hoc comparisons using the Games-Howell test indicated that the mean IOP was significantly different between the controls and all other groups. Furthermore, the mean IOP was significantly different between definite OAG and participants with GON without iGVFL ($P=0.014$). There was no significant difference in IOP between definite OAG and iGVFL without GON ($P=0.09$) and iGVFL without GON and GON without iGVFL ($P=0.67$).

Table 3. Results of cox-regression models with different aspects of glaucoma (see Figure 2; in all models, controls were participants without iGVFL and without GON [n=3548]).

	iGVFL (n=140)		GON (n=299)		iGVFL and GON (n=48)		iGVFL without GON (n=92)		GON without iGVFL (n=251)	
	Hazard ratio (95% CI)	P-value	Hazard ratio (95% CI)	P-value	Hazard ratio (95% CI)	P-value	Hazard ratio (95% CI)	P-value	Hazard ratio (95% CI)	P-value
Age (years)	1.09 (1.06-1.12)	***	1.11 (1.10-1.13)	***	1.09 (1.04-1.14)	**	1.09 (1.06-1.13)	***	1.12 (1.10-1.14)	***
Gender (female)	0.78 (0.56-1.10)	0.16	0.96 (0.76-1.21)	0.72	0.89 (0.49-1.60)	0.69	0.74 (0.49-1.12)	0.15	0.97 (0.75-1.25)	0.80
IOP (mmHg)	1.14 (1.10-1.19)	***	1.11 (1.08-1.15)	***	1.18 (1.11-1.24)	***	1.13 (1.06-1.20)	**	1.09 (1.05-1.13)	***
IOP Rx	2.61 (1.35-5.04)	*	1.57 (0.92-2.71)	0.10	3.00 (1.07-8.44)	0.04	2.43 (1.00-5.92)	0.05	1.11 (0.54-2.30)	0.77
FH	2.15 (1.37-3.38)	**	1.67 (1.17-2.37)	*	2.85 (1.40-5.79)	*	1.85 (1.01-3.38)	0.05	1.49 (0.99-2.24)	0.06
Low myopia	0.97 (0.64-1.49)	0.90	0.98 (0.73-1.32)	0.89	1.24 (0.62-2.47)	0.55	0.83 (0.48-1.44)	0.51	0.93 (0.67-1.30)	0.67
High myopia	1.53 (0.80-2.95)	0.20	1.46 (0.93-2.29)	0.10	1.45 (0.44-4.75)	0.54	1.54 (0.71-3.38)	0.28	1.47 (0.90-2.39)	0.12
DBP	1.00 (0.98-1.01)	0.81	1.00 (0.99-1.01)	0.58	0.99 (0.96-1.01)	0.30	1.00 (0.99-1.02)	0.65	1.01 (0.99-1.02)	0.27
BMI	0.94 (0.89-0.99)	0.02	0.96 (0.93-0.99)	0.01	0.92 (0.84-1.01)	0.09	0.94 (0.88-1.00)	0.07	0.96 (0.93-1.00)	0.05

ABBREVIATIONS	GON	glaucomatous optic neuropathy	*	significant associations at a p-value of <0.01
95% CI	iGVFL	incident glaucomatous visual field loss	**	significant associations at a P<0.001
BMI	IOP	intraocular pressure	***	significant associations at P<0.0001
DBP	IOP Rx	intraocular pressure lowering treatment		
FH		positive family history for glaucoma		

DISCUSSION

In this study, the 12-years incidences of GVFL and definite OAG were 3.5% and 1.2%, respectively, and the corresponding incidence rates 2.9 and 1.0 per 1000 person years. The 12-years incidence of GVFL increased from 0.8 to 12.7% in the age range studied. Unilateral GVFL occurred as often in the right eye as in the left eye; GVFL affecting predominantly the superior hemifield was as common as GVFL affecting predominantly the inferior hemifield. About one-third of the cases with iGVFL had GON. Our data do not support the hypothesis that OAG with dominating GVFL or dominating GON are different entities, as depicted by the finding that the various phenotypes did not differ noticeably in their associations with the OAG risk factors studied.

The incidence rate of 2.9 per 1000 person years was similar to the incidence rate after 10 years of follow-up in the Rotterdam Study¹. Cedrone et al. found a 12-years incidence of OAG of 3.8% (95% CI 2.3-6.2)¹¹, quite similar to our 3.5%. Their definition of OAG was GVFL plus IOP \geq 21 mmHg or VCDR \geq 0.5 or VCDR asymmetry \geq 0.2. Hence, their incidence of GVFL without other criteria would probably be higher. On the other hand, they only performed visual field testing in suspect glaucoma (IOP \geq 21 mmHg or VCDR \geq 0.5 or VCDR asymmetry \geq 0.2) and at random in 50% of the other individuals. In this way they will have missed some iGVFL cases, being the cases without elevated IOP and without a clearly excavated ONH.

In the study from Cedrone et al.¹¹, 53% of the incident OAG cases had unilateral visual field loss. Data concerning the occurrence in right or left eyes is missing. A ratio of 1:1 for uni- and bilateral OAG was also found in the Blue Mountains Eye Study¹². We found a greater percentage (81%) of unilateral cases than these studies. This difference could be explained by the fact that we examined our individuals on regular time intervals and thus detected the GVFL in an earlier stage of the disease. The time between the two examinations in the study from Cedrone et al. was 12 years, while the Blue Mountains Eye Study described also prevalent cases. In the Blue Mountains Eye Study, 34.2% of 152 eyes with GVFL had defects in only the upper hemifield, 40.1% in only the lower hemifield ($P=0.13$), and 25.7% had defects in both hemifields. This absence of a clear hemifield preference agrees with our study.

It has been postulated that NTG differs from HTG in optic nerve head appearance. Caprioli et al. found thinner optic disc rim in NTG patients ($n=34$) compared to HTG patients ($n=41$), especially in the inferior and inferotemporal area¹³. Iester et al. compared HRT parameters between HTG patients ($n=132$) and NTG patients ($n=50$) and found no statistically significant differences in any of the parameters¹⁴. This is in line with the results of our unbiased study (as argued in the Introduction section, NTG might bias towards more pronounced ONH abnormalities in a clinical setting). We were not able to locate studies addressing asymmetry in left/right eye and/or inferior/superior hemifield occurrence of GVFL.

We found no association between myopia and any of the OAG phenotypes. A meta-analysis showed that myopia was associated with glaucoma (odds ratio of 1.9 for any myopia)¹⁵. Previously, we also found an association between high myopia and OAG in the Rotterdam Study (HR 2.3 [1.2-4.5], $P=0.011$). However, of the 32 participants who developed GVFL during the latest follow-up round only one had high myopia and therefore the effect of the

association disappeared. Our finding suggests that (high) myopia may mainly play a role in the development of OAG at a younger age. After all, the mean age of the participants at the latest follow-up round (RS-I-5) was 79.5 years (to be compared to 66 years at baseline). A similar phenomenon occurred for gender. We previously identified male gender as a risk factor for glaucoma (HR 1.62 [1.10-2.38], $P=0.015$). The current study found a higher IR among males but yielded no significant associations for gender in the risk factor analysis, apparently related to an excess of females (27) amongst the 32 most recently diagnosed iGVFL cases (72%). This suggests that males tend to develop OAG at an earlier age. However, the wide confidence intervals in the individual age and gender categories do not permit firm conclusions.

We found a nominally significant association between BMI and GVFL and BMI ($P=0.02$) and GON ($P=0.01$), which were not significant after correction for multiple testing. The associations between BMI and the other OAG subtypes were not significant. However, the hazard ratios were all in the same – protective – direction (0.92-0.96). Other studies also found a protective effect of BMI on OAG¹⁶⁻²⁰. Furthermore, previous studies found that a higher BMI was associated with small cup-disc ratios or cup areas²¹⁻²⁴, which is in line with our finding that a higher BMI is protective for GON.

In our study, diastolic blood pressure was not associated with OAG. A recent meta-analysis, which included 27 studies that investigated the relationship between blood pressure and glaucoma, found a pooled relative risk of 1.16 (95% CI 1.05-1.28) for the effect of hypertension (not separately studied for SDP and DBP) on OAG²⁵. However, they showed some heterogeneity across studies (I^2 34.5%; 18 studies reported a positive association and 9 studies reported an inverse or no association) and the effect was only significant in cross-sectional studies; the pooled relative risk of two longitudinal studies was 1.05 (0.69-1.59). Clearly, the power was limited here, but – generally speaking – longitudinal studies are more informative concerning a causal relationship between a risk factor and a disease. Our results, together with the previous results from the two longitudinal studies, suggest that there is no clear association between blood pressure and OAG. Studying blood pressure as a linear variable implies the risk of overlooking non-linear associations, for example an increased risk for those with a very low or a very high blood pressure. In our study, entering DBP in quartiles did not reveal any association either (data not shown), suggesting the absence of a clear nonlinear relationship between OAG and DBP.

A strong point of our study is that all participants underwent visual field testing, regardless of ONH abnormalities or IOP measurements. We showed that two-third of the iGVFL cases had no ONH abnormalities exceeding the 97.5th percentile. Studies who performed only visual field testing in subjects with suspicious ONH findings may thus miss many OAG cases. A limitation of the study is the relatively low number of cases, which is inherent to the low incidence of OAG in the general population but hampers detailed risk factor analyses.

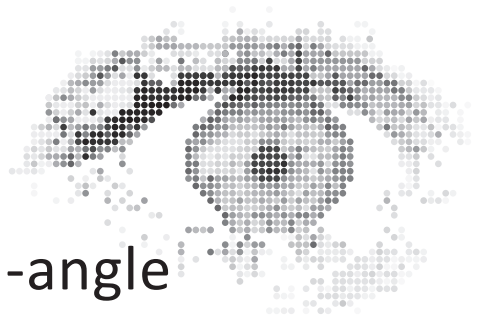
In conclusion, we found a 12-years incidence of 3.5% for GVFL. We confirmed the associations between GVFL and age, IOP, and family history. We found no association between GVFL and either gender or myopia, and hypothesized that these factors may particularly be related to GVFL with a younger age of onset.

References

1. Czudowska, M.A. et al. Incidence of glaucomatous visual field loss: a ten-year follow-up from the Rotterdam Study. *Ophthalmology* 117, 1705-12 (2010).
2. de Voogd, S. et al. Incidence of open-angle glaucoma in a general elderly population: the Rotterdam Study. *Ophthalmology* 112, 1487-93 (2005).
3. Hofman, A. et al. The Rotterdam Study: 2016 objectives and design update. *Eur J Epidemiol* 30, 661-708 (2015).
4. Wolfs, R.C. et al. Changing views on open-angle glaucoma: definitions and prevalences--The Rotterdam Study. *Invest Ophthalmol Vis Sci* 41, 3309-21 (2000).
5. Skenduli-Bala, E. et al. Causes of incident visual field loss in a general elderly population: the Rotterdam study. *Arch Ophthalmol* 123, 233-8 (2005).
6. Müskens, R.P.H.M. Some diagnostic and therapeutic controversies in glaucoma addressed. (2008).
7. Ramdas, W.D. et al. Heidelberg Retina Tomograph (HRT3) in population-based epidemiology: normative values and criteria for glaucomatous optic neuropathy. *Ophthalmic Epidemiol* 18, 198-210 (2011).
8. Rothman, K.J. & Greenland, S. *Modern Epidemiology*. 2nd ed Philadelphia:Lippincott-Raven.(1998).
9. Wieberdink, R.G., Ikram, M.A., Hofman, A., Koudstaal, P.J. & Breteler, M.M. Trends in stroke incidence rates and stroke risk factors in Rotterdam, the Netherlands from 1990 to 2008. *Eur J Epidemiol* 27, 287-95 (2012).
10. Ramdas, W.D. et al. Ocular perfusion pressure and the incidence of glaucoma: real effect or artifact? The Rotterdam Study. *Invest Ophthalmol Vis Sci* 52, 6875-81 (2011).
11. Cedrone, C. et al. The 12-year incidence of glaucoma and glaucoma-related visual field loss in Italy: the Ponza eye study. *J Glaucoma* 21, 1-6 (2012).
12. Lee, A.J. et al. Patterns of glaucomatous visual field defects in an older population: the Blue Mountains Eye Study. *Clin Experiment Ophthalmol* 31, 331-5 (2003).
13. Caprioli, J. & Spaeth, G.L. Comparison of the optic nerve head in high- and low-tension glaucoma. *Arch Ophthalmol* 103, 1145-9 (1985).
14. Iester, M. & Mikelberg, F.S. Optic nerve head morphologic characteristics in high-tension and normal-tension glaucoma. *Arch Ophthalmol* 117, 1010-3 (1999).
15. Marcus, M.W., de Vries, M.M., Junoy Montolio, F.G. & Jansonius, N.M. Myopia as a risk factor for open-angle glaucoma: a systematic review and meta-analysis. *Ophthalmology* 118, 1989-1994 e2 (2011).
16. Charlson, E.S. et al. The primary open-angle african american glaucoma genetics study: baseline demographics. *Ophthalmology* 122, 711-20 (2015).
17. Gasser, P., Stumpfig, D., Schotzau, A., Ackermann-Liebrich, U. & Flammer, J. Body mass index in glaucoma. *J Glaucoma* 8, 8-11 (1999).
18. Leske, M.C., Connell, A.M., Wu, S.Y., Hyman, L.G. & Schachat, A.P. Risk factors for open-angle glaucoma. The Barbados Eye Study. *Arch Ophthalmol* 113, 918-24 (1995).
19. Pasquale, L.R., Willett, W.C., Rosner, B.A. & Kang, J.H. Anthropometric measures and their relation to incident primary open-angle glaucoma. *Ophthalmology* 117, 1521-9 (2010).
20. Wu, S.Y. & Leske, M.C. Associations with intraocular pressure in the Barbados Eye Study. *Arch Ophthalmol* 115, 1572-6 (1997).
21. Amerasinghe, N. et al. Determinants of the optic cup to disc ratio in an Asian population: the Singapore Malay Eye Study (SiMES). *Arch Ophthalmol* 126, 1101-8 (2008).
22. Khawaja, A.P. et al. Laser scanning tomography in the EPIC-Norfolk Eye Study: principal components and associations. *Invest Ophthalmol Vis Sci* 54, 6638-45 (2013).
23. Xu, L., Wang, Y.X., Wang, S. & Jonas, J.B. Neuroretinal rim area and body mass index. *PLoS One* 7, e30104 (2012).
24. Zheng, Y., Cheung, C.Y., Wong, T.Y., Mitchell, P. & Aung, T. Influence of height, weight, and body mass index on optic disc parameters. *Invest Ophthalmol Vis Sci* 51, 2998-3002 (2010).
25. Zhao, D., Cho, J., Kim, M.H. & Guallar, E. The association of blood pressure and primary open-angle glaucoma: a meta-analysis. *Am J Ophthalmol* 158, 615-27 e9 (2014).

CHAPTER 3.2

Relationship between sleep apnea and open-angle glaucoma: a population-based cohort study



Henriët Springelkamp, Lisette A. Zuurbier, Annemarie I. Luik, Roger C.W. Wolfs, Albert Hofman, Caroline C.W. Klaver, Henning Tiemeier, Nomdo M. Jansonius.

Submitted

ABSTRACT

Purpose. Brief episodes of cessation of breath during sleep (sleep apnea) can lead to hypoxia; hypoxia of the optic nerve may induce or accelerate glaucoma. The purpose of our study was to determine the relationship between sleep apnea and glaucoma in a large population-based study.

Methods. We performed a logistic regression analysis to determine the association between subjective sleep apnea symptoms, as assessed with the Pittsburgh Sleep Quality Index questionnaire, and glaucomatous visual field loss (GVFL), cross-sectionally in 1,662 individuals (of which 54 had prevalent GVFL) and longitudinally in 721 individuals (of which 26 had incident GVFL). We performed linear regression analyses to determine the associations between the apnea hypopnea index (AHI; assessed with polysomnography [PSG] in 767 individuals) and several continuous glaucoma parameters: linear cup-disc ratio (LCDR) and peripapillary retinal nerve fiber layer (pRNFL) thickness as assessed with the Heidelberg Retina Tomograph, and intraocular pressure (IOP).

Results. There was no association between subjective sleep apnea symptoms and prevalent GVFL (Odds Ratio [95% confidence interval] = 1.17 [0.49-2.78]) or incident GVFL (OR 1.00 [0.29-3.42]). No associations were found between AHI and LCDR (effect of 10 units increase in AHI was 0.00 [-0.01 to 0.01]), pRNFL thickness (-0.01 [-0.38 to 0.36] μm), and IOP (0.13 [-0.02 to 0.29] mmHg).

Conclusions. In this large population-based study, we did not find any associations between sleep apnea and glaucoma.

INTRODUCTION

Glaucoma is a disease of the optic nerve leading to visual field loss and eventually blindness. Primary open-angle glaucoma is the most common form of glaucoma in the elderly Western population, with a prevalence of 1-3%¹. Risk factors for the disease include an elevated intraocular pressure (IOP), age, a positive family history of glaucoma, African descent, and myopia²⁻⁴. The treatment of glaucoma patients focuses on lowering of the IOP. However, up to half of the glaucoma patients have a normal IOP, and a significant percentage of the patients develop visual field loss progression or blindness despite IOP lowering therapy^{5,6}. The identification of new risk factors could lead to a new target for therapy.

Sleep apnea is characterized by brief episodes of cessation of breath. This can lead to recurrent hypoxia and may thus damage the optic nerve. In 1982, Walsh and Montplaisir reported about the co-occurrence of glaucoma and sleep apnea in five members of one family⁷. Since then, sleep apnea has been indicated as a risk factor for glaucoma in several small studies, but the results of large study populations are scarce, as is the case for population-based studies, and the results are conflicting. Most of the studies did not use polysomnography (PSG), the golden standard to assess sleep apnea, but used questionnaires or insurance databases.

The aim of this study was to determine the relationship between sleep apnea and glaucoma in a large population-based sample. Sleep apnea was assessed with a sleep questionnaire, focusing on snoring and respiratory pauses, and with PSG. We determined the associations between these parameters and (1) the prevalence and incidence of glaucoma, and (2) continuous glaucoma endophenotypes, being the linear cup-disc ratio (LCDR), the peripapillary retinal nerve fiber layer (pRNFL) thickness, and IOP.

METHODS

Study population

The current study was embedded in the Rotterdam Study, a prospective population-based cohort in Rotterdam, the Netherlands⁸. It comprises three separate cohorts (RS-I, RS-II, and RS-III) consisting of participants aged 45 years and older. The Rotterdam Study was conducted in accordance with the Declaration of Helsinki and has been approved by the Medical Ethics Committee of the Erasmus MC and by the Ministry of Health, Welfare and Sport of the Netherlands, implementing the “Wet Bevolkingsonderzoek: ERGO (Population Studies Act: Rotterdam Study)”. All participants provided written informed consent to participate in the study and to obtain information from their treating physicians.

Sleep apnea assessment

Pittsburgh Sleep Quality Index (PSQI)

Subjective sleep apnea symptoms were measured with items from the Pittsburgh Sleep Quality Index (PSQI), a self-rated questionnaire⁹. We analyzed the PSQI assessed during RS-I-4 (RS-I, fourth examination). In total, 2,167 participants were invited to answer the questionnaire; 1,672 participants (77.2%) responded to the questions about snoring and

respiratory pauses. We considered subjective sleep apnea symptoms to be present if participants reported that they snored loudly at least 2 nights per week and if they reported occasional respiratory pauses or respiratory pauses during sleep at least 1 night per week¹⁰.

Polysomnography

From January 2012 until December 2013, 1,355 persons from the second cohort (RS-II, third examination) and the third cohort (RS-III, second examination) were invited to participate in a polysomnographic (PSG) sleep study; 787 participants (58.1%) agreed. Persons who participated in the PSG study did not significantly differ in age or sex from persons who refused to participate in the PSG study. We excluded 20 participants because the PSG recording was of insufficient quality. In total, data of 767 participants were available for analysis.

A home visit for the ambulant PSG was planned within 6 months (median 1 month) after agreement to enter the PSG sleep study. During the home visit, a trained research-assistant placed the sensors and prepared the Vitaport 4[®] (Temec, Kerkrade, The Netherlands) to record a PSG. The ambulant PSG included respiratory belts on the chest and abdomen, oximetry, and a nasal pressure transducer and oronasal thermocouple to measure airflow¹¹.

Apnea was defined as a reduction of airflow of at least 90% of the baseline lasting at least 10 seconds. Hypopnea was defined as a reduction in airflow of at least 30% of the baseline for at least 10 seconds and a desaturation of at least 3% of the pre-event baseline or an arousal¹². We calculated the AHI as the total number of apneas and hypopneas per hour of sleep using Prana software (PhiTools, Strasbourg, France).

Glaucoma assessment

Optic nerve head, retinal nerve fiber layer, and intraocular pressure

Participants visiting the research center underwent an extensive ophthalmic examination. Details of the eye examinations have been described elsewhere¹. The optic nerve head was examined with the Heidelberg Retina Tomograph (HRT; Engineering, Dossenheim, Germany). A priori selected parameters included the linear cup-disc ratio (LCDR¹³) and the peripapillary retinal nerve fiber layer (pRNFL) thickness. HRT examinations with a topographic standard deviation > 50 μm were excluded. IOP was measured with Goldmann applanation tonometry (Haag-Streit, Bern, Switzerland). It was measured trice per eye and the median was taken. IOP lowering treatment was defined as current use of IOP lowering medication or prior laser or surgery. For this study, the mean LCDR of both eyes was used, as well as the mean pRNFL thickness and mean IOP.

Visual field testing

All participants underwent visual field testing using the Humphrey Field Analyzer (HFA; Carl Zeiss Meditec, Jena, Germany). Details have been published before². In short, the visual field of both eyes from each participant was screened with a 52-point supra-threshold test, which tests 52 points from the Glaucoma Hemifield Test. If a participant did not respond to a light stimulus (6 dB above a threshold-related estimate of the hill of vision) in three or more contiguous points, or four when the defect contained the blind spot, a second supra-threshold test was performed. If the second supra-threshold test showed at least partially (one or more test locations) overlapping abnormalities in the same hemifield, full-

threshold HFA was performed on both eyes. The full-threshold HFA tests were classified as abnormal if at least one of three criteria was met: 1) a Glaucoma Hemifield Test 'outside normal limits', 2) a minimum of three contiguous points in the pattern deviation probability plot with a sensitivity decreased to $P < 0.05$ of which at least one point to $P < 0.01$, or 3) a Pattern Standard Deviation $P < 0.05$. Visual field loss was considered to be present if it was reproducible, that is, the abnormalities had to be present on the full-threshold test and on both supra-threshold tests. Also, defects had to be in the same hemifield and at least one depressed test point had to have exactly the same location on all fields. Fields had to be reliable, that is, false positives and false negatives had to be $< 33\%$ and fixation losses $< 20\%$. Fundus photographs, ophthalmic examination reports, medical histories, and – if available – MRI scans of the brain were checked for disorders that could explain the visual field loss. If no other cause could be identified, and no homonymous defects and artefacts like rim artefacts were found, the visual field loss was considered glaucomatous visual field loss (GVFL). Discrepancies were resolved by consensus. Ophthalmic histories were checked for signs of angle-closure and secondary glaucoma. The current study only included GVFL due to open-angle glaucoma (OAG).

Covariates

Covariates that were considered as potential confounders included age, gender, BMI, systolic blood pressure, smoking, alcohol use, coffee use, mini-mental state examination, use of sleep medication, stroke, diabetes mellitus, and myocardial infarction. Body mass index (BMI) was calculated as weight (in kilograms) divided by the square of height (in meters). Height and weight were measured with indoor clothing and no shoes. Blood pressure was measured after the participant had been seated for at least 5 minutes. Systolic blood pressure was measured twice on the right arm using a random-zero sphygmomanometer with a 14x38 cm cuff. The mean of two values was used in the analysis. Smoking, alcohol, and coffee were assessed by means of a questionnaire. Smoking was defined as current, before, or never. Alcohol use was defined as drinking of alcohol yes or no; for the PSG analysis it was defined as drinking of alcohol during the night (starting at 6 pm) of the PSG (yes/no). Coffee was defined as the average number of cups per day; for the PSG analysis it was defined as drinking of coffee during the night (starting at 6 pm) of the PSG (yes/no). The mini-mental state examination (MMSE) was performed during the visit to the research center to measure cognitive function. The use of sleep medication (anatomical therapeutic chemical (ATC) codes N05 and N06) (ref NOW, World Health Organization. ATC/DDD Index 2014. World Health Organization Collaborating Centre for Drug Statistics Methodology cited 2014; Available from: http://www.whocc.no/atc_ddd_index/) was assessed at a home-interview. The history of stroke, diabetes mellitus, and myocardial infarction were determined during the center visit and by medical records. The number of missing values never exceeded 8%. Missing values for continuous covariates were replaced by the mean, and for missing values of categorical covariates a separate missing category was defined.

Statistical analyses

We determined the relationship between sleep apnea and glaucoma in two different ways using 1) subjective sleep apnea symptoms measured with the PSQI questionnaire, and 2) the AHI extracted from the PSG. The correlation between subjective sleep apnea symptoms and AHI was calculated in the subset of participants who underwent PSG using the

Pearson correlation coefficient r . In the first analysis (PSQI), we used GVFL – the most obvious glaucoma outcome. In the second analysis (PSG), we used several continuous glaucoma parameters that were available in most of the participants as outcome (only four participants who underwent a PSG were diagnosed with GVFL). There was no overlap in individuals between the two different analyses because the examinations were performed in different study cohorts (RS-I versus RS-II/RS-III-2).

For the analysis investigating the association between subjective sleep apnea symptoms and GVFL, we used the PSQI questionnaire conducted during RS-I-4. Firstly, we analysed the association between subjective sleep apnea symptoms (yes/no) and prevalent GVFL at RS-I-4 (yes/no) using logistic regression. Secondly, we analysed the association between subjective sleep apnea symptoms at RS-I-4 and incident GVFL at RS-I-5 (RS-I, fifth examination; on average 6.6 years after RS-I-4) using logistic regression. In this second analysis, participants with GVFL at RS-I-4 were excluded. Next, age and gender were included as covariates in both analyses. Finally, stroke and smoking were also included. Use of alcohol or coffee, use of sleep medication, BMI, diabetes mellitus, myocardial infarct, and MMSE were not included in the model, since these factors did not change the effect estimates by more than ten percent.

For the analysis investigating the association between sleep apnea measured with the AHI and several continuous glaucoma parameters (LCDR, pRNFL thickness, and IOP), we used data from RS-II-3 and RS-III-2. We performed regression analysis for proportion data with AHI as determinant and LCDR as outcome (LCDR is a continuous variable with range 0 to 1), and linear regression analysis with AHI as determinant and pRNFL thickness or IOP as outcome. We also tested the difference in LCDR, pRNFL thickness, and IOP between participants with severe sleep apnea (AHI > 30) and no sleep apnea (AHI < 5) using a linear regression model. In a second model, age, gender, and IOP lowering therapy for the IOP analyses were included as additional covariates. In a final model, BMI, smoking, alcohol, MMSE, and systolic blood pressure were also included as covariates. Stroke, myocardial infarction, diabetes mellitus, the use of coffee, and the use of sleep medication were not included in the model, since these factors did not change the effect estimates by more than ten percent. Individuals who were treated with continuous positive airway pressure (CPAP) therapy were excluded from all analyses investigating the AHI ($n=4$).

The regression model for proportion data was performed using R (version 3.2.1; R Foundation for Statistical Computing, Vienna, Austria); all other analyses were performed using IBM SPSS Statistics Release 20.0.0 (IBM Corp., Armonk, NY).

RESULTS

The correlation between subjective sleep apnea and AHI was $r = 0.28$ ($P < 0.001$).

At RS-I-4, 1,672 individuals answered the questions about snoring and respiratory pauses in the PSQI questionnaire. Of these individuals, 1,662 had reliable visual field testing at RS-I-4. Their mean age (standard deviation [SD]) was 74.5 (5.5) years; 54% was female. Fifty-four individuals had GVFL; their mean (SD) age was 77.9 (5.5) years and 44% was females. There

was no significant association between subjective sleep apnea symptoms and prevalent GVFL (Odds Ratio [OR; 95% confidence interval (CI)] = 1.17 [0.49-2.78], $P=0.72$). Of the 1,608 individuals without GVFL at RS-I-4, 721 individuals had reliable visual field testing at RS-I-5 (mean age [SD] at RS-1-4 72.2 [4.4] years; 55% female). The median time between visual field testing at RS-I-4 and RS-I-5 was 6.5 years; 26 individuals developed GVFL (mean age [SD] 73.6 [5.2] years; 73% female). There was no significant association between subjective sleep apnea at RS-I-4 and incident GVFL at RS-I-5 (OR [95% CI] = 1.00 [0.29-3.42], $P=1.00$). The effects remained non-significant after additional correction for age, gender, smoking, and stroke (Table 1).

In total, 787 consecutive individuals underwent PSG. In our study sample, four participants were using a CPAP mask. All of these four individuals had normal visual fields and the LCDR (0.21-0.47) and IOP (11.5-15.0 mmHg) were within the normal range. After exclusion of these four individuals, 741 individuals with HRT data available and 751 individuals with IOP data available were included in the analysis. The mean (SD) age, LCDR, pRNFL thickness, and IOP of these participants were 62 (5.5) years, 0.43 (0.17), 251.6 (66.2) μm , and 13.6 (2.8) mmHg. The median AHI was 9, 54% was woman, and 24 individuals were treated with IOP lowering medication or underwent IOP lowering surgery or laser.

Figure 1 shows the correlation between AHI and LCDR. There was no correlation ($r = 0.008$, $P=0.82$). No associations were found between AHI and LCDR, pRNFL thickness, and IOP in crude and fully adjusted models. The effect per ten units increase in AHI on LCDR and pRNFL thickness was 0.00 ($P=0.82$) and $-0.01 \mu\text{m}$ ($P=0.94$), respectively (Table 2). In the IOP analysis, the effect of ten units increase in AHI was 0.13 mmHg ($P=0.09$). The effects remained non-significant after additional correction for age, gender, IOP lowering therapy, BMI, smoking, alcohol, MMSE, and SBP (Table 2).

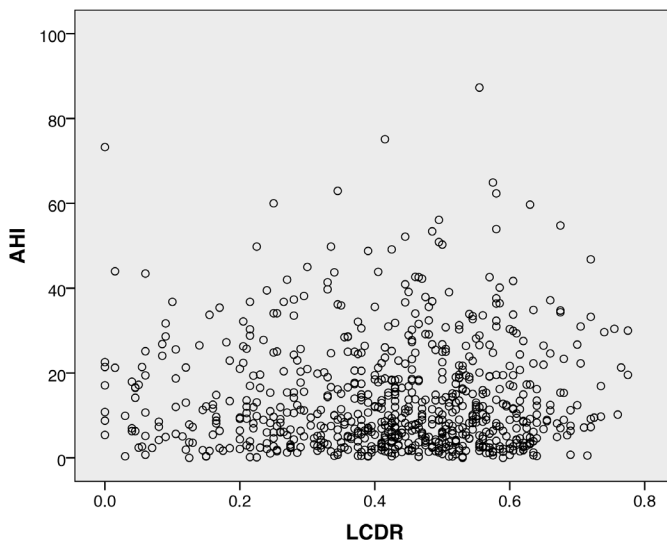
There was no statistically significant association between LCDR, pRNFL thickness, and IOP and severe sleep apnea (AHI > 30; $n = 113$) versus no sleep apnea (AHI < 5; $n = 184$) (Table 3). In the persons that underwent PSG, only four individuals had GVFL. Figure 2 shows the AHI distributions of these four individuals and of the individuals without GVFL. One individual with GVFL had severe sleep apnea (AHI 43), the others with GVFL had mild or moderate sleep apnea (AHI values of 9, 9, and 20).

Table 1. The association between subjective sleep apnea and glaucomatous visual field loss (GVFL).

		Prevalent GVFL (OR [95% CI]; $n=54$)	Incident GVFL (OR [95% CI]; $n=26$)
Sleep apnea	Crude	1.17 (0.49 to 2.78)	1.00 (0.29 to 3.42)
	adjusted for age and gender	1.39 (0.57 to 3.43)	1.58 (0.44 to 5.77)
	adjusted for age, gender, smoking, and stroke	1.50 (0.60 to 3.71)	1.66 (0.45 to 6.08)

ABBREVIATIONS

CI confidence interval
OR odds ratio

Figure 1. Apnea hypopnea index (AHI) versus linear cup-disc ratio (LCDR).**Table 2.** The effect of the apnea hypopnea index on LCDR, peripapillary RNFL thickness, and IOP.

		LCDR	pRNFL thickness (μm)	IOP (mmHg)
		(β [95% CI]; n=741)	(β [95% CI]; n=741)	(β [95% CI]; n=751)
Apnea (AHI per 10 units)	Crude	0.00 (-0.01 to 0.01)	-0.01 (-0.38 to 0.36)	0.13 (-0.02 to 0.29)
	adjusted for age, gender, and in the IOP analysis also for IOP lowering therapy	0.00 (-0.01 to 0.01)	0.17 (-0.21 to 0.55)	0.09 (-0.07 to 0.25)
	adjusted for age, gender, BMI, smoking, use of alcohol, MMSE, and SBP	0.00 (-0.01 to 0.01)	0.17 (-0.23 to 0.57)	-0.06 (-0.22 to 0.11)

ABBREVIATIONS

AHI apnea hypopnea index
BMI body mass index
CI confidence interval
IOP intraocular pressure

LCDR linear cup-disc ratio
MMSE mini-mental state examination
PRNFL peripapillary retinal nerve fiber layer
SBP systolic blood pressure

Figure 2. Distribution of the apnea hypopnea index (AHI) in individuals with and without glaucomatous visual field loss (GVFL). The box depicts the interquartile range, the whiskers denote the lowest and highest value in the data without outliers. The line in the box represents the median. The outliers (the circles and *) are defined as values greater than 1.5 interquartile ranges away from the 25th or 75th percentile.

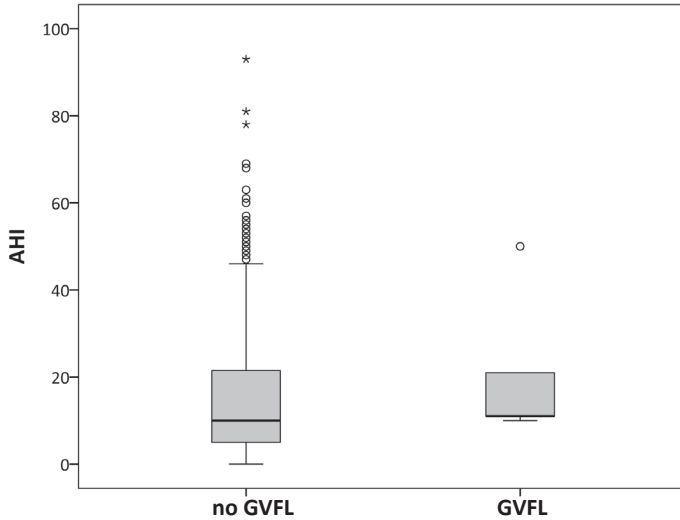


Table 3. The effect of severe sleep apnea (apnea hypopnea index > 30) versus no sleep apnea (apnea hypopnea index < 5) on LCDR, peripapillary RNFL thickness, and IOP.

		LCDR	pRNFL thickness (µm)	IOP (mmHg)
		(β [95% CI]; n=295)	(β [95% CI]; n=295)	(β [95% CI]; n=301)
Severe versus no sleep apnea	Crude	0.01 (-0.03 to 0.05)	-1.17 (-16.4 to 14.0)	0.50 (-0.15 to 1.15)
	adjusted for age and gender, and in the IOP analysis also for IOP lowering therapy	0.01 (-0.03 to 0.06)	2.10 (-14.2 to 18.3)	0.32 (-0.40 to 1.03)
	adjusted for age, gender, BMI, smoking, use of alcohol, MMSE, and SBP, and in the IOP analysis also for IOP lowering therapy	0.02 (-0.03 to 0.07)	3.60 (-14.0 to 21.1)	-0.45 (-1.19 to 0.28)

ABBREVIATIONS

BMI body mass index
IOP intraocular pressure
LCDR linear cup-disc ratio

MMSE mini-mental state examination
PRNFL peripapillary retinal nerve fiber layer
SBP systolic blood pressure

DISCUSSION

In this large population-based study, we found no association between subjective sleep apnea symptoms, based on a questionnaire, and GVFL. We confirmed this negative finding in a subset of participants who underwent PSG. In this subset we found no association between sleep apnea based on the AHI and three continuous parameters depicting glaucoma endophenotypes (LCDR, pRNFL thickness, and IOP).

A recently published literature review and meta-analysis showed a significant association between sleep apnea and OAG¹⁴. It included six case-control studies¹⁵⁻²⁰, one longitudinal study²¹, and nine cross-sectional studies²²⁻³⁰. The majority of the studies included less than 100 sleep apnea or glaucoma patients or controls. The largest case-control study¹⁶ found no association between sleep apnea and glaucoma in 667 glaucoma patients and 6,667 age-matched controls. The longitudinal study²¹ included 1,012 patients who were diagnosed with sleep apnea by PSG and visited an ophthalmologist and 6,072 controls who visited an ophthalmologist according to a health insurance database. After five years of follow-up, a higher incidence rate of glaucoma was observed in the sleep apnea patients compared to controls (11.3% versus 6.8%, respectively). The meta-analysis also included the largest study so far³⁰. In this cross-sectional study 156,336 individuals were included which had an ICD-9CM sleep apnea diagnosis in an insurance database. There was no difference in glaucoma incidence rate in patients with and without sleep apnea. Two other studies with more than 100 sleep apnea patients or controls were published after the inclusion date of the review and found also no association^{31,32}. In line with these studies, we did not find an association between sleep apnea and OAG (defined as GVFL).

In our study, AHI was not associated with the employed parameters LCDR and pRNFL thickness. A significant association between sleep apnea and a decrease in pRNFL thickness was found in nine studies^{27,29,33-39}. Four of these studies also found an association between the severity of OSAS and RNFL thickness^{29,35-37}. One study reported no association between sleep apnea and RNFL thickness⁴⁰. Two studies investigated the association between sleep apnea and cup-disc ratio^{29,37}, of which one found a significant correlation with AHI²⁹.

We found no association between AHI and IOP, which is in line with the studies from Lin et al.²⁷ and Nowak et al.⁴⁰. An increased IOP in patients with sleep apnea has been found in five studies^{29,33,35,37,38}. Huseynoglu et al.³⁵ found only a higher IOP in 15 mild sleep apnea patients compared to 27 moderate and 59 severe sleep apnea patients and 20 patients without sleep apnea, suggesting a chance finding. The other four studies found a higher IOP in all sleep apnea patients together. However, they did not adjust for BMI. A higher BMI is associated with a higher IOP and a higher prevalence of sleep apnea⁴¹. Therefore, the association found in these studies might be explained by BMI as confounder.

A strong point of our study is the large number of participants. The largest study about the association between AHI or sleep apnea and RNFL thickness or cup-disc ratio included 108 patients with sleep apnea and 108 controls³⁹. We included 754 participants in the PSG analysis, of which 113 had severe sleep apnea (AHI > 30). Another strength is our population-based design. All the participants underwent the same examinations, which

avoids information bias. Another strong point is the use of PSG. Two other studies included more than 100 sleep apnea cases diagnosed with PSG^{21,27}, but one of these studies included only 38 subjects without sleep apnea. It might be that most of the participants do not recognize that they have sleep apnea. This can result in referral bias. In our study, 102 of the 113 individuals classified with severe sleep apnea were not known with sleep apnea. Furthermore, 7 of the 25 individuals who were previously diagnosed with sleep apnea had no ($n = 5$) or mild ($n = 2$) sleep apnea based on AHI. Since most published studies used questionnaires or databases for the diagnosis, there could be misclassification of sleep apnea. On the other hand, since most studies did not perform visual field testing in all participants, misclassification of glaucoma could be a problem. In the Rotterdam study, most of the GVFL cases were unaware of having GVFL⁴². Furthermore, it might be possible that individuals diagnosed with glaucoma according to databases have non-arteriitic anterior ischemic optic neuropathy (NAION). Sleep apnea is associated with NAION⁴³ and visual field defects caused by NAION can be confused with visual field defects by glaucoma.

One of the limitations of our study is the relatively young age of participants with PSG data and therefore the low number of glaucoma cases. Most of our glaucoma cases did not undergo PSG. We found no association between subjective sleep apnea symptoms and glaucoma. Although we could not test the association between glaucoma and AHI, the combination of the results of both analyses (PSQI and PSG) suggests that there is no association. The cross-sectional design of our PSG study is another limitation. It might take some time to develop damage to the optic nerve after hypoxia. However, since the effect estimates of AHI for the continuous glaucoma parameters were negligible, we do not expect a much larger, statistically significant, effect after a few years.

In conclusion, in this population-based study, no association was found between sleep apnea and glaucoma or glaucoma-related parameters. Further research in large samples with PSG data is necessary to confirm or depreciate the associations between sleep apnea and glaucoma, which has been reported in several case-control studies.

References

1. Wolfs, R.C. et al. Changing views on open-angle glaucoma: definitions and prevalences--The Rotterdam Study. *Invest Ophthalmol Vis Sci* 41, 3309-21 (2000).
2. Czudowska, M.A. et al. Incidence of glaucomatous visual field loss: a ten-year follow-up from the Rotterdam Study. *Ophthalmology* 117, 1705-12 (2010).
3. Marcus, M.W., de Vries, M.M., Junoy Montolio, F.G. & Jansonius, N.M. Myopia as a risk factor for open-angle glaucoma: a systematic review and meta-analysis. *Ophthalmology* 118, 1989-1994 e2 (2011).
4. Tielsch, J.M. et al. Racial variations in the prevalence of primary open-angle glaucoma. The Baltimore Eye Survey. *JAMA* 266, 369-74 (1991).
5. Anderson, D.R. & Normal Tension Glaucoma, S. Collaborative normal tension glaucoma study. *Curr Opin Ophthalmol* 14, 86-90 (2003).
6. Cheng, J.W., Cai, J.P. & Wei, R.L. Meta-analysis of medical intervention for normal tension glaucoma. *Ophthalmology* 116, 1243-9 (2009).
7. Walsh, J.T. & Montplaisir, J. Familial glaucoma with sleep apnoea: a new syndrome? *Thorax* 37, 845-9 (1982).
8. Hofman, A. et al. The Rotterdam Study: 2016 objectives and design update. *Eur J Epidemiol* 30, 661-708 (2015).
9. Buysse, D.J., Reynolds, C.F., 3rd, Monk, T.H., Berman, S.R. & Kupfer, D.J. The Pittsburgh Sleep Quality Index: a new instrument for psychiatric practice and research. *Psychiatry Res* 28, 193-213 (1989).
10. Fogelholm, M. et al. Sleep-related disturbances and physical inactivity are independently associated with obesity in adults. *Int J Obes (Lond)* 31, 1713-21 (2007).
11. Luik, A.I., Zuurbier, L.A., Whitmore, H., Hofman, A. & Tiemeier, H. REM sleep and depressive symptoms in a population-based study of middle-aged and elderly persons. *J Sleep Res* 24, 305-8 (2015).
12. Iber, C., Ancoli-Israel, S., Chesson, A.L. & Quan, S.F. The aasm manual for the scoring of sleep and associated events: Rules, terminology and technical specifications. Westchester: American Academy of Sleep Medicine (2007).
13. Ramdas, W.D. et al. Heidelberg Retina Tomograph (HRT3) in population-based epidemiology: normative values and criteria for glaucomatous optic neuropathy. *Ophthalmic Epidemiol* 18, 198-210 (2011).
14. Shi, Y., Liu, P., Guan, J., Lu, Y. & Su, K. Association between glaucoma and obstructive sleep apnea syndrome: a meta-analysis and systematic review. *PLoS One* 10, e0115625 (2015).
15. Bilgin, G. Normal-tension glaucoma and obstructive sleep apnea syndrome: a prospective study. *BMC Ophthalmol* 14, 27 (2014).
16. Girkin, C.A., McGwin, G., Jr., McNeal, S.F. & Owsley, C. Is there an association between pre-existing sleep apnoea and the development of glaucoma? *Br J Ophthalmol* 90, 679-81 (2006).
17. Khandgave, T.P., Puthran, N., Ingole, A.B. & Nicholson, A.D. The assessment of sleep apnoea as a risk factor in glaucoma. *J Clin Diagn Res* 7, 1391-3 (2013).
18. Marcus, D.M. et al. Sleep disorders: a risk factor for normal-tension glaucoma? *J Glaucoma* 10, 177-83 (2001).
19. Onen, S.H. et al. High prevalence of sleep-disordered breathing in patients with primary open-angle glaucoma. *Acta Ophthalmol Scand* 78, 638-41 (2000).
20. Roberts, T.V., Hodge, C., Graham, S.L., Burlutsky, G. & Mitchell, P. Prevalence of nocturnal oxygen desaturation and self-reported sleep-disordered breathing in glaucoma. *J Glaucoma* 18, 114-8 (2009).
21. Lin, C.C., Hu, C.C., Ho, J.D., Chiu, H.W. & Lin, H.C. Obstructive sleep apnea and increased risk of glaucoma: a population-based matched-cohort study. *Ophthalmology* 120, 1559-64 (2013).
22. Aptel, F. et al. Association between glaucoma and sleep apnea in a large French multicenter prospective cohort. *Sleep Med* 15, 576-81 (2014).
23. Boonyaleephan, S. & Neruntarat, C. The association of primary open-angle glaucoma / normal tension glaucoma and obstructive sleep apnea in Thai patients. *Journal of Medicine and Health Sciences* 15, 87-94 (2008).
24. Boyle-Walker, M., Semes, L.P., Clay, O.J., Liu, L. & Fuhr, P. Sleep apnea syndrome represents a risk for glaucoma in a veterans' affairs population. *ISRN Ophthalmol* 2011, 920767 (2011).
25. Kadyan, A., Asghar, J., Dowson, L. & Sandramouli, S. Ocular findings in sleep apnoea patients using continuous positive airway pressure. *Eye (Lond)* 24, 843-50 (2010).
26. Karakucuk, S. et al. Ocular blood flow in patients with obstructive sleep apnea syndrome (OSAS). *Graefes Arch Clin Exp Ophthalmol* 246, 129-34 (2008).
27. Lin, P.W. et al. Normal tension glaucoma in patients with obstructive sleep apnea/hypopnea syndrome. *J Glaucoma* 20, 553-8 (2011).

28. Muniesa, M., Sanchez-de-la-Torre, M., Huerva, V., Lumbierres, M. & Barbe, F. Floppy eyelid syndrome as an indicator of the presence of glaucoma in patients with obstructive sleep apnea. *J Glaucoma* 23, e81-5 (2014).
29. Sergi, M. et al. Prevalence of normal tension glaucoma in obstructive sleep apnea syndrome patients. *J Glaucoma* 16, 42-6 (2007).
30. Stein, J.D. et al. The association between glaucomatous and other causes of optic neuropathy and sleep apnea. *Am J Ophthalmol* 152, 989-998 e3 (2011).
31. Gross, N.J. et al. [Prevalence of glaucoma in obstructive sleep apnea]. *Ophthalmologe* 112, 580-4 (2015).
32. Wang, Y.X. et al. Snoring and glaucoma. *PLoS One* 9, e88949 (2014).
33. Casas, P. et al. Retinal and optic nerve evaluation by optical coherence tomography in adults with obstructive sleep apnea-hypopnea syndrome (OSAHS). *Graefes Arch Clin Exp Ophthalmol* 251, 1625-34 (2013).
34. Gutierrez-Diaz, E., Perez-Rico, C., de Atauri, M.J., Mencia-Gutierrez, E. & Blanco, R. Evaluation of the visual function in obstructive sleep apnea syndrome patients and normal-tension glaucoma by means of the multifocal visual evoked potentials. *Graefes Arch Clin Exp Ophthalmol* 250, 1681-8 (2012).
35. Huseyinoglu, N. et al. Optic disc and retinal nerve fiber layer parameters as indicators of neurodegenerative brain changes in patients with obstructive sleep apnea syndrome. *Sleep Breath* 18, 95-102 (2014).
36. Kargi, S.H. et al. Retinal nerve fibre layer measurements are reduced in patients with obstructive sleep apnoea syndrome. *Eye (Lond)* 19, 575-9 (2005).
37. Lin, P.W. et al. Decreased retinal nerve fiber layer thickness in patients with obstructive sleep apnea/hypopnea syndrome. *Graefes Arch Clin Exp Ophthalmol* 249, 585-93 (2011).
38. Moghimi, S. et al. Retinal nerve fiber thickness is reduced in sleep apnea syndrome. *Sleep Med* 14, 53-7 (2013).
39. Sagiv, O. et al. Retinal nerve fibre layer thickness measurements by optical coherence tomography in patients with sleep apnoea syndrome. *Clin Experiment Ophthalmol* 42, 132-8 (2014).
40. Nowak, M.S., Jurowski, P., Gos, R., Prost, M.E. & Smigielski, J. Pulsatile ocular blood flow in subjects with sleep apnoea syndrome. *Arch Med Sci* 7, 332-6 (2011).
41. Klein, B.E., Klein, R. & Linton, K.L. Intraocular pressure in an American community. The Beaver Dam Eye Study. *Invest Ophthalmol Vis Sci* 33, 2224-8 (1992).
42. de Voogd, S. et al. Incidence of open-angle glaucoma in a general elderly population: the Rotterdam Study. *Ophthalmology* 112, 1487-93 (2005).
43. Waller, E.A., Bendel, R.E. & Kaplan, J. Sleep disorders and the eye. *Mayo Clin Proc* 83, 1251-61 (2008).

CHAPTER 3.3

Associations with intraocular pressure across Europe: The European Eye Epidemiology (E³) Consortium



Anthony P. Khawaja, Henriët Springelkamp, Catherine Creuzot-Garcher, Cécile Delcourt, Albert Hofman, René Höhn, Adriana I. Iglesias, Roger C.W. Wolfs, Jean-François Korobelnik, Rufino Silva, Fotis Topouzis, Katie M. Williams, Alain M. Bron, Gabriëlle H.S. Buitendijk, M. Luz Cachulo, Audrey Cougnard-Grégoire, Jean-François Dartigues, Christopher J. Hammond, Norbert Pfeiffer, Angeliki Salonikiou, Cornelia M. van Duijn, Johannes R. Vingerling, Robert N. Luben, Alireza Mirshahi, Julia Lamparter, Caroline C. W. Klaver, Nomdo M. Jansonius, Paul J. Foster.

ABSTRACT

Importance. Understanding associations with IOP and variations in IOP between countries may teach us about mechanisms underlying glaucoma.

Objective. To examine systemic and ocular factors associated with IOP in European men and women, and to examine any geographical trends in IOP across Europe.

Design, Setting and Participants. A total of 43,500 phakic participants from 12 population-based cross-sectional studies across Europe were included in primary analyses. The studies were members of the European Eye Epidemiology (E³) consortium and represented 6 countries. IOP was measured using Goldmann applanation tonometry in 6 studies and non-contact tonometry in 6 studies. Each study conducted multivariable linear regression analyses with IOP as the outcome variable, and age, sex, height, body mass index (BMI), systolic blood pressure (SBP) and spherical equivalent (SE) as explanatory variables. Results from each study were pooled using random effects meta-analysis. A standardized IOP was calculated for each study using set values for covariables (age 65 years, sex 1.5, SBP 135 mmHg, height 165 cm, BMI 25 Kg/m², SE 0.0 Dioptres) and association of standardized IOP with latitude was tested using meta-regression.

Main Outcome and Measures. Mean IOP of right and left eyes

Results. Higher IOP was observed in men (0.18 mmHg; 95% CI 0.06, 0.31; $P=0.004$) and with higher BMI (0.21 mmHg per 5 Kg/m²; 95% CI 0.14, 0.28; $P<0.001$), shorter height (-0.17 mmHg per 10 cm; 95% CI 0.25, -0.08; $P<0.001$), higher SBP (0.17 mmHg per 10 mmHg; 95% CI 0.12, 0.22; $P<0.001$) and more myopic refraction (0.06 mmHg per Dioptre; 95% CI 0.03, 0.09; $P<0.001$). An inverted U-shaped trend was observed between age and IOP, with IOP increasing up to the age of 60 and decreasing in participants older than 70 years. We found no significant association between standardized IOP and study location latitude ($P=0.76$).

Conclusions and Relevance. We report a novel association of lower IOP in taller people, and an inverted-U shaped association of IOP with age. We found no evidence of significant variation in IOP across Europe, supporting the necessary collaborative pooling of data from studies examining the genetic determinants of IOP in Europeans.

INTRODUCTION

Raised intraocular pressure (IOP) is an important risk factor for the incidence¹ and progression² of primary open-angle glaucoma (POAG). Understanding which systemic and ocular parameters are associated with IOP gives us insight into the pathophysiological mechanisms underlying IOP and may ultimately lead to new targets or treatment methods for POAG. Examining geographic trends in disease may also shed light on disease risk and aetiology. For example, differential rates of coronary heart disease mortality across Europe gave impetus to research demonstrating a beneficial effect of a Mediterranean diet³.

Several European population studies have reported IOP data^{4–8}. However, individual studies suffer from limited sample size and results may only apply to the geographical region examined. We therefore conducted a study of IOP data from 12 population-based studies across Europe, maximising power to detect small associations and increasing generalisability to European populations. We also aimed to compare IOP between studies, in particular comparing IOP in Northern Europe with Southern Europe, reflecting differences in lifestyle, such as diet⁹, as well as latitude.

METHODS

The European Eye Epidemiology (E³) consortium is a collaborative network of 38 population-based studies across Europe with the overarching aim of developing and analysing large pooled datasets to increase understanding of eye disease and vision loss. Data on IOP were available from 12 E³ studies from 6 countries (Table 1). Detailed methods for the studies are given in the Supplementary Text. All studies adhered to the tenets of the Declaration of Helsinki and had local ethical committee approval. All participants gave written informed consent.

IOP was measured using Goldmann applanation tonometry (GAT) in 6 studies and non-contact tonometry (NCT) in 6 studies (Table 1). We defined participant IOP as the mean of right and left eye values. Participants with an inter-eye difference in IOP of >6 mmHg were excluded as this may indicate undiagnosed ocular disease or artefact (the 6 mmHg cutoff was based on approximately twice the standard deviation).

Factors to be tested for association with IOP were decided a priori, based on common measures available in all studies with IOP data available; these were age, sex, height, body mass index (BMI), systolic blood pressure (SBP), refractive error (mean spherical equivalent [SE] of right and left eyes), and history of cataract surgery.

For initial analyses, we excluded participants with a history of a glaucoma therapy (laser, surgery or medication) or intraocular surgery (other than cataract surgery) in either eye. After examining the association of cataract surgery with IOP, we further excluded all participants with a history of cataract surgery, given the strong effect on IOP. Our main analyses were conducted on phakic patients only.

To examine the associations between IOP and the variables of interest, we used linear regression. Primary multivariable models included all the main variables of interest (age, sex, height, BMI, SBP and SE; referred to as “Model 1”). We also further adjusted for central corneal thickness (CCT) in the subset of participants with CCT data available (“Model 2”). Regression analyses were conducted for each individual study, and then random-effects meta-analysis was used to combine the effect estimates. A random effects approach was decided a priori given the between study heterogeneity in IOP measurement methods. We further examined the association between age and IOP, stratified into age groups based on initial results. Additionally, to address the potential bias of participants with the highest IOP being excluded due to using IOP-lowering therapy, we repeated analyses including participants on IOP-lowering medication; for these participants we imputed pre-treatment IOP by dividing measured IOP by 0.7 (“Model 3”). This approach assumes an average IOP reduction of 30% on medical treatment and has been used successfully in the study of genetic associations with IOP¹⁰. For the Coimbra Eye Study, data on SBP were not available and multivariable adjusted effect estimates were adjusted for age, sex, height, BMI and SE only; we therefore conducted sensitivity analyses of excluding the Coimbra Eye Study from the meta-analyses. Regression analyses for data from the Twins UK study included data from both twins in each pair and therefore used a clustered analysis approach to account for any correlation between twins. We explored the shapes of the associations with IOP by plotting random effects meta-analysed IOP levels with 95% confidence intervals by ordinal categories of the variables.

We calculated a standardized IOP for each study using multivariable linear regression, based on fixed covariables parameters; these parameters were set to values likely to be included within the range values of values for each study (age 65 years, sex 1.5, SBP 135 mmHg, height 165 cm, BMI 25 Kg/m², SE 0). To compare IOP in different regions in Europe, we divided the studies into Northern and Southern Europe groups using an arbitrary latitude cut-point of 50° to derive two similarly sized groups. We used random-effects meta-analysis to derive pooled standardized IOP estimates, and these were compared using the independent samples t-test. We examined the association between standardized IOP and latitude as a continuous variable using meta-regression. We also compared standardized IOP in GAT studies with predicted IOP in NCT studies, and further examined the association between latitude and predicted IOP stratified by tonometry method.

Stata version 13.1 (StataCorp LP, College Station, TX) was used for all analyses.

RESULTS

A total of 46,081 participants from 12 population-based studies were included. The mean age of participants ranged from 49 to 81 years, and 57% were women (Table 1). Mean IOP ranged from 13.6 mmHg in the Rotterdam Study III to 16.0 mmHg in the EPIC-Norfolk Eye Study (Table 1). In total, 2581 participants (5.6%) had undergone cataract surgery in at least one eye; on average, these participants had 0.61 mmHg lower IOP (Table 2). All but four studies had CCT measurements available (Figure 1). On average, IOP was measured 0.96 mmHg higher per 40µm thicker CCT (Table 2).

Table 1. Descriptive data for contributing studies.

Study	Years	City/Country	IOP measurements		N	Women (%)	Mean age in years (SD)	Mean IOP in mmHg (SD)
			Type	Details				
Alienor Study ³⁹	2006-2008	Bordeaux, France	NCT (KT 800, Kowa)	1 measurement by a trained technician	797	55.9	79.1 (4.0)	14.1 (2.4)
Coimbra Eye Study	2009-2011	Coimbra, Portugal	NCT (Nidek Tonoref II)	Mean of ≥3 measurements per eye (up to 5 readings taken if any outliers)	2,839	56.6	68.3 (8.2)	14.9 (2.9)
EPIC-Norfolk Eye Study ⁴⁰	2004-2011	Norfolk, UK	NCT (ORA)	Best signal value of ≥3 IOPg measurements per eye.	7,253	55.1	67.5 (7.4)	16.0 (3.5)
Erasmus Rucphen Family Study ^{41,42}	2002-2005	Rucphen, Netherlands	GAT	Median of 3 measurements per eye	2,122	56.1	48.2 (14.0)	15.0 (2.9)
Gutenberg Health Study ⁴	2007-2012	Mainz, Germany	NCT (Nidek NT-2000)	Mean of 3 measurements per eye	13,600	49.4	54.4 (10.9)	14.2 (2.7)
Montrachet 3C Study	2009-2013	Montrachet, France	NCT (Nidek Tonoref II)	1 measurement by a trained technician	937	58.1	81.3 (3.3)	15.2 (3.1)
POLA Study ⁴³	1995-1998	Sète, France	GAT	1 measurement by an ophthalmologist	2,208	56.1	70.2 (6.5)	14.7 (2.6)
Rotterdam Study I ⁴⁴	1993-1995	Rotterdam, Netherlands	GAT	Median of 3 measurements per eye	5,198	58.5	69.5 (8.0)	14.5 (2.9)
Rotterdam Study II ⁴⁴	2000-2001	Rotterdam, Netherlands	GAT	Median of 3 measurements per eye	2,496	54.3	63.9 (7.2)	14.1 (2.9)
Rotterdam Study III ⁴⁴	2006-2008	Rotterdam, Netherlands	GAT	Median of 3 measurements per eye	3,386	56.5	56.6 (6.3)	13.6 (2.7)
Thessaloniki Eye Study ⁴⁵	1999-2005	Thessaloniki, Greece	GAT	Mean of 3 measurements per eye	1,993	45.1	70.0 (5.3)	15.0 (3.0)
Twins UK	2001-2014	UK (multiple cities)	NCT (ORA)	Mean of 2 measurements per eye	3,252	97.5	56.2 (12.1)	15.5 (3.2)

ABBREVIATIONS

EPIC European Prospective Investigation of Cancer
GAT Goldmann applanation tonometry
IOP intraocular pressure

NCT non-contact tonometry
ORA Ocular Response Analyzer
SD standard deviation

Table 2. Meta-analysed associations with intraocular pressure (IOP). Results are for all phakic participants (n=43,500), except for cataract surgery (includes pseudophakic participants in addition)* and CCT (a subset of phakic participants)**.

Age group (years)	Unadjusted Difference in IOP (95% CI), mmHg	P-value	Model 1 Difference in IOP (95% CI), mmHg	P-value	Model 2 Difference in IOP (95% CI), mmHg	P-value
Phakic participants						
Age (per decade)	0.06 (-0.03, 0.16)	0.21	-0.05 (-0.16, 0.06)	0.34	0.00 (-0.19, 0.19)	0.97
Female sex	0.00 (-0.13, 0.13)	1	-0.18 (-0.31, -0.06)	0.004	-0.04 (-0.20, 0.12)	0.65
BMI (per 5 Kg/m ²)	0.29 (0.22, 0.35)	<0.001	0.21 (0.14, 0.28)	<0.001	0.25 (0.18, 0.31)	<0.001
Height (per 10 cm)	-0.12 (-0.19, -0.04)	0.003	-0.17 (-0.25, -0.08)	<0.001	-0.14 (-0.25, -0.04)	0.008
SBP (per 10 mmHg)	0.19 (0.15, 0.23)	<0.001	0.17 (0.12, 0.22)	<0.001	0.19 (0.13, 0.25)	<0.001
Spherical equivalent (per dioptre)	-0.04 (-0.07, -0.01)	0.007	-0.06 (-0.09, -0.03)	<0.001	-0.07 (-0.08, -0.06)	<0.001
Phakic and pseudophakic participants						
Cataract surgery*	-0.61 (-0.81, -0.41)	<0.001	-0.63 (-0.87, -0.40)	<0.001	-0.68 (-1.13, -0.23)	0.003
Phakic participants with CCT data						
CCT (per 40 µm)**	0.96 (0.57, 1.35)	<0.001	-	-	0.97 (0.59, 1.35)	<0.001

ABBREVIATIONS

UNADJUSTED results are from univariable regression models

MODEL 1 results from multivariable regression models adjusted for age, sex, body mass index (BMI), height, systolic blood pressure (SBP) and spherical equivalent

MODEL 2 adjusted for central corneal thickness (CCT) in addition to covariables adjusted for in Model 1 (n=21,332)

* analyses carried out on data from phakic and pseudophakic participants (n=46,081 for unadjusted and Model 1; n=21,332 for Model 2)

** analyses carried out on data from 21,332 phakic participants with complete data for CCT in addition to other covariables

Figure 1. Forest plots for associations with intraocular pressure (IOP). All associations were adjusted for age, sex, body mass index (BMI), systolic blood pressure (SBP), height and spherical equivalent unless otherwise indicated. SBP was not measured or adjusted for in the Coimbra Eye Study. Results are for phakic participants (n= 43,500).

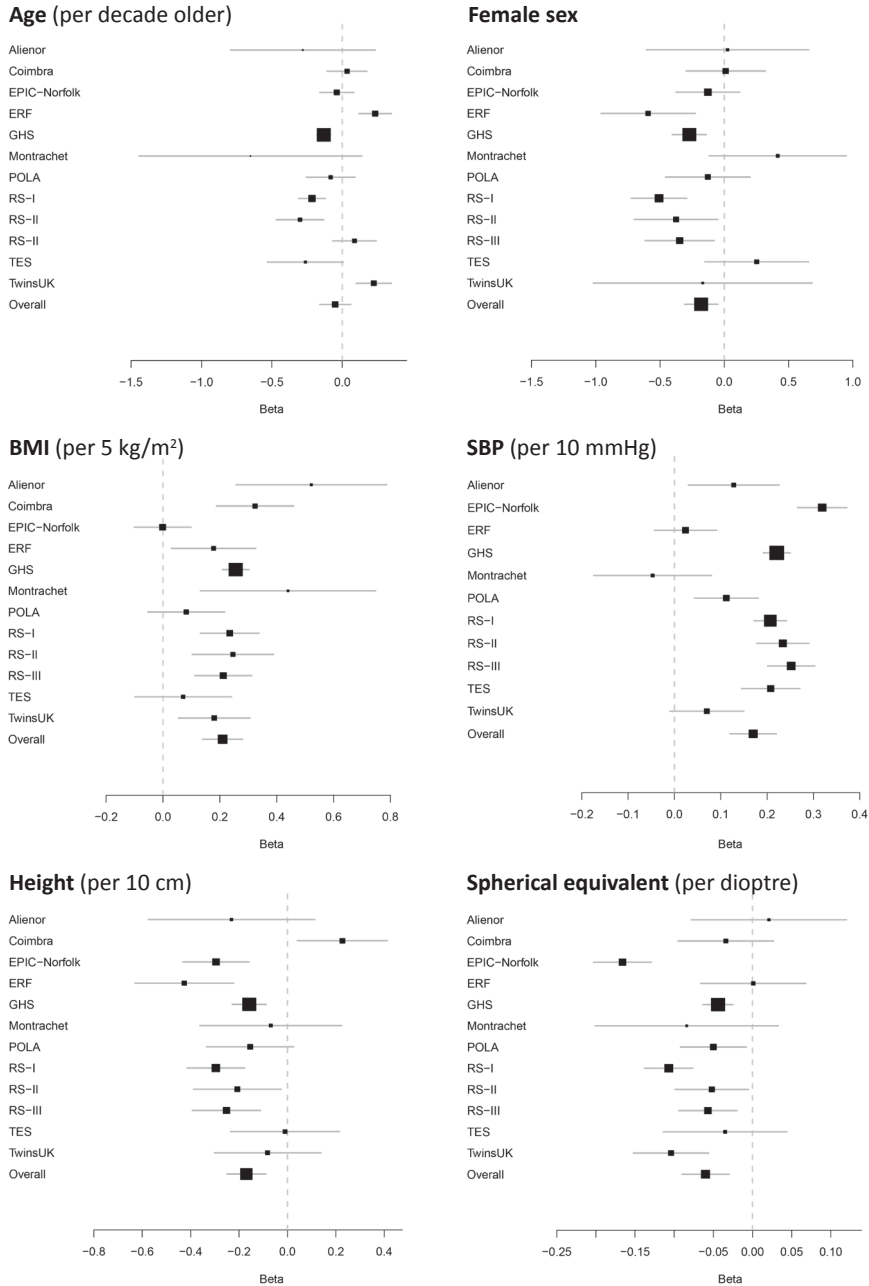


Table 3. Associations between age and intraocular pressure (IOP), stratified by age-group.

Age group (years)	Unadjusted		Model 1	
	Difference in IOP per decade older (95% CI), mmHg	P-value	Difference in IOP per decade older (95% CI), mmHg	P-value
<60	0.27 (0.08, 0.46)	0.005	0.13 (-0.07, 0.33)	0.22
60-69	0.12 (-0.05, 0.29)	0.16	0.01 (-0.17, 0.19)	0.91
≥70	-0.21 (-0.35, -0.07)	0.003	-0.28 (-0.44, -0.12)	0.001

ABBREVIATIONS

MODEL 1 results from multivariable regression models adjusted for sex, body mass index (BMI), height, systolic blood pressure (SBP) and spherical equivalent (n= 43,500)

MODEL 2 adjusted for central corneal thickness in addition to covariables adjusted for in Model 1 (n=21,332)

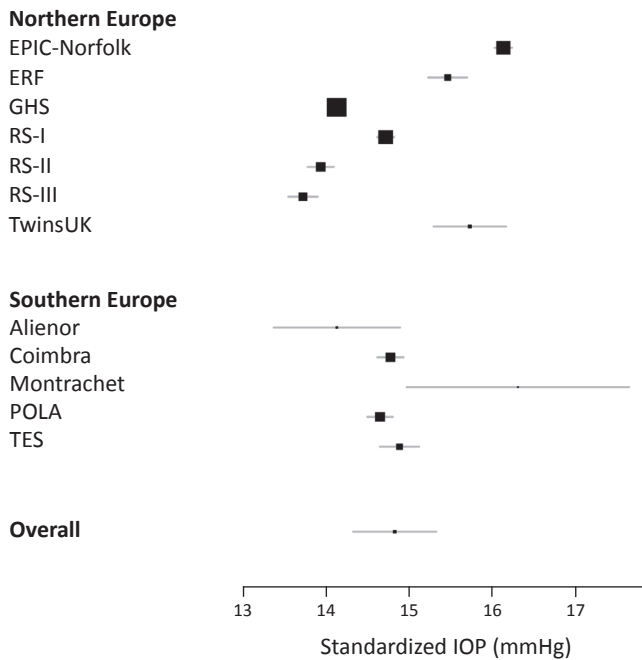


Figure 2. Forest plot of standardized intraocular pressure (IOP), stratified by latitude. Pooled associations for Northern Europe, Southern Europe, and overall were derived using random effects meta-analysis. The right column presents standardized IOP in mmHg (95% confidence interval).

Table 3. (continued)

Age group (years)	Model 2		Model 3	
	Difference in IOP per decade older (95% CI), mmHg	P-value	Difference in IOP per decade older (95% CI), mmHg	P-value
<60	0.00 (-0.07, 0.07)	0.91	0.28 (0.17, 0.39)	<0.001
60-69	0.24 (-0.27, 0.75)	0.35	0.23 (0.01, 0.45)	0.038
≥70	-0.59 (-1.04, -0.14)	0.01	-0.25 (-0.41, -0.09)	0.002

MODEL 3 including participants taking IOP-lowering medication (with imputed pre-treatment IOP), adjusted for sex, BMI, height, SBP and spherical equivalent (n=44,143)

For subsequent analyses, we excluded participants with a history of cataract surgery; results below refer to a total of 43,500 phakic participants for primary analyses and 21,332 participants with CCT data also available for further adjustment.

Table 2 presents crude and adjusted meta-analysed associations with IOP. Figure 1 presents the Forest plots for the meta-analyses adjusted for age, sex, BMI height, SBP and SE. Age was not significantly associated with IOP in these linear analyses. Sex was only associated with IOP in adjusted analyses; women had 0.18 mmHg lower IOP ($P=0.004$). Both BMI and SBP were positively associated with IOP in crude and adjusted analyses (all $P<0.001$). Height was negatively associated with IOP in crude and adjusted analyses (Model 1 $P<0.001$; Model 2 $P=0.008$). A more myopic refraction was associated with higher IOP ($P<0.001$ for adjusted analyses). The R^2 for IOP in the maximally adjusted multivariable models for each study ranged from 0.09 in the Rotterdam Study II to 0.27 in the Gutenberg Health Study.

Supplementary Figure 1 illustrates the shapes of the associations with IOP. There were clear linear associations with IOP across the whole ranges of height, BMI, SBP and SE. There was a suggestion of an inverted-U shaped association between age and IOP. To further explore this potential non-linear relationship, we examined the association between age and IOP stratified into 3 age categories (Table 3). We found evidence for increasing IOP with older age in participants under 60 years, though this was only statistically significant for the crude analysis ($P=0.005$). There was consistent evidence for decreasing IOP with older age in participants 70 years or older (all $P<0.01$). There did not appear to be a significant relationship between IOP and age for participants aged 60-69 years in primary analyses. To further explore whether the reduction of IOP with increasing age in the oldest participants was due to exclusion of participants with higher IOP following commencement of IOP-lowering medication, we repeated the analysis including participants on IOP-lowering medication and imputing their pre-treatment IOP, and observed similar associations (Table 3, Model 3).

Figure 2 presents the standardized IOP for each country in a Forest plot, stratified by latitude. Standardized IOP varied between 13.7 mmHg in Rotterdam Study III to 16.3 mmHg in the Montrachet Study. The meta-analysed standardized IOP for all European studies was 14.8 mmHg (95% CI 14.3, 15.3), and there was no significant difference between Northern European studies (meta-analysed IOP 14.80 mmHg) and Southern European studies (meta-analysed IOP 14.75 mmHg), as shown in Figure 2 ($P=0.95$). We also carried out a meta-regression to examine whether standardized IOP was associated with latitude considered as a continuous variable (Supplementary Figure 2); we found no significant association ($P=0.76$). As shown in Supplementary Figure 3, the standardized IOP for all studies that used NCT (15.2 mmHg; 95% CI 14.2, 16.2) was higher than the standardized IOP for all studies that used GAT (14.5 mmHg; 95% CI 14.1, 15.0), though the difference was not statistically significant ($P=0.32$). We therefore also compared Northern versus Southern Europe standardized IOP stratified by tonometry method (Supplementary Figure 3); there were no significant differences for either the GAT studies ($P=0.56$) or the NCT studies ($P=0.83$). Further, we also carried out meta-regressions using latitude as a continuous variable, stratified by tonometry method (Supplementary Figure 4); there was no significant association for the GAT studies ($P=0.51$) or the NCT studies ($P=0.85$).

DISCUSSION

In this large study examining IOP in over 40,000 participants from 6 European countries, we confirmed previously reported relationships of IOP with SBP, BMI, refractive error and previous cataract surgery. More novel findings include a negative association between IOP and height and an inverted-U-shaped association between IOP and age. The mean standardised IOP was 14.8 mmHg across all studies, and we did not find any significant geographical trends.

While the IOP-lowering effect of cataract extraction in individuals has been consistently reported in longitudinal surgical case series¹¹, it is less clear whether people who have undergone cataract surgery have lower IOP than people who have not within a population. The 0.6 mmHg lower IOP we found in pseudophakic compared to phakic participants is significant at a population level, and would translate into around a 10% reduction in the 5-year incidence of glaucoma based on data from the Rotterdam Study¹, all other factors being equal.

There is no consensus on the direction of association between IOP and age in the literature, with studies reporting increasing IOP^{12–15}, decreasing IOP^{4,7,16–19} or no association of IOP²⁰ with older age. Possible reasons for this inconsistency are differential associations by population, or a non-monotonic relationship between age and IOP such that different studies of different aged participants yield different results. An inverted-U shaped relationship between age and IOP was suggested by data from the Beijing Eye Study, though these results were unadjusted and only certain between group comparisons were statistically significant²¹. We found strong evidence for an inverted-U shaped relationship, with IOP increasing linearly with age up to the age of 60 years, IOP linearly decreasing with age above 70 years, and a plateau with no significant association between the ages of 60 and 70 years. The decrease in IOP with

age in the oldest age groups was still observed even after including participants receiving IOP-lowering medication, reducing the chance that the association is a result of bias due to participants with the highest IOP being excluded in older age due to commencement of therapy. If we assume that participants with higher IOP were more likely to undergo cataract surgery, it remains a possibility that the decline in IOP with age in people older than 70 years is due to exclusion of pseudophakic participants.

The reported association between IOP and sex is also inconsistent between studies; most studies (not included in the current meta-analysis) have reported higher IOP in women^{13,15,16,19,20}, though higher IOP in men^{4,14} or no association between IOP and sex have also been reported¹⁷. We found higher IOP in men, but only in adjusted analyses, and not in the subset with CCT available for further adjustment. This inconsistency raises the possibility of a chance finding. While higher IOP in men is in agreement with a higher risk of POAG in men²², it is possible that a higher prevalence of angle-closure in women²³ also contributes to a sex-differential for IOP; iridocorneal drainage angle width may be an important determinant of IOP, even among healthy participants.

We found a significant decrease in IOP with greater height, even after adjustment for possible confounders. This is a relatively novel finding; while a negative crude association of height with IOP was reported in the Tanjong Pagar Study, this was not significant after adjustment for confounders¹². Our finding is in agreement with the lower prevalence of POAG reported in taller participants of the Beijing Eye Study²⁴. The mechanism underlying lower IOP in taller people is not clear, but may be related to the distance between the eye and the heart. We hypothesise that ciliary body perfusion and resultant aqueous production is lower the higher the eye is above the heart, and that this distance is larger in taller people. This is in agreement with the findings that IOP is lower in the sitting position compared with supine²⁵, and that IOP is lower in the higher eye of study participants in the lateral decubitus position²⁶.

The significant associations we found between IOP and BMI, SBP and spherical equivalent are consistent with the literature. The majority of published studies have reported higher IOP with higher BMI^{13,15–18,20,27,28}, higher SBP^{12,13,15,16,18,20,29,30}, and more myopic refraction^{21,28} or longer axial length¹⁸. We have further examined the shapes of these relationships with IOP and found linear associations for BMI, SBP and spherical equivalent (Supplementary Figure 1). The linear relationship between BMI and IOP across the whole range of BMI is of particular interest. It has been suggested that the relationship between BMI and IOP is due to artefactual high IOP readings in people of high BMI due to an induced Valsalva manoeuvre at slit lamp examination³¹. However, our findings of higher IOP with BMI even at the lower end of the BMI range argue against the Valsalva hypothesis. For example, it would not be expected that a participant of normal BMI would have a greater degree of Valsalva manoeuvre induced at slit lamp examination than an underweight participant. Furthermore, the association between BMI and IOP was seen in studies using NCT, which may be less prone to inducing a Valsalva manoeuvre. The mechanism by which higher BMI increases IOP remains unclear, but may be related to metabolic syndrome in general³². A meta-analysis of epidemiological data suggests an increased risk of glaucoma in myopic people³³. Higher IOP in myopic eyes may be the mechanism by which glaucoma risk is increased. What remains unclear is why IOP is higher in myopic eyes. A possible hypothesis

is that abnormal elongation of the eye is associated with a degree of malformation of drainage angle microstructure.

We did not find striking variability of IOP levels between the European countries participating in this study, and did not find any variation in IOP with latitude. This may be in part due to relative genetic and cultural homogeneity among the predominantly Caucasian populations in this study, and in contrast to the significant difference seen in IOP of Japanese people compared with Europeans³⁴. It is also likely that between study heterogeneity in IOP ascertainment limits meaningful comparisons of absolute IOP values, and reduces statistical power to identify small differences. One such difference in study methods is GAT versus NCT, and while we did repeat analyses stratified by tonometry method, the number of studies within each group was small and limited power for finding any differences. Despite our negative findings, and the limitations of this approach, comparing IOP levels between countries remains an important method of potentially identifying new environmental associations with IOP.

The major strengths of our study are the large pooled sample size allowing identification of small effect associations, and the increased generalisability derived from demonstrating associations across multiple populations. Many epidemiological studies are limited by the possibility of chance findings or that findings are only relevant in the reported population. We have reported associations that were present when considering data from 6 different countries together, and could also examine the results from each study alone in relation to the pooled findings using the Forest plots. We can therefore be more certain that our results were not due to chance, and are likely applicable to many Caucasian populations within and outside Europe. There are also limitations to our study. Meta-analysis of summary data is a useful approach, but post-hoc analysis is limited by the pre-specified analysis compared with pooling of raw data. However, the feasibility of sharing raw participant data between studies is limited by local study ethics arrangements. Another issue with meta-analysis is between study heterogeneity, which can limit the validity of statistically combining results. The degree of heterogeneity in the meta-analyses we conducted was variable, with I^2 statistics ranging from 0% to 98%. While random effects meta-analysis assumes a distribution of the true effect due to between study heterogeneity, it may not always be appropriate to statistically combine results from studies that used vastly different methods. For this reason, we also ran analyses for the major associations (Table 2 and Figure 1) stratified by tonometry method (GAT studies and NCT studies separately); this yielded very similar results (data not shown). While absolute IOP values may vary between GAT and NCT, the direction and strength of association of measured IOP with systemic factors did not appear to differ significantly. Another limitation is that Eastern European populations were not represented in our study sample.

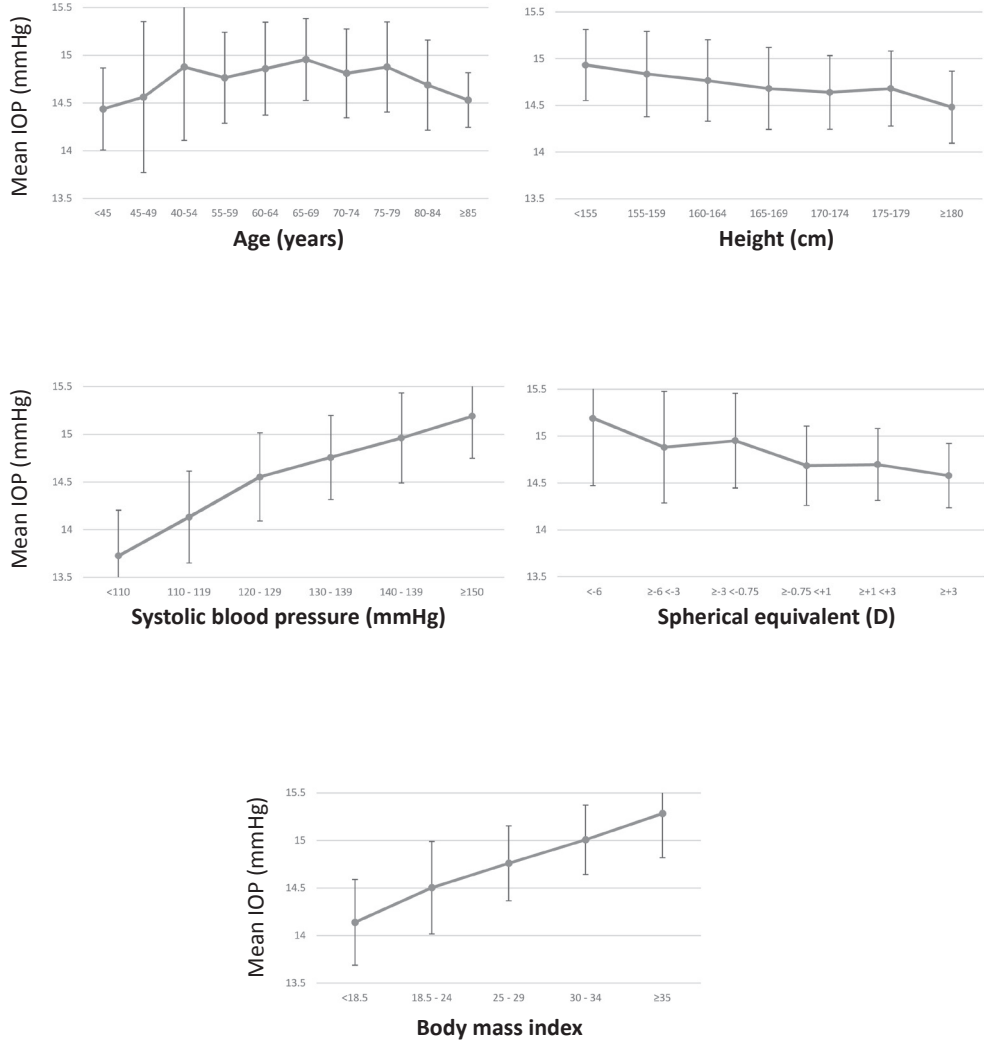
In summary, novel findings from this large pan-European study included an inverted-U shaped association of IOP with age, and lower IOP in taller participants. We did not find significant variation in IOP across Europe. Our findings have implications for the design of future studies seeking novel aetiological factors for IOP, such as genetic association studies; depending on the study age-range, linear adjustment for age may not be appropriate, and pooling of data from studies of people of European descent may be appropriate given the lack of variation in IOP we have observed across Europe.

References

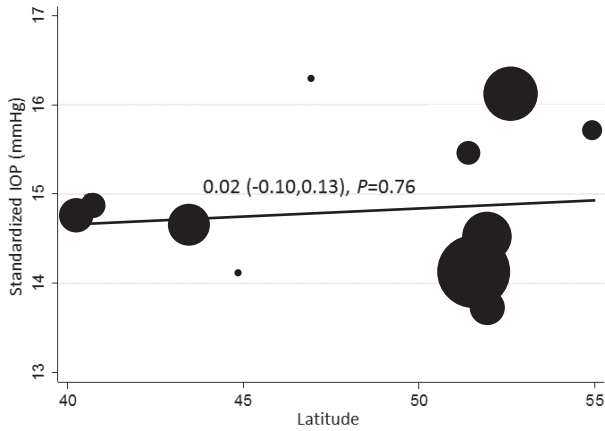
1. de Voogd, S. et al. Incidence of open-angle glaucoma in a general elderly population: the Rotterdam Study. *Ophthalmology* 112, 1487-93 (2005).
2. Leske, M.C. et al. Predictors of long-term progression in the early manifest glaucoma trial. *Ophthalmology* 114, 1965-72 (2007).
3. Trichopoulou, A. et al. Modified Mediterranean diet and survival: EPIC-elderly prospective cohort study. *BMJ* 330, 991 (2005).
4. Hoehn, R. et al. Distribution of intraocular pressure and its association with ocular features and cardiovascular risk factors: the Gutenberg Health Study. *Ophthalmology* 120, 961-8 (2013).
5. Dielemans, I. et al. Primary open-angle glaucoma, intraocular pressure, and diabetes mellitus in the general elderly population. The Rotterdam Study. *Ophthalmology* 103, 1271-5 (1996).
6. Topouzis, F. et al. Prevalence of open-angle glaucoma in Greece: the Thessaloniki Eye Study. *Am J Ophthalmol* 144, 511-9 (2007).
7. Foster, P.J. et al. Intraocular pressure and corneal biomechanics in an adult British population: the EPIC-Norfolk eye study. *Invest Ophthalmol Vis Sci* 52, 8179-85 (2011).
8. Carbonaro, F., Andrew, T., Mackey, D.A., Spector, T.D. & Hammond, C.J. Heritability of intraocular pressure: a classical twin study. *Br J Ophthalmol* 92, 1125-8 (2008).
9. Bach-Faig, A. et al. Mediterranean diet pyramid today. Science and cultural updates. *Public Health Nutr* 14, 2274-84 (2011).
10. van Koolwijk, L.M. et al. Common genetic determinants of intraocular pressure and primary open-angle glaucoma. *PLoS Genet* 8, e1002611 (2012).
11. Slabaugh, M.A. & Chen, P.P. The effect of cataract extraction on intraocular pressure. *Curr Opin Ophthalmol* 25, 122-6 (2014).
12. Foster, P.J. et al. Determinants of intraocular pressure and its association with glaucomatous optic neuropathy in Chinese Singaporeans: the Tanjong Pagar Study. *Invest Ophthalmol Vis Sci* 44, 3885-91 (2003).
13. Wu, S.Y. & Leske, M.C. Associations with intraocular pressure in the Barbados Eye Study. *Arch Ophthalmol* 115, 1572-6 (1997).
14. Bonomi, L. et al. Prevalence of glaucoma and intraocular pressure distribution in a defined population. The Egna-Neumarkt Study. *Ophthalmology* 105, 209-15 (1998).
15. Memarzadeh, F., Ying-Lai, M., Azen, S.P., Varma, R. & Los Angeles Latino Eye Study, G. Associations with intraocular pressure in Latinos: the Los Angeles Latino Eye Study. *Am J Ophthalmol* 146, 69-76 (2008).
16. Lin, H.Y. et al. Intraocular pressure measured with a noncontact tonometer in an elderly Chinese population: the Shihpai Eye Study. *Arch Ophthalmol* 123, 381-6 (2005).
17. Kawase, K. et al. Ocular and systemic factors related to intraocular pressure in Japanese adults: the Tajimi study. *Br J Ophthalmol* 92, 1175-9 (2008).
18. Tomoyose, E. et al. Intraocular pressure and related systemic and ocular biometric factors in a population-based study in Japan: the Kumejima study. *Am J Ophthalmol* 150, 279-86 (2010).
19. Suh, W., Kee, C., Namil Study, G. & Korean Glaucoma, S. The distribution of intraocular pressure in urban and in rural populations: the Namil study in South Korea. *Am J Ophthalmol* 154, 99-106 (2012).
20. Klein, B.E., Klein, R. & Linton, K.L. Intraocular pressure in an American community. The Beaver Dam Eye Study. *Invest Ophthalmol Vis Sci* 33, 2224-8 (1992).
21. Xu, L. et al. Intraocular pressure in Northern China in an urban and rural population: the Beijing eye study. *Am J Ophthalmol* 140, 913-5 (2005).
22. Tham, Y.C. et al. Global prevalence of glaucoma and projections of glaucoma burden through 2040: a systematic review and meta-analysis. *Ophthalmology* 121, 2081-90 (2014).
23. Day, A.C. et al. The prevalence of primary angle closure glaucoma in European derived populations: a systematic review. *Br J Ophthalmol* 96, 1162-7 (2012).
24. Jonas, J.B. et al. Body height, estimated cerebrospinal fluid pressure and open-angle glaucoma. The Beijing Eye Study 2011. *PLoS One* 9, e86678 (2014).
25. Prata, T.S., De Moraes, C.G., Kanadani, F.N., Ritch, R. & Paranhos, A., Jr. Posture-induced intraocular pressure changes: considerations regarding body position in glaucoma patients. *Surv Ophthalmol* 55, 445-53 (2010).
26. Lee, J.Y., Yoo, C., Jung, J.H., Hwang, Y.H. & Kim, Y.Y. The effect of lateral decubitus position on intraocular pressure in healthy young subjects. *Acta Ophthalmol* 90, e68-72 (2012).
27. Wang, D. et al. Intraocular pressure, central corneal thickness, and glaucoma in chinese adults: the liwan eye

- study. *Am J Ophthalmol* 152, 454-462 e1 (2011).
28. Jonas, J.B. et al. Intraocular pressure and associated factors: the central India eye and medical study. *J Glaucoma* 20, 405-9 (2011).
 29. Xu, L., Wang, H., Wang, Y. & Jonas, J.B. Intraocular pressure correlated with arterial blood pressure: the Beijing eye study. *Am J Ophthalmol* 144, 461-2 (2007).
 30. Dielemans, I. et al. Primary open-angle glaucoma, intraocular pressure, and systemic blood pressure in the general elderly population. The Rotterdam Study. *Ophthalmology* 102, 54-60 (1995).
 31. dos Santos, M.G., Makk, S., Berghold, A., Eckhardt, M. & Haas, A. Intraocular pressure difference in Goldmann applanation tonometry versus Perkins hand-held applanation tonometry in overweight patients. *Ophthalmology* 105, 2260-3 (1998).
 32. Klein, B.E., Klein, R. & Moss, S.E. Intraocular pressure in diabetic persons. *Ophthalmology* 91, 1356-60 (1984).
 33. Marcus, M.W., de Vries, M.M., Junoy Montolio, F.G. & Jansonius, N.M. Myopia as a risk factor for open-angle glaucoma: a systematic review and meta-analysis. *Ophthalmology* 118, 1989-1994 e2 (2011).
 34. Iwase, A. et al. The prevalence of primary open-angle glaucoma in Japanese: the Tajimi Study. *Ophthalmology* 111, 1641-8 (2004)

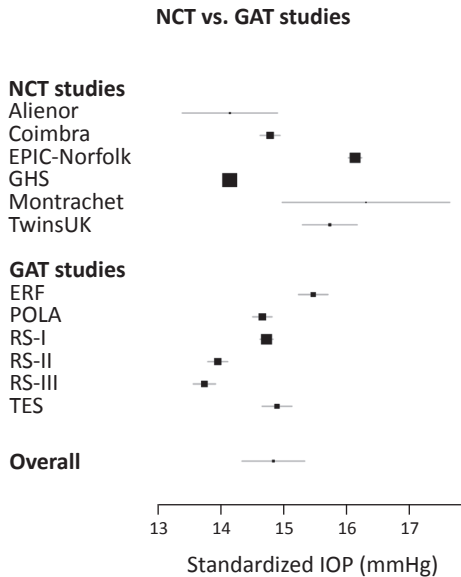
Supplementary Figure 1. Mean intraocular pressure (IOP) and 95% confidence intervals plotted for ordinal categories of explanatory variables.



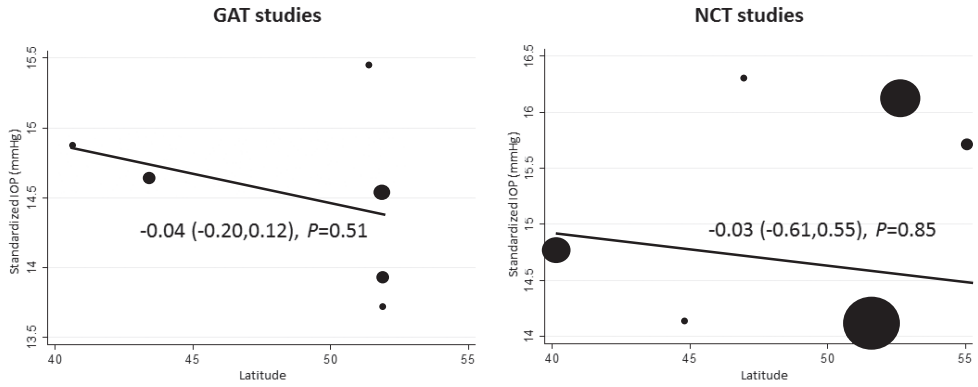
Supplementary Figure 2. Meta-regression for the association between latitude and standardized intraocular pressure (IOP).



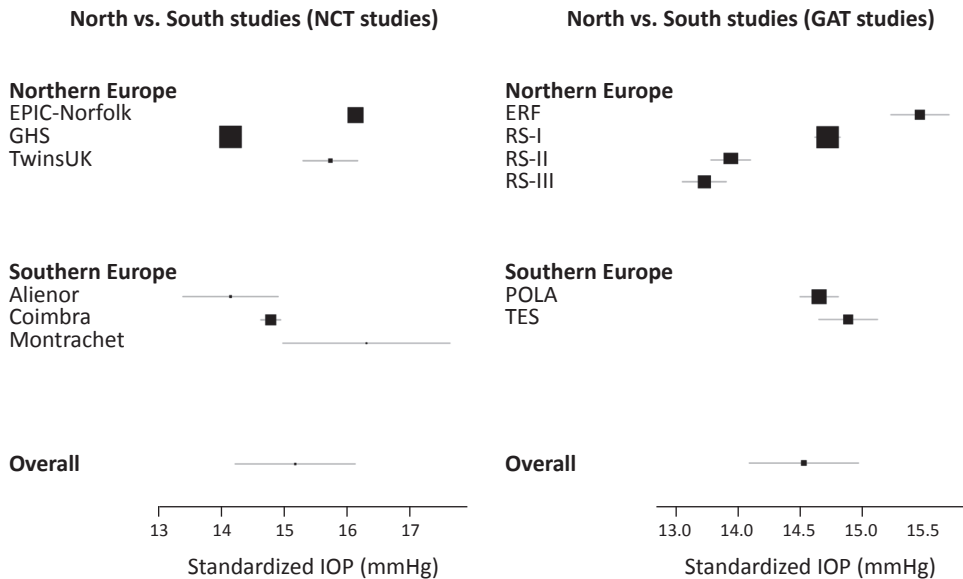
Supplementary Figure 3. Forest plots for standardized intraocular pressure (IOP), stratified by tonometry type and latitude. GAT – Goldmann applanation tonometry, NCT – non-contact tonometry.



Supplementary Figure 4. Meta-regressions for the association between latitude and standardized intraocular pressure (IOP), stratified by tonometry method. GAT = Goldmann applanation tonometry, NCT = non-contact tonometry.



Supplementary Figure 3. (continued)



SUPPLEMENTARY TEXT

The Alienor study

The Alienor (Antioxydants, Lipides Essentiels, Nutrition et maladies OculaiRes) Study is a population-based prospective study aiming at assessing the associations of age-related eye diseases (age-related maculopathy, glaucoma, cataract, dry eye syndrome) with nutritional factors (in particular antioxidants, macular pigment and fatty acids), determined from plasma measurements and estimation of dietary intakes. It also takes into account other major determinants of eye diseases, including gene polymorphisms, environmental factors and vascular factors. The methods of this study have been published elsewhere¹.

Subjects of the Alienor Study were recruited from an ongoing population-based study on the vascular risk factors for dementia, the Three-City (3C) Study². The 3C Study included 9,294 subjects aged 65 years or more from three French Cities (Bordeaux, Dijon and Montpellier), among whom 2,104 were recruited in Bordeaux. They were initially recruited in 1999-2001 and followed-up about every two years since. The Alienor Study consists of eye examinations, which are proposed to all participants of the 3C cohort in Bordeaux since the third follow-up (2006-2008). Among the 1,450 participants re-examined between October 2006 and May 2008, 963 (66.4%) participated in the Alienor Study's baseline eye examination. The design of this study has been approved by the Ethical Committee of Bordeaux (Comité de Protection des Personnes Sud-Ouest et Outre-Mer III) in May 2006.

Intraocular pressure (IOP) was measured with pneumotonometer (KT 800, Kowa, Japan). Central corneal thickness (CCT) was measured using Pachpen (Accutome Inc., Malvern Pa, USA). Refraction was measured using autorefractometer (Speedy K, Luneau, France) and refined subjectively when measuring best-corrected visual acuity. Cataract surgery was ascertained by the absence of the natural lens at slit lamp. Blood pressure was measured after the participant had been seated for at least 5 minutes. Systolic blood pressure was measured twice on the right arm using a digital electronic tensiometer (OMRON M4, France). The mean of two values was used for the analysis.

Coimbra Eye Study

The Coimbra Eye Study is a cross-sectional, single-center, population-based study. The study was approved by the ethics committee. Between August 2009 and April 2011, subjects aged 55 years or older were recruited from the primary healthcare center of Mira. All participants underwent complete bilateral ophthalmologic examination. Best-corrected visual acuity (BCVA) was tested in each eye separately using the Early Treatment Diabetic Retinopathy Study (ETDRS) chart. If the BCVA of either eye was less than logMAR 0.2 refraction was performed with an autorefractor - NIDEK TONOREF II (autoref/kerato/tonometer), and the amended BCVA was recorded. Evaluation also included anterior segment biomicroscopy, tonometry with the same NIDEK TONOREF II (autoref/kerato/tonometer), and colour fundus photography, after pharmacological mydriasis. Two 35° non-simultaneous stereoscopic color fundus photographs were taken from fields 1M (centered on the optic disc), 2 (centered on the macula) and 3M (temporal to the macula), using a digital mydriatic Topocon fundus camera (TRC-50EX; Topcon Corporation, Tokyo, Japan). Fundus reflex photographs were similarly obtained to document media opacities.

EPIC-Norfolk Eye Study

The European Prospective Investigation into Cancer (EPIC) study is a pan-European prospective cohort study designed to investigate the aetiology of major chronic diseases³. EPIC-Norfolk, one of the UK arms of EPIC, recruited and examined 25,639 participants aged 40-79 years between 1993 and 1997 for the baseline examination⁴. Recruitment was via general practices in the city of Norwich and the surrounding small towns and rural areas, and methods have been described in detail previously⁵. Since virtually all residents in the UK are registered with a general practitioner through the National Health Service, general practice lists serve as population registers. Ophthalmic assessment formed part of the third health examination and this has been termed the EPIC-Norfolk Eye Study⁶. In total, 8,623 participants were seen for the ophthalmic examination, between 2004 and 2011. The EPIC-Norfolk Eye Study was carried out following the principles of the Declaration of Helsinki and the Research Governance Framework for Health and Social Care. The study was approved by the Norfolk Local Research Ethics Committee (05/Q0101/191) and East Norfolk & Waveney NHS Research Governance Committee (2005EC07L).

IOP was measured using a non-contact instrument, the Ocular Response Analyser (ORA; Reichert, Corp., Buffalo, NY). Three readings were taken per eye and the best signal value of the Goldmann-correlated parameter used (based on the best quality pressure waveform as assessed by the ORA software). Height and weight were measured with participants wearing light clothing and no shoes. Height was measured to 0.1 cm using a stadiometer, and weight was measured to the nearest 0.1 kg using digital scales (Tanita UK Ltd., Middlesex, UK). Body mass index was calculated as weight/height². Blood pressure was measured with the participant seated resting using an objective measurement device (Accutorr Plus; Datascope Patient Monitoring, Mindray UK, Ltd., Huntington, UK) on two separate occasions during the health examination and the mean of the two measurements considered. Refractive error was measured using a Humphrey Auto-Refractor 500 (Humphrey Instruments, San Leandro, California, USA). Central corneal thickness was measured using ultrasound pachymetry in a subset of participants meeting referral criteria for a hospital clinic examination (Pachmate DGH 55; DGH Technology, Exton, PA; mean of 10 readings per eye).

Erasmus Rucphen Family (ERF) Study

The ERF Study is a family-based cohort in a genetically isolated population in the southwest of the Netherlands with over 3,000 participants aged between 18 and 86 years. The rationale and study design of this study have been described elsewhere^{7,8}. Cross-sectional examination took place between 2002 and 2005. IOP was measured with Goldmann applanation tonometry (Haag-Streit, Bern, Switzerland). IOP was measured twice per eye. If the two measurements in one eye differed, a third measurement was performed, and the median value was recorded. Refractive error was measured using a Topcon RM-A2000 autorefractor (non-dilated). Height and weight were measured with the participant in light underclothing. Blood pressure was measured twice on the right arm in a sitting position after at least 5 min rest using an automated device (OMRON 711). The average of the 2 measures was used in the analyses. All measurements in these studies were conducted after the Medical Ethics Committee of the Erasmus University had approved the study protocols.

Gutenberg Health Study

The Gutenberg Health Study (GHS) is an ongoing, population-based, prospective, observational cohort study in the Rhine-Main Region in midwestern Germany with a total of 15,010 participants⁹. The study sample was recruited from subjects aged between 35 and 74 years at the time of the examination. Exclusion criteria were insufficient knowledge of the German language to understand explanations and instructions, and physical or psychic inability to participate in the examinations in the study center.

All participants underwent an ophthalmological investigation of 25 minutes' duration taking place between 11:00 a.m. and 8:00 p.m. The IOP measurement was performed with a non-contact tonometer with automatic air-puff control (Nidek NT-2000™, Nidek Co., Japan)¹⁰. The mean of three measurements within a range of 3 mmHg was obtained for each eye. Refractive error was measured non-dilated using a Humphrey® Automated Refractor/Keratometer (HARK) 599 (Carl Zeiss Meditec, Jena, Germany). Central corneal thickness was measured by optical pachymetry (Scheimpflug imaging with the Pachycam™, Oculus, Wetzlar, Germany). The measurement with the best quality (at least above 90%) per eye was selected for analysis.

The systolic blood pressure was determined as mean value of two standardized measurements (Omron HEM 705-CP II, OMRON, Mannheim, Germany) after 8 and 11 minutes of rest. Calibrated digital scales (Seca 862, Seca Germany) and a measuring stick (Seca 220, Seca, Germany) were used to take anthropometric measurements.

The study was approved by the Medical Ethics Committee of the state chamber of physicians of Rhineland-Palatinate and by the local and federal data safety commissioners.

The Montrachet 3C Study

Subjects of the Montrachet (Maculopathy Optic Nerve nuTRition neurovAsCular and HEArT diseases) study were recruited from an ongoing population-based study, the Three-City (3C) study, on the vascular risk factors for dementia². The 3C-Study was designed to examine the relationship between vascular diseases and dementia in a community housing 9,294 persons aged 65 years and over. The participants were selected from the electoral rolls and were only urban since they lived in 3 French cities, Bordeaux, Dijon and Montpellier. The 3C-Study began in 1999 and participants were evaluated every two years. A subgroup underwent ocular assessment in Bordeaux (Alienor study; see above)¹ and Dijon (Montrachet study).

In Dijon 4,934 subjects participated to the first run of the 3C-Study in 1999. They were followed every 2 years and at the fourth run undertaken in 2006/2007 they were still 3,137. Among them, 1,604 (51.1%) underwent an MRI at baseline and at the fourth year. We decided to include preferentially the participants having had an MRI and to complete the recruitment with participants without MRI. Therefore from October 22th, 2009 until March 31th, 2013, 913 volunteers with an MRI were recruited in the Montrachet study and 236 without and MRI. After approval by the regional ethics committee, the study was registered as 2009-A00448-49. Intraocular pressure was measured by air tonometry (Tonoref II, Nidek, Aichi, Japan) and CCT was measured with an ultrasonic contact pachymeter (DGH 500, DGH Technology, Exton, PA, USA); the mean of 3 measurements was recorded for each eye. Refractive error was determined using an autorefractor without cycloplegia (Tonoref II, Nidek, Aichi, Japan). Height and weight were measured with participants wearing light clothes and no shoes. Systolic and diastolic blood pressures were recorded with a sphygmomanometer with participants resting seated for five minutes.

The POLA Study

The Pathologies Oculaires Liées à l'Age (POLA) Study is a population-based study aimed at identifying the risk factors of age-related eye diseases. The methods of this study have been published elsewhere¹¹. For inclusion in the study, participants needed to be a resident of Sète (South of France) and aged 60 years and over. According to the 1990 population census, there were almost 12,000 eligible residents, of whom our objective was to recruit 3,000. The population was informed of the study through the local media. We also contacted 4,543 residents individually by mail and telephone, using the electoral roll. The baseline examinations took place in a mobile unit equipped with ophthalmologic devices. Between June 1995 and July 1997, 2,584 participants were recruited. The study was approved by the ethics committee of the University Hospital of Montpellier, France.

One IOP measurement was performed with Goldmann applanation tonometry in each eye. Refractive error was measured using a Topcon RM-A7000 autorefractor, and refined subjectively when assessing best-corrected visual acuity. Systolic and diastolic blood pressures were measured at the right arm after the participant had been seated for at least 5 minutes. Cataract surgery was ascertained by the absence of the natural lens at slit lamp.

The Rotterdam Study I/II/III

The Rotterdam Study is a population-based study established in Rotterdam, the Netherlands¹². It consists of three cohorts. The original cohort, RS-I, started in 1990 and includes 7,983 subjects aged 55 years and older. The second cohort, RS-II, was added in 2000 and includes 3,011 subjects aged 55 years and older. The last cohort, RS-III, includes 3,932 subjects of 45 years of age and older and started in 2006. In all three cohorts, IOP was measured for both eyes with Goldmann applanation tonometry (Haag-Streit, Bern, Switzerland). The measurement was done twice. If the second measurement was different from the first measurement, a third measurement was performed and the median of all three values was taken. Refractive error was measured using a Topcon RM-A2000 autorefractor (non-dilated). A subset of participants from RS-I underwent CCT measurements at baseline using ultrasound pachymetry (Allergan Humphrey 850, Carl Zeiss Meditec, Dublin, CA, USA). Another subset of participants from RS-I, RS-II and RS-III underwent CCT measurements at follow-up using a non-contact biometer (Lenstar LS900, Haag-Streit, Köniz, Switzerland). Height and weight were measured with indoor clothing and no shoes. Blood pressure was measured after the participant had been seated for at least 5 minutes. Systolic blood pressure was measured twice on the right arm using a random-zero sphygmomanometer with a 14x38 cm cuff. The mean of two values was used for the analysis. Other ophthalmic baseline and follow-up examinations, which are still ongoing, were described previously¹³. The Rotterdam Study has been approved by the institutional review board (Medical Ethics Committee) of the Erasmus Medical Center and by the review board of The Netherlands Ministry of Health, Welfare and Sports.

Thessaloniki Eye Study

The Thessaloniki Eye Study (TES) is a cross-sectional, population-based, epidemiologic study of chronic eye diseases in the Greek population of Thessaloniki. According to the National Statistical Service of Greece, Thessaloniki which is a major urban center in Northern Greece is considered representative of the general population in the country.

The initial recruitment frame of the TES consisted of 5,000 people, 60 years of age or older, who were identified randomly in February 1999 from approximately 321,000 persons registered in the municipality registers of the city of Thessaloniki. Subject recruitment is described in detail elsewhere¹⁴. In summary, randomization was provided by the municipality statistical service. From the initial recruitment sample of the 5,000 names, 3,617 subjects were eligible and finally 2,554 participated in the study (participation rate 71%)¹⁵. Study examination and data collection ended in March 2005. The study was approved by the Aristotle University Hospital Ethics Committee and the University of California Los Angeles Human Subject Protection Committee.

Visual acuity was measured with the Early Treatment of Diabetic Retinopathy Study (ETDRS) charts. If visual acuity was less than 20/30 with habitual correction, a full refraction was performed, and best-corrected visual acuity was measured. Intraocular pressure (IOP) was measured using a calibrated Goldmann applanation tonometer (Haag-Streit, Bern, Switzerland). The mean IOP of three readings in each eye was defined as the pressure for that eye. Blood pressure (BP) was considered as the average of two readings taken with an automated sphygmomanometer (model 705CP; OMRON Matsusaka Co Ltd, Matsusaka City, Japan) at least five minutes apart in the same arm, with the cuff approximately level with the heart. The readings were obtained before instillation of mydriatic drops and after the participant was seated for 10 minutes. Somatometric data were also measured as part of the TES protocol: Height and weight were measured with participants wearing light clothing and shoes. Height was measured using a stadiometer, and weight was measured using a 351 TERRAIL digital scales. Central corneal thickness was measured using ultrasound pachymetry in a subset of participants (A-scan, Quantel Medical, France; mean of 5 readings per eye).

TwinsUK

The TwinsUK adult twin registry, based at St. Thomas' Hospital in London, comprises over 12,000 predominantly female Caucasian ancestry twins, from throughout the United Kingdom¹⁶. Twins largely volunteered unaware of the eye studies at the time of enrolment and gave fully informed consent under a protocol reviewed by the St. Thomas' Hospital Local Research Ethics Committee (EC04/015), which was performed in accordance with the Helsinki Declaration.

Various eye phenotypes have been collected on a subset of twins. IOP was measured between 2006 and 2010 with a non-contact air-puff tonometer, the Ocular Response Analyser (ORA, Reichert®, Buffalo, NY). The mean (Goldmann-equivalent) IOP was calculated from 4 readings (2 from each eye) for each participant; where quality indicators were poor or the two IOPs differed by more than 2mmHg, a third reading was taken. CCT was measured using an ultrasound pachymetry device provided with the ORA instrument. Refractive error was measured using non-cycloplegic autorefractometry (ARM-10 autorefractor, Takagi Seiko, Japan). Blood pressure (measured three times with the automated Omron blood pressure machine, and the mean of second and third blood pressures used), height and weight were measured as part of other phenotype study visits. These examinations were not always performed on the same day as the eye examination, but in 87% of individuals measurements were recorded within a year of the eye examination. Body mass index was calculated as weight/height².

References

1. Delcourt, C. et al. Nutrition and age-related eye diseases: the Alienor (Antioxydants, Lipides Essentiels, Nutrition et maladies OculaiRes) Study. *J Nutr Health Aging* 14, 854-61 (2010).
2. 3C Study Group. Vascular factors and risk of dementia: design of the Three-City Study and baseline characteristics of the study population. *Neuroepidemiology* 22, 316-25 (2003).
3. Riboli, E. & Kaaks, R. The EPIC Project: rationale and study design. *European Prospective Investigation into Cancer and Nutrition. Int J Epidemiol* 26 Suppl 1, S6-14 (1997).
4. Day, N. et al. EPIC-Norfolk: study design and characteristics of the cohort. *European Prospective Investigation of Cancer. Br J Cancer* 80 Suppl 1, 95-103 (1999).
5. Hayat, S.A. et al. Cohort profile: A prospective cohort study of objective physical and cognitive capability and visual health in an ageing population of men and women in Norfolk (EPIC-Norfolk 3). *Int J Epidemiol* 43, 1063-72 (2014).
6. Khawaja, A.P. et al. The EPIC-Norfolk Eye Study: rationale, methods and a cross-sectional analysis of visual impairment in a population-based cohort. *BMJ Open* 3(2013).
7. Aulchenko, Y.S. et al. Linkage disequilibrium in young genetically isolated Dutch population. *Eur J Hum Genet* 12, 527-34 (2004).
8. Pardo, L.M., MacKay, I., Oostra, B., van Duijn, C.M. & Aulchenko, Y.S. The effect of genetic drift in a young genetically isolated population. *Ann Hum Genet* 69, 288-95 (2005).
9. Wild, P.S. et al. [The Gutenberg Health Study]. *Bundesgesundheitsblatt Gesundheitsforschung Gesundheitsschutz* 55, 824-9 (2012).
10. Hoehn, R. et al. Distribution of intraocular pressure and its association with ocular features and cardiovascular risk factors: the Gutenberg Health Study. *Ophthalmology* 120, 961-8 (2013).
11. Delcourt, C., Diaz, J.L., Ponton-Sanchez, A. & Papoz, L. Smoking and age-related macular degeneration. The POLA Study. *Pathologies Oculaires Liees a l'Age. Arch Ophthalmol* 116, 1031-5 (1998).
12. Hofman, A. et al. The Rotterdam Study: 2016 objectives and design update. *Eur J Epidemiol* 30, 661-708 (2015).
13. Wolfs, R.C. et al. Changing views on open-angle glaucoma: definitions and prevalences--The Rotterdam Study. *Invest Ophthalmol Vis Sci* 41, 3309-21 (2000).
14. Topouzis, F. et al. Association of blood pressure status with the optic disk structure in non-glaucoma subjects: the Thessaloniki eye study. *Am J Ophthalmol* 142, 60-67 (2006).
15. Topouzis, F. et al. Prevalence of open-angle glaucoma in Greece: the Thessaloniki Eye Study. *Am J Ophthalmol* 144, 511-9 (2007).
16. Moayyeri, A., Hammond, C.J., Hart, D.J. & Spector, T.D. The UK Adult Twin Registry (TwinsUK Resource). *Twin Res Hum Genet* 16, 144-9 (2013).

PART 4

**GENETICS OF INTRAOCULAR
PRESSURE AND OPTIC NERVE
HEAD MEASUREMENTS**

CHAPTER 4.1

Genome-wide analysis of multi-ancestry cohorts identifies new loci influencing intraocular pressure and susceptibility to glaucoma



Pirro G Hysi*, Ching-Yu Cheng*, Henriët Springelkamp*, Stuart Macgregor*, Jessica N Cooke Bailey*, Robert Wojciechowski*, Veronique Vitart, Abhishek Nag, Alex W Hewitt, René Höhn, Cristina Venturini, Alireza Mirshahi, Wishal D. Ramdas, Gudmar Thorleifsson, Eranga Vithana, Chiea-Chuen Khor, Arni B Stefansson, Jiemin Liao, Jonathan L Haines, Najaf Amin, Ya Xing Wang, Philipp S Wild, Ayse B Ozel, Jun Z Li, Brian W Fleck, Tanja Zeller, Sandra E Staffieri, Yik-Ying Teo, Gabriel Cuellar-Partida, Xiaoyan Luo, R Rand Allingham, Julia E Richards, Andrea Senft, Lennart C Karssen, Yingfeng Zheng, Céline Bellenguez, Liang Xu, Adriana I Iglesias, James F Wilson, Jae H Kang, Elisabeth M van Leeuwen, Vesteyn Jonsson, Unnur Thorsteinsdottir, Dominiek D.G. Despriet, Sarah Ennis, Syoko E Moroi, Nicholas G Martin, Nomdo M Jansonius, Seyhan Yazar, E-Shyong Tai, Philippe Amouyel, James Kirwan, Leonieke M.E. van Koolwijk, Michael A Hauser, Fridbert Jonasson, Paul Leo, Stephanie J Loomis, Rhys Fogarty, Fernando Rivadeneira, Lisa Kearns, Karl J Lackner, Paulus T.V.M. de Jong, Claire L Simpson, Craig E Pennell, Ben A Oostra, André G Uitterlinden, Seang-Mei Saw, Andrew J Lotery, Joan E Bailey-Wilson, Albert Hofman, Johannes R Vingerling, Cécilia Maubaret, Norbert Pfeiffer, Roger C.W. Wolfs, Hans G Lemij, Terri L Young, Louis R Pasquale, Cécile Delcourt, Timothy D Spector, Caroline C.W. Klaver, Kerrin S Small, Kathryn P Burdon, Kari Stefansson, Tien-Yin Wong, BMES GWAS Group, NEIGHBORHOOD Consortium, Wellcome Trust Case Control Consortium, Ananth Viswanathan‡, David A Mackey‡, Jamie E Craig‡, Janey L Wiggs‡, Cornelia M van Duijn‡, Christopher J Hammond‡, Tin Aung‡.

* These authors contributed equally.

‡ These authors jointly directed this work.

Nat Genet. 2014 Oct;46(10):1126-30. doi: 10.1038/ng.3087

Supplementary files and figures can be found at:

<http://www.nature.com/ng/journal/v46/n10/full/ng.3087.html>

ABSTRACT

Elevated intraocular pressure (IOP) is an important risk factor in developing glaucoma, and variability in IOP might herald glaucomatous development or progression. We report the results of a genome-wide association study meta-analysis of 18 population cohorts from the International Glaucoma Genetics Consortium (IGGC), comprising 35,296 multi-ancestry participants for IOP. We confirm genetic association of known loci for IOP and primary open angle glaucoma (POAG) and identify four new IOP-associated loci located on chromosome 3q25.31 within the *FNDC3B* gene ($P=4.19 \times 10^{-8}$ for rs6445055), two on chromosome 9 ($P=2.80 \times 10^{-11}$ for rs2472493 near *ABCA1* and $P=6.39 \times 10^{-11}$ for rs8176693 within *ABO*) and one on chromosome 11p11.2 (best $P=1.04 \times 10^{-11}$ for rs747782). Separate meta-analyses of 4 independent POAG cohorts, totaling 4,284 cases and 95,560 controls, showed that 3 of these loci for IOP are also associated with POAG.

INTRODUCTION

Primary open angle glaucoma (POAG) is the leading cause of irreversible blindness in the world¹. The only modifiable risk factor for the development and progression of glaucoma is high intraocular pressure (IOP)², and lowering IOP is currently the only therapy that can reduce glaucomatous progression, even in forms of glaucoma that have IOP close to the statistical norm for the population (normal-tension glaucoma, or NTG)^{3,4}. POAG and IOP are highly heritable; the lifetime risk of developing POAG is 22% among first degree relatives of cases⁵, which is approximately ten times higher than the risk for the rest of the population¹. Heritability for IOP is estimated to be approximately 55%⁶. Genetic studies have shown that the genetic risk for POAG and IOP are partly shared; polymorphisms within the *TMCO1* gene are associated with both POAG risk⁷ and IOP⁸. Studying genetic determinants of IOP is therefore likely to provide critical insights into the genetic architecture of POAG and open new avenues for therapeutic intervention.

In this study, we present the results from a meta-analysis of genome-wide association studies (GWAS) of IOP from 18 studies participating in the International Glaucoma Genetics Consortium (IGGC) and an assessment of the importance of the genetic findings for susceptibility to POAG (Figure 1). The IOP meta-analysis include 35,296 subjects (7,738 Asians and 27,558 of European descent) drawn from the general populations of 7 countries. The demographic characteristics of these population-based cohorts are given in Supplementary Table 1. Genotyping assays and imputation to HapMap2 haplotypes were performed at individual sites. Association analyses were performed using an additive model with IOP as the outcome and the number of alleles at each polymorphic site as the predictor, adjusting for age and sex. IOP levels for participants who were receiving IOP-lowering therapy at the time of the study and for whom data on baseline, pretreatment levels were not available were imputed as previously described⁸. Subjects who had undergone surgery or had other eye diseases that could affect IOP were excluded (Supplementary Note). Secondary analyses were carried out adjusting for central corneal thickness (CCT), which is known to influence IOP measurements⁹.

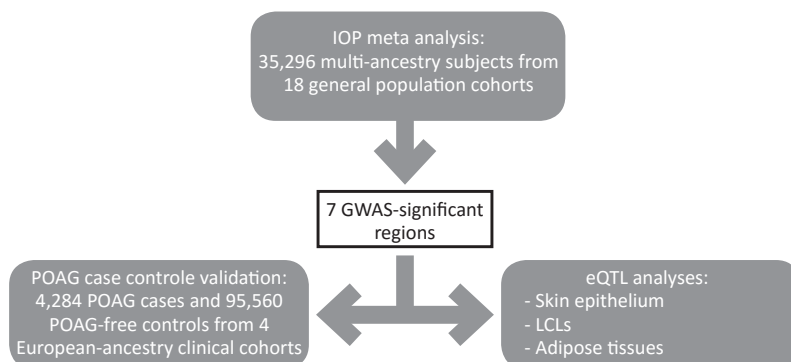


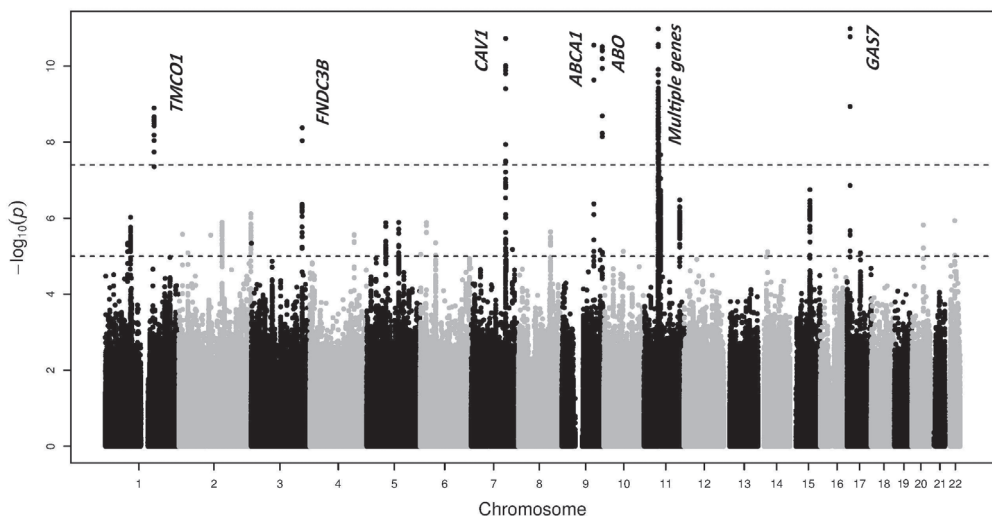
Figure 1. Flow chart of the analyses. Associated SNPs in a meta-analysis of IOP in participants from 18 general-population cohorts were validated in 4 clinical case-control cohorts and examined for transcription regulation activity in 3 tissues from 856 white British subjects.

RESULTS AND DISCUSSION

After applying conventional quality control filters, we performed a fixed effects meta-analysis of the 22 autosomes across the cohorts with approximately 2.5 million markers. Within-study genomic inflation factors¹⁰ ranged between 0.992 and 1.043 (Supplementary Table 2 and Supplementary Figure 1), indicating a lack of major population stratification bias within each study. SNPs available in fewer than 16 cohorts or showing large effect heterogeneity (defined as $I^2 > 75\%$ ¹¹) were removed. We found 145 SNPs (Supplementary Table 3) whose association crossed the conventional genome-wide significance threshold of association ($P < 5 \times 10^{-8}$)¹². All of these SNPs clustered around seven separate regions of the genome (Figure 2). Two of the regions associated with IOP in our meta-analysis had previously been implicated in IOP variability: the region near the *TMCO1* locus^{7,8} ($P = 2.19 \times 10^{-9}$ for rs7555523), and near the *GAS7* gene⁸ ($P = 1.03 \times 10^{-11}$ for rs9913911). A third associated locus, new for IOP, was near the *CAV1* and *CAV2* genes ($P = 1.87 \times 10^{-11}$ for rs10258482) which had previously been associated with POAG¹³.

New associations were identified within a large linkage disequilibrium (LD) block on chromosome 11 encompassing, among other genes, *AGBL2*, *SPI1* and *PTPRJ* (best $P = 1.04 \times 10^{-11}$ for rs747782) (Supplementary Figure 1). Two additional loci were mapped on chromosome 9: one at 9q31.1 upstream of *ABCA1* ($P = 2.80 \times 10^{-11}$ for rs2472493) and the other at 9q34.2 within the *ABO* blood group gene ($P = 3.08 \times 10^{-11}$ for rs8176743). A fourth region was detected on 3q25.31, within *FNDC3B* ($P = 4.19 \times 10^{-8}$ for rs6445055).

Figure 2. Manhattan plot of the results from the meta-analysis of data from 18 multi-ancestry cohorts from IGGC.



The 22 autosomes are plotted along the x axis, and the values on the y axis denote the $-\log_{10}$ -transformed p-values from the meta-analysis of association with IOP observed for each of the SNPs.

Interestingly, of all the loci previously associated with glaucoma or related quantitative traits¹⁴, *CDKN2B-AS1* and *SIX1/SIX6* were not associated with IOP in the meta-analysis. It is possible that these two loci exert their influence on PAOG through mechanisms unrelated to IOP.

Genome-wide significant SNPs from the IOP meta-analysis were then investigated for their effect on the clinical outcome of POAG in 4 independent cohorts representing a combined 4,284 POAG cases (NTG and high-tension glaucoma) and 95,560 controls (details about these cohorts in the Supplementary Information). Associations with POAG were found for the newly discovered regions near *ABCA1* ($P=4.15 \times 10^{-9}$ for rs2472493), near *FNDC3B* ($P=0.03$ for rs6445055) and at the chromosome 11 cluster ($P=0.008$ for rs12419342). We did not find significant statistical evidence of association of POAG with the *ABO* locus. The case-control analyses reinforced association evidence at the previously identified loci on *TMCO1* ($P=1.34 \times 10^{-16}$ for rs7555523), *CAV1/CAV2* ($P=6.27 \times 10^{-9}$ for rs10258482) and *GAS7* ($P=5.22 \times 10^{-13}$ for rs12150284). All alleles associated with higher IOP levels also increased glaucoma risk (Table 1).

We then examined whether the effect sizes of SNPs on IOP levels (β_{IOP}) were linearly related to their effect sizes on POAG (β_{POAG}) using a causal inference framework as previously described¹⁵. In a linear regression analysis, we observed a significant association between β_{IOP} and β_{POAG} ($P=0.03$, Supplementary Table 4), suggesting that the strength of a SNPs' effect on IOP levels is correlated with its effects on risk for POAG.

We subsequently investigated the relationship between variants within the seven regions associated with IOP and *cis* regulation of mRNA expression in three tissues (adipose, lymphoblastoid cell lines [LCLs] and skin) from a sample of 856 British subjects¹⁶. The most significant expression quantitative trait locus (eQTL) associations were generally observed in LCLs for most loci, except for *CAV1*, where effects were strongest in adipose and skin tissues (Table 2). Significant eQTL association was observed for rs4656461 and rs7555523 ($P=0.003$ and $P=0.0001$ with *TMCO1* and *ALDH9A1* transcript expressions in skin and LCLs respectively), rs2024211 ($P=5.43 \times 10^{-16}$ and $P=3.84 \times 10^{-13}$ with *CAV1* transcript levels in adipose and skin tissues, respectively), rs2472493 ($P=3.67 \times 10^{-5}$ with *ABCA1* transcript levels in LCLs) and rs1681630 on chromosome 11 ($P=2.72 \times 10^{-10}$ with the *SPI1* transcript levels in LCLs), among others (Table 2, Supplementary Table 5A). These SNPs also had the strongest eQTL effects for their respective transcripts (Supplementary Table 5B).

We measured the mRNA expression levels of the identified genes in adult ocular tissues using RT-PCR. We found that most of the identified genes, including *TMCO1*, *FNDC3B*, *CAV1/CAV2*, *ABCA1* and *GAS7*, were expressed in most ocular tissues (Supplementary Table 6). The genes within the chromosome 11 locus showed varied expression levels across ocular tissues. Gene-based tests or enrichment for Gene Ontology terms did not identify any new genes or pathways after correction for multiple testing (Supplementary Tables 7 and 8).

Altogether, these SNPs explain approximately 1.2% of the heritability for IOP in the TwinsUK cohort¹⁷, 1.5% of the IOP phenotypic variability in the Rotterdam study¹⁸ and between 0.6 and 1.2% of the phenotypic variability in Asians. *FNDC3B* has been associated with CCT¹⁹,

Table 1. Results for association with IOP from the general-population cohorts for SNPs significant at a multiple-testing correction level ($P < 5 \times 10^{-8}$) and their association with POAG in case-control validation meta-analyses.

SNP			Association with IOP in the discovery cohort				Association in POAG case-control cohorts		
Chr/position	rsID	A1/A2	Nearest gene	β	SE	P-value	Heterogeneity I^2	OR (95% CI)	P-value
1/165687205	rs4656461	G/A	<i>TMCO1</i>	0.228	0.039	6.51×10^{-9}	0.46	1.38 (1.28-1.50)	2.55×10^{-15}
1/165718979	rs7555523	C/A	<i>TMCO1</i>	0.235	0.039	2.19×10^{-9}	0.55	1.40 (1.30-1.52)	1.34×10^{-16}
3/171992387	rs6445055	A/G	<i>FNDCC3B</i>	-0.177	0.030	4.19×10^{-8}	0.17	0.92 (0.85-0.99)	0.03
7/116150095	rs10258482	A/C	<i>CAV1</i>	0.196	0.029	1.87×10^{-11}	0.81	1.20 (1.13-1.28)	6.27×10^{-9}
7/116150952	rs10262524	A/C	<i>CAV1</i>	0.186	0.029	9.69×10^{-11}	0.67	1.20 (1.13-1.28)	1.39×10^{-8}
9/107695848	rs2472493	G/A	<i>ABCA1</i>	0.159	0.024	2.80×10^{-11}	4×10^{-5}	1.24 (1.16-1.34)	4.15×10^{-9}
9/136131415	rs8176743	T/C	<i>ABO</i>	0.261	0.039	3.08×10^{-11}	0.53	1.07 (0.96-1.19)	0.20
11/47468545	rs12419342	C/T	<i>RAPSN</i>	0.153	0.026	4.77×10^{-9}	0.75	1.09 (1.02-1.16)	0.008
11/47940925	rs747782	C/T	<i>NUP160, PTPRJ</i>	0.203	0.030	1.04×10^{-11}	0.95	1.03 (0.96-1.11)	0.36
11/47969152	rs1681630	T/C	<i>PTPRJ</i>	0.144	0.026	1.69×10^{-8}	0.60	1.06 (0.99-1.12)	0.08
11/48004369	rs7946766	T/C	<i>PTPRJ</i>	0.230	0.035	2.71×10^{-11}	0.35	1.03 (0.95-1.12)	0.43
17/10031183	rs9913911	G/A	<i>GAS7</i>	-0.179	0.026	1.03×10^{-11}	4×10^{-4}	0.80 (0.75-0.85)	2.98×10^{-13}

ABBREVIATIONS

A1/A2	reference/alternative alleles	OR	odds ratio
β	linear regression coefficient (mmHg)	POAG	primary open-angle glaucoma
Chr	chromosome	SE	standard error of the regression coefficient (mmHg)
IOP	intraocular pressure	SNP	single nucleotide polymorphism
		95% CI	95% confidence interval for OR

Table

				eQTL effect p values			
SNP	A1/A2	Nearest gene	Adipose	LCLs	Skin	Probe ID	Gene
Chr/position	rsID						
1/165687205	rs4656461	TMCO1	0.004	0.12	0.003	ILMN_1793829	TMCO1
1/165718979	rs7555523	TMCO1	0.39	0.0001	0.05	ILMN_1761804	ALDH9A1
3/171992387	rs6445055	FNDC3B	NS	NS	NS	-	-
7/116150095	rs10258482	CAV1	NS	NS	NS	-	-
7/116150952	rs10262524	CAV1	5.79x10 ⁻¹⁶	8.54x10 ⁻⁵	3.91x10 ⁻¹³	ILMN_1687583	CAV1
9/107695848	rs2472493	ABCA1	0.19	3.67x10 ⁻⁵	0.36	ILMN_1766054	ABCA1
9/136131415	rs8176743	ABO	NS	NS	NS	-	-
11/47468545	rs12419342	RAPSN	0.002	4.32x10 ⁻⁸	0.0003	ILMN_1696463	SPI1
11/47940925	rs747782	NUP160, PTPRJ	NS	NS	NS	-	-
11/47969152	rs1681630	PTPRJ	0.006	2.72x10 ⁻¹⁰	0.002	ILMN_1696463	SPI1
11/48004369	rs7946766	PTPRJ	0.66	2.02x10 ⁻⁵	0.0066	ILMN_1688627	AGBL2
17/10031183	rs9913911	GAS7	NS	NS	NS	-	-

ABBREVIATIONS

- A1/A2 reference/alternative alleles
- Chr chromosome
- LCLs lymphoblastoid cell lines
- NS no significant association detected
- SNP single nucleotide polymorphism

and, as CCT has a significant effect on IOP measurements²⁰, we performed an additional meta-analysis of IOP adjusted for age, sex and CCT in a smaller subsample that had CCT measures (19,563 subjects from 13 population cohorts). The association for rs6445055 remained nominally significant, although it was weaker ($P=9.87\times 10^{-4}$, $\beta=-0.121$ in comparison to -0.177 before adjustment for CCT). This finding suggests that this locus has at least some CCT-independent effect over IOP levels. The association evidence remained consistent, although slightly weaker, for the other loci (Supplementary Table 9).

We report association of variants within the *ABCA1* gene with IOP and POAG. A strong eQTL effect was observed in LCLs ($P=3.67\times 10^{-5}$) for the most highly associated SNP (rs2472493) in our analyses. *ABCA1* is expressed in many tissues²¹ and its expression in leukocytes is significantly up-regulated in glaucoma patients²².

Associations for a number of SNPs within the ABO blood group gene and IOP, although statistically significant and homogeneous across the participating cohorts, were not observed in the glaucoma case-control meta-analysis. This might be owing to type I error in the initial meta-analysis or insufficient power to detect a primarily IOP-led effect in cases that included individuals with NTG, resulting in a type II error in the latter analysis. Four of the nine GWAS polymorphisms associated at genome-wide significance in the ABO locus were non-synonymous variants, determining the B blood group²³. This finding might be relevant, given previous observations that the B blood group is epidemiologically associated with glaucoma, including POAG²⁴, although the mechanisms remain unclear.

Association was found between IOP and variants lying over a large region on chromosome 11. Of the many genes in that region, eQTL analyses singled out *SPI1* and *AGBL2* as possible candidates for prioritization in future studies. eQTL analyses also raised the possibility of *ALDH9A1* as a candidate for IOP regulation, given its strong expression in ciliary body²⁵ and location just downstream of the *TMCO1*-associated variant. The eQTL results also suggest that *CAV1* is a stronger candidate than *CAV2*, although transcription regulation might not be the only mechanism influencing IOP at this locus.

Although IOP and POAG are strongly genetically correlated²⁶, we further explored their shared genetic backgrounds. Using independent SNPs (not in LD) with association $P < 10^{-6}$ in the IOP GWAS meta-analysis as described elsewhere²⁷, we found a statistically significant polygenic overlap between IOP and POAG in the ANZRAG cohort ($P=4.33\times 10^{-5}$). The variance explained in POAG was 0.7%, which changed little if less significant SNPs were progressively included in the model (Supplementary Table 10).

There are potential limitations to this study. First, there was variability across the studies in terms of IOP measurement methods, although the differences are likely to be small²⁸. In addition, we maximized power to discover genetic variants of small effect size by including multi-ancestry cohorts, at the risk of introducing heterogeneity into the study. Heterogeneity was however generally low (Table 1) for most of the loci reported, so we consider our results to be conservative. Second, assessment of clinical importance using panels of POAG cases is not equivalent to a formal replication. Even in this case, we expect our results to be conservative at the price of reduced sensitivity, which could be a possible reason for non-

validation of our associations with IOP in the *ABO* blood group locus. Finally, we based our eQTL analysis on sample tissue availability rather than analyzing the ideal ocular tissue types. Tissues such as trabecular meshwork would have been preferable, but they are impractical because they are generally less accessible. We tried to circumvent this limitation by studying three different tissues, but caution is required when interpreting eQTL results.

Despite these considerations, our report of seven loci associated with IOP and glaucoma, of which four are newly discovered, is a key step toward better understanding the mechanisms of IOP regulation, currently the only modifiable risk factor for POAG.

METHODS

IGGC participants

All studies participating in this meta-analysis are part of the International Glaucoma Genetics Consortium. The discovery cohorts included 27,558 individuals of European ancestry from 14 studies (ALIENOR, BATS, BMES^{29,30}, ERF^{31,32}, Framingham Family Study³³, GHS1, GHS2, ORCADES³⁴, RAINE³⁵⁻³⁷, RS-I, RS-II, RS-III³⁸, TEST³⁹ and TwinsUK⁴⁰). In addition, 7,738 individuals of Asian ancestry from four cohorts (BES⁴¹, SCES⁴², SiMES⁴³, SINDI⁴²) were included. In addition, four case-control population panels were used, all of European ancestry: ANZRAG⁷, MEEI, NEIGHBOR and deCode. General methods, demographics and phenotyping of the study cohorts have previously been described extensively and are provided briefly in Supplementary Table 1 (see Supplementary Note for more details). All studies were performed with the approval of their local Medical Ethics Committees and written informed consent was obtained from all participants in accordance with the Declaration of Helsinki.

Phenotype measurements

Eligible participants underwent an ophthalmologic examination including measurements of IOP and, for most but not all studies, measurements of central corneal thickness (CCT). Each participating cohort was phenotyped separately and IOP measurement methods used by each are described in the Supplementary Table 1.

Genotyping & imputation

The study samples were genotyped on either the Illumina (San Diego, CA, USA) or Affymetrix (Santa Clara, CA, USA) platforms. Each study performed single nucleotide polymorphism (SNP) imputation using the genotype data, together with the HapMap Phase II ethnically matched reference panels (CEU, JPT+CHB, or the 4 HapMap populations) on the basis of build 36 databases (release 22 or 24). The Markov Chain Haplotyping software, IMPUTE^{44,45} or MACH⁴⁶, were adopted for imputation. A detailed description regarding genotyping platforms and imputation procedures for each study is provided on Supplementary Table 1. Stringent quality control of genotype data was applied in each cohort. Samples with low call rates (<95%) or with gender discrepancies were excluded. Cryptically related samples and outliers in population structure from principal component analyses were also excluded. SNPs flagged with missingness >5%, gross departure from Hardy Weinberg Equilibrium (p-value <10⁻⁶) and minor allele frequency (MAF) <1% were removed from further analyses.

Statistical analysis

For each study, an allele-dosage regression model at each directly genotyped or imputed SNP was conducted to determine its association with IOP. Eyes with prior glaucoma surgery or laser were excluded. For subject receiving IOP-lowering medication, we added 25% to the measured IOP levels to estimate pre-treatment IOP, based on a reported average of 17% to 33% IOP reduction caused by IOP lowering medication in a meta-analysis of clinical trials⁴⁷. The mean of the right and left IOP measurements was used. When data from only one eye were available, the IOP measurement from the available eye was used.

For the analyses, we assumed an additive genetic model where the dosage of each SNP is a continuous variable ranging from 0 to 2 for minor alleles carried. Primary analysis for IOP was adjusted for age and sex. Additional adjustment for principal components was carried out by a few participating cohorts to correct for subtle population substructure.

Per-SNP meta-analyses were performed using the GWAMA software with weighted inverse-variance approach, assuming fixed effects, as for initial discovery purposes as the fixed-effects model is preferred for increased statistical power⁴⁸. A Cochran's Q test and I^2 were used to assess heterogeneity across studies⁴⁹. For each participating cohort, only SNPs with sufficient imputation quality scores (proper-info of IMPUTE or R^2 of MACH >0.3) were included into the meta-analysis.

Gene-based testing was conducted using VEGAS software⁵⁰ on the European ancestry and Asian ancestry meta-analysis results separately. VEGAS incorporates information from the full set of markers within a gene and accounts for LD between markers by using simulations from the multivariate normal distribution. For samples of European descent, we used the HapMap 2 CEU population as the reference to estimate patterns of LD. For Asian ancestry groups, we used the combined HapMap 2 JPT and CHB populations as the reference population to approximate LD patterns. To include gene regulatory regions, SNPs were included if they fell within 50 kb of a gene. We performed meta-analysis on the two sets of gene-based P-values using Fisher's method.

VEGAS-Pathway analysis^{19,50} was carried out using prespecified pathways from Gene Ontology. Pathways of with 10 to 1,000 components were selected, yielding 4,628 pathways. Pathway analysis was based on combining gene-based test results from VEGAS. Pathway p-values were computed by summing χ^2 test statistics derived from VEGAS p-values. Empirical VEGAS-Pathway p-values for each pathway were computed by comparing the summed χ^2 test statistics from real data with those generated in 500,000 simulations where the relevant number (according to the size of the pathway) of randomly drawn χ^2 test statistics was summed. To ensure that clusters of genes did not adversely affect results, within each pathway, gene sets were pruned such that each gene was >500 kb away from all other genes in the pathway. Where required, all but one of the clustered genes was dropped at random when genes were clustered. We performed meta-analysis on the two sets of pathway p-values using Fisher's method.

To investigate shared genetic background by using a large number of autosomal SNPs, we performed a systematic evaluation of the overlap between IOP and POAG on the basis of

profile scores, following previously described approaches²⁷. We estimated the relative risk for each SNP of interest on the basis of a discovery set (IOP), with a profile score computed for every individual in a target set of interest (POAG). For each target set individual, the profile score was computed as the number of risk alleles weighted by the effect size estimated in the discovery set. The discovery set comprised the European ancestry-derived samples from our meta-analysis, and the target set was a set of 590 glaucoma cases and 3,956 controls, as previously described⁷. To ensure that there was not a high degree of dependence between the SNPs included in the profile score, we filtered the set of SNPs used in the profile score so that only a set of 149,571 SNPs in LD ($r^2 < 0.5$) was used. We constructed models progressively including more SNPs by lowering the threshold of inclusion (i.e. $P < 0.000001$, $P < 0.00001$, $P < 0.0001$, $P < 0.001$, $P < 0.01$, $P < 0.1$, $P < 0.05$). Profiles derived from IOP SNP effects were tested for association with the phenotype (here, POAG) using a logistic regression. Variance explained was assessed using Nagelkerke's pseudo R^2 measure⁵¹.

To assess whether and to what degree IOP levels confer POAG risk, we performed a causal inference analysis using an instrumental variable framework as previously described¹⁵. In brief, we obtained estimates of effect size (β_{IOP}) for the association of a given SNP with IOP from the meta-analysis of the 18 discovery cohorts. For the association of a given SNP with POAG, we obtained estimates of the effect size (β_{POAG}) from the four case-control panels as described above. We selected the SNP with the strongest association from each of the loci with genome-wide significant association with IOP that we identified. To assess whether the strength of a SNP's association with IOP predicted risk of POAG, we conducted linear regression analysis using the effect size of each SNP for IOP (β_{IOP}) as an independent variable and the effect size for POAG (β_{POAG}) as a dependent outcome variable. A total of seven independent IOP-associated SNPs were used for this analysis, including rs7555523 (*TMCO1*), rs6445055 (*FNDC3B*), rs10258482 (*CAV1*), rs2472493 (*ABCA1*), rs8176743 (*ABO*), rs747782 (*NUP160-PTPRJ*) and rs9913911 (*GAS7*).

Gene expression in human tissues

Adult ocular samples were obtained from the normal eyes of an 82-year-old European-ancestry female from the North Carolina Eye Bank. All adult ocular samples were stored in RNAlater (Qiagen) within 6.5 h of collection and shipped on dry ice overnight to the laboratory. Isolated tissues were snap frozen and stored at -80°C until RNA extraction. RNA was extracted from each tissue sample independently using the Ambion mirVana total RNA extraction kit. Tissue samples were homogenized in Ambion lysis buffer using an Omni Bead Ruptor Tissue Homogenizer according to the provided protocol. Reverse-transcription reactions were performed with the Invitrogen SuperScript III First-Strand Synthesis kit. Expression of the identified genes was assessed by running 10- μl reactions with Qiagen PCR products consisting of 1.26 μl of water, 1.0 μl of 10 \times buffer, 1.0 μl of dNTPs, 0.3 μl of MgCl_2 , 2.0 μl of Q-Solution, 0.06 μl of Taq polymerase, 1.0 μl of forward primer, 1.0 μl of reverse primer and 1.5 μl of cDNA. Reactions were run on an Eppendorf MasterCycler Pro S thermocycler with touchdown PCR decreasing the annealing temperature by 1°C per cycle from 72°C to 55°C followed by 50 cycles of 94°C for 30 s, 55°C for 30 s and 72°C for 30 s with a final elongation of 7 min at 72°C . All primer sets were designed using Primer3⁵². Products were run on a 2% agarose gel at 70 V for 35 min. Primer sets were run on a custom tissue panel including Human MTC Panel I and Fetal MTC Panel I (Clontech) and an ocular tissue panel.

References

1. Quigley, H.A. & Broman, A.T. The number of people with glaucoma worldwide in 2010 and 2020. *Br J Ophthalmol* 90, 262-7 (2006).
2. Heijl, A., Leske, M.C., Bengtsson, B., Hyman, L. & Hussein, M. Reduction of intraocular pressure and glaucoma progression: results from the Early Manifest Glaucoma Trial. *Arch Ophthalmol* 120, 1268-79 (2002).
3. Collaborative Normal-Tension Glaucoma Study Group. The effectiveness of intraocular pressure reduction in the treatment of normal-tension glaucoma. Collaborative Normal-Tension Glaucoma Study Group. *Am J Ophthalmol* 126, 498-505 (1998).
4. Kass, M.A. et al. The Ocular Hypertension Treatment Study: a randomized trial determines that topical ocular hypotensive medication delays or prevents the onset of primary open-angle glaucoma. *Arch Ophthalmol* 120, 701-13; discussion 829-30 (2002).
5. Wolfs, R.C. et al. Genetic risk of primary open-angle glaucoma. Population-based familial aggregation study. *Arch Ophthalmol* 116, 1640-5 (1998).
6. Sanfilippo, P.G., Hewitt, A.W., Hammond, C.J. & Mackey, D.A. The heritability of ocular traits. *Surv Ophthalmol* 55, 561-83 (2010).
7. Burdon, K.P. et al. Genome-wide association study identifies susceptibility loci for open angle glaucoma at TMC01 and CDKN2B-AS1. *Nat Genet* 43, 574-8 (2011).
8. van Koolwijk, L.M. et al. Common genetic determinants of intraocular pressure and primary open-angle glaucoma. *PLoS Genet* 8, e1002611 (2012).
9. Shah, S. et al. Relationship between corneal thickness and measured intraocular pressure in a general ophthalmology clinic. *Ophthalmology* 106, 2154-60 (1999).
10. Devlin, B. & Roeder, K. Genetic control for association studies. *Biometrics* 55, 997-1004 (1999)
11. Higgins, J.P. & Thompson, S.G. Quantifying heterogeneity in a meta-analysis. *Stat Med* 21, 1539-58 (2002).
12. Dudbridge, F. & Gusnanto, A. Estimation of significance thresholds for genomewide association scans. *Genet Epidemiol* 32, 227-34 (2008).
13. Thorleifsson, G. et al. Common variants near CAV1 and CAV2 are associated with primary open-angle glaucoma. *Nat Genet* 42, 906-9 (2010).
14. Ozel, A.B. et al. Genome-wide association study and meta-analysis of intraocular pressure. *Hum Genet*. 133. 41-57 (2014).
15. Do, R. et al. Common variants associated with plasma triglycerides and risk for coronary artery disease. *Nat. Genet.* 45, 1345–1352 (2013).
16. Grundberg, E. et al. Mapping cis- and trans-regulatory effects across multiple tissues in twins. *Nat Genet* 44, 1084-1089 (2012).
17. Moayyeri, A., Hammond, C.J., Hart, D.J. & Spector, T.D. The UK Adult Twin Registry (TwinsUK Resource). *Twin Res Hum Genet* 16, 144-9 (2013).
18. Hofman, A. et al. The Rotterdam Study: 2012 objectives and design update. *Eur J Epidemiol* 26, 657-86 (2011).
19. Lu, Y. et al. Genome-wide association analyses identify multiple loci associated with central corneal thickness and keratoconus. *Nat Genet* 45, 155-63 (2013).
20. Tonnu, P.A. et al. The influence of central corneal thickness and age on intraocular pressure measured by pneumotonometry, non-contact tonometry, the Tono-Pen XL, and Goldmann applanation tonometry. *Br J Ophthalmol* 89, 851-4 (2005).
21. Denis, M. et al. Expression, regulation, and activity of ABCA1 in human cell lines. *Mol Genet Metab* 78, 265-74 (2003).
22. Yeghiazaryan, K. et al. An enhanced expression of ABC 1 transporter in circulating leukocytes as a potential molecular marker for the diagnostics of glaucoma. *Amino Acids* 28, 207-11 (2005).
23. Denomme, G.A. et al. Consortium for Blood Group Genes (CBGG): 2009 report. *Immunohematology* 26, 47-50 (2010).
24. Khan, M.I. et al. Association of ABO blood groups with glaucoma in the Pakistani population. *Can J Ophthalmol* 44, 582-6 (2009).
25. Janssen, S.F. et al. Gene expression and functional annotation of the human ciliary body epithelia. *PLoS One* 7, e44973 (2012).
26. Charlesworth, J. et al. The path to open-angle glaucoma gene discovery: endophenotypic status of intraocular pressure, cup-to-disc ratio, and central corneal thickness. *Invest Ophthalmol Vis Sci* 51, 3509-14 (2010).
27. Purcell, S.M. et al. Common polygenic variation contributes to risk of schizophrenia and bipolar disorder. *Nature* 460, 748–752 (2009).
28. Carbonaro, F., Andrew, T., Mackey, D.A., Spector, T.D. & Hammond, C.J. Comparison of three methods of intraocular pressure measurement and their relation to central corneal thickness. *Eye (Lond)* 24, 1165-70 (2010).
29. Mitchell, P., Smith, W., Attebo, K. & Wang, J.J. Prevalence of age-related maculopathy in Australia. The Blue Mountains Eye Study. *Ophthalmology* 102, 1450-60 (1995).

30. Foran, S., Wang, J.J. & Mitchell, P. Causes of visual impairment in two older population cross-sections: the Blue Mountains Eye Study. *Ophthalmic Epidemiol* 10, 215-25 (2003).
31. Aulchenko, Y.S. et al. Linkage disequilibrium in young genetically isolated Dutch population. *Eur J Hum Genet* 12, 527-34 (2004).
32. Pardo, L.M., MacKay, I., Oostra, B., van Duijn, C.M. & Aulchenko, Y.S. The effect of genetic drift in a young genetically isolated population. *Ann Hum Genet* 69, 288-95 (2005).
33. Leibowitz, H.M. et al. The Framingham Eye Study monograph: An ophthalmological and epidemiological study of cataract, glaucoma, diabetic retinopathy, macular degeneration, and visual acuity in a general population of 2631 adults, 1973-1975. *Surv Ophthalmol* 24, 335-610 (1980).
34. Vitart, V. et al. New loci associated with central cornea thickness include COL5A1, AKAP13 and AVGR8. *Hum Mol Genet* 19, 4304-11 (2010).
35. Evans, S., Newnham, J., MacDonald, W. & Hall, C. Characterisation of the possible effect on birthweight following frequent prenatal ultrasound examinations. *Early Hum Dev* 45, 203-14 (1996).
36. Newnham, J.P., Evans, S.F., Michael, C.A., Stanley, F.J. & Landau, L.I. Effects of frequent ultrasound during pregnancy: a randomised controlled trial. *Lancet* 342, 887-91 (1993).
37. Williams, L.A., Evans, S.F. & Newnham, J.P. Prospective cohort study of factors influencing the relative weights of the placenta and the newborn infant. *BMJ* 314, 1864-8 (1997).
38. Hofman, A. et al. The Rotterdam Study: 2014 objectives and design update. *Eur. J. Epidemiol.* 28, 889–926 (2013).
39. Mackey, D.A. et al. Twins eye study in Tasmania (TEST): rationale and methodology to recruit and examine twins. *Twin Res Hum Genet* 12, 441-54 (2009).
40. Spector, T.D. & Williams, F.M. The UK Adult Twin Registry (TwinsUK). *Twin Res Hum Genet* 9, 899-906 (2006).
41. Wang, Y.X., Xu, L., Yang, H. & Jonas, J.B. Prevalence of glaucoma in North China: the Beijing Eye Study. *Am J Ophthalmol* 150, 917-24 (2010).
42. Lavanya, R. et al. Methodology of the Singapore Indian Chinese Cohort (SiCC) eye study: quantifying ethnic variations in the epidemiology of eye diseases in Asians. *Ophthalmic Epidemiol* 16, 325-36 (2009).
43. Foong, A.W. et al. Rationale and methodology for a population-based study of eye diseases in Malay people: The Singapore Malay eye study (SiMES). *Ophthalmic Epidemiol* 14, 25-35 (2007).
44. Marchini, J., Howie, B., Myers, S., McVean, G. & Donnelly, P. A new multipoint method for genome-wide association studies by imputation of genotypes. *Nature genetics* 39, 906-13 (2007).
45. Howie, B.N., Donnelly, P. & Marchini, J. A flexible and accurate genotype imputation method for the next generation of genome-wide association studies. *PLoS genetics* 5, e1000529 (2009).
46. Li, Y., Willer, C.J., Ding, J., Scheet, P. & Abecasis, G.R. MaCH: using sequence and genotype data to estimate haplotypes and unobserved genotypes. *Genetic epidemiology* 34, 816-34 (2010).
47. van der Valk, R. et al. Intraocular pressure-lowering effects of all commonly used glaucoma drugs: a meta-analysis of randomized clinical trials. *Ophthalmology* 112, 1177-85 (2005).
48. Stephens, M. & Balding, D.J. Bayesian statistical methods for genetic association studies. *Nat Rev Genet* 10, 681-90 (2009).
49. Higgins, J.P., Thompson, S.G., Deeks, J.J. & Altman, D.G. Measuring inconsistency in meta-analyses. *BMJ* 327, 557-60 (2003).
50. Liu, J.Z. et al. A versatile gene-based test for genome-wide association studies. *American journal of human genetics* 87, 139-45 (2010).
51. Nagelkerke, N.J.D. A note on a general definition of the coefficient of determination. *Biometrika* 78, 691-692 (1991).
52. Rozen, S. & Skaletsky, H. Primer3 on the WWW for general users and for biologist programmers. *Methods in molecular biology* 132, 365-86 (2000).

CHAPTER 4.2

Meta-analysis of genome-wide association studies identifies novel loci that influence cupping and the glaucomatous process



Henriët Springelkamp*, René Höhn*, Aniket Mishra*, Pirro G. Hysi*, Chiea-Chuen Khor*, Stephanie J. Loomis*, Jessica N. Cooke Bailey, Jane Gibson, Gudmar Thorleifsson, Sarah F. Janssen, Xiaoyan Luo, Wishal D. Ramdas, Eranga Vithana, Monisha E. Nongpiur, Grant W. Montgomery, Liang Xu, Jenny E. Mountain, Puya Gharahkhani, Yi Lu, Najaf Amin, Lennart C. Karssen, Kar-Seng Sim, Elisabeth M. van Leeuwen, Adriana I. Iglesias, Virginie J.M. Verhoeven, Michael A. Hauser, Seng-Chee Loon, Dominiek D.G. Despriet, Abhishek Nag, Cristina Venturini, Paul G. Sanfilippo, Arne Schillert, Jae H. Kang, John Landers, Fridbert Jonasson, Angela J. Cree, Leonieke M.E. van Koolwijk, Fernando Rivadeneira, Emmanuelle Souzeau, Vesteyn Jonsson, Geeta Menon, Blue Mountains Eye Study – GWAS group, Robert N. Weinreb, Paulus T.V.M. de Jong, Ben A. Oostra, André G. Uitterlinden, Albert Hofman, Sarah Ennis, Unnur Thorsteinsdottir, Kathryn P. Burdon, NEIGHBORHOOD Consortium, Wellcome Trust Case Control Consortium 2 (WTCCC2), Timothy D. Spector, Alireza Mirshahi, Seang-Mei Saw, Johannes R. Vingerling, Yik-Ying Teo, Jonathan L. Haines, Roger C.W. Wolfs, Hans G. Lemij, E-Shyong Tai, Nomdo M. Jansonius, Jost B. Jonas, Ching-Yu Cheng, Tin Aung, Ananth C. Viswanathan, Caroline C.W. Klaver, Jamie E. Craig, Stuart Macgregor, David A. Mackey, Andrew J. Lotery, Kari Stefansson, Arthur A.B. Bergen, Terri L. Young, Janey L. Wiggs, Norbert Pfeiffer‡, Tien-Yin Wong‡, Louis R. Pasquale‡, Alex W. Hewitt‡, Cornelia M. van Duijn‡, Christopher J. Hammond‡.

* These authors contributed equally.

‡ These authors jointly directed this work.

Nat Commun. 2014 Sep 22;5:4883. doi: 10.1038/ncomms5883

Supplementary files and figures can be found at:

<http://www.nature.com/ncomms/2014/140922/ncomms5883/full/ncomms5883.html>

ABSTRACT

Glaucoma is characterized by irreversible optic nerve degeneration and is the most frequent cause of irreversible blindness worldwide. Here, the International Glaucoma Genetics Consortium (IGGC) conducts a meta-analysis of genome-wide association studies of vertical cup-disc ratio (VCDR), an important disease-related optic nerve parameter. In 21,094 individuals of European ancestry and 6,784 individuals of Asian ancestry, we identify ten new loci associated with variation in VCDR. In a separate risk-score analysis of five case-control studies, Caucasians in the highest quintile have a 2.5-fold increased risk of primary open-angle glaucoma as compared with those in the lowest quintile. This study has more than doubled the known loci associated with optic disc cupping and will allow greater understanding of mechanisms involved in this common blinding condition.

INTRODUCTION

Optic nerve degeneration caused by glaucoma is the most common cause of irreversible blindness worldwide¹. Glaucomatous optic neuropathy is recognized by changes in the morphology of the optic nerve head, or optic disc, caused by loss of retinal ganglion cells and thinning of the retinal nerve fiber layer. In glaucoma, the nerve fiber layer typically thins in the superior and inferior regions of the nerve creating a vertically elongated depression (the cup). The ratio of the cup to the overall nerve size (the disc), called the vertical cup-disc ratio (VCDR), is a key factor in the clinical assessment and follow-up of patients with glaucoma. VCDR has been shown to be heritable with h^2 scores ranging between 0.48 and 0.66²⁻⁷. At least seven loci have been associated with VCDR in previous genome-wide association studies (GWAS) and three of these were subsequently implicated in primary open-angle glaucoma (POAG)⁸⁻¹¹. So far, the explained variance of open-angle glaucoma by age, sex, intraocular pressure and established POAG genes is still small (4-6%)¹². As with other complex diseases, large sample sizes are needed to ensure sufficient power to fully define the underlying genetic architecture.

Here, we report the largest genome-wide meta-analysis for VCDR, with data from 14 studies from Europe, the United States, Australia and Asia, as part of the International Glaucoma Genetics Consortium (IGGC). The aim of the study is to identify loci associated with VCDR, and to determine whether these variants are also associated with glaucoma.

We perform the meta-analysis in four stages. In the first stage, we meta-analyse summary data from 10 populations of European ancestry comprising 21,094 individuals. In the second stage, we test the cross-ancestry transferability of the statistically genome-wide significant associations from the first stage in 6,784 individuals from four Asian cohorts. In the third stage, we examine whether the associations are independent of disc area and/or spherical equivalent. We also combine the genome-wide significant effects into a genetic risk score and associate this score with the POAG risk in five populations. Finally, we perform gene-based tests and pathway analysis.

We find ten new loci associated with VCDR, which together increase the risk on POAG 2.5 times. Our findings will help us to unravel the pathogenesis of glaucoma.

RESULTS

Meta-analysis of genome-wide association studies

In stage 1, we analysed approximately 2.5 million HapMap stage 2 single nucleotide polymorphisms (SNPs) – either directly genotyped or imputed in 21,094 subjects of European ancestry (Supplementary Fig. 1, Supplementary Table 1 and Supplementary Methods). The inflation factors (λ) varied between 0.98 and 1.12, implying adequate within-study control of population substructure (Supplementary Table 2 and Supplementary Figures 2 and 3). The overall λ was 1.05. This analysis yielded 440 genome-wide significant SNPs ($P < 5.0 \times 10^{-8}$) located across 15 chromosomal regions (Table 1 and Supplementary Fig. 4a). In stage 2, we investigated the SNP with the strongest association at each region in the Asian

Table 1. Summary of SNPs that showed genome-wide significant ($P < 5 \times 10^{-8}$) association with vertical cup-disc ratio (VCDR) in subjects of European ancestry (stage 1), with results of replication in Asians (stage 2) and the additional SNPs that showed genome-wide significant ($P < 5 \times 10^{-8}$) association in the combined analysis (stage 3) (p-values were calculated by using the z-statistic). We tested for heterogeneous effects between the Asian and European ancestry samples, for which p-values are shown (Cochran's Q-test).

SNP	Chr./position	Nearest Gene	Annotation	A1/A2	Caucasians (n=21,094)				
					MAF	β	SE	P-value	P-value heterogeneity
rs4658101	1/91849997	<i>CDC7/TGFBR3</i>	intergenic	a/g	0.18	0.015	0.002	8.80×10^{-14}	9.34×10^{-2}
rs2623325	3/100614445	<i>COL8A1</i>	intergenic	a/c	0.13	0.018	0.003	7.05×10^{-9}	5.62×10^{-2}
rs17658229	5/172123657	<i>DUSP1</i>	intergenic	c/t	0.05	-0.020	0.004	8.06×10^{-9}	5.95×10^{-1}
rs17756712	6/570071	<i>EXOC2</i>	intronic	g/a	0.18	0.010	0.002	1.98×10^{-8}	6.74×10^{-1}
rs7865618	9/22021005	<i>CDKN2BAS</i>	intronic	g/a	0.43	-0.013	0.001	2.80×10^{-20}	8.93×10^{-1}
rs1900005	10/69668061	<i>ATOH7</i>	intergenic	a/c	0.23	-0.019	0.002	7.21×10^{-31}	2.96×10^{-4}
rs7072574	10/96026296	<i>PLCE1</i>	intronic	a/g	0.33	0.009	0.002	6.17×10^{-9}	1.09×10^{-1}
rs1346	11/65093827	<i>SSSCA1</i>	5upstream	t/a	0.19	-0.014	0.002	2.54×10^{-15}	7.49×10^{-1}
rs4936099	11/129785935	<i>ADAMTS8</i>	intronic	c/a	0.42	-0.009	0.002	6.38×10^{-9}	8.31×10^{-1}
rs11168187	12/46330278	<i>RPAP3</i>	intergenic	g/a	0.16	-0.009	0.002	2.96×10^{-8}	1.00
rs10862688	12/82447043	<i>TMTC2</i>	intergenic	g/a	0.45	0.008	0.001	1.24×10^{-11}	4.80×10^{-2}
rs4901977	14/59858929	<i>SIX1/6</i>	intergenic	t/c	0.31	0.010	0.002	1.98×10^{-11}	7.86×10^{-1}
rs1345467	16/50039822	<i>SALL1</i>	intergenic	g/a	0.27	0.010	0.002	2.70×10^{-12}	1.68×10^{-1}
rs6054374	20/6526556	<i>BMP2</i>	intergenic	t/c	0.42	-0.009	0.002	1.79×10^{-8}	1.26×10^{-1}
rs1547014	22/27430711	<i>CHEK2</i>	intronic	t/c	0.30	-0.013	0.001	2.98×10^{-18}	1.93×10^{-1}
rs301801	1/8418532	<i>RERE</i>	intronic	c/t	0.33	0.008	0.001	1.61×10^{-7}	2.46×10^{-2}
rs868153	6/122431654	<i>HSF2</i>	intergenic	g/t	0.36	-0.007	0.001	5.08×10^{-6}	9.27×10^{-1}
rs5756813	22/36505423	<i>CARD10</i>	intergenic	g/t	0.39	0.006	0.001	1.60×10^{-5}	8.22×10^{-1}

ABBREVIATIONS

A1 reference allele
A2 other allele
 β effect size on VCDR based on allele A1
Chr. chromosome
MAF average minor allele frequency

Nearest gene reference NCBI build 37
SE standard error of the effect size
 The last three rows indicate the SNPs that reached genome-wide significance in the combined analysis, but not in stage 1 or stage 2

Table 1. (continued)

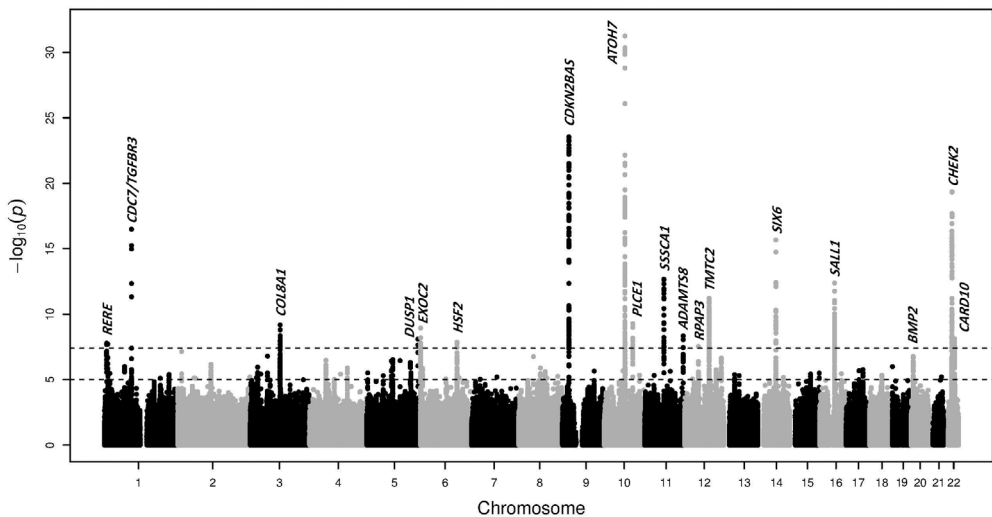
Asians (n= 6,784)					Combined (n= 27,878)				
MAF*	β	SE	P-value	P-value heterogeneity	β	SE	P-value	P-value heterogeneity	I ²
0.14	0.016	0.005	3.13x10 ⁻³	4.26x10 ⁻¹	0.015	0.002	1.06x10 ⁻¹⁵	1.68x10 ⁻¹	0.54
0.16	0.011	0.005	1.46x10 ⁻²	3.43x10 ⁻¹	0.016	0.003	6.61x10 ⁻¹⁰	7.01x10 ⁻²	0.42
0.00	-0.086	0.133	5.17x10 ⁻¹	**	-0.020	0.004	8.06x10 ⁻⁹	5.95x10 ⁻¹	0
0.14	0.011	0.005	1.76x10 ⁻²	4.05x10 ⁻¹	0.010	0.002	1.13x10 ⁻⁹	7.23x10 ⁻¹	0
0.15	-0.021	0.005	8.11x10 ⁻⁶	3.31x10 ⁻¹	-0.013	0.001	4.97x10 ⁻²⁴	6.97x10 ⁻¹	0
0.32	-0.010	0.004	2.08x10 ⁻²	1.58x10 ⁻¹	-0.018	0.002	5.51x10 ⁻³¹	8.54x10 ⁻⁵	0.69
0.38	0.007	0.003	4.80x10 ⁻²	8.18x10 ⁻¹	0.009	0.001	1.02x10 ⁻⁹	2.56x10 ⁻¹	0.18
0.16	0.003	0.005	5.23x10 ⁻¹	7.19x10 ⁻¹	-0.012	0.002	4.89x10 ⁻¹³	1.51x10 ⁻¹	0.28
0.09	-0.007	0.009	4.15x10 ⁻¹	1.14x10 ⁻¹	-0.009	0.002	4.61x10 ⁻⁹	6.79x10 ⁻¹	0
0.18	-0.005	0.004	2.80x10 ⁻¹	6.19x10 ⁻¹	-0.009	0.002	2.96x10 ⁻⁸	9.98x10 ⁻¹	0
0.56	0.004	0.003	2.48x10 ⁻¹	1.20x10 ⁻¹	0.008	0.001	1.49x10 ⁻¹¹	2.61x10 ⁻²	0.44
0.53	0.017	0.003	2.64x10 ⁻⁷	3.82x10 ⁻²	0.011	0.001	2.13x10 ⁻¹⁶	2.02x10 ⁻¹	0.22
0.13	0.011	0.006	5.53x10 ⁻²	4.13x10 ⁻¹	0.010	0.001	4.19x10 ⁻¹³	2.48x10 ⁻¹	0.18
0.72	0.001	0.004	8.66x10 ⁻¹	5.99x10 ⁻¹	-0.007	0.001	1.69x10 ⁻⁷	8.19x10 ⁻²	0.37
0.17	-0.013	0.004	4.26x10 ⁻³	8.11x10 ⁻¹	-0.013	0.001	4.77x10 ⁻²⁰	3.90x10 ⁻¹	0.06
0.13	0.012	0.005	2.59x10 ⁻²	5.38x10 ⁻¹	0.008	0.001	1.66x10 ⁻⁸	5.23x10 ⁻²	0.39
0.39	-0.013	0.003	1.44x10 ⁻⁴	4.96x10 ⁻¹	-0.007	0.001	1.39x10 ⁻⁸	7.96x10 ⁻¹	0
0.32	0.017	0.004	1.71x10 ⁻⁶	1.84x10 ⁻¹	0.008	0.001	7.73x10 ⁻⁹	1.98x10 ⁻¹	0.22

* note that, for the sake of keeping the same reference allele, MAF values may be greater than 0.50 in the Asian populations

** for this SNP, only one Asian study is contributing to the meta-analysis, so p-value for heterogeneity could not be calculated for this SNP in stage 2

populations and found that eight were nominally significant ($P < 0.05$) with an effect in the same direction and generally the same order of magnitude (Table 1 and Supplementary Fig. 4b). Five of the seven loci that did not reach nominal significance in those of Asian descent had a similar effect in the same direction. Supplementary Table 3 shows the most significant SNPs in Asians within 100,000 basepairs from the most significant associated SNP in Europeans. Meta-analysis of only the Asian populations did not result in new genome-wide significant findings. The combined analysis of the European and Asian populations resulted in three additional genome-wide significant associations on chromosome 1, 6 and 22 (Table 1 and Fig. 1). The level of heterogeneity across the samples are shown in Table 1. Of the 18 genome-wide significant loci, 10 are novel for the VCDR outcome (*COL8A1*, *DUSP1*, *EXOC2*, *PLCE1*, *ADAMTS8*, *RPAP3*, *SALL1*, *BMP2*, *HSF2* and *CARD10*) (Supplementary Fig. 5). There were no significant differences in terms of allele frequencies across the different cohorts (Supplementary Table 4). The effect estimates from the participating cohorts appear not to be influenced by main demographic characteristics, such as mean age and sex ratio (Supplementary Fig. 6).

Figure 1. Manhattan plot of the GWAS meta-analysis for vertical cup-disc ratio in the combined analysis ($n = 27,878$).



The plot shows $-\log_{10}$ -transformed p-values for all SNPs (z-statistic). The upper black dotted horizontal line represents the genome-wide significance threshold of $P < 5.0 \times 10^{-8}$; the lower black dotted line indicates p-value of 1×10^{-5} .

Adjustment for disc area and spherical equivalent

Four of the 18 genome-wide significant loci have been previously associated with optic disc area (*CDC7/TGFBR3*, *ATOH7*, *SALL1* and *CARD10*)^{10,13}. Because the size of the optic nerve varies between individuals and is correlated to the VCDR¹⁴, we adjusted the association to VCDR for optic nerve (disc) area. This resulted in a reduced effect size and significance ($P=3.48 \times 10^{-11}$ to $P=9.00 \times 10^{-3}$) at the *CDC7-TGFBR3* locus, suggesting the VCDR association at this locus is explained primarily by its known association with disc area (Supplementary Table 5a,b,c). A similar reduction in effect was seen for *ATOH7*. However, for this locus there remains a significant disc area independent effect ($P=7.28 \times 10^{-9}$). There was no change in association significance for any of the 10 new loci reported here, suggesting they do not act primarily on disc area.

It is of interest that two genes (*SIX6* and *BMP2*) overlap with those implicated in myopia¹⁵, an important risk factor for POAG¹⁶. The correlation between VCDR and spherical equivalent is low (Supplementary Table 6), and adjusting for spherical equivalent did not lead to any major changes in the effects for these or other loci in European populations (Supplementary Table 7a), suggesting a joint genetic etiology for POAG and myopia. In Asian cohorts the direction of effect on VCDR at the chromosome 11 locus (*MIR612-SSSCA1* region) was not consistent with the European populations (Supplementary Table 7b). However, after adjusting for spherical equivalent the direction of effect on VCDR was similar to both populations. At the *BMP2* myopia locus, we observed a large difference in allele frequency between those of European and Asian ancestry (Table 1), which may explain the difference in effect direction.

Risk for primary open-angle glaucoma

The 18 loci, together with age and sex, explain 5.1-5.9% of the VCDR phenotypic variability in Europeans (measured in the Rotterdam Study I, II and III), of which 1.6-1.8% is explained by the new loci. The phenotypic variability explained by all common SNPs is 41-53% in these cohorts, which is in line with the heritability estimates from family-based studies. In addition to confirming the previously published *CDKN2BAS* and *SIX1/6* POAG risk loci, we found nominally significant ($P < 0.05$) associations with POAG for six newly identified genetic variants ($P=8.1 \times 10^{-5}$ from binomial test for chance of seeing six or more such nominally significant associations in 16 tests) (Supplementary Table 8), with odds ratios varying between 0.73 and 1.20. In the combined case-control studies, we found that the sum of all effects of these genes increased the risk of POAG 2.5 fold (Supplementary Table 9) for those in the highest quintile compared to those in the lowest quintile.

Gene-based test

To identify new loci not previously found through individual SNP based tests, we performed gene-based tests using VEGAS software¹⁷. Because of the smaller number of tests (17,872 genes tested), our gene-based significance threshold is $P_{\text{gene-based}} < 0.05/17,872 = 2.80 \times 10^{-6}$. In addition to the SNPs identified as significant ($P < 5 \times 10^{-8}$) in a SNP-based test, we also found two new genes significantly associated with VCDR using the VEGAS gene-based test (Supplementary Table 10). These were *REEP5* ($P=7.48 \times 10^{-7}$) and *PITPNB* ($P=4.89 \times 10^{-7}$). *PITPNB* is approximately 800kb from another gene with a significant SNP association (*CHEK2*, rs1547014) (Supplementary Fig. 7). Although the association signal

centred over *CHEK2* extends a long distance toward *PITPNB*, a separate association peak over *PITPNB* can be observed, which is unrelated (no linkage disequilibrium (LD)) to the *CHEK2* peak. The results we obtained using the specified definition of the gene unit were substantially the same when alternative cutoff points from the transcription initiation and end sites were used (Supplementary Table 11). The *REEP5* gene showed no association with POAG (Supplementary Table 12). The *PITPNB* gene showed evidence for association with POAG in ANZRAG ($P=0.03$) in the gene-based test, with a best single SNP p-value of 0.003, but this was not confirmed in two other studies.

Pathway analysis

To test whether gene-based statistics identified were enriched in 4,628 prespecified Gene Ontology pathways we performed pathway analysis using Pathway-VEGAS¹⁸. We used a pathway-wide significance threshold to be 1.08×10^{-5} ($0.05/4,628$). The only pathway exceeding the pathway-wide significance level was “negative regulation of cyclin-dependent protein kinase activity” (Supplementary Table 13). The second top-pathway “negative regulation of epithelial cell proliferation” is related to the top pathway, both suggesting retardation of cell growth. The “negative regulation of cyclin-dependent protein kinase activity” finding was driven not only by the result at the *CDKN2A* locus but also by the result at *APC*, a gene close to *REEP5*.

Regulatory elements and expression data

Six of the 18 most associated SNPs are located in DNase I hypersensitivity sites (Supplementary Table 14). The retinal pigment epithelium has the highest signal of all 125 available cell lines in one of these DNase I hypersensitivity sites. Thus, these results are suggesting that some of the SNPs may have their effect on VCDR by altering regulatory functions. We investigated the expression of the genes implicated in VCDR by these analyses in human ocular gene expression databases or the published literature. Most of these genes are expressed in eye tissues, including the optic nerve (Supplementary Table 15 and 16).

DISCUSSION

This study reports 10 novel loci associated with VCDR, with an additional two loci identified using gene-based testing. Pathway analysis suggests retardation of cell growth as a major biological mechanism. The results for the most associated pathways “negative regulation of cyclin-dependent protein kinase activity” and “negative regulation of epithelial cell proliferation” are primarily driven by the *CDKN2A* and *CDKN2B* genes, respectively, but in both pathways the gene-based result at *APC* ($P=7.20 \times 10^{-5}$ in Caucasians and $P=8.80 \times 10^{-3}$ in Asians) also contributes to the pathway result. The *APC* gene has previously been reported to be a critical gene regulating retinal pigment epithelium proliferation and development¹⁹. These results add to our earlier findings on the role of growth and the transforming growth factor beta (TGFB) pathways in VCDR¹⁰. Various new genes fall into these pathways. The protein encoded by the *BMP2* (bone morphogenetic protein 2) gene on chromosome 20 belongs to the TGFB super-family. Two other new genes regulate apoptosis: *RPAP3* (RNA polymerase II-associated protein 3)²⁰ on chromosome 12 and *CARD10*, a gene that was previously found to be associated with disc area¹³. Another new VCDR association previously associated with disc area is *SALL1*¹⁰. This gene is implicated in ocular development.

Our findings offer new insights in the etiology of optic nerve degeneration. *COL8A1* (collagen, type VIII, alpha 1) is part of a collagen pathway recently implicated in corneal thickness¹⁸, an ocular trait also associated with glaucoma risk. Missense mutations in *COL8A2* (collagen, type VIII, alpha2) were found in POAG patients with a very thin central corneal thickness (CCT)²¹. The collagen SNP (rs2623325) was not significantly associated with CCT (in Caucasians: $\beta=-0.044$, $P=0.19$; in Asians: $\beta=0.007$, $P=0.89$) or intraocular pressure (in Caucasians and Asians combined: $\beta=-0.02$, $P=0.73$) in largely the same cohorts^{18,22}, suggesting that the collagen involvement in VCDR is not due to influence by CCT or intraocular pressure. We also found several genes involved in cellular stress response. *DUSP1* (dual specificity phosphatase 1) is the nearest gene to the most strongly associated SNP on chromosome 5. This gene, inducible by oxidative stress and heat shock, may play a role in environmental stress response²³, and may also participate in the negative regulation of cellular proliferation. *HSF2* (heat shock transcription factor 2), one of the genes at the chromosome 6 locus, also is part of the cellular stress response pathway. Deficiency of this factor causes various central nervous system defects in mice^{24,25}. Another pathway emerging in this study is that of exocytosis. The SNP on the other chromosome 6 locus is located in *EXOC2* (exocyst complex component 2). The encoded protein is one of the eight proteins of the exocyst complex²⁶. This multi-protein complex is important for directing exocytic vesicles to the plasma membrane, a mechanism that also has been implicated in neuronal degeneration in the brain²⁷. Lipid metabolism emerges as another pathway. The gene on chromosome 10, *PLCE1* (phospholipase C, epsilon 1), belongs to the phospholipase C family, which plays a role in the generation of second messengers²⁸. Various processes affecting cell growth, differentiation and gene expression are regulated by these second messengers. From a clinical perspective, the findings on *ADAMTS8* are of interest. *ADAMTS* enzymes have different functions, including the formation and turnover of the extracellular matrix²⁹. Strikingly, a variant in *ADAMTS10* has been linked to a form of glaucoma in dogs^{30,31}.

In summary, we have now identified 10 novel loci associated with cupping of the optic nerve, a key determinant of glaucoma. Together, these genetic risk variants increased the risk of POAG in case-control validation studies. Pathway analysis implicated negative regulation of cell growth and cellular response to environmental stress as key pathological pathways in glaucoma, and that novel therapies targeting these pathways may be neuro-protective in glaucoma.

METHODS

Study design

We performed a meta-analysis on directly genotyped and imputed SNPs from individuals of European ancestry in 10 studies, with a total of 21,094 individuals. Subsequently, we evaluated significantly associated SNPs in 6,784 subjects of Asian origin including four different studies and performed a meta-analysis on all studies combined.

Subjects and phenotyping

All studies included in this meta-analysis are part of the International Glaucoma Genetics Consortium (IGGC). The ophthalmological examination of each study included an assessment of the optic nerve head to measure the VCDR (Supplementary Table 17a). Unreliable optic nerve data were excluded.

The meta-analysis of stage 1 was based on 10 studies of European ancestry: Brisbane Adolescent Twin Study (BATS), Blue Mountains Eye Study (BMES), Erasmus Rucphen Family (ERF) Study, Gutenberg Health Study (GHS I/GHS II), Glaucoma Genes and Environment (GLAUGEN; controls only), National Eye Institute (NEI) Glaucoma Human Genetics Collaboration (NEIGHBOR; controls only), Raine Study, Rotterdam Study (RS-I/RS-II/RS-III), Twins Eye Study in Tasmania (TEST) and TwinsUK. Stage 2 comprised four Asian studies: Beijing Eye Study (BES), Singapore Chinese Eye Study (SCES), Singapore Malay Eye Study (SIMES) and Singapore Indian Eye Study (SINDI). For each SNP with the strongest association at each locus the association with POAG was tested in five case-control studies: Australian & New Zealand Registry of Advanced Glaucoma (ANZRAG), deCODE, Massachusetts Eye and Ear Infirmary (MEEI), NEIGHBOR and Southampton.

Information on general methods, demographics, phenotyping and genotyping methods of the study cohorts can be found in Supplementary Table 1 and 17 and the Supplementary Note. All studies were performed with the approval of their local medical ethics committee, and written informed consent was obtained from all participants in accordance with the Declaration of Helsinki.

Genotyping and imputation

Information on genotyping in each cohort and the particular platforms used to perform genotyping can be found in more detail in Supplementary Table 17b. To produce consistent data sets and enable a meta-analysis of studies across different genotyping platforms, the studies performed genomic imputation on available HapMap Phase 2 genotypes with MACH³² or IMPUTE³³, using the appropriate ancestry groups as templates.

Each study applied stringent quality control procedures before imputation, including minor allele frequency cutoffs, Hardy-Weinberg equilibrium, genotypic success rate, mendelian inconsistencies, exclusion of individuals with >5% shared ancestry (exception made for family-based cohorts in which due adjustment for family relationship was made) and removal of all individuals whose ancestry as determined through genetic analysis did not match the prevailing ancestry group of the corresponding cohort (Supplementary Note). SNPs with low imputation quality were filtered using metrics specific to the imputation method and thresholds used in previous GWAS analyses. For each cohort, only SNPs with imputation quality scores >0.6 (proper-info of IMPUTE) or $R^2 > 0.6$ (MACH) were included into the meta-analysis.

Statistical analysis

In subjects drawn from their respective populations in which the prevalence of glaucomatous changes is relatively low, the correlation between left and right eye is high³⁴. Therefore, we used the mean VCDR of both eyes. In cases of missing or unreliable data for one eye, data of the other eye was taken. Each individual study did a linear regression model between the VCDR and the SNPs under the assumption of an additive model for the effect of the risk allele. Analyses were adjusted for age, sex and the first two principal components (for population-based studies) or family structure (for family-based studies). Secondary analyses were done with adjustments for disc area or spherical equivalent. In the Rotterdam Studies, we calculated the phenotypic variability explained by the new loci, and explained by all common SNPs using the 'Genome-wide Complex Trait Analysis' tool^{35,36}.

We performed an inverse variance weighted fixed-effect meta-analysis. This was performed with METAL software³⁷. P-values for the association results were calculated by using the z-statistic. P-values for heterogeneity were calculated by using the Cochran's Q-test for heterogeneity. In addition to this, I^2 values were calculated to assess heterogeneity³⁸. F_{st} values were calculated to assess the genetic variation due to subdivision of populations. All study effect estimates were corrected using genomic control and were oriented to the positive strand of the NCBI Build 36 reference sequence of the human genome, which was the genomic build on which most available genotyping platforms were based. Coordinates and further annotations for the SNPs were converted into Build 37, the most recent version of the available builds at the time of this study.

In stage 1, a p-value $< 5.0 \times 10^{-8}$ (the genome-wide threshold of association) was considered significant. In stage 2, a p-value < 0.05 was considered significant. Manhattan, regional and forest plots were made using R³⁹, LocusZoom⁴⁰ and Stata/SE 12.0 (StataCorp LP, College Station, TX, USA).

Risk score models

In five case-control studies, a weighted genetic risk score per individual was calculated. Standardized regression coefficients were used as weighting factor. The weighted risk scores were divided into quintiles. Odds ratios were calculated for each quintile, using the first quintile as a reference.

Gene-based Test using VEGAS

There are different gene-based tests of which VEGAS is one of the most powerful tests⁴¹. We therefore performed gene-based testing using VEGAS software¹⁷, which combines the test statistics of all SNPs present within and 50 kb upstream/downstream of each gene. LD between the markers is accounted for through simulations from the multivariate normal distribution, based on estimates of LD from reference populations. Since Asian and European ancestry populations show different LD patterns, we performed separate gene-based tests for each population. Hapmap 2 CEU population was used as a reference to calculate LD for European ancestry data, whereas Hapmap 2 JPT and CHB combined population was used as a reference for Asian ancestry data. After calculation of gene-based test statistics for Asian and European ancestry populations separately, meta-analysis was conducted using Fisher's method for combining p-values. VEGAS was applied to the summary data from the full VCDR analysis (as in Table 1) and to three of the POAG data sets; Australian & New Zealand Registry of Advanced Glaucoma (ANZRAG), Massachusetts Eye and Ear Infirmary (MEEI) glaucoma clinic and Glaucoma Genes and Environment (GLAUGEN) (Supplementary Note).

Pathway-analysis using Pathway-VEGAS

Prespecified pathways from the Gene Ontology database with size ranging in 5-500 genes were used to perform pathway analysis. Pathway-VEGAS combines VEGAS gene-based test statistics based on prespecified biological pathways¹⁸. Pathway p-values were computed by summing χ^2 test statistics derived from VEGAS p-values. Empirical "VEGAS-pathway" p-values for each pathway were computed by comparing the real data summed χ^2 test statistics with 500,000 simulations where the relevant number (as per size of pathway) of randomly drawn χ^2 test statistics was summed. To ensure clusters of genes did not adversely affect results, within each pathway, gene-sets were pruned such that each gene was >500kb from all other genes in the pathway. Where required, all but one of the clustered genes was dropped at random when genes were clustered. Pathway-VEGAS was performed separately for European and Asian ancestry datasets. Meta-analysis was conducted using Fisher's method for combining p-values.

Regulatory functions

We used the ENCYclopedia Of DNA Elements (ENCODE)⁴² data in the UCSC Genome Browser⁴³ to look at DNase I hypersensitivity sites and other functional elements.

Gene expression in human eye tissue

We examined the expression of genes that reached significance in the individual SNP based test or gene-based test. We used published literature or human ocular gene expression databases (Supplementarys Table 15 and 16).

References

1. Quigley, H.A. & Broman, A.T. The number of people with glaucoma worldwide in 2010 and 2020. *Br J Ophthalmol* 90, 262-7 (2006).
2. Chang, T.C. et al. Determinants and heritability of intraocular pressure and cup-to-disc ratio in a defined older population. *Ophthalmology* 112, 1186-91 (2005).
3. Charlesworth, J. et al. The path to open-angle glaucoma gene discovery: endophenotypic status of intraocular pressure, cup-to-disc ratio, and central corneal thickness. *Invest Ophthalmol Vis Sci* 51, 3509-14 (2010).
4. Coleman, A.L. Glaucoma. *Lancet* 354, 1803-10 (1999).
5. Klein, B.E., Klein, R. & Lee, K.E. Heritability of risk factors for primary open-angle glaucoma: the Beaver Dam Eye Study. *Invest Ophthalmol Vis Sci* 45, 59-62 (2004).
6. van Koolwijk, L.M. et al. Major genetic effects in glaucoma: commingling analysis of optic disc parameters in an older Australian population. *Invest Ophthalmol Vis Sci* 50, 5275-80 (2009).
7. Sanfilippo, P.G., Hewitt, A.W., Hammond, C.J. & Mackey, D.A. The heritability of ocular traits. *Surv Ophthalmol* 55, 561-83 (2010).
8. Burdon, K.P. et al. Genome-wide association study identifies susceptibility loci for open angle glaucoma at TMC01 and CDKN2B-AS1. *Nat Genet* 43, 574-8 (2011).
9. Macgregor, S. et al. Genome-wide association identifies ATOH7 as a major gene determining human optic disc size. *Hum Mol Genet* 19, 2716-24 (2010).
10. Ramdas, W.D. et al. A genome-wide association study of optic disc parameters. *PLoS Genet* 6, e1000978 (2010).
11. Ramdas, W.D. et al. Common genetic variants associated with open-angle glaucoma. *Hum Mol Genet* 20, 2464-71 (2011).
12. Ramdas, W.D. et al. Clinical implications of old and new genes for open-angle glaucoma. *Ophthalmology* 118, 2389-97 (2011).
13. Khor, C.C. et al. Genome-wide association studies in Asians confirm the involvement of ATOH7 and TGFBR3, and further identify CARD10 as a novel locus influencing optic disc area. *Hum Mol Genet* 20, 1864-72 (2011).
14. Ramdas, W.D. et al. Heidelberg Retina Tomograph (HRT3) in population-based epidemiology: normative values and criteria for glaucomatous optic neuropathy. *Ophthalmic Epidemiol* 18, 198-210 (2011).
15. Verhoeven, V.J. et al. Genome-wide meta-analyses of multiancestry cohorts identify multiple new susceptibility loci for refractive error and myopia. *Nat Genet* 45, 314-8 (2013).
16. Kwon, Y.H., Fingert, J.H., Kuehn, M.H. & Alward, W.L. Primary open-angle glaucoma. *N Engl J Med* 360, 1113-24 (2009).
17. Liu, J.Z. et al. A versatile gene-based test for genome-wide association studies. *Am J Hum Genet* 87, 139-45 (2010).
18. Lu, Y. et al. Genome-wide association analyses identify multiple loci associated with central corneal thickness and keratoconus. *Nat Genet* 45, 155-63 (2013).
19. Marcus, D.M. et al. Retinal pigment epithelium abnormalities in mice with adenomatous polyposis coli gene disruption. *Arch Ophthalmol* 115, 645-50 (1997).
20. Ni, L. et al. RPAP3 interacts with Reptin to regulate UV-induced phosphorylation of H2AX and DNA damage. *J Cell Biochem* 106, 920-8 (2009).
21. Desronvil, T. et al. Distribution of COL8A2 and COL8A1 gene variants in Caucasian primary open angle glaucoma patients with thin central corneal thickness. *Mol Vis* 16, 2185-91 (2010).
22. Hysi, P. et al. Genome-wide analysis of multi-ancestry cohorts identifies new loci influencing intraocular pressure and susceptibility to glaucoma. *Nat. Genet.* doi: 10.1038/ng.3087 (2014).
23. Keyse, S.M. & Emslie, E.A. Oxidative stress and heat shock induce a human gene encoding a protein-tyrosine phosphatase. *Nature* 359, 644-7 (1992).
24. Kallio, M. et al. Brain abnormalities, defective meiotic chromosome synapsis and female subfertility in HSF2 null mice. *EMBO J* 21, 2591-601 (2002).
25. Wang, G., Zhang, J., Moskophidis, D. & Mivechi, N.F. Targeted disruption of the heat shock transcription factor (hsf)-2 gene results in increased embryonic lethality, neuronal defects, and reduced spermatogenesis. *Genesis* 36, 48-61 (2003).
26. Lipschutz, J.H. & Mostov, K.E. Exocytosis: the many masters of the exocyst. *Curr Biol* 12, R212-4 (2002).
27. Coleman, P.D. & Yao, P.J. Synaptic slaughter in Alzheimer's disease. *Neurobiol Aging* 24, 1023-7 (2003).
28. Lopez, I., Mak, E.C., Ding, J., Hamm, H.E. & Lomasney, J.W. A novel bifunctional phospholipase c that is regulated by Galpha 12 and stimulates the Ras/mitogen-activated protein kinase pathway. *J Biol Chem* 276, 2758-65 (2001).
29. Apte, S.S. A disintegrin-like and metalloprotease (reprolysin type) with thrombospondin type 1 motifs: the ADAMTS family. *Int J Biochem Cell Biol* 36, 981-5 (2004).
30. Kuchtey, J. et al. Screening ADAMTS10 in dog populations supports Gly661Arg as the glaucoma-causing variant in beagles. *Invest Ophthalmol Vis Sci* 54, 1881-6 (2013).
31. Kuchtey, J. et al. Mapping of the disease locus and identification of ADAMTS10 as a candidate gene in a canine model of primary open angle glaucoma. *PLoS Genet* 7, e1001306 (2011).

32. Li, Y., Willer, C.J., Ding, J., Scheet, P. & Abecasis, G.R. MaCH: using sequence and genotype data to estimate haplotypes and unobserved genotypes. *Genet Epidemiol* 34, 816-34 (2010).
33. Marchini, J., Howie, B., Myers, S., McVean, G. & Donnelly, P. A new multipoint method for genome-wide association studies by imputation of genotypes. *Nat Genet* 39, 906-13 (2007).
34. Li, H., Healey, P.R., Tariq, Y.M., Teber, E. & Mitchell, P. Symmetry of optic nerve head parameters measured by the heidelberg retina tomograph 3 in healthy eyes: the Blue Mountains Eye study. *Am J Ophthalmol* 155, 518-523 e1 (2013).
35. Yang, J., Lee, S.H., Goddard, M.E. & Visscher, P.M. GCTA: a tool for genome-wide complex trait analysis. *Am J Hum Genet* 88, 76-82 (2011).
36. Yang, J. et al. Common SNPs explain a large proportion of the heritability for human height. *Nat Genet* 42, 565-9 (2010).
37. Willer, C.J., Li, Y. & Abecasis, G.R. METAL: fast and efficient meta-analysis of genomewide association scans. *Bioinformatics* 26, 2190-1 (2010).
38. Higgins, J.P. & Thompson, S.G. Quantifying heterogeneity in a meta-analysis. *Stat Med* 21, 1539-58 (2002).
39. R Core Team. R: A Language and Environment for Statistical Computing. <http://www.R-project.org> 2014.
40. Pruim, R.J. et al. LocusZoom: regional visualization of genome-wide association scan results. *Bioinformatics* 26, 2336-7 (2010).
41. Li, M.X., Gui, H.S., Kwan, J.S. & Sham, P.C. GATES: a rapid and powerful gene-based association test using extended Simes procedure. *Am J Hum Genet* 88, 283-93 (2011).
42. Consortium, E.P. A user's guide to the encyclopedia of DNA elements (ENCODE). *PLoS Biol* 9, e1001046 (2011).
43. Kent, W.J. et al. The human genome browser at UCSC. *Genome Res* 12, 996-1006 (2002).

CHAPTER 4.3

Meta-analysis of genome-wide association studies identifies novel loci associated with optic disc morphology



Henriët Springelkamp*, Aniket Mishra*, Pirro G. Hysi*, Puya Gharahkhani*, René Höhn*, Chiea-Chuen Khor*, Jessica N. Cooke Bailey*, Xiaoyan Luo, Wishal D. Ramdas, Eranga Vithana, Victor Koh, Seyhan Yazar, Liang Xu, Hannah Forward, Lisa S Kearns, Najaf Amin, Adriana I. Iglesias, Kar-Seng Sim, Elisabeth M. van Leeuwen, Ayse Demirkan, Sven van der Lee, Seng-Chee Loon, Fernando Rivadeneira, Abhishek Nag, Paul G. Sanfilippo, Arne Schillert, Paulus T.V.M. de Jong, Ben A. Oostra, André G. Uitterlinden, Albert Hofman, NEIGHBORHOOD Consortium, Tiger Zhou, Kathryn P. Burdon, Timothy D. Spector, Karl J. Lackner, Seang-Mei Saw, Johannes R. Vingerling, Yik-Ying Teo, Louis R. Pasquale, Roger C.W. Wolfs, Hans G. Lemij, E-Shyong Tai, Jost B. Jonas, Ching-Yu Cheng, Tin Aung, Nomdo M. Jansonius, Caroline C.W. Klaver, Jamie E. Craig, Terri L. Young, Jonathan L. Haines, Stuart MacGregor, David A. Mackey, Norbert Pfeiffer‡, Tien-Yin Wong‡, Janey L. Wiggs‡, Alex W. Hewitt‡, Cornelia M. van Duijn‡, Christopher J. Hammond‡.

* These authors contributed equally.

‡ These authors jointly directed this work.

Genet Epidemiol. 2015 Mar;39(3):207-16. doi: 10.1002/gepi.21886.

Supplementary files and figures can be found at:

<http://onlinelibrary.wiley.com/doi/10.1002/gepi.21886/full>

ABSTRACT

Primary open-angle glaucoma is the most common optic neuropathy and an important cause of irreversible blindness worldwide. The optic nerve head or optic disc is divided in two parts: a central cup (without nerve fibers) surrounded by the neuroretinal rim (containing axons of the retinal ganglion cells). The International Glaucoma Genetics Consortium conducted a meta-analysis of genome-wide association studies consisting of 17,248 individuals of European ancestry and 6,841 individuals of Asian ancestry. The outcomes of the genome-wide association studies were disc area and cup area. These specific measurements describe optic nerve morphology in another way than the vertical cup-disc ratio, which is a clinically used measurement, and may shed light on new glaucoma mechanisms. We identified 10 new loci associated with disc area (*CDC42BPA*, *F5*, *DIRC3*, *RARB*, *ABI3BP*, *DCAF4L2*, *ELP4*, *TMTC2*, *NR2F2*, and *HORMAD2*) and another 10 new loci associated with cup area (*DHRS3*, *TRIB2*, *EFEMP1*, *FLNB*, *FAM101*, *DDHD1*, *ASB7*, *KPNB1*, *BCAS3*, and *TRIOBP*). The new genes participate in a number of pathways and future work is likely to identify more functions related to the pathogenesis of glaucoma.

INTRODUCTION

The optic nerve is a white matter tract approximately 55 millimeters in length that transmits visual information from the eye to the brain. Various diseases – the most common of which is glaucoma – affect the optic nerve morphology and function. There are many types of glaucoma and in this manuscript we focus on primary open-angle or simple glaucoma, which is one of the leading causes of irreversible blindness worldwide. The optic nerve head, often referred to as the optic disc, is the place where the retinal ganglion cell axons leave the eye and bundle together to form the optic nerve. It is visible at the back of the eye by ophthalmoscopy and is valuable in the assessment of optic nerve-related diseases. Additionally, the optic nerve morphology is a major target of imaging devices (including the Heidelberg Retina Tomography and Optical Coherence Tomography) in screening and follow-up of glaucoma-suspect persons and glaucoma patients. The optic disc consists of two morphologically distinct parts: the cup in the center of the disc, without nerve fibers, and the (neuroretinal) rim, carrying the axons of the retinal ganglion cells. There is a small, age-related decline in the number of axons during life: the decrease is about one third of axons in 100 years^{1,2}. Glaucoma is characterized by an accelerated loss of retinal ganglion cell axons, resulting in an enlarged cup and a reduced rim area. The heritability of optic nerve morphological features is estimated to be 52-83% for the disc area, 66-77% for the cup area, and 34-39% for the rim area^{3,4}. The majority of genetic studies has focused on the vertical cup-disc ratio (VCDR), which is a measure used to assess glaucoma clinically. However, different mechanisms (growth vs. degeneration) may underlie the disc, cup, and rim area. This raises the question whether gene discovery focusing on other measures (parameters) describing the optic disc than only the VCDR may shed light on the development and pathogenesis and mechanisms of diseases of the optic nerve. To date, genome-wide association studies (GWAS) have identified four loci for disc area within or near to the genes *ATOH7*, *CARD10*, *CDC7/TGFBR3* and *SALL1* and one locus for rim area (*RERE*)⁵⁻⁸. We performed a meta-analysis of GWAS for these disc area parameters within the International Glaucoma Genetics Consortium (IGGC).

METHODS

Study design

We performed a meta-analysis on directly genotyped and imputed SNPs from individuals of European ancestry in seven studies, with a total of 17,248 individuals (stage 1). Subsequently, we evaluated significantly associated SNPs in 6,841 subjects of Asian origin including four different studies (stage 2) and performed a meta-analysis on all individual studies from stage 1 and stage 2 (stage 3).

Participants and phenotyping

All studies included in this meta-analysis are part of the International Glaucoma Genetics Consortium (IGGC). The ophthalmic examination of each study included an assessment of the optic nerve head (Supplementary Table 1b).

The meta-analysis of stage 1 was based on 7 studies of European ancestry: Brisbane Adolescent Twin Study (BATS), Erasmus Rucphen Family (ERF) Study, Gutenberg Health Study (GHS I/

GHS II), Raine Study, Rotterdam Study (RS-I/RS-II/RS-III), Twins Eye Study in Tasmania (TEST), and TwinsUK. Stage 2 comprised 4 Asian studies: the Beijing Eye Study (BES), Singapore Chinese Eye Study (SCES), Singapore Malay Eye Study (SIMES), and Singapore Indian Eye Study (SINDI).

Information on general methods, demographics, phenotyping and genotyping methods of the study cohorts can be found in Supplementary Table 1 and 2 and the Supplementary Note. All studies were performed with the approval of their local medical ethics committee, and written informed consent was obtained from all participants in accordance with the Declaration of Helsinki.

Genotyping and imputation

Information on genotyping in each cohort, the particular platforms used to perform genotyping and the methods of imputation can be found in more detail in Supplementary Table 1c. To produce consistent data sets and enable a meta-analysis of studies across different genotyping platforms, the studies performed genomic imputation on available HapMap Phase 2 genotypes with MACH⁹ or IMPUTE¹⁰, using the appropriate ancestry groups as templates. Each study applied stringent quality control procedures for imputation (Supplementary Note). For the meta-analysis, only single nucleotide polymorphisms (SNPs) with minor allele frequency $\geq 1\%$, Hardy Weinberg Equilibrium p -value $> 10^{-6}$, and imputation quality scores ≥ 0.3 (proper-info of IMPUTE) or $R^2 \geq 0.3$ (MACH) were included.

Statistical analysis

As the rim area is the difference between the disc area and cup area, there are two independent variables. Of these, we selected (essentially arbitrarily from a mathematical point of view) disc area and cup area. Moreover, disc and cup area are clearly correlated (Pearson correlation coefficient is 0.59 in Rotterdam Study I). For that reason, we analyzed (1) disc area and (2) cup area adjusted for disc area. We used the mean of the measurements of both eyes. Unreliable optic nerve head data were excluded (e.g. images with standard deviation > 50 for the Heidelberg Retina Tomograph). In cases of missing or unreliable data for one eye, data for the other eye were taken. Each individual study did a linear regression model between the outcomes and approximately 2.5 million HapMap stage 2 SNPs under the assumption of an additive model for the effect of the risk allele. Analyses were adjusted for age, sex and the first two principal components (for population-based studies) or family structure (for family-based studies) to correct for population substructure. Adding additional principal components did not appreciably change the lambda. Glaucoma is characterized by an increased cupping independent of the size of the disc. Therefore, in the linear regression analysis with cup area as outcome, we used disc area as an extra covariate.

All study effect estimates were oriented to the positive strand of the NCBI Build 36 reference. Positioning and annotations for the SNPs were done using the NCBI Build 37 reference. We performed an inverse variance weighted fixed-effect meta-analysis using METAL software¹¹. We used the 'genomiccontrol' option in METAL that estimates the inflation of the test statistic of each individual study and corrects the standard error of each individual study for the inflation. In stage 1, a $P < 5.0 \times 10^{-8}$ (the genome-wide threshold of association) was considered significant. In the replication stage 2, a nominal $P < 0.05$ was considered significant given the already high prior probabilities of association from stage 1. Genome-wide significant SNPs

for disc area were tested for cup area, and vice versa. In total, there were 36 independent SNPs. Therefore, our Bonferonni corrected significant threshold for this analysis was $0.05 / 36 = 1.39 \times 10^{-3}$. Manhattan, regional and forest plots were made using R (<http://www.r-project.org/>), LocusZoom¹² and Stata/SE 12.0 (StataCorp LP, College Station, TX, USA), respectively.

Gene-based test using VEGAS

Gene-based testing was performed using VEGAS software¹³, which combines the test statistics of all SNPs present within and 50 kb upstream or downstream of each gene. Linkage disequilibrium (LD) between the markers was accounted for through simulations from the multivariate normal distribution, based on estimates of LD from reference populations. Because Asian and European ancestry populations show different LD patterns, we performed separate gene-based tests for each population. Hapmap 2 CEU population was used as a reference to calculate LD for European ancestry data, whereas Hapmap 2 JPT and CHB combined population was used as a reference for Asian ancestry data. After calculation of gene-based test statistics for Asian and European ancestry populations separately, meta-analysis was conducted using Fisher's method for combining p-values. VEGAS was applied to the summary data from the full disc and cup area analysis (as in Table 1 and 2).

Phenotypic variability

To evaluate whether the different optic nerve head area parameters have a shared genetic component with primary open angle glaucoma, two genetic risk scores were calculated based on the GWAS results for disc area and cup area. The genotyped SNPs from the discovery cohort were categorized into 17 categories according to p-values, and risk scores for each category were calculated in the ANZRAG study consisting of 1,155 glaucoma cases and 1,992 controls and NEIGHBOR consisting of 2,131 glaucoma cases and 2,290 controls as target cohorts (see Supplementary Information). To maximize the overlap between the genotyped SNPs from the discovery cohort and the SNPs included in the target cohorts, the imputed SNPs with imputation quality score > 0.8 in the target cohort were used for risk score calculation to replace SNPs that were not genotyped in the target cohort. For each individual, the score for a particular SNP was calculated as the effect estimate of the SNP multiplied by the dosage of the effect allele of that SNP. The risk score was defined as the mean of the scores for all SNPs. Logistic regression analyses with glaucoma as outcome adjusted for sex as covariate were performed to calculate the Nagelkerke R-square for the two risk scores (disc area and cup area).

Pathway-analysis using Pathway-VEGAS

Prespecified pathways from the Gene Ontology database with size ranging in 5-500 genes were used to perform pathway analysis. Pathway-VEGAS combines VEGAS gene-based test statistics based on prespecified biological pathways¹⁴. Pathway p-values were computed by summing χ^2 test statistics derived from VEGAS p-values. Empirical "VEGAS-pathway" p-values for each pathway were computed by comparing the real data summed χ^2 test statistics with 500,000 simulations where the relevant number (as per size of pathway) of randomly drawn χ^2 test statistics was summed. To ensure clusters of genes did not adversely affect the result, gene-sets were pruned such that each gene was > 500 kb from all other genes in the pathway. When genes were clustered, only one of the clustered genes was included for that pathway. Pathway-VEGAS was performed separately for European and Asian ancestry datasets. Meta-analysis was conducted using Fisher's method for combining p-values.

RESULTS

This work followed two parallel directions that corresponded to multistage meta-analyses of two phenotypes of interest. Although there were superimpositions in the genetic risk of each of these phenotypes leading to regulation of optic disc morphology in the populations, results will be broken down and reported individually for each. As described in the Methods, we tested for association using linear regression models adjusting for age, sex, and two principal components or family structure.

Disc area

Stage 1 included 17,248 individuals of European ancestry. We analyzed approximately 2.5 million directly genotyped or imputed (HapMap) SNPs. The inflation factors (λ) varied between 0.98 and 1.06 (1.10 for the meta-analysis), implying adequate within-study control of population substructure (Supplementary Table 2 and Supplementary Figures 2a, b, and c). This analysis yielded 296 genome-wide significant ($P < 5.0 \times 10^{-8}$) SNPs located across five chromosomal regions (*CDC7/TGFBR3*, *CDC42BPA*, *DCAF4L2*, *ATOH7*, and *SALL1*) (Table 1, Supplementary Fig. 1a and Supplementary Table 3).

Stage 2 included 6,841 individuals of Asian ancestry. The λ varied between 1.00 and 1.03. Of the most significantly associated SNPs at each of the five chromosomal regions in Europeans, three reached nominal significance ($P < 0.05$) in the Asians: *CDC7/TGFBR3*, *CDC42BPA*, and *ATOH7*. The SNP with the most significant association at the chromosome 8 region (*DCAF4L2*) in stage 1 was not imputed in the Asian population. The second most associated SNP in Europeans (rs12547416, $\beta = -0.03$, $P = 3.25 \times 10^{-8}$) at this region was significant in the Asian population ($\beta = -0.03$, $P = 2.95 \times 10^{-4}$).

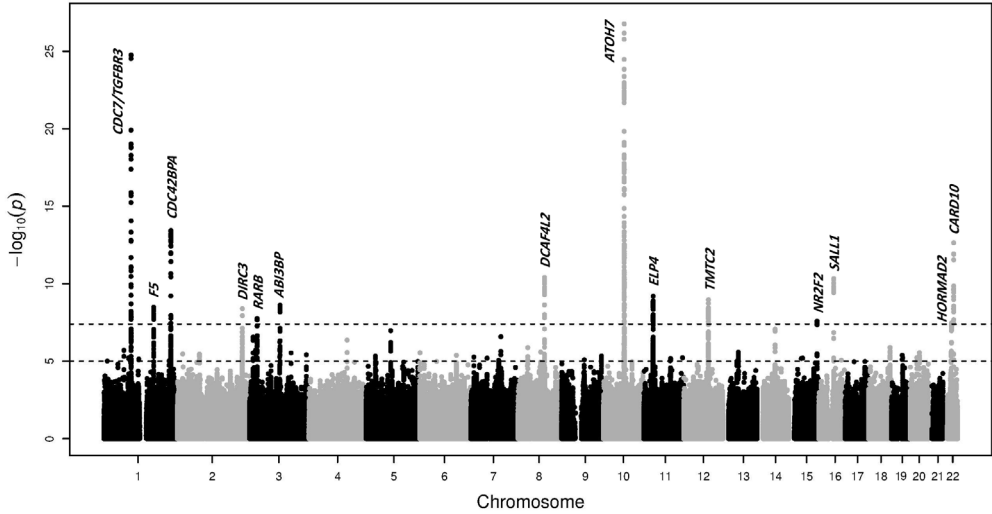
The combined analysis in stage 3 (overall λ 1.10) resulted in nine additional genome-wide significant chromosomal regions (Figure 1). The results of these SNPs were genome-wide suggestive ($P < 5.0 \times 10^{-5}$) in the individuals of European ancestry and nominally significant in individuals of Asian ancestry ($P < 0.05$). Of the 14 associated regions (five associated in Europeans and Asians and nine identified using all cohorts), 10 were not previously related to disc area: *CDC42BPA* (chr. 1) and *DCAF4L2* (chr. 8) identified in stage 1, and *F5* (chr.1), *DIRC3* (chr. 2), *RARB* (chr.3), *ABI3BP* (chr. 3), *ELP4* (chr. 11), *TMTC2* (chr. 12), *NR2F2* (chr. 15), and *HORMAD2* (chr. 22) identified in stage 3.

In order to identify new loci that were not found through per-SNP test, we performed a gene-based test using VEGAS software. Because of the smaller number of genes tested (17,872), our gene-based significance threshold $P_{\text{gene-based}}$ was 2.80×10^{-6} ($0.05 / 17,872$). Supplementary Table 5 shows 23 genes with a p-value below 2.80×10^{-6} for the gene-based test. Of these 23 genes, 22 genes were located in loci identified by the GWAS. In addition to the loci already identified, we found a gene-based significant association of *PAX6* with disc area (gene-based test $P = 5.15 \times 10^{-8}$).

Cup area

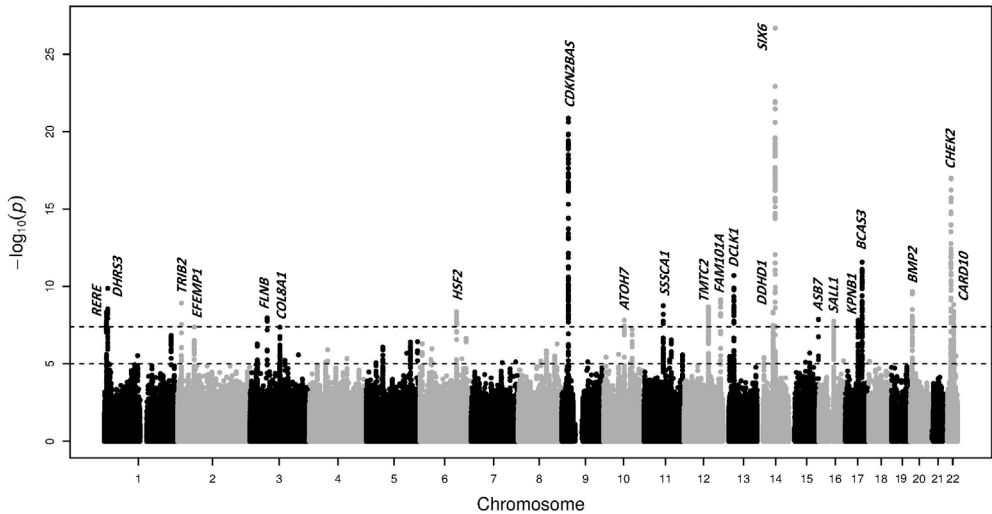
Stage 1 included 17,218 individuals of European ancestry, with λ -values varying between 0.98 and 1.06 (1.10 for the meta-analysis), implying adequate within-study control of

Figure 1. Manhattan plot of the GWAS meta-analysis for disc area in the combined analysis (n = 24,089 subjects of European and Asian ancestry).



The plot shows $-\log_{10}$ -transformed p-values for all single nucleotide polymorphisms. The upper black dotted horizontal line represents the genome-wide significance threshold of $P < 5.0 \times 10^{-8}$; the lower black dotted line indicates p-value of 1×10^{-5} .

Figure 2. Manhattan plot of the GWAS meta-analysis for cup area (adjusted for disc area) in the combined analysis (n = 23,831 subjects of European and Asian ancestry).



The plot shows $-\log_{10}$ -transformed p-values for all single nucleotide polymorphisms. The upper black dotted horizontal line represents the genome-wide significance threshold of $P < 5.0 \times 10^{-8}$; the lower black dotted line indicates p-value of 1×10^{-5} .

Table 1. Summary of SNPs that showed genome-wide significant ($P < 5 \times 10^{-8}$) association with disc area in the combined analysis ($n = 24,089$ subjects with European and Asian descent).

SNP	Chr./Position	Annotation	Nearest Gene	A1/A2	Europeans	Asians
					MAF	MAF
rs1192419	1/92080059	Intergenic	<i>CDC7/TGFBR3</i>	a/g	0.18	0.19
rs6671926	1/227386971	Intronic	<i>CDC42BPA*</i>	a/g	0.08	0.03
rs9969524	8/88746846	Intronic	<i>DCAF4L2*</i>	t/a	0.46	NA
rs1900004	10/70000881	Intronic	<i>ATOH7</i>	t/c	0.23	0.26
rs1362756	16/51458290	Intergenic	<i>SALL1</i>	c/g	0.29	0.15
rs12406092	1/169543131	Intronic	<i>F5*</i>	a/g	0.30	0.23
rs1549733	2/218472172	Intronic	<i>DIRC3*</i>	t/c	0.21	0.21
rs11129176	3/25049310	Intronic	<i>RARB*</i>	a/g	0.29	0.22
rs9860250	3/100637871	Intronic	<i>ABI3BP*</i>	g/a	0.18	0.08
rs11031436	11/31663882	Intronic	<i>ELP4*</i>	t/a	0.22	0.32
rs1511589	12/84061431	Intergenic	<i>TMTC2*</i>	a/g	0.46	0.18
rs8034595	15/96719229	Intronic	<i>NR2F2*</i>	a/c	0.28	0.30
rs2412970	22/30486826	Intronic	<i>HORMAD2*</i>	g/a	0.43	0.41
rs9607469	22/37919267	Upstream gene variant	<i>CARD10</i>	a/g	0.15	0.23

We tested for heterogeneous effects, for which p-values and I^2 are shown. Results for the combined meta-analysis of cup area are shown. The first five SNPs were genome-wide significant in stage 1 (meta-analysis of subjects with European descent); the last nine SNPs reached genome-wide significance in stage 3 (meta-analysis of subjects with European and Asian descent). SNP, single nucleotide polymorphism; nearest gene, reference NCBI build 37; A1, reference allele; A2, other allele; MAF, average minor allele frequency; NA, not available; β , effect size on disc area based on allele A1 based on a fixed-effect meta-analysis; β (R), effect size on disc area based on allele A1 based on a random-effect meta-analysis; P-value (R) is the p-value based on a random-effect meta-analysis; SE, standard error of the effect size; * are the newly identified loci.

Table 1. (continued)

Combined (n = 24,089)					Heterogeneity		Cup area combined (n = 23,831)		
β	SE	P-value	β (R)	P-value (R)	P-value	I ²	β	SE	P-value
0.087	0.006	7.98×10^{-56}	0.087	7.98×10^{-56}	8.51×10^{-1}	0	0.006	0.003	4.58×10^{-2}
-0.067	0.009	3.69×10^{-14}	-0.065	9.21×10^{-14}	5.95×10^{-1}	0	0.025	0.005	2.33×10^{-7}
0.030	0.005	1.54×10^{-8}	0.032	4.36×10^{-7}	2.79×10^{-1}	19	0.006	0.003	4.24×10^{-2}
-0.097	0.005	1.13×10^{-73}	-0.097	7.27×10^{-39}	6.43×10^{-2}	40.4	-0.016	0.003	4.92×10^{-8}
0.033	0.005	9.27×10^{-11}	0.033	5.84×10^{-10}	3.91×10^{-1}	5.6	0.011	0.003	4.66×10^{-5}
0.028	0.005	3.32×10^{-9}	0.028	3.3×10^{-9}	4.60×10^{-1}	0	0.003	0.003	2.88×10^{-1}
0.031	0.005	4.03×10^{-9}	0.031	4.03×10^{-9}	6.74×10^{-1}	0	-0.001	0.003	6.99×10^{-1}
0.026	0.005	1.74×10^{-8}	0.026	1.74×10^{-8}	7.99×10^{-1}	0	0.011	0.003	1.12×10^{-5}
-0.036	0.006	2.42×10^{-9}	-0.036	2.42×10^{-9}	4.59×10^{-1}	0	-0.004	0.003	2.05×10^{-1}
0.033	0.005	6.43×10^{-10}	0.032	3.63×10^{-7}	2.47×10^{-1}	19.4	0.003	0.003	3.26×10^{-1}
-0.028	0.005	1.08×10^{-9}	-0.028	5.40×10^{-8}	3.22×10^{-1}	12	-0.012	0.003	5.34×10^{-6}
-0.026	0.005	2.54×10^{-8}	-0.026	2.54×10^{-8}	4.99×10^{-1}	0	0.003	0.003	2.20×10^{-1}
0.024	0.004	3.40×10^{-8}	0.024	3.40×10^{-8}	6.75×10^{-1}	0	0.007	0.002	3.52×10^{-3}
0.041	0.006	2.29×10^{-13}	0.041	1.31×10^{-8}	1.17×10^{-1}	32.3	0.005	0.003	1.03×10^{-1}

Table 2. Summary of SNPs that showed genome-wide significant ($P < 5 \times 10^{-8}$) association with cup area (adjusted for disc area) in the combined analysis (n = 23,831 subjects with European and Asian descent).

SNP	Chr./Position	Annotation	Nearest Gene	A1/A2	Europeans	Asians
					MAF	MAF
rs301801	1/8495945	Intronic	<i>RERE</i>	c/t	0.33	0.15
rs3924048	1/12614848	Intergenic	<i>DHRS3*</i>	g/a	0.40	0.58
rs2113818	2/12890860	Intergenic	<i>TRIB2*</i>	t/c	0.49	0.29
rs2623325	3/99131755	Intergenic	<i>COL8A1</i>	a/c	0.11	0.18
rs7865618	9/22031005	Intronic	<i>CDKN2B-AS1</i>	g/a	0.44	0.16
rs3858145	10/70011838	Regulatory	<i>ATOX7</i>	g/a	0.25	0.34
rs1346	11/65337251	Upstream	<i>SSSCA1</i>	t/a	0.19	0.34
rs7972528	12/84131036	Intergenic	<i>TMTC2</i>	t/c	0.47	0.11
rs9546434	13/36694391	Intronic	<i>DCLK1</i>	t/c	0.23	0.44
rs10483727	14/61072875	Upstream	<i>SIX6</i>	t/c	0.40	0.71
rs11646917	16/51428908	Intergenic	<i>SALL1</i>	t/g	0.27	NA
rs11870935	17/45732605	Intronic	<i>KPNB1*</i>	g/a	0.47	0.35
rs11651885	17/59286263	Intronic	<i>BCAS3*</i>	g/a	0.23	0.29
rs6054383	20/6584604	Intergenic	<i>BMP2</i>	t/g	0.42	0.61
rs1033667	22/29130300	Intronic	<i>CHEK2</i>	t/c	0.28	0.18
rs1346786	2/56108333	Intronic	<i>EFEMP1*</i>	t/c	0.31	0.63
rs6764184	3/58006266	Intronic	<i>FLNB*</i>	t/g	0.24	0.46
rs1402538	6/122388851	Intergenic	<i>HSF2</i>	a/g	0.38	0.40
rs10846617	12/124662131	Intronic	<i>FAM101A*</i>	c/g	0.44	0.28
rs10130556	14/53970675	Intronic	<i>DDHD1/BMP4*</i>	g/c	0.41	0.47
rs11247230	15/101197005	Intergenic	<i>ASB7*</i>	g/a	0.34	0.71
rs5756813	22/38175477	Downstream	<i>TRIOBP*</i>	g/t	0.39	0.34

We tested for heterogeneous effects, for which p-values and I^2 are shown. Results for the combined meta-analysis for cup area are shown. The first fifteen SNPs were genome-wide significant in stage 1 (meta-analysis of subjects with European descent); the last seven SNPs reached genome-wide significance in stage 3 (meta-analysis of subjects with European and Asian descent). SNP, single nucleotide polymorphism; nearest gene, reference NCBI build 37; A1, reference allele; A2, other allele; MAF, average minor allele frequency; NA, not available; β , effect size on cup area based on allele A1 based on a fixed-effect meta-analysis; β (R), effect size on cup area based on allele A1 based on a random-effect meta-analysis; P-value (R) is the p-value based on a random-effect meta-analysis; SE, standard error of the effect size; * are the newly identified loci.

Table 2.(continued)

Combined (n = 23,831)					Heterogeneity		Disc area combined (n = 24,089)		
β	SE	P-value	β (R)	P-value (R)	P-value	I ²	β	SE	P-value
0.016	0.003	4.55x10 ⁻⁹	0.016	4.55x10 ⁻⁹	4.56x10 ⁻¹	0	0.004	0.005	3.80x10 ⁻¹
-0.016	0.003	1.34x10 ⁻¹⁰	-0.016	1.34x10 ⁻¹⁰	7.55x10 ⁻¹	0	-0.003	0.005	4.68x10 ⁻¹
0.015	0.002	1.19x10 ⁻⁹	0.015	1.19x10 ⁻⁹	7.90x10 ⁻¹	0	0.005	0.004	2.70x10 ⁻¹
0.025	0.005	4.36x10 ⁻⁸	0.024	1.33x10 ⁻⁵	1.71x10 ⁻¹	27.9	0.025	0.008	1.92x10 ⁻³
-0.023	0.002	1.37x10 ⁻²¹	-0.022	9.36x10 ⁻¹⁷	3.12x10 ⁻¹	12.9	-0.010	0.005	2.01x10 ⁻²
-0.015	0.003	7.83x10 ⁻⁸	-0.014	1.56x10 ⁻⁵	1.65x10 ⁻¹	18.6	-0.09	0.005	5.14x10 ⁻⁷⁵
-0.019	0.003	1.78x10 ⁻⁹	-0.019	7.50x10 ⁻⁹	4.02x10 ⁻¹	4.4	-0.020	0.006	3.84x10 ⁻⁴
-0.014	0.003	4.03x10 ⁻⁸	-0.011	9.34x10 ⁻³	8.02x10 ⁻³	55.4	-0.020	0.005	4.24x10 ⁻⁵
0.021	0.003	1.98x10 ⁻¹¹	0.020	2.11x10 ⁻¹¹	6.38x10 ⁻¹	0	-0.012	0.006	2.80x10 ⁻²
0.026	0.002	2.10x10 ⁻²⁷	0.025	2.41x10 ⁻¹⁰	4.80x10 ⁻³	56.6	-0.023	0.004	1.14x10 ⁻⁷
-0.018	0.003	1.71x10 ⁻⁸	-0.018	1.84x10 ⁻⁸	4.36x10 ⁻¹	0.2	-0.020	0.006	8.53x10 ⁻⁴
0.013	0.002	1.57x10 ⁻⁸	0.013	1.57x10 ⁻⁸	5.81x10 ⁻¹	0	0.001	0.004	8.82x10 ⁻¹
-0.018	0.003	4.49x10 ⁻¹¹	-0.017	1.09x10 ⁻⁴	9.27x10 ⁻³	54.6	0.012	0.005	1.75x10 ⁻²
-0.015	0.002	2.13x10 ⁻¹⁰	-0.014	2.51x10 ⁻⁷	2.04x10 ⁻¹	0	0.002	0.004	6.88x10 ⁻¹
-0.023	0.003	1.13x10 ⁻¹⁷	-0.024	5.48x10 ⁻¹²	1.19x10 ⁻¹	32.1	-0.020	0.005	6.18x10 ⁻⁵
-0.014	0.003	4.26x10 ⁻⁸	-0.014	4.26x10 ⁻⁸	5.20x10 ⁻¹	0	0.008	0.005	9.66x10 ⁻²
0.015	0.003	1.10x10 ⁻⁸	0.015	2.48x10 ⁻⁷	2.94x10 ⁻¹	14.6	0.003	0.005	5.25x10 ⁻¹
-0.014	0.002	4.33x10 ⁻⁹	-0.014	4.33x10 ⁻⁹	7.51x10 ⁻¹	0	-0.015	0.004	8.57x10 ⁻⁴
-0.014	0.002	7.17x10 ⁻¹⁰	-0.014	7.17x10 ⁻¹⁰	4.71x10 ⁻¹	0	-0.003	0.004	5.31x10 ⁻¹
-0.014	0.002	4.53x10 ⁻⁹	-0.014	4.53x10 ⁻⁹	6.46x10 ⁻¹	0	0.006	0.005	2.07x10 ⁻¹
0.014	0.003	1.34x10 ⁻⁸	0.014	1.34x10 ⁻⁸	8.46x10 ⁻¹	0	0.017	0.004	1.41x10 ⁻⁴
0.014	0.002	1.49x10 ⁻⁹	0.014	1.49x10 ⁻⁹	9.61x10 ⁻¹	0	0.013	0.004	2.39x10 ⁻³

population substructure (Supplementary Table 2 and Supplementary Figures 6a, b, and c). In total, 342 SNPs located across 15 chromosomal regions were genome-wide significant (Table 2, Supplementary Fig. 5a and Supplementary Table 4).

Stage 2 consisted of 6,613 individuals of Asian ancestry (λ 1.01-1.03). Nine of the 15 most associated SNPs across the 15 chromosomal regions were nominal significant in this Asian population. The most significantly associated SNP on chromosome 16 in Europeans could not be imputed with sufficient accuracy for use in individuals of Asian ancestry (*SALL1*). The second most significant associated SNP in the Europeans (rs4238758, β =-0.02, $P=4.83 \times 10^{-8}$) did not replicate in individuals of Asian ancestry (β =-0.02, $P=3.11 \times 10^{-1}$).

In stage 3, the combined analysis (meta-analysis λ 1.10) yielded seven additional genome-wide significant loci (Figure 2). Of the 22 (15+7) chromosomal regions, 12 were previously genome-wide significant associated with the VCDR, the clinically used optic disc parameter¹⁵. The VCDR is highly correlated to cup area ($r=0.78$, calculated in the Rotterdam Study I). The other 10 loci were new: *DHRS3* (chr.1), *TRIB2* (chr.2), *KPNB1* (chr.17) and *BCAS3* (chr.17) identified in stage 1, and *EFEMP1* (chr. 2), *FLNB* (chr.3), *FAM101A* (chr.12), *DDHD1* (chr.14), *ASB7* (chr.15), and *TRIOBP* (chr.22) identified in stage 3. In the gene-based analysis, *FAT4* was significantly associated with cup area, but this association disappeared after correction for disc area. This gene is also associated with disc area (nominal significant; $P=6.69 \times 10^{-3}$) suggesting that *FAT4* acts primarily through its effect on disc area. For the cup area adjusted for disc area analysis, 27 genes were significant but all of them are located in regions identified by the GWAS.

From genes to glaucoma

To investigate the relevance of the disc area and cup area SNPs in the clinical disease glaucoma, we calculated the explained variance of glaucoma in ANZRAG and NEIGHBOR. The top SNPs from the disc area analysis ($P < 10^{-8}$) explained 0.1% (ANZRAG) and 0.07% (NEIGHBOR) of the variance of glaucoma (Table 3). The top SNPs from the cup area analyses ($P < 10^{-8}$), explained 2.1% (ANZRAG) and 3.2% (NEIGHBOR) of the variance. The top SNPs mainly consisted of SNPs in *CDKN2B-AS1* and *SIX6*. To investigate the effect of other SNPs, we removed SNPs within 1 MB from *CDKN2B-AS1* and *SIX6* in ANZRAG. The explained variance of glaucoma decreased from 1.5% to 1.0% (SNPs $P < 0.1$), but was still significant ($P=1.36 \times 10^{-6}$). In the Rotterdam Study I, the 10 new cup area SNPs explained an additional 0.9% of the VCDR phenotypic variability compared to known VCDR SNPs¹⁵.

Pathway analysis

To test whether the genes found through the VEGAS gene-based approach were enriched in 4,628 prespecified Gene Ontology pathways we performed a pathway analysis using Pathway-VEGAS¹⁴. We used a pathway-wide significance threshold of 1.08×10^{-5} ($0.05 / 4628$). One pathway exceeded the pathway-wide significance level for disc area: "Entrainment of circadian clock" ($P=8.00 \times 10^{-6}$). This pathway result was driven by the strong association signal at *ATO7H*. For cup area (unadjusted for disc area), the top pathway is "Negative regulation of cyclin-dependent protein kinase activity" that is also associated with VCDR¹⁵. After adjustment for disc area, the top pathway for cup area was "G1/S transition checkpoint" ($P=4.66 \times 10^{-5}$) (Supplementary Table 6). The known POAG gene *CDKN2B-AS1* is part of this pathway.

Table 3. The explained variance (Nagelkerke R²) for glaucoma in ANZTRAG (1,155 cases and 1,992 controls) and NEIGHBOR (2,131 cases and 2,290 controls) determined by the single nucleotide polymorphisms from the genome-wide association analysis for disc area and cup area.

P-value threshold	Disc area				Number of tested SNPs	Cup area				
	ANZTRAG		NEIGHBOR			ANZTRAG		NEIGHBOR		
	Beta	R ²	P-value	R ²		P-value	Beta	R ²	P-value	
<10 ⁻⁸	-0.15	0.0011	1.08x10 ⁻¹	0.0007	1.25x10 ⁻¹	1.96	0.0207	4.08x10 ⁻¹²	0.0316	<2.00x10 ⁻¹⁶
<10 ⁻⁷	-0.14	0.0010	1.24x10 ⁻¹	0.0007	1.34x10 ⁻¹	1.82	0.0207	4.22x10 ⁻¹²	0.0353	<2.00x10 ⁻¹⁶
<10 ⁻⁶	-0.12	0.0009	1.52x10 ⁻¹	0.0008	1.02x10 ⁻¹	1.56	0.0179	1.23x10 ⁻¹⁰	0.0355	<2.00x10 ⁻¹⁶
<10 ⁻⁵	-0.09	0.0005	2.62x10 ⁻¹	0.0014	2.95x10 ⁻²	1.43	0.0190	3.30x10 ⁻¹¹	0.0348	<2.00x10 ⁻¹⁶
<10 ⁻⁴	-0.04	0.0001	5.87x10 ⁻¹	0.0019	1.29x10 ⁻⁴	1.09	0.0180	1.11x10 ⁻¹⁰	0.0313	<2.00x10 ⁻¹⁶
<10 ⁻³	-0.01	0.0000	9.22x10 ⁻¹	0.0034	7.72x10 ⁻⁴	0.88	0.0211	2.48x10 ⁻¹²	0.0316	<2.00x10 ⁻¹⁶
<10 ⁻²	0.07	0.0015	6.67x10 ⁻²	0.0040	2.85x10 ⁻⁴	0.49	0.0183	7.84x10 ⁻¹¹	0.0284	<2.00x10 ⁻¹⁶
<0.1	0.07	0.0055	3.71x10 ⁻⁴	0.0038	3.87x10 ⁻⁴	0.21	0.0151	3.42x10 ⁻⁹	0.0165	1.52x10 ⁻¹³
<0.2	0.05	0.0048	8.39x10 ⁻⁴	0.0049	5.73x10 ⁻⁵	0.15	0.0132	3.14x10 ⁻⁸	0.0149	2.44x10 ⁻¹²
<0.3	0.04	0.0038	2.94x10 ⁻³	0.0054	2.54x10 ⁻⁵	0.13	0.0114	2.94x10 ⁻⁷	0.0142	7.10x10 ⁻¹²
<0.4	0.04	0.0041	2.20x10 ⁻³	0.0053	2.76x10 ⁻⁵	0.11	0.0107	6.76x10 ⁻⁷	0.0137	1.87x10 ⁻¹¹
<0.5	0.04	0.0042	1.97x10 ⁻³	0.0057	1.42x10 ⁻⁵	0.11	0.0110	4.51x10 ⁻⁷	0.0127	1.01x10 ⁻¹⁰
<0.6	0.04	0.0042	1.93x10 ⁻³	0.0059	1.05x10 ⁻⁵	0.11	0.0112	3.60x10 ⁻⁷	0.0123	1.83x10 ⁻¹⁰
<0.7	0.04	0.0042	1.96x10 ⁻³	0.0058	1.30x10 ⁻⁵	0.11	0.0110	4.82x10 ⁻⁷	0.0126	1.19x10 ⁻¹⁰
<0.8	0.04	0.0042	1.83x10 ⁻³	0.0058	1.19x10 ⁻⁵	0.11	0.0111	4.26x10 ⁻⁷	0.0127	9.37x10 ⁻¹¹
<0.9	0.04	0.0042	1.96x10 ⁻³	0.0058	1.15x10 ⁻⁵	0.11	0.0109	4.96x10 ⁻⁷	0.0125	1.23x10 ⁻¹⁰
<1.0	0.04	0.0041	2.04x10 ⁻³	0.0058	1.15x10 ⁻⁵	0.11	0.0110	4.73x10 ⁻⁷	0.0126	1.19x10 ⁻¹⁰

DISCUSSION

This study identified new genetic loci associated with two parameters describing the morphology of the optic nerve head. In total, we identified 10 new disc area loci and 10 new cup area loci. Gene-based analysis identified one additional region associated with disc area.

Of the 10 new disc area loci, two were identified in stage 1 and did replicate in stage 2. The eight other new loci were identified in stage 3 and therefore replication is missing because of lack of samples. In the cup area analysis, four new loci were identified in stage 1 and the *KPNB1* and *BCAS3* SNPs did not replicate in stage 2. However, the effect estimates are similar and in the same direction in Caucasian and Asian populations so this might be due to lack of power since we included less samples in stage 2. For the six other new loci from stage 3, replication is also missing. Although there is lack of replication for the new loci identified in stage 3, the p-values of the associations from stage 1 are low for these SNPs and the effect estimates are similar and in the same direction in stage 2, suggesting that these new loci are real new loci. Some SNPs showed heterogeneity. Therefore, we ran also a random-effect meta-analysis. For the new loci, most effect estimates and p-values remain similar after the random-effect meta-analysis. Only the p-value for *BCAS3* (cup area) decreased from 4.49×10^{-11} to 9.27×10^{-3} , but the effect estimate remained similar (-0.018 vs. -0.017), which is compatible with the heterogeneity as measured with the I^2 .

We investigated the expression of the genes implicated in the parameters for optic nerve head areas by these analyses in various eye tissues using published literature or human ocular gene expression databases (Supplementary Table 7 and 8)¹⁶⁻¹⁹. The highest expression in the optic nerve was found for *ABI3BP*. Most of the other genes were also expressed in the optic nerve or other glaucoma-related eye tissues like the trabecular meshwork and the cornea.

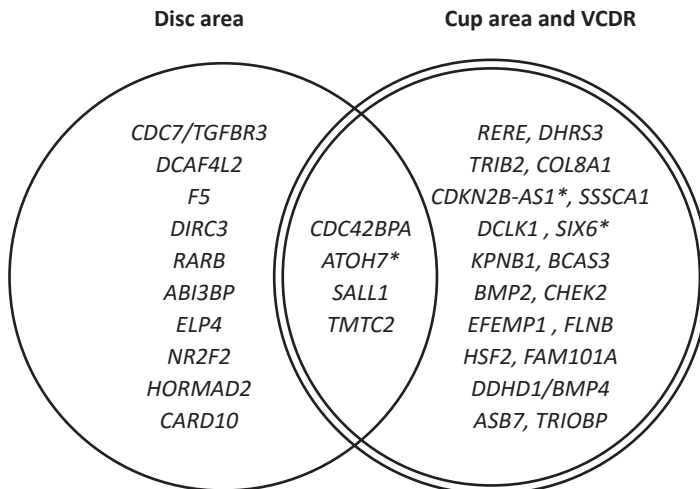
The genes in the new disc area loci have different functions. An interesting gene is *RARB*, which limits cell growth by regulating gene expression. Also *NR2F2* plays a role in gene regulation. *PAX6* was identified by gene-based analysis. Although *PAX6* is a neighboring gene (with linkage disequilibrium extending across this region) to *ELP4*, which was associated with disc area in the GWAS, the strong biological relevance of *PAX6* to eye development (it is expressed in developing eyes, and rare mutations cause aniridia, a rare developmental eye disorder²⁰) suggests that genetic variation in this region more likely influences the regulation of *PAX6* rather than other genes in the region.

Our study shows that studies of optic nerve head parameters may shed light on clinical outcomes. The genetic overlap between disc area and glaucoma is small, but the direction of the significant risk scores (P threshold < 0.1 and higher) might suggest that a larger disc area increases the risk of glaucoma. There is a strong genetic overlap between the cup area and glaucoma: 2.1% and 3.2% of the variance of glaucoma is explained by the most significant SNPs for cup area in two independent glaucoma case-control studies (ANZRAG and NEIGHBOR, respectively). This is mostly explained by the known genes *CDKN2B-AS1* and *SIX6*, but SNPs in other genes explain also 1.0% of the variance, based on a polygenic risk

score comprising all SNPs associated at $P < 0.1$ with cup area. The loci that are associated with cup area are also associated with VCDR (Supplementary Table 9). The region on chromosome 22 (with the top SNP rs5756813) contains the *CARD10* gene that was previously reported to be associated with disc area. However, it seems that the *TRIOBP* gene is responsible for the association with cup area. Its protein interacts with trio, which is interesting because of the role of trio in neural tissue development²¹. The nearest gene to the top SNP on chromosome 14 (rs10130566) is *DDHD1*, but the association might be explained by the *BMP4* gene. This gene is a member of the bone morphogenetic protein family, which is part of the transforming growth factor-beta superfamily. Another member of this family is *BMP2*, which is also associated with VCDR¹⁵. While the top SNP on chromosome 15 is located near to the *ASB4* gene, the *ADAMTS17* in this region may contribute more to disease susceptibility. This gene belongs to the same family of *ADAMTS10*, which is associated with VCDR¹⁵. Furthermore, *ADAMTS17* is already linked to some forms of (syndromal) glaucoma²². Pathway analysis implicated that cell growth and death is an important mechanism associated with cup area.

Figure 3 shows the overlap between the different optic nerve head area parameters. Overall, most loci were only associated with disc area or cup area. *ATOH7* was associated with disc and cup area as well as with glaucoma²³. *SIX6* and *CDKN2B-AS1* were associated with cup area and glaucoma^{24,25}. The figure shows only genome-wide significant SNPs, but it is likely that other SNPs affect also more than one trait, including rs11129176 (*RARB*), which is genome-wide significant in disc area and reached a p-value of 1.12×10^{-5} in the cup area analysis.

Figure 3. Overlap between the different optic nerve head parameters. Genes that reached genome-wide significance are shown.



VCDR = vertical cup-disc ratio, * = genes that have been previously associated with glaucoma. All SNPs associated with cup area, are also associated with VCDR (Supplementary Table 9).

In summary, we found 20 new loci associated with optic nerve head area and/or cupping which explain a further proportion of the missing heritability of glaucoma. These results showed that investigation of more refined measurements of optic nerve head morphology, especially the cup area, is a fruitful approach to discover new glaucoma-related loci, in addition to the crude VCDR linear measurement commonly used in clinical practice and previously investigated¹⁵. The new loci contain many genes with different functions, and while there appears to be one strong candidate causal gene in some regions, there are several possible candidate genes in others. Further research including exome sequencing and functional studies is necessary to unravel the causative associations in the gene-dense regions and the mechanism of these genes in the pathophysiology of glaucoma. Our findings are an important step towards a better understanding of the disease.

References

1. Jonas, J.B., Muller-Bergh, J.A., Schlotzer-Schrehardt, U.M. & Naumann, G.O. Histomorphometry of the human optic nerve. *Invest Ophthalmol Vis Sci* 31, 736-44 (1990).
2. Jonas, J.B., Schmidt, A.M., Muller-Bergh, J.A., Schlotzer-Schrehardt, U.M. & Naumann, G.O. Human optic nerve fiber count and optic disc size. *Invest Ophthalmol Vis Sci* 33, 2012-8 (1992).
3. Sanfilippo, P.G., Hewitt, A.W., Hammond, C.J. & Mackey, D.A. The heritability of ocular traits. *Surv Ophthalmol* 55, 561-83 (2010).
4. van Koolwijk, L.M. et al. Genetic contributions to glaucoma: heritability of intraocular pressure, retinal nerve fiber layer thickness, and optic disc morphology. *Invest Ophthalmol Vis Sci* 48, 3669-76 (2007).
5. Axenovich, T. et al. Linkage and association analyses of glaucoma related traits in a large pedigree from a Dutch genetically isolated population. *J Med Genet* 48, 802-9 (2011).
6. Khor, C.C. et al. Genome-wide association studies in Asians confirm the involvement of ATOH7 and TGFBR3, and further identify CARD10 as a novel locus influencing optic disc area. *Hum Mol Genet* 20, 1864-72 (2011).
7. Ramdas, W.D. et al. A genome-wide association study of optic disc parameters. *PLoS Genet* 6, e1000978 (2010).
8. Macgregor, S. et al. Genome-wide association identifies ATOH7 as a major gene determining human optic disc size. *Hum Mol Genet* 19, 2716-24 (2010).
9. Li, Y., Willer, C.J., Ding, J., Scheet, P. & Abecasis, G.R. MaCH: using sequence and genotype data to estimate haplotypes and unobserved genotypes. *Genet Epidemiol* 34, 816-34 (2010).
10. Marchini, J., Howie, B., Myers, S., McVean, G. & Donnelly, P. A new multipoint method for genome-wide association studies by imputation of genotypes. *Nat Genet* 39, 906-13 (2007).
11. Willer, C.J., Li, Y. & Abecasis, G.R. METAL: fast and efficient meta-analysis of genomewide association scans. *Bioinformatics* 26, 2190-1 (2010).
12. Pruim, R.J. et al. LocusZoom: regional visualization of genome-wide association scan results. *Bioinformatics* 26, 2336-7 (2010).
13. Liu, J.Z. et al. A versatile gene-based test for genome-wide association studies. *Am J Hum Genet* 87, 139-45 (2010).
14. Lu, Y. et al. Genome-wide association analyses identify multiple loci associated with central corneal thickness and keratoconus. *Nat Genet* 45, 155-63 (2013).
15. Springelkamp, H. et al. Meta-analysis of genome-wide association studies identifies novel loci that influence cupping and the glaucomatous process. *Nat Commun* 5, 4883 (2014).
16. Bowes Rickman, C. et al. Defining the human macula transcriptome and candidate retinal disease genes using EyeSAGE. *Invest Ophthalmol Vis Sci* 47, 2305-16 (2006).
17. Liu, Y. et al. Serial analysis of gene expression (SAGE) in normal human trabecular meshwork. *Mol Vis* 17, 885-93 (2011).
18. Wagner, A.H. et al. Exon-level expression profiling of ocular tissues. *Exp Eye Res* 111, 105-11 (2013).
19. Young, T.L. et al. Whole Genome Expression Profiling of Normal Human Fetal and Adult Ocular Tissues. *Exp Eye Res* 116, 265-78 (2013).
20. Jordan, T. et al. The human PAX6 gene is mutated in two patients with aniridia. *Nat Genet* 1, 328-32 (1992).
21. Seipel, K., O'Brien, S.P., Iannotti, E., Medley, Q.G. & Streuli, M. Tara, a novel F-actin binding protein, associates with the Trio guanine nucleotide exchange factor and regulates actin cytoskeletal organization. *J Cell Sci* 114, 389-99 (2001).
22. Morales, J. et al. Homozygous mutations in ADAMTS10 and ADAMTS17 cause lenticular myopia, ectopia lentis, glaucoma, spherophakia, and short stature. *Am J Hum Genet* 85, 558-68 (2009).
23. Ramdas, W.D. et al. Common genetic variants associated with open-angle glaucoma. *Hum Mol Genet* 20, 2464-71 (2011).
24. Burdon, K.P. et al. Genome-wide association study identifies susceptibility loci for open angle glaucoma at TMC01 and CDKN2B-AS1. *Nat Genet* 43, 574-8 (2011).
25. Wiggs, J.L. et al. Common variants at 9p21 and 8q22 are associated with increased susceptibility to optic nerve degeneration in glaucoma. *PLoS Genet* 8, e1002654 (2012).

CHAPTER 4.4

ARHGEF12 influences the risk of glaucoma by increasing intraocular pressure



Henriët Springelkamp*, Adriana I. Iglesias*, Gabriel Cuellar-Partida, Najaf Amin, Kathryn P. Burdon, Elisabeth M. van Leeuwen, Puya Gharakhani, Aniket Mishra, Sven van der Lee, Alex W. Hewitt, Fernando Rivadeneira, Ananth C. Viswanathan, Roger C.W. Wolfs, Nicholas G. Martin, Wishal D. Ramdas, Leonieke M. van Koolwijk, Craig E. Pennell, Johannes R. Vingerling, Jenny E. Mountain, André G. Uitterlinden, Albert Hofman, Paul Mitchell, Hans G. Lemij, Jie Jin Wang, Caroline C.W. Klaver, David A. Mackey, Jamie E. Craig, Cornelia M. van Duijn‡, Stuart MacGregor‡.

* These authors contributed equally.

‡ These authors jointly directed this work.

Hum Mol Genet. 2015 May 1;24(9):2689-99. doi: 10.1093/hmg/ddv027.

Supplementary files and figures can be found at:

<http://hmg.oxfordjournals.org/content/24/9/2689.long>

ABSTRACT

Primary open-angle glaucoma (POAG) is a blinding disease. Two important risk factors for this disease are a positive family history and elevated intraocular pressure (IOP), which is also highly heritable. Genes found to date associated with IOP and POAG are *ABCA1*, *CAV1/CAV2*, *GAS7*, and *TMC01*. However, these genes explain only a small part of the heritability of IOP and POAG. We performed a genome-wide association study of IOP in the population-based Rotterdam Study I and Rotterdam Study II using single nucleotide polymorphisms (SNPs) imputed to 1000 Genomes. In this discovery cohort ($n = 8,105$) we identified a new locus associated with IOP. The most significantly associated SNP was rs58073046 ($\beta=0.44$, $P=1.87 \times 10^{-8}$, minor allele frequency = 0.12), within the gene *ARHGEF12*. Independent replication in five population-based studies ($n = 7,471$) resulted in an effect size in the same direction that was significantly associated ($\beta=0.16$, $P=0.04$). The SNP was also significantly associated with POAG in two independent case-control studies ($n = 1,225$ cases and $n = 4,117$ controls; OR = 1.53, $P=1.99 \times 10^{-8}$), especially with high-tension glaucoma (OR = 1.66, $P=2.81 \times 10^{-9}$; for normal-tension glaucoma OR = 1.29, $P=4.23 \times 10^{-2}$). *ARHGEF12* plays an important role in the RhoA/RhoA kinase pathway, which has been implicated in IOP regulation. Furthermore, it binds to *ABCA1* and links the *ABCA1*, *CAV1/CAV2*, and *GAS7* pathway to Mendelian POAG genes (*MYOC*, *OPTN*, *WDR36*). In conclusion, this study identified a novel association between IOP and *ARHGEF12*.

INTRODUCTION

Glaucoma is a heritable eye disease affecting the optic nerve, which leads to irreversible visual field loss and eventually to blindness. Primary open-angle glaucoma (POAG) is the most common form of glaucoma. Individuals with a first-degree family member affected with POAG have a ten-fold increased risk of developing the disease¹. Variants in *MYOC*, *OPTN*, and *WDR36* explain some familial forms of POAG²⁻⁷. However, disease-causing mutations in these genes are rare in POAG patients and therefore explain only a small part of the overall heritability. Genome-wide association studies (GWAS) have identified *CAV1/CAV2*, *TMCO1*, *SIX6* and *CDKN2B-AS1* as POAG genes, and recently *ABCA1*, *AFAP1*, and *GMD5* were added to the list⁸⁻¹².

Elevated intraocular pressure (IOP) is an important risk factor for glaucoma and the target of glaucoma therapy is lowering the IOP. IOP is highly heritable with heritability estimates ranging between 0.29-0.67^{13,14}. *TMCO1*, *GAS7*, *FAM125B* were implicated in IOP, as well as the *CAV1/CAV2* region^{12,15}. The International Glaucoma Genetics Consortium (IGGC) recently published a meta-analysis of IOP, reporting four new genes for IOP (*FNDC3B*, *ABCA1*, *ABO*, and a region on chromosome 11.p11.2 with many genes in it), and showed that one of the new genes (*ABCA1*) also influences the risk of developing POAG¹⁶. This has shown that investigating the genetics of IOP is a fruitful approach to discover genes related to POAG.

The IGGC meta-analysis utilised data imputed to the HapMap 2 reference panel. In this study we aimed to identify new genetic variants associated with IOP using 1000 Genomes reference panel to increase the number of variants analysed in the population-based Rotterdam Study.

RESULTS

After exclusion of 95 subjects with a history of IOP-lowering laser or surgery, 8,105 subjects were included in the meta-analysis of the discovery cohorts (Rotterdam Study I [RS-I] and Rotterdam Study II [RS-II]). The demographics of all individual studies are shown in Table 1. The inflation factor (λ) was 1.03 for RS-I and 1.01 for RS-II, indicating good control of population substructures. The λ of the meta-analysis was 1.04 (Supplementary Figure 1). In the meta-analysis, 3 single nucleotide polymorphisms (SNPs) reached genome-wide significance (Figure 1). These 3 SNPs were located on chromosome 11q23.3 in the *ARHGEF12* gene. The most significantly associated SNP was the intronic variant rs58073046 ($\beta=0.44$, $P=1.87 \times 10^{-8}$, minor allele frequency [MAF] = 0.12; Figure 2 and Table 2). Since IOP can be influenced by the central corneal thickness (CCT) we adjusted for CCT. Adjustment for CCT was possible in only 25% of the dataset. In this small subset, by chance the effect of rs58073046 on IOP without adjustment for CCT was smaller ($\beta=0.34$, $P=4.44 \times 10^{-2}$, $n = 2,036$). After adjustment for CCT, the effect estimate was 0.36 and remained marginally significant despite the small sample size (p-value for effect of rs58073046 on IOP corrected for CCT = 3.35×10^{-2} , $n = 2,036$).

Figure 1. Manhattan plot of the meta-analysis of genome-wide association studies for intraocular pressure in the discovery phase ($n = 8,105$). Each dot represents a single nucleotide polymorphism (SNP). The plot shows $-\log_{10}$ -transformed p-values for all SNPs. The upper black-dotted horizontal line represents the threshold of genome-wide significance ($P < 5.0 \times 10^{-8}$); the lower black-dotted horizontal line represents a p-value of 1×10^{-5} .

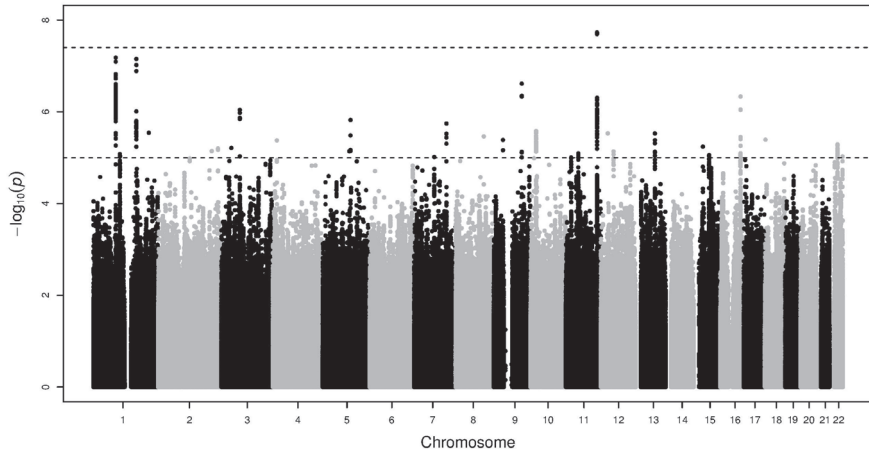


Figure 2. Regional association and recombination plot of the 11q23.3 region in the meta-analysis of the discovery cohorts. Plots are centered on rs58073046 (purple diamond), the most significantly associated single nucleotide polymorphism (SNP) in this region, and flanked by the meta-analysis results for SNPs in the 400-kb region surrounding it. SNPs are shaded according to their pairwise correlation (r^2) with rs58073046. The blue line represents the estimated recombination rates; the gene annotations are shown below the figure.

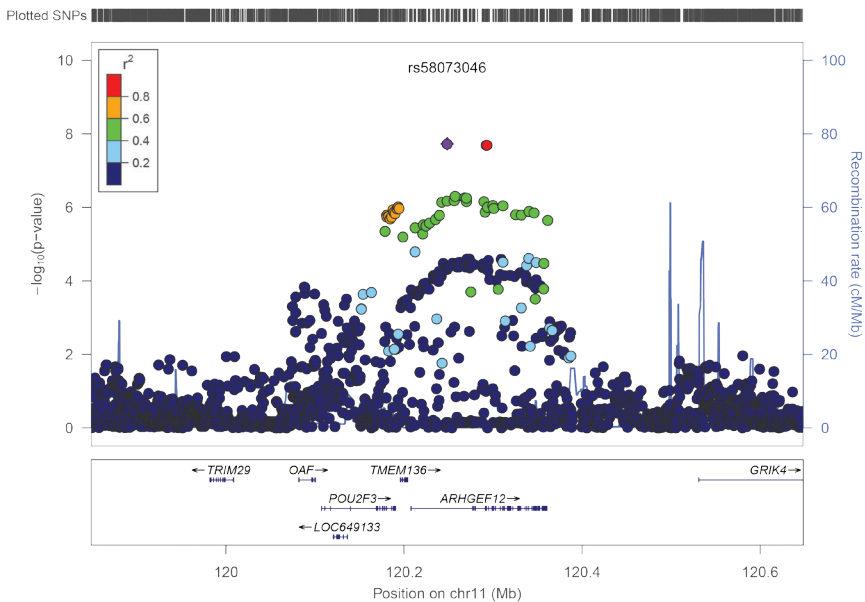


Table 1. Characteristics of the discovery and replication studies.

ABBREVIATIONS: **BATS** Brisbane Adolescent Twins Study; **BMES** Blue Mountains Eye Study; **IOP** intraocular pressure; **n** number of samples; **RS** Rotterdam Study; **SD** standard deviation; **TEST** Twins Eye Study in Tasmania.

	Discovery cohorts (n = 8,105)		Replication cohorts (n = 7,471)				
	RS-I	RS-II	RS-III	BATS	BMES	Raine	TEST
n included in analysis	6010	2095	2992	1152	1769	895	663
mean age (SD)	69.2 (9.0)	64.8 (7.9)	57.2 (6.8)	20.1 (4.0)	64.0 (8.3)	20.0 (0.4)	25.6 (18.8)
% male	40	46	44	53	43	49	60
mean IOP (SD)	14.7 (3.2)	14.2 (3.1)	13.6 (2.9)	15.8 (2.9)	16.1 (2.7)	14.9 (4.7)	15.8 (3.1)
n of participants with IOP lowering medication	112	40	35	-	38	-	-
n of participants with IOP lowering laser/surgery	59	36	12	-	18	-	-

Table 2. Summary of the discovery and replication findings of the genome-wide search for intraocular pressure related genes using data imputed to the 1000 Genomes reference.

ABBREVIATIONS: **A1** allele 1, the effect allele; **A2** allele 2; **β** effect size on intraocular pressure based on allele 1; **Chr** chromosome; **MAF** minor allele frequency (=A1); **I²** I² for heterogeneity between all samples; **pos** position; **SE** standard error; **SNP** single nucleotide polymorphism.

SNP	Chr/pos	A1/ A2	MAF	Discovery stage (n = 8,105)			Replication stage (n = 7,471)			Meta-analysis (n = 15,576)			
				β	SE	P-value	β	SE	P-value	β	SE	P-value	I ²
rs58073046	11/120248493	g/a	0.12	0.44	0.08	1.87x10 ⁻⁸	0.16	0.08	4.13x10 ⁻²	0.30	0.06	6.22x10 ⁻⁸	41.6

Table 3. The explained variance of intraocular pressure in the Rotterdam Study I (RS-I) and Rotterdam Study II (RS-II). Models with different predictors were tested and the p-value shows the p-value of the difference in explained variance for model 2, model 3, and model 4 compared to model 1. ABBREVIATIONS: **BATS** Brisbane Adolescent Twins Study; **BMES** Blue Mountains Eye Study; **RS** Rotterdam Study; **TEST** Twins Eye Study in Tasmania.

	RS-I		RS-II	
	Explained variance (%)	P-value	Explained variance (%)	P-value
Model 1 = rs58073046	0.4		0.3	
Model 2 = model 1 + promotor flanking region SNPs	0.6	0.28	0.4	0.89
Model 3 = model 2 + enhancers + CTCF binding site	1.0	0.19	0.6	0.82
Model 4 = model 3 + all other SNPs (93 in total)	2.2	0.06	2.6	0.16

Figure 3. Forest plot for rs58073046 (chromosome 11q23.3). For each study, the square shows the beta linear regression coefficient or the average difference in intraocular pressure for each additional copy of the minor allele (G) and the lines represent the standard error of the estimate.

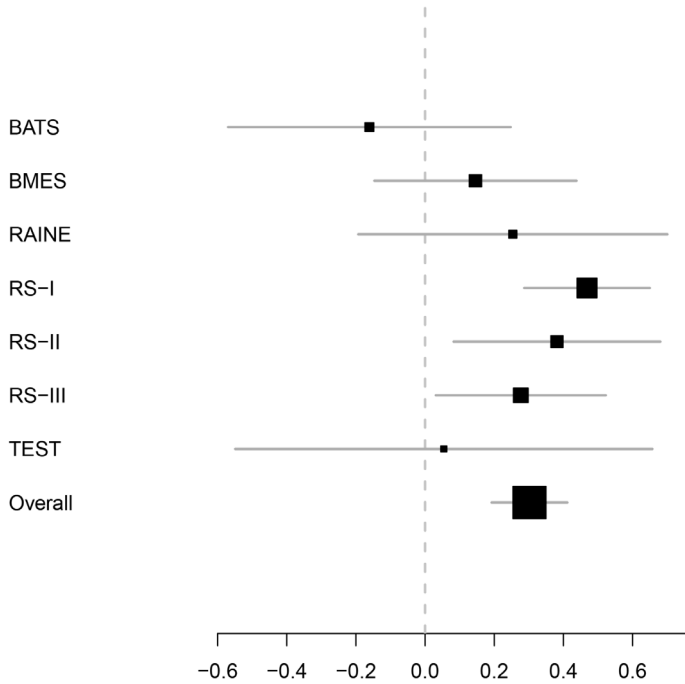


Table 4. Result of the association of rs58073046 with primary open-angle glaucoma (POAG). The table shows the association result for all POAG, as well as for the subtypes high-tension glaucoma (intraocular pressure >21 mmHg) and normal-tension glaucoma (intraocular pressure ≤21 mmHg). ABBREVIATIONS: **ANZRAG** Australian & New Zealand Registry of Advanced Glaucoma; **CI** confidence interval; **ERF/GRIP** Erasmus Rucphen Family study and Genetic Research in Isolated Populations; **HTG** high-tension glaucoma; **NTG** normal-tension glaucoma; **OR** Odds Ratio; **POAG** primary open-angle glaucoma. Please note that the sum of HTG and NTG is not equal to the total number of cases in the ANZRAG cohort, since peak IOP measures were only available for 1,039 of the 1,155 cases.

	All POAG		OR	95% CI	P-value
	controls (n)	cases (n)			
ANZRAG	1,992	1,115	1.54	1.32-1.80	3.14x10 ⁻⁷
ERF/GRIP	2,125	110	1.46	0.91-2.35	1.27x10 ⁻¹
Meta-analysis	4,117	1,225	1.53	1.32-1.78	1.99x10 ⁻⁸

Figure 4. Network map of protein-protein interactions between *ARHGEF12* with a) previously known genes associated with IOP and glaucoma (*ABCA1*, *CAV1/CAV2*, *GAS7*), and b) known genes involved in familial forms of glaucoma (*MYOC*, *OPTN*, *WDR36*). Map was built using Ingenuity Pathway Analysis. Solid lines imply direct relationships between proteins (e.g. physical protein-protein interaction or enzyme-substrate); dotted lines imply indirect functional relationships, such as co-expression, phosphorylation/dephosphorylation, activation/deactivation, transcription or inhibition. Proteins in bold correspond to known glaucoma genes. Meaning of symbols is shown on the right side of the figure.

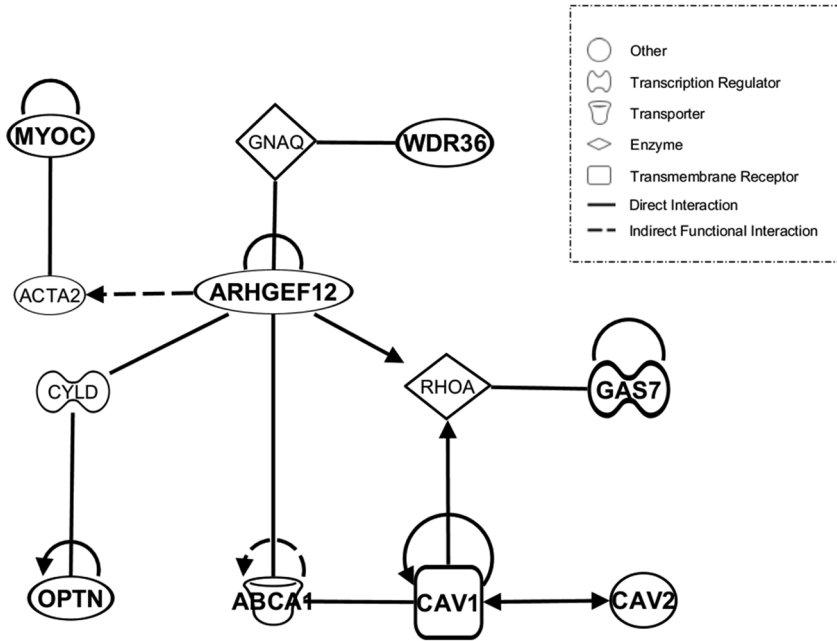


Table 4. (continued).

HTG cases (n)	OR	95% CI	P-value	NTG cases (n)	OR	95% CI	P-value
709	1.65	1.38-1.97	2.12x10 ⁻⁷	330	1.33	1.03-1.72	3.01x10 ⁻²
68	1.79	1.04-3.09	4.10x10 ⁻²	42	0.92	0.41-2.06	8.36x10 ⁻¹
777	1.66	1.41-1.97	2.81x10 ⁻⁹	372	1.29	1.01-1.64	4.23x10 ⁻²

When combining the results of the validation cohort, rs58073046 was replicated ($\beta=0.16$, $P=4.13 \times 10^{-2}$, $n = 7,471$; Table 2). The effect estimates of each individual study are shown in Figure 3. Figure 2 shows that 93 SNPs in the chromosome 11q23.3 region reached a p-value below 5.0×10^{-5} in the discovery cohort. All 93 SNPs were included in the combined meta-analysis of the discovery and replication cohorts (see Supplementary Table 1). The two most significant associations are two SNPs in linkage disequilibrium (pairwise correlation r^2 is 1 in 1000 Genomes Pilot 1 in Northern Europeans) which has thus similar effect sizes and p-values (rs58073046: $\beta=0.30$, $P=6.12 \times 10^{-8}$; rs11217863: $\beta=0.30$ for the minor allele, $P=6.22 \times 10^{-8}$; for all studies together). Twenty-four of the 93 SNPs included in the combined meta-analysis are located in regulatory elements, particularly at enhancers (16/24) and promoter flanking regions (7/24), and one at a CTCF-binding site, suggesting an effect on IOP by altering regulation of *ARHGEF12* or other genes.

Expression profile of human *ARHGEF12* was investigated using UniGene, an expressed sequence tag (EST) database from NCBI. Positive expression was found in various tissues, being particularly high in the eye, vascular tissue, ear, adipose tissue, mouth, uterus, and skin (Supplementary Table 2). Eye specific expression of *ARHGEF12* was examined through the eye-centric genome browser, EyeBrowse, which showed that *ARHGEF12* is expressed in the cornea, lens, iris, trabecular meshwork, retina, optic nerve, and human fetal eye (Supplementary Table 3a). Compared to other genes in the neighbourhood (*POU2F3* and *TMEM136*) *ARHGEF12* presents the highest EST counts in the eye (Supplementary Table 3b). This finding is consistent with microarray data from the Ocular Tissue Database in which the highest expression of *ARHGEF12* occurred in the trabecular meshwork (Supplementary Table 4).

The most significantly associated SNP (rs58073046) explained 0.4% (RS-I) and 0.3% (RS-II) of the variance in IOP (Table 3). The explained phenotypic variance increased to 1.0% (RS-I) and 0.6% (RS-II) by adding the 24 regulatory variants at 11q23.3, and to 2.2% (RS-I) and 2.6% (RS-II) by adding all the other 11q23.3 variants which reached a p-value below 5.0×10^{-5} in the discovery cohort, but the differences in explained variance are not statistically significant between the models.

The SNP (rs58073046) was also genome-wide significantly associated with POAG in 1,225 cases and 4,117 controls (Odds Ratio [OR] = 1.53, $P=1.99 \times 10^{-8}$; see Table 4). The association of rs58073046 was stronger for high-tension glaucoma (HTG) (OR = 1.66, $P=2.81 \times 10^{-9}$) than for normal-tension glaucoma (NTG) (OR = 1.29, $P=4.23 \times 10^{-2}$).

Figure 4 shows a network map of protein interactions created using the Ingenuity Pathway Analysis (IPA) software. *ARHGEF12* binds directly to *ABCA1* and RhoA proteins, and interacts through other proteins with genes implicated in POAG by GWAS (*CAV1/CAV2*, *GAS7*) or linkage analysis (*MYOC*, *OPTN* and *WDR36*). No evidence was found for interactions with protein products of other known IOP genes such as *ABO*, *TMCO1* or *FNDC3B*.

DISCUSSION

The aim of this study was to identify new genetic variants that influence IOP using GWAS datasets imputed to the 1000 Genomes reference panel. We have identified a new region, chromosome 11q23.3, associated with IOP. The SNP rs58073046 is located in *ARHGEF12*. This gene was previously associated with POAG but the findings did not replicate⁸. The association of the region with IOP is new.

Gharahkhani et al. previously reported an association between POAG and rs11827818 (OR 1.52, $P=9.2 \times 10^{-9}$), an intronic SNP located within the *TMEM136* gene near to *ARHGEF12*, in 1,155 cases and 1,992 controls from the ANZRAG study⁸. We checked the association between the variant found by Gharahkhani et al. and POAG in the Genetic Research in Isolated Populations (GRIP)/Erasmus Rucphen Family (ERF) study consisting of 110 POAG cases. The magnitude for rs11827818 was smaller (OR 1.15 for overall glaucoma and OR 1.36 for HTG) than the magnitude of the most associated SNP rs58073046 observed in our study (OR 1.46 for overall POAG and OR 1.79 for HTG). These two SNPs (rs11827818 and rs58073046) are in partial linkage disequilibrium (pairwise correlation r^2 is 0.51 in 1000 Genomes Pilot 1 in Northern Europeans). Gharahkhani et al. used the genotyped SNP rs2276035 within *ARHGEF12* for replication in other POAG case-control studies, however, this SNP did not clearly replicate. In our GRIP/ERF study, rs2276035 was not associated with POAG (OR 0.99 for overall POAG and OR 1.22 for those with HTG).

In our analysis of IOP, the SNP found by Gharahkhani et al. (rs11827818) was associated with an increased mean IOP level in our discovery cohorts but did not reach genome-wide significance ($\beta=0.30$, $P=6.41 \times 10^{-6}$). In our replication cohorts the effect of rs58073046 on IOP was heterogeneous between studies, particularly in one small study (BATS) in which the effect was in the opposite direction. The I^2 for heterogeneity was 41.5 in the combined analysis of all studies. However, after removal of BATS the heterogeneity I^2 was 0.0 and the p-value became 5.04×10^{-9} . BATS is a relatively small and younger sample, which might explain the failure to replicate the findings. The effect estimates from all other replication cohorts were in the same direction as that from our discovery cohorts, though smaller in magnitude.

ARHGEF12 (Rho guanine nucleotide exchange factor (GEF) 12; previously known as Leukemia-Associated Rho Guanine Nucleotide Exchange Factor or LARG) may regulate RhoA GTPases¹⁷. Rho proteins are important for numerous cellular processes. Activation of RhoA protein will lead to the activation of ROCK, a RhoA kinase. It has been shown that RhoA/RhoA kinase signalling plays a role in regulation of trabecular meshwork plasticity, fibrogen activity, and myofibroblast activation¹⁸. Activation of RhoA proteins can also decrease the permeability of Schlemm's canal cells¹⁹. This links *ARHGEF12* to POAG as the regulation of IOP is a balance between the production of aqueous humour by the ciliary body and the outflow through the trabecular meshwork and Schlemm's canal cells. The changes in trabecular meshwork and Schlemm's canal cells lead to an increased resistance for the aqueous humour outflow and subsequently an elevated IOP. ROCK-inhibitors can decrease IOP by inducing relaxation of trabecular meshwork and ciliary body muscles and seems to be a good new target for IOP-lowering therapy²⁰.

Interestingly, *ARHGEF12* links the *ABCA1*, *CAV1/CAV2*, and *GAS7* genes, which has been previously associated with IOP as well as with POAG, to Mendelian POAG genes (*MYOC*, *OPTN*, and *WDR36*). The *ARHGEF12* gene interacts with *ABCA1*. *ARHGEF12* can extend the half-life of the *ABCA1* protein, by binding to its C terminus and subsequently activating RhoA, which in turn prevents *ABCA1* degradation²¹. *ABCA1* plays a role in the transport of different molecules across extra- and intra-cellular membranes and the interference of *ARHGEF12* in the degradation of *ABCA1* protein might extend the transportation of molecules. *ABCA1* is not the only glaucoma gene that has a role in the transport of vesicles. *CAV1*, *CAV2*, and *FAM125B* have been also implicated in vesicle transport¹⁵.

In flies, RhoGEF2 is the single homologue of mammalian *ARHGEF1*, *ARHGEF11* and *ARHGEF12*, and has been extensively studied in the context of tumorigenesis²². Flies lacking RhoGEF2 showed an early embryonic lethality^{23,24}, while overexpression of this gene in eye resulted in small eyes, ablation of eye tissue, aberrant proliferation patterns, tissue morphology, and partially blocked differentiation²². Overexpression of Rho1 GTPase results in a rough eye phenotype with reduced retinal thickness²⁵, but in the presence of RhoGEF2 the retina thickness is recovered²³, supporting the role of RhoGEF2 as upstream activator of Rho1 in the developing eye. No data about eye morphology or histology has been described in either knockout flies or mice. Absence of *arhgef12* in mice leads to embryonic lethality with incomplete penetrance, which might be explained by redundancy of *arhgef11* and *arhgef12*²⁶. These findings suggest that *arhgef12* expression is required during eye and general development and that its absence may impact animal viability.

POU2F3 is another gene in the region on chromosome 11. It is a member of the POU domain family of transcription factors, which regulate cell type-specific differentiation pathways. *POU2F3* specifically regulates differentiation of keratinocytes²⁷. *POU2AF1* is a POU class-associating factor and is associated with CCT²⁸. Because IOP is related to CCT, we performed an additional analysis with extra adjustment for CCT in the discovery cohorts. Only a small subset of the discovery cohorts had CCT data available, therefore the association did not reach genome-wide significance after this additional adjustment. However, the beta was similar, suggesting that the signal of association on chromosome 11 is independent of CCT.

TMEM136 (transmembrane protein 136) is the gene between *ARHGEF12* and *POU2F3*. Compared to *TMEM136* and *POU2F3*, *ARHGEF12* showed the highest expression in the eye and particularly in the trabecular meshwork and ciliary body (Supplementary Table 3b and 4). These findings, besides its interaction with known POAG and IOP genes, are compatible with the view that *ARHGEF12* is most likely the gene causing the association signal. Nonetheless, further functional studies focusing on eye phenotypes are needed to clarify the role of chromosome 11q23.3 in the regulation of IOP and its influence on the risk of glaucoma.

In summary, our meta-analysis of GWAS has identified a new locus that may be important for the regulation of IOP and the risk of glaucoma. *ARHGEF12* is the most likely gene causing the association signal. It plays a role in the RhoA/RhoA kinase signalling which has been proven to be an important new target for glaucoma therapy. Our study shows that investigating the genetics of IOP is a fruitful way to elucidate the genetics of glaucoma.

METHODS

We performed a meta-analysis of GWAS in two discovery cohorts – RS-I and RS-II – which are identical in population structure. Our replication cohorts include the Brisbane Adolescent Twins Study (BATS), Blue Mountains Eye Study (BMES), the Western Australian Pregnancy Cohort (Raine) Study, the Rotterdam Study III (RS-III), and Twins Eye Study in Tasmania (TEST). Next, we validated our findings in the Australian & New Zealand Registry of Advanced Glaucoma (ANZRAG) and GRIP/ERF POAG case-control studies. All studies adhered to the tenets of the Declaration of Helsinki and written, informed consent was obtained from all participants.

The Rotterdam Study

The Rotterdam Study is a population-based study established in Rotterdam, the Netherlands²⁹. It consists of three cohorts. The original cohort, RS-I, started in 1990 and includes 7,983 subjects aged 55 years and older. The second cohort, RS-II, was added in 2000 and includes 3,011 subjects aged 55 years and older. The last cohort, RS-III, includes 3,932 subjects of 45 years of age and older and started in 2006. In all three cohorts, IOP was measured for both eyes with Goldmann applanation tonometry (Haag-Streit, Bern, Switzerland). The measurement was done twice. If the second measurement was different from the first measurement, a third measurement was performed and the median of all three values was taken. A subset of participants from RS-I underwent CCT measurements at baseline using ultrasound pachymetry (Allergan Humphrey 850, Carl Zeiss Meditec, Dublin, CA, USA). Another subset of participants from RS-I, RS-II and RS-III underwent CCT measurements at follow-up using a non-contact biometer (Lenstar LS900, Haag-Streit, Köniz, Switzerland). Other ophthalmic baseline and follow-up examinations, which are still ongoing, were described previously³⁰. DNA was isolated from whole blood according to standard procedures. Genotyping of SNPs was performed using the Illumina Infinium II HumanHap550 array (RS-I), the Illumina Infinium HumanHap 550-Duo array (RS-I, RS-II), and the Illumina Infinium Human 610-Quad array (RS-I, RS-III). Samples with low call rate (<97.5%), with excess autosomal heterozygosity (>0.336), or with sex-mismatch were excluded, as were outliers identified by the identity-by-state clustering analysis (outliers were defined as being >3 standard deviation (s.d.) from population mean or having identity-by-state probabilities >97%). A set of genotyped input SNPs with call rate >98%, MAF >0.001 and Hardy-Weinberg Equilibrium (HWE) $P > 10^{-6}$ was used for imputation. The Markov Chain Haplotyping (MACH) package version 1.0 software (Rotterdam, The Netherlands; imputed to plus strand of NCBI build 37, 1000 Genomes phase I version 3) and minimac version 2012.8.6 were used for the analysis. GWAS analyses were performed using the ProbABEL package³¹. The analyses were adjusted for age, sex, and the first five principal components. The Rotterdam Study has been approved by the institutional review board (Medical Ethics Committee) of the Erasmus Medical Center and by the review board of The Netherlands Ministry of Health, Welfare and Sports.

Brisbane Adolescent Twins Study and Twins Eye Study in Tasmania

The Australian Twin Eye Study comprises participants examined as part of TEST or BATS. In most participants, the IOP was measured with the TONO-PEN XL (Reichert, Inc. New York, USA)³². The Australian twin cohorts were genotyped on the Illumina Human Hap610W Quad array.

The inclusion criteria for the SNPs were a $MAF > 0.01$, $HWE P \geq 10^{-6}$, and a SNP call rate $> 95\%$ or Illumina Beadstudio Gencall Score ≥ 0.7 , resulting in 543,862 SNPs. Imputation was done with reference to the August 4, 2010 version of the publicly released 1000 Genomes Project European genotyping using MACH. For BATS data, 1,152 people from 517 families were included in the analyses. For TEST data, 663 individuals from 350 families were included. Association analyses were performed in Merlin (<http://www.sph.umich.edu/csg/abecasis/merlin/>) by using the `-fastassoc` option. Ancestry, initially determined through self-reporting, was verified through Principal Component decomposition. The analyses were adjusted for age, sex, the technique of IOP measurement, and the first five principal components. The studies were approved by the human ethics committees of the University of Tasmania, Royal Victorian Eye and Ear Hospital, and Queensland Institute of Medical Research.

Blue Mountains Eye Study

The Blue Mountains Eye Study is a population-based cohort study of common eye diseases in older Australians living in the Blue Mountains region, west of Sydney, Australia. IOP was measured using Goldmann applanation tonometry (Haag-Streit, Bern, Switzerland)³³. DNA was extracted from whole blood and quality was validated by Sequenom iPLEX assay. Genotyping was performed on the Illumina Infinium platform using the Human660W-Quad, a Wellcome Trust Case Control Consortium 2 designed custom chip containing Human550 probes with 60,000 additional probes to capture common copy-number variations from the Structural Variation Consortium³⁴. Genotyped data were filtered to include SNPs with genotyping rate ≥ 0.97 , $MAF \geq 1\%$, $HWE P \geq 10^{-6}$. Samples with call rates less than 95% were excluded from analysis. Relatedness filtering based on estimated identity by descent was performed so that no pairs of individuals shared more than 20% of their genome. Ancestry outliers with > 6 s. d. from 1000 Genomes northern European ancestry samples were removed. The IMPUTE2 software was used for imputation of data on 1000 Genomes phase 1 release version 3^{35,36}. The association test was performed using SNPTTEST_v2.5-beta4^{37,38}. The analyses were adjusted for age, sex, and the first five principal components. The study was approved by the Human Research Ethics Committees of the University of Sydney and Sydney West Area Health Service.

Raine

The Western Australian Pregnancy Cohort (Raine) Study is an ongoing prospective cohort study of pregnancy, childhood, adolescence and young adulthood in Perth, Western Australia³⁹. At the initiation of the study, 2,900 pregnant women were recruited at 16-18 weeks' gestation from the state's largest public women's hospital and surrounding private practices for a randomized clinical trial investigating effects of intensive ultrasound and Doppler studies in pregnancy outcomes. Following this study, the offspring of the recruited individuals have been evaluated in detail during childhood and adolescence. At the 20-year review of the cohort, Raine participants underwent a comprehensive ocular examination for the first time⁴⁰. As part of this examination, IOP was measured using an Icare TAO1i Tonometer (Icare Finland Oy, Helsinki, Finland). DNA samples and consents for GWAS studies were available from the previous assessments. Genotype data were generated using the genome-wide Illumina 660 Quad Array at the Centre for Applied Genomics (Toronto, Ontario, Canada). Relatedness filtering based on estimated identity

by descent was performed so that no pairs of individuals shared more than 20% of their genome. We also excluded people who had a high degree of missing genotyping data (>3%). The data were filtered for a HWE $P > 1 \times 10^{-6}$, SNP call rate >95%, and a MAF >0.01. GWAS imputation was performed in the MACH v1.0.16 software using the November 23, 2010 version of the 1000 Genome Project European genotyping. The association analyses were adjusted for age, sex, and the first two principal components. This study was approved by the Human Research Ethics Committee of the University of Western Australia.

Australian & New Zealand Registry of Advanced Glaucoma

ANZRAG recruits cases of advanced glaucoma Australia-wide through ophthalmologist referral. The cohort also included participants enrolled in the Glaucoma Inheritance Study in Tasmania (GIST) who met the criteria for ANZRAG. This cohort has been described previously⁹. Advanced POAG was defined as best-corrected visual acuity worse than 6/60 due to POAG, or a reliable 24-2 Visual Field with a mean deviation of worse than -22db or at least 2 out of 4 central fixation squares affected with a Pattern Standard Deviation of < 0.5%. The less severely affected eye was also required to have signs of glaucomatous disc damage. Clinical exclusion criteria for this advanced POAG study were: i) pseudoexfoliation or pigmentary glaucoma, ii) angle closure or mixed mechanism glaucoma; iii) secondary glaucoma due to aphakia, rubella, rubeosis or inflammation; iv) infantile glaucoma, v) glaucoma in the presence of a known associated syndrome. The ANZRAG cohort included 1,155 ANZRAG glaucoma cases and 1,992 controls genotyped on Illumina Omni1M or OmniExpress arrays and imputed against 1000 Genomes Phase 1 Europeans. The case set included all samples from the previously published GWAS⁹. Controls were drawn from the Australian Cancer Study (225 oesophageal cancer cases, 317 Barrett's oesophagus cases and 552 controls) or from a study of inflammatory bowel diseases (303 cases and 595 controls). The quality control methods were performed in PLINK by removing individuals with more than 3% missing genotypes, SNPs with call rate <97%, MAF < 0.01 and HWE $P < 0.0001$ in controls and HWE $P < 5 \times 10^{-10}$ in cases⁴¹. The same quality control protocol was used before merging the cases and controls to avoid mismatches between the merged data sets. After merging, the genotypes for 569,249 SNPs common to the arrays were taken forward for analysis. Relatedness filtering based on estimated identity by descent was performed so that no pairs of individuals shared more than 20% of their genome. Principal components were computed for all participants and reference samples of known northern European ancestry (1000G British, CEU and Finland participants) using the smartpca package from EIGENSOFT software^{42,43}. Participants with principal component 1 or 2 values >6 s.d. from the known northern European ancestry group were excluded. Imputation was conducted using IMPUTE2 in 1-Mb sections, with the 1000 Genomes phase 1 Europeans (March 2012 release) used as the reference panel^{35,36}. SNPs with imputation quality score >0.8 and MAF > 0.01 were carried forward for analysis. Association testing on the imputed data was performed in SNPTEST_v2.5-beta3 using an additive model (-frequentist 1) and full dosage scores (-method expected) with sex and the first six principal components fitted as covariates^{37,38}. All were Australians of European ancestry. Approval was obtained from the Human Research Ethics Committees of Southern Adelaide Health Service/Flinders University, University of Tasmania, QIMR Berghofer Institute of Medical Research (Queensland Institute of Medical Research) and the Royal Victorian Eye and Ear Hospital.

Peak IOP measures were available for 1,039 of the 1,155 cases in the ANZRAG cohort. Of these cases, 330 (31.8%) had NTG (IOP \leq 21 mm Hg) and 709 (68.2%) had HTG (IOP $>$ 21 mm Hg). Association testing for NTG and HTG was performed in SNPTEST _v2.5-beta3 as explained above, using 1,992 shared population controls.

Erasmus Rucphen Family study and Genetic Research in Isolated Populations program

The ERF study is a family-based cohort in a genetically isolated population in the southwest of the Netherlands with over 3,000 participants aged between 18 and 86 years^{44,45}. In the region of the ERF population, a total of 110 patients with glaucoma who did not participate in the ERF study were recruited in three local hospitals. Their visual fields were tested with standard automated perimetry (Humphrey Field Analyzer c24-2 SITA Standard test program) or the Octopus 101 (G2 program with TOP strategy) (Haag-Streit, Bern, Switzerland). The diagnosis of glaucoma was made by the patient's ophthalmologist and confirmed by a glaucoma specialist (HGL). It was based on a glaucomatous appearance of the optic disc (notching or thinning of the neuroretinal rim), combined with a matching glaucomatous visual field defect, and open-angles seen by gonioscopy. Classification of HTG (IOP $>$ 21 mmHG) and NTG (IOP \leq 21 mmHG) was based on IOP at the time of diagnosis. Participants from the ERF study were used as control group (n = 2,125). Genotyping was performed with the 318K array of the Illumina Infinium II whole-genome genotyping assay (HumanHap300-2). Samples with low call rate ($<$ 97.5%), with excess autosomal heterozygosity ($>$ 0.336), or with sex-mismatch were excluded. A set of genotyped input SNPs with call rate $>$ 98%, with MAF $>$ 0.01, and with HWE $P >$ 10^{-6} was used for imputation. We used the MACH package version 1.0.18.c software (Rotterdam, The Netherlands; imputed to plus strand of NCBI build 37, 1000 Genomes Phase I version 3) and minimac version 2012.8.15 for the analyses. Association tests were performed using the ProbABEL package³¹. The analyses were adjusted for age and sex. All measurements in these studies were conducted after the Medical Ethics Committee of the Erasmus University had approved the study protocols.

Expression data

We investigated the expression profile of several genes using NCBI's UniGene⁴⁶, which is an organized view of the transcriptome that evaluates semi quantitatively the EST calculated as number of transcripts per million (online available at <http://www.ncbi.nlm.nih.gov/unigene/>). The EST data for "Breakdown by body site" that shows the approximate gene expression pattern in different tissues was chosen.

Expression of genes in eye tissues was evaluated using two databases: the EyeBrowse and the Ocular Tissue Database. The EyeBrowse is a customized eye-centric version of the UCSC Genome Browser, which includes A) eye-derived ESTs from the National Eye Institute (47) and B) the EyeSage project^{48,49}. The EyeBrowse is available at <http://eyebrowse.cit.nih.gov/>. We only selected human data. In the Ocular Tissue Database, the gene expression is indicated as Affymetrix Probe Logarithmic Intensity Error (PLIER) normalized value. The PLIER normalization method was described by Wagner et al⁵⁰. The Ocular Tissue Database is available at <https://genome.uiowa.edu/otdb/>.

Ensembl Genome Browser

The Ensembl Genome Browser release version 77 was used to investigate regulatory variants in genome-wide significant regions⁵¹.

Ingenuity Pathway Analysis

Network map was created using the IPA software (Ingenuity Systems, <http://www.ingenuity.com>, Redwood City, CA, USA), where a) *ARHGEF12*, b) known IOP associated genes (*ABO* and *FNDC3B*), c) known genes associated with both IOP and POAG (*ABCA1*, *CAV1/CAV2*, *GAS7* and *TMCO1*), as well as d) known genes involved in familial forms of glaucoma (*OPTN*, *TMCO1*, *WDR36*) were selected. The “Path explorer” function (shortest +1) was used to map protein-protein interactions between *ARHGEF12* and the rest of included genes. All direct and indirect interactions are supported by at least one reference from the literature, a textbook, or canonical information stored in the Ingenuity Pathways Knowledge Base.

Statistical analysis

We used the mean IOP of right and left eye for the analysis. If IOP was missing for one eye, the IOP of the other eye was used. For participants receiving IOP-lowering medication, we added 30% to the IOP measurement to estimate a pre-medication IOP value⁵². Participants who underwent IOP-lowering laser or surgery were excluded from the analysis. GWAS was performed on each individual study as described above under the assumption of an additive model for the effect of the risk allele. In a secondary analysis in the discovery phase CCT was included as an extra covariate. We used METAL software to carry-out an inverse variance weighted fixed-effect meta-analysis between RS-I and RS-II⁵³. SNPs with MAF <0.01 or with imputation quality score $R^2 < 0.5$ were excluded. For the meta-analysis of RS-I and RS-II a p-value of $< 5.0 \times 10^{-8}$ (threshold of genome-wide significance) was considered statistically significant. Next, we validated the association results of the SNPs that reached genome-wide significance in five other studies (BMES, BATS, Raine, RS-III, and TEST). In the validation phase, a $P < 0.05$ was considered statistically significant. Furthermore, in the discovery and validation cohorts we meta-analysed all the SNPs with $P < 5.0 \times 10^{-5}$ in the region that reached genome-wide significance in the discovery cohort. We calculated the explained variance (R^2) of IOP by the new SNPs in RS-I and RS-II. In the first model, we calculated the explained variance for the most significantly associated SNP. Next, we added SNPs located within a regulatory element or all SNPs with $P < 5.0 \times 10^{-5}$ to the model. The nested models were compared using an F test. Finally, we investigated the effect of the genome-wide significant SNPs on POAG in ANZRAG and ERF. A Manhattan plot, regional plots and forest plots were made using R⁵⁴ and LocusZoom⁵⁵.

References

1. Wolfs, R.C. et al. Genetic risk of primary open-angle glaucoma. Population-based familial aggregation study. *Arch Ophthalmol* 116, 1640-5 (1998).
2. Kubota, R. et al. A novel myosin-like protein (myocilin) expressed in the connecting cilium of the photoreceptor: molecular cloning, tissue expression, and chromosomal mapping. *Genomics* 41, 360-9 (1997).
3. Monemi, S. et al. Identification of a novel adult-onset primary open-angle glaucoma (POAG) gene on 5q22.1. *Hum Mol Genet* 14, 725-33 (2005).
4. Rezaie, T. et al. Adult-onset primary open-angle glaucoma caused by mutations in optineurin. *Science* 295, 1077-9 (2002).
5. Sarfarazi, M. et al. Localization of the fourth locus (GLC1E) for adult-onset primary open-angle glaucoma to the 10p15-p14 region. *Am J Hum Genet* 62, 641-52 (1998).
6. Sheffield, V.C. et al. Genetic linkage of familial open angle glaucoma to chromosome 1q21-q31. *Nat Genet* 4, 47-50 (1993).
7. Stone, E.M. et al. Identification of a gene that causes primary open angle glaucoma. *Science* 275, 668-70 (1997).
8. Gharahkhani, P. et al. Common variants near ABCA1, AFAP1 and GMDS confer risk of primary open-angle glaucoma. *Nat Genet* 46, 1120-5 (2014).
9. Burdon, K.P. et al. Genome-wide association study identifies susceptibility loci for open angle glaucoma at TMCO1 and CDKN2B-AS1. *Nat Genet* 43, 574-8 (2011)..
10. Ramdas, W.D. et al. Common genetic variants associated with open-angle glaucoma. *Hum Mol Genet* 20, 2464-71 (2011).
11. Thorleifsson, G. et al. Common variants near CAV1 and CAV2 are associated with primary open-angle glaucoma. *Nat Genet* 42, 906-9 (2010).
12. van Koolwijk, L.M. et al. Common genetic determinants of intraocular pressure and primary open-angle glaucoma. *PLoS Genet* 8, e1002611 (2012).
13. Sanfilippo, P.G., Hewitt, A.W., Hammond, C.J. & Mackey, D.A. The heritability of ocular traits. *Surv Ophthalmol* 55, 561-83 (2010).
14. van Koolwijk, L.M. et al. Genetic contributions to glaucoma: heritability of intraocular pressure, retinal nerve fiber layer thickness, and optic disc morphology. *Invest Ophthalmol Vis Sci* 48, 3669-76 (2007).
15. Nag, A. et al. A genome-wide association study of intra-ocular pressure suggests a novel association in the gene FAM125B in the TwinsUK cohort. *Hum Mol Genet* 23, 3343-8 (2014).
16. Hysi, P.G. et al. Genome-wide analysis of multi-ancestry cohorts identifies new loci influencing intraocular pressure and susceptibility to glaucoma. *Nat Genet* 46, 1126-30 (2014).
17. Fukuhara, S., Chikumi, H. & Gutkind, J.S. Leukemia-associated Rho guanine nucleotide exchange factor (LARG) links heterotrimeric G proteins of the G(12) family to Rho. *FEBS Lett* 485, 183-8 (2000).
18. Pattabiraman, P.P., Maddala, R. & Rao, P.V. Regulation of plasticity and fibrogenic activity of trabecular mesh work cells by Rho GTPase signaling. *J Cell Physiol* 229, 927-42 (2014).
19. Kumar, J. & Epstein, D.L. Rho GTPase-mediated cytoskeletal organization in Schlemm's canal cells play a critical role in the regulation of aqueous humor outflow facility. *J Cell Biochem* 112, 600-6 (2011).
20. Wang, J., Liu, X. & Zhong, Y. Rho/Rho-associated kinase pathway in glaucoma (Review). *Int J Oncol* 43, 1357-67 (2013).
21. Okuhira, K. et al. Binding of PDZ-RhoGEF to ATP-binding cassette transporter A1 (ABCA1) induces cholesterol efflux through RhoA activation and prevention of transporter degradation. *J Biol Chem* 285, 16369-77 (2010).
22. Brumby, A.M. et al. Identification of novel Ras-cooperating oncogenes in *Drosophila melanogaster*: a RhoGEF/Rho-family/JNK pathway is a central driver of tumorigenesis. *Genetics* 188, 105-25 (2011).
23. Barrett, K., Leptin, M. & Settleman, J. The Rho GTPase and a putative RhoGEF mediate a signaling pathway for the cell shape changes in *Drosophila* gastrulation. *Cell* 91, 905-15 (1997).
24. Hacker, U. & Perrimon, N. DRhoGEF2 encodes a member of the Dbl family of oncogenes and controls cell shape changes during gastrulation in *Drosophila*. *Genes Dev* 12, 274-84 (1998).
25. Hariharan, I.K. et al. Characterization of rho GTPase family homologues in *Drosophila melanogaster*: overexpressing Rho1 in retinal cells causes a late developmental defect. *EMBO J* 14, 292-302 (1995).
26. Mikelis, C.M. et al. PDZ-RhoGEF and LARG are essential for embryonic development and provide a link between thrombin and LPA receptors and Rho activation. *J Biol Chem* 288, 12232-43 (2013).
27. Cabral, A., Fischer, D.F., Vermeij, W.P. & Backendorf, C. Distinct functional interactions of human Skn-1 isoforms with Ese-1 during keratinocyte terminal differentiation. *J Biol Chem* 278, 17792-9 (2003).
28. Lu, Y. et al. Genome-wide association analyses identify multiple loci associated with central corneal thickness and keratoconus. *Nat Genet* 45, 155-63 (2013).
29. Hofman, A. et al. The Rotterdam Study: 2014 objectives and design update. *Eur J Epidemiol* 28, 889-926 (2013).
30. Wolfs, R.C. et al. Changing views on open-angle glaucoma: definitions and prevalences--The Rotterdam Study. *Invest Ophthalmol Vis Sci* 41, 3309-21 (2000).

31. Aulchenko, Y.S., Struchalin, M.V. & van Duijn, C.M. ProbABEL package for genome-wide association analysis of imputed data. *BMC Bioinformatics* 11, 134 (2010).
32. Mackey, D.A. et al. Twins eye study in Tasmania (TEST): rationale and methodology to recruit and examine twins. *Twin Res Hum Genet* 12, 441-54 (2009).
33. Mitchell, P., Smith, W., Attebo, K. & Wang, J.J. Prevalence of age-related maculopathy in Australia. The Blue Mountains Eye Study. *Ophthalmology* 102, 1450-60 (1995).
34. Conrad, D.F. et al. Origins and functional impact of copy number variation in the human genome. *Nature* 464, 704-12 (2010).
35. Howie, B., Marchini, J. & Stephens, M. Genotype imputation with thousands of genomes. *G3 (Bethesda)* 1, 457-70 (2011).
36. Howie, B.N., Donnelly, P. & Marchini, J. A flexible and accurate genotype imputation method for the next generation of genome-wide association studies. *PLoS Genet* 5, e1000529 (2009).
37. Marchini, J. & Howie, B. Genotype imputation for genome-wide association studies. *Nat Rev Genet* 11, 499-511 (2010).
38. Wellcome Trust Case Control, C. Genome-wide association study of 14,000 cases of seven common diseases and 3,000 shared controls. *Nature* 447, 661-78 (2007).
39. McKnight, C.M. et al. Birth of a cohort--the first 20 years of the Raine study. *Med J Aust* 197, 608-10 (2012).
40. Yazar, S. et al. Raine eye health study: design, methodology and baseline prevalence of ophthalmic disease in a birth-cohort study of young adults. *Ophthalmic Genet* 34, 199-208 (2013).
41. Purcell, S. et al. PLINK: a tool set for whole-genome association and population-based linkage analyses. *Am J Hum Genet* 81, 559-75 (2007).
42. Patterson, N., Price, A.L. & Reich, D. Population structure and eigenanalysis. *PLoS Genet* 2, e190 (2006).
43. Price, A.L. et al. Principal components analysis corrects for stratification in genome-wide association studies. *Nat Genet* 38, 904-9 (2006).
44. Aulchenko, Y.S. et al. Linkage disequilibrium in young genetically isolated Dutch population. *Eur J Hum Genet* 12, 527-34 (2004).
45. Pardo, L.M., MacKay, I., Oostra, B., van Duijn, C.M. & Aulchenko, Y.S. The effect of genetic drift in a young genetically isolated population. *Ann Hum Genet* 69, 288-95 (2005).
46. Coordinators, N.R. Database resources of the National Center for Biotechnology Information. *Nucleic Acids Res* (2014).
47. Wistow, G. et al. NEI Bank: genomics and bioinformatics resources for vision research. *Mol Vis* 14, 1327-37 (2008).
48. Bowes Rickman, C. et al. Defining the human macula transcriptome and candidate retinal disease genes using EyeSAGE. *Invest Ophthalmol Vis Sci* 47, 2305-16 (2006).
49. Liu, Y. et al. Serial analysis of gene expression (SAGE) in normal human trabecular meshwork. *Mol Vis* 17, 885-93 (2011).
50. Wagner, A.H. et al. Exon-level expression profiling of ocular tissues. *Exp Eye Res* 111, 105-11 (2013).
51. Flicek, P. et al. Ensembl 2014. *Nucleic Acids Res* 42, D749-55 (2014).
52. van der Valk, R. et al. Intraocular pressure-lowering effects of all commonly used glaucoma drugs: a meta-analysis of randomized clinical trials. *Ophthalmology* 112, 1177-85 (2005).
53. Willer, C.J., Li, Y. & Abecasis, G.R. METAL: fast and efficient meta-analysis of genomewide association scans. *Bioinformatics* 26, 2190-1 (2010).
54. R core team. R: a language and environment for statistical computing. <http://www.R-project.org>. (2014).
55. Pruim, R.J. et al. LocusZoom: regional visualization of genome-wide association scan results. *Bioinformatics* 26, 2336-7 (2010).

CHAPTER 4.5

New insights into genetics of primary open-angle glaucoma based on meta-analyses of intraocular pressure and optic disc characteristics



Henriët Springelkamp*, Adriana I. Iglesias*, Aniket Mishra*, René Höhn*, Robert Wojciechowski*, Anthony P. Khawaja, Abhishek Nag, Ya Xing Wang, Jie Jin Wang, Gabriel Cuellar-Partida, Jane Gibson, Jessica N. Cooke Bailey, Eranga N. Vithana, Puya Gharahkhani, Thibaud Boutin, Wishal D. Ramdas, Tanja Zeller, Robert N. Luben, Ekaterina Yonova-Doing, Ananth C. Viswanathan, Seyhan Yazar, Angela J. Cree, Jonathan L. Haines, Jia Yu Koh, Emmanuelle Souzeau, James F. Wilson, Najaf Amin, Christian Müller, Cristina Venturini, Lisa S. Kearns, Jae Hee Kang, NEIGHBORHOOD Consortium, Yih Chung Tham, Tiger Zhou, Elisabeth M. van Leeuwen, Stefan Nickels, Paul Sanfilippo, Jiemin Liao, Herma van der Lind, Wanting Zhao, Leonieke M.E. van Koolwijk, Li Zheng, Fernando Rivadeneira, Mani Baskaran, Sven van der Lee, Shamira Perera, Paulus T.V.M. de Jong, Ben A. Oostra, André G. Uitterlinden, Qiao Fan, Albert Hofman, E-Shyong Tai, Johannes R. Vingerling, Xueling Sim, Roger C.W. Wolfs, Yik Ying Teo, Hans G. Lemij, Chiea Chuen Khor, Rob Willemsen, Karl J Lackner, Tin Aung, Nomdo M. Jansonius, Grant Montgomery, Philipp S Wild, Terri L. Young, Kathryn P. Burdon, Pirro G. Hysi, Louis R. Pasquale, Tien Yin Wong, Caroline C.W. Klaver, Alex W. Hewitt, Jost B. Jonas, Paul Mitchell, Andrew J Lotery, Paul J. Foster, Veronique Vitart, Norbert Pfeiffer, Jamie E. Craig, David A. Mackey‡, Christopher J. Hammond±, Janey L. Wiggs‡, Ching-Yu Cheng‡, Cornelia M. van Duijn‡, Stuart MacGregor‡.

* These authors contributed equally.

‡ These authors jointly supervised this work.

ABSTRACT

Primary open-angle glaucoma (POAG), the most common optic neuropathy, is a highly heritable disease. Intraocular pressure (IOP) and optic nerve head characteristics are used clinically to predict POAG risk. We conducted a genome-wide association meta-analysis of IOP and optic disc parameters and validated our findings in POAG cases. We identified 21 new genomic regions associated with optic nerve head variation and with IOP. Several genomic regions affect both IOP and the optic disc and we found that pathways involved in these endophenotypes are not distinct as assumed. We further identified a novel association with POAG and *CDKN1A*. Using a zebrafish model we demonstrate an in vivo interaction between *six6b* (associated with POAG and optic nerve head variation) and *cdkn1a*.

INTRODUCTION

In primary open-angle glaucoma (POAG), loss of retinal ganglion cells and nerve fibers causes damage to the optic nerve, which leads to visual field loss and, eventually, blindness. The optic nerve damage is characterized by an increase in cup size, the central area of the optic nerve head (or optic disc). This damage can be quantified by the vertical cup-disc ratio (VCDR), comparing the vertical diameter of the cup with the vertical diameter of the total optic disc.

Elevated intraocular pressure (IOP) is a well-recognized risk factor and current POAG therapies lower IOP by various mechanisms. POAG is highly heritable¹ and several genome-wide association studies (GWAS) have identified new POAG genes by examining POAG directly or studying endophenotypes like VCDR and IOP²⁻¹¹. Several genes associated with VCDR and IOP – *CDKN2B-AS1*, *SIX6* (VCDR); and *CAV1/CAV2*, *TMCO1*, *ABCA1* and *ARHGEF12* (IOP) – are highly significantly associated with POAG. Notably, no genes have been significantly (genome-wide) associated with both VCDR and IOP. Charlesworth et al. previously found a genetic correlation between VCDR and IOP (RhoG = 0.45, $P=0.0012$), however, genes underlying this relationship have not yet been identified¹².

The aims of this study were to (1) identify new genes associated with the POAG endophenotypes IOP, VCDR, cup area, and disc area, and ultimately POAG, using the 1000 Genomes imputations reference panel, and (2) investigate the genetic overlap between the different endophenotypes. To accomplish these aims we performed a meta-analysis of GWAS of these four traits within the International Glaucoma Genetics Consortium (IGGC).

METHODS

Study design

We performed a meta-analysis on directly genotyped and imputed SNPs to the 1000 Genomes reference panel. We analyzed four outcomes: IOP, VCDR, cup area, and disc area. In the first stage, we included 22,489-29,578 individuals with European ancestry. Subsequently, we evaluated the genome-wide significant SNPs from the first stage in 7,307-8,373 individuals with Asian ancestry. Finally, we performed a meta-analysis of GWAS summary findings from all individual studies including individuals with European and Asian ancestry. We subsequently tested the effect of all genome-wide significant SNPs on POAG in four independent case-control studies.

Subjects, phenotyping and genotyping

All studies included in this meta-analysis are part of the IGGC (Supplementary Table 1a). Details for each individual study can be found in Supplementary Table 1b and the Supplementary Note. The ophthalmological examinations included measurements of IOP and optic nerve head assessment. Studies performed genomic imputation using 1000 Genomes phase 1 reference samples. Study-specific quality control can be found in the Supplementary Note. All studies were performed with the approval of their local medical ethics committee, and written informed consent was obtained from all participants in accordance with the Declaration of Helsinki.

Statistical analysis

In the IOP analysis, individuals who underwent IOP-lowering laser or surgery were removed from the analysis; in individuals receiving IOP-lowering medication, the IOP value was multiplied by 1.3 to estimate a pre-medication IOP value¹³. The mean IOP, VCDR, cup area, and disc area of both eyes was used for the analyses. SNPs with MAF < 0.01 and imputation quality scores < 0.3 (proper-info of IMPUTE) or $R^2 < 0.3$ (MACH) were removed from the analyses.

Each individual study performed a linear regression between each endophenotype (IOP, VCDR, cup area, and disc area) and the SNPs, under the assumption of an additive model for the effect of the risk allele. Analyses were adjusted for age, sex and the first five principal components (for population-based studies) or family structure (for family-based studies).

We performed an inverse variance weighted fixed-effect meta-analysis with METAL software¹⁴. P-values for heterogeneity were calculated by using the Cochran's Q-test for heterogeneity. SNPs with a p-value for heterogeneity < 0.001 were removed from the results, as well as SNPs only present in three studies. We used the 'genomic control' option in METAL to correct the standard error of each individual study for estimated genomic inflation. In the meta-analyses of individuals with European ancestry, a $P < 5.0 \times 10^{-8}$ (the genome-wide threshold of association) was considered significant. In the second stage, these genome-wide significant SNPs were validated in individuals with Asian ancestry, and in this look-up a $P < 0.05$ was considered significant. Finally, in the meta-analysis of individuals with European and Asian ancestry a p-value of $< 5.0 \times 10^{-8}$ was considered significant. In total, we identified 75 independent SNPs across different genomic regions for all the traits together. Therefore, the threshold for significance in the POAG analysis was $(0.05 / 75) 6.67 \times 10^{-4}$. Manhattan, regional and forest plots were made using R¹⁵ and LocusZoom¹⁶.

Gene-based test using VEGAS

A gene-based test was performed using VEGAS2 software¹⁷, with a 50kb gene boundary. The 1000 Genomes European and Asian populations were used as a reference to calculate LD for European and Asian ancestry data respectively. After calculation of gene-based test statistics for Asian and European ancestry populations separately, meta-analyses were conducted using Fisher's method for combining p-values.

In silico analysis of *CDKN2B* and *CDKN1A* promoters

Analysis of *CDKN2B* and *CDKN1A* promoter sequences was performed using the ConTra promoter alignment analysis tool (<http://www.dnbr.ugent.be/prx/bioit2-public/contrav2/index.php>), using the highest stringency settings (i.e. minimize false positives (minFP), which only uses the TRANSFAC database).

Expression of *cdkn1a* in zebrafish

We investigated the expression of *cdkn1a* in a *six6b* knockdown zebrafish. To achieve this knockdown, we injected 6ng of a previously described morpholino designed to target the translation site of *six6b* (*six6b* SB-MO= 5'-TGTAATCTGGAAACGCACCTGTT-3')¹⁸ into the yolk of one to two cells stage using a pneumatic picopump (World Precision Instruments, Berlin, Germany).

For evaluation of *cdkn1a* expression, total RNA was isolated after dissection of eye tissue from approximately 50 injected and wild-type embryos at 3dpf; in all extractions an RNA-Bee (Tri-Test, Inc) protocol was used. Synthesis of cDNA was performed using Superscript III reverse transcriptase (Invitrogen, California USA). To measure mRNA levels, qRT-PCR on cDNA samples was carried out using SYBR® select Master Mix for CFX (applied Biosystems, Inc, USA). Samples were analyzed on the Bio-Rad CFX96 qPCR detection system. The relative expression software tool (REST-384©) was used to estimate the relative changes in mRNA levels of *cdkn1a*, *cdkn2b* and *six6b*¹⁹. All RT- qPCR experiments were undertaken in triplicate.

Primers used for qRT-PCR were designed using Primer3Plus tool²⁰. Oligonucleotide sequences have been published elsewhere¹⁸.

Gene-set enrichment

Gene-set enrichment was performed using the DEPICT framework²¹. DEPICT uses reconstituted versions of known molecular pathways, details of the method have been published elsewhere²¹. Per trait two separate analyses were performed: 1) an analysis based on independent genome-wide significant SNPs, and 2) an analysis based on all independent SNPs with a $P < 1.0 \times 10^{-5}$. In the first analysis a total of 24 IOP SNPs, 119 VCDR SNPs, 78 cup area SNPs and 46 disc area SNPs were analysed with DEPICT. Due to the high correlation between VCDR and cup area, we analysed 139 independent SNPs associated with either VCDR, cup area or both. To evaluate potentially overlapping pathways between the endophenotypes, we performed two additional analyses: a) SNPs genome-wide associated with VCDR, cup area or disc area ($n=157$), and b) SNPs genome-wide associated with VCDR, cup area or IOP ($n=175$). In the second analysis, a total of 131 suggestive IOP SNPs, 333 VCDR SNPs, 250 cup area SNPs and 175 disc area SNPs with a $P < 1.0 \times 10^{-5}$ were included. As in the first analysis, we evaluated overlapping pathways or gene sets between VCDR and cup area ($n=392$ SNPs) and VCDR, cup area and disc area ($n=421$ SNPs). Analysis of the overlapping pathways between VCDR, cup area, and IOP was performed using SNPs with a $P < 7.0 \times 10^{-6}$ ($n=458$). This threshold was selected to fulfil the amount of unique loci supported by DEPICT. To reduce redundancies among pathways we used the Affinity Propagation (AP) clustering algorithm as described previously²¹⁻²³. The pairwise Pearson correlation between significant pathways was calculated and then the AP algorithm was used to cluster similar pathways into meta-pathways. Clusters were named by their representative pathway, which was automatically selected by the AP algorithm. In addition, correlation between the meta-pathways was calculated to create a network. The Cytoscape tool was used to visualize the networks.

RESULTS

Intraocular pressure

After removal of single nucleotide polymorphisms (SNPs) with minor allele frequency (MAF) < 0.01 and low imputation quality, approximately 8 million SNPs were included. Whilst the analysis of individuals of European descent yielded no novel associations, combined analysis of individuals of European and Asian descent ($n = 37,930$, $\lambda = 1.07$; Supplementary Figures 1 and 2, yielded nine genomic regions reaching genome-wide significance, of which eight genomic

regions were already known (Supplementary Table 2)^{4,6,8}. The peak SNP in the new genomic region was rs55796939 on chromosome 11q25 near *ADAMTS8* (Supplementary Figure 3).

Vertical cup-disc ratio

In the meta-analysis of individuals of European descent ($n = 23,899$, $\lambda = 1.10$), 21 genomic regions were genome-wide significant (Supplementary Table 2). Five genomic regions were novel (near to the genes *RPE65* on chr. 1p31, *F5* on chr. 1q23, *PDZD2* on chr. 5p13.3, *RREB1* on chr. 6p25, and *DGKB* on chr. 7p21.2) (Supplementary Figure 3); the other genomic regions have been previously associated with VCDR or cup area, two highly correlated traits²⁴⁻²⁶. Of the five novel genomic regions, *RREB1* ($P=4.00 \times 10^{-3}$) was nominally significant in the analysis of individuals of Asian descent ($n = 8,373$, $\lambda = 1.02$). In the combined analysis ($n = 32,272$, $\lambda = 1.08$), another four novel genomic regions, near to the genes *VCAN* on chr. 5q14.3, *PSCA* on chr. 8q24.2, *ENO4* on chr. 10q25.3, and *RBM23* on chr. 14q11.2 (Supplementary Figure 2 and 3), were genome-wide significant leading to a total of nine (5+4) novel genomic regions associated with VCDR. Of these novel genomic regions, *F5* has been associated with disc area previously²⁶. Disc area influences the VCDR²⁷, and therefore we corrected VCDR for disc area in a secondary analysis. After correction for disc area, the β (p-value) decreased from -0.007 (2.48×10^{-9}) to -0.002 (5.60×10^{-2}) in the subset with disc area available, suggesting that *F5* acts primarily on disc area and secondary to VCDR through its relation to disc area.

Cup area

The meta-analysis of individuals of European descent ($n = 22,489$, $\lambda = 1.09$) yielded 20 genome-wide significant regions of which 17 regions were already implicated for cup area or VCDR (Supplementary Table 2)^{25,26}. There were three novel associations on chr. 1q42.11 near *CDC42BPA*, chr. 8q21.11 near *CRISPLD1*, and on chr. 15q26.3 near *FAM169B* (Supplementary Figure 3). *CDC42BPA* has previously been associated with disc area and the fact that the association with cup area adjusting for disc area is genome wide significant suggests an independent effect on cup area. In the combined analysis of European and Asian individuals ($n = 29,828$, $\lambda = 1.08$, Supplementary Figures 2 and 3) all loci except *FAM169B* remained genome-wide significant, and there were two additional genome-wide significant SNPs at chr. 6p21.2 (*CDKN1A*) and chr. 9q34.2 (*ABO*; previously associated to IOP).

Disc area

The meta-analysis of individuals of European descent ($n = 22,504$, $\lambda = 1.09$) resulted in 13 genome-wide significant regions, of which two were not previously associated with disc area: *UGT8* on chr. 4q26 and *CTNNA3* on chr. 10q22.2 (Supplementary Figure 2 and Supplementary Table 2). These SNPs were not significant in the meta-analysis of individuals of Asian descent ($n = 7,307$, $\lambda = 1.03$). An additional four SNPs reached genome-wide significance in the combined meta-analysis ($n = 29,811$, $\lambda = 1.09$): *PRDM16* on chr. 1p36.23-p33, *GADD45A* on chr. 1p31.2, *VGLL4* on chr. 3p25.3, and *ASB7* on chr. 15q26.3 (Supplementary Figures 2 and 3).

Gene-based test

To identify new loci not found through per-SNP tests, we performed gene-based testing using VEGAS2. Reflecting the smaller number of tests, our gene-based significance threshold is $P_{\text{gene-based}} < 0.05/24,769 = 2.02 \times 10^{-6}$ (24,769 genes tested). Using the gene-based test we

found several novel loci (Supplementary Table 3). *C9* was significantly associated with IOP ($P=1.61 \times 10^{-6}$); *RARB* ($P=1.86 \times 10^{-6}$) and *HORMAD2-AS1* ($P=1.04 \times 10^{-6}$) were associated with VCDR. These genes were previously associated with disc area, so the novel associations with VCDR could possibly be driven by the influence of disc area on VCDR²⁶. In the cup area analysis, the genes *LRP10* ($P=1.20 \times 10^{-6}$) and *REM2* ($P=1.55 \times 10^{-6}$), and *THSD4* ($P=5.44 \times 10^{-8}$) were significantly associated. The first two genes are located near to *RBM23*, which was significant in the per-SNP test. *THSD4* is located near to *KPNB1*, which was associated with VCDR in our previous meta-analysis²⁵. In the disc area analysis we found two genes that were significantly associated with disc area: *ANKRA2* ($P=8.42 \times 10^{-7}$) and *LOC149950* ($P=3.87 \times 10^{-7}$).

Characterizing the overlap in biological pathways involved in glaucoma endophenotypes

In total, 86 SNPs were associated with one or more of the above endophenotypes. The effect estimates and p-values of these SNPs for all four endophenotypes are shown in Table 1. *ADAMTS8* (IOP and VCDR) and *ABO* (IOP and cup area) were genome-wide significantly associated with two traits. Of note is that there were different variants involved in *ADAMTS8*: rs55796939 for IOP and rs4936099 for VCDR ($r^2=0.03$ between these SNPs in 1000G European samples). Figure 1 shows the overlap in associations across endophenotypes – we depict annotated genes for which at least one SNP was genome-wide significant in at least one trait. Overlap is defined as nominal significance or stronger for the second trait. The figure shows as expected a strong overlap in variants associated to disc area, cup area and VCDR. Further, overlap is noted in genes associated to IOP, cup area and VCDR.

To further characterize the overlap in biological functions, gene set enrichment of loci associated with IOP and optic disc parameters was performed using DEPICT¹⁷. We first investigated enriched pathways or gene sets using only genome-wide associated SNPs. No significant pathways were found after FDR correction. However, pathways involved in metabolic processes such as “increased circulating leptin level”, “abnormal fat cell morphology” and “increased insulin sensitivity” were suggestive when we analyzed the list of SNPs associated with VCDR, cup area and disc area (FDR<0.2, see Supplementary Table 4). We next searched for enriched pathways using suggestive SNPs ($P<1.0 \times 10^{-5}$). We further investigated potential overlap in pathways across the endophenotypes, and found 57 significant pathways when using VCDR, cup area and IOP variants; and 100 pathways when analysing suggestive VCDR, cup area and disc area variants. Note that in the first analysis we investigated pathways enriched when IOP genes are taken into account, while in the second one we analysed genes influencing the optic nerve head characteristics. Due to a high degree of redundancy between pathways, we clustered the significant pathways into meta-pathways, resulting in 11 meta-pathways for VCDR, cup area and IOP and 17 for VCDR, cup area, and disc area (Figure 2, Supplementary Table 5). Most of the gene sets found in both analyses highlighted pathways involved in cell differentiation, notch signaling, regulatory DNA binding and embryonic development, which reflects the pathways found when VCDR and CA variants are analyzed (Supplementary Figure 4). Furthermore, we found “abnormal fat cell morphology” and “abnormal liver morphology” significantly enriched; a key gene in these pathways is *ABCA1*. When IOP genes are included the elongation factor, “RNA Polymerase II (ELL2) protein complex” shows an enrichment. When disc area genes are included, pathways such as “blood vessel development”, “protein import into nucleus”,

Table 1. Single nucleotide polymorphisms (SNPs) that are genome-wide significantly associated with at least one trait are shown in this table. For these SNPs, the associations with the other traits are also included. SNPs that are Bonferroni significantly associated with other traits are shown in bold. In the first rows, the SNPs genome-wide significantly associated with intraocular pressure (IOP) are shown. Next, SNPs associated with IOP, vertical cup-disc ratio (VCDR), and cup area); VCDR, cup area, and disc area; VCDR and cup area; VCDR and disc area; cup area and disc area; and finally SNPs associated with only disc area, are shown.

SNP	Nearest gene	A1/A2	IOP		P-value	VCDR
			β	SE		β
rs10918274	<i>TMCO1</i>	t/c	0.26	0.04	3.40×10^{-12}	0.005
rs7635832	<i>FNDC3B</i>	g/t	-0.22	0.03	3.84×10^{-13}	-0.001
rs10281637	<i>CAV1/CAV2</i>	c/t	0.20	0.03	2.53×10^{-13}	0.004
8:78380944	<i>PKIA</i>	i/r	1.00	0.17	6.06×10^{-9}	0.000
rs7815043	<i>PKIA</i>	c/t	0.10	0.03	3.64×10^{-5}	-0.001
rs7944735	Many genes	c/g	0.20	0.03	3.97×10^{-11}	0.001
11:120357425	<i>ARHGEF12</i>	d/r	0.18	0.03	1.54×10^{-9}	0.001
rs12794618	<i>ARHGEF12</i>	c/t	0.17	0.03	6.72×10^{-9}	0.001
rs55796939	<i>ADAMTS8</i>	t/c	0.36	0.06	1.92×10^{-8}	0.003
rs2472496	<i>ABCA1</i>	g/a	-0.17	0.02	1.47×10^{-13}	0.005
rs8176741	<i>ABO1</i>	a/g	0.24	0.04	2.55×10^{-10}	0.007
rs9913911	<i>GAS7</i>	g/a	-0.17	0.02	4.95×10^{-12}	-0.006
rs6804624	<i>COL8A1</i>	c/t	-0.01	0.02	6.63×10^{-1}	0.008
rs7916697	<i>ATOH7</i>	a/g	0.01	0.03	7.39×10^{-1}	-0.018
10:96008348	<i>PLCE1</i>	d/r	0.01	0.03	5.81×10^{-1}	0.007
rs324780	<i>TMTC2</i>	g/a	0.03	0.02	2.85×10^{-1}	-0.011
rs4299136	<i>ASB7</i>	c/g	-0.03	0.03	4.13×10^{-1}	0.010
16:51461915	<i>SALL1</i>	r/i	0.02	0.03	4.23×10^{-1}	0.010
rs4784295	<i>SALL1</i>	c/g	0.02	0.03	5.61×10^{-1}	0.010
rs5752773	<i>CHEK2</i>	g/c	0.01	0.03	6.89×10^{-1}	-0.012
rs2092172	<i>CARD10</i>	a/g	0.00	0.03	8.88×10^{-1}	0.009
rs7717697	<i>VCAN</i>	c/t	0.01	0.02	7.27×10^{-1}	-0.007
rs1681739	<i>ENO4</i>	t/c	0.03	0.02	2.19×10^{-1}	0.006
rs60779155	<i>ASB7</i>	a/g	-0.02	0.03	6.57×10^{-1}	0.010
rs7916697	<i>ATOH7</i>	a/g	0.01	0.03	7.39×10^{-1}	-0.018
10:96008348	<i>PLCE1</i>	d/r	0.01	0.03	5.81×10^{-1}	0.007
rs1830890	<i>PLCE1</i>	g/a	0.01	0.02	8.27×10^{-1}	0.006
rs482507	<i>TMTC2</i>	c/t	0.02	0.02	3.52×10^{-1}	-0.011
rs4436712	<i>SIX6</i>	t/g	-0.04	0.02	1.40×10^{-1}	0.009
rs738722	<i>CHEK2</i>	t/c	0.02	0.03	3.61×10^{-1}	-0.012
rs6804624	<i>COL8A1</i>	c/t	-0.01	0.02	6.63×10^{-1}	0.008
rs2684249	<i>HSF2</i>	c/t	0.03	0.02	2.10×10^{-1}	-0.006
rs34222435	<i>ASB7</i>	t/c	-0.03	0.03	3.77×10^{-1}	0.010
rs7916410	<i>ATOH7</i>	t/c	0.00	0.03	9.76×10^{-1}	-0.018
rs442376	<i>TMTC2</i>	c/t	-0.03	0.03	3.15×10^{-1}	0.011
rs1345467	<i>SALL1</i>	g/a	0.01	0.03	6.55×10^{-1}	0.009
rs5762752	<i>CHEK2</i>	c/g	0.01	0.03	6.58×10^{-1}	-0.011
rs11129176	<i>RARB</i>	a/g	0.02	0.03	4.11×10^{-1}	0.005
rs1997404	<i>COL8A1</i>	g/t	-0.02	0.03	3.28×10^{-1}	0.008
rs34935520	<i>SIX6</i>	g/a	-0.04	0.02	1.09×10^{-1}	0.009
rs4960295	<i>RREB1</i>	a/g	0.02	0.02	4.65×10^{-1}	0.007
rs10274998	<i>DGKB</i>	t/c	0.02	0.03	4.31×10^{-1}	0.008
rs2157719	<i>CDKN2B-AS1</i>	c/t	-0.04	0.02	9.20×10^{-2}	-0.013
rs3891783	<i>PLCE1</i>	g/c	0.04	0.02	1.01×10^{-1}	0.007
rs1346	<i>SSSCA1</i>	t/a	-0.05	0.03	1.11×10^{-1}	-0.013

Table 1. (continued)

		CA		DA			
SE	P-value	β	SE	P-value	β	SE	P-value
0.002	8.60×10^{-3}	0.010	0.003	2.20×10^{-3}	-0.001	0.006	9.13×10^{-1}
0.001	3.33×10^{-1}	-0.004	0.003	1.22×10^{-1}	0.002	0.005	7.12×10^{-1}
0.001	4.97×10^{-3}	0.006	0.003	1.13×10^{-2}	-0.003	0.005	5.81×10^{-1}
0.010	9.77×10^{-1}	-0.017	0.017	3.23×10^{-1}	0.018	0.031	5.50×10^{-1}
0.001	3.23×10^{-1}	-0.001	0.002	8.24×10^{-1}	-0.002	0.004	5.65×10^{-1}
0.001	4.53×10^{-1}	0.006	0.003	2.97×10^{-2}	0.000	0.005	9.73×10^{-1}
0.001	5.70×10^{-1}	0.001	0.003	6.27×10^{-1}	0.001	0.005	8.20×10^{-1}
0.001	3.77×10^{-1}	0.002	0.003	4.62×10^{-1}	0.004	0.005	4.24×10^{-1}
0.003	3.77×10^{-1}	0.006	0.006	3.06×10^{-1}	-0.003	0.010	8.00×10^{-1}
0.001	5.69×10^{-5}	0.010	0.002	6.40×10^{-7}	0.003	0.004	4.71×10^{-1}
0.002	4.06×10^{-5}	0.019	0.003	5.65×10^{-8}	0.004	0.006	5.25×10^{-1}
0.001	1.62×10^{-7}	-0.008	0.002	1.79×10^{-4}	-0.001	0.004	8.45×10^{-1}
0.001	4.69×10^{-12}	0.013	0.002	1.66×10^{-8}	0.020	0.004	4.93×10^{-7}
0.001	5.22×10^{-46}	-0.017	0.002	7.42×10^{-13}	-0.094	0.004	7.36×10^{-110}
0.001	3.50×10^{-8}	0.013	0.002	1.11×10^{-8}	0.015	0.004	1.61×10^{-4}
0.001	3.08×10^{-23}	-0.016	0.002	7.62×10^{-14}	-0.029	0.004	8.39×10^{-14}
0.002	1.72×10^{-12}	0.018	0.003	3.02×10^{-10}	0.024	0.005	2.39×10^{-6}
0.001	1.45×10^{-13}	0.013	0.003	5.18×10^{-7}	0.032	0.005	5.19×10^{-13}
0.001	2.22×10^{-13}	0.013	0.002	1.19×10^{-7}	0.031	0.004	1.99×10^{-12}
0.001	7.90×10^{-21}	-0.024	0.003	1.25×10^{-21}	-0.024	0.004	5.28×10^{-8}
0.001	1.92×10^{-12}	0.011	0.003	2.91×10^{-5}	0.032	0.005	3.84×10^{-12}
0.001	4.39×10^{-9}	-0.009	0.002	1.12×10^{-5}	-0.018	0.004	2.16×10^{-6}
0.001	2.12×10^{-8}	0.011	0.002	3.32×10^{-7}	0.019	0.004	1.04×10^{-6}
0.002	2.67×10^{-10}	0.019	0.003	2.92×10^{-9}	0.030	0.005	3.28×10^{-8}
0.001	5.22×10^{-46}	-0.017	0.002	7.42×10^{-13}	-0.094	0.004	7.36×10^{-110}
0.001	3.50×10^{-8}	0.013	0.002	1.11×10^{-8}	0.015	0.004	1.61×10^{-4}
0.001	2.49×10^{-8}	0.012	0.002	6.52×10^{-8}	0.014	0.004	3.60×10^{-4}
0.001	1.03×10^{-19}	-0.017	0.002	1.15×10^{-14}	-0.030	0.004	5.03×10^{-14}
0.001	3.58×10^{-14}	0.025	0.002	1.88×10^{-30}	-0.018	0.004	3.71×10^{-6}
0.001	2.78×10^{-20}	-0.024	0.003	2.35×10^{-22}	-0.021	0.004	1.59×10^{-6}
0.001	4.69×10^{-12}	0.013	0.002	1.66×10^{-8}	0.020	0.004	4.93×10^{-7}
0.001	1.47×10^{-7}	-0.012	0.002	1.96×10^{-8}	-0.015	0.004	9.56×10^{-5}
0.002	1.95×10^{-12}	0.019	0.003	7.65×10^{-11}	0.025	0.005	1.29×10^{-6}
0.001	2.23×10^{-46}	-0.017	0.002	3.57×10^{-12}	-0.097	0.004	1.97×10^{-114}
0.001	6.80×10^{-18}	0.017	0.002	1.59×10^{-12}	0.032	0.004	9.79×10^{-15}
0.001	2.91×10^{-12}	0.012	0.003	8.53×10^{-7}	0.032	0.004	1.19×10^{-13}
0.001	2.29×10^{-18}	-0.021	0.002	2.58×10^{-19}	-0.023	0.004	1.17×10^{-8}
0.001	3.14×10^{-5}	0.010	0.002	8.59×10^{-6}	0.023	0.004	1.02×10^{-8}
0.001	1.36×10^{-11}	0.013	0.002	6.58×10^{-8}	0.024	0.004	7.31×10^{-9}
0.001	5.41×10^{-14}	0.025	0.002	9.85×10^{-30}	-0.022	0.004	2.39×10^{-8}
0.001	1.93×10^{-10}	0.009	0.002	2.52×10^{-5}	0.012	0.004	2.26×10^{-3}
0.001	3.91×10^{-8}	0.012	0.003	5.87×10^{-6}	0.011	0.005	2.09×10^{-2}
0.001	1.30×10^{-35}	-0.024	0.002	5.41×10^{-29}	-0.008	0.004	2.61×10^{-2}
0.001	8.01×10^{-11}	0.011	0.002	2.09×10^{-7}	0.012	0.004	8.58×10^{-4}
0.001	3.88×10^{-18}	-0.019	0.003	5.20×10^{-11}	-0.016	0.005	1.59×10^{-3}

Table 1. (continued)

SNP	Nearest gene	A1/A2	IOP		P-value	VCDR β
			β	SE		
rs4936099	<i>ADAMTS8</i>	c/a	-0.03	0.03	2.31x10 ⁻¹	-0.007
13:36629905	<i>DCLK1</i>	d/r	-0.02	0.03	5.76x10 ⁻¹	0.007
rs7323428	<i>DCLK1</i>	t/g	-0.02	0.03	4.12x10 ⁻¹	0.007
rs8015152	<i>SIX6</i>	t/c	-0.06	0.02	2.03x10 ⁻²	0.010
rs6107845	<i>BMP2</i>	a/g	0.03	0.02	2.89x10 ⁻¹	-0.009
rs6764184	<i>FLNB</i>	t/g	0.05	0.03	5.25x10 ⁻²	0.007
rs7311936	<i>FAM101A</i>	c/g	-0.03	0.02	1.56x10 ⁻¹	-0.006
14:23388793	<i>RBM23</i>	r/d	0.02	0.03	4.00x10 ⁻¹	0.007
rs3794453	<i>RBM23</i>	a/t	0.01	0.02	7.29x10 ⁻¹	0.007
rs2252865	<i>RERE</i>	t/c	0.05	0.02	3.75x10 ⁻²	0.005
rs4846112	<i>DHRS3</i>	a/g	-0.02	0.03	5.23x10 ⁻¹	-0.005
rs13016883	<i>TRIB2</i>	c/g	0.02	0.03	5.48x10 ⁻¹	0.006
rs35084382	<i>DUSP1</i>	c/t	-0.10	0.07	1.25x10 ⁻¹	-0.018
rs117598310	<i>CRISPLD1</i>	t/g	-0.05	0.05	3.09x10 ⁻¹	0.009
rs1360589	<i>CDKN2B-AS1</i>	c/t	-0.04	0.02	7.91x10 ⁻²	-0.013
rs1346	<i>SSSCA1</i>	t/a	-0.05	0.03	1.11x10 ⁻¹	-0.013
rs11613189	<i>FAM101A</i>	t/c	-0.03	0.03	2.08x10 ⁻¹	-0.005
rs7323428	<i>DCLK1</i>	t/g	-0.02	0.03	4.12x10 ⁻¹	0.007
rs2251069	<i>DDHD1</i>	c/t	0.01	0.02	7.33x10 ⁻¹	-0.006
rs6598351	<i>FAM169B</i>	t/c	-0.02	0.03	5.30x10 ⁻¹	0.006
rs11646917	<i>SALL1</i>	t/g	-0.01	0.03	6.71x10 ⁻¹	-0.009
rs11867840	<i>BCAS3</i>	g/a	0.04	0.03	1.04x10 ⁻¹	-0.006
rs6054375	<i>BMP2</i>	t/g	0.03	0.03	2.57x10 ⁻¹	-0.010
rs3791679	<i>EFEMP1/PNPT1</i>	g/a	0.04	0.03	1.66x10 ⁻¹	-0.005
rs12494328	<i>FLNB</i>	a/g	0.04	0.03	1.56x10 ⁻¹	0.006
6:36592986	<i>CDKN1A</i>	d/r	-0.02	0.03	5.08x10 ⁻¹	0.006
rs72852338	<i>CDKN1A</i>	c/a	-0.02	0.03	5.19x10 ⁻¹	0.006
rs4936099	<i>ADAMTS8</i>	c/a	-0.03	0.03	2.31x10 ⁻¹	-0.007
rs1074407	<i>TRIOBP</i>	t/a	0.11	0.02	3.42x10 ⁻⁶	0.006
rs1192414	<i>CDC7/TGFBFR3</i>	a/g	0.06	0.03	5.39x10 ⁻²	0.014
rs10753787	<i>F5</i>	t/c	-0.03	0.02	1.80x10 ⁻¹	-0.007
rs2920293	<i>PSCA</i>	g/c	0.00	0.02	8.67x10 ⁻¹	-0.006
rs4658101	<i>CDC7/TGFBFR3</i>	a/g	0.06	0.03	4.24x10 ⁻²	0.013
1:169530520	<i>F5/SELP</i>	i/r	0.02	0.03	4.44x10 ⁻¹	0.007
rs2239854	<i>F5/SELP</i>	a/g	0.03	0.03	2.73x10 ⁻¹	0.006
rs9843102	<i>ABI3BP</i>	a/g	0.00	0.03	9.91x10 ⁻¹	-0.006
8:88744441	<i>DCAF4L2</i>	d/r	-0.01	0.02	6.98x10 ⁻¹	0.006
rs6468996	<i>DCAF4L2</i>	t/c	0.00	0.02	9.19x10 ⁻¹	0.005
rs61101201	<i>ELP4/PAX6</i>	g/t	0.02	0.03	5.33x10 ⁻¹	0.006
rs56385951	<i>CARD10</i>	a/g	-0.06	0.04	8.65x10 ⁻²	0.011
1:3046430	<i>PRDM16</i>	i/r	-0.04	0.04	4.19x10 ⁻¹	0.007
rs12028027	<i>PRDM16</i>	c/t	-0.03	0.04	5.03x10 ⁻¹	0.007
1:227562773	<i>CDC42BPA</i>	d/r	-0.10	0.05	2.74x10 ⁻²	0.003
rs73102394	<i>CDC42BPA</i>	t/c	-0.09	0.04	3.92x10 ⁻²	0.003
rs11811982	<i>CDC42BPA</i>	a/c	-0.12	0.05	1.21x10 ⁻²	0.004
rs10021731	<i>UGT8</i>	c/t	0.01	0.02	8.26x10 ⁻¹	-0.002
rs12220165	<i>CTNNA3</i>	g/c	0.02	0.03	5.94x10 ⁻¹	-0.004
rs787541	<i>U6_GADD45A</i>	c/g	0.07	0.03	7.17x10 ⁻³	0.002
rs1367187	<i>DIRC3</i>	c/t	-0.07	0.03	9.01x10 ⁻³	0.002
rs2443724	<i>VGLL4</i>	c/g	0.00	0.02	8.77x10 ⁻¹	-0.003
rs1013830	<i>CTNNA3</i>	t/c	0.00	0.05	9.53x10 ⁻¹	-0.007

Table 1. (continued)

		CA		DA			
SE	P-value	β	SE	P-value	β	SE	P-value
0.001	5.16x10 ⁻⁹	-0.013	0.002	3.34x10 ⁻⁸	-0.006	0.004	1.50x10 ⁻¹
0.001	2.45x10 ⁻⁸	0.018	0.002	1.12x10 ⁻¹⁴	-0.005	0.004	2.26x10 ⁻¹
0.001	1.56x10 ⁻⁸	0.019	0.002	8.63x10 ⁻¹⁶	-0.005	0.004	2.08x10 ⁻¹
0.001	1.34x10 ⁻¹⁸	0.024	0.002	2.01x10 ⁻²⁶	-0.011	0.004	5.18x10 ⁻³
0.001	2.12x10 ⁻¹⁷	-0.017	0.002	1.45x10 ⁻¹⁵	-0.014	0.004	3.22x10 ⁻¹
0.001	1.50x10 ⁻⁸	0.015	0.002	1.01x10 ⁻¹⁰	0.010	0.004	1.51x10 ⁻²
0.001	1.87x10 ⁻⁹	-0.013	0.002	2.35x10 ⁻⁹	0.003	0.004	5.21x10 ⁻¹
0.001	2.13x10 ⁻⁸	0.013	0.003	1.47x10 ⁻⁷	0.009	0.004	3.48x10 ⁻²
0.001	5.85x10 ⁻⁸	0.011	0.002	2.10x10 ⁻⁷	0.009	0.004	2.65x10 ⁻²
0.001	1.95x10 ⁻⁵	0.014	0.002	6.69x10 ⁻¹⁰	0.003	0.004	5.13x10 ⁻¹
0.001	2.22x10 ⁻⁴	-0.012	0.002	1.67x10 ⁻⁷	0.005	0.004	2.21x10 ⁻¹
0.001	2.53x10 ⁻⁶	0.016	0.002	1.05x10 ⁻¹¹	0.001	0.004	8.23x10 ⁻¹
0.003	1.56x10 ⁻⁸	-0.034	0.006	1.16x10 ⁻⁸	-0.030	0.011	4.57x10 ⁻³
0.002	1.00x10 ⁻⁴	0.021	0.004	1.32x10 ⁻⁶	0.022	0.008	4.96x10 ⁻³
0.001	5.05x10 ⁻³⁵	-0.024	0.002	4.51x10 ⁻²⁹	-0.008	0.004	3.65x10 ⁻²
0.001	3.88x10 ⁻¹⁸	-0.019	0.003	5.20x10 ⁻¹¹	-0.016	0.005	1.59x10 ⁻³
0.001	4.79x10 ⁻⁶	-0.016	0.002	8.66x10 ⁻¹³	0.002	0.004	6.49x10 ⁻¹
0.001	1.56x10 ⁻⁸	0.019	0.002	8.63x10 ⁻¹⁶	-0.005	0.004	2.08x10 ⁻¹
0.001	7.12x10 ⁻⁸	-0.013	0.002	5.69x10 ⁻¹⁰	0.001	0.004	7.33x10 ⁻¹
0.001	2.34x10 ⁻⁵	0.012	0.003	1.19x10 ⁻⁵	-0.004	0.005	3.83x10 ⁻¹
0.001	3.43x10 ⁻¹⁰	-0.015	0.003	2.54x10 ⁻⁹	-0.015	0.005	1.16x10 ⁻³
0.001	3.89x10 ⁻⁶	-0.018	0.002	1.15x10 ⁻¹³	0.012	0.004	7.36x10 ⁻³
0.001	4.10x10 ⁻¹⁵	-0.018	0.002	8.77x10 ⁻¹⁶	-0.003	0.004	4.72x10 ⁻¹
0.001	1.02x10 ⁻⁴	-0.013	0.002	2.94x10 ⁻⁸	0.003	0.004	4.93x10 ⁻¹
0.001	1.43x10 ⁻⁶	0.016	0.002	4.39x10 ⁻¹¹	0.009	0.004	3.96x10 ⁻²
0.001	1.60x10 ⁻⁵	0.015	0.003	7.85x10 ⁻⁹	-0.006	0.005	2.04x10 ⁻¹
0.001	2.74x10 ⁻⁵	0.014	0.003	2.26x10 ⁻⁸	-0.005	0.005	2.96x10 ⁻¹
0.001	5.16x10 ⁻⁹	-0.013	0.002	3.34x10 ⁻⁸	-0.006	0.004	1.50x10 ⁻¹
0.001	2.66x10 ⁻⁷	0.012	0.002	1.17x10 ⁻⁸	0.008	0.004	3.15x10 ⁻²
0.001	8.18x10 ⁻²⁴	0.007	0.003	1.07x10 ⁻²	0.087	0.005	3.78x10 ⁻⁷⁴
0.001	2.11x10 ⁻⁹	-0.005	0.002	1.84x10 ⁻²	-0.019	0.004	9.12x10 ⁻⁷
0.001	4.95x10 ⁻⁹	-0.007	0.002	7.60x10 ⁻⁴	-0.015	0.004	5.41x10 ⁻⁵
0.001	2.35x10 ⁻²³	0.007	0.003	1.09x10 ⁻²	0.089	0.005	2.35x10 ⁻⁸²
0.001	6.29x10 ⁻⁷	0.005	0.003	5.33x10 ⁻²	0.032	0.005	5.13x10 ⁻¹³
0.001	6.94x10 ⁻⁷	0.005	0.002	4.94x10 ⁻²	0.030	0.004	3.43x10 ⁻¹³
0.002	2.01x10 ⁻⁴	-0.002	0.003	5.89x10 ⁻¹	-0.036	0.005	3.99x10 ⁻¹²
0.001	4.50x10 ⁻⁷	0.006	0.002	4.47x10 ⁻³	0.026	0.004	7.15x10 ⁻¹²
0.001	1.86x10 ⁻⁷	0.006	0.002	2.11x10 ⁻³	0.025	0.004	8.07x10 ⁻¹²
0.001	1.85x10 ⁻⁶	0.005	0.002	3.91x10 ⁻²	0.028	0.004	3.52x10 ⁻¹¹
0.002	1.36x10 ⁻¹¹	0.008	0.003	8.50x10 ⁻³	0.047	0.006	2.48x10 ⁻¹⁷
0.002	5.00x10 ⁻⁴	-0.001	0.004	7.18x10 ⁻¹	0.044	0.007	5.15x10 ⁻¹⁰
0.002	2.02x10 ⁻⁴	-0.001	0.004	8.62x10 ⁻¹	0.043	0.007	6.02x10 ⁻¹⁰
0.002	2.39x10 ⁻¹	0.024	0.004	4.60x10 ⁻⁹	-0.055	0.007	4.93x10 ⁻¹⁴
0.002	1.60x10 ⁻¹	0.022	0.004	2.53x10 ⁻⁸	-0.053	0.007	6.79x10 ⁻¹⁴
0.002	5.48x10 ⁻²	0.027	0.004	1.32x10 ⁻¹⁰	-0.062	0.008	1.74x10 ⁻¹⁶
0.001	5.60x10 ⁻²	-0.002	0.002	2.63x10 ⁻¹	-0.020	0.004	2.44x10 ⁻⁷
0.002	1.41x10 ⁻²	-0.004	0.003	1.76x10 ⁻¹	-0.023	0.005	1.75x10 ⁻⁵
0.001	7.26x10 ⁻²	0.002	0.002	5.06x10 ⁻¹	0.023	0.004	3.16x10 ⁻⁸
0.001	2.63x10 ⁻¹	-0.002	0.003	4.79x10 ⁻¹	0.026	0.005	5.96x10 ⁻⁹
0.001	1.50x10 ⁻²	0.000	0.002	9.47x10 ⁻¹	-0.022	0.004	1.40x10 ⁻⁸
0.002	4.70x10 ⁻³	-0.004	0.005	3.96x10 ⁻¹	-0.045	0.008	2.00x10 ⁻⁸

“Thrombospondin 1 (THBS1) and SMAD3 protein complex”, and “abnormal eye morphology” were significant. Key genes in the latter include: *CDKN2B*, *FAT4*, *LRIG3*, *SIX6*, *COL8A1*, *SOX11*, *RND3*, *BOC*, *WNT2B* and *CYP26A1*.

From endophenotypes to primary open-angle glaucoma

Of the 75 independent (i.e. $R^2 < 0.8$) SNPs that were associated with one or more of the endophenotypes, 32 were nominal significantly associated with POAG in a meta-analysis of 6,429 cases and 41,404 controls ($P < 0.05$; the chance that 32 SNPs of 75 SNPs have a $P < 0.05$ is $< 2.2 \times 10^{-16}$), and 11 independent SNPs were Bonferroni significantly associated with POAG (p-value $0.05/75 = 6.67 \times 10^{-4}$) (Table 2). The association between *CDKN1A* and POAG is novel ($OR = 1.14$, $P = 7.4 \times 10^{-7}$). In our previous paper, the SNP rs6054374 near to *BMP2* was already associated with POAG ($OR = 0.92$, $P = 3.74 \times 10^{-3}$), but the most significantly associated SNP in the current meta-analysis rs6107845 near to *BMP2* shows a slightly larger effect on POAG ($OR = 0.89$, $P = 8.52 \times 10^{-6}$). *CDKN1A* is a novel gene in the same gene family as *CDKN2B*, a gene previously associated to glaucoma. Both *CDKN1A* and *CDKN2B* are cell-cycle genes.

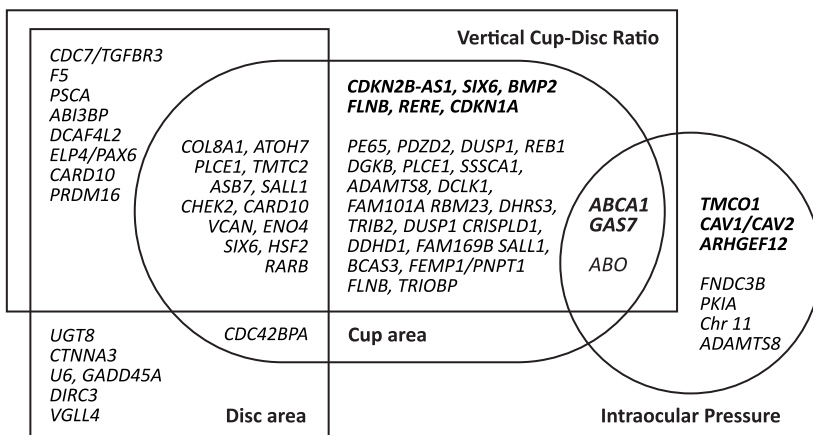


Figure 1. Overlap between the genes associated with one or more endophenotypes. Genes with genome-wide significant association for at least one trait are shown. These genes are counted as overlapping genes if they are Bonferroni significantly associated with the other trait(s). Chr 11 (see intraocular pressure circle) means a region on chromosome 11 that is associated with IOP and has many genes in it; the likely causative gene in this region is not identified yet. Genes in bold are genes associated with primary open-angle glaucoma in our meta-analysis of four case-control studies.

Figure 2. Pathways significantly enriched for: A) Loci associated with vertical cup-disc ratio, cup area and intraocular pressure ($P < 7.0 \times 10^{-6}$ in the GWAS). In total 11 meta-pathways were identified after clustering the 59 pathways identified by DEPICT. B) Loci associated with vertical cup-disc ratio, cup area and disc area ($P < 1.0 \times 10^{-5}$). In total 17 meta-pathways were identified after clustering the 107 pathways identified by DEPICT. In both figures meta-pathways are represented by nodes coloured according to statistical significance, and edges are scaled according to the correlation between meta-pathways. *The pathway “Abnormal eye morphology” clustered with the meta-pathway “Chordate embryonic development”. USP5= ubiquitin specific peptidase 5, EGFR=Epidermal Growth Factor Receptor, DVL2= Dishevelled Segment Polarity Protein 2, THBS1=Thrombospondin 1, RFX2= Regulatory Factor X, 2.

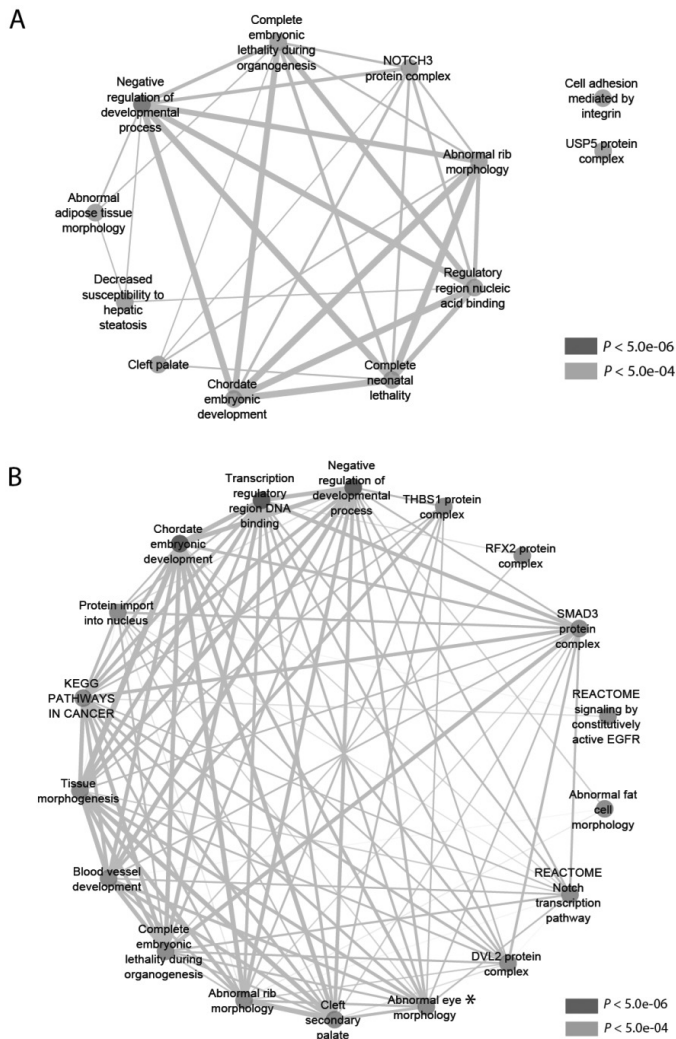


Table 2. Association with primary open-angle glaucoma in a meta-analysis of four independent glaucoma case-control studies (ANZRAG, NEIGHBORHOOD, Singapore, and Southampton). Results are shown for the most significantly associated single nucleotide polymorphisms from the endophenotype analyses.

	Nearest gene	A1/A2	OR	95% CI	P-value	Direction	I ²	P-value of heterogeneity
IOP SNPs								
rs10918274	<i>TMCO1</i>	t/c	1.39	1.30-1.50	2.75x10 ⁻¹⁹	++++	38.4	1.82x10 ⁻¹
rs7635832	<i>FNDC3B</i>	g/t	0.89	0.83-0.95	1.41x10 ⁻³	---?	33.9	2.20x10 ⁻¹
rs10281637	<i>CAV1/CAV2</i>	c/t	1.13	1.07-1.20	2.32x10 ⁻⁵	++++	0	4.89x10 ⁻¹
rs2487048	<i>ABCA1</i>	a/g	1.26	1.19-1.33	2.65x10 ⁻¹⁵	++++	82.9	5.53x10 ⁻⁴
rs8176741	<i>ABO1</i>	a/g	1.07	0.99-1.17	7.36x10 ⁻²	+++	58.5	6.51x10 ⁻²
rs7944735	Many genes (<i>NUP160, PTPRJ</i>)	c/g	1.06	1.01-1.13	2.99x10 ⁻²	++++	0	8.99x10 ⁻¹
11:120357425	<i>ARHGEF12</i>	d/r	1.16	1.09-1.23	1.52x10 ⁻⁶	++++	83.2	4.65x10 ⁻⁴
rs55796939	<i>ADAMTS8</i>	t/c	1.07	0.94-1.24	2.72x10 ⁻¹	+?--	78.6	9.35x10 ⁻³
rs9913911	<i>GAS7</i>	g/a	0.80	0.76-0.84	1.08x10 ⁻¹⁷	----	0	7.50x10 ⁻¹
VCDR SNPs								
rs1925953	<i>RPE65</i>	t/a	1.07	1.02-1.13	4.21x10 ⁻³	++++	46.7	1.31x10 ⁻¹
rs1192414	<i>CDC7/TGFB3</i>	a/g	1.08	1.02-1.16	9.26x10 ⁻³	++++	0	7.27x10 ⁻¹
rs10753787	<i>F5</i>	t/c	0.97	0.93-1.03	3.67x10 ⁻¹	----	0	9.92x10 ⁻¹
rs6804624	<i>COL8A1</i>	c/t	0.99	0.94-1.05	8.14x10 ⁻¹	----	0	8.42x10 ⁻¹
rs72759609	<i>PDZD2</i>	c/t	0.90	0.83-0.99	3.20x10 ⁻²	----	0	9.53x10 ⁻¹
rs114503346	<i>DUSP1</i>	t/c	1.00	0.80-1.25	9.99x10 ⁻¹	+?+	42	1.78x10 ⁻¹
rs4960295	<i>RREB1</i>	a/g	0.99	0.95-1.05	9.50x10 ⁻¹	-++	4.6	3.70x10 ⁻¹
rs10274998	<i>DGKB</i>	t/c	1.03	0.98-1.10	2.16x10 ⁻¹	+++	0	5.38x10 ⁻¹
rs2157719	<i>CDKN2B-AS1</i>	c/t	0.69	0.66-0.74	1.29x10 ⁻⁴⁰	----	0	5.67x10 ⁻¹
rs1900005	<i>ATOH7</i>	a/c	1.01	0.96-1.07	6.98x10 ⁻¹	+++	5.1	3.67x10 ⁻¹
10:96008348	<i>PLCE1</i>	d/r	1.02	0.97-1.09	3.38x10 ⁻¹	++?	35.3	2.13x10 ⁻¹
rs1346	<i>SSSCA1</i>	t/a	0.90	0.85-0.97	2.41x10 ⁻³	----	0	9.04x10 ⁻¹
rs4936099	<i>ADAMTS8</i>	c/a	0.94	0.9-1.00	5.75x10 ⁻²	----	0	9.63x10 ⁻¹
rs324780	<i>TMTC2</i>	g/a	0.93	0.89-0.99	1.35x10 ⁻²	----	0	7.69x10 ⁻¹
13:36629905	<i>DCLK1</i>	d/r	0.99	0.94-1.05	7.53x10 ⁻¹	--+	6.2	3.62x10 ⁻¹
rs8015152	<i>SIX6</i>	t/c	1.21	1.16-1.28	3.90x10 ⁻¹⁵	++++	62.4	4.62x10 ⁻²
rs4299136	<i>ASB7</i>	c/g	1.03	0.97-1.10	3.55x10 ⁻¹	+++	0	8.29x10 ⁻¹
16:51461915	<i>SALL1</i>	i/r	0.94	0.89-1.00	3.85x10 ⁻²	----	0	7.82x10 ⁻¹
rs6107845	<i>BMP2</i>	a/g	0.89	0.85-0.94	1.02x10 ⁻⁵	----	43.1	1.53x10 ⁻¹
rs5752773	<i>CHEK2</i>	g/c	0.92	0.88-0.98	4.63x10 ⁻³	----	0	9.12x10 ⁻¹
rs2092172	<i>CARD10</i>	a/g	0.97	0.92-1.04	4.35x10 ⁻¹	--+	0	7.76x10 ⁻¹
rs6764184	<i>FLNB</i>	t/g	1.07	1.02-1.13	5.73x10 ⁻³	+++	86.1	8.14x10 ⁻⁵
rs7717697	<i>VCAN</i>	c/t	0.98	0.93-1.04	5.26x10 ⁻¹	---?	0	7.30x10 ⁻¹
rs2920293	<i>PSCA</i>	g/c	1.03	0.98-1.09	2.25x10 ⁻¹	++?	0	3.79x10 ⁻¹
rs1681739	<i>ENO4</i>	t/c	1.02	0.97-1.08	3.92x10 ⁻¹	+--	49.2	1.16x10 ⁻¹
rs7311936	<i>FAM101A</i>	c/g	0.99	0.95-1.04	8.12x10 ⁻¹	+++	11	3.38x10 ⁻¹
14:23388793	<i>RBM23</i>	r/d	1.03	0.98-1.1	1.83x10 ⁻¹	+++?	0	4.61x10 ⁻¹
CA SNPs								
rs2252865	<i>RERE</i>	t/c	1.11	1.06-1.18	5.76x10 ⁻⁵	+++	59.3	6.10x10 ⁻²
rs4846112	<i>DHRS</i>	a/g	0.95	0.91-1.01	1.18x10 ⁻¹	----	0	5.53x10 ⁻¹
1:227562773	<i>CDC42BPA</i>	d/r	0.87	0.79-0.97	1.14x10 ⁻²	--?	48.6	1.43x10 ⁻¹
rs13016883	<i>TRIB2</i>	c/g	1.08	1.03-1.14	4.25x10 ⁻³	+++?	0	8.63x10 ⁻¹
rs35084382	<i>DUSP1</i>	c/t	1.04	0.85-1.29	6.72x10 ⁻¹	+?+	0	3.91x10 ⁻¹

Table 2. (continued)

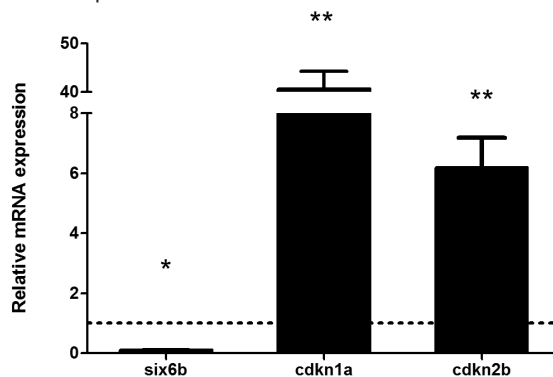
	Nearest gene	A1/A2	OR	95% CI	P-value	Direction	I^2	P-value of heterogeneity
rs117598310	<i>CRISPLD1</i>	t/g	1.08	1.00-1.19	5.39×10^{-2}	+++	0	8.01×10^{-1}
rs1360589	<i>CDKN2B-AS1</i>	c/t	0.69	0.66-0.73	1.90×10^{-42}	----	0	6.47×10^{-1}
rs10998036	<i>ATOH7</i>	c/g	1.01	0.96-1.08	5.42×10^{-1}	+---	26	2.55×10^{-1}
10:96008348	<i>PLCE1</i>	d/r	1.02	0.97-1.09	3.38×10^{-1}	+--+?	35.3	2.13×10^{-1}
rs1346	<i>SSSCA1</i>	t/a	0.90	0.85-0.97	2.41×10^{-3}	----	0	9.04×10^{-1}
rs482507	<i>TMTC2</i>	c/t	0.94	0.89-0.99	2.03×10^{-2}	----	0	7.46×10^{-1}
rs11613189	<i>FAM101A</i>	t/c	0.99	0.95-1.05	8.25×10^{-1}	+--+	18.5	2.98×10^{-1}
rs7323428	<i>DCLK1</i>	t/g	0.99	0.94-1.05	7.83×10^{-1}	+--+	13.6	3.25×10^{-1}
rs2251069	<i>DDHD1</i>	c/t	0.95	0.91-1.00	7.62×10^{-2}	--+	0	4.08×10^{-1}
rs4436712	<i>SIX6</i>	t/g	1.24	1.19-1.31	5.77×10^{-18}	++++	48.8	1.19×10^{-1}
rs6598351	<i>FAM169B</i>	t/c	0.99	0.93-1.06	8.06×10^{-1}	+--	0	7.11×10^{-1}
rs11646917	<i>SALL1</i>	t/3g	0.98	0.93-1.04	5.49×10^{-1}	--+	0	5.97×10^{-1}
rs11867840	<i>BCAS3</i>	g/a	1.06	1.01-1.13	1.83×10^{-2}	++++	8.3	3.51×10^{-1}
rs6054375	<i>BMP2</i>	t/g	0.89	0.85-0.94	8.52×10^{-6}	----	47.1	1.29×10^{-1}
rs738722	<i>CHEK2</i>	t/c	0.93	0.89-0.99	1.26×10^{-2}	----	0	9.05×10^{-1}
rs3791679	<i>EFEMP1/PNPT1</i>	a/g	0.96	0.92-1.02	2.23×10^{-1}	----	0	5.51×10^{-1}
rs12494328	<i>FLNB</i>	a/g	1.13	1.07-1.20	1.28×10^{-5}	+++	26.9	2.50×10^{-1}
rs6804624	<i>COL8A1</i>	c/t	0.99	0.94-1.05	8.14×10^{-1}	----	0	8.42×10^{-1}
6:36592986	<i>CDKN1A</i>	d/r	1.14	1.09-1.21	7.74×10^{-7}	++++	36.6	1.93×10^{-1}
rs2684249	<i>HSF1</i>	c/t	0.92	0.88-0.97	1.08×10^{-3}	----	63.3	4.25×10^{-2}
rs8176672	<i>ABO</i>	t/c	1.00	0.91-1.11	9.49×10^{-1}	+--?	0	3.69×10^{-1}
rs4936099	<i>ADAMTS8</i>	c/a	0.94	0.90-1.00	5.75×10^{-2}	----	0	9.63×10^{-1}
rs34222435	<i>ASB7</i>	t/c	1.03	0.97-1.10	3.66×10^{-1}	+++	0	8.74×10^{-1}
rs1074407	<i>TRIOBP</i>	t/a	1.04	1.00-1.10	4.92×10^{-2}	++++	32.9	2.15×10^{-1}
DA SNPs								
rs4658101	<i>CDC7/TGFBR3</i>	a/g	1.08	1.02-1.16	7.81×10^{-3}	++++	0	7.22×10^{-1}
1:169530520	<i>F5/SELP</i>	i/r	1.01	0.96-1.08	5.40×10^{-1}	+--+?	0	7.14×10^{-1}
rs11811982	<i>CDC42BPA</i>	a/c	0.87	0.80-0.97	1.19×10^{-2}	--+	20.5	2.87×10^{-1}
rs9843102	<i>ABI3BP</i>	a/g	0.92	0.86-0.98	1.37×10^{-2}	----	0	6.24×10^{-1}
rs10021731	<i>UGT8</i>	c/t	1.01	0.96-1.06	6.82×10^{-1}	----	0	6.50×10^{-1}
8:88744441	<i>DCAF4L2</i>	d/r	1.03	0.99-1.09	1.23×10^{-1}	+++	4.9	3.68×10^{-1}
rs12220165	<i>CTNNA3</i>	g/c	1.08	1.01-1.16	1.14×10^{-2}	++++	0	9.04×10^{-1}
rs7916410	<i>ATOH7</i>	t/c	1.00	0.96-1.06	7.63×10^{-1}	+++	3.9	3.73×10^{-1}
rs61101201	<i>ELP4/PAX6</i>	g/t	1.00	0.94-1.06	9.77×10^{-1}	+--?	0	9.63×10^{-1}
rs442376	<i>TMTC2</i>	c/t	1.04	0.99-1.10	7.94×10^{-2}	+++	0	6.82×10^{-1}
rs1345467	<i>SALL1</i>	g/a	1.07	1.01-1.14	1.86×10^{-2}	++++	0	8.73×10^{-1}
rs5762752	<i>CHEK2</i>	c/g	0.92	0.88-0.98	4.90×10^{-3}	----	0	8.29×10^{-1}
rs56385951	<i>CARD10</i>	a/g	0.99	0.92-1.07	9.15×10^{-1}	+--+	0	9.88×10^{-1}
1:3046430	<i>PRDM16</i>	i/r	0.97	0.87-1.10	7.13×10^{-1}	+--+?	63.9	6.28×10^{-2}
rs787541	<i>U6, GADD45A</i>	c/g	0.98	0.94-1.04	6.10×10^{-1}	--+	50.7	1.08×10^{-1}
rs1367187	<i>DIRC3</i>	c/t	0.95	0.90-1.01	1.11×10^{-1}	+--+	46.1	1.35×10^{-1}
rs2443724	<i>VGLL4</i>	c/g	0.91	0.87-0.97	1.04×10^{-3}	--+	38	1.84×10^{-1}
rs11129176	<i>RARB</i>	a/g	0.99	0.94-1.05	8.85×10^{-1}	+---	40.4	1.69×10^{-1}
rs1997404	<i>COL8A1</i>	g/t	1.00	0.95-1.06	9.60×10^{-1}	----	0	6.18×10^{-1}
rs34935520	<i>SIX6</i>	g/a	1.26	1.20-1.33	2.82×10^{-20}	++++	21.5	2.81×10^{-1}
rs60779155	<i>ASB7</i>	a/g	1.02	0.96-1.10	4.52×10^{-1}	+--+	0	5.02×10^{-1}

Expression of *cdkn1a* after knockdown of *six6b* in zebrafish

We used our previously characterized zebrafish model, in which knockdown of *six6b* was achieved using morpholino technology¹⁸. Knockdown embryos showed a small eye phenotype and a downregulation of the expression levels of *cdkn2b*, as observed in previous studies^{18,28}. Both *six6b* and *cdkn2b* are part of the abnormal eye morphology pathway found with DEPICT, which is in line with previous findings. In silico analyses showed that *SIX6* binds to both *CDKN2B* (core score = 1) and *CDKN1A* (core score = 0.812). In this paper, we tested the hypothesis of an in vivo interaction between *six6b* and *cdkn1a*. We evaluated the expression levels of *cdkn1a* in *six6b* deficient embryos by RT-qPCR. A 41-fold overexpression of *cdkn1a* in the eye of *six6b* knockdown embryos was found ($P=0.001$) (Figure 3), showing that in vivo downregulation of *six6b* affects expression levels not only of *cdkn2b* but also of *cdkn1a*, likely by binding to their sequence, repressing their expression.

Figure 3. *cdkn1a* mRNA expression change

Overexpression of *cdkn1a* and *cdkn2b* in response to *six6b* depletion is shown. All samples expression were normalized to the control gene *sdha*. Relative expression was calculated by setting the wild-type expression level at 1. Values represent mean \pm standard error of the mean. * $P<0.05$; ** $P<0.005$.



DISCUSSION

This meta-analysis within the IGGC identified a novel genomic region associated with IOP, nine genomic regions associated with VCDR, five with cup area, and six with disc area. Eleven genomic regions were associated with POAG. Of these regions, the association between *CDKN1A* and POAG is novel.

We identify some specific loci that underlie the genetic correlation between IOP and VCDR described earlier¹². *ADAMTS8* and *ABO* were genome-wide significant for both IOP and VCDR or cup area. Furthermore, *TRIOBP* is genome-wide significant for cup area, and reached a p-value of 3.42×10^{-6} for IOP. Interestingly, *TRIOBP* is approximately 180 kb away from *CARD10* which is associated with disc area. There is a large overlap between VCDR/cup area and disc area. Since VCDR is related to disc area, it might be that the effect found for VCDR is due to the effect of disc area. Most of these overlapping genes are still Bonferroni significant in the cup area analysis in which we corrected for disc area. Only *CDC7/TGFBR3* and *F5* are genome-wide significant for VCDR as well as for disc area, but the effect is negligible after correction for disc area, suggesting that these two genes play primarily a role in disc area.

When suggestive SNPs ($P < 1.0 \times 10^{-5}$) for VCDR and cup area are analyzed together using DEPICT, we found an enrichment of pathways involved in cell differentiation, development, regulatory DNA binding and Notch signaling. Including disc area SNPs to the VCDR and cup area analysis reveals additional joint pathways: 1) eye and blood vessel development, 2) cancer, 3) protein import into nucleus, and 4) thrombospondin 1 and SMAD3 complexes, related to the extracellular matrix. Of interest, known POAG genes also fit in these pathways identified in this paper based on endophenotypes: *GAS7* and *SIX6* play a role during development^{18,29}, *TGFBR3* has been implicated in extracellular matrix regulation^{30,31} and in cancer as well as GMDS³².

The extracellular matrix pathway has been previously implicated in optic nerve degeneration²⁵, and emerges in the DEPICT analyses. Both *ADAMTS8* and *COL8A1* have a role in this pathway. The encoded protein of the novel identified gene *VCAN* (versican) is also a major component of the extracellular matrix. Another member of the ADAMTS family (*ADAMTS5*) plays a role in the regulation of versican³³. Interestingly, mutations in *VCAN* have been implicated in several ophthalmologic disorders, including congenital glaucoma³⁴.

The gene *CDKN2B* encodes a cyclin-dependent kinase inhibitor. Its antisense (*CDKN2B-AS1*) was one of the first POAG genes identified by GWAS. The gene *CDKN1A*, also known as *p21*, *CIP-1* or *WAF-1*, is a gene from the same family as *CDKN2B* and also encodes a cyclin-dependent kinase inhibitor. Upregulation of *CDKN1A* causes G1 arrest and inhibits proliferation of the cell. Herein, for the first time, we provide genome-wide significant evidence for association of *CDKN1A* variants with cup area. Two prior small cohort studies suggested a possible role of *CDKN1A* in POAG. Tsai et al.³⁵ found an association between a codon 31 polymorphism in *CDKN1A* and POAG in 58 patients and 59 controls from China (OR = 2.39 [1.14-5.01]). Saglar et al. found no statistically significant association between the codon 31 polymorphism and POAG in 75 patients and 119 controls from Turkey (OR = 1.70, $P=0.25$)³⁶. Our study provides strong evidence for the role of *CDKN1A* in POAG risk in

a large sample consisting of 6,429 cases and 41,404 controls and shows the first convincing evidence for association of *CDKN1A* and POAG in individuals of European descent. In addition, our *in vivo* studies in zebrafish showed that knockdown of *six6b* upregulates both *cdkn2b* and *cdkn1a*.

The synthesis of *CDKN1A* is increased by the binding of p53 to p53-specific DNA consensus sequence^{37,38}. It has been suggested that p53 plays a role in POAG, especially in POAG with paracentral visual field loss³⁹. Other genes also play a role in p53. *GADD45A* is involved in growth arrest through p53 dependent and independent mechanisms^{37,40} and can interact via *CDKN1A*⁴¹. Other novel identified genes might also play a role in p53-induced apoptosis. It has been shown that the secreted pdzd2 protein activates p53 by transcriptional regulation⁴². Also *RREB1* has an effect on p53 by binding to its promotor and transactivates its expression⁴³. This gene encodes a zinc finger transcription factor. This can bind to the RAS-responsive element of the calcitonin gene promotor which subsequently increases the expression of calcitonin. Calcitonin may be involved in the Ras/Raf signaling cascade that plays a role in the morphogenesis of retinal ganglion cells, the cell type affected by glaucoma, during neurogenesis⁴⁴. Also *PSCA* is probably involved in p53-related pathways⁴⁵. Other genes play a role in apoptosis or cell growth via other pathways than p53: *VGLL4* inhibits Bax- and TNF α -induced apoptosis⁴⁶ and *DGKB* is a regulator of diacylglycerol, which is important for cell growth and differentiation. *UGT8* plays a role in the biosynthesis of the sphingolipids of myelin membranes of the central and peripheral nervous system; sphingolipids are also implicated in apoptosis⁴⁷.

Another interesting novel gene is *RPE65* (retinal pigment epithelium -specific protein 65kDa). This gene has been associated with retinitis pigmentosa (RP)⁴⁸ and Leber congenital amaurosis type 2 (LCA2)⁴⁹. As the name implies, the encoded protein is located in the retinal pigment epithelium⁵⁰. It is involved in the conversion of all-trans retinal to 11-cis retinal, which is a necessary step in the visual cycle. Both diseases (RP and LCA2) are not characterized by an excavation of the optic nerve head. Future studies are necessary to confirm our finding.

Of the genes identified by gene-based testing, *C9* (complement component 9) is an interesting one. Its protein is part of the membrane attack complex (MAC), together with the proteins C5b, C6, C7, and C8. This complex activates several steps that lead to cell death, and cells protect themselves by removing the complex through endocytosis. Caveolin is one of the proteins involved in endocytosis and the *CAV1/CAV2* genes are associated with IOP and POAG. It has been shown that inhibition of caveolin-1 inhibits the endocytosis of MAC⁵¹.

To our best knowledge, this meta-analysis is the largest study of IOP and optic nerve head parameters to date, using well-characterized datasets from populations world-wide. A limitation of our study is the lack of an available dataset for replication of the novel associations detected by combined European and Asian ancestry samples. However, the heterogeneity of these novel genomic regions is generally low in the meta-analysis. For VCDR, cup area, and disc area we have identified novel SNPs in the analysis of individuals with European ancestry. Of the nine novel associations found in these populations (*RPE65*, *PDZD2*, *RREB1*, *DGKB* for VCDR; *CDC42BPA*, *CRISPLD1* and *FAM169B* for cup area;

and *CTNNA3* and *UGT8* for disc area), only *RREB1* was nominally significant in the individuals with Asian ancestry. Five of the seven non-significant SNPs in the individuals with Asian ancestry had an effect estimate in the same direction. As the analysis in individuals with Asian ancestry contains a smaller number of individuals, this could be due to lack of power.

In conclusion, we have found novel genomic regions associated with IOP, VCDR, cup area, and disc area. The overlap between IOP and the optic disc parameters is small. Of the novel associations, *CDKN1A* is strongly associated with POAG. The synthesis of this gene is increased by a p53-dependent cascade. Also other novel genes are implicated in p53 mechanisms. The understanding of the role of this pathway in POAG and other genes may inform the development of new therapies for POAG.

References

1. Wolfs, R.C. et al. Genetic risk of primary open-angle glaucoma. Population-based familial aggregation study. *Arch Ophthalmol* 116, 1640-5 (1998).
2. Burdon, K.P. et al. Genome-wide association study identifies susceptibility loci for open angle glaucoma at TMCO1 and CDKN2B-AS1. *Nat Genet* 43, 574-8 (2011).
3. Gharahkhani, P. et al. Common variants near ABCA1, AFAP1 and GMDS confer risk of primary open-angle glaucoma. *Nat Genet* 46, 1120-5 (2014)
4. Hysi, P.G. et al. Genome-wide analysis of multi-ancestry cohorts identifies new loci influencing intraocular pressure and susceptibility to glaucoma. *Nat Genet* 46, 1126-30 (2014).
5. Thorleifsson, G. et al. Common variants near CAV1 and CAV2 are associated with primary open-angle glaucoma. *Nat Genet* 42, 906-9 (2010).
6. van Koolwijk, L.M. et al. Common genetic determinants of intraocular pressure and primary open-angle glaucoma. *PLoS Genet* 8, e1002611 (2012).
7. Ramdas, W.D. et al. Common genetic variants associated with open-angle glaucoma. *Hum Mol Genet* 20, 2464-71 (2011).
8. Springelkamp, H. et al. ARHGEF12 influences the risk of glaucoma by increasing intraocular pressure. *Hum Mol Genet* 24, 2689-99 (2015).
9. Wiggs, J.L. et al. Common variants near CAV1 and CAV2 are associated with primary open-angle glaucoma in Caucasians from the USA. *Hum Mol Genet* 20, 4707-13 (2011).
10. Wiggs, J.L. et al. Common variants at 9p21 and 8q22 are associated with increased susceptibility to optic nerve degeneration in glaucoma. *PLoS Genet* 8, e1002654 (2012).
11. Chen, Y. et al. Common variants near ABCA1 and in PMM2 are associated with primary open-angle glaucoma. *Nat Genet* 46, 1115-9 (2014).
12. Charlesworth, J. et al. The path to open-angle glaucoma gene discovery: endophenotypic status of intraocular pressure, cup-to-disc ratio, and central corneal thickness. *Invest Ophthalmol Vis Sci* 51, 3509-14 (2010).
13. van der Valk, R. et al. Intraocular pressure-lowering effects of all commonly used glaucoma drugs: a meta-analysis of randomized clinical trials. *Ophthalmology* 112, 1177-85 (2005).
14. Willer, C.J., Li, Y. & Abecasis, G.R. METAL: fast and efficient meta-analysis of genomewide association scans. *Bioinformatics* 26, 2190-1 (2010).
15. Team., R.C. R: a language and environment for statistical computing, <http://www.R-project.org>. (2014).
16. Pruim, R.J. et al. LocusZoom: regional visualization of genome-wide association scan results. *Bioinformatics* 26, 2336-7 (2010).
17. Mishra, A. & Macgregor, S. VEGAS2: Software for More Flexible Gene-Based Testing. *Twin Res Hum Genet* 18, 86-91 (2015).
18. Iglesias, A.I. et al. Exome sequencing and functional analyses suggest that SIX6 is a gene involved in an altered proliferation-differentiation balance early in life and optic nerve degeneration at old age. *Hum Mol Genet* 23, 1320-32 (2014).
19. Pfaffl, M.W., Horgan, G.W. & Dempfle, L. Relative expression software tool (REST) for group-wise comparison and statistical analysis of relative expression results in real-time PCR. *Nucleic Acids Res* 30, e36 (2002).
20. Untergasser, A. et al. Primer3Plus, an enhanced web interface to Primer3. *Nucleic Acids Res* 35, W71-4 (2007).
21. Pers, T.H. et al. Biological interpretation of genome-wide association studies using predicted gene functions. *Nat Commun* 6, 5890 (2015).
22. Bodenhofer, U., Kothmeier, A. & Hochreiter, S. APcluster: an R package for affinity propagation clustering. *Bioinformatics* 27, 2463-4 (2011).
23. Frey, B.J. & Dueck, D. Clustering by passing messages between data points. *Science* 315, 972-6 (2007).
24. Ramdas, W.D. et al. A genome-wide association study of optic disc parameters. *PLoS Genet* 6, e1000978 (2010).
25. Springelkamp, H. et al. Meta-analysis of genome-wide association studies identifies novel loci that influence cupping and the glaucomatous process. *Nat Commun* 5, 4883 (2014).
26. Springelkamp, H. et al. Meta-analysis of Genome-Wide Association Studies Identifies Novel Loci Associated With Optic Disc Morphology. *Genet Epidemiol* 39, 207-16 (2015).
27. Ramdas, W.D. et al. Heidelberg Retina Tomograph (HRT3) in population-based epidemiology: normative values and criteria for glaucomatous optic neuropathy. *Ophthalmic Epidemiol* 18, 198-210 (2011).
28. Carnes, M.U. et al. Discovery and functional annotation of SIX6 variants in primary open-angle glaucoma. *PLoS Genet* 10, e1004372 (2014).
29. Hung, F.C., Cheng, Y.C., Sun, N.K. & Chao, C.C. Identification and functional characterization of zebrafish Gas7 gene in early development. *J Neurosci Res* 91, 51-61 (2013).
30. Wiggs J.L. Glaucoma Genes and Mechanisms. *Prog Mol Biol Transl Sci* 134, 315-42 (2015)
31. Coulson-Thomas, V.J. et al. Fibroblast and prostate tumor cell cross-talk: fibroblast differentiation, TGF-beta,

- and extracellular matrix down-regulation. *Exp Cell Res* 316, 3207-26 (2010).
32. Nakayama, K. et al. Mutation of GDP-mannose-4,6-dehydratase in colorectal cancer metastasis. *PLoS One* 8, e70298 (2013).
 33. Hattori, N. et al. Pericellular versican regulates the fibroblast-myofibroblast transition: a role for ADAMTS5 protease-mediated proteolysis. *J Biol Chem* 286, 34298-310 (2011).
 34. Black, G.C. et al. A novel hereditary developmental vitreoretinopathy with multiple ocular abnormalities localizing to a 5-cM region of chromosome 5q13-q14. *Ophthalmology* 106, 2074-81 (1999).
 35. Tsai, F.J., Lin, H.J., Chen, W.C., Tsai, C.H. & Tsai, S.W. A codon 31ser-arg polymorphism of the WAF-1/CIP-1/p21/ tumour suppressor gene in Chinese primary open-angle glaucoma. *Acta Ophthalmol Scand* 82, 76-80 (2004).
 36. Saglar, E. et al. Association of polymorphisms in APOE, p53, and p21 with primary open-angle glaucoma in Turkish patients. *Mol Vis* 15, 1270-6 (2009).
 37. Smith, M.L. et al. Interaction of the p53-regulated protein Gadd45 with proliferating cell nuclear antigen. *Science* 266, 1376-80 (1994).
 38. Chen, J., Jackson, P.K., Kirschner, M.W. & Dutta, A. Separate domains of p21 involved in the inhibition of Cdk kinase and PCNA. *Nature* 374, 386-8 (1995).
 39. Wiggs, J.L. et al. The p53 codon 72 PRO/PRO genotype may be associated with initial central visual field defects in caucasians with primary open angle glaucoma. *PLoS One* 7, e45613 (2012).
 40. Kastan, M.B. et al. A mammalian cell cycle checkpoint pathway utilizing p53 and GADD45 is defective in ataxia-telangiectasia. *Cell* 71, 587-97 (1992).
 41. Kearsey, J.M., Coates, P.J., Prescott, A.R., Warbrick, E. & Hall, P.A. Gadd45 is a nuclear cell cycle regulated protein which interacts with p21Cip1. *Oncogene* 11, 1675-83 (1995).
 42. Tam, C.W., Liu, V.W., Leung, W.Y., Yao, K.M. & Shiu, S.Y. The autocrine human secreted PDZ domain-containing protein 2 (sPDZD2) induces senescence or quiescence of prostate, breast and liver cancer cells via transcriptional activation of p53. *Cancer Lett* 271, 64-80 (2008).
 43. Liu, H. et al. DNA damage signalling recruits RREB-1 to the p53 tumour suppressor promoter. *Biochem J* 422, 543-51 (2009).
 44. Pimentel, B. et al. c-Raf regulates cell survival and retinal ganglion cell morphogenesis during neurogenesis. *J Neurosci* 20, 3254-62 (2000).
 45. Feng, H.C. et al. Overexpression of prostate stem cell antigen is associated with gestational trophoblastic neoplasia. *Histopathology* 52, 167-74 (2008).
 46. Jin, H.S. et al. A novel inhibitor of apoptosis protein (IAP)-interacting protein, Vestigial-like (Vgl)-4, counteracts apoptosis-inhibitory function of IAPs by nuclear sequestration. *Biochem Biophys Res Commun* 412, 454-9 (2011).
 47. Gomez-Munoz, A., Kong, J.Y., Salh, B. & Steinbrecher, U.P. Ceramide-1-phosphate blocks apoptosis through inhibition of acid sphingomyelinase in macrophages. *J Lipid Res* 45, 99-105 (2004).
 48. Gu, S.M. et al. Mutations in RPE65 cause autosomal recessive childhood-onset severe retinal dystrophy. *Nat Genet* 17, 194-7 (1997).
 49. Marlhens, F. et al. Mutations in RPE65 cause Leber's congenital amaurosis. *Nat Genet* 17, 139-41 (1997).
 50. Hamel, C.P. et al. Molecular cloning and expression of RPE65, a novel retinal pigment epithelium-specific microsomal protein that is post-transcriptionally regulated in vitro. *J Biol Chem* 268, 15751-7 (1993).
 51. Moskovich, O., Herzog, L.O., Ehrlich, M. & Fishelson, Z. Caveolin-1 and dynamin-2 are essential for removal of the complement C5b-9 complex via endocytosis. *J Biol Chem* 287, 19904-15 (2012).

Supplementary Table 1a. Study descriptives.

ABBREVIATIONS: **CA** cup area. **DA** disc area. **IOP** intraocular pressure. **N** number of subjects. **na** not applicable. **sd** standard deviation. **VCDR** vertical cup-disc ratio.

Study	n	Mean age (sd)	Age range	% Men	Mean IOP (sd)	IOP range
BATS	1152	20.1 (4.0)	10-36	46.0%	15.8 (2.9)	6-24.5
BMES	1769	64.0 (8.3)	49-91	43.2%	16.1 (2.7)	8-29.9
EPIC	1096	69.6 (7.9)	50-91	42.9%	16.4 (4.0)	7.4-48.4
ERF	2589	49.1 (14.3)	17-87	45.0%	15.1 (3.0)	6.5-25.4
Framingham	2771	54.7 (9.2)	23-84	45.0%	13.8 (3.5)	5.0-40.0
GHS I	2720	55.5 (10.8)	35-74	51.4%	14.2 (2.8)	7.4-25.1
GHS II	1128	54.9 (10.8)	35-74	49.7%	13.9 (2.7)	5.9-25.6
ORCADES	1073	55.2 (14.2)	18-87	38.0%	15.0 (2.7)	7.5-29.0
RAINE	1009	20.0 (0.43)	18-22	48.1%	15.4 (3.3)	8.0-32.0
RS-I	6010	69.2 (9.0)	55-101	40.3%	14.7 (3.2)	5.0-28.6
RS-II	2095	64.8 (7.9)	55-95	45.9%	14.2 (3.1)	7.0-31.5
RS-III	2992	57.2 (6.8)	46-97	43.7%	13.6 (2.9)	4.5-30.0
TEST	663	25.6 (18.8)	5-81	39.5%	15.8 (3.1)	8.0-30.0
TwinsUK	2511	57.0 (11.6)	16-85	2.2%	15.6 (3.3)	5.4-37.0
BES	817	58.3 (9.2)	45-86	35.7%	15.7 (3.0)	7.0-29.0
SCES (610)	1867	58.4 (9.5)	44-85	51.0%	14.6 (3.0)	4.0-32.5
SCES (Omniexpress)	613	60.3 (9.6)	46-86	51.4%	13.6 (2.9)	5.0-27.0
SIMES	2531	59.1 (11.0)	40-80	49.5%	15.5 (3.5)	5.0-48.5
SINDI	2524	58.0 (10.0)	43-84	51.2%	15.8 (2.8)	7.5-34.0

Study	n	Mean age (sd)	Age range	% Men	Mean VCDR (sd)	VCDR range
BATS	966	20.8 (3.8)	13-34	45.9%	0.46 (0.13)	0.09-0.75
BMES	1784	64.1 (8.3)	49-91	43.2%	0.43 (0.13)	0.09-0.94
EPIC	954	68.6 (7.5)	49-88	41.8%	0.34 (0.23)	0.00-0.94
ERF	2131	47.3 (14.0)	18-85	44.4%	0.31 (0.20)	0.00-0.87
Framingham	834	60.9 (6.0)	53-84	39.0%	0.26 (0.15)	0.00-1.00
GHS I	2678	55.4 (10.8)	35-74	51.3%	0.44 (0.11)	0.19-0.81
GHS II	1024	54.5 (10.8)	35-74	50.2%	0.43 (0.11)	0.19-0.75
ORCADES	na	na	na	na	na	na
RAINE	1003	20.1 (0.4)	18-22	48.3%	0.28 (0.20)	0.00-0.78
RS-I	5573	68.0 (8.4)	55-99	40.9%	0.50 (0.13)	0.05-0.87
RS-II	1987	64.7 (7.7)	55-96	46.1%	0.50 (0.13)	0.10-0.86
RS-III	2873	57.2 (6.6)	46-90	43.9%	0.29 (0.21)	0.00-1.00
TEST	376	20.9 (17.4)	5-79	41.4%	0.44 (0.12)	0.09-0.88
TwinsUK	1716	57.0 (11.2)	16-83	1.5%	0.34 (0.11)	0.04-0.7
BES	624	62.7 (8.9)	50-90	34.0%	0.48 (0.49)	0.12-0.77
SCES (610)	1885	58.5 (9.5)	44-85	51.2%	0.40 (0.13)	0.10-0.94
SCES II (Omniexpress)	614	60.3 (9.5)	46-85	51.3%	0.40 (0.13)	0.13-0.86
SIMES	2531	59.5 (11.0)	40-81	49.5%	0.40 (0.14)	0.08-1.00
SINDI	2514	58.0 (10.0)	43-83	51.2%	0.43 (0.11)	0.16-0.97

Supplementary Table 1a. (continued)

Study	n	Mean age (sd)	Age range	% Men	Mean CA (sd)	CA range
BATS	985	20.1 (3.8)	13-34	45.8%	0.46 (0.30)	0.01-1.64
BMES	1765	64.0 (8.3)	49-91	43.3%	0.39 (0.27)	0.01-1.82
EPIC	954	68.6 (7.5)	49-88	41.8%	0.47 (0.35)	0.00-1.96
ERF	2131	47.3 (14.0)	18-85	44.4%	0.43 (0.31)	0.00-2.06
Framingham	na	na	na	na	na	na
GHS I	2350	55.9 (10.9)	35-74	51.5%	0.54 (0.33)	0.07-1.89
GHS II	791	55.1 (10.9)	35-74	50.0%	0.53 (0.32)	0.07-1.63
ORCADES	na	na	na	na	na	na
RAINE	1003	20.1 (0.4)	18-22	48.3%	0.40 (0.31)	0.00-1.73
RS-I	5555	68.0 (8.4)	55-99	40.9%	0.61 (0.34)	0.01-1.98
RS-II	1979	64.7 (7.7)	55-96	46.0%	0.57 (0.32)	0.03-1.94
RS-III	2870	57.2 (6.6)	46-90	43.8%	0.40 (0.30)	0.00-1.90
TEST	385	21.3 (17.4)	5-79	41.2%	0.41 (0.27)	0.01-1.91
TwinsUK	1716	57.0 (11.2)	16-83	1.5%	0.31 (0.24)	0.01-2.43
BES	822	58.3 (9.17)	45-86	35.4%	0.60 (0.37)	0.00-2.84
SCES (610)	1703	58.2 (9.4)	44-85	51.3%	0.55 (0.37)	0.00-2.63
SCES II (Omniexpress)	na	na	na	na	na	na
SIMES	2384	59.1 (10.9)	40-81	50.2%	0.59 (0.39)	0.00-2.80
SINDI	2424	57.8 (9.9)	43-84	51.4%	0.64 (0.39)	0.00-3.35

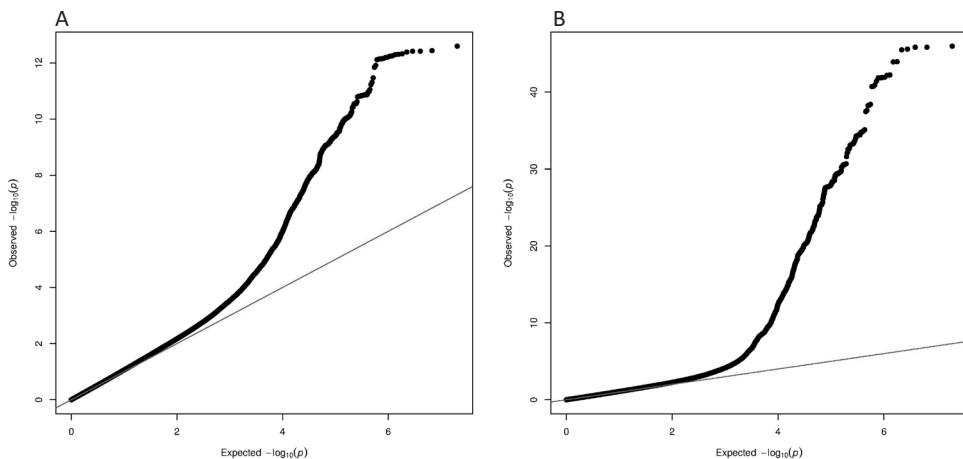
Study	n	Mean age (sd)	Age range	% Men	Mean DA (sd)	DA range
BATS	985	20.1 (3.8)	13-34	45.8%	2.07 (0.39)	1.15–3.56
BMES	1766	64.0 (8.3)	49-91	43.2%	2.07 (0.43)	0.38-4.14
EPIC	954	68.6 (7.5)	49-88	41.8%	1.91 (0.42)	0.54-3.72
ERF	2131	47.3 (14.0)	18-85	44.4%	1.91 (0.35)	1.07-3.95
Framingham	na	na	na	na	na	na
GHS I	2354	55.4 (10.6)	35-74	52.2%	2.32 (0.44)	1.26-4.14
GHS II	792	54.9 (10.8)	35-74	50.0%	2.35 (0.46)	1.07-4.20
ORCADES	na	na	na	na	na	na
RAINE	1003	20.1 (0.4)	18-22	48.3%	1.91 (0.50)	0.86-4.17
RS-I	5563	68.0 (8.4)	55-99	41.0%	2.42 (0.47)	0.58-5.13
RS-II	1983	64.7 (7.7)	55-96	46.1%	2.33 (0.46)	1.13-5.19
RS-III	2872	57.2 (6.6)	46-90	43.8%	1.92 (0.40)	0.75-4.22
TEST	385	21.3 (17.4)	5-79	41.2%	2.06 (0.37)	1.33-3.43
TwinsUK	1716	57.0 (11.2)	16-83	1.5%	2.58 (0.64)	0.59-5.31
BES	791	58.0 (8.9)	45-86	35.5%	2.52 (0.49)	1.05-5.78
SCES (610)	1703	58.2 (9.4)	44-85	51.3%	1.99 (0.42)	0.74-5.48
SCES (Omniexpress)	na	na	na	na	na	na
SIMES	2384	59.1 (10.9)	40-81	50.2%	2.07 (0.45)	0.86-4.39
SINDI	2424	57.8 (9.9)	43-84	51.4%	1.97 (0.41)	0.91-4.71

Supplementary Table 1b. Phenotyping and genotyping methods, and study specific genetic inflation factors (λ).

ABBREVIATIONS: **CA** cup area. **DA** disc area. **GAT** Goldmann applanation tonometry. **HRT** Heidelberg Retina Tomograph. **IOP** intraocular pressure. **NA** not applicable. **ONH** optic nerve head. **VCDR** vertical cup-disc ratio.

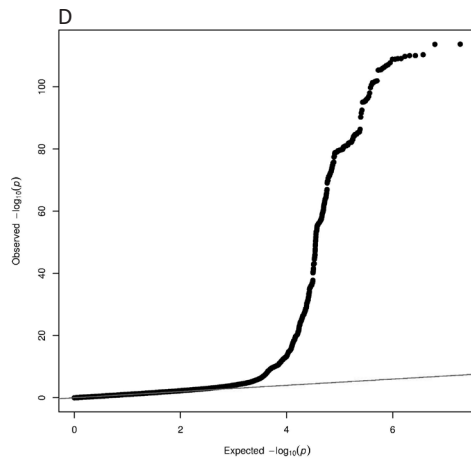
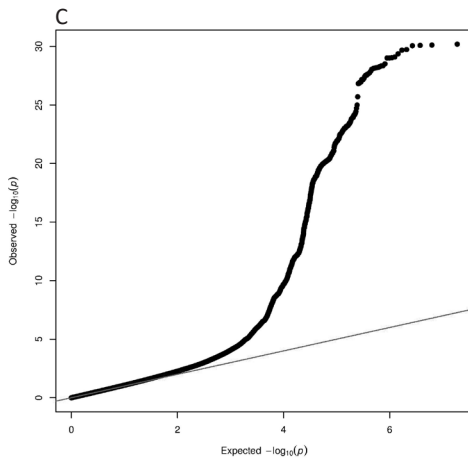
Study	IOP measurement	ONH assessment
BATS	TONO-PEN XL	Nidek 3-Dx fundus camera with custom planimetric software
BMES	GAT	30° color stereoscopic optic disc photographs taken with a 99 Zeiss FF3 fundus camera
EPIC	Ocular Response Analyzer	HRT2
ERF	GAT	HRT2
Framingham	GAT	Binocular indirect ophthalmoscope and a +14 diopter Nikon lens
GHS I	Non-contact tonometer	Visucam ProNM and Visupac
GHS II	Non-contact tonometer	Visucam ProNM and Visupac
ORCADES	Tono-pen	NA
Raine	Icare TAO1i Tonometer	HRT3
RS-I	GAT	ImageNet and stereoscopic fundus camera
RS-II	GAT	ImageNet and stereoscopic fundus camera
RS-III	GAT	HRT2
TEST	TONO-PEN XL	Nidek 3-Dx fundus camera with custom planimetric software
TwinsUK	Ocular Response Analyser	Nidek 3-Dx fundus camera with custom planimetric software
BES	GAT	Planimetry
SCES (610)	GAT	Slit-lamp biomicroscopy with 78 D lens at X16 magnification, with measuring graticule, and HRT2
SCES (Omniexpress)	GAT	Slit-lamp biomicroscopy
SIMES	GAT	HRT2
SINDI	GAT	HRT

Supplementary Figure 1. The Quantile-Quantile plot for association between the traits and all SNPs analyzed in the combined analysis (Caucasians and Asians). Each black dot represents an observed statistic ($-\log_{10}(P)$) versus the corresponding expected statistic. The black line corresponds to the null distribution. A = intraocular pressure, B = vertical cup-disc ratio, C = cup area, D = disc area.

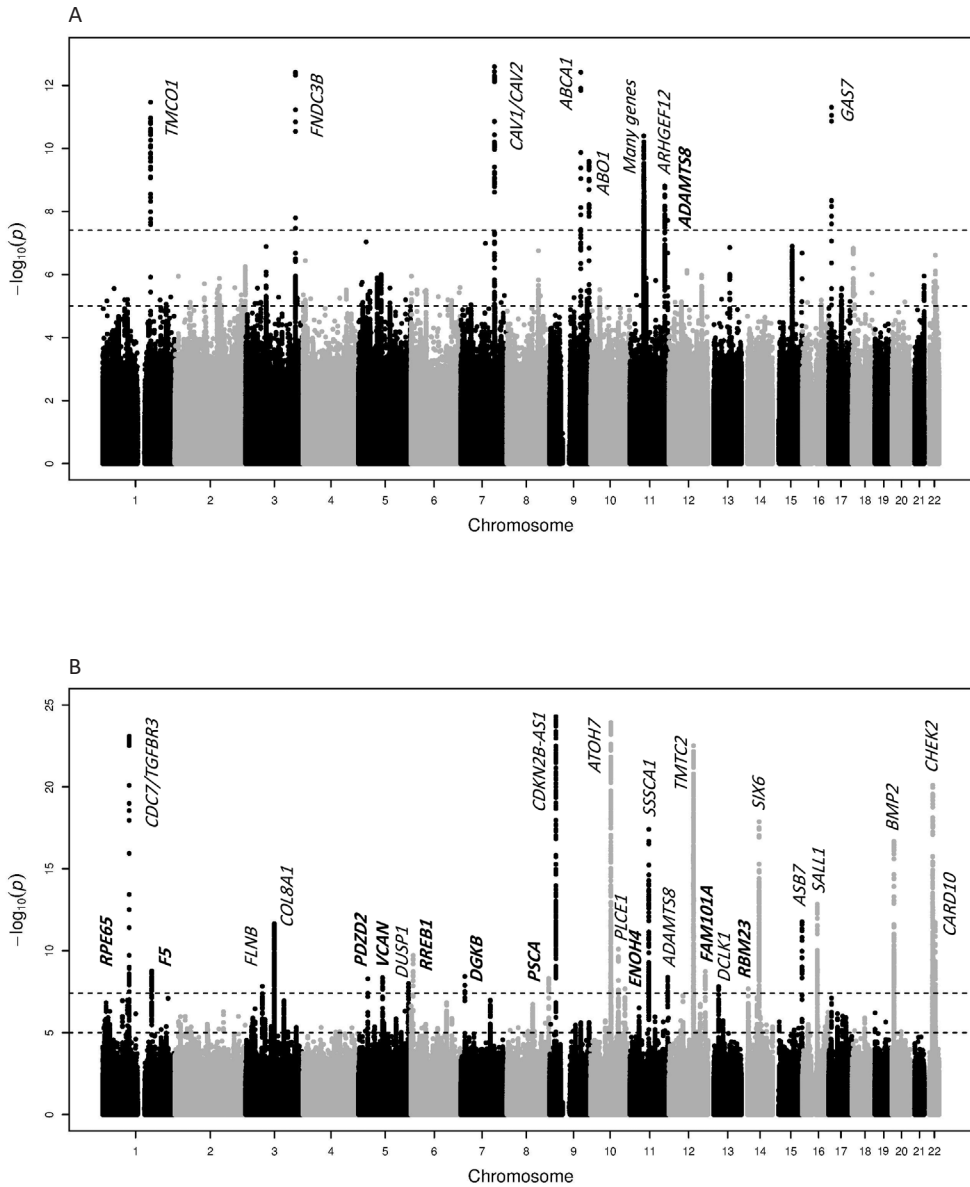


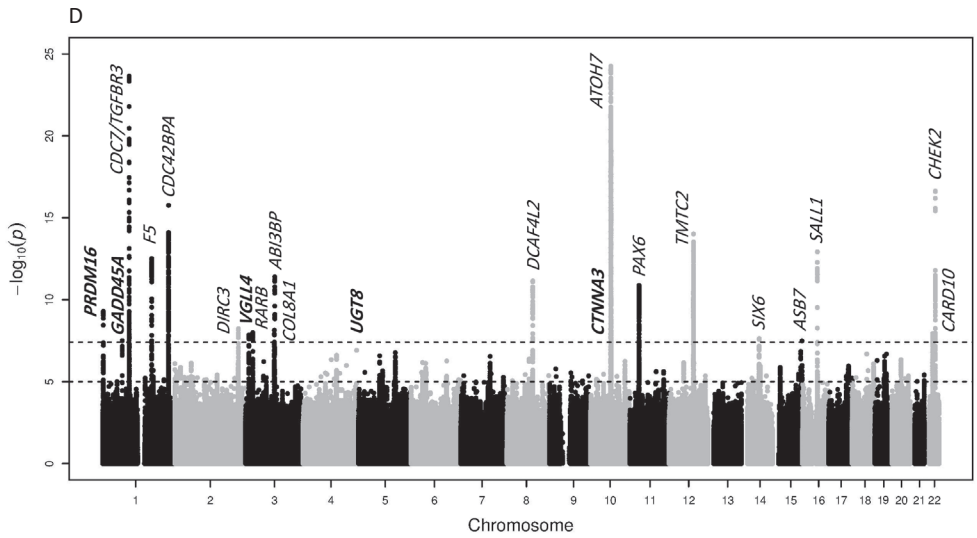
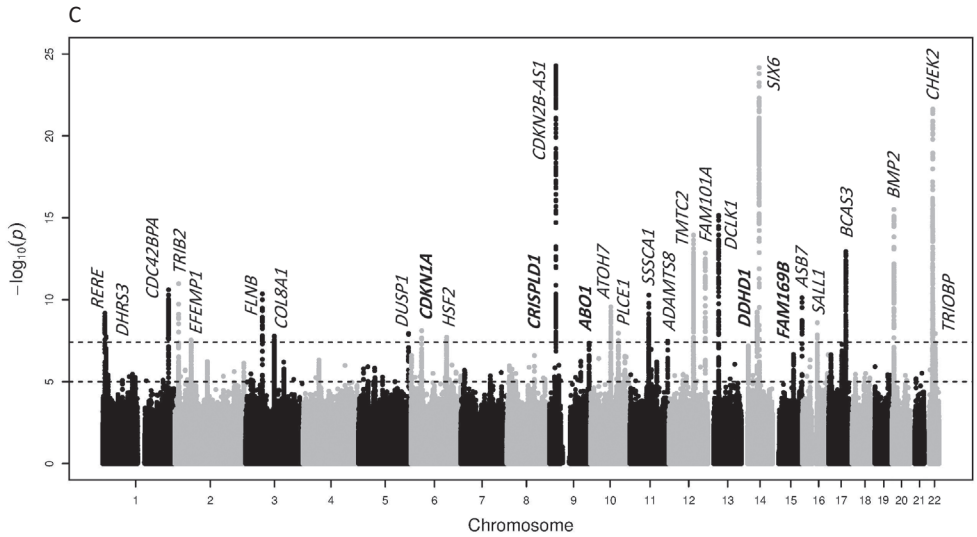
Supplementary Table 1b. (continued)

Genotyping chip	Genetic inflation factor (λ)			
	IOP	VCDR	CA	DA
Illumina HumanHap 610W Quad arrays	1.00	1.01	1.01	1.01
Illumina Human 660W Quad	1.00	1.01	1.00	1.01
Affymetrix GeneChip Human Mapping 500K	1.00	1.01	1.00	1.01
Illumina 6k, 318K and 370K; Affymetrix 250K	1.06	1.05	1.05	1.07
Affymetrix 250k_Nsp 250k_Sty HuGeneFocused50K	1.04	1.06	NA	NA
Affymetrix Genome-Wide Human SNP 6.0 Array	1.02	1.02	1.02	1.02
Affymetrix Genome-Wide Human SNP 6.0 Array	1.00	1.01	1.00	1.01
IlluminaHumanHap300v2, HumanCNV370-Quad, Omni1 and HumanOmniExpress- 12v1	1.00	NA	NA	NA
Illumina 660W Quad Array	1.00	1.01	1.00	0.99
Illumina Infinium II HumanHap550 chip v3.0 array	1.03	0.98	1.06	1.04
HumanHap550 Duo Arrays + Human610-Quad Arrays Illumina	1.01	1.08	0.98	0.99
Human 610 Quad Arrays Illumina	1.01	0.98	1.02	1.01
Illumina HumanHap 610W Quad arrays	1.01	1.00	1.00	1.02
Illumina 300K Duo and HumanHap610-Quad arrays	1.00	1.01	1.00	1.00
Illumina HumanHap 610 Quad	1.00	0.94	1.03	1.03
Illumina HumanHap 610 Quad	1.00	1.02	1.02	1.01
Illumina OmniExpress	1.00	1.02	NA	NA
Illumina HumanHap 610 Quad	1.01	1.01	1.01	0.98
Illumina HumanHap 610 Quad	1.00	1.01	1.01	1.01



Supplementary Figure 2. Manhattan plot of the GWAS meta-analysis for all traits in the combined analysis (Caucasians and Asians). The plot shows $-\log_{10}$ -transformed p-values for all SNPs. The upper dotted horizontal line represents the genome-wide significance threshold of $P < 5.0 \times 10^{-8}$; the lower dotted line indicates p-value of 1×10^{-5} . Only SNPs with a p-value $> 5.0 \times 10^{-25}$ are shown. A = intraocular pressure, B = vertical cup-disc ratio, C = cup area, D = disc area.





Supplementary Table 2. Results of the GWAS meta-analysis for all traits. SNPs that showed genome-wide significant ($P < 5 \times 10^{-8}$) association with any trait in subjects of European ancestry or in the combined analysis (European and Asian ancestry) are shown.

SNP	Chr/pos	Nearest gene	Annotation	A1/A2	Caucasians			P-value
					MAF	β	SE	
Intraocular pressure								
rs10918274	1/165714416	<i>TMCO1</i>	intronic	t/c	0.13	0.27	0.04	9.77×10^{-13}
rs7635832	3/171989276	<i>FNDC3B</i>	intronic	g/t	0.19	-0.25	0.04	1.47×10^{-12}
rs10281637	7/116151338	<i>CAV1/CAV2</i>	intergenic	c/t	0.27	0.20	0.03	9.58×10^{-12}
rs2487048	9/107691823	<i>ABCA1</i>		a/g	0.42	0.16	0.03	3.60×10^{-9}
rs8176741	9/136131461	<i>ABO</i>	synonymous	a/g	0.07	0.26	0.05	1.97×10^{-7}
rs7944735	11/47955608	<i>Many genes</i>	intergenic	c/g	0.20	0.21	0.03	9.23×10^{-10}
11:120357425	11/120357425	<i>ARHGEF12</i>	3'-UTR	d/r	0.18	0.23	0.04	2.68×10^{-10}
rs55796939	11/130284041	<i>ADAMTS8</i>	intronic	t/c	0.04	0.38	0.08	3.16×10^{-6}
rs9913911	17/10031183	<i>GAS7</i>	intronic	g/a	0.36	-0.20	0.03	7.65×10^{-13}
Vertical cup-disc ratio								
rs1925953	1/68848681	<i>RPE65</i>	intergenic	t/a	0.40	0.01	0.001	2.00×10^{-8}
rs1192414	1/92075134	<i>CDC7/TGFBFR3</i>	intergenic	a/g	0.18	0.02	0.002	1.00×10^{-20}
rs10753787	1/169549775	<i>F5</i>	intronic	t/c	0.43	-0.01	0.001	2.00×10^{-9}
rs6804624	3/99159147	<i>COL8A1</i>	intergenic	c/t	0.31	0.01	0.001	8.00×10^{-10}
rs72759609	5/31952051	<i>PDZD2</i>	intronic	c/t	0.09	-0.01	0.002	3.00×10^{-9}
rs114503346	5/172192350	<i>DUSP1</i>	intergenic	t/c	0.04	-0.02	0.004	4.00×10^{-9}
rs4960295	6/7205796	<i>RREB1</i>	intronic	a/g	0.44	0.01	0.001	1.00×10^{-8}
rs10274998	7/14245377	<i>DGKB</i>	intronic	t/c	0.15	0.01	0.002	2.00×10^{-8}
rs2157719	9/22033366	<i>CDKN2B-AS1</i>	intronic	c/t	0.44	-0.01	0.001	2.00×10^{-33}
rs1900005	10/69998055	<i>ATOH7</i>		a/c	0.24	-0.02	0.002	4.00×10^{-43}
10:96008348	10/96008348	<i>PLCE1</i>	intronic	d/r	0.32	0.01	0.002	3.00×10^{-10}
rs1346	11/65337251	<i>SSSCA1</i>	intergenic	t/a	0.19	-0.01	0.002	1.00×10^{-17}
rs4936099	11/130280725	<i>ADAMTS8</i>	intronic	c/a	0.40	-0.01	0.001	2.00×10^{-9}
rs324780	12/84003866	<i>TMTC2</i>	intergenic	g/a	0.46	-0.01	0.001	2.00×10^{-21}
13:36629905	13/36629905	<i>DCLK1</i>	intronic	d/r	0.23	0.01	0.002	5.00×10^{-10}
rs8015152	14/60811999	<i>SIX6</i>	intergenic	t/c	0.32	0.01	0.001	2.00×10^{-13}
rs4299136	15/101201604	<i>ASB7</i>	intergenic	c/g	0.14	0.01	0.002	1.00×10^{-9}
16:51461915	16/51461915	<i>SALL1</i>	intergenic	r/i	0.29	0.01	0.002	1.00×10^{-16}
rs6107845	20/6578741	<i>BMP2</i>	intergenic	a/g	0.41	-0.01	0.001	3.00×10^{-17}
rs5752773	22/29105415	<i>CHEK2</i>	intronic	g/c	0.30	-0.01	0.001	3.00×10^{-21}
rs2092172	22/37907069	<i>CARD10</i>	intronic	a/g	0.20	0.01	0.002	2.00×10^{-8}
rs6764184	3/58006266	<i>FLNB</i>	intronic	t/g	0.24	0.01	0.002	4.00×10^{-6}
rs7717697	5/82744604	<i>VCAN</i>	intergenic	c/t	0.40	-0.01	0.001	2.00×10^{-7}
rs2920293	8/143765414	<i>PSCA</i>	intergenic	g/c	0.45	-0.01	0.001	3.00×10^{-6}
rs1681739	10/118563329	<i>ENO4</i>	intergenic	t/c	0.41	0.01	0.001	1.00×10^{-6}
rs7311936	12/124631597	<i>FAM101A</i>	intronic	c/g	0.43	-0.01	0.001	6.00×10^{-8}
14:23388793	14/23388793	<i>RBM23</i>	intergenic	r/d	0.44	0.01	0.002	4.00×10^{-5}
Cup area								
rs2252865	1/8422676	<i>RERE</i>	intronic	t/c	0.34	0.013	0.002	3.34×10^{-8}
rs4846112	1/12619173	<i>DHRS3</i>	intergenic	a/g	0.28	-0.015	0.003	3.83×10^{-8}
1:227562773	1/227562773	<i>CDC42BPA</i>	intergenic	d/r	0.08	0.029	0.005	3.09×10^{-10}
rs13016883	2/12877307	<i>TRIB2</i>	intronic	c/g	0.46	0.014	0.003	2.09×10^{-8}
rs35084382	5/172197039	<i>DUSP1</i>	intronic	c/t	0.05	-0.034	0.006	1.21×10^{-8}
rs117598310	8/75999096	<i>CRISPLD1</i>	intergenic	t/g	0.06	0.030	0.005	1.07×10^{-8}
rs1360589	9/22045317	<i>CDKN2B-AS1</i>	intronic	c/t	0.44	-0.025	0.002	4.97×10^{-28}
rs10998036	10/70016678	<i>ATOH7</i>	intergenic	c/g	0.22	-0.020	0.003	3.03×10^{-12}

Supplementary Table 2. (continued)

SNP	Asians				Caucasians+Asians			I ²	P _{het} -value
	MAF	β	SE	P-value	β	SE	P-value		
Intraocular pressure									
rs10918274	0.05	0.04	0.14	7.61x10 ⁻¹	0.26	0.04	3.40x10 ⁻¹²	6.2	3.81x10 ⁻¹
rs7635832	0.29	-0.13	0.05	1.36x10 ⁻²	0.22	0.03	3.84x10 ⁻¹³	20.1	2.25x10 ⁻¹
rs10281637	0.15	0.26	0.09	6.14x10 ⁻³	-0.20	0.03	2.53x10 ⁻¹³	2.1	4.31x10 ⁻¹
rs2487048	0.47	0.22	0.05	1.18x10 ⁻⁵	0.17	0.02	3.83x10 ⁻¹³	48.1	1.04x10 ⁻²
rs8176741	0.21	0.21	0.06	2.70x10 ⁻⁴	0.24	0.04	2.55x10 ⁻¹⁰	0	8.38x10 ⁻¹
rs7944735	0.22	0.16	0.06	1.05x10 ⁻²	0.20	0.03	3.97x10 ⁻¹¹	4.8	3.98x10 ⁻¹
11:120357425	0.26	0.08	0.06	1.74x10 ⁻¹	0.18	0.03	1.54x10 ⁻⁹	23.4	1.88x10 ⁻¹
rs55796939	0.11	0.32	0.10	1.55x10 ⁻³	0.36	0.06	1.92x10 ⁻⁸	30.4	1.08x10 ⁻¹
rs9913911	0.39	-0.06	0.05	2.08x10 ⁻¹	0.17	0.02	4.95x10 ⁻¹²	41.2	3.53x10 ⁻²
Vertical cup-disc ratio									
rs1925953	0.65	0.00	0.002	4.53x10 ⁻¹	0.01	0.001	1.00x10 ⁻⁷	14	2.90x10 ⁻¹
rs1192414	0.22	0.01	0.003	3.94x10 ⁻⁵	0.01	0.001	8.00x10 ⁻²⁴	46.2	1.70x10 ⁻²
rs10753787	0.32	0.00	0.003	1.94x10 ⁻¹	-0.01	0.001	2.00x10 ⁻⁹	0	9.89x10 ⁻¹
rs6804624	0.34	0.01	0.002	1.20x10 ⁻³	0.01	0.001	5.00x10 ⁻¹²	0	5.68x10 ⁻¹
rs72759609	0.06	-0.01	0.005	2.33x10 ⁻¹	-0.01	0.002	5.00x10 ⁻⁹	0	7.73x10 ⁻¹
rs114503346	0.01	0.00	0.017	9.65x10 ⁻¹	-0.02	0.004	1.00x10 ⁻⁸	35.2	1.26x10 ⁻¹
rs4960295	0.74	0.01	0.002	4.00x10 ⁻³	0.01	0.001	2.00x10 ⁻¹⁰	7.9	3.61x10 ⁻¹
rs10274998	0.36	0.00	0.002	8.51x10 ⁻²	0.01	0.001	4.00x10 ⁻⁸	2.0	2.20x10 ⁻¹
rs2157719	0.18	-0.01	0.003	3.24x10 ⁻⁴	-0.01	0.001	1.00x10 ⁻³⁵	0	8.51x10 ⁻¹
rs1900005	0.27	-0.01	0.002	3.61x10 ⁻⁷	-0.02	0.001	1.00x10 ⁻⁴⁶	58.2	1.05x10 ⁻³
10:96008348	0.36	0.00	0.002	5.16x10 ⁻¹	0.01	0.001	4.00x10 ⁻⁸	50.2	1.38x10 ⁻²
rs1346	0.15	-0.01	0.003	1.38x10 ⁻²	-0.01	0.001	4.00x10 ⁻¹⁸	0	4.84x10 ⁻¹
rs4936099	0.21	0.00	0.003	4.00x10 ⁻¹	-0.01	0.001	5.00x10 ⁻⁹	0	9.56x10 ⁻¹
rs324780	0.24	-0.01	0.003	1.35x10 ⁻³	-0.01	0.001	3.00x10 ⁻²³	38.4	5.95x10 ⁻²
13:36629905	0.42	0.00	0.002	3.67x10 ⁻¹	0.01	0.001	2.00x10 ⁻⁸	47.9	2.00x10 ⁻²
rs8015152	0.51	0.01	0.002	1.60x10 ⁻⁶	0.01	0.001	1.00x10 ⁻¹⁸	0	5.30x10 ⁻¹
rs4299136	0.54	0.01	0.002	1.20x10 ⁻⁴	0.01	0.002	2.00x10 ⁻¹²	0	4.67x10 ⁻¹
16:51461915	0.16	0.00	0.003	9.77x10 ⁻¹	0.01	0.001	1.00x10 ⁻¹³	44.9	3.08x10 ⁻²
rs6107845	0.56	0.00	0.002	2.14x10 ⁻²	-0.01	0.001	2.00x10 ⁻¹⁷	9.6	3.42x10 ⁻¹
rs5752773	0.15	-0.01	0.003	4.05x10 ⁻²	-0.01	0.001	8.00x10 ⁻²¹	0	5.58x10 ⁻¹
rs2092172	0.23	0.01	0.002	1.49x10 ⁻⁵	0.01	0.001	2.00x10 ⁻¹²	35.1	7.12x10 ⁻²
rs6764184	0.46	0.01	0.002	1.00x10 ⁻³	0.01	0.001	1.00x10 ⁻⁸	4.1	4.07x10 ⁻¹
rs7717697	0.20	-0.01	0.003	6.65x10 ⁻³	-0.01	0.001	4.00x10 ⁻⁹	23.6	1.75x10 ⁻¹
rs2920293	0.34	-0.01	0.002	2.81x10 ⁻⁴	-0.01	0.001	5.00x10 ⁻⁹	0	5.19x10 ⁻¹
rs1681739	0.26	0.01	0.002	5.38x10 ⁻³	0.01	0.001	2.00x10 ⁻⁸	36.4	6.25x10 ⁻²
rs7311936	0.27	-0.01	0.002	9.71x10 ⁻³	-0.01	0.001	2.00x10 ⁻⁹	8.1	3.59x10 ⁻¹
14:23388793	0.26	0.01	0.003	4.26x10 ⁻⁵	0.01	0.001	2.00x10 ⁻⁸	18.2	2.55x10 ⁻¹
Cup area									
rs2252865	0.17	0.017	0.006	4.81x10 ⁻³	0.014	0.002	6.69x10 ⁻¹⁰	51.5	9.04x10 ⁻³
rs4846112	0.25	-0.004	0.005	3.94x10 ⁻¹	-0.012	0.002	1.67x10 ⁻⁷	46.9	2.00x10 ⁻²
1:227562773	0.07	0.005	0.009	5.69x10 ⁻¹	0.024	0.004	4.60x10 ⁻⁹	9.2	3.54x10 ⁻¹
rs13016883	0.29	0.021	0.005	6.18x10 ⁻⁵	0.016	0.002	1.05x10 ⁻¹¹	0	8.38x10 ⁻¹
rs35084382	0.02	-0.019	0.039	6.27x10 ⁻¹	-0.034	0.006	1.16x10 ⁻⁸	12.3	3.21x10 ⁻¹
rs117598310	0.11	0.002	0.008	8.12x10 ⁻¹	0.021	0.004	1.32x10 ⁻⁶	38.4	8.50x10 ⁻²
rs1360589	0.17	-0.015	0.006	7.50x10 ⁻³	-0.024	0.002	4.51x10 ⁻²⁹	29	1.33x10 ⁻¹
rs10998036	0.19	0.002	0.006	7.34x10 ⁻¹	-0.016	0.003	1.10x10 ⁻⁹	54.6	4.59x10 ⁻³

Supplementary Table 2. Results of the GWAS meta-analysis for all traits. SNPs that showed genome-wide significant ($P < 5 \times 10^{-8}$) association with any trait in subjects of European ancestry or in the combined analysis (European and Asian ancestry) are shown.

SNP	Chr/pos	Nearest gene	Annotation	A1/A2	Caucasians			P-value
					MAF	β	SE	
10:96008348	10/96008348	<i>PLCE1</i>	intronic	d/r	0.32	0.015	0.003	7.90×10^{-9}
rs1346	11/65337251	<i>SSSCA1</i>	intergenic	t/a	0.19	-0.023	0.003	9.32×10^{-13}
rs482507	12/83979286	<i>TMTC2</i>	intergenic	c/t	0.47	-0.019	0.002	2.67×10^{-15}
rs11613189	12/124642803	<i>FAM101A</i>	intronic	t/c	0.37	-0.016	0.002	1.76×10^{-10}
rs7323428	13/36643601	<i>DCLK1</i>	intronic	t/g	0.24	0.021	0.003	1.82×10^{-14}
rs2251069	14/53988050	<i>DDHD1</i>	intergenic	c/t	0.44	-0.013	0.002	2.91×10^{-8}
rs4436712	14/60808002	<i>SIX6</i>	intergenic	t/g	0.38	0.023	0.002	1.61×10^{-20}
rs6598351	15/98808111	<i>FAM169B</i>	intergenic	t/c	0.16	0.019	0.003	9.83×10^{-9}
rs11646917	16/51428908	<i>SALL1</i>	intergenic	t/g	0.28	-0.016	0.003	4.81×10^{-9}
rs11867840	17/59273265	<i>BCAS3</i>	intronic	g/a	0.23	-0.021	0.003	6.46×10^{-14}
rs6054375	20/6578629	<i>BMP2</i>	intergenic	t/g	0.40	-0.021	0.003	1.26×10^{-16}
rs738722	22/29130012	<i>CHEK2</i>	intronic	t/c	0.28	-0.025	0.003	3.86×10^{-19}
rs3791679	2/56096892	<i>EFEMP1/PNPT1</i>	intronic	g/a	0.23	-0.014	0.003	4.75×10^{-7}
rs12494328	3/58035497	<i>FLNB</i>	intronic	a/g	0.22	0.014	0.003	3.59×10^{-6}
rs6804624	3/99159147	<i>COL8A1</i>	intergenic	c/t	0.31	0.012	0.003	4.91×10^{-6}
6:36592986	6/36592986	<i>CDKN1A</i>	intergenic	d/r	0.21	0.015	0.003	6.36×10^{-7}
rs2684249	6/122392511	<i>HSF2</i>	intergenic	c/t	0.41	-0.012	0.002	1.32×10^{-6}
rs8176672	9/136142185	<i>ABO</i>	intronic	t/c	0.07	0.018	0.005	7.84×10^{-5}
rs4936099	11/130280725	<i>ADAMTS8</i>	intronic	c/a	0.40	-0.013	0.003	7.02×10^{-8}
rs34222435	15/101200873	<i>ASB7</i>	intergenic	t/c	0.14	0.019	0.004	6.42×10^{-7}
rs1074407	22/38156183	<i>TRIOBP</i>	intronic	t/a	0.38	0.011	0.002	6.99×10^{-6}
Disc area								
rs4658101	1/92077409	<i>CDC7/TGFB3</i>	intergenic	a/g	0.18	0.089	0.005	1.05×10^{-61}
1:169530520	1/169530520	<i>F5/SELP</i>	intronic	i/r	0.28	0.033	0.005	1.73×10^{-10}
rs11811982	1/227581520	<i>CDC42BPA</i>	intergenic	a/c	0.08	-0.063	0.008	3.96×10^{-15}
rs9843102	3/100650929	<i>ABI3BP</i>	intronic	a/g	0.19	-0.034	0.006	1.19×10^{-9}
rs10021731	4/115481915	<i>UGT8</i>	intergenic	c/t	0.41	-0.025	0.004	1.00×10^{-8}
8:88744441	8/88744441	<i>DCAF4L2</i>	intergenic	d/r	0.47	0.027	0.004	7.78×10^{-10}
rs12220165	10/69339164	<i>CTNNA3</i>	intronic	g/c	0.16	-0.037	0.007	3.94×10^{-8}
rs7916410	10/69995667	<i>ATOX7</i>	intergenic	t/c	0.23	-0.101	0.005	3.73×10^{-92}
rs61101201	11/31480349	<i>IMMP1L</i> , near to <i>PAX6</i>	intronic	g/t	0.24	0.033	0.005	1.33×10^{-10}
rs442376	12/83978117	<i>TMTC2</i>	intergenic	c/t	0.49	0.034	0.005	1.99×10^{-13}
rs1345467	16/51482321	<i>SALL1</i>	intergenic	g/a	0.26	0.035	0.005	2.13×10^{-13}
rs5762752	22/29100977	<i>CHEK2</i>	intronic	c/g	0.34	-0.028	0.005	1.30×10^{-9}
rs56385951	22/37909539	<i>CARD10</i>	intronic	a/g	0.10	0.046	0.007	1.60×10^{-10}
1:3046430	1/3046430	<i>PRDM16</i>	intronic	i/r	0.08	0.041	0.011	8.41×10^{-5}
rs787541	1/68051230	<i>U6, GADD45A</i>	intergenic	c/g	0.32	0.022	0.005	1.95×10^{-6}
rs1367187	2/218466221	<i>DIRC3</i>	intronic	c/t	0.22	0.027	0.005	2.25×10^{-7}
rs2443724	3/11655351	<i>VGLL4</i>	intronic	c/g	0.27	-0.021	0.005	8.78×10^{-6}
rs11129176	3/25049310	<i>RARB</i>	intergenic	a/g	0.29	0.024	0.005	1.14×10^{-7}
rs1997404	3/99161022	<i>COL8A1</i>	intergenic	g/t	0.30	0.024	0.005	3.21×10^{-7}
rs34935520	14/61091401	<i>SIX6</i>	intergenic	g/a	0.40	-0.020	0.005	1.12×10^{-5}
rs60779155	15/101199737	<i>ASB7</i>	intergenic	a/g	0.14	0.023	0.007	1.25×10^{-3}

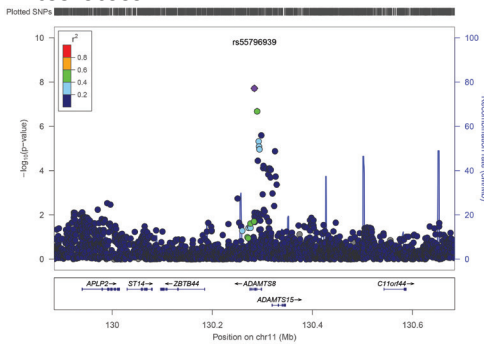
ABBREVIATIONS: **A1** reference allele; **A2** other allele; β effect size based on allele A1; **Chr.** chromosome; **DA** disc area; **MAF** minor allele frequency; **P** p-value; **P_{het}**-value p-value for heterogeneity; **Pos** position; **SE** standard error; **SNP** single nucleotide polymorphism.

Supplementary Table 2. (continued)

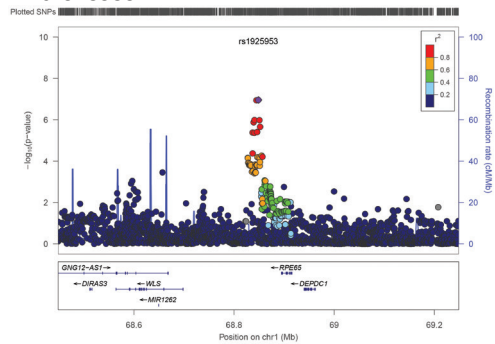
SNP	Asians				Caucasians+Asians			I ²	P _{het} -value
	MAF	β	SE	P-value	β	SE	P-value		
10:96008348	0.36	0.007	0.004	1.38x10 ⁻¹	0.013	0.002	1.11x10 ⁻⁸	43.3	4.28x10 ⁻²
rs1346	0.15	-0.002	0.006	7.01x10 ⁻¹	-0.019	0.003	5.20x10 ⁻¹¹	25.8	1.70x10 ⁻¹
rs482507	0.25	-0.007	0.006	2.42x10 ⁻¹	-0.017	0.002	1.15x10 ⁻¹⁴	33.8	1.05x10 ⁻¹
rs11613189	0.26	-0.015	0.005	1.26x10 ⁻³	-0.016	0.002	8.66x10 ⁻¹³	1.8	4.31x10 ⁻¹
rs7323428	0.46	0.013	0.005	4.21x10 ⁻³	0.019	0.002	8.63x10 ⁻¹⁶	27.7	1.45x10 ⁻¹
rs2251069	0.46	-0.012	0.004	5.50x10 ⁻³	-0.013	0.002	5.69x10 ⁻¹⁰	0.2	4.49x10 ⁻¹
rs4436712	0.67	0.033	0.005	2.20x10 ⁻¹²	0.025	0.002	1.88x10 ⁻³⁰	41.4	4.74x10 ⁻²
rs6598351	0.32	-0.003	0.005	6.02x10 ⁻¹	0.012	0.003	1.19x10 ⁻⁵	46	2.63x10 ⁻²
rs11646917	0.14	-0.010	0.007	1.73x10 ⁻¹	-0.015	0.003	2.54x10 ⁻⁹	0	6.57x10 ⁻¹
rs11867840	0.24	-0.009	0.005	8.41x10 ⁻²	-0.018	0.002	1.15x10 ⁻¹³	25.7	1.65x10 ⁻¹
rs6054375	0.60	-0.008	0.005	1.13x10 ⁻¹	-0.018	0.002	8.77x10 ⁻¹⁶	56.5	6.39x10 ⁻³
rs738722	0.19	-0.021	0.006	1.11x10 ⁻⁴	-0.024	0.003	2.35x10 ⁻²²	0	9.31x10 ⁻¹
rs3791679	0.57	-0.011	0.005	1.77x10 ⁻²	-0.013	0.002	2.94x10 ⁻⁸	0	6.55x10 ⁻¹
rs12494328	0.42	0.021	0.004	1.03x10 ⁻⁶	0.016	0.002	4.39x10 ⁻¹¹	0	6.07x10 ⁻¹
rs6804624	0.33	0.017	0.005	6.37x10 ⁻⁴	0.013	0.002	1.66x10 ⁻⁸	0.9	4.42x10 ⁻¹
6:36592986	0.31	0.014	0.005	3.47x10 ⁻³	0.015	0.003	7.85x10 ⁻⁹	0	4.99x10 ⁻¹
rs2684249	0.39	-0.013	0.004	4.26x10 ⁻³	-0.012	0.002	1.96x10 ⁻⁸	0	7.56x10 ⁻¹
rs8176672	0.21	0.020	0.005	1.49x10 ⁻⁴	0.019	0.003	4.49x10 ⁻⁸	0	7.69x10 ⁻¹
rs4936099	0.19	-0.010	0.008	1.99x10 ⁻¹	-0.013	0.002	3.34x10 ⁻⁸	0	9.30x10 ⁻¹
rs34222435	0.53	0.020	0.005	2.73x10 ⁻⁵	0.019	0.003	7.65x10 ⁻¹¹	0	9.31x10 ⁻¹
rs1074407	0.36	0.017	0.005	2.01x10 ⁻⁴	0.012	0.002	1.17x10 ⁻⁸	0	9.40x10 ⁻¹
Disc area									
rs4658101	0.22	0.089	0.009	2.11x10 ⁻²²	0.089	0.005	2.35x10 ⁻⁸²	0	6.32x10 ⁻¹
1:169530520	0.24	0.031	0.009	7.15x10 ⁻⁴	0.032	0.005	5.13x10 ⁻¹³	1.3	4.33x10 ⁻¹
rs11811982	0.05	-0.053	0.021	1.15x10 ⁻²	-0.062	0.008	1.74x10 ⁻¹⁶	24.8	1.93x10 ⁻¹
rs9843102	0.08	-0.046	0.013	5.93x10 ⁻⁴	-0.036	0.005	3.99x10 ⁻¹²	0	7.50x10 ⁻¹
rs10021731	0.33	-0.003	0.008	7.24x10 ⁻¹	-0.020	0.004	2.44x10 ⁻⁷	0	5.44x10 ⁻¹
8:88744441	0.54	0.023	0.007	2.07x10 ⁻³	0.026	0.004	7.15x10 ⁻¹²	0.1	4.47x10 ⁻¹
rs12220165	0.49	0.001	0.009	8.85x10 ⁻¹	-0.023	0.005	1.75x10 ⁻⁵	31.7	1.16x10 ⁻¹
rs7916410	0.27	-0.086	0.009	1.52x10 ⁻²⁴	-0.097	0.004	1.97x10 ⁻¹¹⁴	38.2	6.08x10 ⁻²
rs61101201	0.37	0.018	0.007	1.73x10 ⁻²	0.028	0.004	3.52x10 ⁻¹¹	0	4.76x10 ⁻¹
rs442376	0.74	0.025	0.010	9.44x10 ⁻³	0.032	0.004	9.79x10 ⁻¹⁵	20.1	2.40x10 ⁻¹
rs1345467	0.15	0.019	0.011	8.66x10 ⁻²	0.032	0.004	1.19x10 ⁻¹³	0	7.51x10 ⁻¹
rs5762752	0.20	-0.006	0.009	5.10x10 ⁻¹	-0.023	0.004	1.17x10 ⁻⁸	0	5.09x10 ⁻¹
rs56385951	0.22	0.049	0.009	2.71x10 ⁻⁸	0.047	0.006	2.48x10 ⁻¹⁷	0	5.04x10 ⁻¹
1:3046430	0.22	0.046	0.009	1.43x10 ⁻⁶	0.044	0.007	5.15x10 ⁻¹⁰	0	8.05x10 ⁻¹
rs787541	0.23	0.025	0.009	4.58x10 ⁻³	0.023	0.004	3.16x10 ⁻⁸	0	5.14x10 ⁻¹
rs1367187	0.25	0.025	0.009	7.75x10 ⁻³	0.026	0.005	5.96x10 ⁻⁹	0	8.25x10 ⁻¹
rs2443724	0.57	-0.026	0.007	3.52x10 ⁻⁴	-0.022	0.004	1.40x10 ⁻⁸	13.8	2.95x10 ⁻¹
rs11129176	0.22	0.019	0.009	2.58x10 ⁻²	0.023	0.004	1.02x10 ⁻⁸	0	7.79x10 ⁻¹
rs1997404	0.24	0.024	0.009	6.77x10 ⁻³	0.024	0.004	7.31x10 ⁻⁹	0	7.70x10 ⁻¹
rs34935520	0.70	-0.030	0.008	3.18x10 ⁻⁴	-0.022	0.004	2.39x10 ⁻⁸	0	9.44x10 ⁻¹
rs60779155	0.51	0.040	0.008	2.20x10 ⁻⁶	0.030	0.005	3.28x10 ⁻⁸	0	8.28x10 ⁻¹

Supplementary Figure 3. Regional association and recombination rate plots for all novel identified loci. The figures represent the results from the meta-analysis of studies with European and Asian ancestry. Plots are centered on the most significant single nucleotide polymorphism (SNP) at each locus and flanked by the meta-analysis results for the SNPs in the 400-kb region surrounding it. For each locus, the topSNP (lowest p-value) is depicted as a purple diamond; other SNPs are shaded according to their pairwise correlation (R^2) with the topSNP. The blue line represents the estimated recombination rates; the gene annotations are shown below the figure. Plots were created with Locuszoom (<http://csg.sph.umich.edu/locuszoom>). Figures are shown in the same order as in main Table 1. Only SNPs with p -value $> 1.0 \times 10^{-25}$ are shown. A: intraocular pressure. B-J: vertical cup-disc ratio. K-O: cup area. P-U: disc area

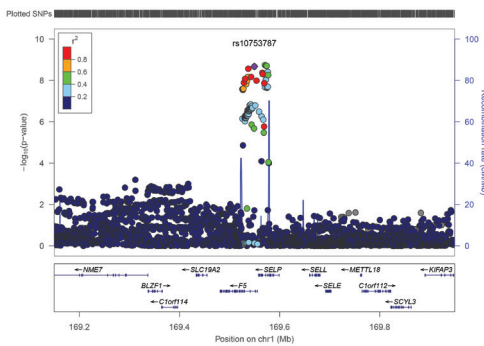
A. rs55796939



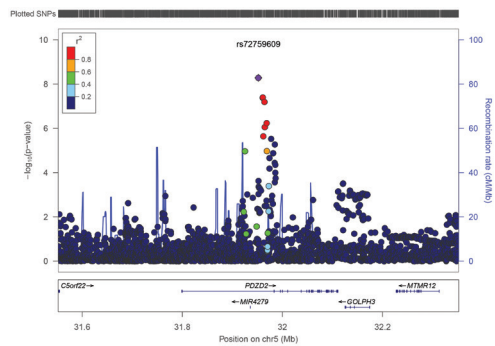
B. rs1925953



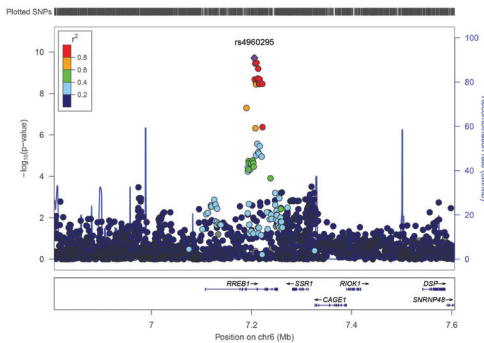
C. rs10753787



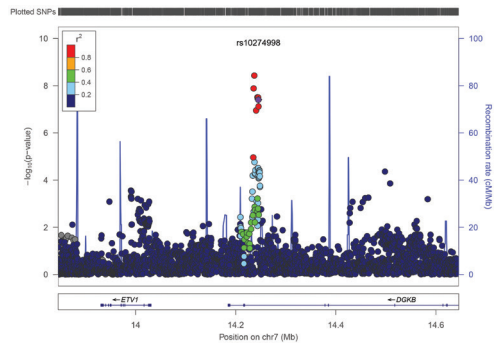
D. rs72759609



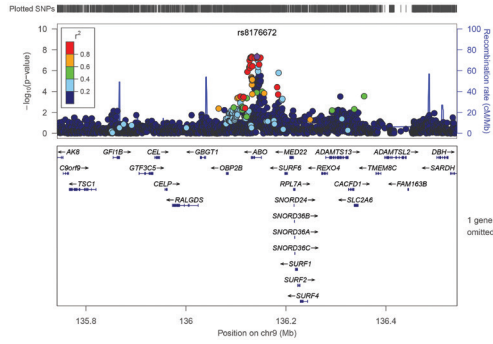
E. rs4960295



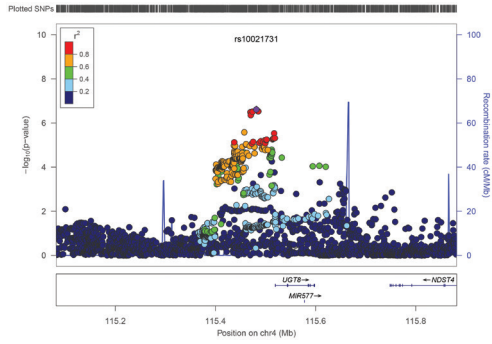
F. rs10274998



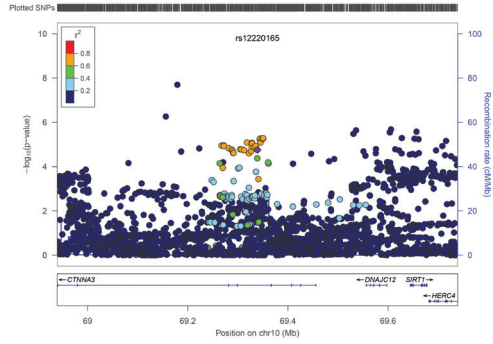
O. rs8176672



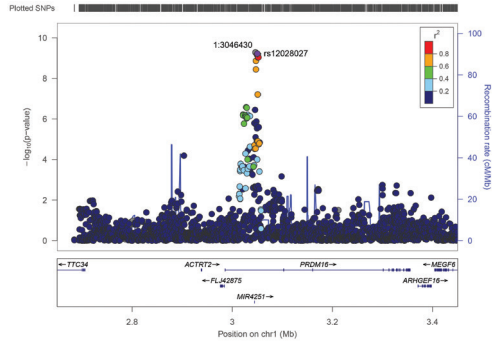
P. rs10021731



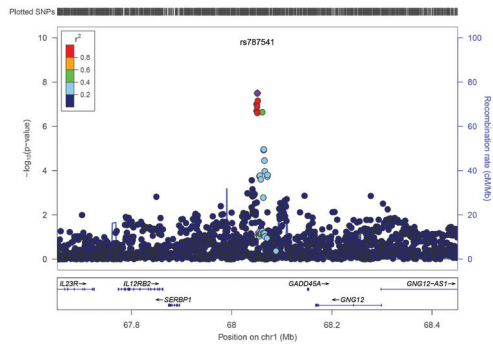
Q. rs12220165



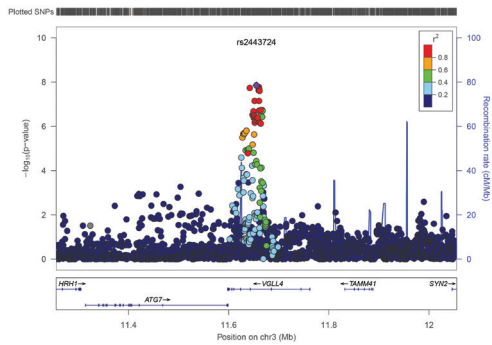
R. 1:3046430



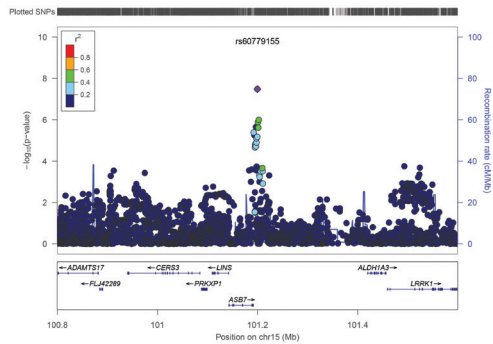
S. rs787541



T. rs2443724



U. rs60779155



Supplementary Table 3. Results of gene-based test using VEGAS. Bonferroni significantly associated genes that show no genome-wide significant evidence for association in the per-SNP test are shown.

Phenotype	Gene	Chromosome (hg19)	Start Position (hg19)	Stop Position (hg19)	P _{gene-based} -value		
					European ancestry cohort	Asian ancestry cohort	Combined
Intraocular pressure	<i>C9</i>	5	39234377	39414655	3.0x10 ⁻⁶	0.03	1.61x10 ⁻⁶
Vertical cup-disc ratio	<i>RARB</i>	3	25165822	25689422	5.0x10 ⁻⁶	0.02	1.86x10 ⁻⁶
	<i>LOC101929664 (HORMAD2-AS1)</i>	22	30354730	30526469	3.0x10 ⁻⁶	0.02	1.04x10 ⁻⁶
Cup area	<i>LRP10</i>	14	23290959	23397291	4.0x10 ⁻⁶	0.01	1.20x10 ⁻⁶
	<i>REM2</i>	14	23302431	23406889	4.0x10 ⁻⁶	0.02	1.55x10 ⁻⁶
	<i>THSD4</i>	15	71383787	72125722	1.0x10 ⁻⁶	2.62x10 ⁻³	5.44x10 ⁻⁸
Disc area	<i>ANKRA2</i>	5	72798024	72911511	7.0x10 ⁻⁶	6.72x10 ⁻³	8.42x10 ⁻⁷
	<i>LOC149950</i>	20	31125280	31246694	1.0x10 ⁻⁶	0.02	3.87x10 ⁻⁷

ABBREVIATION:

hg humane genome

Supplementary Table 4. Gene set enrichment analysis in DEPICT using SNPs with p-value $< 5.0 \times 10^{-8}$. Top four pathways are shown for: IOP, VCDR, cup area, and disc area, while for VCDR/cup area, VCDR/cup area/disc area, VCDR/cup area/IOP the top ten pathways are shown. Top 10 genes and its respective z-score are shown in the table.

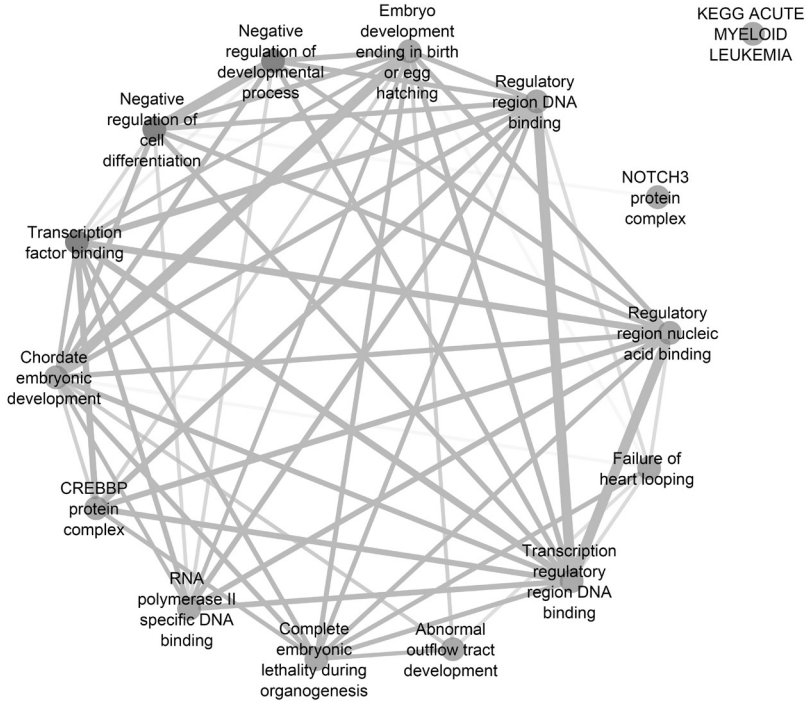
Original pathway description	Nominal P value	False discovery rate	Gene 1 (Z score) until gene 10 (Z score)
Intraocular pressure			
RPL22 protein complex	1.20×10^{-4}	> 0.20	FNBP4 (2.7), PSMC3 (1.7), MEI51 (1.7), NDUFS3 (1.6), ENSG00000226334 (1.5), MYBPC3 (1.4), CAV1 (1.2), ENSG00000230817 (1.1), MED22 (1.1), CELF1 (1.0)
DNAJA3 protein complex	7.52×10^{-4}	> 0.20	GHTM (3.0), SURF6 (2.8), SURF4 (2.4), PTPR1 (1.6), ENSG00000230817 (1.5), ABCA1 (1.4), PTPMT1 (1.4), PSMC3 (1.3), TMCO1 (1.3), MTC2 (1.3)
MARS protein complex	8.49×10^{-4}	> 0.20	PSMC3 (2.0), SURF2 (2.0), GHTM (1.8), CELF1 (1.5), ARS1 (1.5), MED22 (1.4), DDR2 (1.4), TMCO1 (1.4), NUP160 (1.3), MTC2 (1.3)
chemoattractant activity	9.51×10^{-4}	> 0.20	ENSG00000256746 (2.3), ADAMTS8 (2.0), ARS1 (1.7), ENSG00000226334 (1.7), OR4A1P (1.7), SPRY2 (1.6), OSBP10 (1.5), SURF1 (1.5), SURF2 (1.4), FNBP4 (1.4)
Vertical cup-disc ratio			
impaired glucose tolerance	9.08×10^{-5}	> 0.20	CACNB2 (3.3), CABP7 (3.2), CDH22 (2.7), ARL5B (2.6), MGST1 (2.1), TMEM57 (1.9), FLNB (1.9), PHKG1 (1.8), GPR146 (1.8), RERG (1.8)
response to ionizing radiation	1.46×10^{-4}	> 0.20	GTF2H3 (3.0), ZNF43 (2.7), C4orf21 (2.6), ENSG00000240291 (2.4), E2F7 (2.4), ENSG00000256995 (2.4), NPAT (2.3), EYS (2.3), LINC00460 (2.2), CDC7 (2.2)
abnormal heart left ventricle morphology	1.85×10^{-4}	> 0.20	RYR2 (5.1), SGCG (3.8), MYPN (3.3), CACNB2 (2.9), ENSG00000245482 (2.7), VCAN (2.2), KANK1 (1.9), SLURP1 (1.9), CCDC102B (1.9), PTPRO (1.8)
chordate embryonic development	1.90×10^{-4}	> 0.20	IRX3 (3.3), TTC28 (2.9), NEUROG2 (2.6), SIX4 (2.4), SIX1 (2.2), C14orf39 (2.2), FZD8 (2.1), FAM1101A (2.1), RSPO3 (2.0), ENSG00000223850 (2.0)
Cup area			
RBPMS protein complex	3.45×10^{-6}	≤ 0.20	SPSB4 (2.8), SIX1 (2.6), ENSG00000233368 (2.6), SOX13 (2.4), TRIOBP (2.3), RERE (2.3), XAB2 (2.1), FBRSL1 (1.9), SPEN (1.9), KIAA1211 (1.7)
SETDB1 protein complex	1.95×10^{-5}	≤ 0.20	ENSG00000179743 (3.0), TRIOBP (2.6), ZNF664 (2.4), CCD92 (2.4), CHEK2 (2.1), ERCC2 (1.9), FBRSL1 (1.9), SRSF3 (1.7), ENSG00000233368 (1.7), DNA2 (1.6)
MYH14 protein complex	4.22×10^{-5}	≤ 0.20	CKM (4.2), LINC00314 (4.0), FLNB (3.6), DPVSL3 (3.4), FILIP1L (3.3), CDC42BPA (2.9), MYPN (2.8), NQO1 (2.5), STK32A (2.3), CLDN5 (2.1)
positive regulation of cellular component organization	5.48×10^{-5}	≤ 0.20	TRIOBP (2.8), DPVSL3 (2.4), CAMSAP3 (2.3), CD244 (2.2), NFAT5 (2.1), LTBP3 (2.1), NCS1 (2.1), EHP11L (1.8), P2RX2 (1.8), TNFAIP8L1 (1.7)
Disc area			
holoprosencephaly	6.64×10^{-5}	> 0.20	SIX6 (4.4), PAX6 (4.0), C14orf39 (3.1), RCN1 (2.7), SIX4 (2.4), TET1 (2.2), ATOH7 (2.1), SALL1 (2.1), PRDM16 (1.7), DCDC5 (1.6)
abnormal tooth development	1.14×10^{-4}	> 0.20	SIX1 (4.3), ABI3BP (4.2), SIX4 (3.5), TTC28 (2.3), INSC (2.1), VGLL4 (1.6), PSEN2 (1.6), TGFBR3 (1.6), DIRC3 (1.5), COL8A1 (1.1)
small basiphonoid bone	1.49×10^{-4}	> 0.20	SIX1 (4.9), SIX4 (4.0), PRDM16 (3.3), COL8A1 (2.9), PAX6 (2.9), ABI3BP (2.3), C14orf39 (2.0), RARB (1.9), VGLL4 (1.8), DIRC3 (1.8)
abnormal craniofacial bone morphology	1.89×10^{-4}	> 0.20	SIX4 (5.7), SIX1 (4.9), RARB (3.8), TTC28 (3.3), VGLL4 (3.1), PRDM16 (2.5), TET1 (1.7), TMTC2 (1.7), SALL1 (1.7), INSC (1.6)
Vertical cup-disc ratio / cup area			
abnormal fat cell morphology	3.45×10^{-5}	≤ 0.20	SLC16A7 (3.2), MGST1 (3.2), SLC25A16 (2.9), PYGL (2.8), DCLK1 (2.7), GPR146 (2.4), F1IR (2.4), PDZD2 (2.3), SGCG (2.2), DDHD1 (2.0)

Original pathway description	Nominal P value	False discovery rate	Gene 1 (Z score) until gene 10 (Z score)
abnormal myocardium layer morphology	4.24x10 ⁻⁵	<= 0.20	RYR2 (5.6), MYPN (4.2), PLCE1 (3.7), SGGC (3.2), CACNB2 (2.5), ADAMTS8 (2.3), FBRSL1 (2.3), AKAP6 (2.2), F11R (2.0), GPR146 (1.9)
thyroid gland development	8.48x10 ⁻⁵	<= 0.20	ENSG00000229565 (3.3), ENSG00000229775 (2.9), CABP7 (2.6), TSSK6 (2.6), SIX4 (2.2), C14orf39 (2.2), P2RX2 (2.1), CYP2W1 (1.9), SIX6 (1.9), DHR33 (1.9)
MMP14 protein complex	1.12x10 ⁻⁴	<= 0.20	S100A2 (4.0), RIN2 (3.9), PDPN (3.6), COL8A1 (3.5), MITF (3.4), KANK1 (3.0), LTBP3 (2.6), VCAN (2.4), NXPH1 (2.3), C10orf11 (2.3)
increased circulating leptin level	1.25x10 ⁻⁴	<= 0.20	GALR3 (2.8), NAT2 (2.5), ITLN1 (2.4), DHR33 (2.4), CDKN2B (2.3), KANK1 (2.3), GPR146 (2.3), RREB1 (2.3), SIX6 (2.2), ENSG00000247225 (2.1)
fusion of atlas and odontoid process	1.43x10 ⁻⁴	<= 0.20	DHR33 (2.9), FAM101A (2.5), TRIOBP (2.4), NEUROG2 (2.3), SOX13 (2.2), TTC28 (1.8), LINC00315 (1.8), ANO3 (1.7), ODZ4 (1.7), PAX7 (1.6)
impaired glucose tolerance	1.43x10 ⁻⁴	<= 0.20	CACNB2 (3.3), CABP7 (3.2), CDH22 (2.7), ARL5B (2.6), MGST1 (2.1), TMEM57 (1.9), ENSG00000257479 (1.9), FLNB (1.9), PHKG1 (1.8), GPR146 (1.8)
abnormal rib-sternum attachment	1.51x10 ⁻⁴	<= 0.20	SIX1 (4.3), PAX7 (4.1), SIX4 (3.3), IRX3 (3.1), ENSG00000248762 (2.7), SALL1 (2.5), NXPH1 (2.3), DHR33 (2.2), C14orf39 (2.1), LINC00460 (1.9)
decreased susceptibility to diet-induced obesity	1.73x10 ⁻⁴	<= 0.20	ENSG00000229775 (3.2), ENSG00000257479 (2.8), RREB1 (2.5), CCDC102B (2.3), SI (2.2), GPR146 (2.2), SLC16A7 (2.1), LTBP3 (2.1), DMRT1 (2.1), ODZ4 (1.9)
HSPG2 protein complex	1.91x10 ⁻⁴	<= 0.20	COL8A1 (4.2), VCAN (4.2), LTBP3 (3.6), ENSG00000233419 (3.3), KDELC2 (2.5), PDPN (2.3), ENSG00000253741 (2.3), BMP2 (2.1), F11R (2.1), SOX13 (2.0)
Vertical cup-disc ratio / cup area / disc area			
increased circulating leptin level	1.62x10 ⁻⁵	<= 0.20	GALR3 (2.8), NAT2 (2.5), ITLN1 (2.4), DHR33 (2.4), CDKN2B (2.3), KANK1 (2.3), GPR146 (2.3), RREB1 (2.3), SIX6 (2.2), ENSG00000247225 (2.1)
impaired glucose tolerance	1.92x10 ⁻⁵	<= 0.20	TGFB3 (3.4), CACNB2 (3.3), CABP7 (3.2), CDH22 (2.7), ARL5B (2.6), MGST1 (2.1), TMEM57 (1.9), ENSG00000257479 (1.9), FLNB (1.9), PHKG1 (1.8)
abnormal fat cell morphology	2.29x10 ⁻⁵	<= 0.20	SLC16A7 (3.2), MGST1 (3.2), SLC25A16 (2.9), PYGL (2.8), DCLK1 (2.7), TGFB3 (2.6), GPR146 (2.4), F11R (2.4), PDZD2 (2.3), SGGC (2.2)
increased insulin sensitivity	2.97x10 ⁻⁵	<= 0.20	TGFB3 (2.8), MITF (2.5), CACNB2 (2.2), XYLTI (2.1), CCDC102B (2.1), PLCE1 (2.0), SLC16A7 (2.0), HSPA12A (1.9), PDZD2 (1.8), DUSP1 (1.8)
abnormal myocardium layer morphology	3.53x10 ⁻⁵	<= 0.20	RYR2 (5.6), MYPN (4.2), CTNNA3 (4.1), PLCE1 (3.7), SGGC (3.2), CACNB2 (2.5), ADAMTS8 (2.3), FBRSL1 (2.3), AKAP6 (2.2), F11R (2.0)
abnormal heart left ventricle morphology	3.79x10 ⁻⁵	<= 0.20	RYR2 (5.1), SGGC (3.8), MYPN (3.3), CACNB2 (2.9), ENSG00000245482 (2.7), F11R (2.4), VCAN (2.2), KANK1 (1.9), SLURP1 (1.9), CCDC102B (1.9)
decreased susceptibility to diet-induced obesity	4.81x10 ⁻⁵	<= 0.20	ENSG00000229775 (3.2), ENSG00000257479 (2.8), RREB1 (2.5), CCDC102B (2.3), SI (2.2), GPR146 (2.2), SLC16A7 (2.1), LTBP3 (2.1), DMRT1 (2.1), ODZ4 (1.9)
decreased circulating free fatty acid level	7.77x10 ⁻⁵	<= 0.20	PHKG1 (3.2), PYGL (3.1), CPB2 (3.1), DHR33 (2.8), ODZ4 (2.5), RREB1 (2.2), GADD45A (2.1), DUSP1 (2.1), AHNK (2.0), F5 (1.9)
MMP14 protein complex	8.08x10 ⁻⁵	<= 0.20	S100A2 (4.0), RIN2 (3.9), PDPN (3.6), COL8A1 (3.5), MITF (3.4), KANK1 (3.0), LTBP3 (2.6), VCAN (2.4), NXPH1 (2.3), C10orf11 (2.3)
hyperglycemia	8.23x10 ⁻⁵	<= 0.20	GPR146 (2.9), SGGC (2.8), SLC16A7 (2.7), MGST1 (2.6), CABP7 (2.4), KANK1 (2.3), ENSG00000257479 (2.3), MYO16 (2.3), LINC00460 (2.2), RHCE (2.1)

Supplementary Table 4. Gene set enrichment analysis in DEPICT using SNPs p-value $< 5.0 \times 10^{-8}$. Top four pathways are shown for: IOP, VCDR, cup area, and disc area, while for VCDR/cup area, VCDR/cup area/disc area, VCDR/cup area/IOP the top ten pathways are shown. Top 10 genes and its respective z-score are shown in the table. (continued)

Original pathway description	Nominal P value	False discovery rate	Gene 1 (Z score) until gene 10 (Z score)
decreased circulating free fatty acid level	7.77×10^{-5}	≤ 0.20	PHKG1 (3.2), PYGL (3.1), CPB2 (3.1), DHRS3 (2.8), ODZ4 (2.5), RREB1 (2.2), GADD45A (2.1), DUSP1 (2.1), AHNAK (2.0), F5 (1.9)
MMP14 protein complex	8.08×10^{-5}	≤ 0.20	S100A2 (4.0), RIN2 (3.9), PDPN (3.6), COL8A1 (3.5), MITF (3.4), KANK1 (3.0), LTBP3 (2.6), VCAN (2.4), NXP1 (2.3), C10orf11 (2.3)
hyperglycemia	8.23×10^{-5}	≤ 0.20	GPR146 (2.9), SGGC (2.8), SLC16A7 (2.7), MGST1 (2.6), CABP7 (2.4), KANK1 (2.3), ENSG0000257479 (2.3), MYO16 (2.3), LINC00460 (2.2), RHCE (2.1)
decreased circulating free fatty acid level	7.77×10^{-5}	≤ 0.20	PHKG1 (3.2), PYGL (3.1), CPB2 (3.1), DHRS3 (2.8), ODZ4 (2.5), RREB1 (2.2), GADD45A (2.1), DUSP1 (2.1), AHNAK (2.0), F5 (1.9)
MMP14 protein complex	8.08×10^{-5}	≤ 0.20	S100A2 (4.0), RIN2 (3.9), PDPN (3.6), COL8A1 (3.5), MITF (3.4), KANK1 (3.0), LTBP3 (2.6), VCAN (2.4), NXP1 (2.3), C10orf11 (2.3)
hyperglycemia	8.23×10^{-5}	≤ 0.20	GPR146 (2.9), SGGC (2.8), SLC16A7 (2.7), MGST1 (2.6), CABP7 (2.4), KANK1 (2.3), ENSG0000257479 (2.3), MYO16 (2.3), LINC00460 (2.2), RHCE (2.1)
Vertical cup-disc ratio / cup area / intraocular pressure			
RBPM5 protein complex	4.61×10^{-6}	≤ 0.20	SPSB4 (2.8), SIX1 (2.6), ENSG0000233368 (2.6), SOX13 (2.4), TRIOBP (2.3), RERE (2.3), NEUROG2 (2.2), XAB2 (2.1), FBRSL1 (1.9), SPEN (1.9)
MDFI protein complex	1.73×10^{-5}	≤ 0.20	PAX7 (3.6), PPP1R16A (3.6), LRRC14 (3.4), ZNF100 (3.2), SIX4 (3.2), ZNF43 (2.8), ZNF492 (2.7), DMRT2 (2.3), XAB2 (2.2), ZMAT5 (2.1)
cell fate commitment	1.33×10^{-4}	≤ 0.20	PAX7 (4.6), NEUROG2 (3.9), DMRT2 (3.8), SIX6 (3.7), SOX13 (3.1), FZD8 (3.0), ENSG00000179743 (3.0), SIX1 (2.9), ABO (2.8), PCDH15 (2.8)
abnormal sclerotome morphology	1.56×10^{-4}	≤ 0.20	NXP1 (3.4), FAM101A (3.1), CARD10 (2.8), TMCO1 (2.8), FAM70B (2.5), PCDH15 (2.5), NEUROG2 (2.4), S100A2 (2.4), GPT (2.3), TMEM57 (2.2)
decreased circulating leptin level	1.61×10^{-4}	≤ 0.20	PYGL (3.3), SLC16A7 (2.8), XYLT1 (2.6), GPT (2.6), MGST1 (2.6), GPR146 (2.3), RERG (2.3), C8orf82 (2.2), ANO3 (2.2), DGKB (2.0)
embryo development ending in birth or egg hatching	1.66×10^{-4}	≤ 0.20	SOX13 (3.1), IRX3 (3.1), DMRT2 (3.0), TTC28 (2.8), NEUROG2 (2.7), SIX4 (2.4), SPEN (2.2), SIX1 (2.2), C14orf39 (2.1), RSP03 (2.1)
cell differentiation in spinal cord	2.06×10^{-4}	≤ 0.20	CDH22 (4.2), PAX7 (3.7), ENSG0000253741 (3.2), ATP5G2P1 (3.1), CLV51 (2.9), ENSG00000179743 (2.9), NEUROG2 (2.8), NLGN1 (2.7), SPSB4 (2.7), ENSG0000226764 (2.5)
chordate embryonic development	2.08×10^{-4}	≤ 0.20	IRX3 (3.3), SOX13 (3.1), DMRT2 (3.0), TTC28 (2.9), NEUROG2 (2.6), SIX4 (2.4), SPEN (2.2), SIX1 (2.2), C14orf39 (2.2), MEIS1 (2.1)
fusion of atlas and odontoid process	2.38×10^{-4}	≤ 0.20	MEIS1 (3.0), DHRS3 (2.9), FAM101A (2.5), TRIOBP (2.4), NEUROG2 (2.3), SOX13 (2.2), TTC28 (1.8), LINC00315 (1.8), ANO3 (1.7), ADAMTS13 (1.7)
neuron fate commitment	2.54×10^{-4}	≤ 0.20	PAX7 (4.3), NEUROG2 (4.0), PCDH15 (3.8), ENSG0000226764 (3.2), SOX13 (3.2), CDH13 (3.1), PRAMEF12 (3.1), ABO (3.0), SIX6 (2.8), C9orf7 (2.8)

Supplementary Figure 4. Pathways significantly enriched for loci associated with vertical cup-disc ratio and cup area ($P < 1.0 \times 10^{-5}$). In total 15 pathways were found enriched using DEPICT. Pathways are represented by nodes coloured according to statistical significance, and edges are scaled according to the correlation between meta-pathways. Only correlations > 0.3 are shown.



Supplementary Table 5. Meta pathways significantly enriched using DEPICT. Meta-pathways were named by their representative pathway which was automatically selected by the Affinity Propagation clustering algorithm.

Meta-pathways	Significant pathways clustered in the meta-pathway
Vertical cup-disc ratio / cup area / intraocular pressure Negative regulation of developmental process	negative regulation of developmental process (GO:00511093), absent spleen (MP:0000690), neuron fate commitment (GO:0048663), regulation of anatomical structure morphogenesis (GO:0022603), negative regulation of cell differentiation (GO:0045596), regulation of cell development (GO:0060284) abnormal liver morphology (MP:0000598)
Abnormal liver morphology Regulatory region nucleic acid binding	regulatory region nucleic acid binding (GO:0001067), KEGG ACUTE MYELOID LEUKEMIA (KEGG_ACUTE_MYELOID_LEUKEMIA), transcription factor binding (GO:0008134), transcription regulatory region DNA binding (GO:0044212), sequence-specific DNA binding RNA polymerase II transcription factor activity (GO:0000981), regulatory region DNA binding (GO:0000975), CREBBP protein complex (ENSG00000005339), ETV7 protein complex (ENSG00000010030), negative regulation of transcription from RNA polymerase II promoter (GO:0000122).
Chordate embryonic development	chordate embryonic development (GO:0043009) DVL3 protein complex (ENSG00000161202), embryo development ending in birth or egg hatching (GO:0009792).
NOTCH3 protein complex Complete embryonic lethality during organogenesis	NOTCH3 protein complex (ENSG00000074181), DTX1 protein complex (ENSG00000135144). complete embryonic lethality during organogenesis (MP:0011098), prenatal lethality (MP:0002080), hemorrhage (MP:0001914), trabecula carnea hypoplasia (MP:0000295), decreased embryo size (MP:0001698), pale yolk sac (MP:0001722), embryonic growth retardation (MP:0003984), partial lethality throughout fetal growth and development (MP:0011109), abnormal neural tube morphology/development (MP:0002151), edema (MP:0001785), complete lethality throughout fetal growth and development (MP:0011099).
Complete neonatal lethality	complete neonatal lethality (MP:0011087), double outlet heart right ventricle (MP:0000284), respiratory distress (MP:0001954), cyanosis (MP:0001575), ATN1 protein complex (ENSG00000111676), positive regulation of cellular component organization (GO:0051130), developmental growth (GO:0048589).
Abnormal rib morphology	abnormal rib morphology (MP:0000150), lordosis (MP:0000162), abnormal vertebral arch morphology (MP:0004599), abnormal thoracic vertebrae morphology (MP:0003047), abnormal lumbar vertebrae morphology (MP:0003049), abnormal scrotome morphology (MP:0006029), abnormal caudal vertebrae morphology (MP:0002759), abnormal vertebrae morphology (MP:0000137), abnormal vertebral body morphology (MP:0000141), abnormal pterygoid process morphology (MP:0004452), abnormal sternbra morphology (MP:0004322).
Cleft palate	Cleft palate, (SPECCL1 protein complex: ENSG00000100014), FAM55B protein complex (ENSG00000204361), HTRA1 protein complex (ENSG00000166033), MYH14 protein complex (ENSG00000105357), TPM2 protein complex (ENSG00000198467).
Cell adhesion mediated by integrin ELL2 protein complex	cell adhesion mediated by integrin (GO:0033627) ELL2 protein complex (ENSG00000118985)
Vertical cup-disc ratio / cup area / disc area Negative regulation of developmental process	negative regulation of developmental process (GO:00511093), negative regulation of cell differentiation (GO:0045596), positive regulation of cell differentiation (GO:0045597).
Transcription regulatory region DNA binding	transcription regulatory region DNA binding (GO:0044212), chromatin binding (GO:0003682), regulatory region nucleic acid binding (GO:0001067), transcription factor binding (GO:0008134), sequence-specific DNA binding RNA polymerase II transcription factor activity (GO:0000981), regulatory region DNA binding (GO:0000975), RNA polymerase II distal enhancer sequence-specific DNA binding transcription factor activity (GO:0003705), transcription factor complex (GO:0005667), negative regulation of transcription from RNA polymerase II promoter (GO:0000122).

Supplementary Table 5. Meta pathways significantly enriched using DEPICT. Meta-pathways were named by their representative pathway which was automatically selected by the Affinity Propagation clustering algorithm.

Meta-pathways	Significant pathways clustered in the meta-pathway
Chordate embryonic development	chordate embryonic development (GO:0043009), abnormal eye morphology (MP:0002092), in utero embryonic development (GO:0001701), embryonic organ development (GO:0048568), embryo development ending in birth or egg hatching (GO:0009792), pattern specification process (GO:0007389).
Complete embryonic lethality during organogenesis	complete embryonic lethality during organogenesis (MP:0011098), abnormal outflow tract development (MP:0006126), prenatal lethality (MP:0002080), enlarged heart (MP:0000274), pericardial effusion (MP:0005312), abnormal embryogenesis/development (MP:0001672), trabecula carnea hypoplasia (MP:0000295), decreased embryo size (MP:0001698), failure of heart looping (MP:0004251), pale yolk sac (MP:0001722), embryonic growth retardation (MP:0003984), partial prenatal lethality (MP:0011101), partial lethality throughout fetal growth and development (MP:0011109), abnormal neural tube morphology/development (MP:0002151), edema (MP:0001785), abnormal spongiotrophoblast layer morphology (MP:0004255), complete lethality throughout fetal growth and development (MP:0011099), complete prenatal lethality (MP:0011091).
REACTOME Notch transcription pathway	REACTOME NOTCH:HLH TRANSCRIPTION PATHWAY, KEGG DORSO VENTRAL AXIS FORMATION, KEGG NOTCH SIGNALING PATHWAY, REACTOME NICD TRAFFICS TO NUCLEUS, NOTCH3 protein complex (ENSG00000074181).
Protein import into nucleus	protein import into nucleus (GO:006606), protein localization to nucleus (GO:0034504), nuclear import (GO:0051170).
Abnormal rib morphology	abnormal rib morphology (MP:0000150), abnormal vertebral arch morphology (MP:0004599), abnormal thoracic vertebrae morphology (MP:0003047), abnormal sternum morphology (MP:0000157), abnormal phalanx morphology (MP:0005306), abnormal vertebrae morphology (MP:0000137), abnormal styloid process morphology (MP:0008023), abnormal vertebral body morphology (MP:0000141), abnormal rib-sternum attachment (MP:0008148), rib fusion (MP:0000154), abnormal sternebra morphology (MP:0004322).
KEGG pathways in cancer	KEGG PATHWAYS IN CANCER, KEGG RENAL CELL CARCINOMA, KEGG ACUTE MYELOID LEUKEMIA, KEGG MELANOMA
SMAD3 protein complex	SMAD3 protein complex (ENSG0000166949), GSK3B protein complex (ENSG00000082701), CREBBP protein complex (ENSG0000005339), HDAC1 protein complex (ENSG00000116478), SMAD2 protein complex (ENSG00000175387).
Tissue morphogenesis	tissue morphogenesis (GO:0048729), double outlet heart right ventricle (MP:0000284), perimembraneous ventricular septal defect (MP:0010418), WWTR1 protein complex (ENSG00000018408), developmental growth (GO:0048589), heart valve morphogenesis (GO:0003179), morphogenesis of an epithelium (GO:0002009), cell fate commitment (GO:0045165) cleft secondary palate (MP:0009890), respiratory distress (MP:0001954), abnormal basisphenoid bone morphology (MP:0000106), abnormal pterygoid process morphology (MP:0004452), complete neonatal lethality (MP:0011087), cyanosis (MP:0001575), palatal shelves fail to meet at midline (MP:0009888).
Cleft secondary palate	THBS1 protein complex (ENSG00000137801), abnormal liver morphology (MP:0000598), NOV protein complex (ENSG00000136999), COL4A1 protein complex (ENSG00000187498).
THBS1 protein complex	MDF1 protein complex
MDF1 protein complex	Blood vessel development (GO:0001568), hydrops fetalis (MP:0002192), abnormal angiogenesis (MP:0000260), decreased angiogenesis (MP:0005602), dilated heart right ventricle (MP:0002754), abnormal heart left ventricle morphology (MP:0003921), angiogenesis (GO:0001525), blood vessel morphogenesis (GO:0048514), cell adhesion mediated by integrin (GO:0033627), regulation of anatomical structure morphogenesis (GO:0022603), muscle cell proliferation (GO:0033002).
Blood vessel development	RFX2 protein complex (ENSG000000087903)
RFX2 protein complex	abnormal fat cell morphology (MP:0009115)
Abnormal fat cell morphology	DVL2 protein complex (ENSG00000004975), DVL3 protein complex (ENSG00000161202)
DVL2 protein complex	

SUPPLEMENTARY NOTE

The studies including individuals from with European ancestry were Brisbane Adolescent Twin Study (BATS), Blue Mountains Eye Study (BMES), EPIC (European Prospective Investigation into Cancer), Erasmus Rucphen Family (ERF) Study, Framingham Eye Study, Gutenberg Health Study I and II (GHS I and GHS II), Orkney Complex Disease Study (ORCADES), the Western Australian Pregnancy Cohort (Raine) Study, the Rotterdam Study I, II, and III (RS-I, RS-II, RS-III), Twins Eye Study in Tasmania (TEST), and TwinsUK. The studies including individuals from with Asian ancestry were Beijing Eye Study (BES), Singapore Chinese Eye Study, Singapore Malay Eye Study (SIMES) and Singapore Indian Eye Study (SINDI). The four POAG case control studies were Australian & New Zealand Registry of Advanced Glaucoma (ANZRAG), National Eye Institute Glaucoma Human Genetics Collaboration Heritable Overall Operational Database (NEIGHBORHOOD), Singapore and Southampton.

Population-based studies

Beijing Eye Study (BES)

The BES is a population-based cohort of Han Chinese in the rural region and in the urban region of Beijing in North China^{1,2}. The Medical Ethics Committee of the Beijing Tongren Hospital approved the study protocol and all participants gave informed consent, according to the Declaration of Helsinki. At baseline (2001), 4439 individuals out of 5324 eligible individuals aged 40 years or older participated (response rate: 83.4%). In the years 2006 and 2011, the study was repeated by re-inviting all participants from the survey from 2001 to be re-examined. Out of the 4439 subjects examined in 2001, 3251 (73.2%) subjects returned for the follow-up examination in 2006, and 2695 (60.7%) subjects returned for the follow-up examination in 2011. All study participants underwent an ophthalmic examination including refractometry, pneumotometry, slit-lamp biomicroscopy, and photography of the cornea, lens, optic disc, and macula. Intraocular pressure (IOP) was measured using a non-contact pneumotonometer (CT-60 computerized tonometer, Topcon Ltd., Japan) by an experienced technician. Three measurements were taken, and the mean of the three measurements was taken for further statistical analysis. If the measurements were higher than 25 mmHg, tonometry was repeated. A questionnaire included questions for self-reported diseases, including topical anti-glaucomatous medications, and previous ocular surgery. Optic disc parameters were measured using Planimetry and the vertical cup-disc ratio was manually calculated. Blood samples were taken from 2,929 (90.1%) participants, and DNA was extracted from blood leucocytes according to standard procedures. We performed genotyping using Illumina Human610-Quad BeadChip in 988 subjects³. 151 individuals with cryptic relatedness were excluded during sample QC procedure. After the removal of samples, SNPs were excluded based on (i) high rates of missingness (>5%); (ii) monomorphism; (iii) gross departure from HWE of $P < 10^{-6}$. Imputation was performed using the genotyped data passed the quality control filtering, together with the 1000 genomes phase 1 cosmopolitan panel haplotypes (March 2012 release). The Markov Chain Haplotyping software was used in the imputation procedure (Minimac software, <http://genome.sph.umich.edu/wiki/Minimac>).

Blue Mountains Eye Study

The Blue Mountains Eye Study is a population-based cohort study of common eye diseases in older Australians living in the Blue Mountains region, west of Sydney, Australia. IOP was measured using Goldmann applanation tonometry (Haag-Streit, Bern, Switzerland)⁴. Optic disc measurements were obtained after pupil dilation from 30° color stereoscopic optic disc photographs taken with a 99 Zeiss FF3 fundus camera (Carl Zeiss Meditec, Dublin, CA). Further details have been described elsewhere⁵. DNA was extracted from whole blood and quality was validated by Sequenom iPLEX assay. Genotyping was performed on the Illumina Infinium platform using the Human660W-Quad, a Wellcome Trust Case Control Consortium 2 designed custom chip containing Human550 probes with 60,000 additional probes to capture common copy-number variations from the Structural Variation Consortium⁶. Genotyped data were filtered to include SNPs with genotyping rate ≥ 0.97 , MAF $\geq 1\%$, HWE p -value $\geq 10^{-6}$. Samples with call rates less than 95% were excluded from analysis. Relatedness filtering based on estimated identity by descent was performed so that no pairs of individuals shared more than 20% of their genome. Ancestry outliers with >6 s. d. from 1000 Genomes northern European ancestry samples were removed. The IMPUTE2 software was used for imputation of data on 1000 Genomes phase 1 release version 3^{7,8}. The association test was performed using SNPTTEST_v2.5-beta4^{9,10}. The study was approved by the Human Research Ethics Committees of the University of Sydney and Sydney West Area Health Service.

Brisbane Adolescent Twins Study (BATS) and Twins Eye Study in Tasmania (TEST)

The Australian Twin Eye Study comprises participants examined as part of TEST or BATS. In most participants, the IOP was measured with the TONO-PEN XL (Reichert, Inc. New York, USA)¹¹. A Nidek 3-Dx fundus camera (Nidek, Gamagori, Japan) was used to obtain simultaneous stereoscopic optic disc photographs. All images were captured on colour 35 mm slides (Ektachrome, Eastman Kodak, Rochester, NY, USA) and digitized using a Nikon CoolScan IV ED slide scanner (Nikon Corp., Tokyo, Japan). Optic discs were analysed stereoscopically with custom planimetric software (StereoDx, using a Z-screen; StereoGraphics Corp., Beverly Hills, CA, USA), where the inner margin of the optic disc and the neuroretinal rim were delineated at the depth of the scleral plane, and images were modified for magnification using refraction and keratometry data. The Australian twin cohorts were genotyped on the Illumina Human Hap610W Quad array. The inclusion criteria for the SNPs were a MAF >0.01 , HWE p -value $\geq 10^{-6}$, and a SNP call rate $>95\%$ or Illumina Beadstudio Gencall Score ≥ 0.7 , resulting in 543,862 SNPs. Imputation was done with reference to the August 4, 2010 version of the publicly released 1000 Genomes Project European genotyping using MACH. Association analyses were performed in Merlin (<http://www.sph.umich.edu/csg/abecasis/merlin/>) by using the `-fastassoc` option. Ancestry, initially determined through self-reporting, was verified through Principal Component decomposition. The studies were approved by the human ethics committees of the University of Tasmania, Royal Victorian Eye and Ear Hospital, and Queensland Institute of Medical Research.

EPIC-Norfolk Eye Study

The European Prospective Investigation into Cancer (EPIC) study is a pan-European prospective cohort study designed to investigate the aetiology of major chronic diseases¹². EPIC-Norfolk, one of the UK arms of EPIC, recruited and examined 25,639 participants aged 40-79 years between 1993 and 1997 for the baseline examination¹³. Recruitment was via

general practices in the city of Norwich and the surrounding small towns and rural areas, and methods have been described in detail previously¹⁴. Since virtually all residents in the UK are registered with a general practitioner through the National Health Service, general practice lists serve as population registers. Ophthalmic assessment formed part of the third health examination and this has been termed the EPIC-Norfolk Eye Study¹⁵. In total, 8,623 participants were seen for the ophthalmic examination, between 2004 and 2011.

IOP was measured using the Ocular Response Analyzer (ORA, Reichert, New York, USA; software V.3.01). Three readings were taken per eye following a demo puff. ORA measurements with a poor quality pressure waveform were repeated. The best signal value for each eye was considered for each eye. Scanning laser ophthalmoscopy (Heidelberg Retinal Tomograph (HRT) II, Heidelberg Engineering, Heidelberg, Germany) was used to assess optic nerve head anatomy. The participant's keratometry was entered prior to scanning. If the image quality was poor (topography SD >40 μm) a repeat scan was undertaken. Contours around the disc margins were manually drawn and subsequently checked by an ophthalmologist (and redrawn if necessary). The HRT software was subsequently updated to Glaucoma Module Premium Edition (software V.3.1) and data exported following this. These data are equivalent to HRT3-derived parameters.

Genotyping on a subset of the cohort was undertaken using the Affymetrix GeneChip Human Mapping 500K Array Set. Data were pre-phased with SHAPEIT version 2 and imputed to the March 2012 build of the 1000 Genomes project using IMPUTE version 2.2.2. The EPIC-Norfolk Eye Study was carried out following the principles of the Declaration of Helsinki and the Research Governance Framework for Health and Social Care. The study was approved by the Norfolk Local Research Ethics Committee (05/Q0101/191) and East Norfolk & Waveney NHS Research Governance Committee (2005EC07L). All participants gave written, informed consent.

Erasmus Rucphen Family Study

The Erasmus Rucphen Family (ERF) Study is a family-based cohort in a genetically isolated population in the southwest of the Netherlands with over 3,000 participants aged between 18 and 86 years^{16,17}. Cross-sectional examination took place between 2002 and 2005. The IOP was measured with Goldmann applanation tonometry (Haag-Streit, Bern, Switzerland). IOP was measured twice per eye. If the two measurements in one eye differed, a third measurement was performed, and the median value was recorded. Heidelberg Retina Tomograph 2 was used to measure the VCDR. Details have been described elsewhere¹⁸. All measurements in these studies were conducted after the Medical Ethics Committee of the Erasmus University had approved the study protocols and all participants had given a written informed consent in accordance with the Declaration of Helsinki. DNA was genotyped on one of four different platforms (Illumina 6k, Illumina 318K, Illumina 370K and Affymetrix 250K), which were then merged. Samples with low call rate (<97.5%), with excess autosomal heterozygosity (>0.336), or with sex-mismatch were excluded. A set of genotyped input SNPs with call rate >98%, with MAF >0.01, and with HWE p-value >10⁻⁶ was used for imputation. We used the MACH package version 1.0.18.c software (Rotterdam, The Netherlands; imputed to plus strand of NCBI build 37, 1000 Genomes Phase I version 3) and minimac version 2012.8.15 for the analyses. Association tests were performed using the ProbABEL package¹⁹. GWAS analyses were performed using the ProbABEL package. Mmscore models were used to correct for family structure.

Framingham Family Study (Framingham Heart Study, FHS; Framingham Eye Study, FES)

The Framingham Eye Study²⁰ (FES) was nested within the Framingham Heart Study (FHS, <http://www.framinghamheartstudy.org>), which began its first round of extensive physical examinations in 1948 by recruiting 5,209 men and women from the town of Framingham, MA, USA. Surviving participants from the original cohort returned for biennial exams, which continue to the present. A total of 2675 FHS participants were also examined as part of the FES between 1973 and 1975. The FES was designed to evaluate ocular characteristics of examinees such as: senile cataract; age-related macular disease; glaucoma; and retinopathy. Between 1989 and 1991, 1603 offspring of original cohort participants also received ocular examinations. All data — including IOP, VCDR, demographics and genotypes — were retrieved from the database of Genotypes and Phenotypes (dbGaP, <http://www.ncbi.nlm.nih.gov/gap>) after approval for controlled access to individual-level data. All study protocols are in compliance with the World Medical Association Declaration of Helsinki. Since 1971, written consent has been obtained from participants before each examination. The research protocols of the Framingham Heart Study are reviewed annually by the Institutional Review Board of the Boston University Medical Center and by the Observational Studies Monitoring Board of the National Heart, Lung and Blood Institute.

Genotyping was conducted as part of the NHLBI Framingham SNP Health Association Resource (SHARe). This sub-study contains genotype data for approximately 550000 SNPs (Affymetrix 500K mapping arrays [Mapping250k_Nsp and Mapping250K_Sty] plus Affymetrix 50K supplemental human gene-focused array) in over 9200 FHS participants. Samples were chosen based on pedigree information and genotyping quality; samples with a genotypic call rate below 95% were not chosen for analysis. The mean call rate for analyzed samples was 99.2% (SD=0.4%). Genotype data cleaning was carried-out in several steps. The final marker list contained 436,494 high-quality SNPs with a minor-allele frequency ≥ 0.01 , a Mendelian error rate below 2% across all pedigrees, a genotype call rate above 95%, and whose distribution was consistent with Hardy-Weinberg expectations ($P > 0.0001$). Genotype imputation to the 1000 Genomes Project integrated reference panel (phase 1, version 3) was carried out in a two-step process using SHAPEIT (v2) and IMPUTE (version 2.3.0) software. First, haplotype estimation (pre-phasing) was carried out using SHAPEIT (v2) and 1000 genomes reference haplotypes²¹. Missing 1000 genomes genotypes were then imputed using the pre-phased data and IMPUTE. A total of approximately 11 million variants were successfully imputed. Statistical analyses were conducted with the R statistical software (version 2.7) and the GenABEL (version 1.7-2) and MixABEL (version 0.1-1) packages for linear mixed model association analyses. Linear mixed models included age, sex, and the first three eigenvectors from principal components analyses of genotype data.

IOP measurements were taken using Goldmann Applanation Tonometry (GAT) or (rarely) using Schiottz tonometry in non-ambulatory participants. IOP was taken under topical anesthesia with one drop of a combined proparacaine and fluorescein ophthalmic solution. Only GAT measurements were considered in the analyses. IOP measurements were taken three times and each reading was rated as 'reliable' or 'unreliable' by the examiner. A detailed description of the IOP measurement procedure can be found in the original published FES protocol²⁰. The protocol for the Framingham Offspring eye study is unavailable. This study also used GAT and the protocol appears to have been based on the original FES. The final unilateral IOPs were coded as the mean of all reliable readings in each eye, in millimeters of mercury (mmHg). Unilateral IOPs were truncated (Winsorized) at 40 mmHg. The mean

of both unilateral IOPs were used in the analyses. Individual eyes were excluded if: all readings were unreliable; there was a history or evidence of previous intraocular surgery (including cataract surgery); best-corrected monocular distance visual acuity was 20/200 or worse; and/or if stromal corneal opacities were present. In addition, one participant was excluded because of extreme IOP measurements (76 mmHg) which were subject to the range limitations of GAT.

Details of fundus examination and optic nerve head parameter estimation has been published in the Framingham Eye Study Monograph²⁰. Estimation of cup/disc ratio was performed using a binocular indirect ophthalmoscope and a +14 diopter Nikon lens. The ratio was measured in two meridians, horizontal and vertical. Both were recorded in tenths. The fundus examination was considered adequate if performed through a dilated pupil, and all features of the disc, macula and posterior fundus were seen clearly with the direct ophthalmoscope.

Gutenberg Health Study I and II

The GHS is a population-based, prospective, observational cohort study in the Rhine-Main Region in midwestern Germany with a total of 15,010 participants and follow-up after five years. The study sample is recruited from subjects aged between 35 and 74 years at the time of the exam. The sample was drawn randomly from local governmental registry offices and stratified by gender, residence (urban and rural) and decade of age. Exclusion criteria were insufficient knowledge of the German language to understand explanations and instructions, and physical or psychic inability to participate in the examinations in the study center. The study was approved by the Medical Ethics Committee of the University Medical Center Mainz and by the local and federal data safety commissioners. According to the tenets of the Declaration of Helsinki, written informed consent was obtained from all participants prior to entering the study.

Within GHS, DNA was extracted from buffy-coats from EDTA blood samples as described earlier²². Genetic analysis was conducted in the first 5,000 study participants. For these, 3,463 individuals were genotyped in 2008 (GHS I) and further 1,439 individuals in 2009 (GHS II). Genotyping was performed for GHS I and GHS II using the Affymetrix Genome-Wide Human SNP Array 6.0. Genotypes were called using the Affymetrix Birdseed-V2 calling algorithm. Individuals with a call rate below 97% or a too high autosomal heterozygosity (3 SD from mean) and sex-mismatches were excluded. After applying standard quality criteria (MAF >1%, genotype call rate >98% and p-value of deviation from HWE of >10⁻⁴), 557,988 autosomal SNPs in 2,996 individuals from GHS I and 567,771 autosomal SNPs in 1,179 individuals from GHS II remained for analysis. Imputation of missing genotypes was performed using MACH version 1.0.18.c based on 1000G Phase I Integrated Release Version 2, NCBI Build 37.

All participants underwent an ophthalmological investigation of 25 minutes' duration taking place between 11:00 a.m. and 8:00 p.m. This examination was based on standard operating procedures, including 30° and 45° color photographs by a non-mydratic fundus camera (Visucam PRO NM™, Carl Zeiss Meditec AG, Jena, Germany) centered around the optic nerve head (ONH). The vertical cup to disc ratio, disc area, and cup area were measured semiautomatically with Visupac™ (Carl Zeiss Meditec AG, Jena, Germany). The IOP measurement was performed with a non-contact tonometer with automatic airpuff control (Nidek NT-2000™, Nidek Co., Japan). The mean of three measurements within a range of 3 mmHg was obtained for each eye.

Orkney Complex Disease Study (ORCADES)

The Orkney Complex Disease Study (ORCADES) is a population-based, cross-sectional study in the Scottish archipelago of Orkney, including 1,285 individuals with eye measurements. The study received approval from relevant ethics committees in Scotland and followed the tenets of the Declaration of Helsinki. Informed consent and blood samples were provided by Orcadian volunteers.

IOP was measured with a tonopen. Measures on eyes with a history of trauma were removed and the analysis was done on the average of both eye measures, or on one eye measure only when the fellow-eye measurement was missing. 1111 individuals which had been genotyped and had IOP measurements were used in this analysis. Genome-wide association analysis was performed using the “mmscore” function of ProbABEL under an additive model for the SNP allelic effect. This score test for family based association takes into account relationship structure and allowed unbiased estimations of SNP allelic effect when relatedness is present between examinees. The relationship matrix used in this analysis was generated by the “ibs” function of GenABEL (using weight= “freq” option), which uses genomic data to estimate the realized pair-wise kinship coefficients.

Individuals were genotyped with either the Illumina HumanHap300v2 or 370CNV-Quad beadchips (n=890) or the Illumina Omni1 (n=304) or Illumina OmniExpress beadchips (n=1073). Alleles were called in BeadStudio/GenomeStudio (Hap300/Omni) using Illumina cluster files. Subjects were excluded if they fulfilled any of the following criteria: genotypic call rate <98%, mismatch between reported and genotypic sex, unexpectedly low genomic sharing with first degree relatives, excess autosomal heterozygosity, or outliers identified by IBS clustering analysis. We excluded SNPs on the basis of minor allele frequency (<0.01/monomorphism), HWE ($P < 10^{-6}$), call rate (<97%). Given the very high overlap in SNPs between the two Omni chips, the intersection of QC'd SNPs was used to impute and phase individuals genotyped on the Omni arrays together, whilst the Hap300 individuals were phased and imputed separately. Samples were phased using shapeit v2. Imputation was carried out using impute2 and the 1,000 genomes all ancestries phase1 integrated v3 reference panel, with a secondary reference panel of local exome sequences, sequenced using the Agilent SureSelect All Exon Kit v2.0 and Illumina 100 bp paired end reads (average 30x depth), derived from 90 ORCADES subjects chosen to optimally represent the haplotypes present. Imputations for the Hap300 and Omni subjects were then combined to form a combined panel of 37.5m SNPs for 2222 subjects. The impute2mach GENABEL function was used to convert the impute2 outputs to the MACH format that is used in the ABEL suite (<http://www.genabel.org/packages>).

Raine

The Western Australian Pregnancy Cohort (Raine) Study is an ongoing prospective cohort study of pregnancy, childhood, adolescence and young adulthood in Perth, Western Australia²³. At the initiation of the study, 2,900 pregnant women were recruited at 16-18 weeks' gestation from the state's largest public women's hospital and surrounding private practices for a randomized clinical trial investigating effects of intensive ultrasound and Doppler studies in pregnancy outcomes. Following this study, the offspring of the recruited individuals have been evaluated in detail during childhood and adolescence. At the 20-year review of the cohort, Raine participants underwent a comprehensive ocular examination for the first time²⁴. As part of this examination, IOP was measured using an

Icare TAO1i Tonometer (Icare Finland Oy, Helsinki, Finland) and a baseline glaucoma analysis was done on each participant using the Heidelberg Retina Tomography 3 (Heidelberg Engineering, Heidelberg, Germany). Participant was appropriately positioned in front of the camera and instructed to stare at the flashing light. The position of the camera was adjusted to illuminate and sharpen the image of the optic disc. Poor images were repeated. Each scan was reviewed at the end and the mean standard deviation of less than 20 μm was maintained for quality check.

DNA samples and consents for GWAS studies were available from the previous assessments. Genotype data were generated using the genome-wide Illumina 660 Quad Array at the Centre for Applied Genomics (Toronto, Ontario, Canada). Relatedness filtering based on estimated identity by descent was performed so that no pairs of individuals shared more than 20% of their genome. We also excluded people who had a high degree of missing genotyping data ($> 3\%$). The data were filtered for a HWE p-value $> 1 \times 10^{-6}$, SNP call rate $> 95\%$, and a MAF > 0.01 . GWAS imputation was performed in the MACH v1.0.16 software using the November 23, 2010 version of the 1000 Genome Project European genotyping. This study was approved by the Human Research Ethics Committee of the University of Western Australia.

Rotterdam Study I, II, and III

The Rotterdam Study is a population-based study established in Rotterdam, the Netherlands²⁵. It consists of three cohorts. The original cohort, RS-I, started in 1990 and includes 7,983 subjects aged 55 years and older. The second cohort, RS-II, was added in 2000 and includes 3,011 subjects aged 55 years and older. The last cohort, RS-III, includes 3,932 subjects of 45 years of age and older and started in 2006. In all three cohorts, IOP was measured for both eyes with Goldmann applanation tonometry (Haag-Streit, Bern, Switzerland). The measurement was done twice. If the second measurement was different from the first measurement, a third measurement was performed and the median of all three values was taken. The optic nerve head was assessed with ImageNet (RS-I and RS-II) or Heidelberg Retina Tomograph 2 (RS-III). Details of this assessment have been described elsewhere¹⁸. DNA was isolated from whole blood according to standard procedures. Genotyping of SNPs was performed using the Illumina Infinium II HumanHap550 array (RS-I), the Illumina Infinium HumanHap 550-Duo array (RS-I, RS-II), and the Illumina Infinium Human 610-Quad array (RS-I, RS-III). Samples with low call rate ($< 97.5\%$), with excess autosomal heterozygosity (> 0.336), or with sex-mismatch were excluded, as were outliers identified by the identity-by-state clustering analysis (outliers were defined as being > 3 standard deviation (s.d.) from population mean or having identity-by-state probabilities $> 97\%$). A set of genotyped input SNPs with call rate $> 98\%$, MAF > 0.001 and Hardy-Weinberg Equilibrium (HWE) p-value $> 10^{-6}$ was used for imputation. The Markov Chain Haplotyping (MACH) package version 1.0 software (Rotterdam, The Netherlands; imputed to plus strand of NCBI build 37, 1000 Genomes phase I version 3) and minimac version 2012.8.6 were used for the analysis. GWAS analyses were performed using the ProbABEL package¹⁹. The Rotterdam Study has been approved by the Medical Ethics Committee of the Erasmus MC and by the Ministry of Health, Welfare and Sport of the Netherlands, implementing the “Wet Bevolkingsonderzoek: ERGO (Population Studies Act: Rotterdam Study)”. All participants provided written informed consent to participate in the study and to obtain information from their treating physicians.

Singapore Malay Eye Study (SIMES), Singapore Indian Eye Study (SINDI), and Singapore Chinese Eye Study (SCES)

SIMES is a population-based prevalence survey of Malay adults aged 40 to 79 years living in Singapore that was conducted between August of 2004 and June of 2006²⁶. From a Ministry of Home Affairs random sample of 16,069 Malay adults in the Southwestern area, an age-stratified random sampling strategy was used in selecting 1400 from each decade from age 40 years onward (40–49, 50–59, 60–69, and 70–79 years). The 4,168 eligible participants from the sampling frame, while 3,280 (78.7%) participated. Genome-wide genotyping was performed in 3,072 individuals using the Illumina Human 610 Quad Beadchips^{3,27,28}. After genotyping, we removed a total of 530 individuals including those of subpopulation structure (n=170), cryptic relatedness (n=279), excessive heterozygosity or high missingness rate > 5% (n=37), and gender discrepancy (n=44). After the removal of these samples, SNP QC was then applied on a total of 579,999 autosomal SNPs for the 2,542 post-QC samples. SNPs were excluded based on (i) high rates of missingness (>5 %) (ii) monomorphism or MAF <1%; or (iii) genotype frequencies deviated from HWE ($P < 1 \times 10^{-6}$), leaving 557,824 autosomal SNPs for analysis.

SINDI is a population-based survey of major eye diseases in ethnic Indians aged 40 to 80 years living in the South-Western part of Singapore and was conducted from August 2007 to December 2009²⁹. In brief, 4,497 Indian adults were eligible and 3,400 participated. Genome-wide genotyping was performed in 2,953 individuals²⁷. The Illumina Human610 Quad Beadchips was used for genotyping all DNA samples from SINDI (n=2,593). We excluded 415 subjects from the total of 2,953 genotyped samples based on: excessive heterozygosity or high missingness rate >5% (n=34), cryptic relatedness (n=326), issues with population structure ascertainment (n=39) and gender discrepancies (n=16). This left a total of 2,538 individuals with 579,999 autosomal SNPs. During SNP QC procedure, SNPs were excluded based on the same (i) high rates of missingness (>5%); (ii) monomorphism or MAF <1%; or (iii) genotype frequencies deviated from HWE ($p < 1 \times 10^{-6}$), leaving 559,119 SNPs for analysis.

Similar to SINDI, the SCES is a population-based cross-sectional study of eye diseases in Chinese adults 40 years of age or older residing in the southwestern part of Singapore. The methodology of the SCES study has been described in detail previously²⁹. Between 2009 and 2011, 3,353 (72.8%) of 4,605 eligible individuals underwent a comprehensive ophthalmologic examination, using the same protocol as SINDI. Genome-wide genotyping using was done in a subset of SCES participants using Illumina Human610-Quad BeadChip 38 (n=1,952) and Illumina OmniExpress (n = 635). From a starting number of 1,952 individuals genotyped by Illumina OmniExpress, three samples failed when being loaded into Beadstudio. Samples were excluded if they had missingness > 5% (n=8) or excessive heterozygosity (n=11), cryptic relatedness (41), evidence of admixture or genetic outlier, high heterogeneity and gender discrepancies (n=2). SNP QC was then performed on 579,999 autosomal SNPs following similar criteria as in SIMES and SINDI. This left 538,408 SNPs on 1,889 samples for analysis. For those samples genotyped by Illumina OmniExpress, using the sample QC criteria, samples were removed due to samples were removed due to missingness >5% and unusual heterozygosity (n=10), cryptic relatedness (7), evidence of genetic outlier (n=1), and gender gender discrepancies (n=2). SNP QC was performed on 690,511 autosomal SNPs following similar criteria as above. This left 633,783 SNPs on 615 samples for analysis.

IOP readings were obtained by Goldmann applanation tonometry (Haag-Streit, König, Switzerland) before pupil dilation in for SIMES, SINDI and SCES. Optic discs were assessed using slit-lamp biomicroscopy with 78 D lens at X16 magnification, with measuring graticule after pupil dilation. Optic nerve head was also evaluated using Heidelberg Retina Tomography 2 (HRT 2), as previously described^{30,31}.

For all studies, imputation was performed using the genotyped data passed the quality control filtering, together with the 1000 genomes phase 1 cosmopolitan panel haplotypes (March 2012 release). The Markov Chain Haplotyping software was used in the imputation procedure (Minimac software, <http://genome.sph.umich.edu/wiki/Minimac>).

All three studies adhere to the Declaration of Helsinki. Ethics approvals have been obtained from the Institutional Review Boards of the Singapore Eye Research Institute Singapore. In all cohorts, participants provided written, informed consent at the recruitment into the studies.

TwinsUK

The TwinsUK adult twin registry based at St. Thomas' Hospital in London is a volunteer cohort of over 10,000 twins from the general population³². Twins largely volunteered unaware of the eye studies, gave fully informed consent under a protocol reviewed by the St. Thomas' Hospital Local Research Ethics Committee. Out of the original 1,951 subjects for whom phenotype and genotype information was available, 1,922 subjects were included in the study; 29 subjects were excluded after failing quality control. Genotyping was carried out using three genotyping platforms from Illumina: the HumanHap 300k Duo for part of the UK Twin Cohort and the HumanHap610-Quad array for the rest of the UK Twin Cohort. Genotype imputation was done after pre-phasing (using Shapelt software) with reference to the complete 1000 genomes Phase I integrated variant set haplotypes (March 2012) using IMPUTE version 2. Individuals were included if their genotyping success rate exceeded 95%, did not show excess or low heterozygosity (defined by the interval of 0.2-04). We measured IOP with a non-contact air-puff tonometer. The Ocular Response Analyser (ORA, Reichert®, Buffalo, NY) ejects an air impulse in order to flatten the cornea, which is detected by an electro-optical collimation system. The mean IOP was calculated from 4 readings (2 from each eye) for each participant. IOP for subjects receiving IOP-lowering medications (26 out of 2774) was imputed by increasing the measured value by 30%, based on efficacy data from commonly prescribed therapies. Optic disc parameters in the subjects was measured from stereo disc photographs using the Nidek-3DX stereo camera, with digitized images scanned from Polaroid images and StereoDx stereoscopic planimetric software (StereoDx) using a Z-screen (StereoGraphics Corp) and software obtained from James Morgan from Cardiff University software, Wales, UK³³.

POAG case-control studies

Australian & New Zealand Registry of Advanced Glaucoma

ANZRAG recruits cases of advanced glaucoma Australia-wide through ophthalmologist referral. The cohort also included participants enrolled in the Glaucoma Inheritance Study in Tasmania (GIST) who met the criteria for ANZRAG. This cohort has been described previously³⁴. Advanced POAG was defined as best-corrected visual acuity worse than 6/60 due to POAG, or a reliable 24-2 Visual Field with a mean deviation of worse than -22db or at least 2 out of 4 central fixation squares affected with a Pattern Standard Deviation of < 0.5%. The less severely affected eye was also required to have signs of glaucomatous disc damage.

Clinical exclusion criteria for this advanced POAG study were: i) pseudoexfoliation or pigmentary glaucoma, ii) angle closure or mixed mechanism glaucoma; iii) secondary glaucoma due to aphakia, rubella, rubeosis or inflammation; iv) infantile glaucoma, v) glaucoma in the presence of a known associated syndrome. The ANZRAG cohort included 1,155 ANZRAG glaucoma cases and 1,992 controls genotyped on Illumina Omni1M or OmniExpress arrays and imputed against 1000 Genomes Phase 1 Europeans. The case set included all samples from the previously published GWAS³⁴. Controls were drawn from the Australian Cancer Study (225 oesophageal cancer cases, 317 Barrett's oesophagus cases and 552 controls) or from a study of inflammatory bowel diseases (303 cases and 595 controls). The quality control methods were performed in PLINK by removing individuals with more than 3% missing genotypes, SNPs with call rate <97%, MAF < 0.01 and HWE p-value < 0.0001 in controls and HWE p-value < 5×10^{-10} in cases³⁵. The same quality control protocol was used before merging the cases and controls to avoid mismatches between the merged data sets. After merging, the genotypes for 569,249 SNPs common to the arrays were taken forward for analysis. Relatedness filtering based on estimated identity by descent was performed so that no pairs of individuals shared more than 20% of their genome. Principal components were computed for all participants and reference samples of known northern European ancestry (1000G British, CEU and Finland participants) using the smartpca package from EIGENSOFT software^{36,37}. Participants with principal component 1 or 2 values >6 s.d. from the known northern European ancestry group were excluded. Imputation was conducted using IMPUTE2 in 1-Mb sections, with the 1000 Genomes phase 1 Europeans (March 2012 release) used as the reference panel^{7,8}. SNPs with imputation quality score >0.8 and MAF > 0.01 were carried forward for analysis. Association testing on the imputed data was performed in SNPTEST _v2.5-beta3 using an additive model (-frequentist 1) and full dosage scores (-method expected) with sex and the first six principal components fitted as covariates^{9,10}. All were Australians of European ancestry. Approval was obtained from the Human Research Ethics Committees of Southern Adelaide Health Service/Flinders University, University of Tasmania, QIMR Berghofer Institute of Medical Research (Queensland Institute of Medical Research) and the Royal Victorian Eye and Ear Hospital.

NEIGHBORHOOD (National Eye Institute (NEI) Glaucoma Human Genetics Collaboration Heritable Overall Operational Database)

The NEIGHBORHOOD dataset is the meta-analysis of imputed GWAS summary data for 8 independent studies (total sample = 3,853 cases and 33,480 controls)³⁹⁻⁴⁰. The study was approved by the Massachusetts Eye and Ear Infirmary institutional review board and all subjects signed consent forms approved by the local IRB prior to enrolling in the study. For all enrollees, primary open angle glaucoma (POAG) cases were defined as individuals for whom reliable visual field (VF) tests show characteristic VF defects consistent with glaucomatous optic neuropathy. Individuals were classified as affected if the VF defects were reproduced on a subsequent test or if a single qualifying VF was accompanied by a cup-disc ratio (CDR) of 0.7 or more in at least one eye. For some cases VFs were not reliable and these cases had either CDR > 0.7 in both eyes or a difference in CDR of at least 0.2 between the eyes. In the OHTS study (one of the 8 NEIGHBORHOOD datasets) an alternative case definition based on progression of optic nerve degeneration was also used⁴⁰. Patients with clinical features of secondary glaucoma based on the examination of the ocular anterior segment were excluded from this study. Elevation of IOP was

not a criterion for inclusion; however, 67% of cases did have a history of elevated IOP (≥ 22 mm Hg) measured in a clinical setting (typically between the hours of 8AM and 5PM) and were classified as high-pressure glaucoma (HPG). For all datasets genome-wide genotypes were obtained from either Illumina or Affymetrix platforms. For each dataset, site-specific quality control (sample and genotype call rates $\geq 95\%$), principal components analysis (EIGENSTRAT), and imputation (IMPUTE2 or MACH) were completed using the 1000 Genomes Project reference panel (March 2012). Imputed variants with minor allele frequencies $< 5\%$ or imputation quality scores (r^2) < 0.7 were removed prior to analysis. Dosage data, in the form of estimated genotypic probabilities, were analyzed in ProbABEL for each dataset using logistic regression models, adjusting for age, sex, any significant eigenvectors and study-specific covariates. Genomic inflation was less than 1.05 (λ -value) for each individual dataset. Estimated genotypic probabilities for 6,425,680 variants were meta-analyzed in METAL using the inverse variance weighted method.

SINGAPORE

POAG including NTG patients were from the Singapore National Eye Center glaucoma clinics. Ethical approval for the collection of patient information and blood samples was provided by the local institutional ethics review committee (CIRB) and study was conducted in accordance with revised Declaration of Helsinki. Patients with POAG over the age of 40 years old were recruited. Patients with POAG were defined by the following criteria: the presence of glaucomatous optic neuropathy (defined as a loss of neuroretinal rim with a vertical cup: disc ratio of > 0.7 or an inter-eye asymmetry of > 0.2 , and/ or notching attributable to glaucoma) with compatible visual field loss, open angles on gonioscopy, and absence of secondary causes of glaucomatous optic neuropathy. Diurnal IOP measurements were recorded hourly between 8.00 am to 5.00 pm with non-contact air puff tonometry (Topcon CT-80 Computerized Non-Contact Tonometer, Topcon). Patients were excluded if they were unable to give informed consent or had either neurological/retinal disease that had visual field sequelae, or secondary glaucoma (such as pigmentary, uveitic, neovascular or post-traumatic).

1224 Singaporean Chinese POAG patients were recruited under the above criteria, and their genomic DNA samples were genotyped using the Illumina Human OmniExpress Beadchips. 1037 cases passed quality control filters and were brought forward for downstream analyses. Controls were ascertained from an on-going population based study of Chinese persons aged 40 years and older (SCES)²⁹. 2587 SCES samples were genotyped with Illumina Human OmniExpress or Human610-Quad BeadChips. 2543 that passed quality check were used in subsequent genetic analyses. The imputation and phasing of genotypes were carried out using IMPUTE2 (http://mathgen.stats.ox.ac.uk/impute/impute_v2.html) with cosmopolitan population haplotypes based on data from 2535 individuals from 26 distinct populations around the world obtained from the 1000 Genomes project Phase 3 (Jun 2014) release for reference panel construction. Imputed genotypes were called with impute probability thresholds of 0.90 with all other genotypes classified as missing. Additional quality control filters were applied to remove SNPs with a call rate of $< 99\%$ should the SNP have a minor allele frequency (MAF) below 5% in either cases or controls. For common SNPs with MAF above 5%, the exclusion filtering criteria were set at less than 95% call rate.

Southampton

Primary open-angle (POAG) and normal tension glaucoma patients were recruited from the Southampton University Hospital Trust Eye Clinic and satellite regional glaucoma clinics. Ethical approval for the collection of patient information and blood samples was provided by the Southampton and South West Hampshire Local Research Ethics Committee (05/Q1702/8) and Cohort Recruitment commenced in August 2005. Each patient was examined by an experienced glaucoma specialist. Diagnoses were made on the basis of characteristic visual field loss/glaucomatous optic disc damage/increased IOP. Patients presenting with narrow-angle, developmental or secondary glaucoma or any other known abnormalities of the anterior segment were excluded. Patients with unambiguous glaucoma, but normal tension were included in sample collection later. Furthermore, to select for patients with typical POAG or normal-tension glaucoma (NTG), only patients diagnosed over the age of 40 years were included. Both conditions are rare before this age. DNA was extracted according to the standard methods, dissolved in TE buffer, and stored at -20°C. Primary open angle glaucoma patients (n=400) were genotyped on the Affymetrix SNP 6.0 array, all data were exported on the forward strand. These data were combined with the Affymetrix SNP 6.0 data publically available for the WTCCC2 controls. The Genome-wide association data previously described⁴¹ was further filtered to ensure removal of individuals with more than 5% missing genotypes, SNPs with more than 3% missing samples, SNPs with a minor allele frequency of <1% and a Hardy-Weinberg p-value < 1×10^{-6} . SNPs were all on the forward strand and locations were lifted over from hg18 to hg19 using the UCSC liftover tool. SNPs with complementary alleles were also excluded (A/T and G/C).

The data used for imputation included 384 cases and 3389 controls, and 533,774 SNPs. Pre-phasing was carried out using Shapeit (v2, r790) and imputation was carried out using Impute2 (v2.3.1), using 1000 Genomes Phase I integrated haplotypes (produced using SHAPEIT2), b37 Dec 2013, downloaded from the impute2 website. Imputation was carried out over the genome in 5Mb chunks as per the best practices on the impute2 website. The imputed data was then converted to plink format using GTOOL. Case-control analysis was carried out using logistic regressions for the selected replication SNPs and Indels with sex as a covariate, using PLINK (v1.90b3b 64-bit (15 Jan 2015)).

References

- Xu, L. et al. Visual acuity in northern China in an urban and rural population: the Beijing Eye Study. *Br J Ophthalmol* 89, 1089-93 (2005).
- Xu, L., Zhang, H., Wang, Y.X. & Jonas, J.B. Central corneal thickness and glaucoma in adult Chinese: the Beijing Eye Study. *J Glaucoma* 17, 647-53 (2008).
- Cornes, B.K. et al. Identification of four novel variants that influence central corneal thickness in multi-ethnic Asian populations. *Hum Mol Genet* 21, 437-45 (2012).
- Mitchell, P., Smith, W., Attebo, K. & Wang, J.J. Prevalence of age-related maculopathy in Australia. The Blue Mountains Eye Study. *Ophthalmology* 102, 1450-60 (1995).
- van Koolwijk, L.M. et al. Major genetic effects in glaucoma: commingling analysis of optic disc parameters in an older Australian population. *Invest Ophthalmol Vis Sci* 50, 5275-80 (2009).
- Conrad, D.F. et al. Origins and functional impact of copy number variation in the human genome. *Nature* 464, 704-12 (2010).
- Howie, B.N., Donnelly, P. & Marchini, J. A flexible and accurate genotype imputation method for the next generation of genome-wide association studies. *PLoS Genet* 5, e1000529 (2009).
- Howie, B., Marchini, J. & Stephens, M. Genotype imputation with thousands of genomes. *G3 (Bethesda)* 1, 457-70 (2011).
- Marchini, J. & Howie, B. Genotype imputation for genome-wide association studies. *Nat Rev Genet* 11, 499-511 (2010).
- Wellcome Trust Case Control, C. Genome-wide association study of 14,000 cases of seven common diseases and 3,000 shared controls. *Nature* 447, 661-78 (2007).
- Mackey, D.A. et al. Twins eye study in Tasmania (TEST): rationale and methodology to recruit and examine twins. *Twin Res Hum Genet* 12, 441-54 (2009).
- Riboli, E. & Kaaks, R. The EPIC Project: rationale and study design. *European Prospective Investigation into Cancer and Nutrition. Int J Epidemiol* 26 Suppl 1, S6-14 (1997).
- Day, N. et al. EPIC-Norfolk: study design and characteristics of the cohort. *European Prospective Investigation of Cancer. Br J Cancer* 80 Suppl 1, 95-103 (1999).
- Hayat, S.A. et al. Cohort profile: A prospective cohort study of objective physical and cognitive capability and visual health in an ageing population of men and women in Norfolk (EPIC-Norfolk 3). *Int J Epidemiol* 43, 1063-72 (2014).
- Khawaja, A.P. et al. The EPIC-Norfolk Eye Study: rationale, methods and a cross-sectional analysis of visual impairment in a population-based cohort. *BMJ Open* 3(2013).
- Aulchenko, Y.S. et al. Linkage disequilibrium in young genetically isolated Dutch population. *Eur J Hum Genet* 12, 527-34 (2004).
- Pardo, L.M., MacKay, I., Oostra, B., van Duijn, C.M. & Aulchenko, Y.S. The effect of genetic drift in a young genetically isolated population. *Ann Hum Genet* 69, 288-95 (2005).
- Ramdas, W.D. et al. A genome-wide association study of optic disc parameters. *PLoS Genet* 6, e1000978 (2010).
- Aulchenko, Y.S., Struchalin, M.V. & van Duijn, C.M. ProbABEL package for genome-wide association analysis of imputed data. *BMC Bioinformatics* 11, 134 (2010).
- Leibowitz, H.M. et al. The Framingham Eye Study monograph: An ophthalmological and epidemiological study of cataract, glaucoma, diabetic retinopathy, macular degeneration, and visual acuity in a general population of 2631 adults, 1973-1975. *Surv Ophthalmol* 24, 335-610 (1980).
- O'Connell, J. et al. A general approach for haplotype phasing across the full spectrum of relatedness. *PLoS Genet* 10, e1004234 (2014).
- Zeller, T. et al. Genetics and beyond--the transcriptome of human monocytes and disease susceptibility. *PLoS One* 5, e10693 (2010).
- McKnight, C.M. et al. Birth of a cohort--the first 20 years of the Raine study. *Med J Aust* 197, 608-10 (2012).
- Yazar, S. et al. Raine Eye Health Study: Design, Methodology and Baseline Prevalence of Ophthalmic Disease in a Birth-cohort Study of Young Adults. *Ophthalmic Genet* (2013).
- Hofman, A. et al. The Rotterdam Study: 2014 objectives and design update. *Eur J Epidemiol* 28, 889-926 (2013).
- Foong, A.W. et al. Rationale and methodology for a population-based study of eye diseases in Malay people: The Singapore Malay eye study (SiMES). *Ophthalmic Epidemiol* 14, 25-35 (2007).
- Khor, C.C. et al. Genome-wide association studies in Asians confirm the involvement of ATOH7 and TGFBR3, and further identify CARD10 as a novel locus influencing optic disc area. *Hum Mol Genet* 20, 1864-72 (2011).
- Vithana, E.N. et al. Collagen-related genes influence the glaucoma risk factor, central corneal thickness. *Hum Mol Genet* 20, 649-58 (2011).
- Lavanya, R. et al. Methodology of the Singapore Indian Chinese Cohort (SICC) eye study: quantifying ethnic variations in the epidemiology of eye diseases in Asians. *Ophthalmic Epidemiol* 16, 325-36 (2009).
- Zheng, Y. et al. Influence of diabetes and diabetic retinopathy on the performance of Heidelberg retina tomography II for diagnosis of glaucoma. *Invest Ophthalmol Vis Sci* 51, 5519-24 (2010).

31. Zheng, Y. et al. Diagnostic ability of Heidelberg Retina Tomography in detecting glaucoma in a population setting: the Singapore Malay Eye Study. *Ophthalmology* 117, 290-7 (2010).
32. Spector, T.D. & Williams, F.M. The UK Adult Twin Registry (TwinsUK). *Twin Res Hum Genet* 9, 899-906 (2006).
33. Morgan, J.E., Sheen, N.J., North, R.V., Choong, Y. & Ansari, E. Digital imaging of the optic nerve head: monoscopic and stereoscopic analysis. *Br J Ophthalmol* 89, 879-84 (2005).
34. Burdon, K.P. et al. Genome-wide association study identifies susceptibility loci for open angle glaucoma at TMCO1 and CDKN2B-AS1. *Nat Genet* 43, 574-8 (2011).
35. Purcell, S. et al. PLINK: a tool set for whole-genome association and population-based linkage analyses. *Am J Hum Genet* 81, 559-75 (2007).
36. Patterson, N., Price, A.L. & Reich, D. Population structure and eigenanalysis. *PLoS Genet* 2, e190 (2006).
37. Price, A.L. et al. Principal components analysis corrects for stratification in genome-wide association studies. *Nat Genet* 38, 904-9 (2006).
38. Wiggs, J.L. et al. The NEIGHBOR consortium primary open-angle glaucoma genome-wide association study: rationale, study design, and clinical variables. *J Glaucoma* 22, 517-25 (2013).
39. Wiggs, J.L. et al. Common variants at 9p21 and 8q22 are associated with increased susceptibility to optic nerve degeneration in glaucoma. *PLoS Genet* 8, e1002654 (2012).
40. Feuer, W.J. et al. The Ocular Hypertension Treatment Study: reproducibility of cup/disk ratio measurements over time at an optic disc reading center. *Am J Ophthalmol* 133, 19-28 (2002).
41. Gibson, J. et al. Genome-wide association study of primary open angle glaucoma risk and quantitative traits. *Mol Vis* 18, 1083-92 (2012).

PART 5

**FUNCTIONAL
CONSEQUENCES OF
GENETIC VARIANTS**

CHAPTER 5.1

Exome sequencing and functional analyses suggest *SIX6* is a gene involved in an altered proliferation-differentiation balance early in life and optic nerve degeneration at old age



Adriana I. Iglesias, Henriët Springelkamp, Herma van der Linde, Lies-Anne Severijnen, Najaf Amin, Ben Oostra, Christel E.M. Kockx, Mirjam C.G.N. van den Hout, Wilfred F. J. van IJcken, Albert Hofman, André G. Uitterlinden, Rob M. Verdijk, Caroline C.W. Klaver, Rob Willemsen and Cornelia M. van Duijn.

Hum Mol Genet. 2014 Mar 1;23(5):1320-32. doi: 10.1093/hmg/ddt522

Supplementary files and figures can be found at:

<http://hmg.oxfordjournals.org/content/23/5/1320.long>

ABSTRACT

Primary open-angle glaucoma (POAG) is a hereditary neurodegenerative disease, characterized by optic nerve changes including increased excavation, notching and optic disc haemorrhages. The excavation can be described by the vertical cup-disc ratio (VCDR). Previously, genome-wide significant evidence for the association of rs10483724 in *SIX1-SIX6* locus with VCDR and subsequent POAG was found. Using 1000 genomes-based imputation of 4 independent population-based cohorts in the Netherlands, we identified a missense variant rs33912345 (His141Asn) in *SIX6* associated with VCDR ($P_{\text{meta}}=7.74\times 10^{-7}$; n=11,473) and POAG ($P_{\text{meta}}=6.09\times 10^{-3}$; n=292). Exome sequencing analysis revealed another missense variant rs146737847 (Glu129Lys) also in *SIX6* associated with VCDR ($P=5.09\times 10^{-3}$; n=1,208). These two findings point to *SIX6* as the responsible gene for the previously reported association signal. Functional characterization of *SIX6* in zebrafish revealed that knockdown of *six6b* led to a small eye phenotype. Histological analysis showed retinal lamination, implying an apparent normal development of the eye, but an underdeveloped lens and reduced optic nerve diameter. Expression analysis of morphants at 3dpf showed a 5.5-fold up-regulation of *cdkn2b*, a cyclin-dependent kinase inhibitor, involved in cell cycle regulation and previously associated with VCDR and POAG in genome-wide association studies. Since both *six6b* and *cdkn2b* play a key role in cell proliferation, we assessed the proliferative activity in eye of morphants and found an alteration of the proliferative pattern of retinal cells. Our findings in humans and zebrafish suggest a functional involvement of *six6b* in early eye development, and open new insights into the genetic architecture of POAG.

INTRODUCTION

Primary open-angle glaucoma (POAG) is a neurodegenerative disease¹ characterized by loss of retinal ganglion cells, optic nerve degeneration, and as a consequence, visual field loss and eventually blindness. It is recognized as a complex disease in which multiple genetic and environmental factors interact²⁻⁴. Known risk factors include age, race, myopia, high intraocular pressure (IOP), decreased central corneal thickness and positive family history¹. First degree relatives of affected individuals are estimated to have a 10-fold increased risk of POAG compared to the general population⁵. Heritability estimates of related quantitative traits as disc area (DA), vertical cup-disc ratio (VCDR), IOP and central corneal thickness are high (52-59%; 48-80%; 35-42% and 68-72%, respectively⁶⁻⁹).

Developments in the field of genomics have opened opportunities to uncover the genetic mechanisms involved in POAG. To date, at least 20 genetic loci have been linked to POAG, including 3 causative genes (*MYOC*, *OPTN*, *WDR36*)¹⁰⁻¹². In addition, genome-wide association studies (GWAS) have allowed the identification of candidate genes, such as *CAV1/CAV2*^{13,14} which are expressed in the trabecular meshwork as well as in retinal ganglion cells, and *TMCO1* which is also expressed in retinal ganglion cells¹⁵.

As in other disorders, GWAS of POAG have targeted on endophenotypes, i.e., heritable quantitative determinants of POAG. This approach has facilitated the identification of genes that were subsequently implicated in POAG. Three of the six loci that have been associated with neurodegeneration of the optic nerve (VCDR)¹⁶ were also associated with POAG¹⁷. The strongest associations were seen for the single nucleotide polymorphism (SNPs) rs1900004, within 10kb of the *ATOH7* gene; the rs10483727 near *SIX1-SIX6* genes; and the rs1063192, in the 3'UTR region of *CDKN2B* gene.

Two of these variants point to pathways involved in growth and development of the optic nerve. *ATOH7* and *SIX1-SIX6* genes are transcription factors involved in eye development¹⁸⁻²². The role of *ATOH7* in eye development and retinal ganglion cell differentiation has been well characterized in several animal models¹⁸⁻²⁰. *SIX1* and *SIX6* are homeoproteins members of the *SIX/sine oculis* family of homeobox transcription factors²². *SIX1* is highly expressed in skeletal muscle²³ and has been involved in myogenesis²⁴, while *SIX6* is highly expressed in the developing eye^{25,26}. To date, it is not clear which one of the two genes is causally related to optic nerve degeneration and POAG, asking for a more in-depth analysis of the *SIX1-SIX6* region.

The protein encoded by *CDKN2B* gene, the third POAG gene identified by GWAS of VCDR, has emerged as a key protein in the pathogenesis of optic nerve degeneration and POAG in different populations^{15-17,27-33}. *CDKN2B* gene is member of the family of cyclin-dependent kinases (CDK) inhibitors which play a role in cell cycle regulation, influencing the proliferation/differentiation balance³⁴. In the *Six6* null mice it was demonstrated that *Six6* repress the transcription of members of the *Cdkn1* family, particularly *Cdkn1b*³⁵. Therefore, it may be speculated that the *SIX1-SIX6* region is potentially related to the *CDKN2B* regulation, although this has not been described.

In this study, we investigated the *SIX1-SIX6* locus in depth in human and zebrafish. First, we fine-mapped the region and performed a conditional, and exome sequencing analysis. As we found two variants that pointed to *SIX6* as best candidate gene, we next characterized the effect of *six6b* knockdown on eye development of zebrafish and evaluated expression levels of several target genes in morphants, including *cdkn2b*.

RESULTS

Fine-mapping of *SIX1-SIX6* region

The results of the analyses in the Rotterdam Study (RS) and the Erasmus Rucphen Family (ERF) study are shown in Table 1. The IOP analysis included 5,782 (RS-I), 2,116 (RS-II), 2,038 (RS-III) and 2,589 (ERF) participants. The optic nerve head analyses included 5,322 (RS-I), 2,054 (RS-II), 1,966 (RS-III) and 2,131 (ERF) participants with reliable data. The case-control studies consisted of 188 cases and 5,548 controls from the RS-I and 104 cases and 2,126 controls from the GRIP/ERF study.

Fine-mapping of the *SIX1-SIX6* region based on imputations of the SNPs using 1000 Genomes Project revealed a missense variant rs33912345 in *SIX6*, this variant is in complete linkage disequilibrium with the previous reported intergenic variant rs10483727 (the two D' and $r^2 = 1$). Both the rs10483727 and the missense variant in *SIX6* rs33912345 were associated with VCDR ($P_{\text{meta}} = 5.56 \times 10^{-7}$ and 7.74×10^{-7} , respectively), DA ($P_{\text{meta}} = 1.69 \times 10^{-3}$ and 3.51×10^{-3} , respectively) and POAG ($P_{\text{meta}} = 6.09 \times 10^{-3}$ and 2.95×10^{-3} , respectively) (see Table 1). The significant association between rs10483727 and VCDR disappeared after adjustment for rs33912345 ($P_{\text{meta}} = 8.72 \times 10^{-1}$), indicating that the *SIX6* variant is most likely responsible for the association. This variant determines an amino acid change (His141Asn) in the homeobox DNA-binding domain of *SIX6*. PolyPhen-2 predicted a benign effect (score=0) for this evolutionarily conserved variant³⁶, based on the Genomic Evolutionary Rate Profiling (GERP)³⁷ score= 5.38. No significant association was found with variants in *SIX1*.

Exome sequencing of *SIX1-SIX6* region

To determine whether there were other unobserved rare variants in *SIX6*, we explored the presence of exonic variants associated with VCDR in this region. In exome sequence data from 1,208 individuals of the ERF study, we found another missense variant, rs146737847 (MAF=0.0023) in *SIX6* ($P = 1.25 \times 10^{-3}$). This evolutionarily conserved variant (GERP= 5.38) determines an amino acid change (Glu129Lys) in the homeobox DNA-binding domain of *SIX6*, which PolyPhen-2 predicted as probably damaging (score =0.971). When conducting a conditional analysis on rs33912345, the rs146737847 variant remained associated with VCDR ($P = 4.58 \times 10^{-3}$), confirming that both variants are independent of each other. Direction of the effect of both variants was the same; rs33912345 (beta= 0.011, se= 0.002) and rs146737847 (beta=0.183, se=0.055). No exonic variants in *SIX1* were significantly associated with VCDR.

eQTL and expression analyses

No significant cis or trans eQTLs effects for rs10483727, rs33912345 or rs14673784 were found in the GTEx project database³⁸. The Ocular Tissue Database³⁹ was used to compare the expression levels of *SIX1* and *SIX6* in different human ocular tissues. We found that *SIX6*

is highly expressed in relevant tissues for POAG, including cornea, optic nerve, trabecular meshwork and retina compared with *SIX1* (PLIER number 27.33 vs 9.65; 22.25 vs 18.32; 25.80 vs 15.43 and 26.08 vs 14.73; respectively).

Exclusion of an eQTL effect of the evaluated SNPs on the gene expression of *SIX1* or *SIX6*, together with the fine-mapping and exome sequencing data suggest that the variants in *SIX6* rather than *SIX1* explain the observed association signal reported in previous studies in the region.

Identification and characterization of zebrafish *six6b*

A zebrafish *six6* ortholog was retrieved from the Ensemble database. Two genes were found, *six6a* and *six6b*. The protein encoded by *six6a* together with the protein encoded by *six6b* were blasted against the human *SIX6* protein, showing that *six6a* and *six6b* independently have 91% identity to the human *SIX6*, while the overall identity of both zebrafish *six6* to the human protein is 88% (Supplementary figure S1). In this study we evaluated the effect of *six6b* depletion.

To evaluate the role of *six6b* at different time points of the development, quantitative reverse transcription PCR (RT-qPCR) was performed. Taking reference expression levels at 1day post fertilization, we found that over time expression of *six6b* gradually increases, reaching a peak at the larvae stage of 3dpf, then decreasing at 5dpf (Figure 3 A).

six6b is required for normal eye development in zebrafish

To evaluate the function of *six6b* during embryonic development, two non-overlapping antisense MOs were designed, the first one targeting the AUG translation initiation site (*six6b* AUG-MO) and the other targeting the exon1/intron1 splice site (*six6b* SB-MO). Since embryos injected with either *six6b* AUG-MO or *six6b* SB-MO developed similar dose-dependent (2-12 ng) small eye size compared with controls, the *six6b* SB-MO (6ng) was selected for further studies as it provided the possibility to quantify the efficiency of knockdown by RT-qPCR. Embryos injected with the highest concentration of the MOs (12ng) showed a severe phenotype (twisted trunk, small head and eye, massive heart edema and lethality at ~4dpf, data not shown).

Eye size difference between injected and control embryos was quantified at 5dpf since the phenotype is then well defined and easy to evaluate (Figure 1 A). 78% of the injected embryos showed a small eye phenotype (n=286). RT-qPCR analysis indicated *six6b* SB-MO reduced *six6b* mRNA levels by 70% (Supplementary figure S2). To elucidate whether morphants showed small eye phenotype secondary to *six6b* knockdown as opposed to an overall delay in development, we measured the ratio of the eye size to body length (E:B) 40. The E:B ratio was measured in 30 embryos of each group (Figure 1 B). Morphants showed small eyes compared with controls, suggesting an eye development delay (mean E:B=0.064 vs 0.092, $P=4.96 \times 10^{-20}$). Other abnormalities were observed as pericardial edema, diffuse pigmentation that resembles an expanded melanophore phenotype, small head, and in some embryos short jaw. To exclude the presence of small head as principal cause of a small eye, we measured the ratio of the eye size to head length (E:H) in ~30 embryos of each group (i.e. wild-type, *six6b* SB-MO injected, and *six6b* SB-MO + *p53*-MO co injected). This measure

Table 1. Evidence of association of *SIX6* with VCDR and POAG in RS and ERF.

SNP	RS-I					RS-II				
	MA	MAF	β	SE	P-value	MAF	β	SE	P-value	
IOP (~ age, sex, PC1, PC2)										
rs33912345	C	0.41	0.034	0.064	5.8×10^{-1}	0.40	-0.039	0.096	6.8×10^{-1}	
rs10483727	T	0.41	0.035	0.064	5.8×10^{-1}	0.40	-0.037	0.096	7.0×10^{-1}	
DA (~ age, sex, PC1, PC2)										
rs33912345	C	0.41	-0.02	0.009	3.2×10^{-2}	0.40	-0.031	0.015	3.4×10^{-2}	
rs10483727	T	0.41	-0.02	0.009	2.7×10^{-2}	0.40	-0.033	0.015	2.6×10^{-2}	
VCDR (~ age, sex, PC1, PC2)										
rs33912345	C	0.41	0.013	0.003	4.2×10^{-7}	0.40	0.008	0.004	4.5×10^{-2}	
rs10483727	T	0.41	0.013	0.003	3.1×10^{-7}	0.40	0.009	0.004	3.1×10^{-2}	
VCDR (~ age, sex, PC1, PC2, spherical equivalent)										
rs33912345	C	0.41	0.013	0.003	2.9×10^{-7}	0.40	0.009	0.004	2.6×10^{-2}	
rs10483727	T	0.41	0.013	0.003	2.2×10^{-7}	0.40	0.010	0.004	1.8×10^{-2}	
VCDR (~ age, sex, PC1, PC2, rs33912345)										
rs10483727	T	0.41	0.000	0.003	9.3×10^{-1}	0.40	0.001	0.004	8.7×10^{-1}	
POAG (~ age, sex, PC1, PC2)										
rs33912345	C	0.41	0.252	0.106	1.8×10^{-2}	NA	NA	NA	NA	
rs10483727	T	0.41	0.246	0.106	2.0×10^{-2}	NA	NA	NA	NA	

ABBREVIATIONS

DA disc area**ERF** Erasmus Rucphen Family**IOP** intraocular pressure**MA** minor allele**MAF** minor allele frequency**NA** not applicable

Table 1. (continued)

RS-III				ERF				Meta-analysis		
MAF	β	SE	P-value	MAF	β	SE	P-value	β	SE	P-value
0.39	-0.070	0.093	4.5×10^{-1}	0.45	-0.251	0.087	4.1×10^{-3}	-0.062	0.041	1.3×10^{-1}
0.39	-0.066	0.093	4.8×10^{-1}	0.44	-0.303	0.106	4.3×10^{-3}	-0.054	0.042	2.0×10^{-1}
0.39	-0.019	0.014	1.6×10^{-1}	0.46	-0.303	0.011	8.0×10^{-1}	-0.017	0.006	3.5×10^{-3}
0.39	-0.018	0.014	1.7×10^{-1}	0.45	-0.020	0.014	6.5×10^{-1}	-0.019	0.006	1.7×10^{-3}
0.39	0.002	0.007	7.8×10^{-1}	0.46	0.013	0.007	3.7×10^{-2}	0.011	0.002	7.7×10^{-7}
0.39	0.001	0.007	8.4×10^{-1}	0.45	0.013	0.008	3.5×10^{-2}	0.011	0.002	5.6×10^{-7}
0.39	0.001	0.007	9.1×10^{-1}	0.46	0.013	0.007	3.7×10^{-2}	0.011	0.002	4.8×10^{-7}
0.39	0.000	0.007	9.7×10^{-1}	0.45	0.013	0.008	3.5×10^{-2}	0.011	0.002	3.5×10^{-7}
0.39	0.000	0.007	9.4×10^{-1}	0.44	0.000	0.008	9.3×10^{-1}	0.000	0.002	8.7×10^{-1}
NA	NA	NA	NA	0.41	0.252	0.164	1.6×10^{-1}	0.244	0.089	6.1×10^{-3}
NA	NA	NA	NA	0.41	0.246	0.164	5.1×10^{-2}	0.277	0.093	2.9×10^{-3}

PC principal component
POAG primary open-angle glaucoma
RS Rotterdam Study

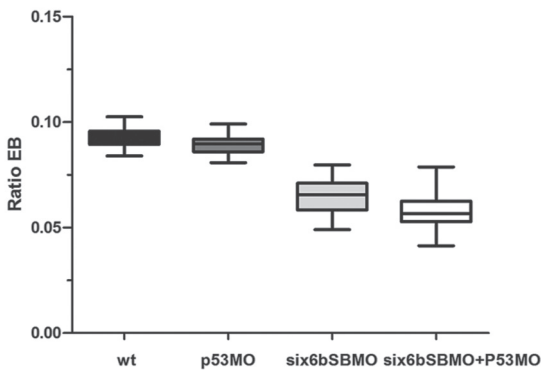
SE standard error
SNP single nucleotide polymorphism
VCDR vertical cup-disc ratio

Figure 1. Phenotype characterization of *six6b* SB-MO injected fish.

(A) *six6b* knockdown results in small eye phenotype, other abnormalities including pericardial edema, diffused pigmentation small head and short jaw were also observed. The small eye phenotype was not rescued after co-injection with *p53*-MO indicating a specific effect of *six6b* SB-MO in eye size. (B) Ratio eye to body size (E:B) in morphants and *p53* co-injected compared to wild-type embryos, n=30 for each group. P-values are indicated in the text. (C) Co-injection of wt *six6b* mRNA and *six6b* SB-MO partially rescued the small eye phenotype. Mean eye area improves from 1.425.747 μm^2 to 1.749.203 μm^2 , $P=0.001$.



B Ratio E:B at 5dpf



C *six6b* SBMO + WT *six6b* mRNA at 3dpf

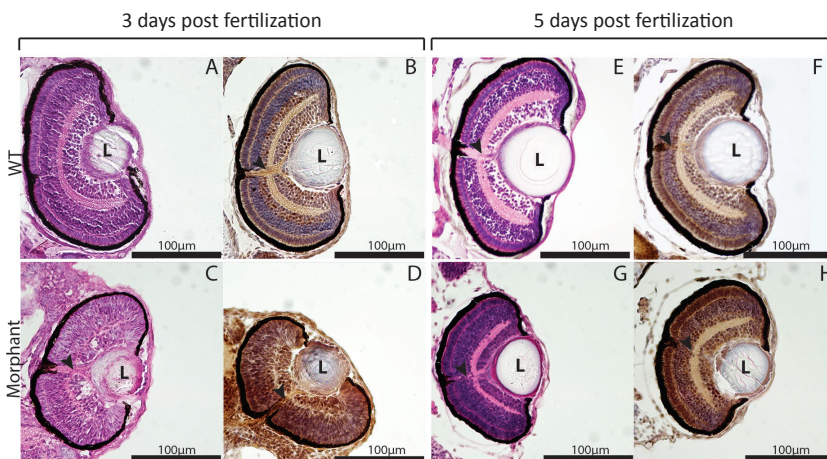


provides the possibility to evaluate the impact of *six6b* knockdown on eye size independent of the head size reduction. The E:H ratio was significantly smaller in morphants compared with wild-type embryos (mean E:H= 0.445 vs 0.530, $P=2.59 \times 10^{-10}$; Supplementary figure S3).

We performed two control experiments; first, a specific *p53*-targeting MO (4ng) was co-injected with the *six6b* SB-MO (6ng) to exclude whether the phenotype observed was due to off-target effects mediated by induction of *p53* expression. The mean ratio E:B in *p53*-MO co-injected embryos was 0.061, showing a small eye phenotype comparable with *six6b* knockdown ($P=2.41 \times 10^{-31}$), excluding a small eye size as consequence of *p53*-mediated apoptosis pathway. Second, we conducted rescue experiments using wild-type *six6b* mRNA. Since no difference in body length was observed between wild-type and morphants at 5dpf (mean = 3.952 mm vs 3.908 mm, respectively; $P=1.95 \times 10^{-1}$), assessment of rescue experiments was focused on eye dimensions only. Co-injection of *six6b* SB-MO with wt-*six6b* mRNA resulted in a partial, but significant, rescue of small eye phenotype (mean eye area improved from 1.425.747 μm^2 to 1.749.203 μm^2 , $P=1 \times 10^{-3}$; Figure 1 C and Supplementary Figure S4).

Figure 2. *six6b* knockdown results in small and underdeveloped eyes.

(A-D) Representative images of histological sections of wild-type (A and B); and morphants (C and D) at 3dpf. Though retinal lamination occurred in morphants, note the cellularized and underdeveloped lens. Panels A and C were Hematoxylin-Eosin (H&E) stained. (E-H) Histological sections of wild type (E and F); and morphants (G and H) at 5dpf. Note that at this age small eye size was the principal difference between the groups, the lens of morphants resembles the wild-type lens. Panels B, D, F and H show immunohistochemical localization of *six6/six3* in both wild type and morphants. The optic nerve is marked by arrowheads; L=Lens.



Loss of *six6b* results in immature and underdeveloped eyes

In order to carry out detailed assessment of the *six6b* SB-MO small eye phenotype, histological analysis was performed on embryos at 3 and 5dpf (Figure 2 A-C-E-G). Histology revealed that retinal lamination in morphants occurred. Therefore, the ganglion cell layer (GCL), inner nuclear layer (INL), and outer nuclear layer (ONL) were visualized by H&E staining. Although the optic nerve was seen leaving the retina, its thickness was decreased compared with wild-type embryos. A semi-quantitative analysis on serial sections of 6-microns showed that optic nerve thickness on wild-type embryos (n=4) was around 21 μm while in morphants (n=4) it was $\sim 12 \mu\text{m}$. In addition, the lens of 3dpf morphants was immature and cellularized compared with controls of the same age, supporting that eyes of morphants were delayed in development. Eyes of morphants at 5dpf showed a conserved general architecture, leaving small size as the principal difference between control embryos and morphants at this age.

Immunohistochemical localization of *six6* was studied using a rabbit anti-*SIX6* polyclonal antibody on sections at 3 and 5dpf (Figure 2 B-D-F-H). Since the rabbit anti-*SIX6* can recognize the protein products of the closely related *six3a* and *six3b* as well, the anti-*SIX6* immunoreactivity was only used to investigate the localization of *six6/3* proteins in the zebrafish retina, not for the efficiency of *six6b* knockdown. Both wild-type and morphants were analysed. Consistent with previous studies in chick embryos, mouse, and human fetal and adult eye^{21,22,41-43}, we found *six6/3* protein localized in the nuclei of the GCL, the nuclei of potential bipolar, amacrine and horizontal cells located in the INL, the nuclei of the photoreceptors and the optic nerve (Figure 2 B-F). In general, labeling in wild-type embryos at 3dpf was stronger than at 5dpf. Morphants at 3dpf presented less intense labeling, as predicted from expression data.

Expression patterns of *six3a* and *six3b* in *six6b* morphants

The *SIX* gene family of homeoproteins is required in both *Drosophila* and vertebrates for eye development. Similar to *SIX6*, *SIX3* has also been involved in eye development^{26,44-46}, both genes share high homology and are expressed during early stages^{21,25}. To determine whether zebrafish *six3* can compensate *six6b* depletion, RT-qPCR of morphants at 3dpf was performed. Two orthologues of the human *SIX3* were retrieved from Ensemble, *six3a* (ENSDARG0000058008) and *six3b* (ENSDARG0000054879). RT-qPCR of morphants compared to wild-type showed an expected down-regulation of *six6b*. Surprisingly, we found down-regulation of *six3a* in morphants as well, while expression levels of *six3b* were not significantly deregulated (Figure 3 B).

Knockdown of *six6b* up-regulate expression of the cell cycle inhibitor *cdkn2b* in zebrafish

Since *Six6/Dacha* interacts with some members of the family of cyclin-dependent kinases (CDK) inhibitors³⁵, we decided to evaluate whether knockdown of *six6b* in zebrafish alters the expression of *cdkn2b*, another member of the CDK inhibitors previously associated in our GWAS studies with VCDR¹⁶ and POAG¹⁷. RT-qPCR was performed at 3dpf on injected and wild-type embryos, showing a 5.5-fold overexpression of *cdkn2b* in morphants compared to wild-type ($P = 1.56 \times 10^{-2}$), while *cdkn2c* and *cdkn2d* (taken as a control) remain unaffected (Figure 3 C). Expression levels of *dacha* and *dachb* at 3dpf showed no differences between morphants and controls (data not shown).

Effect of *six6b* knockdown on cell proliferation in the developing eye of zebrafish

To evaluate whether up-regulation of *cdkn2b* in morphants leads to premature cell cycle exit, we examined the expression of the proliferating cell nuclear antigen (PCNA) in eye by immunostaining. Wild-type embryos and morphants at 2, 3, 4 and 5dpf were analysed. In wild-type fish at 2dpf, almost all retinal progenitor cells showed a strong PCNA immunoreactivity (Figure 4 A). As expected, in wild-type embryos at 3, 4 and 5dpf, cells concentrated in the ciliary marginal zone were PCNA-positive (Figure 4 B-C-D). The ciliary marginal zone is a proliferative zone described in eye of cold-blooded vertebrates⁴⁷. Thus, this finding is consistent with normal retinal differentiation processes in zebrafish^{48,49}. In contrast, morphants at 3 and 4dpf showed numerous PCNA-positive cells in the photoreceptor and inner nuclear layers (Figure 4 F-G), suggesting that proliferation in morphants was not restricted to the ciliary marginal zone, on the contrary, retinas of morphants at 3 and 4dpf showed a PCNA immunoreactivity pattern that resembled 2dpf wild-type retinas. At 5dpf morphants showed PCNA immunoreactivity mostly restricted to the ciliary marginal zone comparable with wild-type embryos (Figure 4 H). We also investigated whether increased apoptosis was the cause of small eye phenotype. Caspase-3 staining did not show an increased apoptosis rate in morphants compared with wild-type embryos (Supplementary Figure S5).

DISCUSSION

In this study, we investigated the *SIX1-SIX6* region in more detail to understand its role in optic nerve degeneration. Fine mapping and conditional analysis revealed a missense variant, rs33912345, in the *SIX6* gene. Further analysis of the *SIX6* exonic region revealed another rare missense variant, rs146737847. Both variants are located in the homeobox DNA-binding domain of *SIX6* and are highly evolutionarily conserved. No common or rare variants in *SIX1* were significantly associated to VCDR or POAG.

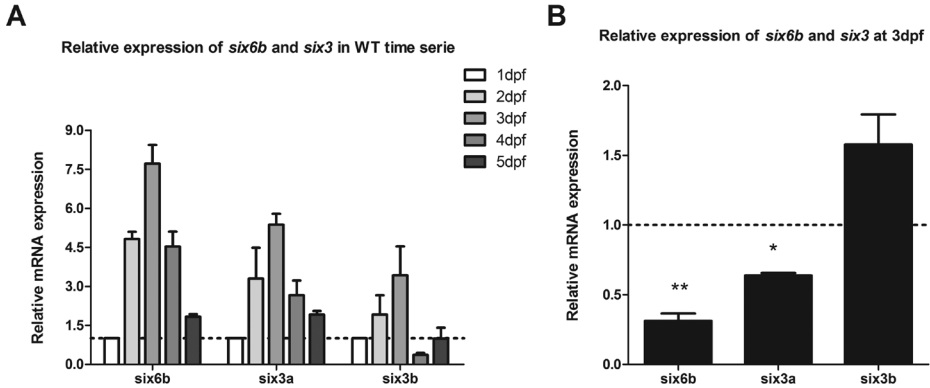
In line with previous findings, the rs33912345 has been described in patients with severe eye malformations, including anophthalmia, microphthalmia and coloboma^{22,50,51}. It is in complete linkage disequilibrium with the reported SNP rs10483727, which is known to be associated with VCDR and POAG^{16,17,30}. The rs146737847 variant has been reported in POAG cases of United States at the American Society of Human Genetics meeting 2012 (<http://www.ashg.org/2012meeting/abstracts/fulltext/f120122353.htm>).

SIX6 in adult human tissues is highly expressed in the choroid, ciliary body, sclera, optic nerve head and retina, particularly GCL, INL and ONL⁴³. Mouse, chick and *Xenopus* studies have demonstrated a role of *Six6* during eye development^{22,26,35,52}, whereas *Six1* is highly expressed in skeletal muscle²³ and plays a role in myogenesis²⁴. Both our findings and the known biological function support the notion that *SIX6*, rather than *SIX1*, may play a role in VCDR and POAG.

To evaluate the function of the *SIX6* gene on eye development and POAG, we used zebrafish as animal model due to its numerous advantages in comparison to mammalian models⁵³. We assessed the effect of *six6b* knockdown in zebrafish. Deficiency of *six6b* in zebrafish

Figure 3. *six6*, *six3a/six3b* and *cdkn2b* mRNA expression change.

(A) Wild-type relative expression of *six6b*, *six3a* and *six3b* over time from 1dpf to 5dpf. Relative expression was calculated by setting the 1dpf expression level at 1. Samples expression were normalized to the control gene β -actin (B) *six6b* knockdown in response to *six6b* SB-MO at 3dpf. In addition, morphants showed downregulation of *six3a* but no *six3b*.

**Figure 4.** *six6b* is involved in proliferation and differentiation of retinal cells in zebrafish.

(A-D) Representative images of PCNA immunoreactivity in wild-type embryos at 2, 3, 4 and 5 dpf; (A) In wild-type embryos at 2dpf almost all cells were PCNA-positive, the lens was cellularized and there was not retinal lamination, while at 3, 4 and 5dpf (B-D) proliferation is restricted to the ciliary marginal zone, marked by arrowheads. Retinal lamination is clear and the lens is mature and not cellularized. In contrast, morphants at 3 and 4 dpf present proliferating cells located outside the ciliary marginal zone (F-G). Note that at 5dpf the morphants resembles the wild-type retina, although some cells located in the central retinal showed a positive PCNA signal (H).

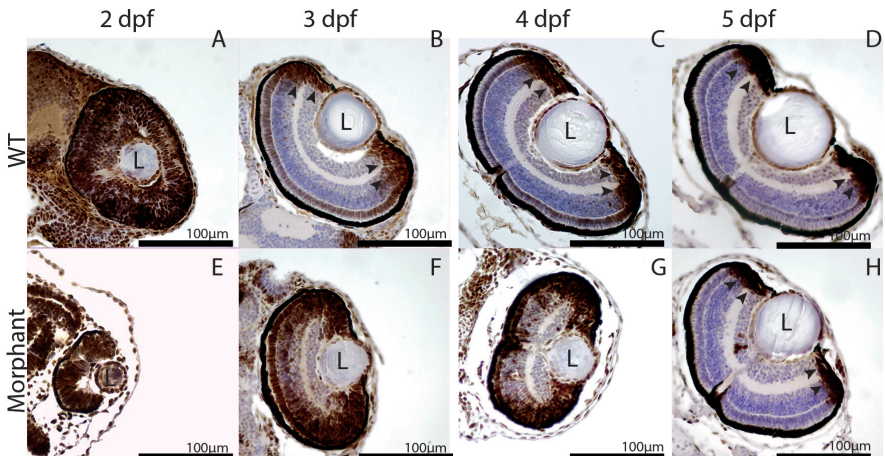
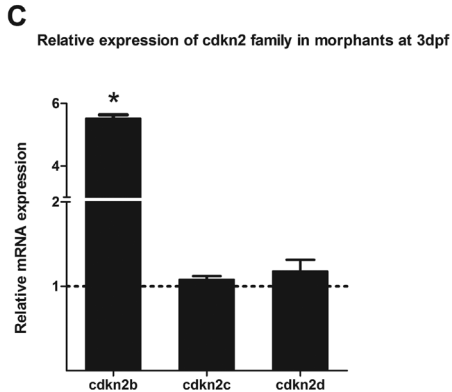
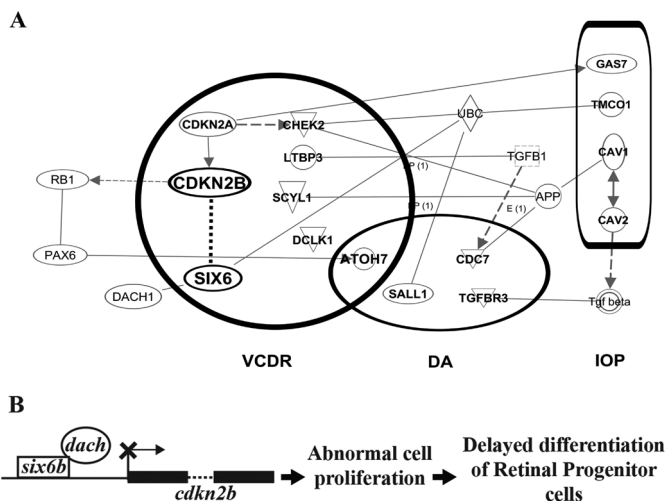


Figure 3. (continued)

(C) Overexpression of *cdkn2b* in response to *six6b* depletion. All sample expression from experiment B and C were normalized to the control gene *sdha*. Relative expression was calculated by setting the wild-type expression level at 1. Values represent means \pm s.e.m. * $P < 0.05$; ** $P < 0.01$.

**Figure 5.** *six6b* and *cdkn2b* interaction.

(A) Ingenuity diagram of the biological interaction of the known genes identified through GWAS of optic disc parameters (VCDR, DA and IOP); the bold dashed line shows the new interaction found in this study using a zebrafish model. The Ingenuity knowledge base is a repository of biological interactions and functional annotations of in vivo and in vitro experiments (www.ingenuity.com). The diagram was generated using the function “Path Explorer”. (B) *six6b* represses *cdkn2b* transcription in association with the co-repressor *dach*. *six6b* and *dach* form a complex that interacts with the regulatory region of *cdkn2b*. This interaction blocks *cdkn2b* transcription and thus controls the proliferative state of retinal progenitor cells. VCDR= Vertical Cup-Disc Ratio; DA= Disc Area; IOP= Intraocular Pressure.



led to a small eye phenotype, associated with small head and pericardial edema. Although morphants showed a small head, we found that the eye of morphants remains smaller independently of the head size. Other abnormalities, including diffused pigmentation were also observed. A clear connection between the visual system, particularly retinal-hypothalamic projections, and the control of pigment cells has been established⁵⁴⁻⁵⁶. In this study, *six6b* depleted embryos showed diffused pigmentation, a feature present in mutants who lack the ability to sense ambient light⁵⁷. This may indicate an abnormal eye function in *six6b* morphants. Furthermore, histological sections of *six6b* morphants at 3dpf showed a rudimentary lens, which indicates a developmental delay of the eye. Also, the optic nerve had a reduced thickness when compared with age-matched controls, which is relevant in the context of the neurodegenerative disease POAG. This finding is consistent with previous analysis of *Six6* null mice³⁵, which showed retinal hypoplasia, with often absence of optic nerve and chiasm. All these results support our hypothesis that the main effect of *six6b* knockdown is in the ocular system.

In flies, *sine oculis (so)* and *Optix* play a central role in eye development^{25,58}. In vertebrates, *Six3* and *Six6* are the homologs of *Optix*. Both *Six3* and *Six6* show high homology and are expressed during early stages of eye development^{25,26}. *Six3* has a wide role in forebrain development, whereas *Six6* has a more specific role in eye development^{35,45,46,52,59-61}. We evaluated the effect of *six6b* knockdown on expression levels of *six3a* and *six3b*. No significant changes in expression levels of *six3b* were found in morphants compared with wild-type embryos. Interestingly, we found down-regulation of *six3a* in *six6b* morphants. However, fourteen mismatches between the *six6b* SB-MO and the *six3a* gene confirmed that our MO did not target *six3a*. Down-regulation of *six3a* in *six6b* morphants might suggest a complex feedback mechanism between *six3a/six3b* and *six6b* in zebrafish. Though both *Six3* and *Six6* might function through similar⁶² and different⁶³ mechanisms, our results show that in zebrafish *six6b* is needed for normal eye development. Neither *six3a* or *six3b* can compensate for *six6b* deficiency, resulting in a small eye phenotype.

Studies in medaka fish indicate that *Six3* and the replication-initiation inhibitor gemini act antagonistically to regulate the balance between proliferation and differentiation during eye development⁶². *Six6* also interacts with gemini⁶², supporting a potential role of *Six6* in cell proliferation and differentiation. Additionally, in the *Six6* null mice it was demonstrated that *Six6* interacts with *Dach1*, a transcriptional co-repressor, to suppress *Cdkn1b* transcription *in vivo*³⁵. *Cdkn1b* is a member of the CDK inhibitor family and controls the cell cycle progression, arresting cell proliferation. *CDKN2B*, a gene known to be associated with VCDR and POAG^{16,17,27,28,30,64}, is also member of the CDK inhibitor family. *CDKN2B* controls G1 progression of the cell cycle and is highly induced by TGF- β ⁶⁵, which in turn is one of the pathways involved in POAG pathogenesis¹⁷. We demonstrated a 5.5-fold overexpression of *cdkn2b* in *six6b* morphants compared to wild-type embryos. This finding is in accordance with a rat model of glaucoma¹⁵, in which overexpression of *Cdkn2b* was described after induction of high IOP. Up-regulation of *cdkn2b* arrests cell cycle progression causing an abnormal proliferation and small eye phenotype. Based on our results we conclude that *Six6* repress the expression not only of *Cdkn1b*, as previously reported³⁵, but also *cdkn2b*. This reveals a new interaction between two known pathways associated with POAG (developmental and TGF- β signaling pathways) (Figure 5 A; www.ingenuity.com).

Next, we evaluated the proliferative activity of retinal cells through PCNA assessment. PCNA allows detection of cells in either G1 or S phase of the cell cycle. We found that knockdown of *six6b* changes the pattern of positive PCNA labeling. Similar results were found in a previous study in which a collagen gene (*drCol15a1b*) was knocked down in zebrafish⁶⁶. It is well established that retinal progenitor cells start a differentiation process when they exit the cell cycle^{66,67}. Analysis of *drCol15a1b* morphants indicated that cells arrested in a proliferative state were undifferentiated⁶⁶. Our results demonstrate an abnormal proliferation in the presence of an efficient knockdown of *six6b* with a recovery at 5dpf. This could be explained by a reduced morpholino activity, as a consequence of its dilution due to cell growth and division. Based on our findings, we hypothesized that decreased expression of *six6b* may lead to fewer differentiated cells as depicted by our proposed model in Figure 5 B. This needs to be assessed in future studies by evaluating the presence of retinal-differentiated cells in the eyes of *six6b* morphants. Caspase-3 assessment did not show an increase number of apoptotic cells in the eye of *six6b*-depleted embryos.

In conclusion, by combining fine-mapping and exome sequence analysis we found that *SIX6*, rather than *SIX1*, is responsible for the association signal previously reported in the *SIX1/SIX6* region. We found two variants located in the DNA-binding homeodomain of *SIX6*, which were significantly associated with VCDR. The rs33912345 variant was also associated with POAG in our study. Knockdown of *six6b* in zebrafish led to a small eye phenotype, as a result of an abnormal proliferative pattern in retinal cells. This alteration may also be associated with a disturbance in the differentiation process of retinal progenitor cells. Additionally, we were able to find an *in vivo* interaction between proteins identified by GWAS (*SIX6* and *CDKN2B*) for POAG. Further biological research is needed to verify the exact mechanism behind this interaction. Our findings from genetic association and functional studies demonstrate that *SIX6* is a susceptibility gene for POAG and is involved in early eye development. This study provides new insight into the complex genetic architecture of POAG.

MATERIALS AND METHODS

Human and Fine-mapping studies

Study populations

The Rotterdam Study (RS) is a prospective cohort study in the district Ommoord of Rotterdam. The rationale and study design are described elsewhere⁶⁸. The original cohort (RS-I) consisted of 7,983 residents aged 55 years and older. In 2000, the cohort was extended with 3,011 residents aged 55 years and older (RS-II). In 2006, the cohort was further expanded with 3,932 residents aged 45-54 years (RS-III). Details about examinations in each one of the cohorts are described elsewhere¹⁶.

The Erasmus Rucphen Family (ERF) Study is a family-based study in a genetically isolated population in the southwest of the Netherlands. It includes over 3,000 participants with age varying between 18 and 86 years old. The cross-sectional examinations took place between 2002 and 2005. The rationale and study design have been described elsewhere^{69,70}.

An independent series of 104 glaucoma cases from an isolated population (the Genetic Research in an Isolated Population [GRIP] study) was used for a case-control analysis. These patients were recruited in three local hospitals in the geographical region of the ERF study. They did not participate in the ERF study. Participants from the ERF study were used as the control population.

Ophthalmic examinations

The ophthalmic assessment in the Rotterdam Study and ERF study included a medical history, autorefractometry, keratometry, IOP measurements, visual field testing, fundus photography and optic nerve head imaging. Details about IOP and optic disc measurements are described elsewhere^{16,71}. In RS-I, glaucoma diagnosis was based on glaucomatous visual field loss (GVFL). The visual field of each eye was screened using a 52-point supra-threshold test that covered the central visual field with a radius of 24°, and that tested the same locations as used in the Glaucoma Hemifield Test. Participants with a reproducible visual field loss in a second supra-threshold test, were evaluated with a Goldmann kinetic perimetry or full-threshold HFA test by a skilled perimetrist on both eyes. We incorporated prevalent glaucoma cases⁷², as well as incident cases⁷³ based on GVFL during at least one of the examination rounds. VCDR per se was not an inclusion criteria of the diagnosis. In GRIP/ERF, the diagnosis was based on the optic disc appearance, visual field testing and angle assessment.

The study protocols were approved by the Medical Ethics Committee of the Erasmus University and all participants have given a written informed consent in accordance with the Declaration of Helsinki.

Genotyping and statistical analysis of fine-mapping studies

Illumina Infinium II HumanHap550 chip v3.0 array was used for DNA genotyping in RS-I, RS-II and RS-III. In the ERF study genotyping was performed using Illumina 318K, Illumina 370K, Illumina 610K and Affymetrix 250K genotyping platforms. Imputation for both studies was done by using 1000 Genomes Phase 1 (v3) as the reference.

We used the mean IOP, VCDR or DA of both eyes. In cases of missing or unreliable data on one eye, the other eye was taken. Participants with a history of glaucoma laser or surgery were excluded for the IOP analysis. IOP measurements of participants with IOP lowering medication were imputed by adding 25% to the value of the measurement. We used 1000 Genomes Phase 1(v3) to perform fine-mapping and modeling of *SIX1/SIX6* locus in relation to these continuous outcomes on an assumed additive model for the effect of the risk allele. Additionally, we examined through logistic regression the association between the *SIX1/SIX6* locus and primary open-angle glaucoma. All analyses were adjusted for age, sex, the first two principal components (RS) or family structure (ERF). Extra adjustments were done with spherical equivalent, as measure of myopia, to evaluate whether the missense variant rs33912345 was independently associated to VCDR. The spherical equivalent was calculated for each eye using the standard formula: spherical equivalent = sphere + 1/2 cylinder. Additionally, independence between rs10483727 and rs33912345 was tested, adjusting for the last one. Then an inverse variance weighted meta-analysis was performed.

Exome sequencing

Exomes of 1,309 individuals from the ERF population were sequenced “in-house” at the Center for Biomix of the Cell Biology department of the Erasmus MC, The Netherlands, using the Aligent version V4 capture kit on an Illumina HiSeq2000 sequencer and the TrueSeq Version3 protocol. The sequences reads were aligned to the human genome build 19 (hg19) using Burrows-Wheeler Aligner⁷⁴ and NARWHAL pipeline⁷⁵. For each sample, at least 4 Gigabases of sequence was aligned to the genome with an average fold-coverage of 74.23x per base. Subsequently, the aligned reads were processed further using the Indel Realigner, Mark Duplicates and Table Recalibration tools from the Genome Analysis Toolkit (GATK)⁷⁶ and Picard (<http://picard.sourceforge.net>) to remove systematic biases and to recalibrate the PHRED quality scores in the alignments. Genetic variants were called using the Unified Genotyper Tool from GATK. Of the 1,309 individuals 1,208 had data on VCDR. As the ERF study included related individuals, association analysis was performed in SOLAR using procedure “polygenic --screen”, and adjusting for age and sex. In total two variants in *SIX1* and seven variant in *SIX6* with a call rate >0.99 were found. Only one of the nine variants at *SIX6*, rs146737847, reached significance levels. In addition, conditional analysis were performed with the rs33912345, previously found in the fine mapping analysis.

eQTL and expression analyses

We used the Genotype-Tissue expression (GTEx) project database (www.broadinstitute.org/gtex/) to examined whether rs10483727, rs33912345 or rs146737847 had a cis or trans eQTL effect. Although the GTEx database does not include eye tissues, it contains more than 10 different brain regions and other tissues. For trans-eQTL analysis a p-value of 5×10^{-13} was considered significant³⁸.

Additionally, we compared expression levels of *SIX1* and *SIX6* using the Ocular Tissue Database (<https://genome.uiowa.edu/otdb/>). The gene expression is indicated as Affymetrix Probe Logarithmic Intensity Error (PLIER) number. The PLIER numbers were calculated by GC-background correction, PLIER normalization, log transformation and z-score calculation³⁹. Larger PLIER numbers represent high expression levels of a particular gene in particular tissue.

Statistical analysis of zebrafish experiments

Statistical analysis was performed using SPSS statistics 20. Analysis of E:B and E:H ratios was performed using the Student’s t-test. Each group (*six6b* SB-MO injected, *p53* MO injected and *six6b* SB-MO + *p53* MO co-injected) was compared individually with the WT group (n=30, in each group). All RT- qPCR experiments were undertaken in triplicate. Results were considered statistically significant when $P < 0.05$, and is denoted in the figures with an asterisk.

Zebrafish maintenance

The zebrafish (*Danio rerio*) strain used for this work was the Tupfel long fin (TL). Adults were maintained at 28°C on a 14 hour-light/10 hour-dark cycle. Embryos were collected from natural mating and raised in system water containing methylene blue at 28°C. Developmental stages were determined according to Kimmel⁷⁷. All procedures and conditions were in accordance with the Dutch animal welfare legislation. The use of zebrafish for this study was approved by the Institutional Review Board for experimental animals of the Erasmus MC, Rotterdam.

Genetic analysis of the zebrafish *SIX6* orthologue

The zebrafish *six6* ortholog was retrieved from Ensemble using the comparative genomics tool⁷⁸. Two genes were found, *six6a* (ENSDARG00000025187) and *six6b* (ENSDARG00000031316). In this study we reported the effect of *six6b* knockdown. We sequenced wild type zebrafish *six6b* to corroborate the reference sequence and select the regions for morpholinos oligonucleotides (MO) design.

Morpholino and mRNA microinjections

Morpholino antisense oligonucleotides were obtained from Gene-Tools (Philomath, OR, USA). Two morpholinos were designed against *six6b*. One morpholino was designed to target the translation initiation site: AUG-MO = 5'-AAATTGGCAACTGAAACATGAAGGC-3'; and the second morpholino targeted exon 1 donor site: SB-MO = 5'-TGTAATCTGGAAAACGCACCTGTT-3'. All MO sequences were aligned with the *Danio rerio* genome using NCBI and UCSC Blast to confirm specificity to the *six6b* genomic region and ratify that neither the AUG-MO nor the SB-MO recognized *six6a*, *six3a* or *six3b*. A previously described MO designed to target the translation site of *p53* (*p53*-MO = 5'-GCGCCATTGCTTTGCAAGAATTG-3' was used for control experiments⁷⁹). Morpholinos were reconstituted in distilled water and further diluted in Danieau solution containing 0.1% Phenol Red for microinjections into embryos.

Indicated dosages of MOs were injected into the yolk of one to two cells stage using a pneumatic picopump (World Precision Instruments, Berlin, Germany). Optimum dose was considered when maximal knockdown efficiency, low mortality rate and small eye phenotype without severe malformations were observed on injected embryos. Six nanograms of either SB or AUG-MO was selected as optimal concentration. In separate experiments, 4ng of *p53*-MO was co-injected with 6ng of *six6b*-specific MO (SB or AUG), in order to detect off-target effects due to activation of *p53* expression.

For MO rescue experiments, wild type *Danio rerio* *six6b* cDNA was ligated into the pCR2.1-TOPO vector (Invitrogen), and subcloned at the site of EcoRI in pCS2+ vector. The fidelity of *six6b*-pCS2 was verified by direct sequencing. Using as template NsiI linearized *six6b*-pCS2, wild type *six6b* mRNA was synthesized with mMESSAGING mMACHINE SP6 kit (Ambion Inc). Double injection of mRNA and MO was carried out in two steps, first 3ng *six6b* SB-MO were injected into the yolk, then a second injection with 9pg *six6b* mRNA into the cell was performed, all embryos were injected in 1-cell stage. Eye size was evaluated at 3 dpf.

RNA isolation and RT-qPCR

Pooled embryos were snap frozen in liquid nitrogen and stored at -80°C. Total RNA from ~60 wild-type embryos at 1,2,3,4 and 5dpf was isolated for time series analyses. For evaluation of *six6b* knockdown, total RNA was isolated from ~60 morphants and wild-type embryos at 3dpf; in all extractions an RNA-Bee (Tri-Test, Inc) protocol was used. Synthesis of cDNA was performed using Superscript III reverse transcriptase (Invitrogen, California USA). To measure mRNA levels, qRT-PCR on cDNA samples was carried out using SYBR® select Master Mix for CFX (applied Biosystems, Inc, USA). All samples were analyzed on the Bio-Rad CFX96 qPCR detection system. Primers used for qRT-PCR were designed using Primer3Plus tool⁸⁰. Primers for the reference genes *sdha* and *b-actin* were designed using Primer Express software (version 2.0.0). Oligonucleotide sequences are shown in detail in Supplementary Table S1.

Eye measurements

Wild-type and morphant embryos at 5dpf were euthanized and fixed in 4% paraformaldehyde at 4°C overnight. Photographs were made at a fixed magnification of the dorsal view of the whole embryo with a camera (Olympus DP72) attached to a dissecting microscope (Olympus SZX 16). The cellSense imaging software (Olympus) was used to measure eye, head and body length for each embryo. Eye length was defined as the longest dimension of the elliptical eye, head length was determined from the most anterior part of the head to the otic vesicles, as previously described⁸¹, and body length was measured from the tip of the head to the end of the trunk. The ratio of the eye size to body length (E:B) was measured to determine the relative size of the eye⁴⁰. The ratio of the eye size to head length (E:H) was measured to evaluate the effect of *six6b* depletion in eye size, independently of the head length.

For the assessment of the rescue experiments three eye measurements from the dorsal view of embryos at 3dpf were made. First, the eye length (defined previously) and called anterior-posterior (AP) length, second the superior-inferior length (SI) defined as the longest dimension along the superior-inferior axis, and third the total eye area. All measurements were traced using the Count & Measure function of the cellSense imaging software.

Histological analysis

Histological analysis was performed using standard protocols. Briefly, embryos were fixed in 4% paraformaldehyde at 4°C overnight, embedded in paraffin using standard procedures and cut in 6 µm sections. Subsequently, histological haematoxylin–eosin staining of the sections was carried out using a standard protocol.

Immunohistochemistry

Briefly, deparaffinized sections were pretreated for antigen retrieval by microwave heating in 0.1 M sodium citrate buffer (pH 6) for time series of 9-3-3 minutes. Expression pattern of *six6* in larvae at 3dpf was evaluated using a rabbit polyclonal antibody against *six6* (1:400, Sigma). Proliferating cells were labeled using a mouse monoclonal antibody to PCNA (1:32000, Sigma). All antibody incubations were overnight at 4°C followed by incubation with secondary antibody (BrightVision Poly-HRP-Anti rabbit IgG or poly-HRP Anti-mouse, respectively) indirect immunoperoxidase labeling and hematoxylin counter stain was performed.

References

1. Kwon, Y.H., Fingert, J.H., Kuehn, M.H. & Alward, W.L. Primary open-angle glaucoma. *N Engl J Med* 360, 1113-24 (2009).
2. Ramdas, W.D. et al. Genetic architecture of open angle glaucoma and related determinants. *J Med Genet* 48, 190-6 (2011).
3. Ramdas, W.D. et al. Lifestyle and risk of developing open-angle glaucoma: the Rotterdam study. *Arch Ophthalmol* 129, 767-72 (2011).
4. Ramdas, W.D. et al. Ocular perfusion pressure and the incidence of glaucoma: real effect or artifact? The Rotterdam Study. *Invest Ophthalmol Vis Sci* 52, 6875-81 (2011).
5. Wolfs, R.C. et al. Genetic risk of primary open-angle glaucoma. Population-based familial aggregation study. *Arch Ophthalmol* 116, 1640-5 (1998).
6. Schwartz, J.T., Reuling, F.H. & Feinleib, M. Size of the physiologic cup of the optic nerve head. hereditary and environmental factors. *Arch Ophthalmol* 93, 776-8 (1975).
7. Freeman, E.E., Roy-Gagnon, M.H., Descovich, D., Masse, H. & Lesk, M.R. The heritability of glaucoma-related traits corneal hysteresis, central corneal thickness, intraocular pressure, and choroidal blood flow pulsatility. *PLoS One* 8, e55573 (2013).
8. Klein, B.E., Klein, R. & Lee, K.E. Heritability of risk factors for primary open-angle glaucoma: the Beaver Dam Eye Study. *Invest Ophthalmol Vis Sci* 45, 59-62 (2004).
9. van Koolwijk, L.M. et al. Genetic contributions to glaucoma: heritability of intraocular pressure, retinal nerve fiber layer thickness, and optic disc morphology. *Invest Ophthalmol Vis Sci* 48, 3669-76 (2007).
10. Stone, E.M. et al. Identification of a gene that causes primary open angle glaucoma. *Science* 275, 668-70 (1997).
11. Rezaie, T. et al. Adult-onset primary open-angle glaucoma caused by mutations in optineurin. *Science* 295, 1077-9 (2002).
12. Monemi, S. et al. Identification of a novel adult-onset primary open-angle glaucoma (POAG) gene on 5q22.1. *Hum Mol Genet* 14, 725-33 (2005).
13. Wiggs, J.L. et al. Common variants near CAV1 and CAV2 are associated with primary open-angle glaucoma in Caucasians from the USA. *Hum Mol Genet* 20, 4707-13 (2011).
14. Thorleifsson, G. et al. Common variants near CAV1 and CAV2 are associated with primary open-angle glaucoma. *Nat Genet* 42, 906-9 (2010).
15. Burdon, K.P. et al. Genome-wide association study identifies susceptibility loci for open angle glaucoma at TMC01 and CDKN2B-AS1. *Nat Genet* 43, 574-8 (2011).
16. Ramdas, W.D. et al. A genome-wide association study of optic disc parameters. *PLoS Genet* 6, e1000978 (2010).
17. Ramdas, W.D. et al. Common genetic variants associated with open-angle glaucoma. *Hum Mol Genet* 20, 2464-71 (2011).
18. Brown, N.L., Patel, S., Brzezinski, J. & Glaser, T. Math5 is required for retinal ganglion cell and optic nerve formation. *Development* 128, 2497-508 (2001).
19. Mao, C.A. et al. Reprogramming amacrine and photoreceptor progenitors into retinal ganglion cells by replacing Neurod1 with Atoh7. *Development* 140, 541-51 (2013).
20. Prasov, L., Nagy, M., Rudolph, D.D. & Glaser, T. Math5 (Atoh7) gene dosage limits retinal ganglion cell genesis. *Neuroreport* 23, 631-4 (2012).
21. Jean, D., Bernier, G. & Gruss, P. Six6 (Optx2) is a novel murine Six3-related homeobox gene that demarcates the presumptive pituitary/hypothalamic axis and the ventral optic stalk. *Mech Dev* 84, 31-40 (1999).
22. Gallardo, M.E. et al. Genomic cloning and characterization of the human homeobox gene SIX6 reveals a cluster of SIX genes in chromosome 14 and associates SIX6 hemizygoty with bilateral anophthalmia and pituitary anomalies. *Genomics* 61, 82-91 (1999).
23. Boucher, C.A., Carey, N., Edwards, Y.H., Siciliano, M.J. & Johnson, K.J. Cloning of the human SIX1 gene and its assignment to chromosome 14. *Genomics* 33, 140-2 (1996).
24. Ridgeway, A.G. & Skerjanc, I.S. Pax3 is essential for skeletal myogenesis and the expression of Six1 and Eya2. *J Biol Chem* 276, 19033-9 (2001).
25. Serikaku, M.A. & O'Tousa, J.E. sine oculis is a homeobox gene required for Drosophila visual system development. *Genetics* 138, 1137-50 (1994).
26. Oliver, G. et al. Six3, a murine homologue of the sine oculis gene, demarcates the most anterior border of the developing neural plate and is expressed during eye development. *Development* 121, 4045-55 (1995).
27. Fan, B.J., Wang, D.Y., Pasquale, L.R., Haines, J.L. & Wiggs, J.L. Genetic variants associated with optic nerve vertical cup-to-disc ratio are risk factors for primary open angle glaucoma in a US Caucasian population. *Invest Ophthalmol Vis Sci* 52, 1788-92 (2011).
28. Cao, D. et al. CDKN2B polymorphism is associated with primary open-angle glaucoma (POAG) in the Afro-Caribbean population of Barbados, West Indies. *PLoS One* 7, e39278 (2012).

29. Pasquale, L.R. et al. CDKN2B-AS1 genotype-glaucoma feature correlations in primary open-angle glaucoma patients from the United States. *Am J Ophthalmol* 155, 342-353 e5 (2013).
30. Osman, W., Low, S.K., Takahashi, A., Kubo, M. & Nakamura, Y. A genome-wide association study in the Japanese population confirms 9p21 and 14q23 as susceptibility loci for primary open angle glaucoma. *Hum Mol Genet* 21, 2836-42 (2012).
31. Burdon, K.P. et al. Glaucoma risk alleles at CDKN2B-AS1 are associated with lower intraocular pressure, normal-tension glaucoma, and advanced glaucoma. *Ophthalmology* 119, 1539-45 (2012).
32. Nakano, M. et al. Common variants in CDKN2B-AS1 associated with optic-nerve vulnerability of glaucoma identified by genome-wide association studies in Japanese. *PLoS One* 7, e33389 (2012).
33. Wiggs, J.L. et al. Common variants at 9p21 and 8q22 are associated with increased susceptibility to optic nerve degeneration in glaucoma. *PLoS Genet* 8, e1002654 (2012).
34. Krimpenfort, P. et al. p15Ink4b is a critical tumour suppressor in the absence of p16Ink4a. *Nature* 448, 943-6 (2007).
35. Li, X., Perissi, V., Liu, F., Rose, D.W. & Rosenfeld, M.G. Tissue-specific regulation of retinal and pituitary precursor cell proliferation. *Science* 297, 1180-3 (2002).
36. Adzhubei, I.A. et al. A method and server for predicting damaging missense mutations. *Nat Methods* 7, 248-9 (2010).
37. Cooper, G.M. et al. Single-nucleotide evolutionary constraint scores highlight disease-causing mutations. *Nat Methods* 7, 250-1 (2010).
38. Consortium, G.T. The Genotype-Tissue Expression (GTEx) project. *Nat Genet* 45, 580-5 (2013).
39. Wagner, A.H. et al. Exon-level expression profiling of ocular tissues. *Exp Eye Res* 111, 105-11 (2013).
40. Veth, K.N. et al. Mutations in zebrafish *Irp2* result in adult-onset ocular pathogenesis that models myopia and other risk factors for glaucoma. *PLoS Genet* 7, e1001310 (2011).
41. Toy, J., Yang, J.M., Leppert, G.S. & Sundin, O.H. The *optx2* homeobox gene is expressed in early precursors of the eye and activates retina-specific genes. *Proc Natl Acad Sci U S A* 95, 10643-8 (1998).
42. Lopez-Rios, J., Gallardo, M.E., Rodriguez de Cordoba, S. & Bovolenta, P. *Six9* (*Optx2*), a new member of the six gene family of transcription factors, is expressed at early stages of vertebrate ocular and pituitary development. *Mech Dev* 83, 155-9 (1999).
43. Aijaz, S. et al. Expression analysis of *SIX3* and *SIX6* in human tissues reveals differences in expression and a novel correlation between the expression of *SIX3* and the genes encoding isocitrate dehydrogenase and cadherin 18. *Genomics* 86, 86-99 (2005).
44. Zhou, X., Hollemann, T., Pieler, T. & Gruss, P. Cloning and expression of *xSix3*, the *Xenopus* homologue of murine *Six3*. *Mech Dev* 91, 327-30 (2000).
45. Lagutin, O. et al. *Six3* promotes the formation of ectopic optic vesicle-like structures in mouse embryos. *Dev Dyn* 221, 342-9 (2001).
46. Carl, M., Loosli, F. & Wittbrodt, J. *Six3* inactivation reveals its essential role for the formation and patterning of the vertebrate eye. *Development* 129, 4057-63 (2002).
47. Amato, M.A., Arnault, E. & Perron, M. Retinal stem cells in vertebrates: parallels and divergences. *Int J Dev Biol* 48, 993-1001 (2004).
48. Raymond, P.A., Barthel, L.K., Bernardos, R.L. & Perkowski, J.J. Molecular characterization of retinal stem cells and their niches in adult zebrafish. *BMC Dev Biol* 6, 36 (2006).
49. Kassen, S.C. et al. The *Tg(ccnb1:EGFP)* transgenic zebrafish line labels proliferating cells during retinal development and regeneration. *Mol Vis* 14, 951-63 (2008).
50. Gallardo, M.E. et al. Analysis of the developmental *SIX6* homeobox gene in patients with anophthalmia/microphthalmia. *Am J Med Genet A* 129A, 92-4 (2004).
51. Aijaz, S. et al. Absence of *SIX6* mutations in microphthalmia, anophthalmia, and coloboma. *Invest Ophthalmol Vis Sci* 45, 3871-6 (2004).
52. Zuber, M.E., Perron, M., Philpott, A., Bang, A. & Harris, W.A. Giant eyes in *Xenopus laevis* by overexpression of *XOptx2*. *Cell* 98, 341-52 (1999).
53. Lieschke, G.J. & Currie, P.D. Animal models of human disease: zebrafish swim into view. *Nat Rev Genet* 8, 353-67 (2007).
54. Guo, S. Linking genes to brain, behavior and neurological diseases: what can we learn from zebrafish? *Genes Brain Behav* 3, 63-74 (2004).
55. Malicki, J. et al. Mutations affecting development of the zebrafish retina. *Development* 123, 263-73 (1996).
56. Neuhauss, S.C. Behavioral genetic approaches to visual system development and function in zebrafish. *J Neurobiol* 54, 148-60 (2003).
57. Haffter, P. et al. The identification of genes with unique and essential functions in the development of the zebrafish, *Danio rerio*. *Development* 123, 1-36 (1996).
58. Cheyette, B.N. et al. The *Drosophila sine oculis* locus encodes a homeodomain-containing protein required for the development of the entire visual system. *Neuron* 12, 977-96 (1994).

59. Kobayashi, M., Toyama, R., Takeda, H., Dawid, I.B. & Kawakami, K. Overexpression of the forebrain-specific homeobox gene *six3* induces rostral forebrain enlargement in zebrafish. *Development* 125, 2973-82 (1998).
60. Loosli, F., Winkler, S. & Wittbrodt, J. *Six3* overexpression initiates the formation of ectopic retina. *Genes Dev* 13, 649-54 (1999).
61. Bernier, G. et al. Expanded retina territory by midbrain transformation upon overexpression of *Six6* (*Optx2*) in *Xenopus* embryos. *Mech Dev* 93, 59-69 (2000).
62. Del Bene, F., Tessmar-Raible, K. & Wittbrodt, J. Direct interaction of *geminin* and *Six3* in eye development. *Nature* 427, 745-9 (2004).
63. Lopez-Rios, J., Tessmar, K., Loosli, F., Wittbrodt, J. & Bovolenta, P. *Six3* and *Six6* activity is modulated by members of the *groucho* family. *Development* 130, 185-95 (2003).
64. Dimasi, D.P. et al. Genetic investigation into the endophenotypic status of central corneal thickness and optic disc parameters in relation to open-angle glaucoma. *Am J Ophthalmol* 154, 833-842 e2 (2012).
65. Hannon, G.J. & Beach, D. *p15INK4B* is a potential effector of TGF-beta-induced cell cycle arrest. *Nature* 371, 257-61 (1994).
66. Gonzalez-Nunez, V., Nocco, V. & Budd, A. Characterization of *drCol 15a1b*: a novel component of the stem cell niche in the zebrafish retina. *Stem Cells* 28, 1399-411 (2010).
67. Agathocleous, M. & Harris, W.A. From progenitors to differentiated cells in the vertebrate retina. *Annu Rev Cell Dev Biol* 25, 45-69 (2009).
68. Hofman, A. et al. The Rotterdam Study: 2012 objectives and design update. *Eur J Epidemiol* 26, 657-86 (2011).
69. Aulchenko, Y.S. et al. Linkage disequilibrium in young genetically isolated Dutch population. *Eur J Hum Genet* 12, 527-34 (2004).
70. Pardo, L.M., MacKay, I., Oostra, B., van Duijn, C.M. & Aulchenko, Y.S. The effect of genetic drift in a young genetically isolated population. *Ann Hum Genet* 69, 288-95 (2005).
71. Rolando, M. et al. Measurement variability in digital analysis of optic discs. *Doc Ophthalmol* 85, 211-22 (1994).
72. Dielemans, I. et al. The prevalence of primary open-angle glaucoma in a population-based study in The Netherlands. The Rotterdam Study. *Ophthalmology* 101, 1851-5 (1994).
73. Czudowska, M.A. et al. Incidence of glaucomatous visual field loss: a ten-year follow-up from the Rotterdam Study. *Ophthalmology* 117, 1705-12 (2010).
74. Li, H. & Durbin, R. Fast and accurate short read alignment with Burrows-Wheeler transform. *Bioinformatics* 25, 1754-60 (2009).
75. Brouwer, R.W., van den Hout, M.C., Grosveld, F.G. & van Ijcken, W.F. NARWHAL, a primary analysis pipeline for NGS data. *Bioinformatics* 28, 284-5 (2012).
76. McKenna, A. et al. The Genome Analysis Toolkit: a MapReduce framework for analyzing next-generation DNA sequencing data. *Genome Res* 20, 1297-303 (2010).
77. Kimmel, C.B., Ballard, W.W., Kimmel, S.R., Ullmann, B. & Schilling, T.F. Stages of embryonic development of the zebrafish. *Dev Dyn* 203, 253-310 (1995).
78. Vilella, A.J. et al. EnsemblCompara GeneTrees: Complete, duplication-aware phylogenetic trees in vertebrates. *Genome Res* 19, 327-35 (2009).
79. Robu, M.E. et al. *p53* activation by knockdown technologies. *PLoS Genet* 3, e78 (2007).
80. Untergasser, A. et al. Primer3Plus, an enhanced web interface to Primer3. *Nucleic Acids Res* 35, W71-4 (2007).
81. van de Water, S. et al. Ectopic Wnt signal determines the eyeless phenotype of zebrafish masterblind mutant. *Development* 128, 3877-88 (2001).

PART 6

GENERAL DISCUSSION

GENERAL DISCUSSION

Open-angle glaucoma (OAG) is an important blinding disease of which the pathophysiology is still largely unknown. In this thesis I have investigated several aspects of OAG. First, I have examined the utility of optical coherence tomography (OCT) in the diagnosis of OAG in the general population. Second, I have explored risk factors for OAG and factors that influence the major OAG risk factor, intraocular pressure (IOP). Next, I have identified novel associations between genetic variants and endophenotypes of OAG. Finally, I have investigated the functional consequence of one of the genes associated with optic nerve degeneration and OAG. In this general discussion, I will summarize and review the main findings described in this thesis. Furthermore, I will address methodological considerations, clinical implications, and suggestions for future research.

MAIN FINDINGS

In OAG, damage of the optic nerve leads to irreversible visual field defects. This can be functionally assessed with perimetry. The morphological changes like thinning of the retinal nerve fiber layer (RNFL) and retinal ganglion cell layer (RGCL) can be quantitatively assessed with techniques such as confocal scanning laser ophthalmoscopy (Heidelberg Retina Tomograph [HRT]¹) or scanning laser polarimetry (GDx Nerve Fiber Analyzer^{2,3}). However, the correlation between functional loss measured by perimetry and structural loss measured by HRT or GDx is – at best – moderate. OCT is another technique that makes it possible to quantify the RNFL and RGCL thicknesses of specific regions of interest. Theoretically, small regions of interest should result in better correlations with functional tests. A too detailed look, however, could also compromise the signal-to-noise ratio. In **Chapter 2.1** I have shown that the size of the scanned region is indeed negatively correlated with the test-retest variability. Taken this into account, I optimized OCT parameters for discriminating between OAG cases and controls. I found that the RGCL thickness averaged over the inferior half of the scanned macular area was the best parameter for detecting OAG cases defined as cases with glaucomatous visual field loss (GVFL) in a population-based setting. Although we detected more OAG cases with OCT than was done in the past with HRT or GDx, still about half of the OAG cases was not detected correctly – at the same specificity of 97.5%.

An elevated IOP is a well-known and important risk factor for OAG. This was confirmed in our data. IOP was associated with the two major OAG characteristics: GVFL and glaucomatous optic neuropathy (GON). Other risk factors for OAG are (old) age, African descent, a thin central corneal thickness (CCT), a low body mass index (BMI) – especially in women, and myopia⁴⁻⁶. Further, there is a long list of putative risk factors for which the relationship with OAG is less clear. As is true with systemic hypertension, there is a state of equipoise regarding the relation of sleep apnea and OAG. I therefore investigated this proposed risk factor in the Rotterdam Study, a study setting without information bias and one of the largest studies with data available to study this association. I found no evidence for an association between sleep apnea and OAG. During the past years, not many new risk factors have been published that are consistently associated with OAG. It is possible that not yet identified risk factors may have a minor effect on OAG, and have therefore not been identified in single studies – with

their inherent limited statistical power due to the low prevalence of glaucoma. One way to overcome this problem is to conduct a meta-analysis with several OAG studies. In **Chapter 3.3** we used this strategy to find new risk factors for IOP. We conducted this meta-analysis within the European Eye Epidemiology (E³) consortium (see **Chapter 1.1**). We found a new association of lower IOP in taller people, which is in line with a reported lower prevalence of OAG in taller people in the Beijing Eye Study⁷.

A positive family history is also a major risk factor for OAG. Major progress has been made in understanding the genetic origin of OAG. In this thesis I used Hapmap and 1000 Genomes imputations to find new genes associated with endophenotypes of OAG. I identified novel single nucleotide polymorphisms (SNPs) that were associated with IOP or optic nerve head parameters (vertical cup-disc ratio [VCDR], cup area [CA], or disc area [DA]) in the largest meta-analyses until today. In total, we identified six novel genomic regions for IOP, eighteen for VCDR, fifteen for CA, and sixteen for DA (see Table 1).

The genes associated with OAG or its endophenotypes play a role in different pathways: Rho/RhoA kinase, vascular tone, TGF- β signaling, extracellular matrix, ubiquitination, heat shock, eye development, cell cycle and cell growth (see Figure 1). Some pathways are connected with each other, and some genes play a role in two pathways.

The gene *ABCA1* appeared an important OAG gene. Two independent case-control studies showed a genome-wide significant association between this gene and OAG. Gharahkhani et al. identified this gene in 1,155 OAG cases and 1,992 controls from Australia, and replicated their findings in two other Australian cohorts (in total 932 cases and 6,862 controls) and two United States cohorts (in total 2,616 cases and 2,634 controls)⁸. Chen et al. found this gene in 1,007 cases with high-tension glaucoma (HTG) and 1,009 controls from China⁹. They replicated the finding in 525 HTG cases and 912 controls from Singapore, and 1,374 OAG cases and 4,053 controls from China. Another study has previously shown that the expression of the *ABCA1* transporter is increased in leucocytes from OAG patients compared to controls¹⁰. Interestingly, this gene binds to *ARHGEF12*, a gene which plays a role in the Rho/RhoA kinase pathway. We found an association between *ARHGEF12* and IOP, and showed that this gene is also associated with OAG.

ABCA1 also binds to *CAV1*¹¹. Both genes play a role in cholesterol binding¹². Alterations in cholesterol hemostasis influence glucose metabolism and it has been shown that *ABCA1* in adipocytes plays a role in glucose metabolism¹³. Also, mutations in *ABCA1* may lead to enhanced β -cell secretory capacity in the pancreas¹⁴. A reduced *ABCA1* expression was found in patients with type 2 diabetes¹⁵, and two smaller studies found associations between *ABCA1* polymorphisms and type 2 diabetes^{16,17}. The *ABO* gene has also been associated with fasting glucose¹⁸ and diabetes¹⁹. Interestingly, *CDKN1A* can triggers β -cell apoptosis in the pancreas²⁰. Gene-set enrichment analysis identified “impaired glucose tolerance” in the analysis of VCDR SNPs, and “increased insulin sensitivity” in the analysis of VCDR, cup area, and disc area SNPs (**Chapter 4.5**). These findings may consolidate the results from two meta-analyses that found an association between diabetes and the risk of glaucoma^{21,22}.

The association between *CAV1/CAV2* and OAG also suggests that vascular tone is an important pathway involved in glaucoma²³. The proteins caveolin-1 and caveolin-2, encoded by the genes *CAV1/CAV2*, interact with endothelial nitric oxide synthase (eNOS, encoded by *NOS3*) which subsequently produce nitric oxide (NO) in the vascular endothelia. NO plays an important role in IOP regulation and OAG: it has been implicated in aqueous humor outflow regulation and OAG patients showed less NO production in the trabecular meshwork and Schlemm's canal^{24,25}. Furthermore, the 17 β -estradiol hormone regulates *CAV1* and *NOS3*²⁶ and the estrogen metabolism might also be important in OAG. This hypothesis is supported by the findings that SNPs in *NOS3* have been associated with OAG subjects with a history of migraine²⁷ and women with high-tension glaucoma²⁸. Furthermore, some studies showed that early menopause, the use of oral contraceptive, and bilateral oophorectomy before the age of 43 years are associated with a higher risk of OAG²⁹⁻³², while the use of postmenopausal hormones reduces the risk of OAG or RNFL defects^{31,33,34}. Another study found a protective effect of 17 β -estradiol eye drops on the RGCL function³⁵. Finally, the estrogen SNP pathway has been found to be associated with POAG among women³⁶. In **Chapter 3.3**, we found a positive linear relationship between IOP and BMI, which is in line with other studies. On the other hand, there might be an inverse relationship between BMI and OAG (**Chapter 3.1**). These contradictory findings might be explained by the fact that obese people have higher postmenopausal estrogen levels³⁷.

The TGF- β pathway is another pathway that has been linked to glaucoma³⁸. It has an important role in the aqueous humor and trabecular meshwork³⁹, and TGF- β 2 was shown to be elevated in the ONH of glaucoma patients⁴⁰. Genes involved in this pathway are associated with ONH morphology (*TGFBR3*, *BMP2*, *BMP4*, and furthermore, *CDKN2B* is induced by TGF- β ⁴¹). Elevation of TGF- β 2 may induce extracellular matrix changes (ECM) in the lamina cribrosa. Extracellular matrix is a pathway that also came up in the genetic association studies: *COL8A1*, *ADAMTS8*, and *VCAN* play a role in ECM and are associated with VCDR and CA. Changes in the ECM have been observed in the optic nerve head, especially in the lamina cribrosa, and it might be that those genes have an effect in this process.

Apart from our studies, Gharahkhani et al. found an association between *AFAP1* and *GMDS* and OAG⁸. Chen et al. showed an association between *PMM2* and HTG⁹. Interestingly, *GMDS* and *PMM2* are both involved in metabolism of mannose. Mannose is a building block of the core glycan structure, which is converted into N-glycan structures. N-glycan has different functions. It plays a role in the structural components of the extracellular matrix. It is also important for targeting of proteins to lysosomes for degradation. This function links these two genes to *OPTN* and *TBK1*. Recently, it has been shown that not only *OPTN* but also *TBK1* is associated with amyotrophic lateral sclerosis. Those genes are activated by TNF- α and play a role in removal of pathological ribonucleoprotein inclusions⁴². Dysfunction leads to aggregation of proteins, which is also a characteristic of other neurodegenerative diseases like Alzheimer's Disease. The ubiquitin-proteasome system (UPS) is involved in protein degradation. Ubiquitin is expressed in retinal ganglion cells⁴³. The E50K mutation in *OPTN* leads to dysfunction of the UPS with apoptosis as a result⁴⁴. Alterations in the UPS also occur in *MYOC* mutations or overexpression⁴⁵. Other genes that are related to UPS are *ASB7*, *GMDS*, *HSF2*, *RPAP3*, *PMM2*, and *TMCO1*. Heat shock proteins are also involved in the prevention of protein aggregation. This pathway was identified in the GWAS for VCDR.

The functional consequences of the genetic variants implicated in OAG or its endophenotypes remains largely unknown. In **Chapter 5.1** we aimed to elucidate the best candidate gene in the region between *SIX1* and *SIX6*. In zebrafish the genome is duplicated and as a consequence there are two orthologs of the human *SIX6*: *six6a* and *six6b*. We conducted a knockdown experiment of *six6b* and found that *SIX6* is involved in early development of the eye – knockdown caused a small eye size – and the proliferation pattern of retinal cells in zebrafish. Another group replicated our findings in an experiment with knockdown of *six6a*. Carnes et al. showed that knockdown of *six6a* causes a small eye phenotype⁴⁶. Other genes that play a role in eye development are *ATOH7*, *SALL1* and *PAX6*.

Interestingly, knockdown of *six6b* upregulated the expression of *cdkn2b*, another gene implicated in optic nerve degeneration and OAG. Both *CDKN2B* and *CDKN1A* are cyclin-dependent kinase inhibitors and are important for cell proliferation. P53 plays a role in the synthesis of *CDKN1A*. Other genes that are involved in (p53-dependent) apoptosis or cell growth are *GADD45A*, *PDZD2*, *RREB1*, *PSCA*, *VGLL4*, *DGKB*, and *UGT8*.

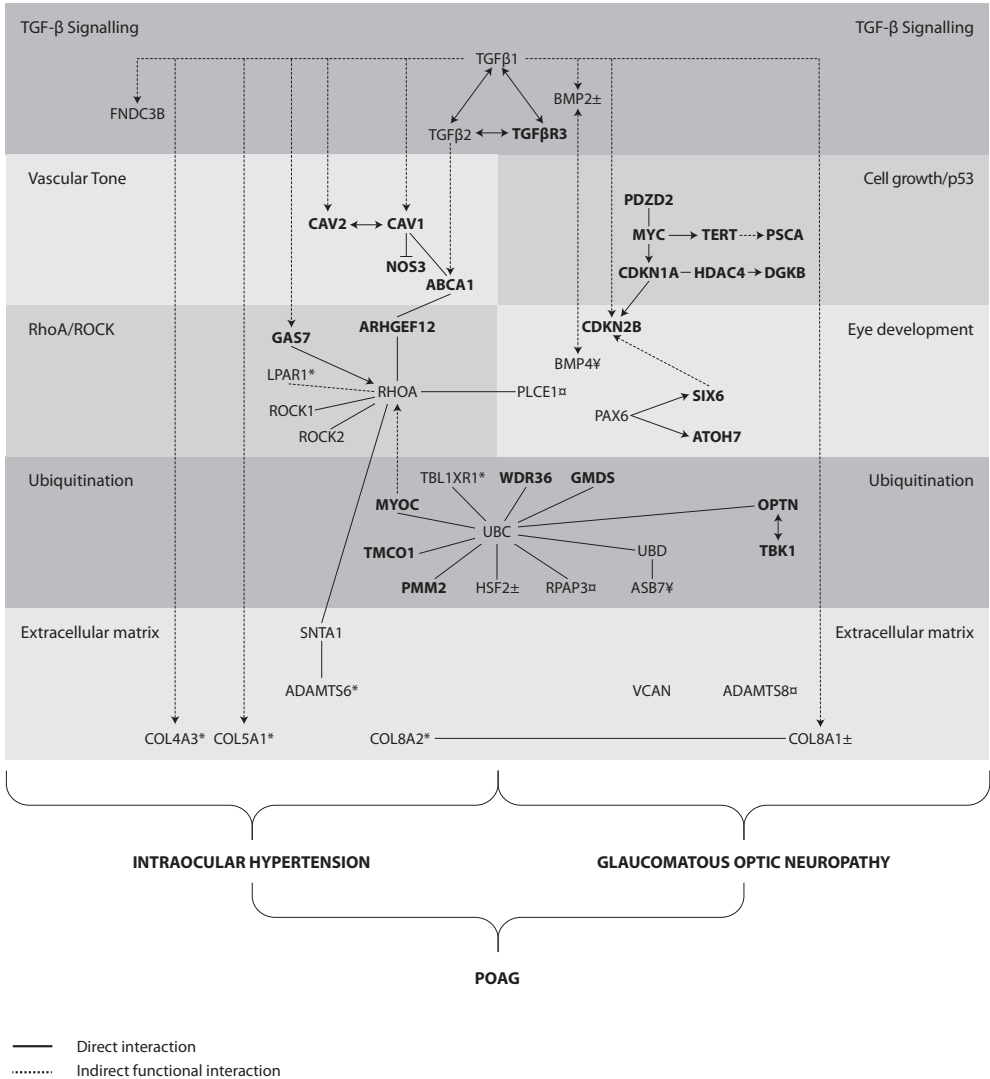
Table 1. Overview of genes located in novel identified genetic loci for intraocular pressure (IOP), vertical cup-disc ratio (VCDR), cup area (CA), disc area (DA), and open-angle glaucoma (OAG) and their putative gene function.

Gene	IOP	VCDR	CA	DA	OAG	Function
<i>ADAMTS8</i>	X	X				Extracellular matrix
<i>ABO</i>	X		X			Blood group system
<i>ABCA1</i>	X				X	Cholesterol binding
<i>ARHGEF12</i>	X				X	Rho/RhoA kinase
<i>FNDC3B</i>	X					?
chr 11	X					-
<i>BMP2</i>		X			X	TGF-beta
<i>CARD10</i>		X				Apoptosis
<i>COL8A1</i>		X				Extracellular matrix
<i>DGKB</i>		X				Apoptosis
<i>DUSP1</i>		X				Cellular stress response
<i>ENO4</i>		X				?
<i>EXOC2</i>		X				Exocyst complex
<i>HSF2</i>		X				Cellular stress response, protein aggregation
<i>PDZD2</i>		X				Apoptosis
<i>PLCE1</i>		X				Cell growth and differentiation
<i>PSCA</i>		X				Apoptosis
<i>RBM23</i>		X				Steroid response
<i>RPAP3</i>		X				Apoptosis
<i>RPE65</i>		X				Conversion of all-trans retinal to 11-cis retinal (visual cycle)
<i>RREB1</i>		X				Apoptosis
<i>SALL1</i>		X				Ocular development
<i>VCAN</i>		X				Extracellular matrix
<i>ASB7</i>			X	X		Ubiquitination
<i>CDC42BPA</i>			X	X		Peripheral actin formation, cytoskeletal reorganization

Table 1. (continued)

Gene	IOP	VCDR	CA	DA	OAG	Function
<i>BCAS3</i>			X			?
<i>CDKN1A</i>			X		X	Cell cycle
<i>CRISPLD1</i>			X			?
<i>DDHD1</i>			X			?
<i>DHRS3</i>			X			Oxidation/reduction of substrates like retinoids and steroids
<i>EFEMP1</i>			X			?
<i>FAM101A</i>			X			?
<i>FAM169B</i>			X			?
<i>FLNB</i>			X		X	Repair of vascular injury
<i>KPNB1</i>			X			Nucleocytoplasmic transport
<i>TRIB2</i>			X			Apoptosis
<i>TRIOBP</i>			X			Neural tissue development
<i>ABI3BP</i>				X		?
<i>CTNNA3</i>				X		Cell-cell adhesion in muscle cells
<i>DCAF4L2</i>				X		?
<i>DIRC3</i>				X		?
<i>ELP4</i>				X		Histone acetyltransferase complex
<i>F5</i>				X		Blood coagulation cascade
<i>GADD45A</i>				X		Apoptosis
<i>HORMAD2</i>				X		?
<i>NR2F2</i>				X		Gene regulation
<i>PRDM16</i>				X		Zinc finger transcription factor
<i>RARB</i>				X		Cell growth
<i>TMTC2</i>				X		?
<i>UGT8</i>				X		Apoptosis
<i>VGLL4</i>				X		Apoptosis

Figure 1. Putative pathways for POAG revealed by linkage and association studies⁹⁰. Seven different biological processes possibly implicated in POAG are shown in the figure. This map was built using Ingenuity Pathway Analysis (IPA). Solid lines imply direct relationships between proteins (e.g. physical protein-protein interaction or enzyme-substrate); dotted lines imply indirect functional relationships, such as co-expression, phosphorylation/dephosphorylation, activation/deactivation, transcription or inhibition. Proteins in bold correspond to known glaucoma genes.



METHODOLOGICAL CONSIDERATIONS

The studies described in this thesis focused on different endophenotypes of OAG. Due to the relatively low prevalence of OAG, the power to investigate the genetics of OAG in large population-based studies is relatively low. Exploring the genetics of endophenotypes which represent early changes in OAG pathogenesis makes it possible to investigate the genetics of OAG indirectly. Furthermore, using endophenotypes also help to overcome problems related to diagnostics that may differ across studies (see below). Using this approach, we identified some novel loci for OAG: *ABCA1* and *ARHGEF12* are highly associated with IOP and OAG. Also *CDKN1A* is associated with OAG, although the effect is smaller. A drawback of studying endophenotypes is that there may not be a straightforward relationship to disease. Some genes associated with endophenotypes (e.g. VCDR) are not associated with the disease (e.g. OAG, see Table 1); other genes associated with the disease may not be identified by studying endophenotypes. Ideally, a large case-control analysis with OAG cases and controls should be performed.

Obviously, there are differences in OAG definition among the case-control studies. Depending on the definition, the OAG prevalence can differ by a factor of ten⁴⁷. It seems that studies containing more advanced cases can identify more genetic variants with a relatively small number of cases (e.g. ANZRAG), presumably related to the fact that phenotyping is difficult in early glaucoma, which makes misclassification inevitable. However, it is harder to collect only advanced cases. The findings of our iGVFL study (**Chapter 2.1**) suggest that – for risk factor studies – it is not necessary to include GON as a confining criterion for diagnosis: cases with GVFL without obvious GON were similarly associated with known OAG risk factors as cases with both GVFL and clear cut GON. Agreement about the glaucoma definition will make collaboration and comparison of findings between studies easier, though, especially because different endophenotypes seem to point to different loci. For example, the separation of high tension glaucoma from normal tension glaucoma leads to different findings: some genes are important in only one of the two entities (e.g. *ARHGEF12* in HTG, see **Chapter 4.4**).

The effect of the individual SNPs identified in this thesis on OAG was low, as was the effect on the different endophenotypes. IOP and VCDR both appeared to be highly polygenic traits in which many variants have a small effect⁴⁸. We previously showed that common variants explain up to 53% of the phenotypic variance of VCDR. Although we published the largest meta-analyses so far, the number of participants included in our studies is still relatively small. The latest GWAS for height, for example, included 180,000 individuals and identified >600 loci⁴⁹. In order to completely unravel the genetics of IOP and VCDR, larger sample sizes are needed.

A strong point of the GWAS in this thesis is the inclusion of individuals from European as well as Asian ancestry. Unfortunately, individuals from African ancestry are missing. The prevalence of OAG in this population is reported to be four to six times higher than in individuals from European ancestry⁵⁰. Furthermore, the onset of the disease is at a younger age and the course is more severe⁵¹. The first studies investigating individuals from African ancestry focused on mutations in *MYOC* and *OPTN*⁵²⁻⁵⁶. Since mutations in *MYOC* are associated with high IOP, and African OAG patients often have a higher IOP, a higher number of

disease-causing mutations in *MYOC* can be expected. However, all reports have concluded that mutations in *MYOC* and *OPTN* play only a limited role in the pathogenesis of OAG. The highest frequency of glaucoma-causing *MYOC* mutations identified was 4.4% in a dataset from Ghana (90 OAG cases and 76 controls⁵⁷) and a dataset from South Africa (131 OAG cases and 131 controls⁵⁸). Liu et al. reported the largest study on glaucoma genetics in individuals from African ancestry⁵⁹. They evaluated SNPs in or near to *CDKN2B-AS1*, *TMCO1*, *CAV1/CAV2*, chromosome 8q22, and *SIX1/SIX6* in a dataset consisting of 1,150 OAG cases and 999 controls of African American ancestry, and 483 OAG cases and 593 controls from Ghana. There was only one association that reached Bonferroni significance: *CDKN2B-AS1* in the African American dataset (OR = 1.21 [95% CI 1.07-1.37]). SNPs in the *TMCO1* and *CAV1/2* regions reached nominal significance in this dataset. In the Ghanaian dataset, SNPs in *CAV1/2* reached nominal significance; none of the associations survived the correction for multiple testing. Williams et al. conducted a candidate gene association study in black South Africans⁶⁰. In 215 OAG cases and 214 controls, they genotyped 198 SNPs in genes known to be associated with OAG, optic nerve parameters or CCT (*TMCO1*, *MYOC*, *CDKN2B*, *CAV1/2*, *CYP1B1*, *WDR36*, *COL1A1*, *COL1A2*, *COL5A1*, *COL8A2*, *ZNF469*, *SIX1/6*, *ATOH7* and chromosome 2p16). Four SNPs reached a $P < 0.05$ but were not Bonferroni significant (rs6693322 in *COL8A2*, rs235917 in *MYOC*, rs16948744 in *COL1A1*, and rs9925231 in *ZNF469*). Since there are no ‘big players’ identified in African samples, more studies are necessary to elucidate the genetic background of OAG in Africans. Therefore, we recently designed a large case-control study: the Genetics In Glaucoma patients of African descent (GIGA) study.

The results from our GWAS have provided a better comprehension of the genetic architecture of OAG. Nevertheless, the exact mechanisms of the genes in OAG remain unclear. We attempted to clarify the role of *SIX6* by using the morpholino technology. With this approach one can knockdown the targeted gene. However, this is only effective for a few days and therefore you can only study the role of the gene in early development. Since OAG is a disease of the elderly, we are interested in the long-term effects. Furthermore, recent studies have shown that the findings after knockdown are not comparable to findings after complete knockout of the gene. Therefore, studying the effects of knockout are indispensable. Although the zebrafish eye is comparable to the human eye (see **Chapter 1.1**), there remain differences which limit the translation of findings to the disease in the human eye. Also, a considerable number of the associated SNPs probably do not have a direct effect on protein function, but may alter gene expression and protein levels. This can be examined by expression quantitative trait loci (e-QTL) analysis. Although there are publically available databases, many do not contain eye tissues which makes it difficult to translate findings to OAG. The availability of ocular tissues, especially tissues related to OAG, would be helpful to unravel the mechanisms leading to OAG.

CLINICAL IMPLICATIONS

In clinical practice, most tools for diagnosis or follow-up of OAG patients are based on optic nerve head or peripapillary RNFL scans. A promising device to measure these parameters is OCT. Based on our findings in **Chapter 2.2**, it is advisable to make an OCT scan of the optic disc and macular area as well and measure the RGCL thickness; for screening, the inferior part of

the macular scan appeared to be the most relevant part. An abnormal macular scan was not uncommon in those with perimetric loss limited to the area outside the central 10 degrees. This might be a true structure-function discrepancy, or just a consequence of the fact that the applied perimetric testing grid (24-2, also the default in clinical care) has only a few points in the central 10 degrees. Adding some centrally located test points to the 24-2 grid may improve the diagnostic performance for OAG.

Investigating the genetics of a disease will help us to learn more about the pathophysiology of the disease, may lead to DNA based diagnostic tests and finally, will help to develop novel mechanism-based therapies. The identification of the novel genes gave us insight into the different pathways involved in OAG.

Janssen et al. created a model for OAG prediction⁶¹. This model included age, gender, IOP, and risk alleles of 65 candidate genes for OAG. They found a high AUC of 0.88, compared to an AUC of 0.68 based on age, gender, and IOP. This indicates a promising future for genetic screening or risk profile assessment, but at this moment there are no such tests commercially available. Genetic variants associated with clinical characteristics of OAG patients have been published, and this can also be used for personalized medicine. Nowak et al. investigated the genetic variant *TP53* Arg72Pro in 186 OAG cases and 188 controls⁶². Although there was no difference in frequency of the risk allele between cases and controls, glaucoma cases carrying the genetic variant showed a statistically significant thinner RNFL. Wiggs et al. examined the same *TP53* variant in 264 OAG cases and 400 controls from the United States and 308 OAG cases and 178 controls from Australia (all of Caucasian descent)⁶³. They found an association between the variant and OAG ($P=0.032$), especially with normal tension glaucoma ($P=0.008$). The risk allele was more common in patients with early stage paracentral scotoma in the patients from the United States (odds ratio 2.2 [95% CI 1.43-3.39]). This finding was replicated in the patients from Australia (OR 2.32 [95% CI 1.24-4.34]). Nowak et al. further showed that genetic variants in *BDNF* and *HSP70-1* are possibly related to OAG progression⁶⁴. Interestingly, *HSP70-1* encodes a heat shock protein. We identified this pathway in our ONH GWAS. Loomis et al. found a stronger effect for SNPs in or near to *CAV1* and *CAV2* in OAG with early paracentral visual field loss (224 cases and 3,430 controls; OR 1.52 [95% CI 1.23-1.89]) than in OAG with peripheral visual field loss only (993 cases and 3,430 controls; OR 1.24 [95% CI 1.09-1.41])⁶⁵. Furthermore, they found that these SNPs were associated with OAG particularly in women. In the future it could be possible to identify individuals, based on genetic risk factors, who have a higher chance of developing progression or high-impact abnormalities, that is, visual field loss close to fixation. In these cases, early treatment may be warranted. A genetic test may also be helpful to identify OAG patients who need more or less frequent clinical examinations.

The goal of OAG treatment is to slow down disease progression to guarantee useful vision at the end of life at minimal side effects. At the moment, lowering the IOP is the only therapeutically approach with proven effectiveness. This can be achieved by medication (in most of the cases eye drops) or IOP lowering laser treatment or surgery. Unfortunately, approximately 15%^{66,67} of the treated patients become visual impaired or blind despite treatment. This demands the development of novel therapies. The *ARHGEF12* gene, associated with IOP and OAG, is part of the RhoA/RhoA kinase pathway. This pathway is implicated in IOP regulation by its effect

on the trabecular meshwork and Schlemm's canal cells. Rho kinase inhibitors increase the aqueous humor drainage through the trabecular meshwork and it has been shown that these inhibitors decrease IOP in monkeys and rabbits^{68,69}. Tanihara et al. investigated the effect of an inhibitor of ROCK, a RhoA kinase, in 45 healthy individuals from Japan⁷⁰. They divided the individuals in six groups with different treatment regimens and found the maximum decrease of IOP (-27%) on day 7 after 4 hours of eye drop instillation in the group that was treated with one drop a day. Williams et al. studied the IOP lowering effect of a Rho kinase inhibitor in patients with glaucoma or ocular hypertension⁷¹. They found an effect of the same magnitude as Tanihara et al., with a maximum effect after 2-4 hours. This effect was dose dependent and higher in the group receiving 2 drops a day compared to 1 drop a day. In both studies ocular hyperemia was an adverse effect, however, this effect disappeared after a few hours. No severe adverse effects were observed. These results seem promising but large randomized control trials, which are still lacking, must confirm these findings. Future studies could stratify individuals to genotype (i.e. the *ARHGEF12* SNP), to see if individuals with the genetic variant will benefit more from treatment targeting the RhoA/RhoA kinase pathway. Pharmacogenetics can also be applied to study the effect of statins. Low levels of high-density lipoprotein cholesterol has been reported to be associated with an increased risk of having glaucoma⁷², and several other studies have shown a beneficial effect of cholesterol-lowering drugs on the development of glaucoma⁷³⁻⁷⁶. This effect remains still controversial since other studies found no effect^{77,78}. The identification of *ABCA1*, important for cholesterol efflux, shed new light into this possible association.

FUTURE RESEARCH

Implementation of OCT can improve OAG diagnosis. This examination is time efficient and does not depend much on patient cooperation. Especially in the elderly it can be difficult to obtain a reliable visual field test. However, the sensitivity of OCT parameters is still not sufficiently high. Many studies have been reported on the utility of OCT testing in clinical practice but most of these studies were small. Therefore, large clinical-based studies should be performed to investigate the possibilities of replacing visual field testing by OCT scanning. The study described in **Chapter 2.2** investigated the role of OCT scanning in the screening, or diagnosis, of OAG, and therefore we cannot conclude that the macula scan is also useful for detection of OAG progression. The question whether the macula OCT scan is also useful for progression detection or not should be addressed in large studies.

If it is possible in the future to diagnose OAG based on OCT scans, harmonizing OAG definitions between studies will be easier. In this scenario, meta-analysis of large OAG case-control studies can be conducted without problems of heterogeneity between studies. This will be helpful in identifying new risk factors for OAG. We were not able to identify new risk factors with a large effect on OAG. We found no association between sleep apnea / apnea-hypopnea index and OAG or OAG related parameters (**Chapter 3.2**). Only a few population-based studies investigating this topic have been published and the association between sleep apnea and OAG still remains unclear. One of the weaknesses of our study was the cross-sectional design. New studies should be focusing on follow-up data in population-based studies. By performing such studies, the question about the relationship may be answered.

In contrast to general risk factors for glaucoma, numerous novel genetic risk factors have been identified for OAG. To unravel the genetics and subsequently understand the pathophysiology of OAG as much as possible, two things are important: 1) to identify novel genetic variants associated with OAG or its endophenotypes, and 2) to clarify the functional consequences of the genetic variants identified.

GCTA analyses in the Rotterdam Study estimated that the phenotypic variability of VCDR that may be explained by common SNPs (i.e. minor allele frequency >1%) is 41-53%, but the phenotypic variability explained by the current significantly identified SNPs is much lower. This suggests that a lot of common variants, that are associated with VCDR, have not yet been identified at the moment. Different strategies can be applied to find novel genetic variants associated with OAG or its endophenotypes: 1) increasing the number of analyzed individuals, including a large meta-analysis of OAG cases, 2) analyzing samples from the disproportionately affected African population, 3) identifying rare variants using exome chip or exome sequencing data, and 4) investigating the interaction between SNPs, and between SNPs and environmental factors. Gender might be a suitable environmental factor, as my findings in **Chapter 3.1** suggest that males might develop OAG at a younger age compared to females. Also, some studies have been published about the interaction of SNPs with estrogen-related measurements. Kang et al. published two papers about this topic. In the first study the authors found an interaction between SNPs in the *NOS3* gene and female gender and postmenopausal hormone use in patients with high tension glaucoma²⁸. In the second study, the authors identified an interaction between SNPs in the *NOS3* gene and age at menarche⁷⁹. In another study, interactions were found between *NOS3* SNPs and hypertension or cigarette smoking for the risk of developing OAG⁸⁰. Since estrogen plays an important role in the pubertal growth spurt⁸¹ and I found that height is related to IOP (**Chapter 3.3**), height (for which data is probably available in more studies) is another environmental factor that can be explored in interaction analyses.

Investigating the macular RGCL thickness as a new endophenotype can also identify novel genetic variants associated with OAG. The RNFL thickness is heritable⁸², and the RGCL thickness may also be heritable. Some studies already showed that *SIX6*, originally identified to be associated with VCDR, is associated with RNFL thickness^{46,83,84}. We have shown in this thesis that RGCL is a better parameter than VCDR for discriminating between OAG cases and controls. OCT examination is relatively easy, making it possible to collect retinal thicknesses on a large scale. Furthermore, studies focusing on other ophthalmological diseases like macular degeneration may have already collected OCT scans instead of IOP and optic nerve head measurements. If large data samples are available, a GWAS on macular RGCL thickness would be a logical next step.

Perhaps the most important challenge is to better understand the functional consequences of the identified genes. One of the approaches is to develop a stable knockout zebrafish model. This approach will allow us to investigate the effect of the absence of a gene of interest not only during embryogenesis but also during adulthood. The transgenic reporter line tg(brn3c:mGFP) makes it possible to visualize the optic nerve in vivo. Once a stable knockout model with optic nerve degeneration has been developed, this can serve as a therapeutic model. The zebrafish can easily absorb drugs from water. Previous studies have suggested that statins may prevent OAG (see above) and they would be one of the drugs suitable for

testing. The drugs can be dissolved in the water and subsequently the effect on the optic nerve can be measured, e.g. with the transgenic reporter line. The zebrafish will allow us to investigate statins and other new therapies on large scale in a relatively short time period before clinical studies with healthy people and glaucoma patients can be conducted.

Other sources of information about functional consequences of genetic variants are databases containing information about DNA methylation, histone modifications, gene expression, and microRNA (miRNA). In total, 1500 miRNAs are known to play a role in gene regulation in humans. The identification of miRNAs that are associated with glaucoma can lead to the discovery of novel mechanisms of the disease and may ultimately lead to novel therapies targeting these mechanisms. Recently, some miRNAs that are altered in retina of glaucomatous eyes have been identified⁸⁵. These miRNAs are also involved in central nervous system injury and play a role in apoptosis and TGF- β signaling, pathways that are also significant in GWAS (see above). Approximately 1% of the SNPs are involved in miRNA regulation in three different ways: 1) changes in the miRNA sequence that alter the folding or production of the miRNA, 2) changes in the binding of miRNA to target mRNA, and 3) changes in the binding site of the target mRNA. Databases can tell us which variants identified in GWAS are located in miRNA or miRNA binding sites. One of the main disadvantages is lack of disease specific tissue, i.e. eye tissue. Collected eye tissues of diseased people are important for further research. Another possibility is the generation of induced pluripotent stem cells (iPSCs). They can be generated from patients with OAG and subsequently differentiated into glaucoma specific cell types like retinal ganglion cells. These differentiated RGCs can give us insight in the molecular mechanisms underlying the disease. Genome editing can be applied to, for example, iPSCs and zebrafish. The relatively new CRISPR/Cas9 system can be used to achieve genome editing⁸⁶. Another method to learn more about the pathophysiology is to analyze metabolomics. Studies have been shown that glaucoma is associated with metabolic factors, including markers related to oxidative stress^{87,88}. The identification of differences in metabolites between OAG cases and controls can point towards novel pathways related to OAG. A previous study showed that serum phospholipids are related to Alzheimer's Disease⁸⁹. To overcome the problem of obtaining glaucoma-related eye tissues, a first good step would be to evaluate serum of OAG cases.

To conclude, I have investigated several aspects of OAG. Although I did not find a new major risk factor for OAG, I have identified numerous genetic variants associated with OAG endophenotypes. The genetic background of these endophenotypes provided new insight into the pathogenesis of OAG. Our findings can serve as starting points for new (functional) studies. The combination of epidemiologic and functional research will help us to unravel the pathogenesis and ultimately lead to the development of new therapies for this blinding disease.

References

1. Rohrschneider, K., Burk, R.O., Kruse, F.E. & Volcker, H.E. Reproducibility of the optic nerve head topography with a new laser tomographic scanning device. *Ophthalmology* 101, 1044-9 (1994).
2. Dreher, A.W. & Reiter, K. Retinal laser ellipsometry: a new method for measuring the retinal nerve fibre layer thickness distribution? *Clin Vis Sci* 7, 481-488 (1992).
3. Weinreb, R.N. et al. Histopathologic validation of Fourier-ellipsometry measurements of retinal nerve fiber layer thickness. *Arch Ophthalmol* 108, 557-60 (1990).
4. Czudowska, M.A. et al. Incidence of glaucomatous visual field loss: a ten-year follow-up from the Rotterdam Study. *Ophthalmology* 117, 1705-12 (2010).
5. Marcus, M.W., de Vries, M.M., Junoy Montolio, F.G. & Jansonius, N.M. Myopia as a risk factor for open-angle glaucoma: a systematic review and meta-analysis. *Ophthalmology* 118, 1989-1994 e2 (2011).
6. Tielsch, J.M. et al. A population-based evaluation of glaucoma screening: the Baltimore Eye Survey. *Am J Epidemiol* 134, 1102-10 (1991).
7. Jonas, J.B. et al. Body height, estimated cerebrospinal fluid pressure and open-angle glaucoma. *The Beijing Eye Study 2011. PLoS One* 9, e86678 (2014).
8. Gharahkhani, P. et al. Common variants near ABCA1, AFAP1 and GMDS confer risk of primary open-angle glaucoma. *Nat Genet* 46, 1120-5 (2014).
9. Chen, Y. et al. Common variants near ABCA1 and in PMM2 are associated with primary open-angle glaucoma. *Nat Genet* 46, 1115-9 (2014).
10. Yeghiazaryan, K. et al. An enhanced expression of ABC 1 transporter in circulating leukocytes as a potential molecular marker for the diagnostics of glaucoma. *Amino Acids* 28, 207-11 (2005).
11. Kuo, C.Y., Lin, Y.C., Yang, J.J. & Yang, V.C. Interaction abolishment between mutant caveolin-1(Delta62-100) and ABCA1 reduces HDL-mediated cellular cholesterol efflux. *Biochem Biophys Res Commun* 414, 337-43 (2011).
12. Murata, M. et al. VIP21/caveolin is a cholesterol-binding protein. *Proc Natl Acad Sci U S A* 92, 10339-43 (1995).
13. de Haan, W., Bhattacharjee, A., Ruddle, P., Kang, M.H. & Hayden, M.R. ABCA1 in adipocytes regulates adipose tissue lipid content, glucose tolerance, and insulin sensitivity. *J Lipid Res* 55, 516-23 (2014).
14. Rickels, M.R. et al. Loss-of-function mutations in ABCA1 and enhanced beta-cell secretory capacity in young adults. *Diabetes* 64, 193-9 (2015).
15. Patel, D.C. et al. Type 2 diabetes is associated with reduced ATP-binding cassette transporter A1 gene expression, protein and function. *PLoS One* 6, e22142 (2011).
16. Ergen, H.A., Zeybek, U., Gok, O. & Karaali, Z.E. Investigation of ABCA1 C69T polymorphism in patients with type 2 diabetes mellitus. *Biochem Med (Zagreb)* 22, 114-20 (2012).
17. Daimon, M. et al. Association of the ABCA1 gene polymorphisms with type 2 DM in a Japanese population. *Biochem Biophys Res Commun* 329, 205-10 (2005).
18. Wessel, J. et al. Low-frequency and rare exome chip variants associate with fasting glucose and type 2 diabetes susceptibility. *Nat Commun* 6, 5897 (2015).
19. Qi, L. et al. Genetic variants in ABO blood group region, plasma soluble E-selectin levels and risk of type 2 diabetes. *Hum Mol Genet* 19, 1856-62 (2010).
20. Hernandez, A.M. et al. Upregulation of p21 activates the intrinsic apoptotic pathway in beta-cells. *Am J Physiol Endocrinol Metab* 304, E1281-90 (2013).
21. Zhao, D., Cho, J., Kim, M.H., Friedman, D.S. & Guallar, E. Diabetes, fasting glucose, and the risk of glaucoma: a meta-analysis. *Ophthalmology* 122, 72-8 (2015).
22. Zhou, M., Wang, W., Huang, W. & Zhang, X. Diabetes mellitus as a risk factor for open-angle glaucoma: a systematic review and meta-analysis. *PLoS One* 9, e102972 (2014).
23. Kang, J.H. et al. Vascular tone pathway polymorphisms in relation to primary open-angle glaucoma. *Eye (Lond)* 28, 662-71 (2014).
24. Nathanson, J.A. & McKee, M. Alterations of ocular nitric oxide synthase in human glaucoma. *Invest Ophthalmol Vis Sci* 36, 1774-84 (1995).
25. Stamer, W.D., Lei, Y., Boussommier-Calleja, A., Overby, D.R. & Ethier, C.R. eNOS, a pressure-dependent regulator of intraocular pressure. *Invest Ophthalmol Vis Sci* 52, 9438-44 (2011).
26. Wang, R. et al. Caveolin-1 functions as a key regulator of 17beta-estradiol-mediated autophagy and apoptosis in BT474 breast cancer cells. *Int J Mol Med* 34, 822-7 (2014).
27. Logan, J.F. et al. Evidence for association of endothelial nitric oxide synthase gene in subjects with glaucoma and a history of migraine. *Invest Ophthalmol Vis Sci* 46, 3221-6 (2005).
28. Kang, J.H. et al. Endothelial nitric oxide synthase gene variants and primary open-angle glaucoma: interactions with sex and postmenopausal hormone use. *Invest Ophthalmol Vis Sci* 51, 971-9 (2010).
29. Hulsman, C.A. et al. Is open-angle glaucoma associated with early menopause? The Rotterdam Study. *Am J*

- Epidemiol 154, 138-44 (2001).
30. Pasquale, L.R. & Kang, J.H. Female reproductive factors and primary open-angle glaucoma in the Nurses' Health Study. *Eye (Lond)* 25, 633-41 (2011).
 31. Pasquale, L.R., Rosner, B.A., Hankinson, S.E. & Kang, J.H. Attributes of female reproductive aging and their relation to primary open-angle glaucoma: a prospective study. *J Glaucoma* 16, 598-605 (2007).
 32. Vajaranant, T.S. et al. Risk of glaucoma after early bilateral oophorectomy. *Menopause* 21, 391-8 (2014).
 33. Newman-Casey, P.A. et al. The potential association between postmenopausal hormone use and primary open-angle glaucoma. *JAMA Ophthalmol* 132, 298-303 (2014).
 34. Na, K.S. et al. The ocular benefits of estrogen replacement therapy: a population-based study in postmenopausal Korean women. *PLoS One* 9, e106473 (2014).
 35. Prokai-Tatrai, K. et al. 17beta-estradiol eye drops protect the retinal ganglion cell layer and preserve visual function in an in vivo model of glaucoma. *Mol Pharm* 10, 3253-61 (2013).
 36. Pasquale, L.R. et al. Estrogen pathway polymorphisms in relation to primary open angle glaucoma: an analysis accounting for gender from the United States. *Mol Vis* 19, 1471-81 (2013).
 37. Ramdas, W.D. et al. Lifestyle and risk of developing open-angle glaucoma: the Rotterdam study. *Arch Ophthalmol* 129, 767-72 (2011).
 38. Fuchshofer, R. & Tamm, E.R. The role of TGF-beta in the pathogenesis of primary open-angle glaucoma. *Cell Tissue Res* 347, 279-90 (2012).
 39. Jampel, H.D., Roche, N., Stark, W.J. & Roberts, A.B. Transforming growth factor-beta in human aqueous humor. *Curr Eye Res* 9, 963-9 (1990).
 40. Pena, J.D., Taylor, A.W., Ricard, C.S., Vidal, I. & Hernandez, M.R. Transforming growth factor beta isoforms in human optic nerve heads. *Br J Ophthalmol* 83, 209-18 (1999).
 41. Hannon, G.J. & Beach, D. p15INK4B is a potential effector of TGF-beta-induced cell cycle arrest. *Nature* 371, 257-61 (1994).
 42. Cirulli, E.T. et al. Exome sequencing in amyotrophic lateral sclerosis identifies risk genes and pathways. *Science* 347, 1436-41 (2015).
 43. Campello, L., Esteve-Rudd, J., Cuenca, N. & Martin-Nieto, J. The ubiquitin-proteasome system in retinal health and disease. *Mol Neurobiol* 47, 790-810 (2013).
 44. Koga, T. et al. Differential effects of myocilin and optineurin, two glaucoma genes, on neurite outgrowth. *Am J Pathol* 176, 343-52 (2010).
 45. Qiu, Y., Shen, X., Shyam, R., Yue, B.Y. & Ying, H. Cellular processing of myocilin. *PLoS One* 9, e92845 (2014).
 46. Carnes, M.U. et al. Discovery and functional annotation of SIX6 variants in primary open-angle glaucoma. *PLoS Genet* 10, e1004372 (2014).
 47. Wolfs, R.C. et al. Changing views on open-angle glaucoma: definitions and prevalences--The Rotterdam Study. *Invest Ophthalmol Vis Sci* 41, 3309-21 (2000).
 48. Ramdas, W.D. et al. Genetic architecture of open angle glaucoma and related determinants. *J Med Genet* 48, 190-6 (2011).
 49. Lango Allen, H. et al. Hundreds of variants clustered in genomic loci and biological pathways affect human height. *Nature* 467, 832-8 (2010).
 50. Tielsch, J.M. et al. Racial variations in the prevalence of primary open-angle glaucoma. The Baltimore Eye Survey. *JAMA* 266, 369-74 (1991).
 51. Herndon, L.W. et al. Survey of glaucoma in an eye clinic in Ghana, West Africa. *J Glaucoma* 11, 421-5 (2002).
 52. Ayala-Lugo, R.M. et al. Variation in optineurin (OPTN) allele frequencies between and within populations. *Mol Vis* 13, 151-63 (2007).
 53. Fingert, J.H. et al. Analysis of myocilin mutations in 1703 glaucoma patients from five different populations. *Hum Mol Genet* 8, 899-905 (1999).
 54. Liu, W. et al. Low prevalence of myocilin mutations in an African American population with primary open-angle glaucoma. *Mol Vis* 18, 2241-6 (2012).
 55. Liu, Y. et al. Optineurin coding variants in Ghanaian patients with primary open-angle glaucoma. *Mol Vis* 14, 2367-72 (2008).
 56. Melki, R. et al. Mutational analysis of the Myocilin gene in patients with primary open-angle glaucoma in Morocco. *Ophthalmic Genet* 24, 153-60 (2003).
 57. Challa, P. et al. Prevalence of myocilin mutations in adults with primary open-angle glaucoma in Ghana, West Africa. *J Glaucoma* 11, 416-20 (2002).
 58. Whigham, B.T. et al. Myocilin mutations in black South Africans with POAG. *Mol Vis* 17, 1064-9 (2011).
 59. Liu, Y. et al. Investigation of known genetic risk factors for primary open angle glaucoma in two populations of African ancestry. *Invest Ophthalmol Vis Sci* 54, 6248-54 (2013).
 60. Williams, S.E., Carmichael, T.R., Allingham, R.R., Hauser, M. & Ramsay, M. The genetics of POAG in black South Africans: a candidate gene association study. *Sci Rep* 5, 8378 (2015).
 61. Janssen, S.F. et al. The vast complexity of primary open angle glaucoma: disease genes, risks, molecular mechanisms and pathobiology. *Prog Retin Eye Res* 37, 31-67 (2013).

62. Nowak, A. et al. The relationship of TP53 and GRIN2B gene polymorphisms with risk of occurrence and progression of primary open-angle glaucoma in a Polish population. *Pol J Pathol* 65, 313-21 (2014).
63. Wiggs, J.L. et al. The p53 codon 72 PRO/PRO genotype may be associated with initial central visual field defects in caucasians with primary open angle glaucoma. *PLoS One* 7, e45613 (2012).
64. Nowak, A. et al. BDNF and HSP gene polymorphisms and their influence on the progression of primary open-angle glaucoma in a Polish population. *Arch Med Sci* 10, 1206-13 (2014).
65. Loomis, S.J. et al. Association of CAV1/CAV2 genomic variants with primary open-angle glaucoma overall and by gender and pattern of visual field loss. *Ophthalmology* 121, 508-16 (2014).
66. Ernest, P.J. et al. Prevalence of end-of-life visual impairment in patients followed for glaucoma. *Acta Ophthalmol* 91, 738-43 (2013).
67. Peters, D., Bengtsson, B. & Heijl, A. Factors associated with lifetime risk of open-angle glaucoma blindness. *Acta Ophthalmol* 92, 421-5 (2014).
68. Tian, B., Wang, R.F., Podos, S.M. & Kaufman, P.L. Effects of topical H-7 on outflow facility, intraocular pressure, and corneal thickness in monkeys. *Arch Ophthalmol* 122, 1171-7 (2004).
69. Tokushige, H. et al. Effects of topical administration of γ -39983, a selective rho-associated protein kinase inhibitor, on ocular tissues in rabbits and monkeys. *Invest Ophthalmol Vis Sci* 48, 3216-22 (2007).
70. Tanihara, H. et al. Intraocular pressure-lowering effects and safety of topical administration of a selective ROCK inhibitor, SNJ-1656, in healthy volunteers. *Arch Ophthalmol* 126, 309-15 (2008).
71. Williams, R.D., Novack, G.D., van Haarlem, T., Kocpczynski, C. & Group, A.R.P.A.S. Ocular hypotensive effect of the Rho kinase inhibitor AR-12286 in patients with glaucoma and ocular hypertension. *Am J Ophthalmol* 152, 834-41 e1 (2011).
72. Kim, M.J., Kim, M.J., Kim, H.S., Jeoung, J.W. & Park, K.H. Risk factors for open-angle glaucoma with normal baseline intraocular pressure in a young population: the Korea National Health and Nutrition Examination Survey. *Clin Experiment Ophthalmol* 42, 825-32 (2014).
73. De Castro, D.K. et al. Effect of statin drugs and aspirin on progression in open-angle glaucoma suspects using confocal scanning laser ophthalmoscopy. *Clin Experiment Ophthalmol* 35, 506-13 (2007).
74. Leung, D.Y. et al. Simvastatin and disease stabilization in normal tension glaucoma: a cohort study. *Ophthalmology* 117, 471-6 (2010).
75. Marcus, M.W. et al. Cholesterol-lowering drugs and incident open-angle glaucoma: a population-based cohort study. *PLoS One* 7, e29724 (2012).
76. McGwin, G., Jr. et al. Statins and other cholesterol-lowering medications and the presence of glaucoma. *Arch Ophthalmol* 122, 822-6 (2004).
77. Iskedjian, M. et al. Effect of selected antihypertensives, antidiabetics, statins and diuretics on adjunctive medical treatment of glaucoma: a population based study. *Curr Med Res Opin* 25, 1879-88 (2009).
78. Owen, C.G. et al. Hypotensive medication, statins, and the risk of glaucoma. *Invest Ophthalmol Vis Sci* 51, 3524-30 (2010).
79. Kang, J.H., Wiggs, J.L., Haines, J., Abdrabou, W. & Pasquale, L.R. Reproductive factors and NOS3 variant interactions in primary open-angle glaucoma. *Mol Vis* 17, 2544-51 (2011).
80. Kang, J.H. et al. Endothelial nitric oxide synthase gene variants and primary open-angle glaucoma: interactions with hypertension, alcohol intake, and cigarette smoking. *Arch Ophthalmol* 129, 773-80 (2011).
81. Simm, P.J., Bajpai, A., Russo, V.C. & Werther, G.A. Estrogens and growth. *Pediatr Endocrinol Rev* 6, 32-41 (2008).
82. van Koolwijk, L.M. et al. Genetic contributions to glaucoma: heritability of intraocular pressure, retinal nerve fiber layer thickness, and optic disc morphology. *Invest Ophthalmol Vis Sci* 48, 3669-76 (2007).
83. Cheng, C.Y. et al. Association of common SIX6 polymorphisms with peripapillary retinal nerve fiber layer thickness: the Singapore Chinese Eye Study. *Invest Ophthalmol Vis Sci* 56, 478-83 (2015).
84. Kuo, J.Z. et al. Quantitative Trait Locus Analysis of SIX1-SIX6 With Retinal Nerve Fiber Layer Thickness in Individuals of European Descent. *Am J Ophthalmol* 160, 123-30 e1 (2015).
85. Jayaram, H., Cepurna, W.O., Johnson, E.C. & Morrison, J.C. MicroRNA Expression Within The Glaucomatous Retina. ARVO annual meeting (2015).
86. Nemudryi, A.A., Valetdinova, K.R., Medvedev, S.P. & Zakian, S.M. TALEN and CRISPR/Cas Genome Editing Systems: Tools of Discovery. *Acta Naturae* 6, 19-40 (2014).
87. Chang, D. et al. The evaluation of the oxidative stress parameters in patients with primary angle-closure glaucoma. *PLoS One* 6, e27218 (2011).
88. Majsterek, I. et al. Evaluation of oxidative stress markers in pathogenesis of primary open-angle glaucoma. *Exp Mol Pathol* 90, 231-7 (2011).
89. Gonzalez-Dominguez, R., Garcia-Barrera, T. & Gomez-Ariza, J.L. Combination of metabolomic and phospholipid-profiling approaches for the study of Alzheimer's disease. *J Proteomics* 104, 37-47 (2014).
90. Iglesias, A.I. et al. Genes, pathways, and animal models in primary open-angle glaucoma. *Eye (Lond)* 29, 1285-98 (2015).

PART 7

**SAMENVATTING
SUMMARY**

**ACKNOWLEDGEMENTS –
DANKWOORD**

PHD PORTFOLIO

LIST OF PUBLICATIONS

ABOUT THE AUTHOR

SAMENVATTING

Open kamerhoek glaucoom is een belangrijke oorzaak van onherstelbare blindheid. In open kamerhoek glaucoom leidt verlies van retinale ganglion cellen tot schade aan de oogzenuw. Dit veroorzaakt gezichtsveldverlies en uiteindelijk blindheid. Veranderingen in de kop van de oogzenuw, de papil genaamd, kunnen worden vast gelegd met confocale scanning laser ophthalmoscopie (Heidelberg Retina Tomograph[HRT]), scanning laser polarimetrie (GDx) of 'Optical Coherence Tomography' (OCT). Belangrijke risicofactoren voor het ontwikkelen van open kamerhoek glaucoom zijn een verhoogde oogdruk, hoge leeftijd, bijziendheid of myopie, etniciteit, een dunne centrale corneadikte en een positieve familie anamnese voor glaucoom. De pathofysiologie van open kamerhoek glaucoom is echter nog grotendeels onbekend.

Doel van het in dit proefschrift beschreven onderzoek was de diagnose van glaucoom te verbeteren en de pathofysiologie van deze blindmakende ziekte beter te begrijpen. De specifieke doelen van het onderzoek zijn: 1) evaluatie van de diagnostische mogelijkheden van de OCT scan voor open kamerhoek glaucoom, 2) ontdekken van nieuwe risicofactoren voor open kamerhoek glaucoom of een verhoogde oogdruk, 3) het identificeren van nieuwe genetische varianten die geassocieerd zijn met open kamerhoek glaucoom, en 4) het onderzoeken van de functionele betekenis van genen geassocieerd met open kamerhoek glaucoom. Het onderzoek werd uitgevoerd in het Erasmus Rotterdam Gezondheid Onderzoek (ERGO), de Erasmus Rucphen Familie (ERF) studie, bevolkingsonderzoeken uit het European Eye Epidemiology (E³) Consortium en bevolkingsonderzoeken en patiënt-controle studies uit het Internationale Glaucoom Genetica Consortium (IGGC).

Hoofdstuk 1 geeft een algemene introductie over open kamerhoek glaucoom (**Hoofdstuk 1.1**) en een samenvatting over de kennis van de genetische achtergrond van open kamerhoek glaucoom tot en met 2011 (**Hoofdstuk 1.2**). In **Hoofdstuk 2** onderzochten wij de bruikbaarheid van de OCT scan in de diagnose van open kamerhoek glaucoom in het ERGO onderzoek. Door dit in een bevolkingsonderzoek te bekijken voorkom je vertekening door selectie. In een klinische studie zullen vooral patiënten opgenomen zijn die voor oogartsen makkelijk herkenbare glaucoomkenmerken hebben. In **Hoofdstuk 2.1** bepaalden we eerst de gebieden van de OCT scan die gesegmenteerd kunnen worden, dat wil zeggen, waarvan de kwaliteit van de meting voldoende is om de dikte van de diverse retinale cellagen te kunnen bepalen. Dit gebied was groter voor de macula scans dan voor de papil scans. Vervolgens analyseerden wij de test-retest variabiliteit van de laagdiktemetingen als functie van de grootte van het geanalyseerde gebied. Zoals verwacht stijgt de test-retest variabiliteit naar mate kleinere gebieden van de OCT scan worden geanalyseerd. Hiermee rekening houdend bepaalden wij in **Hoofdstuk 2.2** hoe je het beste uit een OCT scan informatie over de aan- of afwezigheid van glaucoom kunt halen. Het bleek dat je het beste kunt kijken naar relatief grote gebieden van de maculascan, bijvoorbeeld naar de gemiddelde RGCL-dikte in de hele onderhelft.

In **Hoofdstuk 3** onderzochten wij de risicofactoren voor open kamerhoek glaucoom en een verhoogde oogdruk. Wij berekenden de incidentie van gezichtsvelduitval door glaucoom twee decennia na het begin van het ERGO onderzoek in **Hoofdstuk 3.1**. Ook onderzochten

wij in dit cohort de rol van reeds bekende risicofactoren (leeftijd, geslacht, oogdruk, familie anamnese, myopie, diastolische bloeddruk en body mass index [BMI]) voor verschillende open kamerhoek glaucoom fenotypes, dat wil zeggen gezichtsvelduitval en/of een glaucomateuze papil. De incidentie van gezichtsveld uitval was 2.9 per 1000 persoonsjaren. Oogdruk en leeftijd waren geassocieerd met beide open kamerhoek glaucoom fenotypes (gezichtsvelduitval of een glaucomateuze papil). Een hoge BMI was beschermend voor alle fenotypes, echter niet significant. Geslacht, myopie en diastolische bloeddruk waren met geen van de uitkomsten geassocieerd. In **Hoofdstuk 3.2** onderzochten wij slaap apneu, dat wil zeggen een ademstilstand tijdens het slapen, als een risico factor voor open kamerhoek glaucoom. Verschillende kleine patiënt-controle studies vonden een verhoogde prevalentie van slaap apneu in patiënten met open kamerhoek glaucoom. Wij vonden echter geen associatie tussen slaap apneu en kenmerken van de papil of oogdruk. Dit benadrukt het belang van onderzoek uitgevoerd in grote (bevolkings)onderzoeken waarin mensen lange tijd worden vervolgd. Als laatste onderzochten wij in **Hoofdstuk 3.3** risicofactoren (leeftijd, geslacht, BMI, systolische bloeddruk en brilsterkte) voor de oogdruk in 12 bevolkingsonderzoeken van het E³ consortium. Wij ontdekten dat langere mensen een lagere oogdruk hebben. Verder vonden wij dat de oogdruk stijgt tot de leeftijd van 60 jaar en weer afneemt na het 70ste levensjaar. Er was geen geografisch verschil in oogdruk binnen Europa.

Hoofdstuk 4 was gericht op de genetische risicofactoren van open kamerhoek glaucoom. Om nieuwe genetische varianten geassocieerd met oogdruk of papil kenmerken te identificeren werd het Internationale Glaucoom Genetica Consortium geformeerd. In **Hoofdstuk 4.1, 4.2** en **4.3** werden meta-analyses van ongeveer 2,5 miljoen genetische varianten (als beschreven in de HapMap imputaties) in ruim 35,000 personen uitgevoerd binnen het IGGC; in **Hoofdstuk 4.5** werden meta-analyses van ongeveer 8 miljoen genetische varianten (als beschreven in de 1000 Genomes) binnen het IGGC uitgevoerd. **Hoofdstuk 4.4** was gebaseerd op een meta-analyse binnen het ERGO onderzoek, gebruik makende van 8 miljoen varianten als beschreven in de 1000 Genomes referentie set. In **Hoofdstuk 4.1** ontdekten wij vier nieuwe genetische varianten geassocieerd met oogdruk. Deze varianten lagen in of dichtbij de genen *FNDC3B*, *ABCA1* en *ABO*. Verschillende genen liggen in de buurt van de vierde genetische variant (chromosoom 11p11.2). Drie van de vier genetische varianten waren ook geassocieerd met open kamerhoek glaucoom, waarvan *ABCA1* genoom-wijd significant. In **Hoofdstuk 4.2** worden tien nieuwe genetische varianten voor de verticale cup-disc ratio (VCDR) beschreven: *COL8A1*, *DUSP1*, *EXOC2*, *PLCE1*, *ADAMTS8*, *RPAP3*, *SALL1*, *BMP2*, *HSF2* en *CARD10*. Individuen die veel genetische varianten hebben, hebben een 2,5 keer zo hoog risico op het ontwikkelen van open kamerhoek glaucoom vergeleken met individuen die weinig van deze genetische varianten hebben. Uit dit onderzoek blijkt verder dat ‘negatieve regulatie van celtgroei’ en ‘cellulaire respons op stress’ belangrijke processen zijn in open kamerhoek glaucoom. In een analyse dat ook gebruik maakte van de HapMap referentie set (**Hoofdstuk 4.3**) vonden wij nieuwe genetische varianten voor de papil oppervlakte (*CDC42BPA*, *F5*, *DIRC3*, *RARB*, *ABI3BP*, *DCAF4L2*, *ELP4*, *TMTTC2*, *NR2F2* en *HORMAD2*) en oppervlakte van de uitholling (*DHRS3*, *TRIB2*, *EFEMP1*, *FLNB*, *FAM101*, *DDHD1*, *ASB7*, *KPNB1*, *BCAS3* en *TRIOBP*). Verschillende van deze genen spelen een rol in processen die belangrijk zijn voor open kamerhoek glaucoom. Toekomstig werk gericht op papil of uitholling oppervlakte zal nieuwe mechanismen belangrijk voor open kamerhoek glaucoom identificeren. In **Hoofdstuk 4.4** werd de 1000 Genomes referentie set gebruikt in het ERGO onderzoek om nieuwe

genetische risicofactoren voor oogdruk te identificeren. Een genetische variant in *ARHGEF12* werd gevonden als een nieuwe genetische risicofactor en deze bevinding werd gevalideerd in andere bevolkingsonderzoeken. Dit gen was ook geassocieerd met open kamerhoek glaucoom in twee patiënt-controle studies. Het *ARHGEF12* gen bindt aan *ABCA1* en speelt een rol in de RhoA/RhoA kinase signalering dat een rol speelt in oogdruk regulatie. Deze RhoA/RhoA kinase signalering is een nieuw aanknopingspunt voor oogdruk verlagende medicatie en onze bevinding kan nieuw licht schijnen op therapeutische opties. Tenslotte werden in **Hoofdstuk 4.5** nieuwe genetische varianten voor oogdruk, VCDR, uitholling en papil oppervlakte gevonden binnen het IGGC met behulp van de 1000 Genomes referentie set. Eén van deze nieuwe genen – *CDKN1A* dat genoom-wijd significant geassocieerd was met de oogzenuw uitholling – was ook significant geassocieerd met open kamerhoek glaucoom. In een zebavis model werd een in vivo interactie tussen *six6b* en *cdkn1a* gevonden. Voor de eerste keer vonden wij genen die een rol spelen in oogdruk en papilkenmerken: *ADAMTS8* en *ABO* waren genoom-wijd significant voor oogdruk en VCDR en uitholling oppervlakte.

In **Hoofdstuk 5.1** werden de functionele consequenties van *SIX6*, een gen geassocieerd met VCDR en open kamerhoek glaucoom, onderzocht. Met behulp van een morfolino werd het *six6b* in de zebavis geïnactiveerd. Dit resulteerde in een klein oog, een onderontwikkelde lens en kleinere oogzenuw diameter. Ook was de expressie van *cdkn2b* verhoogd. Dit gen is geassocieerd met VCDR en open kamerhoek glaucoom en speelt een rol in de cel cyclus regulatie. Daarom werd de proliferatie activiteit onderzocht en een veranderd proliferatie patroon van retinale cellen werd gevonden. Deze bevindingen suggereren dat *six6b* is betrokken bij de vroege ontwikkeling van het oog.

Als laatste geeft **Hoofdstuk 6** een algemene interpretatie van deze resultaten. Dit hoofdstuk beschrijft ook de methodologische overwegingen, klinische implicaties en suggesties voor toekomstig onderzoek.

Concluderend zijn er verschillende aspecten van open kamerhoek glaucoom in dit proefschrift onderzocht. We identificeerden veel nieuwe genetische varianten voor de fenotypes (oogdruk, VCDR, oppervlakte van de papil en uitholling van de oogzenuw). Dit zorgt voor nieuwe inzichten in de genetische achtergrond van glaucoom en daardoor voor meer kennis over de pathogenese van glaucoom.

SUMMARY

Open-angle glaucoma (OAG) is an important cause of irreversible blindness. In OAG, loss of retinal ganglion cells leads to damage of the optic nerve. This causes visual field loss and eventually blindness. Changes in the optic nerve head (ONH) can be examined with confocal scanning laser ophthalmoscopy (Heidelberg Retina Tomograph [HRT]), scanning laser polarimetry (GDx) or Optical Coherence Tomography (OCT). Important risk factors for OAG are elevated intraocular pressure (IOP), high age, myopia, ethnicity, thin central corneal thickness, and a positive family history for OAG. However, the pathophysiology still remains largely unknown.

In order to improve the diagnosis and learn more about the pathophysiology of this blinding disease, the main objectives of the research described in this thesis were to: 1) address the diagnostic utility of the OCT scan for OAG, 2) elucidate new risk factors for OAG or IOP, 3) identify novel genetic variants associated with OAG or its endophenotypes, and 4) assess the functional consequences of genetic variants associated with OAG. Our study populations included the population-based Rotterdam Study, the Erasmus Rucphen Family (ERF) Study, population-based studies from the European Eye Epidemiology (E³) Consortium and population-based and OAG case-control studies from the International Glaucoma Genetics Consortium (IGGC).

Chapter 1 gives a general introduction to OAG (**Chapter 1.1**) and discusses the knowledge about the genetic background of OAG until 2011 (**Chapter 1.2**). In **Chapter 2**, we investigated the utility of the OCT scan in the diagnosis of OAG in the Rotterdam Study. By investigating this in a population-based study, you prevent selection bias. In a clinical study, most included patients are patients with clear glaucoma characteristics. In **Chapter 2.1**, we first determined the regions of the OCT scan that can be segmented, i.e., scans with sufficient quality to determine the thickness of several retinal layers. This region was higher in the macular scan than in the ONH scan. Next, we calculated the test-retest variability as a function of the size of regions of interest. As expected, the test-retest variability increases when analyzing smaller regions of interest. Taking this into account, we determined in **Chapter 2.2** the best way to use information from the OCT scan for discrimination between glaucoma patients and controls. It appeared that it works best to investigate relatively large areas of the macular scan, for example the mean RGCL thickness in the inferior half of the scan.

In **Chapter 3**, we explored risk factors for OAG and IOP. We calculated the incidence of visual field loss caused by glaucoma two decades after the onset of the Rotterdam Study in **Chapter 3.1**. We furthermore assessed risk factors (age, gender, baseline IOP, family history, myopia, diastolic blood pressure (DBP), and body mass index [BMI]) for different OAG phenotypes, i.e. visual field loss and/or glaucomatous optic neuropathy (GON). The incidence rate of visual field loss was 2.9 per 1000 person years. IOP and age were associated with both OAG phenotypes. BMI was protective for all OAG phenotypes, although not significant. Gender, myopia, and DBP were not associated at all. We investigated sleep apnea as a risk factor for OAG in **Chapter 3.2**. Although several small case-control studies demonstrated a higher

prevalence of sleep apnea among OAG patients or vice versa, we found no association between sleep apnea and optic nerve head parameters or IOP. This emphasizes the need of research performed in large (population-based) follow-up studies. Finally, in **Chapter 3.3** we assessed risk factors (age, sex, height, BMI, systolic blood pressure, and refractive error) for IOP as outcome in 12 population-based studies across Europe (within the E³ consortium). We discovered a novel association of lower IOP in taller people. Furthermore, IOP increased to the age of 60 years, and decreased in subjects older than 70 years. There was no geographical variation in IOP across Europe.

Chapter 4 focused on genetic risk factors for OAG and associated outcomes. To identify new genetic variants associated with IOP or ONH parameters, the International Glaucoma Genetics Consortium was established. In **Chapter 4.1**, **4.2**, and **4.3** meta-analyses using HapMap as a reference panel were performed within the IGGC; in **Chapter 4.5** meta-analyses using 1000 Genomes as a reference panel were performed within the IGGC. **Chapter 4.4** was based on a meta-analysis in the Rotterdam Study using 1000 Genomes reference panel. In **Chapter 4.1** we identified four novel loci associated with IOP. These loci were located in or near to the genes *FNDC3B*, *ABCA1*, and *ABO*. Many genes are located in the fourth region (chromosome 11p11.2). Three of four loci were also associated with OAG, of which *ABCA1* was genome-wide significant for OAG. In **Chapter 4.2** ten novel loci were identified for the vertical cup-disc ratio (VCDR): *COL8A1*, *DUSP1*, *EXOC2*, *PLCE1*, *ADAMTS8*, *RPAP3*, *SALL1*, *BMP2*, *HSF2*, and *CARD10*. Individuals carrying many of these genetic variants have a 2.5-fold increased risk of OAG compared to individuals carrying only a few of these genetic variants. The research described in this chapter furthermore identified negative regulation of cell growth and cellular response to environmental stress as important pathways in OAG. Another analysis using HapMap as reference panel (**Chapter 4.3**) found novel loci for disc area (*CDC42BPA*, *F5*, *DIRC3*, *RARB*, *ABI3BP*, *DCAF4L2*, *ELP4*, *TMTC2*, *NR2F2*, and *HORMAD2*) and cup area (*DHRS3*, *TRIB2*, *EFEMP1*, *FLNB*, *FAM101*, *DDHD1*, *ASB7*, *KPNB1*, *BCAS3*, and *TRIOBP*). Several genes have a role in pathways implicated in OAG, and it is likely that further work focusing on disc or cup area will identify new pathways important for OAG. In **Chapter 4.4**, 1000 Genomes imputations were used in the Rotterdam Study to identify new risk factors for IOP. A genetic variant in *ARHGEF12* was identified as a new risk factor and was validated in other population-based samples. Furthermore, this gene was associated with OAG in two independent case-control studies. The *ARHGEF12* gene binds to *ABCA1* and plays a role in the RhoA/RhoA kinase pathway that has an important role in IOP regulation. This pathway is a new target for IOP lowering medication and our finding may shed new light into new therapeutic options. Finally, in **Chapter 4.5** novel genetic variants for IOP, VCDR, cup area and disc area were found in the IGGC using 1000 Genomes imputations. One of these new genes – *CDKN1A* that was genome-wide significantly associated with cup area – was also highly significantly associated with OAG. In a zebrafish model, an *in vivo* interaction was found between *six6b* and *cdkn1a*. For the first time, we identified genes associated with two endophenotypes: genetic variants in *ADAMTS8* and *ABO* were genome-wide significant for IOP and ONH (VCDR or cup area).

In **Chapter 5.1** the functional consequences of *SIX6*, a gene associated with VCDR and OAG, were investigated. Knockdown of *six6b* in zebrafish was achieved by using a morpholino targeting the translation initiation site and exon 1 donor site of *six6b*. Knockdown led to a small eye, underdeveloped lens and reduced optic nerve diameter. Furthermore, expression

analysis showed an up-regulation of *cdkn2b*. This gene is also associated with VCDR and OAG and plays a role in cell cycle regulation. Therefore, the proliferative activity was assessed and an alteration of the proliferative pattern of retinal cells was found. Our findings suggest that *six6b* is involved in early eye development.

Finally, **Chapter 6** gives a general interpretation of these results. This chapter also addressed methodological considerations, clinical implications and suggestions for future research.

To conclude, we have investigated several aspects of open-angle glaucoma in this thesis. We identified numerous genetic variants associated with OAG endophenotypes. These findings lead to new insights into the genetic background of OAG and eventually more knowledge about the pathogenesis of OAG.

ACKNOWLEDGEMENTS – DANKWOORD

Na ruim 4 jaar is het opeens tijd om het dankwoord te schrijven. De afgelopen jaren zijn voorbij gevlogen en in deze jaren heb ik ontzettend veel geleerd. Ik heb gemerkt dat onderzoek doen net een schaakpartij is: je hebt de combinatie van stukken nodig om de partij af te ronden. Zo is het ook met mijn onderzoek geweest. Ik heb het niet alleen gedaan, maar heb de hulp gehad van mensen uit vele verschillende hoeken. Het samenwerken heeft geleid tot het afronden van mijn onderzoek en het publiceren van mijn proefschrift. Ik wil iedereen hiervoor bedanken.

In het bijzonder wil ik allereerst mijn promotoren prof.dr.ir. Cornelia van Duijn, prof.dr. Nomdo M. Jansonius en prof.dr. Caroline C.W. Klaver bedanken.

Cock, toen ik in Melbourne een presentatie gaf werd u beschreven als ‘the queen of the genetic epidemiology’. Dat klopt helemaal! Ik sta er altijd weer versteld van hoeveel details u boven water weet te halen en hoe makkelijk u verbanden legt. Bedankt voor uw enthousiasme en bedankt voor de kansen die ik heb gekregen. Niet alleen qua publicaties, maar ook wat betreft mijn tijd in het buitenland en het diner in de Ridderzaal. Dat zal ik niet snel vergeten!

Nomdo, uw kennis, nuchterheid en heldere ideeën maakten het niet erg om uren in de trein richting Groningen te zitten. De Groningsche Mosterdsoep is één van mijn favoriete gerechten geworden. Elke keer als ik dit recept lees moet ik weer lachen vanwege uw humor. Net zoals de ansichtkaart uit Zweden die er voor heeft gezorgd dat het helemaal goed gekomen is met Hoofdstuk 4.3!

Caroline, jouw enthousiasme heeft er voor gezorgd dat ik na mijn keuze-onderzoek besloot om te solliciteren in Rotterdam. Het is mooi om te zien hoe je in een korte tijd zo’n grote onderzoeksgroep hebt opgebouwd. Tijdens de Blind Games werd al snel duidelijk dat iedereen ontzettend fanatiek is en we met elkaar het onderste uit de kan halen. Het is fijn om in zo’n omgeving te werken. Bedankt voor de inspiratie en de mogelijkheden die je mij hebt gegeven.

Beste prof.dr. Robert Hofstra, bedankt dat u wilt plaatsnemen in de kleine commissie en mijn manuscript heeft willen beoordelen. Prof.dr. Paul Foster and prof.dr. Louis Pasquale, thank you for taking part in the inner doctoral committee and thank you for your extensive review that has improved my thesis. Prof.dr. J.R. Vingerling, prof.dr. C.A.B. Webers en prof.dr. R.Q. Hintzen: bedankt voor het plaatsnemen in de grote commissie. Hans, bedankt voor de mogelijkheid om zowel mijn promotie onderzoek als de opleiding tot oogarts in een hele fijne leeromgeving te mogen doen.

Gabriëlle en Virginie, jullie waren mijn kamergenootjes van het eerste uur. Bedankt dat ik met al mijn vragen bij jullie terecht kon. Nog meer bedankt voor alle gezelligheid die er voor zorgde dat ik elke dag met plezier naar het werk toe ging. Ik zal de vele congressen en

vakanties daarna nooit vergeten. Ada en Corina, jullie hebben ontzettend veel data verzameld voor het ERGO onderzoek en mede daardoor kon ik al snel beginnen met het analyseren van data en schrijven van artikelen. Bedankt! Jan Roelof, JR, het was altijd gezellig om jouw huisgenootje te zijn. Freya, mijn vaste Ajax kamergenoot: we gaan snel Oreos bakken! Anna, het was super leuk om samen naar ARVO in Seattle te gaan. Leuk dat we nu samen in opleiding zijn! Annemarie, Laurence, Milly, Pieter, Sheila en Willem: het voelt soms toch wel een beetje raar om uit de onderzoekstoren weg te zijn, maar ik weet zeker dat het met jullie als nieuwe lichten helemaal goed gaat komen met het onderzoek daar boven. Magda, ik heb niet heel direct met je samen gewerkt, maar ik klop wel een keer bij je aan als ik me aan een aanvraag ga wagen ;-) Elza, Maaïke, Nicole en Riet: bedankt dat jullie altijd weer een afspraak voor mij konden regelen ondanks de overvolle agenda's van mijn promotoren.

Ik wil alle andere onderzoekers van de afdeling Epidemiologie bedanken voor de gezelligheid en momenten van afleiding. In het bijzonder team Epi'sch (Annemarie, Lisette, Mariana, Nikkie en Rachel): bedankt voor alle spelletjesavonden. Annemarie en Lisette, het was altijd erg gezellig op het ERGO centrum en ik vind het super leuk dat ik uiteindelijk ook met jullie data onderzoek heb gedaan. Mariana, gezellig dat je weer terug bent in het Erasmus MC! Ik moet binnenkort toch maar eens die thorax telefoon lastig vallen. Nikkie, buuf, nogmaals bedankt dat je mijn redder in nood bent geweest in je pyjama! Rachel, waar gaan we de volgende keer sushi eten? Ik heb nu al honger... Ook wil ik iedereen van de Genetische Epidemiologie bedanken. Ayse, Elisa, Lennart, Linda, Maarten en Sarah: jullie hielpen de oog-meisjes, waaronder ik, altijd weer op weg met lastige scriptjes.. Dankjulliewel! Najaf, the GE02 course was my most favorite course! Thanks for all your help. Sven, na ons Olli avontuur wist ik het zeker: jij zou mijn paranimf worden! Je begrijpt wel dat je als werkechtgenoot altijd een bijzonder plekje in mijn hart houdt ;-) Adriana, thanks for being my glaucoma twin! I wish you all the best with finishing your thesis and I am sure you will make a good choice for your future. Het was super leuk om de laatste maanden bij jullie op de kamer te werken. Bedankt dat jullie vandaag naast mij staan!

Prof.dr. Bert Hofman, ik heb geluk dat ik met zo'n grote wereldstudie mocht werken. Bedankt voor het opzetten van het ERGO onderzoek en bedankt voor de leuke en leerzame epidemiologie cursussen. Anneke en co: de onderzoeksdagen op het ERGO centrum waren altijd een leuke afwisseling van al het computerwerk. Bedankt voor de fijne sfeer! Eric, Frank, Jolande, Nano, René en René: bedankt voor alle onmisbare hulp achter de schermen.

Prof.dr. Rob Willemsen, bedankt voor de mogelijkheid om het epidemiologische onderzoek te combineren met functioneel onderzoek. Ik ben benieuwd wat de vissen ons de komende jaren voor glaucoom gaan brengen!

Dit proefschrift zou niet bestaan zonder alle internationale samenwerkingen. Prof. Michael Abramoff, mijn trip naar Iowa was mijn eerste werk-gerelateerde reis naar het buitenland. Het duurde niet zo heel lang, al moest ik bijna door een sneeuwstorm langer blijven. Bedankt voor de samenwerking die uiteindelijk heeft geresulteerd in een mooi Hoofdstuk 2. I would like to thank everybody from the European Eye Epidemiology Consortium and the International Glaucoma Genetics Consortium. Cécile, thank you for the great meetings in Bordeaux and Rome. Anthony and prof. Paul Foster, it was nice to work with you on Chapter 3.3! Prof. Janey

Wiggs, thank you for organizing all the IGGC meetings, they were really great. Pirro and prof. Chris Hammond, it was great to see you in Rotterdam and London. Stuart, thank you so much for giving me the opportunity to study in Brisbane. It was a very fruitful time and I have learned a lot. Aniket, Gabriel, Pik-Fang, and Puya: you made my time in Australia unforgettable! Thanks for all the tea-times and day- and weekend trips. Lu Yi, I hope to celebrate my PhD with you in Stockholm. Alex, if I was a dinosaur, which one would I be? Prof. David Mackey, thank you for the invitation to visit your lab. Seyhan, you made my trip to Perth so special! Thanks for everything, especially for showing me one of the most beautiful spots in Australia: the Henrietta rocks ;-) I hope to see you soon! Prof. Jamie Craig: next time I'm going to Adelaide!

Ik wil alle arts-assistenten, oogartsen en overige medewerkers van de afdeling Oogheelkunde bedanken voor de interesse in mijn onderzoek en het begrip dat ik me soms niet helemaal op de poli's kon focussen. Het was even wennen om weer terug te zijn in de kliniek, maar mede dankzij jullie is dit helemaal goed gekomen. Speciale dank gaat ook uit naar Emine en Giorgio Porro. Dankzij jullie ben ik terecht gekomen in Rotterdam, dus heel erg bedankt hiervoor! Roger, bedankt voor de vele uren die je hebt gestoken in het classificeren en bediscussiëren van de gezichtsvelden van de ERGO deelnemers en het doornemen van mijn artikelen. Het is leuk om het nu allemaal van de andere kant te bekijken en ik kijk er naar uit om de komende jaren nog heel erg veel te leren. Wishal, overall waar ik kwam kende iedereen jou en was de eerste stap voor een nieuwe samenwerking al gezet. Bedankt dat je de tijd nam om kritisch naar mijn artikelen te kijken.

Ik wil alle arts-onderzoekers Oogheelkunde uit de rest van Nederland bedanken voor de gezelligheid op de (inter)nationale congressen en verdedigingen van elkaar. Gelukkig is het wereldje niet zo groot en blijven we elkaar nog lang zien! In het speciaal wil ik iedereen in Groningen bedanken. Wanneer gaan we weer met z'n allen wadlopen? Nancy, wat heb jij mij in de watten gelegd in Groningen. Het leek wel alsof ik in hotel Aychoua sliep. Bedankt! Benjamin, jij ook bedankt voor de logeerpartijen tijdens mijn bezoeken aan Groningen, al neem ik de volgende keer wel mijn eigen rood-witte kussensloop mee ;-) Ik zal nu helaas niet meer zo vaak in Groningen te vinden zijn, dus het lijkt mij een goed idee om wat vaker pannenkoeken dates te plannen met Martine en Sebastiaan!

Ellen, Jeruëlle, Kirsten, Liliane en Mariska: we moeten snel weer daten! Ik ben blij dat ik nu weer meer tijd heb om met jullie door te brengen. Bedankt voor de vriendschap en jullie interesse in mijn onderzoek! Kirsten, Olga en Susanne: het is weer tijd voor de Suriname en Jordanië reünie! Laila, veel succes met het afronden van jouw onderzoek en het combineren van de opleiding. Marlies, door de drukte kon ik je helaas niet eerder opzoeken in Cannes, maar ik ben blij dat het nog gelukt is voor de eerste verjaardag van Julia ;-) Ik kom je snel weer opzoeken hoor! Daniëlle, het is super leuk dat ik nu dichterbij jou in de buurt woon. Zo is de kans weer wat groter dat we later samen in het bejaardenhuis gaan schaken!

Jessy, jij verdient een speciaal plekje in dit dankwoord! Ontzettend bedankt voor jouw hulp bij het in elkaar zetten van dit proefschrift. Ik ben super blij met het resultaat. Het leek de laatste weken alsof we elkaars huisgenootjes weer waren. Dat wordt wel even afkicken, maar we gaan snel vieren dat we het hebben gehaald en iets super moois hebben neergezet!

Ik heb een hele lieve familie en daar bof ik maar mooi mee. Ik heb nog nooit zoveel verjaardagen moeten afzeggen als in de periode dat ik mijn proefschrift moest afronden, maar dat ga ik snel weer recht zetten! Ik kijk nu al uit naar de barbecue tijdens Oud en Nieuw. Dat wordt een startschot voor een jaar vol fantastische mijlpalen en feestjes. Ik heb er zin in! Roel, Jenny, Esther, Anne en Remco: doe maar gewoon, dan doe je al gek genoeg. Dat is niet hoe mijn eigen familie, maar ook hoe jullie in het leven staan. Daarom voel ik me zo thuis bij jullie. Bedankt dat jullie altijd voor mij klaar staan en mij op alle fronten willen helpen!

Fernando, Francien en Yuran: in een relatief korte tijd verdubbelde ons gezin opeens. Het is super gezellig met z'n allen en daar wil ik jullie graag voor bedanken. Gerdien en Petra, van het Mega Piraten Festijn tot aan het Zand festival, van Guus Meeuwis tot Nick en Simon: bedankt voor alle gezellige muzikale afleiding. Nu ik dit schrijf heb ik mij net ingeschreven voor de Acht van Apeldoorn en besef ik me nog eens extra wat voor grenzen jullie aan het verleggen zijn. Ga zo door! Jaap, nu kan ik jou eindelijk bedanken voor de hulp bij de figuren uit Hoofdstuk 2! Het verbouwen van jullie huis is net zo'n groot project (of eigenlijk groter) als mijn proefschrift geweest. Succes met de laatste loodjes! Lieve papa en mama, bedankt voor jullie onvoorwaardelijke steun. Het is niet altijd makkelijk om aan de andere kant van Nederland te wonen, maar door jullie opvoeding is de Rotterdamse mentaliteit (niet zeuren, maar gewoon werken!) mij niet vreemd. Bedankt dat jullie dit mij hebben meegegeven.

Lieve Paul, woorden schieten tekort om jou voor alles te bedanken. Bedankt dat je me aanmoedigde om naar Australië te gaan (al ga ik echt nooit meer zo lang weg zonder jou!), bedankt voor het runnen van het huishouden waardoor ik de laatste maanden een workaholic kon zijn, bedankt voor jouw luisterende oor, steun en vertrouwen. Op naar 27 mei!

PHD PORTFOLIO

Summary of PhD training and teaching

Name PhD student: Hendrika Springelkamp
 Erasmus MC Departments: Ophthalmology and Epidemiology
 Research School: NIHES
 PhD period: 2011-2015
 Supervisors: prof.dr.ing. C.M. van Duijn, prof.dr. N.M. Jansonius and
 prof.dr. C.C.W. Klaver

PhD training	Year	Workload (ECTS)
Courses		
Master of Health Sciences, Genetic Epidemiology (NIHES)	2011-2013	70
Workshop on Indesign CS5 (Molmed)	2012	0.3
Biomedical English Writing and Communication	2014	4.0
Genome Browsing with Ensembl and Viewing Variation (EBI)	2015	0.3
Seminars, symposia and workshops		
2 nd European Eye Epidemiology Workshop, Bordeaux, France	2012	0.3
PhD Day, Erasmus Medical Center, Rotterdam	2012	0.3
CHARGE Meeting, Rotterdam	2013	0.3
Basiscursus Gezichtsvelonderzoek, Groningen	2013	0.2
3 rd European Eye Epidemiology Workshop, Bordeaux, France (oral presentation)	2013	1.0
Research day Erasmus Medical Center (oral presentation)	2013	1.0
4 th European Eye Epidemiology Workshop, Rome, Italy (oral presentation)	2014	1.0
Australian Neurogenetics Conference, Brisbane, Australia	2014	0.6
Glaucoomzorg met Perimetrie, Groningen	2015	0.2
LVAO course glaucoma, Utrecht	2015	0.3
Research seminars, department of Epidemiology, Erasmus MC	2011-2015	4.5
Weekly seminars, department of Ophthalmology, Erasmus MC	2011-2015	4.5

PhD training	Year	Workload (ECTS)
National conferences		
Nederlands Oogheelkundig Gezelschap (NOG) jaarvergadering, Groningen (poster presentation)	2012	1.0
2 nd Dutch Ophthalmology PhD Students (DOPS) conference, Nijmegen (oral presentation)	2013	1.0
NOG jaarvergadering, Groningen (oral presentation)	2013	1.0
3 rd DOPS conference, Nijmegen (oral presentation)	2014	1.0
NOG jaarvergadering, Maastricht (oral presentation)	2014	1.0
NOG jaarvergadering, Groningen (oral presentation)	2015	1.0
International conferences		
ARVO Annual Meeting, Fort Lauderdale, USA (poster presentation)	2012	1.0
ARVO Annual Meeting, Seattle, USA (oral presentation)	2013	1.0
International Society for Genetic Eye Diseases and Retinoblastoma Meeting, Ghent, Belgium (invited oral presentation)	2013	1.0
ARVO Annual Meeting, Orlando, USA (poster presentation)	2014	1.0
Translation of Genetic Eye Research Annual Meeting, Brisbane, Australia (invited oral presentation)	2014	1.0
ARVO Annual Meeting, Denver, USA (oral presentation)	2015	1.0
Teaching		
Supervising research internship Genetics in Africa project	2012-2014	1.4
Other		
Co-organizer of the 1 st DOPS conference, Nijmegen	2012	3.0
Chair of glaucoma session, ARVO Annual Meeting, Denver, USA	2015	0.1
Side-kick at the 'Avond van de Wetenschap en Maatschappij', Ridderzaal, Den Haag	2015	0.1
Reviewer for several international journals	2012-today	1.0

LIST OF PUBLICATIONS

Publications on which this thesis is based

Buitendijk GH*, **Springelkamp H***, Ho L, Klaver CCW (2013) Age-related macular degeneration and primary open-angle glaucoma: genetics and gene-environment interaction. In: Scholl HP, Massof RW, West S (Eds). *Ophthalmology and the ageing society*, (pp57-82). Berlin Heidelberg. Springer.

Springelkamp H, Lee K, Ramdas WD, Vingerling JR, Hofman A, Klaver CC, Sonka M, Abramoff MD, Jansonius NM. Optimizing the Information Yield of 3D OCT in Glaucoma. *Invest Ophthalmol Vis Sci*. 2012 Dec 13;53(13):8162-71.

Springelkamp H, Lee K, Wolfs RC, Buitendijk GH, Ramdas WD, Hofman A, Vingerling JR, Klaver CC, Abramoff MD, Jansonius NM. Population-based evaluation of retinal nerve fiber layer, retinal ganglion cell layer, and inner plexiform layer as a diagnostic tool for glaucoma. *Invest Ophthalmol Vis Sci*. 2014 Nov 20;55(12):8428-38.

Hysi PG*, Cheng CY*, **Springelkamp H***, Macgregor S*, Bailey JN*, Wojciechowski R*, Vitart V, Nag A, Hewitt AW, Höhn R, Venturini C, Mirshahi A, Ramdas WD, Thorleifsson G, Vithana E, Khor CC, Stefansson AB, Liao J, Haines JL, Amin N, Wang YX, Wild PS, Ozel AB, Li JZ, Fleck BW, Zeller T, Staffieri SE, Teo YY, Cuellar-Partida G, Luo X, Allingham RR, Richards JE, Senft A, Karssen LC, Zheng Y, Bellenguez C, Xu L, Iglesias AI, Wilson JF, Kang JH, van Leeuwen EM, Jonsson V, Thorsteinsdottir U, Despriet DD, Ennis S, Moroi SE, Martin NG, Jansonius NM, Yazar S, Tai ES, Amouyel P, Kirwan J, van Koolwijk LM, Hauser MA, Jonasson F, Leo P, Loomis SJ, Fogarty R, Rivadeneira F, Kearns L, Lackner KJ, de Jong PT, Simpson CL, Pennell CE, Oostra BA, Uitterlinden AG, Saw SM, Lotery AJ, Bailey-Wilson JE, Hofman A, Vingerling JR, Maubaret C, Pfeiffer N, Wolfs RC, Lemij HG, Young TL, Pasquale LR, Delcourt C, Spector TD, Klaver CC, Small KS, Burdon KP, Stefansson K, Wong TY; BMES GWAS Group; NEIGHBORHOOD Consortium; Wellcome Trust Case Control Consortium 2, Viswanathan A, Mackey DA, Craig JE, Wiggs JL, van Duijn CM, Hammond CJ, Aung T. Genome-wide analysis of multi-ancestry cohorts identifies new loci influencing intraocular pressure and susceptibility to glaucoma. *Nat Genet*. 2014 Oct;46(10):1126-30. *contributed equally

Springelkamp H, Höhn R, Mishra A, Hysi PG, Khor CC, Loomis SJ, Bailey JN, Gibson J, Thorleifsson G, Janssen SF, Luo X, Ramdas WD, Vithana E, Nongpiur ME, Montgomery GW, Xu L, Mountain JE, Gharahkhani P, Lu Y, Amin N, Karssen LC, Sim KS, van Leeuwen EM, Iglesias AI, Verhoeven VJ, Hauser MA, Loon SC, Despriet DD, Nag A, Venturini C, Sanfilippo PG, Schillert A, Kang JH, Landers J, Jonasson F, Cree AJ, van Koolwijk LM, Rivadeneira F, Souzeau E, Jonsson V, Menon G; Blue Mountains Eye Study—GWAS group, Weinreb RN, de Jong PT, Oostra BA, Uitterlinden AG, Hofman A, Ennis S, Thorsteinsdottir U, Burdon KP; NEIGHBORHOOD Consortium; Wellcome Trust Case Control Consortium 2 (WTCCC2), Spector TD, Mirshahi A, Saw SM, Vingerling JR, Teo YY, Haines JL, Wolfs RC, Lemij HG, Tai ES, Jansonius NM, Jonas JB, Cheng CY, Aung T, Viswanathan AC, Klaver CC, Craig JE, Macgregor S, Mackey DA, Lotery AJ,

Stefansson K, Bergen AA, Young TL, Wiggs JL, Pfeiffer N, Wong TY, Pasquale LR, Hewitt AW, van Duijn CM, Hammond CJ. Meta-analysis of genome-wide association studies identifies novel loci that influence cupping and the glaucomatous process. *Nat Commun.* 2014 Sep 22;5:4883.

Springelkamp H, Mishra A, Hysi PG, Gharahkhani P, Höhn R, Khor CC, Cooke Bailey JN, Luo X, Ramdas WD, Vithana E, Koh V, Yazar S, Xu L, Forward H, Kearns LS, Amin N, Iglesias AI, Sim KS, van Leeuwen EM, Demirkan A, van der Lee S, Loon SC, Rivadeneira F, Nag A, Sanfilippo PG, Schillert A, de Jong PT, Oostra BA, Uitterlinden AG, Hofman A; NEIGHBORHOOD Consortium, Zhou T, Burdon KP, Spector TD, Lackner KJ, Saw SM, Vingerling JR, Teo YY, Pasquale LR, Wolfs RC, Lemij HG, Tai ES, Jonas JB, Cheng CY, Aung T, Jansonius NM, Klaver CC, Craig JE, Young TL, Haines JL, MacGregor S, Mackey DA, Pfeiffer N, Wong TY, Wiggs JL, Hewitt AW, van Duijn CM, Hammond CJ. Meta-analysis of Genome-Wide Association Studies Identifies Novel Loci Associated With Optic Disc Morphology. *Genet Epidemiol.* 2015 Mar;39(3):207-16.

Springelkamp H, Iglesias AI, Cuellar-Partida G, Amin N, Burdon KP, van Leeuwen EM, Gharahkhani P, Mishra A, van der Lee SJ, Hewitt AW, Rivadeneira F, Viswanathan AC, Wolfs RC, Martin NG, Ramdas WD, van Koolwijk LM, Pennell CE, Vingerling JR, Mountain JE, Uitterlinden AG, Hofman A, Mitchell P, Lemij HG, Wang JJ, Klaver CC, Mackey DA, Craig JE, van Duijn CM, MacGregor S. ARHGEF12 influences the risk of glaucoma by increasing intraocular pressure. *Hum Mol Genet.* 2015 May 1;24(9):2689-99.

Iglesias AI, **Springelkamp H**, van der Linde H, Severijnen LA, Amin N, Oostra B, Kockx CE, van den Hout MC, van Ijcken WF, Hofman A, Uitterlinden AG, Verdijk RM, Klaver CC, Willemsen R, van Duijn CM. Exome sequencing and functional analyses suggest that SIX6 is a gene involved in an altered proliferation-differentiation balance early in life and optic nerve degeneration at old age. *Hum Mol Genet* 2014 Mar 1;23(5):1320-32.

Submitted manuscripts on which this thesis is based

Springelkamp H, Wolfs RCW, Ramdas WD, Hofman A, Vingerling JR, Klaver CCW, Jansonius NM. Incidence of glaucomatous visual field loss after two decades of follow-up: the Rotterdam Study.

Springelkamp H, Zuurbier LA, Luik AI, Wolfs RCW, Hofman A, Klaver CCW, Tiemeier H, Jansonius NM. Relationship between sleep apnea and open-angle glaucoma: a population-based cohort study.

Khawaja AP, **Springelkamp H**, Creuzot-Garcher C, Delcourt C, Hofman A, Höhn R, Iglesias AI, Wolfs RCW, Korobelnik J-F, Silva R, Topouzis F, Williams KM, Bron AM, Buitendijk GHS, Cachulo ML, Cougnard-Grégoire A, Dartigues J-F, Hammond CJ, Pfeiffer N, Salonikiou A, van Duijn CM, Vingerling JR, Luben RN, Mirshahi A, Lamparter J, Klaver CCW, Jansonius NM, Foster PJ. Associations with intraocular pressure across Europe: The European Eye Epidemiology (E³) Consortium.

Springelkamp H, Iglesias AI, Mishra A, Höhn R, Wojciechowski R, Khawaja AP, Nag A, Wang JX, Wang JJ, Cuellar-Partida G, Gibson J, Cooke Bailey JN, Vithana EN, Gharahkhani P, Boutin T, Ramdas WD, Zeller T, Luben RN, Yonova-Doing E, Viswanathan AC, Yazar S, Cree AJ, Haines JL, Koh JY, Souzeau E, Wilson JF, Amin N, Müller C, Venturini C, Kearns LS, Kang JH, NEIGHBORHOOD Consortium, Tham YC, Zhou T, van Leeuwen EM, Nickels S, Sanfilippo P, Liao J, van der Linde H, Zhao W, van Koolwijk LME, Zheng L, Rivadeneira F, Baskaran M, van der Lee S, Perera S, de Jong PTVM, Oostra BA, Uitterlinden AG, Fan Q, Hofman A, Tai E-S, Vingerling JR, Sim X, Wolfs RCW, Teo YY, Lemij HG, Khor CC, Willemsen R, Lackner KJ, Aung T, Jansonius NM, Montgomery G, Wild PS, Young TL, Burdon KP, Hysi PG, Pasquale LR, Wong TY, Klaver CCW, Hewitt AW, Jonas JB, Mitchell P, Lotery AJ, Foster PJ, Vitart V, Pfeiffer N, Craig JE, Mackey DA, Hammond CJ, Wiggs JL, Cheng CY, van Duijn CM, MacGregor S. New insights into genetics of primary open-angle glaucoma based on meta-analyses of intraocular pressure and optic disc characteristics.

Other publications

Iglesias AI, **Springelkamp H**, Ramdas WD, Klaver CC, Willemsen R, van Duijn CM. Genes, pathways, and animal models in primary open-angle glaucoma. 2015 Oct;29(10):1285-98. doi: 10.1038/eye.2015.160.

Cuellar-Partida G, **Springelkamp H**, Lucas SE, Yazar S, Hewitt AW, Iglesias AI, Montgomery GW, Martin NG, Pennell CE, van Leeuwen EM, Verhoeven VJ, Hofman A, Uitterlinden AG, Ramdas WD, Wolfs RC, Vingerling JR, Brown MA, Mills RA, Craig JE, Klaver CC, van Duijn CM, Burdon KP, MacGregor S, Mackey DA. WNT10A exonic variant increases the risk of keratoconus by decreasing corneal thickness. *Hum Mol Genet.* 2015 Sep 1;24(17):5060-8. doi: 10.1093/hmg/ddv211.

Zhang L, Buitendijk GH, Lee K, Sonka M, **Springelkamp H**, Hofman A, Vingerling JR, Mullins RF, Klaver CC, Abramoff MD. Validity of Automated Choroidal Segmentation in SS-OCT and SD-OCT. *Invest Ophthalmol Vis Sci.* 2015 May;56(5):3202-11. doi: 10.1167/iovs.14-15669.

Lu Y, Vitart V, Burdon KP, Khor CC, Bykhovskaya Y, Mirshahi A, Hewitt AW, Koehn D, Hysi PG, Ramdas WD, Zeller T, Vithana EN, Cornes BK, Tay WT, Tai ES, Cheng CY, Liu J, Foo JN, Saw SM, Thorleifsson G, Stefansson K, Dimasi DP, Mills RA, Mountain J, Ang W, Hoehn R, Verhoeven VJ, Grus F, Wolfs R, Castagne R, Lackner KJ, **Springelkamp H**, Yang J, Jonasson F, Leung DY, Chen LJ, Tham CC, Rudan I, Vataavuk Z, Hayward C, Gibson J, Cree AJ, MacLeod A, Ennis S, Polasek O, Campbell H, Wilson JF, Viswanathan AC, Fleck B, Li X, Siscovick D, Taylor KD, Rotter JI, Yazar S, Ulmer M, Li J, Yaspan BL, Ozel AB, Richards JE, Moroi SE, Haines JL, Kang JH, Pasquale LR, Allingham RR, Ashley-Koch A; NEIGHBOR Consortium, Mitchell P, Wang JJ, Wright AF, Pennell C, Spector TD, Young TL, Klaver CC, Martin NG, Montgomery GW, Anderson MG, Aung T, Willoughby CE, Wiggs JL, Pang CP, Thorsteinsdottir U, Lotery AJ, Hammond CJ, van Duijn CM, Hauser MA, Rabinowitz YS, Pfeiffer N, Mackey DA, Craig JE, Macgregor S, Wong TY. Genome-wide association analyses identify multiple loci associated with central corneal thickness and keratoconus. *Nat Genet.* 2013 Feb;45(2):155-63.

ABOUT THE AUTHOR

Hendrika Springelkamp was born on the 17th of June, 1987 in Apeldoorn, the Netherlands. She graduated from secondary school at de Heemgaard, Apeldoorn, in 2005. She subsequently started studying medicine at the University of Utrecht in September 2005. In 2009, she spent 3 months of her medical school in Paramaribo, Suriname. She conducted several internships in the field of Ophthalmology, including a research internship in the Erasmus Medical Center in 2010. After obtaining her medical degree in August 2011, she began her PhD study described in this thesis at the Department of Ophthalmology and the Department of Epidemiology of the Erasmus Medical Center in Rotterdam under supervision of Prof.dr. C.M. van Duijn, Prof.dr. N.M. Jansonius and Prof.dr. C.C.W. Klaver. In 2013, she obtained a Master of Health Sciences in Genetic Epidemiology at the Netherlands Institute for Health Sciences (NIHES). She has presented her work at several national and international meetings. In 2014, she received the Bayer Ophthalmology Research Award (BORA) and the Cultuurfondsbeurs from the Jan de Ruijsscher / Pia Huisman Fonds (Prins Bernhard Cultuurfonds). As part of her PhD study, she worked 3 months at QIMR Berghofer Medical Research Institute in Brisbane, Australia, under supervision of dr. Stuart MacGregor. In March 2015, she started her residency in Ophthalmology at the Department of Ophthalmology at the Erasmus Medical Center, headed by Prof.dr. J.R. Vingerling.

